List of Contributors

Steve C. F. Au-Yeung, *Department of Chemistry, The Chinese University of Hong Kong, Shatin, New Territories, Hong Kong*

Patrick J. Barrie, *Department of Chemical Engineering, University of Cambridge, Pembroke Street, Cambridge CB2 3RA, UK*

Jerry C. C. Chan, *Institut für Physikalische Chemie, Westfälische Wilhelms-Universität, Schlossplatz 7, D48149 Münster, Germany*

Rubén H. Contreras, *Departamento de Física, Facultad de Ciencias Exactas y Naturales, Universidad de Buenos Aires, Buenos Aires, Argentina*

Stephan Dusold, *Bayerisches Geoinstitut, University of Bayreuth, D-95440 Bayreuth, Germany*

Julio C. Facelli, *Center for High Performance Computing, University of Utah, Salt Lake City, Utah 84102, USA*

Caludia G. Giribet, *Departamento de Física, Facultad de Ciencias Exactas y Naturales, Universidad de Buenos Aires, Buenos Aires, Argentina*

Juan E. Peralta, *Departamento de Física, Facultad de Ciencias Exactas y Naturales, Universidad de Buenos Aires, Buenos Aires, Argentina*

Martin C. Ruiz de Azúa, *Departamento de Física, Facultad de Ciencias Exactas y Naturales, Universidad de Buenos Aires, Buenos Aires, Argentina*

Angelika Sebald, *Bayerisches Geoinstitut, University of Bayreuth, D-95440 Bayreuth, Germany*

Preface

Volume 41 of Annual Reports on NMR consists of four reports covering diverse areas of molecular science. The first one is Cobalt-59 NMR Spectroscopy by J. C. C. Chan and S. C. F. Au-Yeung. Following this is an account of Advances in Theoretical and Physical Aspects of Spin–Spin Coupling Constants by R. H. Contreras, J. E. Peralta, C. G. Giribet, M. C. Ruiz de Azua and J. C. Facelli. The third contribution is by S. Dusold and A. Sebald on Dipolar Recoupling under Magic-Angle-Spinning Conditions. The final chapter relates to the Characterization of Porous Media using NMR Methods by P. J. Barrie. It is a very great pleasure for me to have this opportunity to express my gratitude to these reporters for their cerebral accounts which contain many important features making them appealing to a broad scientific audience.

My thanks are also due to the production staff at Academic Press (London) for their efforts in the reification of this volume from the initial concepts.

University of Surrey
Guildford, Surrey
England

G. A. WEBB
May 1999

Cobalt-59 NMR Spectroscopy

JERRY C. C. CHAN[1] and STEVE C. F. AU-YEUNG[2]

[1] *Institut für Physikalische Chemie, Westfälische Wilhelms-Universität Münster, Schlossplatz 7, D48149 Münster, Germany*
[2] *Department of Chemistry, The Chinese University of Hong Kong, Shatin, New Territories, Hong Kong, China*

1. INTRODUCTION

The cobalt-59 nucleus has been one of the key nuclei in the history of NMR, on which the chemical shift concept was developed.[1] ^{59}Co is a quadrupolar nucleus of spin 7/2 and has a natural abundance of 100%. The receptivity of ^{59}Co is better than that of ^{13}C by a factor of 1570. Its resonance frequency is about 71.2 MHz at 7.1 T. The relaxation time of ^{59}Co is relatively short, in

ANNUAL REPORTS ON NMR SPECTROSCOPY
VOLUME 41 ISBN 0-12-505341-X

general less than 1 s for polycrystalline and solution samples. Except in cases when the electric field gradients at the cobalt sites are very large, ^{59}Co is a distinctly 'user-friendly' nucleus by today's standards. ^{59}Co NMR spectroscopy has regularly been reviewed in the literature. Various medium effects on ^{59}Co chemical shifts, such as concentration, temperature, pressure, hydrogen-bonding and ion-pairing, have been incisively discussed by Kidd,[2] Laszlo[3] and Goodfellow.[4] The ligand-field interpretation and parametrization of ^{59}Co chemical shifts were described in detail by Juranic.[5] While Mason illustrated the periodicity in the chemical shielding of transition-metal nuclei,[6] Kidd discerned the dependence of the shielding on metal oxidation states.[7–9] Both authors gave a substantial coverage of ^{59}Co NMR. An extensive database on solution ^{59}Co chemical shifts was constructed and updated by Yamasaki.[10,11] Also, Pregosin concisely summarized several empirical correlations between ^{59}Co chemical shifts and regioselectivity/catalytic activity.[12]

Some years ago, Laszlo commented that the potential of ^{59}Co NMR was largely untapped.[3] While this remark may remain appropriate today, we find it rather difficult to include every aspect of ^{59}Co NMR in a review of reasonable length. Not only is there a wealth of literature on the ^{59}Co hyperfine interaction of cobalt-containing alloys and ferromagnetic materials determined by spin-echo techniques, there is also a considerable volume of work dedicated to *in vivo* ^{59}Co NMR. As we intend to focus on the 'mainstream' of ^{59}Co NMR, regrettably these two topics are considered beyond the scope of the present chapter. The virtues and uniqueness of ^{59}Co NMR have also been well documented and require no replication of what has been reviewed. As such, this contribution is a comprehensive review of the literature on solid-state ^{59}Co NMR so as to complement the existing excellent reviews on solution-state work. A brief account of the recent progress in chemical shift interpretation and relaxation studies is also presented, covering the relevant solution-state studies published in the 1990s, in which particular attention will be given to controversial results. Finally, we summarize the advances in the theoretical calculations of ^{59}Co NMR parameters.

2. SOLID-STATE NMR

Solid-state NMR techniques are nowadays indispensable for the study of a wide variety of crystalline and amorphous systems. In general, a Hamiltonian describing any NMR-active spin system can be expressed as the sum of isotropic and anisotropic terms.[13,14] The anisotropic part of a Hamiltonian, which is averaged to zero in isotropic fluids, contains valuable information about the spatial orientation of the NMR-active species. Although the first ^{59}Co NMR work can be traced back to the 1950s, relatively few solid-state ^{59}Co NMR data have been reported compared with the large body of literature concerning other quadrupolar nuclei such as ^{23}Na or ^{27}Al. The main reasons

for this belated development of ^{59}Co solid-state NMR spectroscopy are twofold: (i) the ^{59}Co nucleus has a nuclear spin of 7/2 and a large quadrupole moment of 0.40×10^{-28} m^2, which degrades the detection sensitivity and the spectral resolution when the electric field gradient (EFG) at the cobalt site is nonzero; (ii) the general coexistence of chemical shift anisotropy and second-order quadrupolar broadening renders nontrivial the numerical simulation of ^{59}Co NMR spectra arising from static powder samples. Because of these problems, single-crystal NMR measurements remained the only reliable method in the early development of solid-state ^{59}Co NMR. Despite the considerable number of single-crystal studies appearing in the literature, most review articles about ^{59}Co NMR have very little coverage of the solid-state aspect. In view of the recent revival of interest in probing structures and bondings by solid-state ^{59}Co NMR, a compilation of the literature data is in order.

In this section, we attempt to review the solid-state ^{59}Co NMR data published up to the end of 1998. The data on chemical shift tensors and quadrupole coupling constants are summarized in Tables 1–4. Data obtained by nuclear quadrupole resonance (NQR) are included wherever appropriate. Readers interested in the spin–spin coupling between spin-1/2 and ^{59}Co nuclei are referred to an article by Wasylishen and colleagues and the references cited therein.[15] The NMR conventions employed in this review are defined in the next section. This is followed by a discussion of the techniques that have been applied to solid-state ^{59}Co NMR studies with emphasis on what has been applied to ^{59}Co systems. A detailed discussion on the techniques and Hamiltonians for quadrupolar nuclei is referred to the comprehensive review by Freude and Haase.[16]

2.1 Definitions and conventions

Chemical shielding and chemical shift. Following the IUPAC convention, the definition of chemical shielding is

$$\sigma/\text{ppm} = 10^6 \frac{(\nu_{\text{nucl}} - \nu_{\text{s}})}{\nu_{\text{nucl}}} \tag{1}$$

where ν_{s} and ν_{nucl} are the resonance frequencies of the sample and the bare nucleus, respectively. Chemical shielding is a tensorial quantity describing the modification of the magnetic field experienced by a nucleus arising from the interaction between the external $\mathbf{B}_0$ field and the electrons in the close vicinity of the nucleus. Since it is impracticable to determine ν_{nucl} experimentally, the relative value of the shielding tensor of the sample with respect to that of a reference standard is measured in practice. This so-called chemical shift, also a

Table 1. Summary of the solid-state ^{59}Co NMR/NQR parameters of Co(III) model systems[a]

Compound	$e^2q_{33}Q/h$ (MHz)	η_Q	δ_{iso} (ppm)	Ω (ppm)	κ	α,β,γ (deg)	Remarks	Ref.
$Co(acac)_3$[b]	5.6(1)	0.20(3)	12505(1)	1159(46)	−0.55(5)	–	MAS, VAS	73
	5.53(7)	0.22(6)	12498(5)	1174(13)	−0.57(5)	72.4, 86.4, 12.9	SNMR	37
$Co(NH_3)_6Cl_3$[c]								
Site 1	0.97(1)	0.10(1)	7899(2)	118	0.05	–	SNMR, MAS	175, 176, 74
Site 2	2.11(1)	0.53(1)	7963(2)	163	0.66			
Site 3	3.37(1)	0.45(1)	7848(2)	308	0.56			
Site 4	17.17(3)	0.57(2)	–	818	−0.22			
$K_3Co(CN)_6$	6.2	0.82	14	96	0.41	74, 66, 14	Static powder	53
$K_3Co(CN)_6$[d]	5.88(1)	0.900(4)	–	178(10)	−0.74(13)	–	SNMR	177, 178
$LaCo(CN)_6$	1.08	0	–	–	–	–	Static powder	47
$Co(en)_3Cl_3$[e]	–	–	–	255	1.0	–	Static powder	44
	2.63	0	–	–	–	–	NQR	46
$Na_3Co(NO_2)_6$	9.4	0	–	180	−1.0	–	Static powder	44
	8.2	0.0	7628	180	−1.0	90, 90, 0	Static powder	50
	8.23	0	7641	177	−1.0	–	3QMAS	72
	8.24	0	–	–	–	–	Nutation	79
	8.15	0.03	7631	186.5	−0.95	–	Static powder	80
$[Co(NH_3)_5Cl]SO_4 \cdot H_2SO_4$[f]	33.43(4)	0.042	–	–	–	–	NQR	52
	34.39(4)	0.089						
$[Co(NH_3)_5CN]Cl_2$	26.57(1)	0.1853(2)	6700	2300	−0.91	–	SNMR	35
$[Co(NH_3)_5Cl]Cl_2$	31.74	0.215	–	–	–	–	NQR	52
	26.9(5)	0.0(1)	8890(5)			–	Q-CPMG	51
$[Co(NH_3)_5H_2O](ClO_4)_3$	54.8	0	9100	3060	1.0	–	SNMR	34
trans-$[Co(NO_2)_4(NH_3)_2]NH_4$	32.7	0	–	–	–	–	SNMR	34
trans-$[Co(NH_3)_4Cl_2]Cl$	59.23	0.136	–	–	–	–	NQR	179
trans-$[Co(tn)_2Cl_2]Cl \cdot HCl \cdot 2H_2O$[g]	61.41	0.132	–	–	–	–	NQR	180
trans-$[Co(en)_2Cl_2]Cl \cdot HCl \cdot 2H_2O$	71.73(5)	0.222(2)	–	–	–	–	NQR	181
	71.679(7)	0.2248(2)	9200	4800	0.87	–	SNMR	34
	71.816	0.2248	–	–	–	–	NQR	182

trans-$[Co(en)_2Cl_2]Cl \cdot HCl \cdot 2H_2O$[h]	71.894	0.2192	–	–	–	–	NQR	182
trans-$[Co(en)_2Cl_2]Cl$	60.63	0.272	–	–	–	–	NQR	179
trans-$[Co(en)_2Cl_2]Br$	60.08	0.204	–	–	–	–	NQR	183
trans-$[Co(en)_2Cl_2]I$	58.41	0.156	–	–	–	–	NQR	183
trans-$[Co(en)_2Cl_2]NO_3$	62.78	0.132	–	–	–	–	NQR	179
trans-$[Co(en)_2Cl_2]SCN$	60.43	0.245	–	–	–	–	NQR	172
trans-$[Co(en)_2Cl_2]BrO_3$	65.15	0.238	–	–	–	–	NQR	172
trans-$[Co(en)_2Cl_2]ClO_4$[c]	60.22	0.149	–	–	–	–	NQR	172
	60.14	0.146						183
	59.92	0.149						172
	59.86	0.148						183
trans-$[Co(en)_2Br_2]Br$	60.36	0.235	–	–	–	–	NQR	179
trans-$[Co(en)_2Br_2]Br \cdot HBr$	72.80	0.244	–	–	–	–	NQR	181
trans-$[Co(en)_2Br_2]ClO_4$	57.38	0.149	–	–	–	–	NQR	172
trans-$[Co(en)_2(NO_2)_2]NO_3$	13.22(1)	0.7272(5)	6300	400	−0.5	–	SNMR	34
	13.3	0.735	6211	400	−0.5	0, 3.5, 90	Static powder	50
	13	0.75	6211	393	−0.48	–	MAS	72
	13.28	0.85	–	–	–	–	Nutation	63
$[Co(C_5H_5)_2]NO_3$	165.61(3)	0.0070(1)	−2500	6500	0.91	–	SNMR	34
$[Co(C_5H_5)_2]ClO_4$	171	0.0	–	–	–	–	NQR	184, 185
cis-$[Co(en)_2Cl_2]Cl \cdot H_2O$	36.05	0.268	–	–	–	–	NQR	186
cis-$[Co(en)_2Cl_2]NO_3$	33.71	0.173	–	–	–	–	NQR	186
$[Co(NH_3)_4CO_3]Br$	18.82(1)	0.7269(2)	9700	1500	0.33	–	SNMR	34

[a] Unless stated otherwise, all the measurements were done at room temperature; the chemical shifts data were referenced to aqueous $K_3[Co(CN)_6]$; the parenthetical figures indicate the error estimation.
[b] acac = $(CH_3COCHCOCH_3)^-$.
[c] Four crystallographically nonequivalent sites.
[d] Doped with 0.079% Cr (by mass).
[e] en = ethylenediamine.
[f] Two crystallographically nonequivalent sites.
[g] tn = trimethylenediamine.
[h] Deuterated sample.

Table 2. Summary of the solid-state ^{59}Co NMR/NQR parameters of cobalt clusters[a]

Compound	$e^2q_{33}Q/h$ (MHz)	η_Q	δ_{iso} (ppm)	Ω (ppm)	κ	α,β,γ (deg)	Remarks	MW	Ref.
$Cl_3SiCo(CO)_4$	130.67	0.13	–	–	–	–	NQR	305.42	195
$(HCCH)Co_2(CO)_6$	84.76(11)	0.551(8)	–	–	–	–	NQR, 273 K	311.97	187
$(CH_3)_3SnCo(CO)_4$	96.8	0.03	–	–	–	–	NQR	334.77	196
$Co_2(CO)_8$									
Site A	90.19(2)	0.3136(3)	−2200	500	−1	–	SNMR, 77 K	341.95	188
Site B	89.30(15)	0.4837(1)	–	–	–	–	NQR, 77 K		189
$Cl_3GeCo(CO)_4$	160.4	0.035	–	–	–	–	NQR	349.92	200
$Co(CO)_4Mn(CO)_5$	128.79(2)	0.12(3)	−3000	100	1	–	SNMR,NQR	365.96	190
$(Bu^tCCH)Co_2(CO)_6$	82.66(28)	0.568(52)	–	–	–	–	NQR, 273 K	368.07	187
$(HOCH_2CCCH_2OH)Co_2(CO)_6$	86.45(40)	0.528(30)	–	–	–	–	NQR, 273 K	372.02	187
$(\pi\text{-}C_7H_8)Co_2(CO)_6$	81.9(8)	0.34(3)	–	–	–	–	NQR, 273 K	378.07	187
$Cl_2GaCo(CO)_4\cdot THF$	107.2	0.10	–	–	–	–	NQR	383.71	191
$Cl_3SnCo(CO)_4$	163.45	0	–	–	–	–	NQR	396.02	195
$Zn[Co(CO)_4]_2$	83.85	0.067	–	–	–	–	NQR	407.33	192
$(\pi\text{-}C_7H_8)_2Co_2(CO)_4$	73.9(7)	0.70	–	–	–	–	NQR, 273 K	414.19	187
$acacGaBrCo(CO)_4$	101.7	0.10	–	–	–	–	NQR	419.71	191
$Ph_3SiCo(CO)_4$	101.09	0	–	–	–	–	NQR	430.38	195
$Co_3(CO)_9(CH)$	77.3	0.18	–	–	–	–	NQR	441.91	193
$(CF_3CCCF_3)Co_2(CO)_6$	64	0.73	–	–	–	–	NQR, 273 K	447.96	187
$Cd[Co(CO)_4]_2$	90.5	0.128	–	–	–	–	NQR	454.36	192
$Co_3(CO)_9(CCH_3)$	77.5	0.15	–	–	–	–	NQR	455.94	93
$(PhCCPh)Co_2(CO)_6$	75(3)	0.67	–	–	–	–	NQR, 273 K	464.16	187
$Co_3(CO)_9(COCH_3)$	83(3)	0.11	–	–	–	–	NQR	471.94	193
$Br_2GaCo(CO)_4\cdot THF$	109.7	0.06	–	–	–	–	NQR	472.61	191
$Ph_3GeCo(CO)_4$	109.63	0.05	–	–	–	–	NQR	474.88	194
$Co_3(CO)_9(CCl)$	76.26	0.068	–	–	–	–	NQR	476.36	193
$Cl_3Si[Co(CO)_3P(n\text{-}C_4H_9)_3]$	113.9	0	–	–	–	–	NQR	479.73	202
$Br_3GeCo(CO)_4$	161.34	0.12	–	–	–	–	NQR	483.28	195

$Cl_2Ge[Co(CO)_4]_2$	150(5)	0.10(6)	–	–	–	–	NQR	485.45	196
$(CH_3)_2Sn[Co(CO)_4]_2$	105.7	0	–	–	–	–	NQR	490.7	196
$Co_3(CO)_9(COCOCH_3)$	78.5	0.15	–	–	–	–	NQR	499.95	193
$Co_3(CO)_9(CCF_3)$	68.1	0.14	–	–	–	–	NQR	509.91	193
$acacGa[Co(CO)_4]_2$	96.4(9)	0.08	–	–	–	–	NQR	510.78	191
$Co_3(CO)_9(CCOOC_2H_5)$	70(3)	0.16	–	–	–	–	NQR	513.98	193
$Co_3(CO)_9(CPh)$	74(2)	0.16	–	–	–	–	NQR	518.01	193
$ClGa[Co(CO)_4]_2 \cdot THF$	102.2	0.15	–	–	–	–	NQR	519.23	191
$Ph_3SnCo(CO)_4$	104.00(2)	0.0285(2)	−3200	200	0	–	SNMR	520.98	200
$Cl_3Ge[Co(CO)_3P(n\text{-}C_4H_9)_3]$	166.0	0	–	–	–	–	NQR	524.23	202
$Br_3SnCo(CO)_4$	159.88(2)	0.0723(2)	−2600	700	0.7	–	SNMR	529.38	200
$Cl_2Sn[Co(CO)_4]_2$	146.9(2)	0.069	–	–	–	–	NQR	531.55	197
$[(CH_3O)_3PCo(CO)_3]_2$	143.982	0.0405	–	–	–	–	NQR	534.08	198
$Hg[Co(CO)_4]_2$	111.4(6)	0.03(2)	–	–	–	–	NQR	542.54	196
$Co_3(CO)_9(CCOPh)^b$	51.21	0.287	–	–	–	–	NQR	546.02	193
	68.93	0.214							
	79.85	0.172							
$acacIn[Co(CO)_4]_2$	101(3)	0.10(2)	–	–	–	–	NQR	555.88	191
$Co_3(CO)_9(CSi(C_2H_5)_3)$	67(2)	0.28	–	–	–	–	NQR	556.17	193
$(PhCH_2)_3SnCo(CO)_4$	100.4	0.15	–	–	–	–	NQR	563.06	199
$BrGa[Co(CO)_4]_2 \cdot THF$	103.3	0.16	–	–	–	–	NQR	563.68	191
$ClIn[Co(CO)_4]_2 \cdot THF$	104(4)	0.10(4)	–	–	–	–	NQR	564.33	191
$HFeCo_3(CO)_{12}$	12.19(12)	0.23(3)	−2833(5)	1739(27)	0.93(1)	0, 43.9(5), 90	Static powder	569.78	26
$Cl_3Sn[Co(CO)_3P(n\text{-}C_4H_9)_3]$	173.6	0	–	–	–	–	NQR	570.33	202
$Co_4(CO)_{12}{}^c$	15(3)[d]	0.8	−715	–	–	–	Nutation	571.86	81
	12.40[d]	0.32	–	–	–	–	Nutation		80
	9(2)[e]	0	−1125	–	–	–	Nutation		81
$ClPhSn[Co(CO)_4]_2$	127.6(7)	0.07(2)	–	–	–	–	NQR	573.20	197
$Cl_3Ge[Co(CO)_3PPh_3]$	156.9(1)	0.08	–	–	–	–	NQR	584.20	202
$BrIn[Co(CO)_4]_2 \cdot THF$	106(3)	0.11(4)	–	–	–	–	NQR	608.78	191
$(C_6H_5)_3PbCo(CO)_4$	110.82	0.05	–	–	–	–	NQR	609.49	195
$(C_6H_5)_2Sn[Co(CO)_4]_2$	112.9(2)	0.08(2)	–	–	–	–	NQR	614.85	197

(*continued*)

Table 2. *Continued*

Compound	e^2qQ/h (MHz)	η_Q	δ_{iso} (ppm)	Ω (ppm)	κ	α,β,γ (deg)	Remarks	MW	Ref.
$HRuCo_3(CO)_{12}$	18.57(4)	0.4(2)	−2916(2)	1745(7)	0.87(1)	0, 39.4(4), 90	Static powder	615.00	26
$Ph_3SnCo(CO)_3P(OCH_3)_3$	104.19	0.04	–	–	–	–	NQR	617.05	194
$(CH_3)_3SnCo(CO)_3P(OPh)_3$	103.88	0.03	–	–	–	–	NQR	617.05	194
$[(C_2H_5O)_3PCo(CO)_3]_2$	141.655	0.0320	–	–	–	–	NQR	618.24	198
$f_4farsCo_2(CO)_6$[f]	89.7(6)	0.48(1)	–	–	–	–	NQR, 273 K	619.95	187
$Br_2Sn[Co(CO)_4]_2$	146.5	0.08(8)	–	–	–	–	NQR	620.45	196
$I_3GeCo(CO)_4$	158.76(2)	0.0487(2)	−2300	1200	0.8	–	SNMR	624.28	200
$In[Co(CO)_4]_3$	103(2)	0.3(1)	–	–	–	–	NQR	627.74	192
$CH_3Sn[Co(CO)_4]_3$	121	0.06	–	–	–	–	NQR	646.65	196
$ClSn[Co(CO)_4]_3$	134.3(1.6)	0.07	–	–	–	–	NQR	667.07	196
$I_3SnCo(CO)_4$	153.04	0.06	–	–	–	–	NQR	670.38	195
$Cl_3SnCo(CO)_3P(OPh)_3$	159.46	0.03	–	–	–	–	NQR	678.30	194
$[(n\text{-}C_4H_9)_3PCo(CO)_3]_2$	140.627	0.0333	–	–	–	–	NQR	690.57	198
$Ph_3SnCo(CO)_3P(n\text{-}C_4H_9)_3$	103.18	0.04	–	–	–	–	NQR, 338 K	695.29	194
$[NEt_4][FeCo_3(CO)_{12}]$	23.25(8)	0.47(1)	−2648(20)	1076(5)	0.86(4)	90, 16.3(6), 0	Static powder	699.02	26
$\{Co(CO)_3[P(OCH_3)_3]_2\}BPh_4$	136.1	0.13	–	–	–	–	NQR	710.35	201
$BrSn[Co(CO)_4]_3$	133.0	0.14	–	–	–	–	NQR	711.52	196
$Ph_3SnCo(CO)_2[P(OCH_3)_3]_2$	104.20	0.37	–	–	–	–	NQR	713.11	194
$Tl[Co(CO)_4]_3$	119(1)	0.22	–	–	–	–	NQR	717.31	192
$Bi[Co(CO)_4]_3$	131(1)	0.09	–	–	–	–	NQR	721.90	192
$f_4fars(PhCCPh)Co_2(CO)_4$	64.881	0.828	–	–	–	–	NQR	742.16	187
$[NEt_4][RuCo_3(CO)_{12}]$	16.75(5)	0.53(2)	−2745(20)	1019(10)	0.93(5)	90, 21.5(4), 0	Static powder	744.25	26

$Ph_3GeCo(CO)_3P(OPh)_3$	113.02	0.25	–	–	–	–	NQR	757.16	194
$Sn[Co(CO)_4]_4$	129.2	0	–	–	–	–	NQR	802.59	196
$Ph_3SnCo(CO)_3P(OPh)_3$	110.44	0.27	–	–	–	–	NQR	803.26	194
$\{Co(CO)_2[P(OCH_3)_3]_3\}BPh_4$	136.3	0.47	–	–	–	–	NQR	806.42	201
$[Co(CO)_3PPh_3]_2$	146.8	0	–	–	–	–	NQR	810.51	202
$[Co(CO)_4][Co(CO)_3(PPh_3)_2]$	159.7	0.05	–	–	–	–	NQR	838.52	202
$HFeCo_3(CO)_9[P(OCH_3)_3]_3$	17.7	0.57	–	–	–	–	Static powder	857.98	63
$Ph_3PbCo(CO)_3P(OPh)_3$	120.28	0.26	–	–	–	–	NQR	891.77	194
$Ph_3POIn[Co(CO)_4]_3$	97(4)	0.15	–	–	–	–	NQR	906.03	191
$[(PhO)_3PCo(CO)_3]_2$	156.230	0.0414	–	–	–	–	NQR	906.51	198
$(Ph_3P)_2Co(CO)_3BPh_4$	157.754	0.219	–	–	–	–	NQR	986.78	198
$\{Co[P(OCH_3)_3]_5\}BPh_4$	153.7	0.04	–	–	–	–	NQR	998.55	201
$Ph_3SnCo(CO)_2[P(OPh)_3]_2$	95.40	0.55	–	–	–	–	NQR	1085.54	194
$Ph_4AsHg[Co(CO)_4]_3$	80.9	0.28	–	–	–	–	NQR	1096.86	192
$Hg[Co(CO)_3P(OPh)_3]_2$[c]	114.65	0.27	–	–	–	–	NQR	1107.10	194
	106.91	0.06							
$In_3Br_3Co_4(CO)_{15}$	115.7(4)	0.09(4)	–	–	–	–	NQR	1240.06	191
$\{ClIn[Co(CO)_4]_2\}_x$	115.5	0.15	–	–	–	–	NQR		191
$\{BrIn[Co(CO)_4]_2\}_x$	116.2	0.15	–	–	–	–	NQR		191

[a] See footnote *a* of Table 1; average values of multiple sites were listed for the NQR data unless stated otherwise; the data are sorted in ascending order of molecular weight (MW).
[b] Three crystallographically nonequivalent sites.
[c] Two crystallographically nonequivalent sites.
[d] Apical site.
[e] Basal site.
[f] $f_4fars = (CH_3)_2AsCCAs(CH_3)_2CF_2CF_2$.

Table 3. Summary of the solid-state ^{59}Co NMR parameters of Co(III) systems of biological interests[a]

Compound	$e^2q_{33}Q/h$ (MHz)	η_Q	δ_{iso} (ppm)	Ω (ppm)	κ	α,β,γ (deg)	Remarks	Ref.
Co(TPP)Im_2	4.9(1.5)[b]	–	8940(6)	2640(60)	0.78(4)	–	MAS	74
Co(TPP)$MeIm_2$	3.1(2.4)[b]	–	8632(6)	2800(60)	0.75(4)	–	MAS	74
Co(OEP)Im_2	6.4(1.2)[b]	–	9220(6)	3300(60)	0.43(4)	–	MAS	74
Co(OEP)$MeIm_2$	3.4(2.2)[b]	–	9027(6)	2800(60)	0.81(4)	–	MAS	74
Co(TMeOPP)Im_2	4.4(1.7)[b]	–	8931(6)	2700(60)	0.73(4)	–	MAS	74
Co(TMeOPP)$MeIm_2$	5.5(1.4)[b]	–	9023(1)	2500(60)	0.87(4)	–	MAS	74
Co(TPP)Py_2	16.5	0.1	8440(50)	2800(60)	0.88(4)	0, 0, 0	Static powder	74
Co(TPP)$IsoQ_2$	26	0.3	8260(50)	4100(60)	0.65(3)	120, 20, 0	Static powder	74
Vitamin B_{12}[c]	17.7(6)	0.2(2)	4800(100)	1280(60)	0.8(2)	45(40), 45(25), 45(40)	Static powder	27
Vitamin B_{12}[d]	26.1(4)	0.1(2)	4650(100)	1000(100)	0.8(2)	20(20), 40(20), 135(25)	Static powder	27
Vitamin B_{12}[d]	27.31(8)	0.243(5)	4549(45)	1173(52)	0.3(0.1)	26(13), 41.4(1.7), 152.7(2.5)	SNMR	39
B_{12} coenzyme[c]	23.5(6)	1.0(2)	4500(100)	1530(60)	−0.3(2)	135(30), 160(20), 135(30)[e,f]	Static powder	27
B_{12} coenzyme[d]	22(2)	0.7(4)	4700(300)	2000(200)	0.0(4)	0(35), 75(35), 135(35)	Static powder	27
Methylcobalamin[c]	19.0(6)	0.4(2)	4340(120)	2790(80)	−0.6(2)	130(40), 150(25), 135(40)[e]	Static powder	27
Methylcobalamin[d]	12.1(4)	0.3(2)	4250(100)	2990(80)	−0.5(2)	0(40), 60(25), 155(40)[e]	Static powder	27
Dicyanocobyrinic acid heptamethylester[c]	26.7(8)	0.9(4)	4300(200)	1600(100)	0.2(2)	0(35), 95(35), 0(35)	Static powder	27
Dicyanocobyrinic acid heptamethylester[d]	26.7(8)	0.9(4)	4300(200)	1600(100)	0.2(2)	0(35), 95(35), 0(35)	Static powder	27
(CH_3)(Py)Co$(DH)_2$[g]	29.6(4)	0.1(2)	3640(100)	1160(50)	−0.6(2)	190(25), 90(25), 150(25)[e]	Static powder	27
(CH_3)(Im)Co$(DH)_2$	32.1(4)	0.1(2)	3620(100)	1160(50)	−0.5(2)	135(25), 90(25), 170(25)[e]	Static powder	27
(CN)(Py)Co$(DH)_2$	27.7(4)	0.0(2)	4100(100)	1100(50)	0.4(2)	130(25), 90(25), 165(25)	Static powder	27
K[$(CN)_2$Co$(DH)_2$]	40.2(4)	0.5(2)	3200(100)	880(50)	0.4(2)	90(25), 0(25), 170(25)	Static powder	27
$(CH_3)(H_2O)$Co$(DH)_2$	18.4(4)	1.0(2)	4220(100)	770(50)	−0.3(2)	190(25), 80(25), 160(25)[e]	Static powder	27
[$(NH_3)_2$Co$(DH)_2$]Cl	30.7(4)	0.6(2)	5320(100)	2510(50)	0.8(2)	90(25), 90(25), 0(25)	Static powder	27
N_3Co$(DH)_2$P$(OEt)_3$	24(2)	–	–	–	–	–	^{31}P MAS	15

$CH_3Co(DH)_2PPh_3$	28.12	0.77	–	–	–	–	NQR	203
$CH_3Co(DH)_2NC_5H_5$	29.52	0.22	–	–	–	–	NQR	203
$CH_3Co(DH)_2S(CH_3)_2$	30.30	0.58	–	–	–	–	NQR	203
$CH_3Co(DH)_2AsPh_3$	[30.59][h]	[0.35]	–	–	–	–	NQR	203
	[32.02]	[0.73]						
$CH_3Co(DH)_2N(CH_3)_3$	[31.0]	[0.15]	–	–	–	–	NQR	203
	[33.3]	[0.84]						
$CH_3Co(DH)_2$-imid[i]	[31.34]	[0.18]	–	–	–	–	NQR	203
	[33.69]	[0.82]						
$CH_3Co(DH)_2P(OCH_2)_3CC_2H_5$	40.24	0.50	–	–	–	–	NQR	203
$CH_3Co(DH)_2CH_3OH$	41.62	0.30	–	–	–	–	NQR	203
$CH_3Co(DH)_2P(OCH_3)_3$	43.33	0.57	–	–	–	–	NQR	203
$CH_3Co(DH)_2P(n\text{-}C_4H_9)_3$	46.20	0.55	–	–	–	–	NQR	203
$CHCl_2Co(DH)_2S(CH_3)_2$	36.93	0.79	–	–	–	–	NQR	203
$N(C_2H_5)_4[Br_2Co(DH)_2]$	75.88	0.68	–	–	–	–	NQR	203
$N(C_2H_5)_4[Cl_2Co(DH)_2]$	73.15	0.72	–	–	–	–	NQR	203
$ClCo(DH)_2NC_5H_5$	64.82	0.63	–	–	–	–	NQR	203
$ClCo(DH)_2PPh_3$	60.45	0.81	–	–	–	–	NQR	203
$ClCo(DH)_2P(n\text{-}C_4H_9)_3$	[41.2]	[0.30]	–	–	–	–	NQR	203
	[43.6]	[0.77]						

[a] See footnote *a* of Table 1.
[b] The reported value corresponds to the second-order quadrupolar shifts, defined as $\chi(1+\eta_Q^2/3)^{1/2}$.
[c] As-purchased samples.
[d] Slowly recrystallized samples.
[e] The reported Euler angles correspond to the convention $|\delta_{33}-\delta_{iso}| \geq |\delta_{11}-\delta_{iso}| \geq |\delta_{22}-\delta_{iso}|$.
[f] The reported Euler angles might be inconsistent to the corresponding spectrum in ref. 27.
[g] DH denotes the dimethylglyoximato ligand.
[h] Values in the square brackets represent data that are equally probable.
[i] Imid = 1-(2-trifluoromethylphenyl)imidazole.
Im, imidazole; MeIm, methylimidazole; TPP, tetraphenylporphyrin; TMeOPP, tetramethoxyphenylporphyrin; OEP, octaethylporphyrin; Py, pyridine; Iso Q, isoquinoline.

Table 4. Summary of the solid-state ^{59}Co NMR/NQR parameters of miscellaneous Co(III) complexes.[a]

Compound	$e^2q_{33}Q/h$ (MHz)	η_Q	δ_{iso} (ppm)	Ω (ppm)	κ	α,β,γ (deg)	Remarks	Ref.
$CsCo(1,2\text{-}B_9C_2H_{11})_2$	161	0.03(1)	–	–	–	–	NQR	184, 185
[18]aneN$_6$[Co(CN)$_6$]	6.2	0.75	45	121	0.97	–	Static powder	53
[16]aneN$_4$[Co(CN)$_6$]	6.4	0.72	16	88	0.48	–	Static powder	53
[12]aneN$_4$[Co(CN)$_6$]	7.0	0.95	−62	250	0.40	–	Static powder	53
[24]aneN$_8$[Co(CN)$_6$]	5.0	0.98	3	100	−1.0	–	Static powder	53
[24]aneN$_6$[Co(CN)$_6$]	9.6	0.56	23	359	0.24	–	Static powder	53
[32]aneN$_8$[Co(CN)$_6$]	5.3	0.98	10	380	0.16	–	Static powder	53
[(Et$_4$N)$_3$Co(CN)$_6$]	–	–	208	–	–	–	Static powder	54
[(nBu$_3$Sn)$_3$Co(CN)$_6$]	–	–	206	–	–	–	Static powder	54
[(Et$_3$Pb)$_3$Co(CN)$_6$]	–	–	−33	–	–	–	Static powder	55
[(Me$_3$Pb)$_3$Co(CN)$_6$]	–	–	−157	–	–	–	Static powder	54
[(Et$_3$Sn)$_3$Co(CN)$_6$]	–	–	−239	–	–	–	Static powder	55
[(Me$_3$Sn)$_3$Co(CN)$_6$]	–	–	−244	–	–	–	Static powder	54
[H$_3$Co(CN)$_6$]	–	–	−258	–	–	–	Static powder	54

[a] See footnote *a* of Table 1.

tensorial quantity, is defined to be

$$\delta/\text{ppm} = 10^6 \frac{(\nu_s - \nu_{ref})}{\nu_{ref}} \tag{2}$$

where ν_{ref} is the resonance frequency of the reference standard. As a result, chemical shielding and chemical shift are related by the following equation

$$\delta = \frac{(\sigma_{ref} - \sigma_s)}{(1 - \sigma_{ref})} \tag{3}$$

The chemical shielding tensor in general has nine components. In most cases only the symmetric part is measurable experimentally[17] and therefore three independent parameters are required to define a chemical shift tensor. Note that high symmetry elements at the nuclear site could reduce the number of these independent parameters.[18] In the literature, there is considerable confusion over the notation and definition of the chemical shift tensors. In this review, we will follow the suggestions proposed by a group of NMR spectroscopists in a meeting at the University of Maryland in 1992.[19,20] Accordingly, all the measured chemical shift tensors and calculated chemical shielding tensors are to be reported in terms of the isotropic (δ_{iso} and σ_{iso}), span (Ω) and skew (κ) values defined by the tensor principal components (δ_{ii}

and σ_{ii}):

$$\sigma_{11} \leqslant \sigma_{22} \leqslant \sigma_{33} \tag{4}$$

$$\delta_{33} \leqslant \delta_{22} \leqslant \delta_{11} \tag{5}$$

$$\sigma_{iso} = \frac{\sigma_{11} + \sigma_{22} + \sigma_{33}}{3} \tag{6}$$

$$\delta_{iso} = \frac{\delta_{11} + \delta_{22} + \delta_{33}}{3} \tag{7}$$

$$\Omega = \sigma_{33} - \sigma_{11} = \delta_{11} - \delta_{33} \geqslant 0 \tag{8}$$

$$\kappa = 3\,\frac{\sigma_{iso} - \sigma_{22}}{\Omega} = 3\,\frac{\delta_{22} - \delta_{iso}}{\Omega} \tag{9}$$

The idea of chemical shift skew and span are depicted in Fig. 1. κ takes the values between $+1$ and -1, where the two limits denote axial symmetries.

Quadrupolar parameters. The nuclear quadrupole coupling is an electrostatic interaction between the nuclear quadrupole moment, eQ, and the EFG tensor,

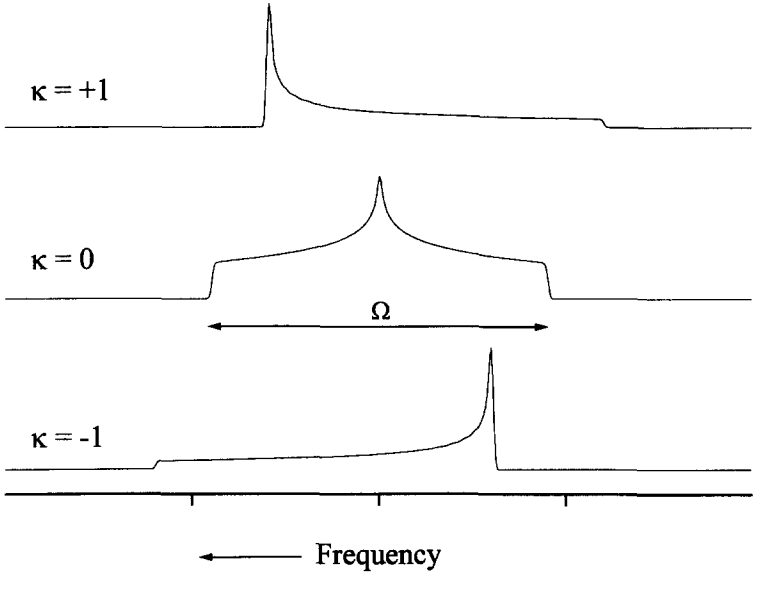

Fig. 1. Schematic illustration of the concepts of chemical shift span and skew. The three traces have the same span and isotropic values. The upper and lower traces correspond to the cases of axial symmetries ($\kappa = \pm 1$).

$e\mathbf{q}$, at a nuclear site. The principal components of $\mathbf{q}$ are defined in a right-handed fashion such that

$$|q_{33}| \geqslant |q_{22}| \geqslant |q_{11}| \tag{10}$$

Because the EFG tensor is traceless and symmetric, two parameters are sufficient to define the magnitude of the principal components, the quadrupole coupling constant, χ, and the asymmetry parameter η_Q:[16,21]

$$\chi = e^2 q_{33} Q/h \tag{11}$$

$$\eta_Q = \frac{q_{11} - q_{22}}{q_{33}} \tag{12}$$

In contrast to the concept of chemical shift skew, η_Q is defined between 0 and +1 and the case of axial symmetry corresponds to vanishing η_Q. Since the sign of χ cannot be determined by NMR experiments except at extremely low temperature,[22] it is usually assumed to be positive.

Euler angles. Without any constraints imposed by symmetry elements, the EFG and chemical shielding tensors at a nuclear site are oriented independently. In general it is necessary to specify three Euler angles (α,β,γ) to define the relative orientation of these two tensors. As pointed out by Man, there are several conventions in the literature concerning the definitions of Euler angles and therefore it is mandatory to clearly specify the convention employed.[23] In this review, Euler angles are reported to transform the principal coordinate of the EFG tensor to that of the chemical shift tensor following *ZYZ* order of rotation.[24] Figure 2 illustrates the transformation of the EFG frame into the chemical shift frame for $(\alpha,\beta,\gamma) = (90°, 90°, 90°)$. Our Euler angles (α,β,γ) have the following relationships with those employed by Wasylishen $(\alpha^W,\beta^W,\gamma^W)$,[25] Hirschinger $(\alpha^H,\beta^H,\gamma^H)$,[26] and Frydman $(\alpha^F,\beta^F,\gamma^F)$,[27] provided that the labels of the chemical shift components are identical:

$$(\alpha,\beta,\gamma) = \left(\alpha^W,\beta^W,\gamma^W + \frac{\pi}{2}\right) \tag{13}$$

$$(\alpha,\beta,\gamma) = \left(\frac{\pi}{2} - \gamma^H,\beta^H,\pi - \alpha^H\right) \tag{14}$$

$$(\alpha,\beta,\gamma) = (\pi - \gamma^F,\beta^F,\pi - \alpha^F) \tag{15}$$

Note that a given relative orientation of two tensors does not produce a unique triplet of Euler angles. Readers are referred to the article by Koons *et al.* for a discussion of the symmetry relationships for Euler angles.[28]

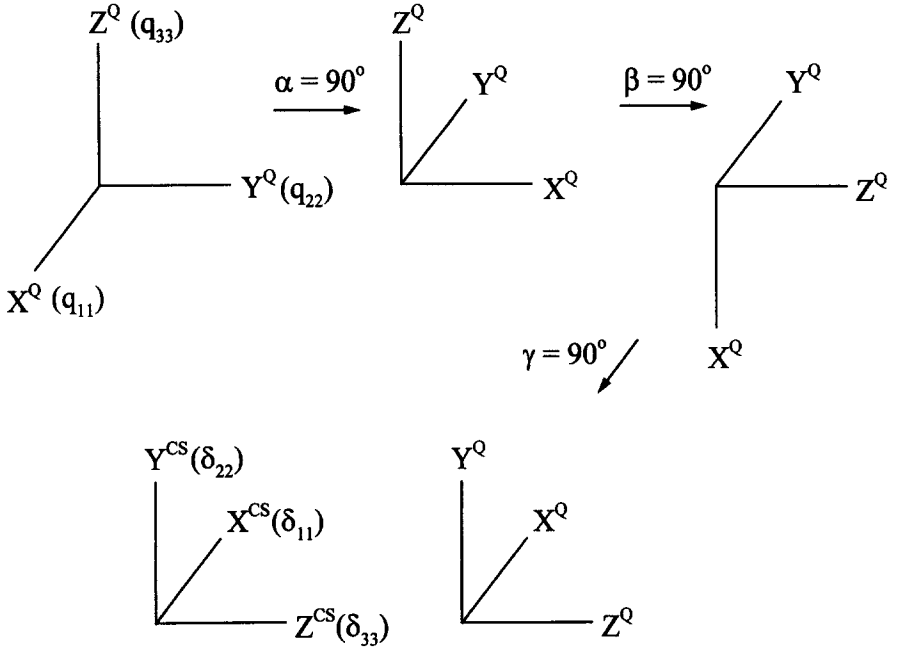

Fig. 2. Pictorial representation of the transformation between the EFG and chemical shift tensors produced by the Euler angles (α,β,γ) defined in this review. The principal coordinate of the EFG tensor ($X^Q Y^Q Z^Q$) is transformed to that of the chemical shift tensor ($X^{CS} Y^{CS} Z^{CS}$) in ZYZ order of rotation.

2.2. Single-crystal NMR

Single-crystal NMR (SNMR) is a powerful method that can provide information for a complete characterization of the tensors of anisotropic interactions. That is, in addition to the magnitudes of the principal tensor components, the tensor orientation with respect to the molecular frame is obtainable by SNMR. The method of analysis, which has been established for over 40 years, is straightforward though tedious.[29] It is therefore not surprising that SNMR enjoyed widespread popularity during the early days of ^{59}Co NMR spectroscopy. The practical aspects and the principles behind SNMR experiments have been discussed by Kennedy and Ellis.[30,31] Here we present results from several ^{59}Co SNMR studies.

The first ^{59}Co SNMR work appears to be the study of $K_3[Co(CN)_6]$ at 4.2 K in 1959.[32] The ^{59}Co quadrupole coupling constant and the asymmetry parameter were determined to be 7.3 MHz and 0.75, respectively, for a pseudo-orthorhombic twin crystal. In a subsequent SNMR study of Cr-doped $K_3[Co(CN)_6]$ at room temperature, the reported quadrupolar parameters were

significantly smaller. This discrepancy may originate from an unknown phase transition of $K_3[Co(CN)_6]$ at low temperature. More recently it has been shown that the crystal structures of $K_3[Co(CN)_6]$ and Cr-doped $K_3[Co(CN)_6]$ are different,[33] questioning the validity of doping the systems of interest with paramagnetic species for NMR study. Several cobalt(III) model compounds had been studied assuming a coincidence of the EFG and chemical shift tensors.[34,35] The authors noticed that the chemical shift anisotropy, defined as the difference between the isotropic value and the principal tensor component along the highest symmetry axis, is apparently proportional to the quadrupole coupling constant (see below). Very interesting results were obtained in studies of $[Co(NH_3)_6]Cl_3$ by Reynhardt.[36] Although the X-ray study shows that the four crystallographically nonequivalent $[Co(NH_3)_6]^{3+}$ octahedra are almost perfect,* very different ^{59}Co quadrupole coupling constants, ranging from 1 to 17 MHz, were observed for these sites. It was concluded that at temperature higher than 330 K the first three sites exhibit rapid isotropic reorientation, whereas the fourth site remains stationary throughout the studied temperature range (93–404 K). In addition to the hexacoordinated Co(III) complexes, several cobalt clusters have been investigated by SNMR and the results are summarized in Table 2. It is rather surprising to find that the literature was virtually devoid of ^{59}Co SNMR studies in the 1980s. Fortunately, the sleeping beauty was eventually awakened. In a reinvestigation of $Co(acac)_3$, Eichele *et al.* successfully resolved the discrepancy concerning the ^{59}Co quadrupolar parameters,[37] showing that the SNMR data of $Co(acac)_3$ reported by Reynhardt is erroneous.[38] Power and co-workers successfully determined the orientation of the ^{59}Co EFG tensor of vitamin B_{12}, indicating that any geometric perturbations of the axial ligands may cause a substantial change of the EFG at the cobalt site.[39]

Although SNMR is usually considered tedious and time-demanding, recent advances in software and instrumentation have greatly improved its efficiency and ease of the data acquisition.[40] Since SNMR is insensitive to any hardware imperfection and is applicable to systems with multiple sites or arbitrarily large quadrupolar interactions, it seems to be the most versatile method for ^{59}Co NMR studies. On the other hand, the requirement of a sizable single crystal is obviously the major disadvantage of this method. Furthermore, in the presence of more than one magnetically nonequivalent sites, it may be difficult to determine the tensor orientation with respect to the molecular frame when there are not enough symmetry constraints at the nuclear sites.[41]

* In ref. 176, however, Reynhardt claimed that there were five crystallographic nonequivalent sites for $[Co(NH_3)_6]Cl_3$. The author unfortunately did not clarify the results in detail.

2.3. Static polycrystalline spectra

Several ^{59}Co static polycrystalline studies on Co(III) complexes were published in the 1960s.[42,43] However, the reliability of these data are questionable because simulation of a static polycrystalline spectrum is not trivial for a ^{59}Co system when it involves two line-broadening mechanisms with comparable magnitudes. Without any symmetry constraints, the quadrupolar and chemical shift interactions must be considered in a general orientation, resulting in an eight-parameter fit (three chemical shift principal tensor components, two quadrupolar parameters and three Euler angles) for any reliable simulation of a one-site ^{59}Co spectrum. Indeed, this kind of general lineshape analysis was not practicable until 1990, which explains why there were very few ^{59}Co static polycrystalline studies of cobalt(III) compounds in recent decades. Nevertheless, without the aid of numerical simulation, Eaton and co-workers were able to get a good estimate of the ^{59}Co NMR parameters of $Co(en)_3Cl_3$ and $Na_3Co(NO_2)_6$ because the spectral analyses were greatly simplified by the presence of high symmetry elements at the cobalt sites.[44] For example, the presence of a D_3 symmetry at the cobalt site of $Co(en)_3Cl_3$[45] implies that the chemical shift and EFG tensors are axially symmetric, as verified by the NMR[44] and NQR[46] experiments, respectively. In addition, a quadrupole coupling constant of 1.08 MHz for $La[Co(CN)_6]$ was readily inferred from the ^{59}Co static Bloch-decay spectrum (Fig. 3), in which the textbook features of the satellite transitions were observed.[47]

In the early 1990s, the research groups of Gerstein,[48] Ellis[49] and Wasylishen[25] independently reported the simulation of NMR static powder spectra, where the chemical shift and the quadrupolar interactions were considered in a general orientation. Hirschinger *et al.* were the first to analyse ^{59}Co static powder spectra without assuming a coincidence of the chemical shift and EFG tensors.[26] For a series of cobalt clusters, the ^{59}Co spectra measured at 4.7 and 7.1 T were analysed in least-squares sense, where the initial estimate of the fitting parameters were obtained by moment analysis. The Euler angles reported are consistent with the presence of a mirror-plane symmetry at the cobalt sites of the clusters. With the help of the computer routine SECQUAD,[25] Chung *et al.* simulated the ^{59}Co static powder spectra of *trans*-$Co[(en)_2(NO_2)_2]NO_3$ and $Na_3Co(NO_2)_6$ measured at 7.1 and 9.5 T.[50] Although the centre of inversion present at the cobalt site of *trans*-$Co[(en)_2(NO_2)_2]NO_3$ does not impose any constraints on the tensorial elements and the relative orientation of these tensors, it was shown that the chemical shift and EFG tensors are coincident for both of these compounds. Furthermore, the chemical shift and EFG tensors of $Na_3Co(NO_2)_6$ are found to be axially symmetric. Since EFG is a functional of charge symmetry, whereas chemical shift originates in electron current density, the axial symmetries exhibited by these two tensors and the fact that they are coincident taken together give a strong hint for the presence of a threefold axis or higher

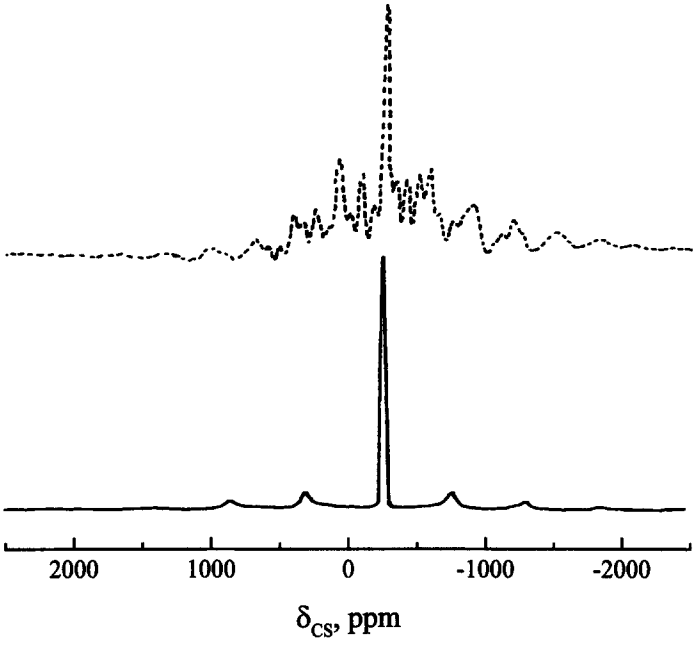

Fig. 3. ^{59}Co solid-state NMR spectra of $LaCo(CN)_6 \cdot 5H_2O$ measured by Bloch decay (bottom, full line) and quad-echo (top, broken line) at 7.1 T. (Reproduced with permission from ref. 47. © 1997 American Chemical Society.)

symmetry element at the cobalt site of $Na_3Co(NO_2)_6$. Nevertheless, this assertion has to be checked by crystallographic study. As a demonstration of the newly developed quadrupolar Carr–Purcell–Meiboom–Gill (QCPMG) technique, the ^{59}Co NMR parameters were determined for $[Co(NH_3)_5Cl]Cl_2$.[51] Although the agreement between the experimental and simulated spectra is fair (see Fig. 4), the reported ^{59}Co quadrupolar parameters differ from the NQR data considerably.[52]

Recently, Frydman *et al.* successfully analysed the ^{59}Co static powder spectra of a series of cobalamins and cobaloximes measured at 4.7, 7.1 and 11.8 T.[27] As pointed out by the authors, there were considerable changes in the ^{59}Co quadrupole coupling constants depending on the crystallization conditions of the cobalamins, whereas the ^{59}Co chemical shift tensors remained fairly constant. It was suggested that the different behaviour of the EFG and chemical shift tensors is due to a different dependence of these tensors on an uncharacterized structural rearrangement when the cobalamins were recrystallized. Furthermore, the close resemblance between the ^{59}Co NMR data of cobalamins and cobaloximes illustrates that cobaloximes are much better model compounds of cobalamins than cobaltoporphyrins. In a study of polyammonium cobalticyanide supercomplexes, Zhou *et al.* combined the use

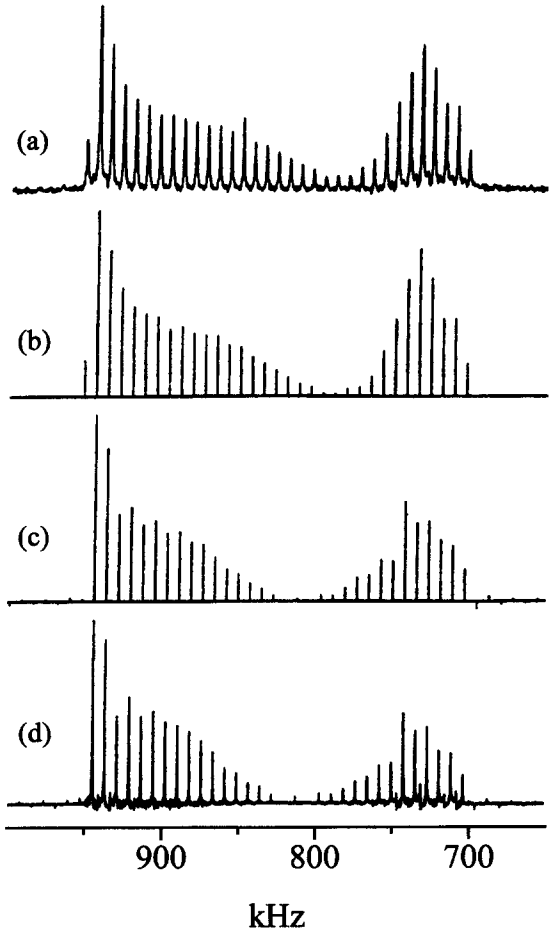

Fig. 4. Comparison of experimental and optimum simulated ^{59}Co QCPMG spectra of $[Co(NH_3)_5Cl]Cl$: (a) experimental spectrum (94.43 MHz); (b) stick-plot of the experimental sideband intensities; (c) stick-plot of the calculated sideband intensities; (d) optimum simulated QCPMG spectrum from which (c) was generated. (Reproduced with permission from ref. 51. © 1997 American Chemical Society.)

of ^{59}Co solid-state NMR methodology and density functional theory calculations to investigate the second-sphere interaction in these supercomplexes.[53] In spite of the relatively low degree of crystallinity, the singularities of the ^{59}Co static powder spectra measured at 7.1 and 9.4 T are reproduced to give an accurate determination of the quadrupolar and chemical shift parameters of the supercomplexes. On the basis of the solid-state ^{59}Co NMR data, it was shown that the splitting of the $^1T_{1g}$ state is most likely the mechanism causing the reduction of the photoaquation quantum yields for $\{[24]aneN_6H_6[Co(CN)_6]\}^{5+}$ and $\{[32]aneN_8H_8[Co(CN)_6]\}^{5+}$, when compared

with $[Co(CN)_6]^{3-}$. It is surprising that rather featureless ^{59}Co spectra were observed for another class of supramolecules containing $[Co(CN)_6]^{3-}$ units.[54,55] Nevertheless, nutation spectroscopy or multiple-quantum magic-angle spinning might be employed to extract the quadrupolar parameters of these systems (see below).

Lineshape analysis

In contrast to the SNMR method, it is crucial to measure an undistorted polycrystalline static spectrum in order to have a reliable spectral analysis when the effects of finite RF pulses and detection bandwidth are ignored in the numerical simulation. Since ^{59}Co static powder spectra in general have well-defined singularities and therefore are suitable for lineshape simulation, the issue of spectral distortion seems to be particularly important for ^{59}Co NMR practitioners. In this section we will give a brief account of lineshape analysis, including experimental considerations and precautions for numerical simulations.

Experimental considerations. Since it is known that the frequency of the central transition (CT) for any half-integer quadrupole system is not affected to first order by the quadrupolar interaction, ^{59}Co spectra are usually dominated by the CT contribution. When the inverse of the signal linewidth is much longer than the spectrometer dead time, a relatively undistorted spectrum may be obtained simply by Bloch decay, provided that the RF field strength is larger than the second-order quadrupolar interaction[56] and the pulse flip-angle is small enough to avoid distortion due to nutation effects.[57] As an example, Fig. 5 shows the Bloch decay spectrum of $K_3[Co(CN)_6]$ measured at 94.939 MHz with dead time delay equal to 5 μs. For the cases with large χ, the dead-time problem could be circumvented by spin-echo technique in conjunction with a 16-step phase cycling.[58,59] The equivalence between an ideal Bloch decay spectrum and the spin-echo spectrum relies on the observation that a truly selectively excited CT can be considered as the magnetization arising from a spin-1/2 system.[22] Of course, this equivalence is no longer valid if the assumption of selective excitation does not hold. The best way to check the pulse selectiveness is to perform a nutation experiment.[60] If the signal linewidth exceeds the detection bandwidth, several spectra measured at different offsets may be co-added to produce the desired undistorted spectrum.[27] The pulse width of a selective $\pi/2$ pulse, $t^{s}_{\pi/2}$, for the central transition, is determined by measuring the $\pi/2$ pulse width of a liquid sample, $t^{liq}_{\pi/2}$, according to the relation

$$t^{s}_{\pi/2} = \frac{t^{liq}_{\pi/2}}{I + \frac{1}{2}} \tag{16}$$

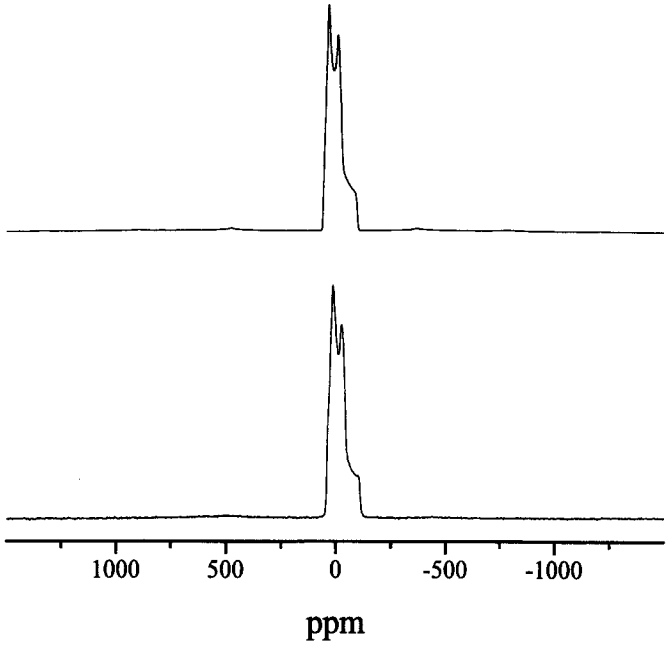

Fig. 5. ^{59}Co static Bloch-decay spectrum of $K_3[Co(CN)_6]$ measured at 9.4 T. The dead-time delay employed was 5 μs. The NMR parameters of the calculated spectrum (upper trace) were taken from Table 1.

As mentioned above, it is advisable to use small pulse flip-angles to measure the spin-echo spectrum. In principle, a selective pulse for CT could be achieved for arbitrarily small χ by reducing the RF strength, but the presence of other internal interactions such as chemical shift anisotropy imposes a lower limit on the pulse strength, sometimes rendering a CT selective excitation impossible for small χ. For partly selective excitation, a 36-step phase cycling (CYCLOP incorporated) may be required for a ^{59}Co spin-echo experiment in order to remove the artefacts originating from unwanted coherence pathways.[61] In view of the very distorted echo spectrum reported by Ganguly and co-workers,[47] $La[Co(CN)_6]$ might be a good test case for the proposed 36-step phase cycling. It is noteworthy that a Bloch decay spectrum under magic-angle spinning would be an attractive alternative for ^{59}Co systems in which χ is less than 8 MHz.

Numerical simulation. Lineshape simulations are useful for spectra with well-defined singularities. Initial parameters for lineshape simulations may be obtained from the published NMR data of similar systems. Alternatively, moment analysis of the spectra could produce a useful initial guess.[26] Since the degree of freedom involved in the spectral analysis of a ^{59}Co spectrum is large,

it is useful to incorporate the feature of iterative least-squares fitting into the simulation routines.* For the same reason, the reliability of the extracted NMR parameters should be verified by simulating spectra measured at multiple $\mathbf{B}_0$ fields or by other independent measurements. The validity of the perturbative approach may be questionable if χ is larger than the Larmor frequency by a factor of 3.5 for ^{59}Co systems.[62] Furthermore, it is mandatory to check that the NMR parameters obtained are compatible with the symmetry elements at the nuclear site.[25] Since the EFG and chemical shift tensors are invariant towards symmetry operations, if there exists a mirror plane (or a C_2 axis) at the nuclear site, one of the principal axes for these two tensors must be perpendicular to the mirror plane (or along the C_2 axis). As such, the Euler angles α and γ would be a multiple of 90° [51] and the presence of a C_3 axis or higher symmetry element would impose axial symmetries on the tensors at the nuclear site. Finally, it is impracticable to analyse a ^{59}Co powder static spectrum by lineshape simulation when more than one site is involved,[63] unless the number of fitting parameters can be reduced considerably.

2.4. Magic/variable angle spinning

Magic-angle spinning

Since the pioneering work of Maricq and Waugh,[64] magic-angle spinning (MAS) has become a standard technique for NMR investigations of half-integer quadrupolar nuclei. This method has the advantage that even a dead time as long as 15 μs would result only in minor baseline distortion of the Bloch decay spectrum. There are several strategies for studies of this kind. (i) If the first-order quadrupolar interaction and chemical shift anisotropy are larger than the spinning speed but smaller than the typical bandwidth of a MAS probe, the quadrupolar and chemical shift parameters can be extracted accurately by the analysis of the sideband envelope.[65] (ii) As the quadrupolar interaction gets larger, the quadrupolar parameters may be estimated by the second-order quadrupolar shift of the satellite transitions.[66] (iii) When the first-order quadrupolar interaction is so large that only the central transition is observable, all the second-ranked interactions may be removed by fast spinning at the magic angle, and the simplified spectrum that is now broadened only by the second-order quadrupolar interaction can be simulated in terms of the quadrupolar parameters;[67] in the most general case the MAS spectrum can be simulated by taking into account all of the internal interactions as well as the

* The revised SECQUAD with iterative fitting incorporated is available upon request from jccchan@qpc048.uni-muenster.de.

RF pulse and spinning speed effects.[68] (iv) When the second-order quadrupolar interaction is much smaller than the chemical shift anisotropy, the quadrupolar parameters can be estimated by monitoring the frequency shift of the centre band as a function of the $\mathbf{B}_0$ field[66] and the chemical shift anisotropy can be determined by Herzfeld–Berger sideband analysis.[69] We shall discuss the applicability of these methods to ^{59}Co systems in turn.

The first strategy may be useful for a ^{59}Co system with χ smaller than 1.2 MHz if we assume the bandwidth of a commercial MAS probe to be 0.5 MHz. It seems that La[Co(CN)$_6$] is a good candidate for this approach. Also, it has long been known that the cobalt site of $K_2Na[Co(NO_2)_6]$ has cubic site symmetry.[70] However, no MAS studies have yet been done for these compounds.

The second strategy is simple to implement. As an illustration, the MAS spectrum of Co(acac)$_3$ measured at 7.1 T is shown in Fig. 6.[71] In the inset, the satellite transition $|5/2| \leftrightarrow |3/2|$ is observed as a small 'spike' next to the peak arising from the satellite transition $|3/2| \leftrightarrow |1/2|$. According to Samoson,[66] the second-order quadrupolar shift for the $|m| \leftrightarrow |m-1|$ transition relative to the isotropic chemical shift in a powder sample is given by

$$\Delta\nu_{m,m-1} = -\frac{3}{40}\frac{\chi^2}{\nu_L}\left\{\frac{I(I+1) - 9m(m-1) - 3}{I^2(2I-1)^2}\right\}(1 + \eta_Q^2/3) \qquad (17)$$

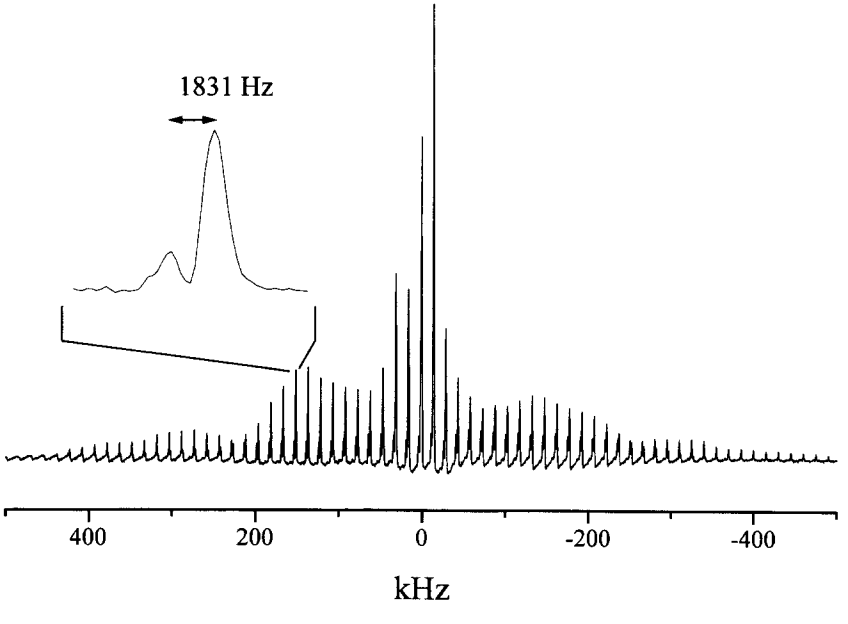

Fig. 6. ^{59}Co MAS spectrum of Co(acac)$_3$ measured at 7.1 T with spinning speed of 15 kHz. The inset illustrates the two peaks arising from the satellite transitions $|5/2| \leftrightarrow |3/2|$ (small peak) and $|3/2| \leftrightarrow |1/2|$ (large peak).

where ν_L is the Larmor frequency. For spin 7/2, the separation between the satellite transitions $|5/2| \leftrightarrow |3/2|$ and $|3/2| \leftrightarrow |1/2|$ is therefore deduced as

$$\Delta\nu_{5/2,3/2} - \Delta\nu_{3/2,1/2} = \frac{9}{1960}\frac{\chi^2}{\nu_L}(1+\eta_Q^2/3) \tag{18}$$

Given that the l.h.s. of Eq. (18) was measured as 1831 Hz (see Fig. 6) and the transmitter frequency was 72.1 MHz, the second-order quadrupolar shift, defined as $\chi(1+\eta_Q^2/3)^{1/2}$, is calculated to be 5.4 MHz for $Co(acac)_3$, in satisfactory agreement with the single-crystal NMR data.

The third strategy requires a relatively high spinning speed to average or partially remove the second-rank interaction such as chemical shift anisotropy. This technique has been applied successfully to the study of $Na_3Co(NO_2)_6$ and *trans*-$[Co(en)_2(NO_2)_2]NO_3$.[72] The MAS spectra of $Na_3Co(NO_2)_6$ shown in Fig. 7,

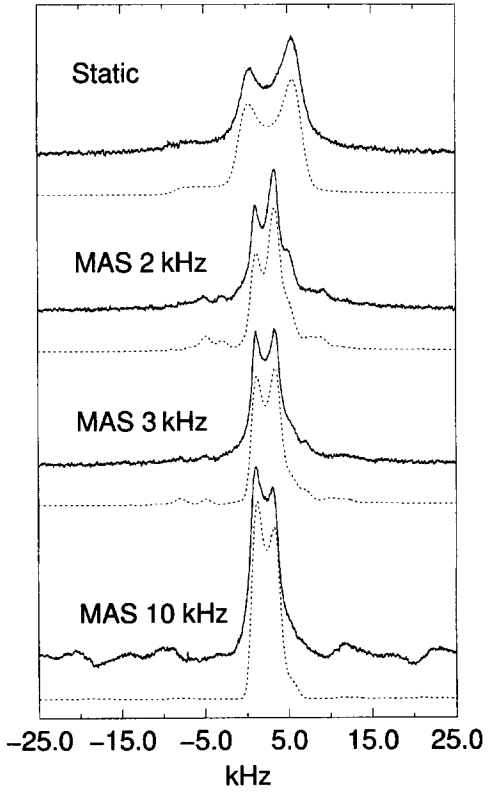

Fig. 7. ^{59}Co experimental (upper spectrum) and simulated (lower spectrum) powder static and MAS spectra of $Na_3Co(NO_2)_6$. (Reproduced from ref. 72, © 1998, with permission from Elsevier Science.)

obtained at various spinning speeds, were simulated with the corresponding NMR parameters reported in Table 1. If the spinning speed is smaller than the chemical shift span of the static spectrum, the next-order sidebands may be added to the centre band to produce a resemblance to the MAS spectrum at infinite spinning speed. However, this method is not very useful if the second-order quadrupolar interaction is too small to produce a characteristic centre band. For example, Hayashi concluded that simulation of the featureless MAS spectrum of $Co(acac)_3$ merely gave an upper bound of the ^{59}Co quadrupole coupling constant, estimated to be 6 MHz.[73]

The fourth strategy has been employed extensively for a systematic study of cobalt(III) porphyrins by Frydman and co-workers.[74] It has been shown that this approach is quite effective when the ^{59}Co quadrupole coupling constant is less than 6 MHz, provided that a large chemical shift anisotropy renders the contribution of the satellite transitions negligible. Thus far, the largest chemical shift span that has been characterized by this method is about 240 kHz.[74] This work indicates that the ^{59}Co paramagnetic shielding in cobaltoporphyrins is influenced by a mechanism that is not active in Werner-type cobalt(III) complexes. In addition, the isotropic chemical shifts of three crystallographic sites of $Co(NH_3)_6Cl_3$ were determined in the same study. Unfortunately, the corresponding chemical shift anisotropies were not reported.

Fast magic-angle spinning (>20 kHz) has been applied to the study of Li_xCoO_2 ($0.48 \leqslant x \leqslant 1.05$), showing that there are nonequivalent CoO_6 octahedra present in this potential material for lithium-ion batteries. However, not much NMR data was extracted owing to the severe overlap of the spinning sideband manifolds.[75]

Variable angle spinning. If a MAS spectrum is complicated by the presence of multiple sites, each resonance signal being broadened by the second-order quadrupolar interaction, it may be useful to spin the sample at other angles in order to simplify the spectral analysis. This approach is known as variable angle spinning (VAS). A comprehensive discussion of VAS was given by Lefebvre and co-workers.[76] A variant of this technique was applied to the study of $Co(acac)_3$, in which the spinning axis was deviated slightly from the magic angle (off-MAS NMR) such that the sideband intensities arising from the satellite transitions were minimized and more spectral features were reintroduced, as shown in Fig. 8.[73] This method yields a very good estimation of the chemical shift and quadrupolar parameters of $Co(acac)_3$.

2.5. Nutation NMR

Nutation NMR spectroscopy was introduced by Samoson and Lippmaa for the study of half-integer quadrupolar nuclei.[77,78] For quadrupolar nuclei in the rotating frame, the nutation frequencies and amplitudes of the excited Zeeman

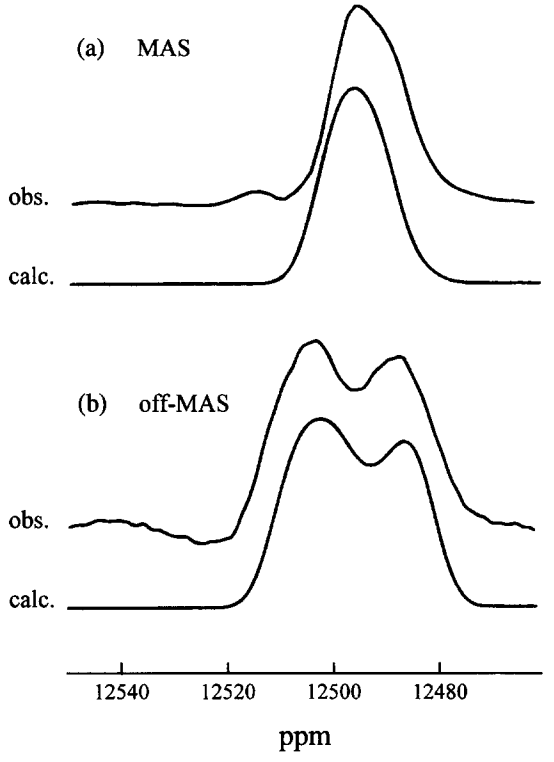

Fig. 8. ^{59}Co NMR MAS and off-MAS spectra and the corresponding simulated results of $Co(acac)_3$ at 94.94 MHz. The experimental lineshapes were obtained by summing the isotropic peak and the spinning sidebands from +5th to −4th order. The spinning rates were (a) 10.00 and (b) 11.00 kHz. (Reproduced with permission from ref. 73. © 1996 John Wiley & Sons Limited.)

transitions are dependent on the quadrupolar parameters during the RF irradiation. If the initial part of the FID is recorded as a function of the irradiation period, χ and η_Q can be obtained by comparing the FID modulation with numerical simulations. For a more detailed discussion of this technique, readers are referred to the review article by Freude and Haase.[16] Nutation spectroscopy has the advantage that basically only the two quadrupolar parameters are involved in the analysis. Nevertheless, it is relatively time consuming from the experimental point of view and therefore not very commonly employed for ^{59}Co NMR work unless the resonance signal is featureless and unsuitable for lineshape simulation. The model compounds $Na_3[Co(NO_2)_6]$ and *trans*-$[Co(en)_2(NO_2)_2]NO_3$ have been studied by nutation spectroscopy and the results are in good agreement with other reported data.[79,80] As an illustration, Fig. 9 shows the results for *trans*-$[Co(en)_2(NO_2)_2]NO_3$. In an application study, Eguchi *et al.* determined the

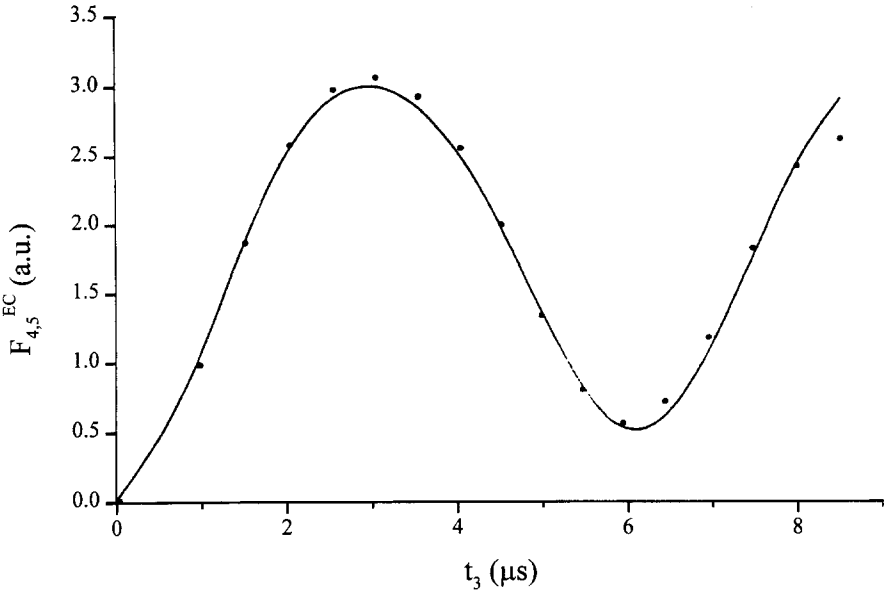

Fig. 9. Experimental ^{59}Co echo amplitude (●) in a polycrystalline sample of *trans*-$[Co(en)_2(NO_2)_2]NO_3$ versus the second pulse length t_3 with $t_1 = 1$ μs and $\tau_2 = 48$ μs. Solid line, calculated amplitude with three parameters: $\chi = 13.28$ MHz, $\eta_Q = 0.85$ and $\omega_1/2\pi = 44.11$ kHz. (Reproduced from ref. 80, © 1997, with permission from Elsevier Science.)

quadrupolar parameters of the two nonequivalent cobalt sites (apical and basal) of $Co_4(CO)_{12}$ by fitting the first-order quadrupolar splitting and measuring the 2D nutation spectrum.[81] From the roughly determined quadrupolar parameters, it was suggested that the Co_4 tetrahedron undergoes rapid reorientation about a pseudo C_3-axis passing through the apical cobalt atom at room temperature. However, in a subsequent nutation study of $Co_4(CO)_{12}$ at 7.1 T, the linewidth of the basal cobalt signal was found to be ~350 kHz,[80] much larger than that inferred from the data reported by Eguchi. As another example, the ^{59}Co nutation measurement of $LiCoO_2$ provided convincing evidence for the presence of two different cobalt environments in the system studied.[47]

2.6. Multiple-quantum magic-angle spinning

The multiple-quantum magic-angle spinning (MQMAS) technique is one of the most important NMR advances for half-integer quadrupolar nuclei that has been made in recent years.[82] Through a correlation between the multiple and single-quantum coherences, the anisotropic second-order quadrupolar

broadening of the central transition is removed in the F1 dimension, resulting in a high-resolution spectrum. The basic two-pulse sequence[83,84]

$$p_1 - t_1 - p_2 - \text{Acquire} \tag{19}$$

and the three-pulse Z-filtering sequence[85]

$$p_1 - t_1 - p_2 - p_3 - \text{Acquire} \tag{20}$$

have been proposed and their corresponding coherence pathways are shown in Fig. 10. For maximum signal sensitivity, the first two pulses that excite and convert the multiple-quantum coherences should be of maximum power.[86,87] The third pulse of the Z-filtering sequence is a soft reading pulse. The presence of a variable interpulse delay (t_1) indicates that MQMAS is a 2D experiment. In this experiment only symmetrical Zeeman transitions such as $1/2 \leftrightarrow -1/2$ ($\pm$1Q), $3/2 \leftrightarrow -3/2$ ($\pm$3Q) and so on are relevant because they are not

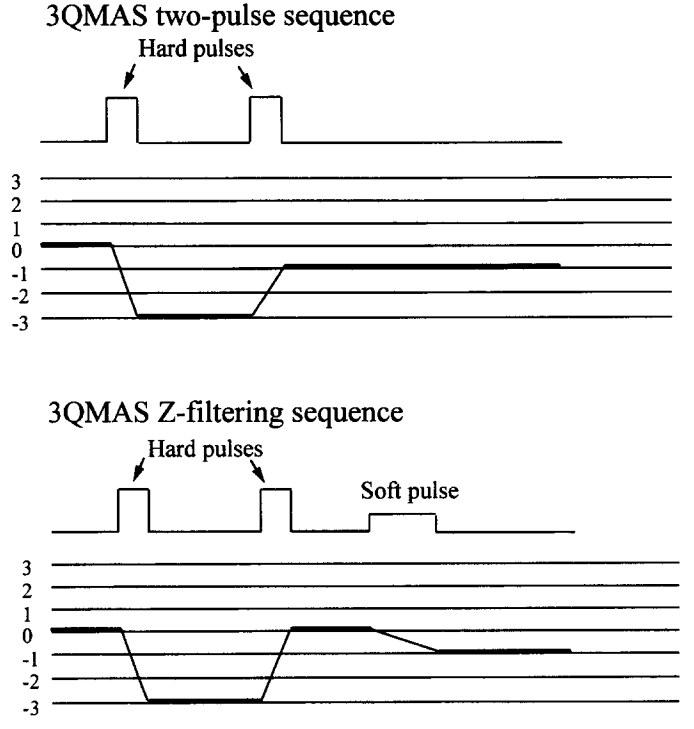

Fig. 10. Coherence pathways of the echo signals associated with two commonly employed MQMAS pulse sequences. The case of spin 3/2 was taken as an illustration.

broadened by the first-order quadrupolar interaction. If we assume that magic-angle spinning averages the anisotropic interactions containing the second-order Legendre polynomial, the precession frequency of a pQ coherence corresponding to a symmetrical Zeeman transition is given as[88]

$$\nu_p = -p\nu_0^{cs} + \nu_0^Q C_0^I(p) + \nu_4^Q(\theta, \phi)C_4^I(p)P_4(\cos\beta) \tag{21}$$

$$\nu_0^Q = -\frac{\chi^2(3+\eta_Q^2)}{10\nu_L[2I(2I-1)]^2} \tag{22}$$

$$C_0^I(p) = -p\left(I(I+1) - \frac{3}{4}p^2\right) \tag{23}$$

$$C_4^I(p) = -p\left(18I(I+1) - \frac{34}{4}p^2 - 5\right) \tag{24}$$

where ν_0^{cs} is the isotropic chemical shielding. The angle β specifies the rotation angle of the sample, the magic angle in this case. $P_4(\cos\beta)$ is the fourth-order Legendre polynomial of $\cos\beta$. The term $\nu_4^Q(\theta,\phi)$ causes the residual quadrupolar broadening of the CT, which is not removed by MAS.[67] The equation of the 2D time domain signal is hence written as

$$\begin{aligned} S(t_1,t_2) = S_{-1,p}(0)&\exp\{-i[-p\nu_0^{cs} + \nu_0^Q C_0^I(p) + \nu_4^Q(\theta,\phi)C_4^I(p)P_4(\cos\beta)]t_1\} \\ &\times \exp\{-i[\nu_0^{cs} + \nu_0^Q C_0^I(-1) + \nu_4^Q(\theta,\phi)C_4^I(-1)P_4(\cos\beta)]t_2\} \end{aligned} \tag{25}$$

$S_{-1,p}(0)$ is the amplitude of the detected coherence, which is a complicated function of RF pulse intensity and duration as well as spinning speed. After Fourier transformation, the second-order quadrupolar and isotropic chemical shifts of any observed signals can be readily inferred from their F1 and F2 positions. This procedure is useful for signals with or without well-defined spectral features. For an exposition of this technique at the introductory level, readers are referred to an article by Chan.[89]

To date, only a few one-site Co(III) complexes have been studied by MQMAS, viz. $K_3[Co(CN)_6]$,[90, 91] $Na_3Co(NO_2)_6$[72] and $[Co(TPP)MeIm_2]BF_4$.[91] The corresponding TQMAS spectra are shown in Figs 11 and 12. These preliminary studies show that the presence of chemical shift anisotropy could severely deteriorate the intensity of the multiple-quantum coherence. Since most ^{59}Co systems have substantial chemical shift anisotropies, the general utility of such experiment in this area remains doubtful at the present stage. Nevertheless, in view of the powerful simulation protocol proposed for 2D MQMAS spectra[72,92] and the launching of commercial MAS probes capable of spinning speed in excess of 30 kHz, more cobalt complexes should soon become accessible by MQMAS at low $\mathbf{B}_0$ field.

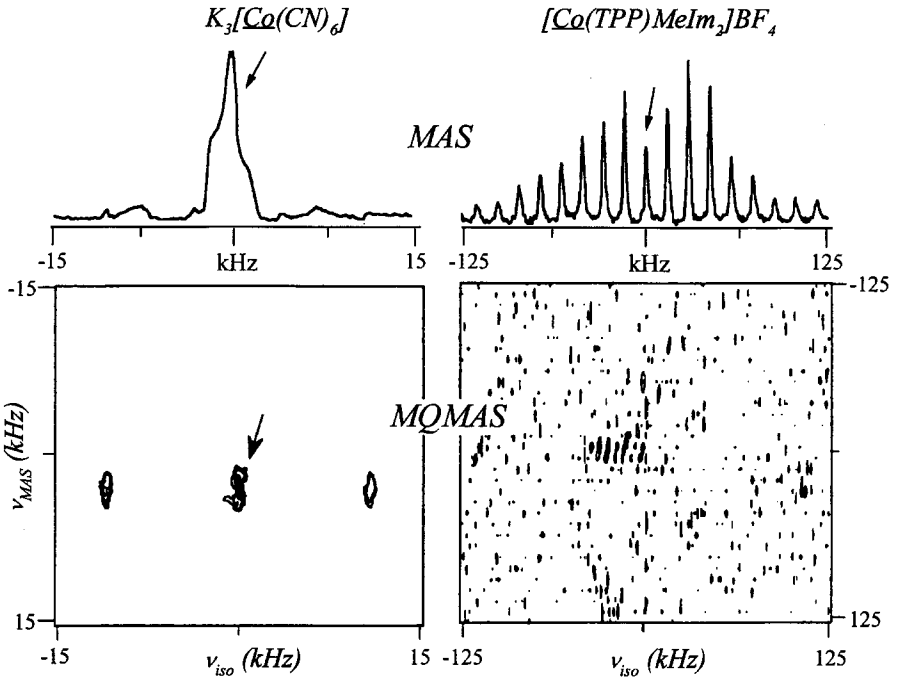

Fig. 11. Comparison between MAS and sheared MQMAS ^{59}Co NMR results observed for two different single-site cobalt complexes ($\mathbf{B}_o$ = 4.7 T, ν_r = 10 kHz). Acquisition of the hexacyano data involved 256 scans for the MAS trace and 1200 scans/t_1 values for the MQMAS. The porphyrin MAS spectrum was collected using 2000 scans while its MQMAS required 67 000 scans/t_1 increment (4 days continuous acquisition). Notice the much poorer S/N of this spectrum, the consequence of the ~3000 ppm shift anisotropy characterizing its cobalt site. Arrows indicate the positions of the spinning centerbands. (Reproduced with permission from ref. 91.)

2.7. Quadrupole coupling constant and chemical shift anisotropy

Interpretation of ^{59}Co quadrupolar parameters has been well documented thanks to NQR spectroscopists.[93] Assuming that the EFG at the nuclear site can be considered as the arithmetic sum of individual ligand contributions, Brown and co-workers proposed a field gradient model to rationalize the observed quadrupolar parameters of a series of cobaloximes. The model explains reasonably well the changes in χ and η_Q when the relative bonding capability of the axial and glyoximato ligands varies. This model and the underlying notions resemble the ligand field approach for the description of ^{59}Co chemical shifts. Thus, it is not surprising that a linear relationship between the quadrupole coupling constant and chemical shift anisotropy had been found experimentally.[35] Since EFG is a ground-state property but a

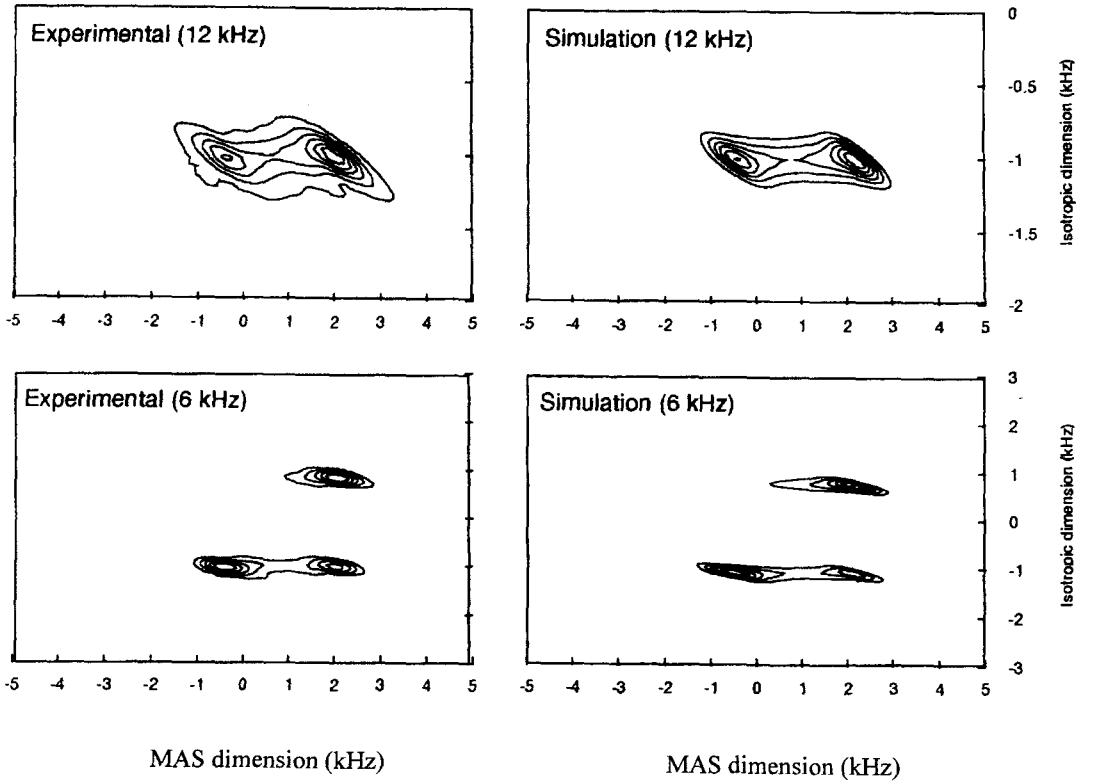

Fig. 12. Experimental (left) and simulated (right) two-dimensional triple-quantum ^{59}Co MAS spectra of $Na_3Co(NO_2)_6$ in which contour lines were drawn every 12.5% starting at 12.5% and ending at 87.5% of the maximum of the spectrum. The spinning speed was $\omega_R = 12$ kHz (top) and 6 kHz (bottom). Spectra were displayed in magnitude mode. (Reproduced with permission from ref. 72, © 1998, with permission from Elsevier Science.)

perturbative description of chemical shielding requires the knowledge of excited states, it is more reasonable to correlate chemical shifts with the quotient of the quadrupole coupling constant and the averaged transition energy.[94] Recently, Au-Yeung and co-workers rationalized this observed proportionality for low-spin Co(III) complexes by manipulating the expressions for the orbital population imbalance in the Townes–Daily theory and the 'atom-in-a-molecule' approximation[95,96] of the Ramsey shielding equation:[50,97]

$$\delta_{iso} - \delta_{//} = A\left(\frac{\chi}{\Delta E_{av}}\right) + B \tag{26}$$

$$A = \frac{14\mu_0\mu_B^2\varepsilon_0 h(P_{xz} - 1)}{e^2 Q(1 - R)} \tag{27}$$

$$B = \frac{8\mu_0\mu_B^2}{3\pi\ \Delta E_{av}} \langle r^{-3}\rangle_{3d}(P_{xz} - P_{x^2-y^2})(P_{xz} - P_{xy}) \tag{28}$$

where $\delta_{//}$ is the principal tensor component along the highest symmetry axis (usually defined as the z-axis); R denotes the Sternheimer correction for the valence contribution to χ; ΔE_{av} represents the averaged electronic transition energy; and P_i is the population of the orbital $3d_i$. The other symbols carry their usual meanings.* There are several assumptions associated with this empirical equation: (i) the averaged excitation energy is identifiable with the weighted average of the magnetically allowed low-lying d–d transition energies; (ii) the chemical shielding and EFG tensors exhibit axial symmetry so that P_{xz} and P_{yz} are always the same; (iii) the lattice contribution to the quadrupole coupling constant is negligible. A rough estimation shows that $(8\mu_0\mu_B^2/3\pi\ \Delta E_{av})\langle r^{-3}\rangle_{3d}$ is on the order of 9000 ppm. In Werner-type Co(III) complexes, the populations of $3d_{xz}$ and $3d_{xy}$ orbitals are expected to be the same if metal–ligand π-bonding is negligible. It is therefore anticipated that Co(III) complexes with and without cobalt–ligand π-bonding will fall on different correlation lines owing to the operation of B in Eq. (26). As an illustration, Fig. 13 illustrates the application of Eq. (26) to several hexacoordinated Co(III) complexes. Although C_3 or higher symmetry elements are assumed in the derivation, Eq. (26) appears to be valid for nonvanishing η_Q as demonstrated in *trans*-$[Co(en)_2(NO_2)_2]NO_3$ ($\eta_Q = 0.735$). It is noteworthy that this empirical relation would be invalidated by the failure of the 'atom-in-a-molecule' description of the chemical shielding. In particular, it was found that

*It is unfortunate that many typographical errors are found in refs 50 and 97 concerning the derivation of the proposed empirical relation. Nevertheless, the resulting empirical equation is shown correctly in the cited references.

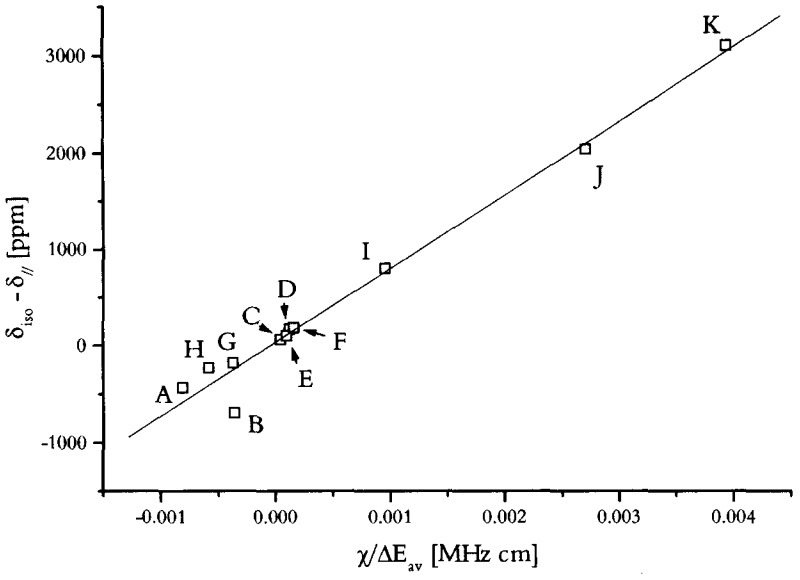

Fig. 13. Correlation of the chemical shift anisotropies and the quotient of the quadrupole coupling constants and the magnetically allowed d–d transition energies. The most up-to-date solid-state NMR data from Table 1 were used, including $[Co(NH_3)_6]Cl_3$ site 4 (A), $Co(acac)_3$ (B), $[Co(NH_3)_6]Cl_3$ site 1 (C), $Co(en)_3Cl_3$ (D), $[Co(NH_3)_6]Cl_3$ site 2 (E), $[Co(NH_3)_6]Cl_3$ site 3 (F), $Na_3Co(NO_2)_6$ (G), *trans*-$[Co(en)_2(NO_2)_2]NO_3$ (H), $[Co(NH_3)_4CO_3]Br$ (I), $[Co(NH_3)_5H_2O](ClO_4)_3$ (J), *trans*-$[Co(en)_2Cl_2]Cl{\cdot}HCl{\cdot}2H_2O$ (K). The correlation line was constructed from the systems with axial symmetries (C, D, G, J and K). χ of A, B, G and H were assumed to be negative. Optical data were taken from refs 50 and 103.

Eq. (26) does not hold in the systems of Co(III) porphyrinates, where the nonlocal contribution to the chemical shielding may be significant owing to the potential interaction between the metal valence electrons and the porphyrin π system.[74]

2.8. Outlook

In the 1970s ^{59}Co NQR spectroscopy was applied extensively to the studies of a wide variety of cobalt clusters (see Table 2). A similar research trend has not yet been observed for solid-state ^{59}Co NMR. However, the foregoing discussion shows that nearly all the solid-state NMR strategies developed for half-integer quadrupolar nuclei are applicable to ^{59}Co systems. The solid-state data compiled cover a broad range of quadrupolar parameters and chemical shifts, constituting different scenarios of spin dynamics awaiting further studies. The ^{59}Co nucleus has many favourable properties such as 100% natural abundance and short relaxation time (<1 s). Together with the fact that

Co(III) compounds are in general easy to prepare and handle, ^{59}Co is an attractive model nucleus for NMR method development.

3. SOLUTION-STATE NMR

3.1. Chemical shift interpretation

The paramagnetic contributions to the chemical shielding of octahedral low spin d^6 Co(III) complexes have commonly been interpreted through the strong-field approximation[98,99] of the Ramsey shielding model:[100]

$$\sigma_{iso}^{p} = -\frac{8\mu_0\mu_B^2}{\pi} \frac{\langle r^{-3}\rangle_{3d} \,|\, \langle {}^1A_{1g} \,|\, L_z \,|\, {}^1T_{1g}\rangle \,|^2}{\Delta E_{({}^1A_{1g} \rightarrow {}^1T_{1g})}} \tag{29}$$

where the d–d transition energy is considered as the spectrochemical factor while the radial factor $\langle r^{-3}\rangle_{3d}$ and the orbital angular momentum integral $|\langle {}^1A_{1g} \,|\, L_z \,|\, {}^1T_{1g}\rangle|^2$ are collectively known as the covalency or the nephelauxetic factor. The classical Freeman–Murray–Richards (FMR) approach[98] emphasizes the dependence of shielding on excitation energies, whereas the independent investigations by Juranic[101,102] and Bramley[103] demonstrated the importance of the nephelauxetic effect in ^{59}Co shielding variation. On the one hand, Taura convincingly showed that the solvent dependence of the ^{59}Co chemical shift for $K_3Co(CN)_6$ arises mainly from the solvent shift of the $^1A_{1g} \rightarrow {}^1T_{1g}$ transition.[104] The ^{59}Co chemical shifts of a wealth of Werner-type Co(III) complexes were successfully rationalized in terms of empirical parameters characterizing the field strength of each ligand type:[105]

$$\sigma_{iso}^{p} = -\frac{1}{3}\left(\frac{1}{S_1 + S_2} + \frac{1}{S_3 + S_4} + \frac{1}{S_5 + S_6}\right) \tag{30}$$

where S_1 and S_2, S_3 and S_4, S_5 and S_6 are parameters characteristic of the ligands on the x-, y-, and z-axes, respectively. This simple but compact scheme, where the product of the integral and radial factor is regarded as a constant, has been applied to over 50 compounds with moderate success.[105] However, Eq. (30) fails to account for the ^{59}Co chemical shift variation of systems with substantial metal–ligand π bonding. On the other hand, it has been shown that the variation of the angular momentum integral $|\langle {}^1A_{1g} \,|\, L_z \,|\, {}^1T_{1g}\rangle|^2$ is negligible in a series of Co(III) pentaammine complexes, leading to the common belief that the covalency effect lies in the variation of $\langle r^{-3}\rangle_{3d}$ and can

be approximated by the nephelauxetic factor β_{35}:[6]

$$\sigma_{iso}^{p} = -\frac{8\mu_0\mu_B^2}{\pi}\frac{\langle r^{-3}\rangle_{3d}}{\beta_{35}}|\langle {}^1A_{1g}|L_z|{}^1T_{1g}\rangle|^2\frac{\beta_{35}}{\Delta E_{({}^1A_{1g}\rightarrow {}^1T_{1g})}} \quad (31)$$

Indeed, the graphs of isotropic chemical shifts versus the quotients of nephelauxetic factors and the d–d transition energies show a better correlation than the conventional FMR plot for Co(III) pentaamine and Co(III) pentacyano complexes.[103,106]

It has been shown that ^{59}Co NMR linewidth at half-height may be invoked to modify the FMR plot in a homologous series of Co(III) complexes with high symmetries.[97] When the quadrupolar relaxation is the dominating relaxation mechanism, the ^{59}Co chemical shifts (δ_{iso}) and linewidths ($\Delta\nu_{1/2}$) have the following relationship for systems containing C_3 or higher symmetry elements:*

$$\delta_{iso} = A\frac{\sqrt{\Delta\nu_{1/2}}}{\Delta E_{av}} + B \quad (32)$$

$$A = \frac{4.86\times 10^{-29}(P_{xz}-1)}{Q(1-R)}\sqrt{\frac{1}{\tau_c}} \quad (33)$$

$$B = \delta_{//} + \frac{31.2\langle r^{-3}\rangle_{3d}}{\Delta E_{av}}(P_{xz}-P_{x^2-y^2})(P_{xz}-P_{xy}) \quad (34)$$

in which τ_c denotes the rotational correlation time; δ_{iso}, $\langle r^{-3}\rangle_{3d}$ and ΔE_{av} are expressed in ppm, atomic units and cm^{-1}, respectively. This empirical correlation is basically an extension of Eq. (26) to solution studies and was verified in a series of $[Co(NH_3)_5X]^{(3+n)+}$, $[Co(CN)_5X]^{(2-n)-}$ and *trans*-$[Co(en)_2X_2]^{(3+2n)+}$ complexes, where n is the formal charge of the ligand X.[97] As shown in Fig. 14, the two correlation lines obtained from the plot of δ_{iso} versus $(\Delta\nu_{1/2})^{1/2}/\Delta E_{av}$ for $[Co(NH_3)_5X]^{(3+n)+}$ divide the ligands X into two classes that are readily categorized by the Pearson hard and soft acid–base concept.[107] Accordingly, $[Co(NH_3)_5]^{3+}$ is considered to be hard and therefore the two correlation lines reveal the hard–hard (HH, mainly ionic bonding[108]) and hard–soft (HS) interactions. The y-intercepts of the two correlation lines are the averaged ^{59}Co $\delta_{//}$ of the corresponding complexes, assuming identical values for P_{xz} and P_{xy}. The smaller $\delta_{//}$ obtained from the HS correlation suggests that the more pronounced partial sigma bonding between Co (hard)

*In ref 97, equation 7 redundantly contains η_Q, which is equal to zero under the assumed symmetries.

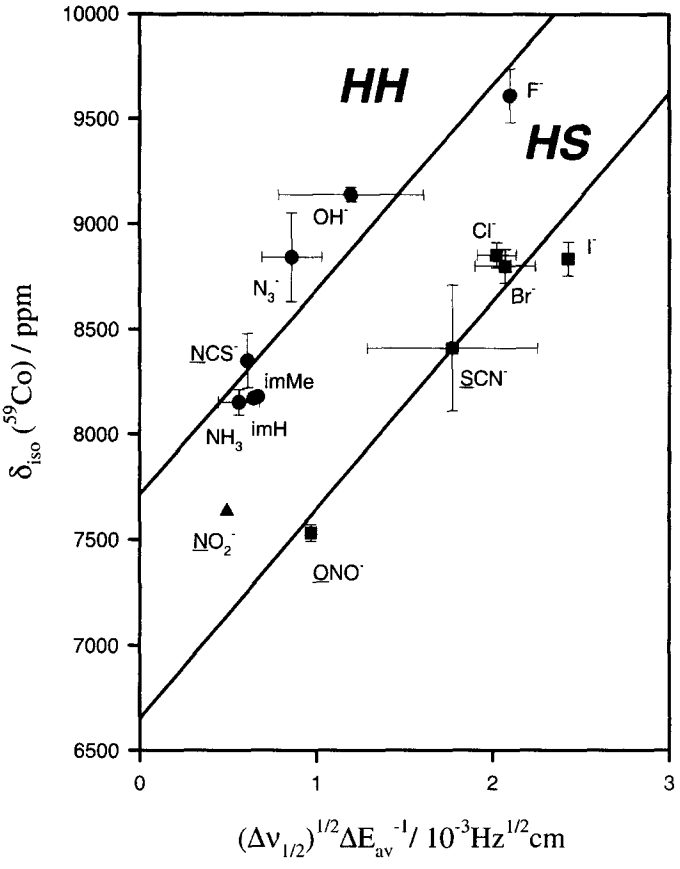

Fig. 14. Plot of $\delta_{iso}(^{59}Co)$ versus $(\Delta\nu_{1/2})^{1/2}\Delta E_{av}^{-1}$ for $[Co(NH_3)_5X]^{(3+n)+}$. The correlation line corresponding to hard–hard interaction type is represented by HH while that of hard-soft type is HS. ● and ■ denotes the hard and soft ligands, respectively. The intermediate case $\underline{N}O_2^-$ (8) is denoted by ▲. (Reproduced with permission from ref. 97.)

and X (soft) induces an upfield NMR shift in the direction perpendicular to the equatorial plane. In other words, $\langle r^{-3}\rangle_{3d}$ of the systems falling on the HS correlation line are diminished owing to the delocalization of the 3d electrons to the ligand X. The difference of the two intercepts, ~1000 ppm, mainly reveals the nephelauxetic effect because the d–d transition energy, $^1A_{1g} \rightarrow {}^1A_{2g}$, to which $\delta_{//}$ is inversely proportional, remains unchanged for $[Co(NH_3)_5X]^{(3+n)+}$. The nephelauxetic effect in Co(III) systems was previously estimated to be 2000 ppm by Kidd.[8] Interestingly, similar correlations were also observed for a series of Co(III) porphyrinates[109] and some of the cobalt clusters.[110] It should be noted, however, that the theory of Deverell[111] also leads to a prediction of direct proportionality between the square root of the

normalized linewidth and the isotropic chemical shift, as a consequence of valence distortion upon solvent–solute interaction.[112,113]

As a justification of the interpretation of the HH and HS correlation lines in Fig. 14, the role of the Co 3d and 4s orbitals in the metal–ligand interactions of $[Co(NH_3)_5X]^{(3+n)+}$ complexes has been examined by density functional theory.[114] The calculated results demonstrated that the participation of the Co 4s orbital will be predominant in a less covalent metal–ligand interaction, whereas the Co 3d orbital will play a more significant role in a covalent environment. Since the s electrons do not contribute to the paramagnetic shielding, the HH and HS correlation lines established for $[Co(NH_3)_5X]^{(3+n)+}$ are mainly the result of the different degrees of metal–ligand bonding involving the participation of 3d orbitals. Both the experimental (the HH and HS correlation lines) and the calculated results indicate that the conventional ligand field description for Co(III) complexes, in which it has been stated that the bonding scheme of the first-row transition metals is carried solely by the 3d electrons,[115] may not be fully justified. Nevertheless, it is also inappropriate to exclude the 3d orbitals from the valence of Co(III) systems.[114,116]

3.2. Strategies for relaxation studies

The microdynamics of solute–solvent interaction have been investigated vigorously by measuring the relaxation of the probe nucleus. Comprehensive discussions on relaxation mechanisms are referred to the listed references.[117,118] It is commonly accepted that quadrupolar relaxation is the predominant relaxation mechanism for ^{59}Co systems with low molecular symmetries.[2] Scalar relaxation of the second kind, spin-rotation and chemical shift anisotropy have been suggested as competing mechanisms for ^{59}Co systems with octahedral symmetry.[3] Since different relaxation mechanisms have different dependences on the temperature and the Larmor frequency, the operating mechanisms for a particular system may be discerned on the basis of the field dependence and temperature dependence measurements. Nevertheless, unequivocal results are not guaranteed because of the high degree of freedom involved in a relaxation process.

Consider the longitudinal relaxation rate, T_Q^{-1} for quadrupolar mechanism under extreme narrowing conditions:[22]

$$T_Q^{-1} = \frac{3\pi^2}{10}\chi^2\left(1+\frac{\eta_Q^2}{3}\right)\left(\frac{2I+3}{I^2(2I-1)}\right)\tau_c \tag{35}$$

in which τ_c is the correlation time characterizing the time-dependent processes. In general, τ_c is either calculated by the Stokes–Einstein–Debye model[119] or assumed to be similar to the correlation time of other processes so that χ could

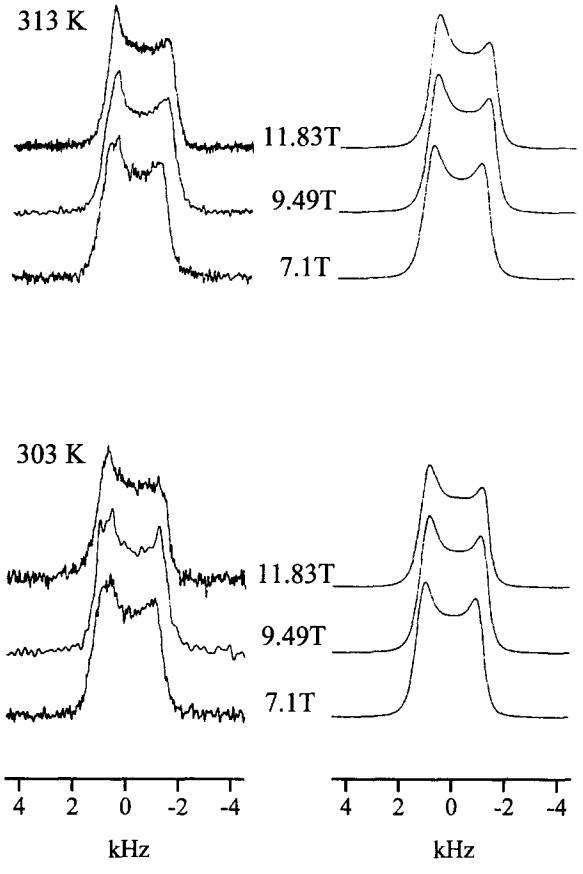

Fig. 15. Experimental $^{31}P\{^1H\}$ NMR spectra of the cluster $HFeCo_3(CO)_{11}PPh_2H$ in CD_2Cl_2. The simulated spectra are characterized by the quadrupolar relaxation rates, the chemical shift anisotropy relaxation rates, the interference term between the quadrupolar interaction and the chemical shift anisotropy, and the indirect spin–spin coupling constants $J(^{31}P-^{59}Co)$. (Reproduced with permission from ref. 123.)

be estimated from T_Q^{-1}. For systems such as $Co(acac)_3$ containing isolated $^{13}C-^1H$ spin pairs, τ_c could be estimated accurately by measuring the relaxation of the methine carbons, because it is very likely that the dipole–dipole relaxation of the methine carbons shares the same correlation time responsible for the ^{59}Co quadrupolar relaxation. On the other hand, the value of χ in Eq. (35) could be determined by solid-state experiment (the so-called static χ) and thus τ_c is determined by the T_Q^{-1} data. This approach is appropriate for systems with large static χ.

Following the approach of Werbelow and co-workers, the lineshape of a spin-1/2 nucleus scalar-coupled to a quadrupolar nucleus may be simulated in terms of the relaxation parameters of the quadrupolar nucleus, provided that

the relaxation rate of the quadrupolar nucleus is not much larger than the scalar-coupling constant.[120] This sensitive method was employed independently by Granger *et al.* and Kofod to analyse the ^{13}C spectra of $K_3[Co(CN)_6]$.[121,122] Although both research groups arrived at the same conclusion, that quadrupolar relaxation is not the only mechanism accounting for the ^{59}Co relaxation rate, different mechanisms, viz. chemical shift anisotropy and spin-rotation, were considered as the additional relaxation process. In spite of this discrepancy, this strategy was shown to be very useful for the study of cobalt clusters containing $^{59}Co-^{31}P$ spin pairs.[63,123] By simulating the ^{31}P spectra shown in Fig. 15, the relative contribution of quadrupolar and chemical shift anisotropy to ^{59}Co relaxation rates were obtained for the cobalt clusters under investigation. Similarly, the scalar-coupling constants $^1J_{Co-C}$ for biological relevant alkylcobalt(III) coordination compounds were determined by simulating the relevant ^{13}C spectrua.[124,125]

As an approximate method for the analyses of the relaxation data of ^{59}Co systems without significant cobalt–ligand π-bonding, $\Delta\nu_{1/2}$ in Eq. (32) has been normalized by the solution bulk viscosity η, leading to the following expression relating $\delta_{iso}(^{59}Co)$ and the viscosity normalized linewidth $\Delta\nu^*_{1/2}$:[97]

$$\delta_{iso} = \frac{4.86 \times 10^{-29}(P_{xz} - 1)}{Q(1 - R)} \sqrt{\frac{\eta}{\tau_c}} \frac{\sqrt{\nu^*_{1/2}}}{\Delta E_{av}} + \delta_{//} \tag{36}$$

For complex ions of similar size within a homologous series, it is expected that η/τ_c remains relatively constant for different solvents at a given temperature, in accordance with the Stokes–Einstein–Debye model. From the slope of the plot δ_{iso} versus $\sqrt{(\Delta\nu^*_{1/2})}/\Delta E_{av}$ shown in Fig. 16, the correlation time constants of a series of *trans*-$[Co(acac)_2XY]$ complexes were estimated and the results were compared favourably with the τ_c obtained from the ^{13}C relaxation measurements of the methene carbons (see Table 5).

Working in dilute solution (< 80 mmol l^{-1}) is recommended whenever the Stokes–Einstein–Debye model is employed for data analysis, as illustrated in the study of ^{59}Co longitudinal relaxation time of $Co(acac)_3$ in CH_3CN.[126]

3.3. Controversial results

Interpretation of relaxation data may be complicated by the presence of hydrogen bonding, ion-pairing effects, anisotropic reorientation, chemical exchange and intramolecular motion. In contrast to the findings of Eaton and co-workers,[127] Kirby *et al.* reported that the ^{59}Co relaxation rates measured for a series of Co(III) complexes with high and low symmetries do not show any dependence on the Larmor frequency, hence ruling out any predominant

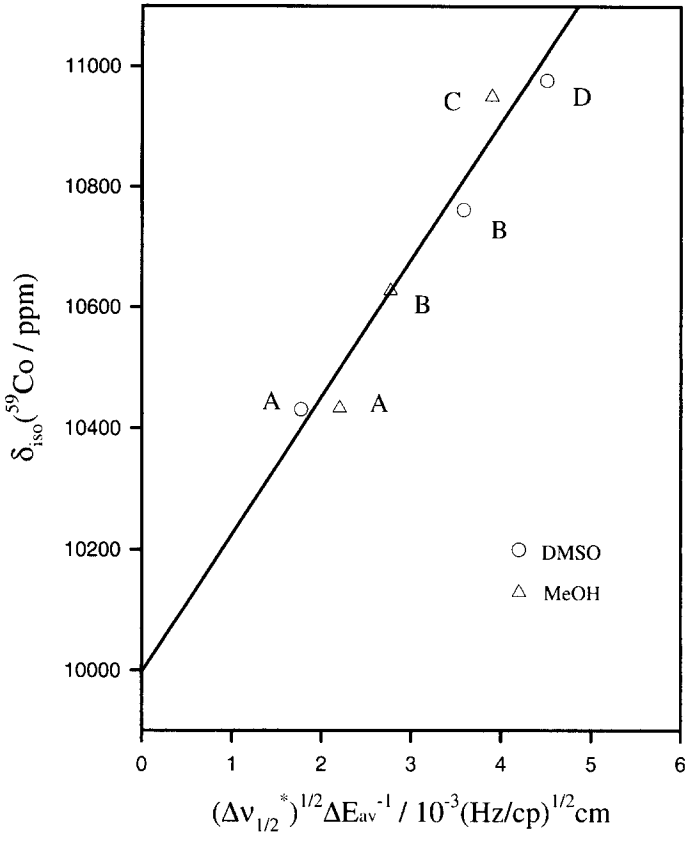

Fig. 16. Plot of $\delta_{iso}(^{59}Co)$ versus $(\Delta\nu_{1/2}{}^{*})^{1/2}\Delta E_{av}^{-1}$ for *trans*-$[Co(acac)_2(\underline{N}O_2)_2]^-$ (A), *trans*-$[Co(acac)_2(NH_3)(\underline{N}O_2)]$ (B), *trans*-$[Co(acac)_2(NH_3)_2]^+$ (C) and *trans*-$[Co(acac)_2(CH_3\underline{N}H_2)_2]^+$ (D) in DMSO and MeOH. (Reproduced with permission from ref. 97.)

Table 5. Summary of the methine carbon longitudinal relaxation rates $T_1(^{13}C_m)$ and the deduced NMR data for *trans*-$[Co(acac)_2(XY)]$ in DMSO and MeOH.[a]

Solvent	X	Y	$T_1(^{13}C_m)$ (s)	Exp. τ_c (ps)	Calc. τ_c (ps)	$\delta_{iso} - \delta_{//}$ (ppm)	χ (MHz)
DMSO	NO_2^-	NO_2^-	0.29(1)	160(8)	150(69)	430	12(3)
	NH_3	NO_2^-	0.34(1)	140(7)	120(55)	760	24(6)
	CH_3NH_2	CH_3NH_2	–	–	120(55)	980	30(7)
MeOH	NO_2^-	NO_2^-	–	–	35(16)	430	15(3)
	NH_3	NO_2^-	–	–	37(17)	630	19(4)
	NH_3	NH_3	–	–	36(16)	950	25(6)

[a] Data reproduced from ref. 97.

contribution of chemical shift anisotropy to ^{59}Co relaxation.[131] The results of Kirby and co-workers are substantiated by the similar observations for cobalt porphyrinates[74] and cobalt clusters.[121] By analysing the ^{59}Co and ^{13}C relaxation rates, Bryant and co-workers reported that the ion-pairing of $[Co(en)_3]^{3+}$ and anions does not lead to any appreciable change in the ^{59}Co quadrupole coupling constant.[128] Later, Masuda and Yamatera argued that the previous analysis is not appropriate for $[Co(en)_3]^{3+}$ and SO_4^{2-} because the rotational reorientation is anisotropic for this ion-pair.[129] They convincingly showed that there is an appreciable decrease (~17%) in the EFG along the C_3 axis of the $[Co(en)_3]^{3+}$ ion upon ion-pair formation. Assuming the same τ_c for $[Co(NH_3)_5CH_3]^{2+}$ and $[Co(NH_3)_6]^{3+}$, Kofod obtained a value of 99.7 MHz for the ^{59}Co quadrupole coupling constant of the former cations,[130] which is rather doubtful in view of the much smaller static χ reported for other similar compounds (see Table 1). In fact, τ_c the data for $[Co(NH_3)_6]^{3+}$ are not expected to be very accurate because they were inferred from other cobaltammine complexes via a hydrodynamic model.[34] Kirby *et al.* extracted the spin-rotation constants of several octahedral Co(III) complexes by performing a bifunctional relaxation time versus inverse temperature fitting.[131] On the basis of these data, the absolute shielding of the reference standard, i.e. 1.0 moll^{-1} aqueous $K_3[Co(CN)_6]$, was inferred to be −1412 ppm, which is quite different from the previous estimate[103] (−5400 ppm) and the latest theoretical results (see below). Most likely, the reported spin-rotation constants are associated with significant errors. Cassidei *et al.* measured the room-temperature ^{13}C spin–lattice relaxation times of various carbons in $[Co(TPP)MeIm_2]^+[BF_4]^-$ and $[Co(TPP)Py_2]^+[BF_4]^-$, and concluded that the axial ligands rotate partially for the former complex and do not rotate at all for the latter complexes.[132] However, a recent ^{1}H NMR study indicated that the pyridine ligand rotation in Co(III) tetraphenylporphyrinates is in fact exceptionally rapid at ambient temperatures.[133] Seemingly, the conclusion of Cassidei and co-workers is not warranted because the ^{59}Co χ values they deduced for the two complexes are much larger than the solid-state data.[74] The ^{59}Co relaxation mechanisms in these systems may be clarified further by the Werbelow approach.

3.4. Miscellaneous

Iida and Tracey studied the Co(III) outer-sphere coordination by observing the ^{59}Co quadrupole splittings in liquid-crystalline medium, covering the complexes of $[Co(en)_3]^{3+}$, $[Co(NH_3)_6]^{3+}$, $[Co(NH_3)_5NO]^{2+}$ and $Co(acac)_3$.[134,135] A typical ^{59}Co spectrum of $Co(NH_3)_6Cl_3$ in potassium dodecanoate mesophase is shown in Fig. 17. Although ^{59}Co quadrupole splitting is more sensitive than the isotropic chemical shift in discriminating the enantiomers of $[Co(en)_3]^{3+}$ in liquid crystalline systems,[136] subsequent studies showed that quadrupole

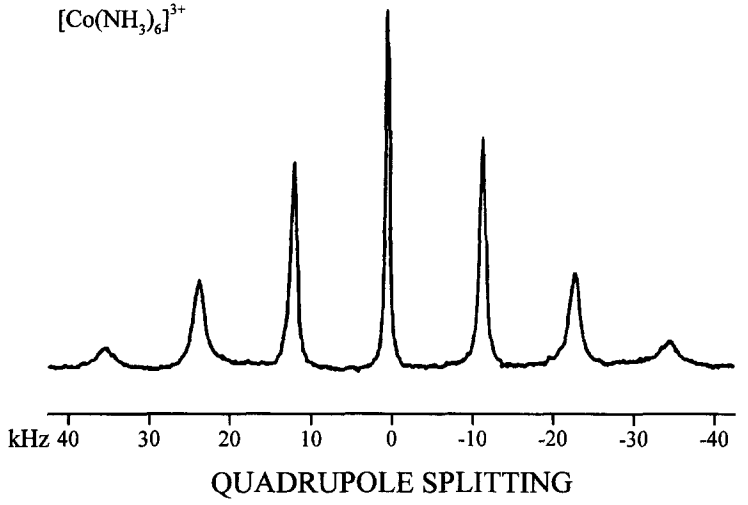

Fig. 17. ^{59}Co NMR spectrum of $[Co(NH_3)_6]^{3+}$ in a potassium dodecanoate mesophase. (Reproduced with permission from ref. 134. © 1991 American Chemical Society.)

splitting is not a sufficient parameter to characterize these systems because the Co(III) ions strongly adsorbed on the micelles do not contribute to the ^{59}Co NMR signals.[137,138] Ion-pairing effects between Co(III) complex cations and bulky anions were also actively investigated by the research group of Iida. It was reported that the ^{59}Co chemical shifts tend to move upfield relative to the free hydrated state if the Co(III) complex cations interact electrostatically with the anions, whereas the converse is true for hydrophobic interaction.[139] From the concentration dependence of the ^{59}Co chemical shifts, it was found that the interactions of the ion-pairs $[Co(chxn)_3]^{3+}$–sulfate/oxalate are electrostatic in nature, where chxn is (R,R)-1,2-cyclohexanediamine. The authors asserted that the lifetime of $[Co(chxn)_3]^{3+}$-oxalate is shorter than the rotational reorientation correlation time in order to explain the observed opposite concentration dependence of the longitudinal relaxation rates of these ion-pairs.[140] The relaxation rates and linewidths of the ^{59}Co signals were measured to deduce the critical micelle concentration values for the aggregation of [Co(R-en)(3,7-diazanonane-1,9-diamine)]$^{3+}$ in water.[141] The effective ^{59}Co quadrupole coupling constants were crudely estimated for $[Co(en)_3]^{3+}$, $[Co(chxn)_3]^{3+}$ and $[Co(phen)_3]^{3+}$ (where phen is 1,10-phenanthroline) in micellar solutions by measuring the ^{59}Co relaxation rates, where τ_c were calculated from the Stokes–Einstein–Debye model.[142] The data trend is consistent with the suggestion that the en and chxn complexes interact with the head groups in the intrafacial region of the micelles, while the phen complex is localized to the interior of the micelles.

A comprehensive discussion of ^{59}Co NMR study of the cobalt cluster chemistry is referred to a review article by Granger and co-workers.[143]

Assuming the similarity of solid-state and solution-state quadrupolar parameters, the rotational reorientation correlation times of several cobalt clusters were determined by measuring the ^{59}Co relaxation times at different temperatures. Motion of hard spheres in a continuous viscous medium was proved to be an appropriate description of the microdynamic motion of the studied clusters.[144, 63] The self-exchange rates for $Co(S_6)^{2+/3+}$ couples were determined by monitoring the linewidth of the ^{59}Co signal as a function of the concentration of the Co(II) species under the slow exchange regime.[145] The two-site exchange system of $Co_2(CO)_8$ and $HCo(CO)_4$ under high-temperature and high-pressure conditions was investigated through NMR line-shape analyses of the ^{59}Co signals, providing insight into the reaction pathway of the catalytic hydroformylation of propylene in supercritical carbon dioxide.[146] The ^{59}Co chemical shifts were measured for $Co(acac)_3$ in 14 organic solvents,[147] where the observed isotropic chemical shifts decreased with the increasing electrophilicity of the solvents. However, the microdynamics of $Co(acac)_3$ in CH_3Cl is yet to be understood.

3.5. Outlook

Since the landmark correlation between ^{59}Co chemical shift and d–d transition proposed in 1957, numerous empirical interpretations have been suggested for discerning the origin of the chemical shift of ^{59}Co nucleus. As the chemical complexity of the currently 'hot' Co(III) systems is getting beyond that of Werner-type compounds, the advancement of ^{59}Co chemical shift interpretation has reached a point where semi-empirical and/or *ab initio* approaches are necessary to make any further progress. Concerning ^{59}Co relaxation studies, we have highlighted in Section 3.3 the difficulties encountered when the number of independent NMR observables is less than the degree of freedom of a relaxation process. Although assumptions of various sophistication are seemingly unavoidable in NMR relaxation studies, independent characterization of the correlation time τ_c by other physical methods might produce further progress in this area. For example, application of laser light scattering for the detection of the hydrodynamic radii of Co(III) supercomplexes in various solvents is underway in the laboratories of Au-Yeung and Wu.[148]

4. THEORETICAL STUDIES

4.1. Chemical shielding

Accurate calculation of chemical shielding tensors is being actively pursued because it facilitates the use of NMR chemical shift data in the studies of structures and bonding. The chemical shifts of hexacoordinated Co(III)

complexes, where the low-spin d^6 complexes have a closed $d(t_{2g})$ sub-shell with energetically low-lying $d(t_{2g}) \rightarrow d(e_g)$ transitions, are known to have a large range of ~12 000 ppm.[9] Although this large chemical shift range provides a stringent test of the reliability of any computation methods, relatively few chemical shielding calculations are found for the ^{59}Co nucleus in the 1990s.[149] The pioneering work by Lamphun and Webb showed that the diamagnetic contribution to the ^{59}Co chemical shielding is significant but that it remains roughly constant among different complexes.[149] However, the calculated results of this INDO[149] study and a subsequent FPT-CNDO/2[150] calculation must be scaled by numerical factors of 4.65 and 4.83, respectively, to achieve a reasonable agreement with the experimental values. The difficulties involved in ^{59}Co chemical shielding calculation are mainly due to the significant electron-correlation effects commonly found in transition-metal systems. Since most of the post-Hartree–Fock methods[151] are too computationally demanding for ^{59}Co systems, and transition metals in general, there is a noticeable absence of any *ab initio* shielding calculations on Co(III) or related complexes in the literature.

In recent years, the density functional theory (DFT) method has been quickly established as an efficient alternative to post-Hartree–Fock methods for the calculations of systems with significant electron-correlation effects.[152] The name DFT is derived from a computational method in which the electron density, rather than the many-body wavefunction, is taken as the variational variable.[153] Within the Kohn–Sham formalism,[154] if the exchange-correlation (XC) functional is known, the ground-state electron density of a many-body system can be obtained. Unfortunately, the exact form of the XC functional is not obtainable and many approximations have been proposed, including local density approximations, generalized gradient approximations and hybrid functionals that are linear combinations of Hartree–Fock exchange and DFT correlation and/or exchange functionals.[155] Owing to the lack of a recipe for a systematic improvement of the approximate XC functionals, future development of the DFT calculation of molecular properties such as chemical shielding relies on an extensive testing of the proposed functionals. The so-called uncoupled-DFT method for chemical shielding calculation was pioneered by Malkin and co-workers.[156,157] As an improvement of the uncoupled-DFT method, Malkin *et al.* proposed the sum-over-states density functional perturbation theory (SOS-DFPT) in which the energy terms in the sum over states were modified by including an empirical parameter.[158] This *ad hoc* energy correction is similar to a level shift correction for the erroneous energy difference, to which the paramagnetic contribution is inversely proportional.[159] Recent studies reveal that the Becke hybrid functionals show a remarkable performance in chemical shielding calculations.[160,161] Other DFT implementations, which have not been applied to ^{59}Co systems, are found in an overview on recent advances of DFT chemical shielding calculations.[162] In the following section we review the efforts to establish an efficient and reliable

method for the calculation of ^{59}Co chemical shielding tensors. For an exposition of the background theory for shielding calculations, readers are referred to the excellent articles by Chesnut.[163,164]

Reference calculations

The first DFT calculations of ^{59}Co chemical shielding constants were done using the SOS-DFPT-IGLO approach.[165] The preliminary results indicated a significant improvement over data previously calculated by INDO[149] and FPT-CNDO/2.[150] Despite this improvement, the calculated ^{59}Co chemical shifts are

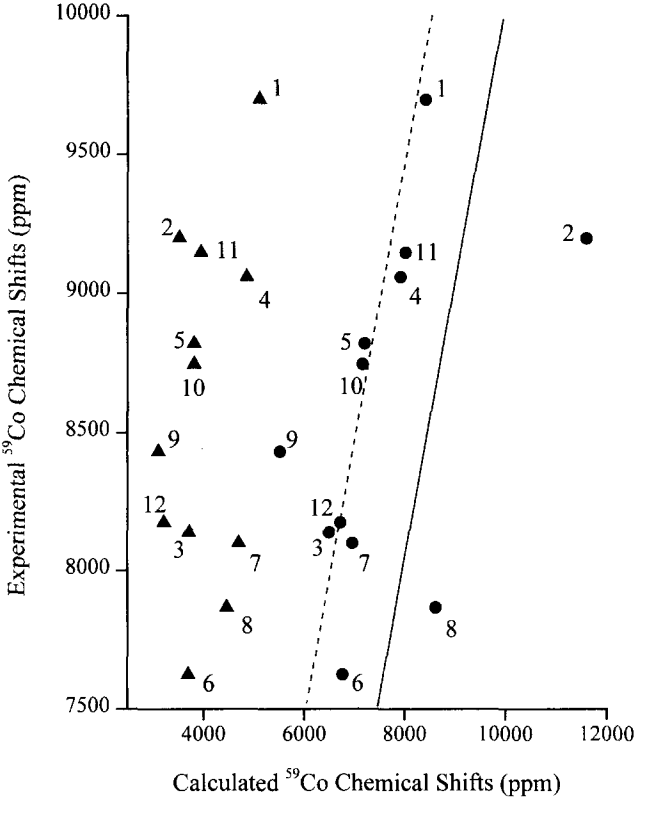

Fig. 18. Graph of experimental isotropic ^{59}Co chemical shifts versus values calculated by SOS-DFPT-IGLO/Becke-Perdew and GIAO/B3LYP. The chemical shift data were referenced to $[Co(CN)_6]^{3-}$. ▲ and ● denote the data calculated by IGLO and GIAO, respectively. The calculated complexes include $[Co(NH_3)_4CO_3]^+$ (1), *trans*-$[Co(en)_2Cl_2]^+$ (2) and $[Co(NH_3)_5X]^{(3+n)+}$: $X = S_2O_3^{2-}$ (3), CO_3^{2-} (4), Cl^- (5), NO_2^- (6), ONO^- (7), NO^- (8), SCN^- (9), N_3^- (10), H_2O (11) and NH_3 (12). The solid line denotes perfect agreement between the experimental and calculated data. (Reproduced with permission from ref. 166, © 1997, with permission from Elsevier Science.)

in general underestimated by a factor of 2 compared with the solution ^{59}Co chemical shifts data.[165] Further testing by calculating the shielding constants of 13 hexacoordinated Co(III) complexes indicated that the hybrid DFT-GIAO method is superior to SOS-DFPT-IGLO, as shown in Fig. 18.[166] The solid line in Fig. 18 depicts the ideal situation in which experimental and calculated results are identical. Since most of the data points deviate from the solid line by ~1500 ppm, it was noted that if $[Co(NH_3)_6]^{3+}$ is employed as the reference instead of $[Co(CN)_6]^{3-}$, the ^{59}Co chemical shifts of 8 out of 12 compounds would be reproduced satisfactorily, as shown by the dotted line drawn parallel to the solid line and passing through the data point of $[Co(NH_3)_6]^{3+}$. Hydrogen bonding is most likely the explanation for the deviation of the data point of *trans* – $[Co(en)_2Cl_2]Cl{\cdot}HCl{\cdot}2H_2O$. Since the experimental absolute shielding scale is not available for the ^{59}Co nucleus, it is difficult to determine whether the magnitude of the shielding constant of $[Co(CN)_6]^{3-}$ was overestimated or the chemical shifts calculated for $Co(NH_3)_5X$ were systematically underestimated by ~1500 ppm. In a follow-up study, the basis set dependence of the calculated chemical shielding tensors of several Co(III) complexes were studied.[167] It was concluded that ^{59}Co shielding tensors could be calculated

Table 6. Summary of the calculated and experimental ^{59}Co chemical shielding tensors[a]

Compounds	σ_{iso}	Ω^{calc} (ppm)	κ^{calc}	δ_{iso}^{expt}	Ω^{expt} (ppm)	κ^{expt}	Ref
$K_3[Co(CN)_6]$	−5208	133	−0.11	14	96	0.41	53
$K_3[Co(CN)_6]$ site 1[b]	−5129	359	−0.19	–	178	−0.74	167
	−5270	361	−0.15				168
$K_3[Co(CN)_6]$ site 2[b]	−5211	344	−0.28	–	178	−0.74	167
	−5349	334	−0.28				168
$K_3[Co(CN)_6]$ site 3[b]	−4997	627	0.52	–	178	−0.74	167
	−5170	634	0.52				168
$[Co(NH_3)_6]Cl_3$ site 1[c]	−11139	252	0.67	7899	118	0.05	168
$[Co(NH_3)_6]Cl_3$ site 2	−12113	64	0.34	7963	163	0.66	167
	−11537	83	−0.04				168
$[Co(NH_3)_6]Cl_3$ site 3	−11696	243	0.56	7848	308	0.56	167
	−11534	102	0.62				168
$[Co(NH_3)_6]Cl_3$ site 4[c]	−11396	568	0.77	–	818	−0.22	168
$Co(acac)_3$	−16614	1115	−0.42	12498	1174	−0.57	167
	−16328	915	−0.38				168
$[Co(NH_3)_4CO_3]Br$	−13886	1562	0.30	9700	1500	0.33	167
	−13046	1416	0.28				168
$[Co(en)_3]Cl_3$	−11068	462	0.51	–	255	1.0	168

[a] All the calculations were performed on the bare complexes; solid-state NMR data were taken for comparison (see Table 1).
[b] Doped with 0.079% Cr (by mass).
[c] The reported bond lengths and angles are inconsistent with the given coordinates in ref. 204.

with reasonable accuracy at the level of B3PW91/6-311 + G* or B3LYP/6-311 + G*. Similar studies were independently carried out by Godbout and Oldfield, who suggested that f-type functions are not essential for ^{59}Co shielding calculations.[168] Some of the calculated results are summarized in Table 6 to reveal the latest progress in this area. The most up-to-date solid-state NMR data, instead of solution data, were taken to evaluate the calculated results because experimental geometries were employed for all the calculations. When the data calculated at the level of B3PW91/6-311 + G* were used to construct the graph in Fig. 19, plotting δ_{iso}^{expt} versus σ_{iso}, the slope and x-intercept were determined to be −1.10(4) and −5500(500) ppm, respectively, with a regression coefficient equal to −0.998. Rewriting Eq. (3)

$$\delta_{iso}^{expt} = -\frac{1}{(1-\sigma_{ref})}\,\sigma_{iso} + \frac{\sigma_{ref}}{(1-\sigma_{ref})} \tag{37}$$

the absolute shielding of the reference standard, aqueous $K_3[Co(CN)_6]$, is calculated to be −5500(500) ppm. This value compares favourably with the most precise experimental result, −5400 ppm[103], and is coherent with the value

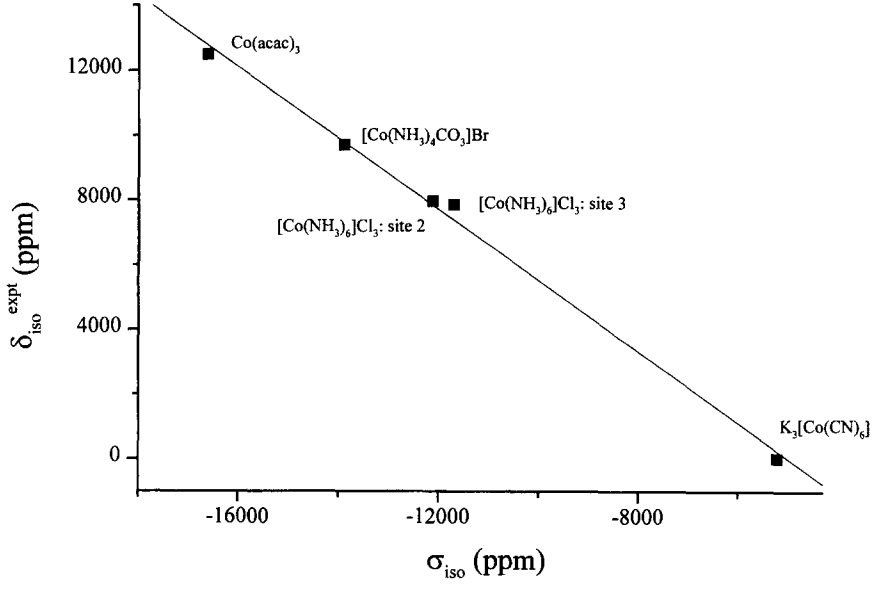

Fig. 19. Correlation between solid-state ^{59}Co isotropic chemical shifts (δ_{iso}^{expt}) and the isotropic chemical shielding constants (σ_{iso}) calculated at 6-311 + G*/B3PW91 level. All the calculations were performed on the bare complexes using experimental geometries. Data were taken from refs 53 and 167, and Table 1.

of −5162 ppm* reported previously.[168] Based on this finding, it seems that there are systematic errors associated with the calculated shielding constants of $Co(NH_3)_5X$ (see above).[166] In addition, the ^{59}Co chemical shift spans of a series of polyammonium macrocycle cobalticyanide supercomplexes were successfully reproduced by calculations at B3PW91/6-311 + G* level, illustrating that the hybrid XC functional is useful to describe small adjustments in structural and electronic properties.[53]

4.2. Quadrupole coupling constant

The classical approach for the calculation of quadrupole coupling constant is to allocate the charges for each atomic species by molecular-orbital calculations and then to calculate the EFG tensors via the Townes–Dailey theory,[169] corrected by the Sternheimer factors.[170] An impressive example had been given by Reynhardt in his study of $Co(NH_3)_6Cl_3$.[36] The experimental quadrupole coupling constants, ranging from 1 to 17 MHz, were nicely reproduced by EFG calculations including point charges and point dipoles. Based on the calculations, it was found that the contributions of point charges and point dipoles within the first ligand-sphere of the metal centre are of the same order of magnitude but of opposite in sign, resulting in relatively small EFGs at three cobalt sites. Owing to the distorted chlorine environment at the fourth site, however, those contributions become additive and therefore result in a relatively large quadrupole coupling constant. This finding illustrates that the almost perfect O_h symmetry of the octahedra does not imply a small intramolecular contribution to the EFG at the nuclear site. The temperature dependence of the ^{59}Co quadrupole coupling constant in $K_3[Co(CN)_6]$ was studied by calculating the effects of bond-stretching and rotational modes of vibration. The results imply the existence of a structural phase transition in $K_3[Co(CN)_6]$ below 100 K.[171] An early EFG calculation suggested that the lattice contribution to χ could be as large as 10 MHz.[172] However, one of the authors later admitted that the previous calculation could not be reproduced and the lattice contribution was re-estimated to be ~5% of the observed χ.[173]

4.3. Outlook

An overview of the recent progress in the theoretical calculations of ^{59}Co chemical shielding tensors has been given. It is encouraging that the DFT approach is useful for rationalizing the entire ^{59}Co chemical shift range of Co(III) complexes. It is desirable to pursue a more accurate description of the

* This value most likely carries an error larger than or equal to 500 ppm.

chemical shift range by testing newly proposed hybrid-XC functionals. Furthermore, an analysis of the calculated shielding tensors in terms of contributions from molecular orbitals is necessary for a complete understanding of the experimental data. In spite of the vast amount of experimental data, no *ab initio*/DFT studies have been reported on ^{59}Co EFG of hexacoordinated Co(III) complexes. Nevertheless, a recent DFT calculation of the EFG and magnetic hyperfine parameters of the square-pyramidal $[Co(CN)_5]^{3-}$ complex may serve as a reference for any pioneering studies.[174]

5. CONCLUDING REMARKS

We have reviewed the progress of ^{59}Co NMR spectroscopy in the 1990s. The focus is on what has been done for ^{59}Co rather than the 'technical details' of the treatments. Since very little has been reported for spin–spin coupling constants involving ^{59}Co nucleus, our solid-state data compilation was done only for chemical shifts and quadrupole coupling constants. For the sake of clarity, we have organized the material into three rather independent sections. However, it is likely that the future trend will be to combine different strategies of solid-state and/or solution-state NMR to provide a unified description of the systems under investigation. In particular, it is anticipated that theoretical calculation will provide a new dimension in ^{59}Co NMR spectroscopy, enabling its application to more complicated systems.

ACKNOWLEDGEMENT

This work was supported by the Alexander von Humboldt Foundation in the form of a research fellowship to J.C.C.C. We express our gratitude to several authors and publishers for granting permission to reproduce some of the figures in this review. We are indebted to Dr T. Charpentier for providing reprints of his work. Thanks are due to Dr S. C. Chung and Dan Shantz for their helpful comments. We thank Dr Timothy C. M. Tam for his assistance in literature searching. We are most grateful to Professor R. E. Wasylishen at Dalhousie University (Halifax, Canada) for a detailed explanation of the data analyses in MAS spectroscopy.

REFERENCES

1. W. G. Proctor and F. C. Yu, *Phys. Rev.*, 1951, **81**, 20.
2. R. G. Kidd and R. J. Goodfellow, in *NMR and the Periodic Table* (eds B. E. Mann and R. K. Harris), Chapter 8, Academic Press, New York, 1978.

3. P. Laszlo, in *NMR of Newly Accessible Nuclei*, Vol. II (ed. P. Laszlo), Chapter 9, Academic Press, New York, 1983.
4. R. J. Goodfellow, in *Multinuclear NMR* (ed. J. Mason), Chapter 20, Plenum Press, New York, 1987.
5. N. Juranic, *Coord. Chem. Rev.*, 1989, **96**, 253.
6. J. Mason, *Chem. Rev.*, 1987, **87**, 1299.
7. R. G. Kidd, in *Annual Reports on NMR Spectroscopy*, Vol. 10A (ed. G. A. Webb), pp. 1–79, Academic Press, London, 1980.
8. R. G. Kidd, in *The Multinuclear Approach to NMR Spectroscopy* (eds. J. B. Lambert and F. G. Riddell), Chapter 21, D. Reidel, Dordrecht, 1983.
9. R. G. Kidd, in *Annual Reports on NMR Spectroscopy*, Vol. 23 (ed. G. A. Webb), pp. 85–132, Academic Press, London, 1991.
10. A. Yamasaki, *Anal. Chim. Acta*, 1981, **133**, 741.
11. A. Yamasaki, *J. Coord. Chem.*, 1991, **24**, 211.
12. P. S. Pregosin, in *Transition Metal Nuclear Magnetic Resonance* (ed. P. S. Pregosin), pp. 144–175, Elsevier, Amsterdam, 1991.
13. M. Mehring, *Principles of High Resolution NMR in Solids*, 2nd edn, Springer-Verlag, Berlin, 1983.
14. K. Schmidt-Rohr and H. W. Spiess, *Multidimensional Solid-State NMR and Polymers*, Academic Press, London, 1994.
15. R. W. Schurko, R. E. Wasylishen and J. H. Nelson, *J. Phys. Chem.*, 1996, **100**, 8057.
16. D. Freude and J. Haase, in *NMR Basic Principles and Progress*, Vol. 29 (eds. P Diehl, E. Fluck, H. Günter, R. Kosfeld and J. Seelig), pp. 1–90, Springer-Verlag, Berlin, 1993.
17. F. A. Anet and D. J. O'Leary, *Concepts Magn. Reson.*, 1991, **3**, 193.
18. W. T. Raynes and R. Ratcliffe, *Mol. Phys.*, 1979, **37**, 571.
19. J. Mason, *Solid State Nucl. Magn. Reson.*, 1992, **2**, 285.
20. C. J. Jameson, *Solid State Nucl. Magn. Reson.*, 1998, **11**, 265.
21. R. K. Harris, J. Kowalewski, S. C. de Menezes, *Solid State Nucl. Magn. Reson.*, 1998, **10**, 111.
22. A. Abragam, *Principles of Nuclear Magnetism*, Oxford University Press, Oxford, 1963.
23. P. P. Man, in *Encyclopedia of Nuclear Magnetic Resonance* (eds D. M. Grant and R. K. Harris), pp. 3838–3848, Wiley, Chichester, 1996.
24. M. E. Rose, *Elementary Theory of Angular Momentum*, Wiley, New York, 1975.
25. W. P. Power, R. E. Wasylishen, S. Mooibroek, B. A. Pettitt and W. Danchura, *J. Phys. Chem.*, 1990, **94**, 591.
26. J. Hirschinger, P. Granger and J. Rosé, *J. Phys. Chem.*, 1992, **96**, 4815.
27. A. Medek, V. Frydman and L. Frydman, *Proc. Natl. Acad. Sci. USA*, 1997, **94**, 14237.
28. J. M. Koons, E. Hughes, H. M. Cho and P. D. Ellis, *J. Magn. Reson.*, 1995, **A114**, 12.
29. G. M. Volkoff, *Can. J. Phys.*, 1953, **31**, 820.
30. M. A. Kennedy and P. D. Ellis, *Concepts Magn. Reson.*, 1989, **1**, 35.
31. M. A. Kennedy and P. D. Ellis, *Concepts Magn. Reson.*, 1989, **1**, 109.
32. T. Sugawara, *J. Phys. Soc. Jpn.*, 1959, **14**, 858.
33. P. Zhou, F. Xue and S. C. F. Au-Yeung, *Acta Crystallogr. C*, 1998, C54, IUC9800062.
34. H. Hartmann and H. Sillescu, *Theor. Chim. Acta*, 1964, **2**, 371.
35. H. W. Spiess, H. Haas and H. Hartmann, *J. Chem. Phys.*, 1969, **50**, 3057.
36. E. C. Reynhardt, *J. Magn. Reson.*, 1977, **28**, 441.
37. K. Eichele, J. C. C. Chan, R. E. Wasylishen and J. F. Britten, *J. Phys. Chem.*, 1997, **101**, 5423.
38. E. C. Reynhardt, *J. Phys. C: Solid State Phys.*, 1974, **7**, 4135.
39. W. P. Power, C. W. Kirby and N. J. Taylor, *J. Am. Chem. Soc.*, 1998, **120**, 9428.
40. T. Vosegaard, E. Hald, V. Langer, H. J. Skov, P. Daugaard, H. Bildsøe and H. J. Jakobsen, *J. Magn. Reson.*, 1998, **135**, 126.
41. S. Kroeker, K. Eichele, R. E. Wasylishen and J. F. Britten, *J. Phys. Chem.*, 1997, **101**, 3727.
42. S. S. Dharmatti, V. Saraswati and R. Vijayaraghavan, in *Proc. XIIIth Colloque Ampère* (ed. L. van Gerven), pp. 133–140, North-Holland, Amsterdam, 1965.

43. V. Saraswati and R. Vijayaraghavan, *Proc. Indian Acad. Sci.*, 1967, **A66**, 253.
44. D. R. Eaton, R. J. Buist and B. G. Sayer, *Can. J. Chem.*, 1987, **65**, 1332.
45. P. A. Whuler, C. Brouty, P. Spinat and P. Herpin, *Acta Crystallogr.*, 1975, **B31**, 2069.
46. B. A. Scott and R. A. Bernheim, *J. Chem. Phys.*, 1966, **44**, 2004.
47. P. Ganguly, T. N. Venkatraman, P. R. Rajamohanan and S. Ganapathy, *J. Phys. Chem.*, 1997, **101**, 11099.
48. P. J. Chu and B. C. Gerstein, *J. Chem. Phys.*, 1989, **91**, 2081.
49. J. T. Cheng, J. C. Edwards and P. D. Ellis, *J. Phys. Chem.*, 1990, **94**, 553.
50. S. C. Chung, J. C. C. Chan, S. C. F. Au-Yeung and X. Xu, *J. Phys. Chem.*, 1993, **97**, 12685.
51. F. H. Larsen, H. J. Jakobsen, P. D. Ellis and N. C. Nielsen, *J. Phys. Chem.*, 1997, **101**, 8597.
52. I. Watanabe, H. Tanaka and T. Shimizu, *J. Chem. Phys.*, 1970, **52**, 4031.
53. P. Zhou, S. C. F. Au-Yeung and X.-P. Xu, *J. Am. Chem. Soc.*, 1999, **121**, 1030.
54. U. Behrens, A. K. Brimah, T. M. Soliman and R. D. Fischer, *Organometallics*, 1992, **11**, 1718.
55. P. Schwarz, E. Siebel, R. d. Fischer, N. A. Davies, D. C. Apperley and R. K. Harris, *Chem. Eur. J.*, 1998, **4**, 919.
56. J. Hasse and E. Oldfield, *J. Magn. Reson.*, 1993, **A104**.
57. N. C. Nielsen, H. Bildsoe and H. J. Jakobsen, *Chem. Phys. Lett.*, 1992, **191**, 205.
58. M. Rance and R. A. Byrd, *J. Magn. Reson.*, 1983, **52**, 221.
59. A. C. Kunwar, G. L. Turner and E. Oldfield, *J. Magn. Reson.*, 1986, **69**, 124.
60. R. Janssen and W. S. Veeman, *J. Chem. Soc., Faraday Trans.*, 1988, **84**, 3747.
61. Y. Dumazy, J.-P. Amoureux and C. Fernandez, *Mol. Phys.*, 1997, **90**, 959.
62. J. Abart, E. Palangie, W. Socher and J. Voitlander, *J. Chem. Phys.*, 1983, **78**, 5468.
63. P. Kempgens, J. Hirschinger, K. Elbayed, J. Raya and P. Granger, *J. Phys. Chem.*, 1996, **100**, 2045.
64. M. M. Maricq and J. S. Waugh, *J. Chem. Phys.*, 1979, **70**, 3300.
65. C. Jäger, in *NMR Basic Principles and Progress*, Vol. 31 (eds P. Diehl, E. Fluck, H. Günter, R. Kosfeld and J. Seelig), pp. 133–170, Springer-Verlag, Berlin, 1994.
66. A. Samoson, *Chem. Phys. Lett.*, 1985, **119**, 29.
67. E. Kundla, A. Samoson and E. Lippmaa, *Chem. Phys. Lett.*, 1981, **83**, 229.
68. J.-P. Amoureux, *Z. Naturforsch.*, 1992, **47a**, 665.
69. J. Herzfeld and A. E. Berger, *J. Chem. Phys.*, 1980, **73**, 6021.
70. S. Ohba, K. Toriumi, S. Sato and Y. Sato, *Acta Crystallogr.*, 1978, **B34**, 3535.
71. J. C. C. Chan and S. C. F. Au-Yeung, unpublished work.
72. T. Charpentier and J. Virlet, *Solid State Nucl. Magn. Reson.*, 1998, **12**, 227.
73. S. Hayashi, *Magn. Reson. Chem.*, 1996, **34**, 791.
74. A. Medek, V. Frydman and L. Frydman, *J. Phys. Chem.*, 1997, **101**, 8959.
75. M. P. J. Peeters, M. J. van Bommel, P. M. C. Neilen-ten Wolde, H. A. M. van Hal, W. C. Keur and A. P. M. Kentgens, *Solid State Ionics*, 1998, **112**, 41.
76. F. Lefebvre, J.-P. Amoureux, C. Fernandez and E. G. Derouane, *J. Chem. Phys.*, 1987, **86**, 6070.
77. A. Samoson and E. Lippmaa, *Phys. Rev.*, 1983, **B28**, 6567.
78. A. Samoson and E. Lippmaa, *Chem. Phys. Lett.*, 1983, **100**, 205.
79. P. P. Man and P. Tougne, *Mol. Phys.*, 1994, **83**, 997.
80. P. Kempgens, J. Hirchinger, P. Granger and J. Rosé, *Solid State Nucl. Magn. Reson.*, 1997, **10**, 95.
81. T. Eguchi, H. Nakayama, H. Ohki, S. Takeda, N. Nakamura, S. Kernaghan and B. T. Heaton, *J. Organometallic Chem.*, 1992, **428**, 207.
82. L. Frydman and J. S. Harwood, *J. Am. Chem. Soc.*, 1995, **117**, 5367.
83. C. Fernandez, and J.-P. Amoureux, *Solid State Nucl. Magn. Reson.*, 1996, **5**, 315.
84. G. Wu, D. Rovnyank, B. Sun and R. G. Griffin, *Chem. Phys. Lett.*, 1995, **249**, 210.
85. J.-P. Amoureux, C. Fernandez and S. Steuernagel, *J. Magn. Reson.*, 1996, **A123**, 116.
86. J.-P. Amoureux, M. Pruski, D. P. Lang and C. Fernandez, *J. Magn. Reson.*, 1998, **131**, 170.

87. J.-P. Amoureux and C. Fernandez, *Solid State Nucl. Magn. Reson.*, 1998, **10**, 211.
88. A. Medek, J. S. Harwood and L. Frydman, *J. Am. Chem. Soc.*, 1995, **117**, 12779.
89. J. C. C. Chan, *Concepts Magn. Reson.*, 1999, **11**, 363–377.
90. J.-P. Amoureux, C. Fernandez and L. Frydman, *Chem. Phys. Lett.*, 1996, **259**, 347.
91. L. Marinelli, A. Medek and L. Frydman, *J. Magn. Reson.*, 1998, **132**, 88.
92. T. Charpentier, C. Fermon and J. Virlet, *J. Chem. Phys.*, 1998, **109**, 3116.
93. T. L. Brown, *Acc. Chem. Res.*, 1974, **7**, 408.
94. J. Mason, *J. Chem. Soc., Faraday Trans.*, 1976, **72**, 2064.
95. M. Karplus and T. P. Das, *J. Chem. Phys.*, 1961, **34**, 1683.
96. C. J. Jameson and H. S. Gutowsky, *J. Chem. Phys.*, 1964, **40**, 1714.
97. J. C. C. Chan and S. C. F. Au-Yeung, *J. Chem. Soc., Faraday Trans.*, 1996, **92**, 1121.
98. R. Freeman, G. R. Murray and R. E. Richards, *Proc. R. Soc. Ser. A.*, 1957, **242**, 455.
99. J. S. Griffith and L. E. Orgel, *Trans. Faraday Soc.*, 1957, **53**, 601.
100. N. F. Ramsey, *Phys. Rev.* 1950, **78**, 699.
101. N. Juranic, *Inorg. Chem.*, 1980, **19**, 1093.
102. N. Juranic, *J. Am. Chem. Soc.*, 1988, **110**, 8341.
103. R. Bramley, M. Brorson, A. M. Sargeson and C. E. Schaffer, *J. Am. Chem. Soc.*, 1985, **107**, 2780.
104. T. Taura, *Bull. Chem. Soc. Jpn.*, 1990, **63**, 1105.
105. S. C. F. Au-Yeung, K. W. Kwong and R. J. Buist, *J. Am. Chem. Soc.* 1990, **112**, 7482 and references therein.
106. T. Fujihara and S. Kaizaki, *J. Chem. Soc., Dalton Trans.*, 1993, **8**, 1275.
107. R. G. Pearson, *J. Am. Chem. Soc.*, 1963, **85**, 3533.
108. R. G. Pearson, *Inorg. Chem.*, 1988, **27**, 734.
109. H. Bang, J. O. Edwards, J. Kim, R. G. Lawler, K. Reynolds, W. J. Ryan and D. A. Sweigart, *J. Am. Chem. Soc.*, 1992, **114**, 2843.
110. T. Richert, K. El Bayed, J. Raya, P. Granger, P. Braunstein and J. Rosé, *Magn. Reson. Chem.*, 1996, **34**, 689.
111. C. Deverell, *Mol. Phys.*, 1969, **16**, 491.
112. A. Delville, C. Detellier, A. Gerstmans and P. Laszlo, *J. Magn. Reson.*, 1981, **42**, 14.
113. K. K. W. Ho, W. Y. Choy, Y. Cui and S. C. F. Au-Yeung, *J. Magn. Reson.*, 1994, **A108**, 196.
114. J. C. C. Chan, P. J. Wilson, S. C. F. Au-Yeung and G. A. Webb, *J. Phys. Chem.*, 1997, **101**, 4196.
115. L. G. Vanquickenborne, M. Hendrickx, I. Hyla-Kryspin and L. Haspeslagh, *Inorg. Chem.*, 1986, **25**, 885.
116. M. Gerloch, *Coord. Chem. Rev.*, 1990, **99**, 117.
117. H. W. Spiess, in *NMR Basic Principles and Progress* (eds P. Diehl, E. Fluck and R. Kosfeld), pp. 55–214, Springer-Verlag, New York, 1978.
118. O. Howarth, in *Multinuclear NMR* (ed. J. Mason), Chapter 5, Plenum Press, New York, 1987.
119. A. Einstein, *Investigations on the Theory of the Brownian Movement*, Dover, New York, 1956.
120. L. G. Werbelow, A. Allouche and G. Pouzard, *J. Chem. Soc., Faraday Trans.*, 1987, **83**, 871.
121. P. Granger, K. El Bayed, J. Raya, P. Kempgens and J. Rosé, *J. Magn. Reson.*, 1995, **A117**, 179.
122. P. Kofod, *J. Magn. Reson.*, 1996, **A119**, 219.
123. K. El Bayed, P. Kempgens, J. Raya, P. Granger and J. Rosé, *J. Magn. Reson.*, 1998, **130**, 209.
124. P. Kofod, E. Larsen, S. Larsen, C. H. Petersen, J. Springborg and D. N. Wang, *Acta Chem. Scand.*, 1992, **46**, 841.
125. P. Kofod, P. Harris and S. Larsen, *Inorg. Chem.*, 1997, **36**, 2258.
126. M. Kanakubo, H. Ikeuchi and G. P. Sato, *J. Magn. Reson.*, 1995, **112**, 13.
127. S. C. F. Au-Yeung, R. J. Buist and D. R. Eaton, *J. Magn. Reson.*, 1983, **55**, 24.
128. K. G. Russell and R. G. Bryant, *J. Phys. Chem.*, 1984, **88**, 4299.
129. Y. Masuda and H. Yamatera, *J. Phys. Chem.*, 1988, **92**, 2067.

130. P. Kofod, *Inorg. Chem.*, 1995, **34**, 2768.
131. C. W. Kirby, C. M. Puranda and W. P. Power, *J. Phys. Chem.*, 1996, **100**, 14618.
132. L. Cassidei, H. Bang, J. O. Edwards and R. G. Lawler, *J. Phys. Chem.*, 1991, **95**, 7186.
133. J. R. Polam, T. K. Shokhireva, K. Raffii, U. Simonis and F. A. Walker, *Inorg. Chim. Acta*, 1997, **263**, 109.
134. M. Iida and A. S. Tracey, *J. Phys. Chem.*, 1991, **95**, 7891.
135. M. Iida, Y. Miyagawa, S. Kohri and Y. Ikemoto, *Bull. Chem. Soc. Jpn.*, 1993, **66**, 2840.
136. M. Iida, T. Nakamori, Y. Mizuno and Y. Masuda, *Chem. Lett.*, 1994, **8**, 481.
137. M. Iida, Y. Mizuno and Y. Miyagawa, *Bull. Chem. Soc. Jpn.*, 1994, **67**, 1531.
138. M. Iida, Y. Mizuno and N. Koine, *Bull. Chem. Soc. Jpn.*, 1995, **68**, 1337.
139. M. Iida, Y. Miyagawa and S. Kohri, *Bull. Chem. Soc. Jpn.*, 1993, **66**, 2398.
140. M. Iida, T. Nakamori, Y. Mizuno and Y. Masuda, *J. Phys. Chem.*, 1995, **99**, 4347.
141. M. Iida, M. Yamamoto and N. Fujita, *Bull. Chem. Soc. Jpn.*, 1996, **69**, 3217.
142. Y. Mizuno and M. Iida, *J. Phys. Chem.*, 1997, **101**, 3919.
143. P. Granger, J. Raya, J. Hirschinger, T. Richert and K. El Bayed, *J. Chim Phys.*, 1994, **91**, 828.
144. P. Granger, T. Richert, K. El Bayed, P. Kempgens, J. Hirschinger, J. Raya, J. Rosé and P. Braunstein, *Mol. Phys.*, 1997, **92**, 895.
145. S. Chandrasekhar and A. McAuley, *Inorg. Chem.*, 1992, **31**, 480.
146. R. J. Klingler and J. W. Rathke, *J. Am. Chem. Soc.*, 1994, **116**, 4772.
147. M. Kanakubo, T. Uda, H. Ikeuchi and G. P. Sato, *J. Solution Chem.*, 1998, **27**, 645.
148. S. C. F. Au-Yeung, Y. Zhang and C. Wu, personal communication.
149. B. N. Lamphun and G. A. Webb, *J. Mol. Structure (Theochem)*, 1983, **104**, 191.
150. X. Xie, S. C. F. Au-Yeung and H. Liu, *J. Mol. Struct. (Theochem)*, 1995, **331**, 181.
151. H. Fukui, *Prog. Nucl. Magn. Reson. Spectrosc.*, 1997, **31**, 317.
152. J. K. Labanowski and J. Andzelm (eds), *Density Functional Methods in Chemistry*, Springer-Verlag, New York, 1991.
153. P. Hohenberg and W. Kohn, *Phys. Rev.*, 1964, **B136**, 864.
154. W. Kohn and L. J. Sham, *Phys. Rev.*, 1965, **A140**, 1133.
155. A. D. Becke, in *Modern Electronic Structure Theory II* (ed. D. R. Yarkony), World Scientific, Singapore, 1995.
156. V. G. Malkin, O. L. Malkina and D. R. Salahub, *Chem. Phys. Lett.*, 1993, **204**, 80.
157. V. G. Malkin, O. L. Malkina and D. R. Salahub, *Chem. Phys. Lett.*, 1993, **204**, 87.
158. V. G. Malkin, O. L. Malkina, M. E. Casida and D. R. Salahub, *J. Am. Chem. Soc.*, 1994, **116**, 5898.
159. L. Olsson and D. Cremer, *J. Chem. Phys.*, 1996, **105**, 8995.
160. J. R. Cheeseman, G. W. Trucks, T. A. Keith and M. J. Frisch, *J. Chem. Phys.*, 1996, **104**, 5497.
161. M. Bühl, *Chem. Phys. Lett.*, 1997, **267**, 251.
162. G. Schreckenbach and T. Ziegler, *Theor. Chem. Acc.*, 1998, **99**, 71.
163. D. B. Chesnut, in *Annual Reports on NMR Spectroscopy*, Vol. 29 (ed. G. A. Webb), pp. 71–122, Academic Press, London, 1994.
164. D. B. Chesnut, in *Reviews in Computational Chemistry*, Vol. 8 (eds. K. B. Lipkowitz and D. B. Boyd), pp. 245–297, VCH, New York, 1996.
165. J. C. C. Chan, S. C. F. Au-Yeung, P. J. Wilson and G. A. Webb, *J. Mol. Struct. (Theochem)*, 1996, **365**, 125.
166. J. C. C. Chan and S. C. F. Au-Yeung, *J. Mol. Struct. (Theochem)*, 1997, **393**, 93.
167. J. C. C. Chan and S. C. F. Au-Yeung, *J. Phys. Chem.*, 1997, **101**, 3637.
168. N. Godbout and E. Oldfield, *J. Am. Chem. Soc.*, 1997, **119**, 8065.
169. C. H. Townes and B. P. Dailey, *J. Chem. Phys.*, 1949, **17**, 782.
170. E. A. C. Lucken, *Nuclear Quadrupole Coupling Constants*, Academic Press, London, 1969.
171. J. A. J. Lourens and E. Smit, *Can. J. Phys.*, 1980, **58**, 68.
172. T. B. Brill and Z. Z. Hugus, Jr., *J. Phys. Chem.*, 1970, **74**, 3022.

173. W. M. Shirley and Z. Z. Hugus, Jr., *J. Magn. Reson.*, 1980, **37**, 529.
174. S. R. Nogueira and D. Guenzburger, *Int. J. Quantum Chem.*, 1995, **54**, 381.
175. E. C. Reynhardt, *Can. J. Phys.*, 1974, **52**, 1398.
176. E. C. Reynhardt, *Solid State Commun.*, 1974, **15**, 643.
177. J. A. J. Lourens and E. C. Reynhardt, *Phys. Stat. Sol.*, 1972, **A11**, 739.
178. J. A. J. Lourens and R. Swanepoel, *Solid State Commun.*, 1969, **7**, 1483.
179. I. Watanabe and Y. Yamagata, *J. Chem. Phys.*, 1967, **46**, 407.
180. T. B. Brill and Z. Z. Hugus, Jr., *Inorg. Nucl. Chem. Lett*, 1970, **6**, 753.
181. H. Hartmann, M. Fleissner and H. Sillescu, *Theor. Chim. Acta*, 1964, **2**, 63.
182. W. M. Shirley, *Spectrochim. Acta*, 1987, **43A**, 565.
183. I. Watanabe, *J. Phys. Soc. Jpn.*, 1970, **29**, 1204.
184. J. Voitländer, H. Klucke, R. Longino and H. Thieme, *Naturwissenschaften*, 1962, **49**, 491.
185. C. B. Harris, *Inorg. Chem.*, 1968, **7**, 1517.
186. I. Watanabe, *J. Chem. Phys.*, 1972, **57**, 3014.
187. L. S. Chia, W. R. Cullen, M. C. L. Gerry and E. C. Lerner, *Inorg. Chem.*, 1975, **14**, 2975.
188. E. S. Mooberry, M. Pupp, J. L. Slater and R. K. Sheline, *J. Chem. Phys.*, 1971, **55**, 3655.
189. E. S. Mooberry, H. W. Spiess, B. B. Garrett and R. K. Sheline, *J. Chem. Phys.*, 1969, **51**, 1970.
190. E. S. Mooberry and R. K. Sheline, *J. Chem. Phys.*, 1972, **56**, 1852.
191. T. B. Brill and D. C. Miller, *Inorg. Chem.*, 1976, **15**, 2553.
192. T. B. Brill and D. C. Miller, *Inorg. Chem.*, 1977, **16**, 1689.
193. D. C. Miller and T. B. Brill, *Inorg. Chem.*, 1978, **17**, 240.
194. T. E. Boyd and T. L. Brown, *Inorg. Chem.*, 1974, **13**, 422.
195. T. L. Brown, P. A. Edwards, C. B. Harris and J. L. Kirsch, *Inorg. Chem.*, 1969, **8**, 763.
196. D. D. Spencer, J. L. Kirsch and T. L. Brown, *Inorg. Chem.*, 1970, **9**, 235.
197. J. D. Graybeal, S. D. Ing and M. W. Hsu, *Inorg. Chem.*, 1970, **9**, 678.
198. L. S. Chia, W. R. Cullen and M. C. L. Gerry, *Can. J. Chem.*, 1974, **52**, 3695.
199. D. L. Lichtenberger, D. R. Kidd, P. A. Loeffler and T. L. Brown, *J. Am. Chem. Soc.*, 1976, **98**, 629.
200. H. W. Spiess and R. K. Sheline, *J. Chem. Phys.*, 1970, **53**, 3036.
201. C. D. Pribula, T. L. Brown and E. Münck, *J. Am. Chem. Soc.*, 1974, **96**, 4149.
202. K. Ogino and T. L. Brown, *Inorg. Chem.*, 1971, **10**, 517.
203. R. A. LaRossa and T. L. Brown, *J. Am. Chem. Soc.*, 1974, **96**, 2072.
204. G. J. Kruger and E. C. Reynhardt, *Acta Crystallogr.*, 1978, **B34**, 915.

Advances in Theoretical and Physical Aspects of Spin–Spin Coupling Constants

RUBÉN H. CONTRERAS,[1] JUAN E. PERALTA,[1] CLAUDIA G. GIRIBET,[1] MARTÍN C. RUIZ DE AZÚA[1] and JULIO C. FACELLI[2]*

[1] *Departamento de Física, Facultad de Ciencias Exactas y Naturales, Universidad de Buenos Aires, Buenos Aires, Argentina*
[2] *Center for High Performance Computing, University of Utah, Salt Lake City, Utah 84102, USA*

ABBREVIATIONS

AO	atomic orbital
CAS	complete active space
CC	coupled clusters
CCD	coupled cluster doubles
CCPPA	coupled cluster polarization propagator approach
CCSD	coupled cluster singles and doubles
CGTO	contracted GTO
CHF	coupled Hartree–Fock
CI	configuration interaction
CID	configuration interaction doubles

*Corresponding author.

ANNUAL REPORTS ON NMR SPECTROSCOPY
VOLUME 41 ISBN 0-12-505341-X

CLOPPA	contributions from localized orbitals within the PP approach
CNDO	complete neglect of differential overlap
DFPT	density functional perturbation theory
DFT	density functional theory
DNA	deoxyribonucleic acid
DSO	diamagnetic spin orbital
ED	energy derivative
EHT	extended Hückel theory
EOM	equation of motion
EPR	electron paramagnetic resonance
FC	Fermi contact
FCI	full configuration interaction
FP	finite perturbation
FPT	finite perturbation theory
GGA	general gradient approximation
GTO	Gaussian-type orbital
HRPA	higher random phase approximation
IGLO	individual gauge for different localized orbitals
INDO	intermediate neglect of differential overlap
IPPP	inner projections of the polarization propagator
IR	infra red
KS	Kohn and Sham
LCAO	linear combination of atomic orbitals
LDA	local density approximation
LMO	localized molecular orbital
MBOHO	maximum bond order hybrid orbital
MBPT	many body perturbation theory
MC	multiconfigurational
MCLR	multiconfigurational linear response
MCSCF	multiconfigurational SCF
MNDO	modified neglect of differential overlap
MO	molecular orbital
MP	Møler–Plesset
NBO	natural bond orbital
NHO	natural hybrid orbital
NMR	nuclear magnetic resonance
NO	natural orbital
NOE	nuclear Overhauser effect
PMO	perturbed molecular orbitals
PP	polarization propagator
PSO	paramagnetic spin orbital
QCI	quadratic configuration interaction
QCISD(T)	quadratic configuration interaction including singles, doubles and triples

RAS	restricted active space
RNA	ribonucleic acid
RPA	random phase approximation
RSPT	Rayleigh–Schrödinger perturbation theory
SCF	self-consistent field
SCPT	self-consistent perturbation theory
SD	spin dipolar
SOPPA	second-order PP approximation
SOS	sum over states
STO	Slater-type orbital
TS	through-space

1. INTRODUCTION

This review is a continuation of the work presented by two of the authors in their 1993 review of the same title.[1] These two reviews cover the theoretical and computational aspects of the NMR spin–spin coupling constants, discussed earlier by Kowalewski,[2,3] as well as the physical aspects involved in the coupling transmission. In this way the review becomes useful not only for theoretically oriented researchers but also for experimentally oriented ones, helping to close the gap that in general has existed between scientists using each methodological approach. Since our previous review appeared,[1] such a gap has been notably narrowed when dealing with molecular problems studied by NMR spectroscopy, as has also happened in other branches of chemistry. To further emphasize this combined approach, in Section 3 of this review we describe trends of coupling constants on the basis of concepts commonly used by chemists in the laboratory.

Since the discovery of nuclear magnetic resonance[4] impressive progress has taken place, both in experimental techniques and in theoretical approaches aimed at understanding the electronic origin of high-resolution NMR parameters. Before the period of this review, many general works were published dealing with the theory of indirect spin–spin coupling constants, with their transmission mechanisms through the molecular electronic system, and with systematic descriptions of experimental trends. A selection of those still frequently quoted in the literature includes refs 2, 3, 5–8.

During the review period the availability of new and powerful computational techniques has produced great advances in the use of theoretical approaches to calculate coupling constants. The advances during this period are essentially improvements in the implementation of previously published theoretical methods that were made possible owing to the unprecedented revolution in computational resources that took place during the same period. Very large calculations that were prohibitively expensive in previous periods are becoming almost routine, not only for theoretical chemists but also for experimentalists.

Ab initio calculations of couplings in small molecules with large basis sets and inclusion of electron correlation effects have reached almost quantitative accuracy. However, different types of couplings in different molecular environments may have very different computational demands in order to obtain such accuracy.

Exceptions to the assertion made above are the DFT-based methods. The use of these methods for chemical applications has increased exponentially in the last decade[9] and several papers have reported its use to calculate coupling constants. For instance, the FPT approach to calculating the FC contribution to different couplings employing a variety of functionals has produced quite promising results.[10–12]

During this period, many review papers have discussed aspects of different types of coupling constants in detail. Of special relevance among these are the contributions on theoretical aspects[13] and on applications of spin–spin coupling constants published in the series of *Specialist Periodical Reports*.[14] Brief general theoretical considerations were also given in ref. 15. *Ab initio* methods for calculating coupling constants were reviewed by Helgaker *et al.*,[16] and applications of the IPPP-CLOPPA method at semiempirical level have also been reviewed.[17] Several aspects of couplings involving thallium nuclei were discussed in Hinton's review.[18] Interesting features of many coupling constants in octahedral complexes and clusters were discussed in the review of Preetz *et al.*[19] Quantum exchange couplings in polyhydride and dihydrogen complexes were reviewed by Sabo-Etienne and Chaudret,[20] while Szsymański reviewed proton tunnelling effects in metal hydrides.[21] Many trends and properties of ^1J(C,C) couplings were comprehensively discussed in Kamienska-Trela's review.[22] The importance of coupling constants in unravelling molecular structures and conformations was stressed in Thomas' review.[23] Several papers reviewing different aspects of spin–spin coupling constants were published in the *Encyclopedia of Nuclear Magnetic Resonance*.[24] Some theoretical aspects as well as some applications in organic chemistry were presented by Barfield.[25] Calculations based on semiempirical approaches were discussed by Facelli.[26] Intermolecular and solvent effects were reviewed by Ando.[27] The transmission of through-space couplings in organic chemistry was reviewed by Mallory and Mallory,[28] while Wasylishen reviewed aspects on how to extract information on the **J** tensor from solid state spectra,[29] and Altona discussed applications of Karplus-type relationship to study molecular conformational problems.[30] The use of spin–spin coupling constants for determining conformational aspects in a variety of compounds, including nucleic acids, was discussed in several review papers.[23,31–33] Stereochemical aspects of J(C,C) couplings were discussed by Krivdin *et al.*[34] Studies of conformational processes in the gas phase were reviewed by True and Suarez.[35] Tvarovska and Taravel[36] discussed the use of J(C,H) couplings for determining conformations in sugar molecules. Conformational analysis of saturated six-membered oxygen containing heterocyclic rings were discussed by Kleinpeter.[37] Changes in ^1J(C,H) couplings of a group

adjacent to a positive charge in a carbocation were discussed in a review by Kelly.[38] Different aspects of couplings involving at least a P nucleus were discussed in different chapters of Quin and Verkade's book.[39] Quantum exchange couplings were discussed in several reviews dealing with hydride complexes.[40] Interesting J(F,F) couplings were discussed in ref. 41. Very valuable information on couplings in organometallic compounds was given by Wrackmeyer.[42] Several types of coupling constants were discussed for azo dyestuffs by Lycka.[43] Heinekey *et al.* discussed some interesting J(H,D) couplings in their review on coordination chemistry of dihydrogen.[40,44] A large set of coupling constants in azoles was collected by Elguero *et al.*[45]

The increase in the use of NMR spectroscopy for analysing chemical structures, as well as other molecular problems, prompted IUPAC to make recommendations about parameters to be reported in publications and on symbols to be used when referring to quantities related with NMR spectroscopy.[46]

The question whether spin–spin coupling interactions are intrinsic properties of a molecular system, i.e. whether they depend on the magnetic field of the spectrometer used to measure them, was addressed by Raynes and Stevens[47] and during the review period by Ding and Ye[48] for both liquids and solids. They found that the change of the interaction tensor is proportional to the external magnetic field and that this effect is more important for quadrupolar spin systems. However, for magnetic fields of the strength that can be obtained at present in the laboratory, such dependence is so small that it is within the experimental error of the couplings.

Progress in different experimental techniques helped to determine relative signs of coupling constants, which in many cases are now determined routinely. This additional information is a significant improvement in using experimental values to obtain insight into different aspects of molecular electronic structure.[49] A few examples are quoted below from the long series of papers by Wrackmeyer *et al.* in which a large number of different coupling signs were determined relative to a known one. Eujen and Hoge[50] determined signs of coupling constants in CF_2H and CF_3 derivatives of silver(III). Other interesting examples can be found in refs. 51–53. Signs of couplings across the metal centre in transition metal complexes were determined, for instance, by Otting *et al.*[54]

The mechanisms governing the newly discovered quantum exchange couplings were poorly understood at the time of publication of the previous report.[1] During the period of this review a number of papers have been published in this area and the significant body of experimental data has been rationalized by comprehensive theoretical models.[20,21,55–57]

The importance of coupling constants as probes to detect configurations, conformations[23] and intra- and intermolecular interactions[58–61] is now well recognized. Their utility is greatly enhanced if measurements are complemented with theoretical analysis. Important progress has been reported in experimental techniques for detecting a large variety of couplings in biologically interesting

compounds and, with the rapidly increasing computational facilities and efficient software, they can now be calculated.[62–64] However, at present it can be envisioned that calculation of couplings in very large compounds will not be necessary since coupling constants, like chemical shifts[65] originate in local interactions. Therefore, if the ground-state molecular wavefunction is known, a given coupling constant can be calculated using a local perturbative calculation such as the IPPP approach.[66]

Unfortunately, to keep the length of this work within reasonable limits, it was not possible to review here all the important papers published during the review period. In most cases a selection of them was chosen or simply very brief comments were made. Unfortunately, this approach might lead to omission of relevant work and the authors apologize for such possible omissions.

2. CALCULATION AND ANALYSIS OF SPIN–SPIN COUPLING CONSTANTS

2.1. Quantum exchange couplings

In the late 1980s, the large and temperature-dependent J(H,H) couplings that were observed in some transition metal hydrides were rationalized in terms of a new nuclear spin–spin coupling mechanism, namely a quantum proton exchange similar to that already known for electron couplings in EPR.[67] This process is possible since the energy barrier separating the two different potential wells, where both identical nuclei are placed, is thermally accessible and the coupled protons can undergo a tunnelling effect. If the two sites are magnetically non-equivalent, their coupling appears in the spectrum. The main features of exchange couplings, J^{EX}(H,H), are that (1) they can be several orders of magnitude larger than those of magnetic origin; (2) they depend strongly on temperature; (3) they are very sensitive to the adduct substituents; and (4) replacement of ^{1}H by ^{2}H or ^{3}H quenches them and only the magnetic contribution remains.

Chaudret *et al.*[68] found the first quantum exchange couplings in dihydride complexes of type $(Cp_2TaH_2L)PF_6$ ($Cp = \eta^5$-C_5H_5; $L = P(OMe)_3$, PMe_2Ph). J^{EX}(H,H) values ranging from 12.5 Hz (178 K) to 76.1 Hz (293 K) for $L = P(OMe)_3$, and from 4.6 Hz (193 K) to 15.6 Hz (310 K) for $L = PMe_2Ph$ were measured, all of them being of the same sign as the corresponding magnetic contribution.[68] Manzano *et al.*[69] used variable-temperature NMR to determine the structure of ruthenium trihydride adducts with metal ions such as Cu^+, Ag^+ and Au^+. They concluded that the presence of a coinage cation does not inhibit the tunnelling phenomenon and, in the case of gold adducts, a very significant increase of J^{EX}(H,H) is observed. Similar conclusions were obtained by Antiñolo *et al.*[70] in niobocene trihydrides and their adducts. Gründemann *et al.*[71] studied J^{EX} (H,H) in the $Cp^*RuH_3(Ppy_3)$ ruthenium (IV) trihydride complex, which displays significantly larger values than those in $Cp^*RuH_3(PCy_3)$ and

$Cp^*RuH_3(PPh_3)$ complexes. The first compounds showing $J^{EX}(H,H)$ coupling in polyhydride derivatives containing nitrogen as donor ligands were reported by Esteruelas *et al.*[72] They found $J^{EX}(H,H)$ in $OsH_6(PPr^i_3)_2$ treated with 2,2′-biimidazole. Sabo-Etienne *et al.*[73] showed that no kinetic isotope effect is observed for the classical rotation of H_2 in tantalum dihydride/dihydrogen complexes.

Wiedenbruch *et al.*[74] measured the pressure dependence of $J^{EX}(H,H)$ in bis(1,3-(trimethylsilyl)niobocene) trihydride. They concluded that the $J^{EX}(H,H)$ pressure dependence is due to a solvent volume effect, i.e. a decrease in that volume hinders the vibrational excitation of the hydrides. This rationalization was made in terms of the model III of Limbach and co-workers.[57]

Heinekey *et al.*[44] studied $J^{EX}(H,H)$ couplings in iridium trihydride complexes. As Manzano *et al.*[69] observed in ruthenium trihydride adducts, they found no significant kinetic isotope effects on the exchange process, but they found important isotope effects both on the $J^{EX}(H,H)$ values and the hydrides chemical shifts. Guari *et al.*[75] observed $J^{EX}(H,H)$ in orthometalated ruthenium complexes between a hydride and protons of a coordinated dihydrogen molecule.

Evidence for enhancement of the quantum exchange process upon formation of hydrogen bonds between a ruthenium trihydride complex and a series of proton donors was reported by Ayllon *et al.*[76] The presence of a hydrogen bond donor, (**1**), causes partial charge transfer from the metal hydride to the hydrogen bond donor. The decrease of the overall electron density at the metal atom could favour the formation of dihydrogen configurations, rendering very large $J^{EX}(H,H)$ couplings. Rationalizations of this type were also made for Lewis acid adducts[77,78] and for changes in the ligand basicity.[57,68] In addition, Ayllon *et al.*[76] found linear correlations between $J^{EX}(H,H)$ and the hydride chemical shifts.

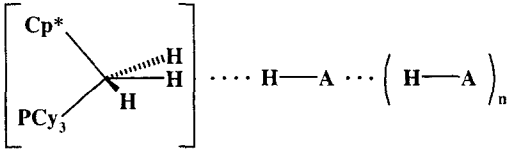

[1]

Many interesting advances in the comprehension of tunnelling mechanisms have been achieved during this period. Limbach *et al.*[57] explored different possible one-dimensional pathways for the hydrogen motion in metal trihydride complexes. The different pathways are shown in scheme (**2**). The reaction coordinate connecting T and T* states corresponds in (**2**:I) to the internuclear H_a–H_b distance, and in (**2**:II) to the rotation angle, θ. Limbach *et al.*[57] proposed pathway (**2**:III), where the reaction takes place in two steps: first, a metastable dihydrogen complex D is formed and subsequently rotational tunnelling takes place from D to D*. Finally, the symmetric state T* is formed. A similar mechanism was proposed by Jarid *et al.*[55,56] to describe

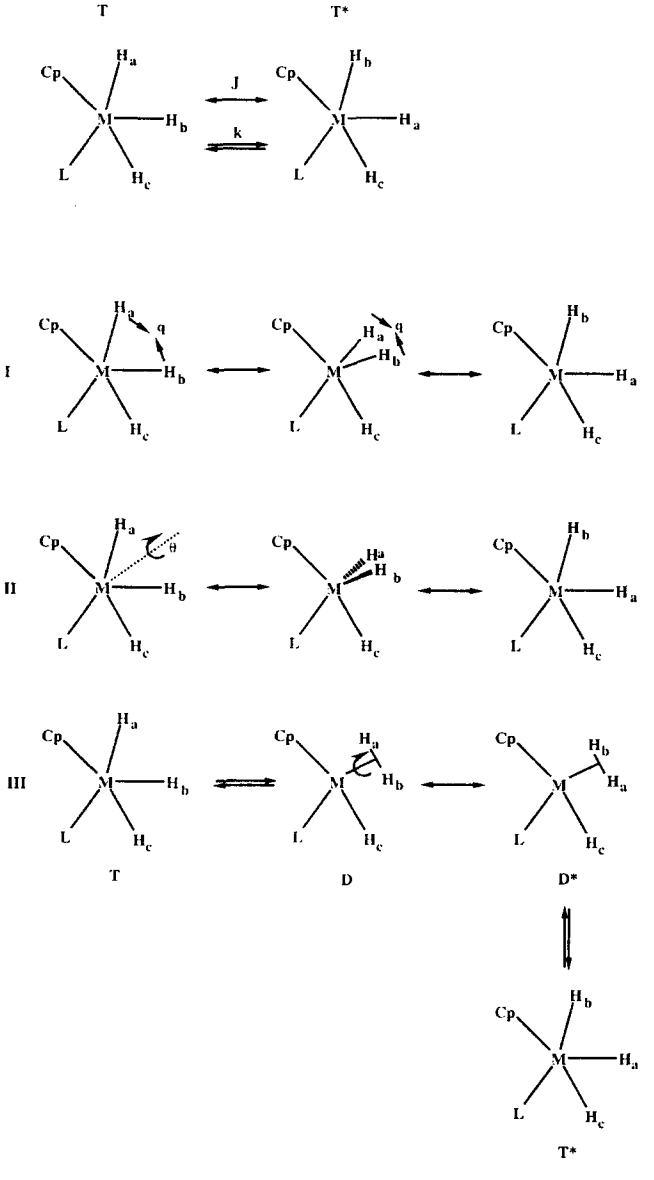

[2]

the exchange in $[(C_5H_5)Ir(L)H_3]^+$ complexes (L = PH_3, CO). They performed HF and MP2 *ab initio* calculations to construct an energy surface for the proton exchange to define the one-dimensional reaction path. For L = PH_3 they obtained the height of the energy barrier as 14.1 kcal mol^{-1} and the corresponding J^{EX}(H,H) as 112.3 Hz, while for L = CO the barrier is

10.7 kcal mol^{-1} and J^{EX}(H,H) = 1279.5 Hz, indicating that the main parameter governing the magnitude of J^{EX}(H,H) is the height of the energy barrier between the two symmetrical states, i.e. the stability of the η^2-H_2 structure. Camanyes *et al.*[79,80] obtained similar conclusions for $[(C_5H_5)_2MH_3]^{n+}$ (M = Mo, W, n = 1; M = Nb, Ta, n = 0) and $Cp_2NbH_3{\cdot}AlH_3$ complexes employing DFT to construct the energy surface.

Physical aspects and the temperature dependence of J^{EX}(H,H) were studied by Hiller and Harris[81–83] in metal trihydrides employing a multiband tight binding model. A thermal bath effect on J^{EX}(H,H) was studied theoretically by Szymański.[84] Clot *et al.*[85] pointed out the similarity between the NMR and inelastic neutron scattering spectra of transition metal hydrides. Limbach *et al.*[86] derived a unified description of the coherent and incoherent dihydrogen quantum exchange and their effects on NMR and inelastic neutron scattering spectra.

One of the most promising applications of measuring J^{EX}(H,H) is the prediction of several characteristics of molecules in the coordination chemistry framework. The high sensitivity of J^{EX}(H,H) to many aspects of the hydride complexes makes it a powerful tool for their study. Kuhlman *et al.*[87] employed the hypersensitivity of J^{EX}(H,H) to several electronic effects for detecting the formation of hydrogen bonds and weak solvent coordination in several osmium trihydrides adducts.

Comprehensive reviews were reported on quantum J^{EX}(H,H) couplings, in polyhydride and dihyrogen complexes by Sabo-Etiene and Chaudret[20] and on proton tunnelling effects in metal hydrides by Szymański.[21]

2.2. Couplings originating in electron–nucleus interactions

At present, theoretical analyses of coupling tensors that are not calculated from a full relativistic formulation continue to be based on the four electron–nucleus interactions described by the Ramsey[88] operators, Eqs. (1–4):

$$H_{DSO} = \frac{\mu_0^2 e\hbar\mu_B}{(4\pi)^2} \sum_{A,B} \gamma_A\gamma_B \sum_k \frac{[(\mathbf{I}_A \cdot \mathbf{I}_B)(\mathbf{r}_{kA} \cdot \mathbf{r}_{kB}) - (\mathbf{I}_A \cdot \mathbf{r}_{kB})(\mathbf{I}_B \cdot \mathbf{r}_{kA})]}{r_{kA}^3 r_{kB}^3} \quad (1)$$

$$H_{PSO} = \frac{\mu_0\hbar\mu_B}{2\pi\,\mathrm{i}} \sum_A \gamma_A \mathbf{I}_A \cdot \sum_k \frac{(\mathbf{r}_{kA} \times \nabla_k)}{r_{kA}^3} \quad (2)$$

$$H_{SD} = \frac{\mu_0\hbar\mu_B}{2\pi} \sum_A \gamma_A \sum_k \left[\frac{3(\mathbf{S}_k \cdot \mathbf{r}_{kA})(\mathbf{I}_A \cdot \mathbf{r}_{kA})}{r_{kA}^5} - \frac{(\mathbf{S}_k \cdot \mathbf{I}_A)}{r_{kA}^3} \right] \quad (3)$$

$$H_{FC} = \frac{4\mu_0\hbar\mu_B}{3} \sum_A \gamma_A \sum_k \delta(\mathbf{r}_{kA}) \frac{(\mathbf{S}_k \cdot \mathbf{I}_A)}{r_{kA}^3} \quad (4)$$

These four interactions, taken as perturbations to the electronic molecular wavefunction, lead to the five terms of the **J** coupling tensor, Eq. (5), which are,

$$\mathbf{J} = \mathbf{J}^{DSO} + \mathbf{J}^{PSO} + \mathbf{J}^{SD} + \mathbf{J}^{FC} + \mathbf{J}^{FC/SD} \tag{5}$$

The diamagnetic and paramagnetic spin–orbit terms, $\mathbf{J}^{DSO}$ and $\mathbf{J}^{PSO}$, respectively, are nonsymmetric tensors; the spin-dipolar, $\mathbf{J}^{SD}$, is also nonsymmetric; the Fermi contact term, $\mathbf{J}^{FC}$, is isotropic; and the cross term between the FC and SD interactions, which yields the $\mathbf{J}^{FC/SD}$ symmetric tensor, is purely anisotropic, i.e. it does not have any effect in the NMR spectra taken in isotropic phase.

All terms in Eq. (5) are proportional to the product of the magnetogyric ratios of both coupled nuclei, γ_A and γ_B. Therefore, the isotropic coupling constant can be of either sign depending both on the signs of both the magnetogyric ratios and on the sign defined by the electronic structure of the molecule containing the coupled nuclei. As the former does not provide any useful molecular information, a reduced coupling constant, Eq. (6), is defined, where J is measured in Hz and K is measured in $T^2 J^{-1}$ if the γ factors are in the SI system.

$$K(A,B) = 4\pi^2 \frac{J(A,B)}{h\gamma_A\gamma_B} \tag{6}$$

One of the open questions about the theory of coupling constants is the relative importance of the different contributions to total couplings. With the very accurate calculations that can be carried out in small compounds containing light atoms, the relative importance of each contribution is reliably known through a theoretical analysis. In other instances, especially for couplings involving heavy nuclei, a large amount of experimental work has been carried out intending to establish the importance of the FC term. In this way, at present it is accepted that couplings such as $^1J(Pt,Si)$,[89] $^1J(^{31}P,^{27}Al)$[90] are dominated by the FC contribution. On the other hand, during the review period a good amount of work was reported about the tensor character of **J**,[29] i.e. the measurement of its large anisotropy, $\Delta\mathbf{J}$, in couplings involving heavy nuclei. A few examples are as follows: $\Delta^1\mathbf{J}(^{199}Hg,^{31}P)$ is ~5.4 kHz in $HgPCy_3(NO_3)_2$ (Cy = cyclohexyl);[91] $\Delta^1\mathbf{J}(^{199}Hg,^{31}P) = (4.0 \pm 0.5)$ kHz in $Hg(PPh_3)_2(NO_3)_2$;[92] $\Delta^1\mathbf{J}(^{199}Hg,^{13}C) = (960 \pm 60)$ Hz in $K_2Hg(CN)_4$;[93] $\Delta^1\mathbf{J}(^{63/65}Cu,^{31}P) = (+750 \pm 100)$ Hz.[94] In many instances, the presence of a large anisotropy is considered to be an indication that the respective isotropic coupling constant has important noncontact contributions,[92,93] while a small anisotropy is taken as an indication that the respective isotropic coupling is dominated by the FC term.[51,95] However, such assertions should be taken with much caution since theoretical analyses show that, in many instances, by far the main contribution to $\Delta\mathbf{J}$ originates in the $\mathbf{J}^{FC/SD}$ term.[1,96–98] In such cases

$\Delta\mathbf{J}$ can be very large, but the isotropic J coupling could be by far dominated by the FC contribution. This situation was nicely exemplified in two papers[97,98] in which $\Delta\mathbf{J}$ was measured in small compounds containing light atoms, i.e. for J(C,C) couplings in benzene[98] and in ethane, ethene and ethyne.[97] These two experimental studies were accompanied by high-quality MCSCF calculations of the different contributions to the **J** tensor. The $\mathbf{J}^{FC/SD}$ contribution is by far the dominant one; for instance, $\Delta^1\mathbf{J}$(C,C) in ethane where $\Delta\mathbf{J}^{DSO} = 3.3$ Hz, $\Delta\mathbf{J}^{PSO} = -2.3$ Hz, $\Delta\mathbf{J}^{SD} = 1.5$ Hz and $\Delta\mathbf{J}^{FC/SD} = 29.6$ Hz.[97] In other cases, for instance, $\Delta^1\mathbf{J}$(C,H) in ethane, important contributions from $\Delta\mathbf{J}^{DSO}$ and $\Delta\mathbf{J}^{PSO}$ were calculated, but these last two contributions tend to cancel each other, again yielding $\Delta\mathbf{J}^{FC/SD}$ as the dominant term. This is the first experimental evidence of the nonnegligible anisotropic contribution to $^1\mathbf{J}$(C,H).[97]

Theoretical evaluation of coupling mechanisms involving the FC interaction at the *ab initio* level faces two main difficulties: the need for inclusion of correlation effects, as the FC interaction couples the singlet ground state with triplet excited states that are very sensitive to such effects; and the need to describe properly the molecular state amplitudes at the positions of the coupled nuclei, i.e. the 'cusp problem'.[2,3] LCAO MOs obtained with truncated GTO basis sets may properly describe the electronic distribution 'in the mean', but it is much more difficult to obtain correct MO amplitudes at a single point in space. Thus AO basis sets must include a large number of uncontracted tight s functions in order to have enough flexibility to correctly describe the FC interaction. Unfortunately, correlated calculations with large AO basis sets imply prohibitive computational costs in polyatomic molecules. However, it seems that the decontraction and/or addition of tight s functions to a given basis set of good quality does not significantly influence the evaluation of electron correlation effects.[99,100] For this reason it is very appealing to find an alternative way of dealing with the FC operator without increasing the basis set size. The possibility of replacing the Dirac δ-operator by a global operator in FC coupling calculations was revisited.[100] In this way, the quality of the result depends on the mean quality of the MOs in a spatial region around the coupled nucleus. A whole class of global operators that can replace the δ one was presented and two particular choices were quantitatively discussed corresponding to a 'Heaviside weighting' and a 'Gaussian weighting' in the HD molecule. Convergence of the SCF and FCI results of the FC term considering different basis sets for the δ-operator and both types of global ones was critically discussed.[100] The improvement and stability of results for the global operators at both levels of approximation are noteworthy and suggest that a correct estimate of correlation effects can be obtained with medium-sized basis sets. An alternative approach to deal with the 'cusp problem' would be to use STOs instead of GTOs. Although no systematic work has yet been reported on the calculation of the FC term with an STO basis set, important advances in this direction were made.[101,102]

The parity nonconservation (PNC) terms of the molecular Hamiltonian originating in electroweak electron–nucleon interactions and their effect on NMR parameters have been discussed.[103] Owing to the short-range nature of such PNC interactions, they occur only when the electron is inside the atomic nucleus. Terms linear and bilinear in the nuclear spins were obtained and their contributions to the **J** tensor were calculated employing RSPT. However, no numerical estimates of their importance were reported.

Sauer[104] introduced an SOS expression for the DSO term. By defining a suitable operator and making use of a resolution of the identity in the state space in terms of eigenstates of the unperturbed Hamiltonian, the ground-state expectation value yielding the DSO term is replaced by an RSPT-like expression. A consistent correlated calculation of all **J** terms is thus possible. However, the DSO contribution may be calculated with a correlated ground-state wavefunction and therefore this method has not so far been used in practical applications.

Hartree–Fock and post-Hartree–Fock approaches

Hartree–Fock and sum-over-states approaches. Although at present many *ab initio* coupling calculations take into account electron correlation effects, several calculations at the CHF or at a lower level of approximation were reported during the review period. Some coupling trends calculated at the CHF level compare favourably with those calculated with approaches that include electron correlation effects, as shown, for example, by Carmichael *et al.*[63]

Battacharyya *et al.*[105] used the FPT scheme to calculate the FC term of ^1J(C,H) couplings in a series of O- and N-containing 5- and 6-membered heterocyclic compounds. The general agreement with experimental trends is good, although many couplings are somewhat overvalued as can be expected for calculations of this type, which do not include electron correlation effects.[106] It is interesting to point out that although these are unsaturated heterocycles, Battacharyya *et al.*[105] did not find non-singlet instability problems.[1]

^1J(X,^{6,7}Li) couplings are used as probes to study the aggregation state of lithium clusters.[107–111] Owing to the large number of atoms involved, only theoretical approaches that can provide reasonably accurate results with rather modest computational requirements were applied. Koizumi *et al.*[112–114] made calculations of the FC contribution to ^1J(C,^{6}Li) couplings using the SCPT scheme[115,116] with a truncated basis set for Li that includes only the 1s function, intended to model the ionic character of the C—Li bond. The good agreement with experimental ^1J(C,Li) couplings suggests that the ionic character of the C—Li bond in alkyllithiums is quite important. Koizumi *et al.*[117] carried out similar calculations for ^1J(^{29}Si,^{7}Li) in H_3SiLi and in $(CH_3)_3SiLi$. Their results are indicative that in (organosilyl)lithiums in solution, the Si—Li bond also

presents an ionic character.[117] Koizumi *et al.*[118] used the same approach with the 6-31G* basis set without any truncation to carry out calculations of $^1J(^{29}Si,^6Li)$ couplings in lithium amide considering different aggregation states.

SCPT calculations of $^1J(X,H)$ and $^2J(H,H)$ in the CH_4, SiH_4, AlH_4^- and GeH_4 hydrides were reported by Nair and Chandra.[119] The importance of uncontracting core functions, including 'bond centred functions' (BFs) and nuclear centred polarization functions (PFs) was analysed. BFs used were of s and p type with exponents optimized by minimizing the molecular ground-state energy. Although their calculations do not include either electron correlation effects or relativistic effects (for the $^1J(Ge,H)$ coupling) they achieved $^1J(X,H)$ couplings in rather good agreement with experimental data. Similar basis set dependence of all terms in all couplings in CH_3F, SiH_3F and CH_3OH at the SCF level was discussed.[120] Addition of BFs in calculations using the uncontracted basis sets yields similar results to the addition of PFs. The simultaneous addition of both BFs and PFs does not further improve the results nor the comparison with experiment. SCF results for $^1J(X,H)$ (X = C, Si) are also reasonably good, but for $^1J(X,F)$ and $^2J(H,H)$ couplings electron correlation effects are of major importance. In CH_3OH, the calculated value of $^1J(O,H)$, with the largest basis set, is −80.14 Hz, while the experimental value is (-85 ± 10) Hz.[121] Calculated $^3J(H,H)$ couplings are also quite close to the experimental values, but for the $^2J(H,H)$ couplings they exceed the experimental values by a factor of 2. Calculations of the couplings in PH_3, PH_4^+, PH_2^- and P_2H_4 were reported.[122,123] Different contraction schemes of the (12s8p)→[6s4p] basis set[124] for P were tested, as well as the addition of PFs and BFs.[123] Calculated results for $^1J(P,H)$ were 209.62 Hz, 554.08 Hz and 81.02 Hz in PH_3, PH_4^+, PH_2^-, respectively, while the corresponding experimental values are 182–195 Hz,[125] 545.7 Hz,[126] and 138–140 Hz.[127] Such comparison indicates that the performance of SCF is very good for PH_4^+, but it is very poor for PH_2^- where the correlation effects are expected to be much larger. In P_2H_4, $^1J^{SD}(P,P)$ is very large (>100 Hz) and of opposite sign to $^1J^{FC}$, but the total calculated value, $^1J^{total}(P,P) = -76.29$ Hz, is far from the experimental value, −108.2 Hz.[128] Except for $^1J(P,H)$, correlation effects seem to be important in P_2H_4. The authors argue that BFs seem to yield better results as they describe the charge distribution in the internuclear region better than PFs. However, results with the largest basis sets indicate that in most cases either addition of PFs or decontraction of s functions to a basis set containing BFs is needed to approach the HF limit.

The SYSMO program,[129] which allows calculations of all the second-order coupling terms using the EOM method[130] at the RPA level,[131] was used in several works. The four terms of all couplings in (**3**) were calculated and, when possible, measured.[132] Good agreement between calculated and experimental values was obtained; however, two features were conspicuous, namely $^1J(C,C)$ was largely overestimated, and the correct trend between both types of $^1J(C,H)$ was only achieved when s AOs were decontracted. Proximity effects on $^1J(C,H)$

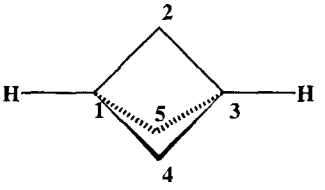

[3]

couplings, when a C—H bond is close to an electronegative atom, were studied[133,134] using the SYSMO program. This program was also modified to allow the use of the IPPP-CLOPPA with *ab initio* wavefunctions.[61,132,135] This scheme was used to study the effect of an electric field on ^1J(C,H) in HCN, considering separately its effect on the σ- and π-transmitted components,[61] and to study the through-space transmission of ^4J(H,H) through the bridgehead carbon atoms in bicyclo[1.1.1]pentane (**3**).[132] The CLOPPA approach was used to study the effect of the pyramidality at the N atom on the bond contributions to ^{1}J(^{15}N,^{1}H) in NH_3.[135] It is interesting to note that at the RPA level, using the 6-31G** basis set, ^{1}J(^{15}N,^{1}H) = −61.81 Hz, which is quite close to the experimental value of −61.26 Hz.[136] Calculations carried out at the EOM-CCSD level[137] show that correlation effects would correct the RPA value by ~15%, and therefore bond contributions to ^{1}J(^{15}N,H) at the RPA level can be considered to be qualitatively correct. It is interesting to note that the different bond and lone pair contributions quite closely follow the trends given by the CLOPPA-INDO method.[17] A remarkable feature of *ab initio* CLOPPA calculations observed in different applications[12] is that LMOs that are linear combinations of only polarization AOs (PLMOs) play a negligible role in the coupling transmission. This seems to indicate that PLMOs can be excluded systematically from the perturbative calculation, i.e. that it is not necessary to include them in the subspace where the PP is inner projected. Therefore, the computational cost can be significantly reduced without affecting the quality of the calculation. However, systematic calculations would be necessary to verify the generality of this assertion.

Weinhold *et al.*[64] used the SOS expression for the FC contribution to J(A,B) couplings (other terms were neglected) given by Eq. (7)[138] to calculate several ^nJ(A,B) (A, B = C, H; n = 1–3) couplings in a variety of hydrocarbons, including differently strained cyclic compounds.[64]

$$J(\mathrm{A,B}) = -\frac{8\eta}{9\pi}\mu_0^2\mu_B^2\gamma_A\gamma_B \sum_i^{\mathrm{occ}} \sum_j^{\mathrm{virt}} \frac{1}{\varepsilon_j - \varepsilon_i} \langle\psi_i \mid \delta(\vec{r}_A) \mid \psi_j\rangle\langle\psi_j \mid \delta(\vec{r}_B) \mid \psi_i\rangle \quad (7)$$

Although within this approach the calculated FC terms are generally in poor agreement with experimental values, they follow several stereochemical trends

rather closely. Therefore, Weinhold *et al.*[64] sought to scale the calculated values, Eq. (8), where the coefficients a and b were obtained by comparison with experimental values.

$$J^{\text{fit}}(\text{A,B}) = aJ^{\text{calc}}(\text{A,B}) + b \tag{8}$$

Employing Eq. (8) and modest basis sets (3-21G and 6-31G*), the fitted ^3J(H,H), ^2J(H,H) and ^1J(C,C) couplings show a high correlation with experimental values in the set of 19 molecules considered. On the other hand, the fit for ^nJ(C,H) ($n = 1-3$) couplings was less successful. Weinhold *et al.*[64] ascribed this poorer performance to neglecting noncontact terms. It should be noted that the FC term of ^2J(C,H) couplings can be of either sign,[139] especially when at least one heteroatom is α to the coupled carbon atom,[140] so when the FC absolute value is close to zero, noncontact contributions can dominate such couplings. It should also be recalled that the SOS scheme neglects the π-transmitted component of the FC term.[141]

Higher random phase approximation, HRPA, calculations. All four terms of all couplings in cubane were calculated[142] within the EOM-HRPA approach, which takes into account a significant portion of electron correlation.[143] In cubane, the C—C—C angles are 90° and therefore the C—H bonds have increased s character while the C—C bonds have decreased s character with respect to those in open-chain, strain-free, systems. The results obtained were related to these features and compared to those in compounds with similar arrangements of bonds. These calculations show that the DSO contribution dominates the ^4J(C,H) and ^5J(H,H) couplings.

Galasso[144,145] analysed all four terms of ^1J(C,C) couplings between the bridgehead C atoms in a series of carbocycles at the EOM-HRPA level[143] to take into account correlation effects that may be important in these highly strained polycyclic compounds. The effects of progressive condensation and of the enlargement of the ring size were discussed. The FC term is by far the most affected, and it takes negative or almost zero values when the C—C bond s character is very small, increasing algebraically when increasing the s character. This feature is consistent with a 'bond contributions' analysis of ^1J couplings presented elsewhere.[17] However, no simple monotonic correlation was found between ^1J(C,C) and the bond s character or geometrical parameters such as bond distances or dihedral angles. Apparently, this arises from the multiple coupling pathways connecting both coupled nuclei.

The same approach was also applied to the calculation of J couplings in a series of cycloalkyl cations with a μ-hydrido-bridged structure containing a three-centre two-electron bond,[146] using geometrical structures optimized at the HF/6-31G** level. The total couplings involving the H_μ proton and the bridge C and H_t terminal atoms, show that $^1J(C,H_\mu)$ is anomalously small (~30(Hz) while $^1J(C,H_t)$ takes a normal alkanic value. This difference is considered to

originate in the remarkably longer distance and increased p character of the C—H_μ bond compared to the C—H_t bond.[146] These results are in good agreement with experimental data.

Møller–Plesset perturbation theory (MP) calculations. Fukui *et al.*[147] analysed the angular dependence of ^3J(H,H) on the dihedral angle ϕ in ethane, using FPT calculations including second- and third-order corrections to the electronic energy according to MP perturbation theory. The calculated values were underestimated by as much as 4–6 Hz compared to experimental ones. Such differences were ascribed to geometric effects (rigid rotations were used) and/or to the lack of higher-order correlation effects in their calculations. Basis set effects were thoroughly discussed in the paper.

^3J(H,H) couplings in methanol (H_3COH) and methylamine (H_3CNH_2) were discussed within the same approach.[148] Completely analogous results to those of ethane were found for ^3J(H,H) in methanol while, in methylamine, correlated results are much closer to the experimental couplings than the SCF values.

Multiconfigurational approaches. Carmichael[62] analysed ^1J(C,C) couplings across saturated C—C bonds, in a wide range of bonding environments using FPT SCF, MP2, CCD and QCISD(T) methods.[149,150] ^1J(C,C) couplings were overestimated at the SCF level, but largely underestimated at the MP2 level. For all ^1J(C,C) couplings considered,[62] ranging from −13.6 Hz to +34.1 Hz, the correlation corrections behave similarly. For instance, in ethane it was found that J(SCF) = 61.6 Hz, J(MP2) = 24.3 Hz, J(CCD) = 28.1 Hz, J(QCISD) = 35.2 Hz, J(QCISD(T)) = 34.1 Hz, and J(exp) = 34.6 Hz. Values for cyclopropane, cyclobutane and bicyclobutane follow quite similar trends. The QCISD FC value for the bridgehead ^1J(C,C) in bicyclobutane (−13.6 Hz) should be compared with that obtained with HRPA (−9.43 Hz).[144] It was also shown[62] that MP2 calculations with poor basis sets may yield fortuitous cancellations of errors and that therefore it is not a reliable procedure.

The ^1J(C,C) dependence on the torsion angle around the C—C bond in HO—C—C—OH fragments was studied theoretically[63] and results were compared with measured couplings in model compounds and in aldofuranose rings (**4a**). Calculations in different conformers of ethanol and in selected conformers of ethylene glycol (**5**) with the QCISD(T) approach show that the electron correlation correction, although important, is almost the same for all conformations. Therefore, SCF calculations were carried out to obtain the full ^1J(C,C) hypersurface as a function of rotations around the C—C and C—O bonds in (**5**), and then 29.8 Hz was subtracted to bring the hypersurface close to the points calculated with the QCISD(T) approach. ^1J(C,C) is larger for a *trans* than for a *gauche* conformation of the C—O bonds, but it shows a larger sensitivity to rotations around the C—O bonds, being largest for a *trans* arrangement of the C—C and O—X bonds. As expected, ^1J(C,C) increases with

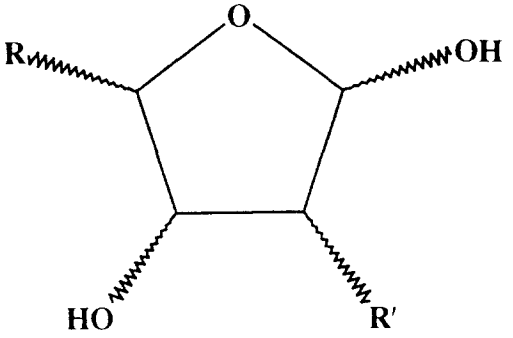

a: R′=OH
b: R=R′=H
c: R=HOH$_2$ C, R′=OH

[4]

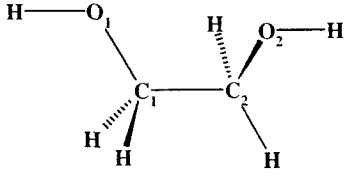

[5]

the number of O substituents attached to the C—C fragment. Experimental support for all these trends and the usefulness of ^1J(C,C) couplings as conformational probes in either fully or selectively ^{13}C-enriched biological compounds were also thoroughly discussed.

The potential of using ^1J(C,H) couplings as conformational probes in furanose rings was studied theoretically using (**4b**) as model compound.[151] Similar studies for ^nJ(C,H) couplings ($n = 1,2,3$) were carried out in (**4c**).[152] In both cases the structures of the different conformations were optimized at the 6-31G*/SCF or MP2 levels and the FC terms of the couplings were calculated. Scaling factors for the couplings were determined to bring MP2 results closer to the QCISD(T) results, using Eq. (9).

$$f_n = \frac{{}^nJ(\text{QCISD(T)}) - {}^nJ(\text{SCF})}{{}^nJ(\text{MP2}) - {}^nJ(\text{SCF})}, \qquad f_n < 1 \tag{9}$$

Differences in ^1J(C,H) couplings for C—H bonds with quasi-axial or quasi-equatorial orientation may differ by as much as 20 Hz. Oxygen lone-pair and exocyclic C—O bond orientations may affect such trends. The most sensitive

^3J(C,H) couplings vary about 4 Hz with ring conformation and follow Karplus-type relationships;[153] several ^2J(C,H) couplings also depend strongly on conformational changes. The potential of ^nJ(C,C) and ^nJ(C,H) ($n = 1,2,3$) couplings as conformational probes was similarly analysed in other derivatives of furanosyl rings.[154,155]

A series of works on calculations of coupling constants based on the MCSCF linear response theory[156] convey a clear idea of its capabilities. These calculations require careful selection of the 'active space' (AS) for making the CI expansion in the MCSCF state and the use of an adequate AO basis set, especially for calculating the FC contribution. The CI expansion carried out in a given calculation is specified dividing the set of MOs into four groups called inactive space, RAS1, RAS2 and RAS3.[157] The first contains MOs that are doubly occupied in all configurations, usually the core orbitals. RAS1 contains a set of MOs from which only a restricted maximum number of electrons is allowed to be excited in any given configuration. RAS2 is the 'fully active' space, that it includes MOs that have no restrictions in their occupancy for a given configuration. RAS3 contains MOs into which only a restricted maximum number of electrons is allowed to be excited for a given configuration. By restricting the MO occupancy in the RAS1 and RAS3 spaces, a larger number of MOs can become active without making the number of configurations in the MCSCF wavefunction prohibitively large. Usually, the active space is selected within the valence shell MOs and/or from the NO occupation numbers at the MP2 level of approximation. In such cases the success of this scheme depends on the capability of these NO occupation numbers to yield an adequate description of the important MOs entering into the MCSCF expansion.

Barszczewicz *et al.*[158] employed the MCSCF method to calculate couplings in cyclopropene, (**6**), that were previously studied[159] using the EOM approach.[143] Progressive enlargements of the active space and/or of the AO basis set were considered. The smallest wavefunction considered was MC1 with [5,3,1,0/2,1,1,1] inactive/active space (i.e., one correlating orbital of each symmetry for 4 electrons). The largest wavefunction used was of the RAS type, with inactive/RAS1/RAS2/RAS3 distribution of MOs [4,2,1,0/0,0,0,0/2,1,1,1/6,4,3,0]. Barszczewicz *et al.*'s results[158] for the FC ^1J(C,C) and

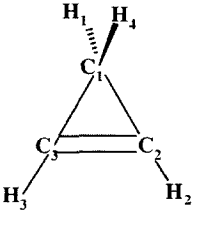

[6]

Table 1. MCSCF and CHF FC contributions[158] to ^1J(C,C) and ^1J(C,H) couplings in (**6**). Noncontact contributions were assumed to be negligible. All values are in Hz

^1J	CHF	RAS	Exp.
C1—C2	30.0	19.6	25[a]
C1—H1	168.7	164.6	167[b]
C2—C3	2093.2	73.0	60[a]
C2—H2	1299.7	216.4	226[c]

[a] Estimated values in ref. 160.
[b] Taken from ref. 161.
[c] Taken from ref. 162.

^1J(C,H) couplings are summarized in Table 1. Interestingly, CHF $^1J(C_1,H)$ couplings differ from all the MCSCF calculated ones by less than 5 Hz, and the CHF $^1J(C_1,C_2)$ is as far from the estimated experimental value as the MCSCF ones. This indicates that the existence of unsaturated bonds leading to non-singlet instabilities or quasi-instabilities does not *a fortiori* imply that the CHF values of all FC terms are devoid of physical meaning. It is important to recall the 'local' character of couplings through only one bond. Apparently, in (**6**) CHF-calculated $^1J(C_1,H)$ and $^1J(C_1,C_2)$ couplings are not affected by such instabilities. Overall agreement of the MCSCF values with experiment is also very good for two- and three-bond couplings.

Vahtras *et al.*[163] performed MCSCF calculations of couplings in N_2 and CO where correlation effects are important, as shown previously with SOPPA calculations.[164] All four contributions, FC, PSO, SD and DSO, were computed since noncontact terms could be significant in multiply bonded systems. Different choices of CAS/RAS spaces were considered.[163] The FC $^1J(^{14}N,^{15}N)$ value ranges from -0.53 Hz to $+0.12$ Hz (the SOPPA value is 0.45 Hz[164]). The PSO and SD terms converged very fast to stable values of ~ -1.90 Hz and 2.70 Hz, respectively, while $^1J^{exp}(^{14}N,^{15}N) = (1.8 \pm 0.6)$ Hz.[165] The geometry dependence was analysed and a zero-point vibrational average was carried out. For the CO molecule, the FC value converged only when large MCSCF expansions were considered. A value of $^1J^{FC}(C,O) = 6.69$ Hz was obtained, which is close to the SOPPA value, 7.30 Hz.[164] DSO, PSO and SD terms depend only slightly on the selected active space and the overall agreement with experiment is quite good, i.e., $J^{calc} = 16.10$ Hz, vs $J^{exp} = 16.4$ Hz.[166]

Coupling constant calculations in HN_3 and in different isomers of H_2CN_2 by Barszczewicz *et al.*[167] are a direct continuation of previous work on magnetic shielding constants[168] within the same MCSCF approach. Different choices of active spaces were considered and a RAS calculation yielded differences smaller than 0.15 Hz in all couplings with respect to a large CAS calculation. Such RAS space was thus chosen for carrying out calculations on the different isomers of H_2CN_2, which are isoelectronic with HN_3. Again, the DSO, PSO and SD values do not depend significantly on the choice of active space, but the

FC value does so strongly. As a general conclusion, the authors suggest a practical procedure for saving computer resources in coupling calculations, i.e. a fairly simple approximate wavefunction can be used to get an idea of the relative importance of different contributions and later the important ones can be calculated at a higher level of approximation.

The MCSCF approach was also applied[169] to calculate the coupling tensors in HCN, HNC and CH_3CN and CH_3NC and an important contribution from $\Delta J^{FC/SD}$ to $\Delta^1J(C{\equiv}N)$ was found that was similar in all four compounds. This contribution is the most sensitive to the choice of active space. A similar study was undertaken for couplings in azide, N_3^-, which is isoelectronic with CH_3CN and CH_3NC.[170] Good agreement with experiment was achieved for the largest calculation that included all valence shell MOs in the RAS2 set and 11 more MOs in the RAS3 set.

All four coupling terms in XH_4 (X = Si, Ge, Sn) were calculated.[171] For Sn an extensive basis set study was carried out starting from a [12s7p5d/6s2p] set and reaching one that had 2s, 1p, 2d and 2f functions. It should be noted that decontraction of this basis set yielded very different results for ^1J(Sn,H).[172] Results for ^1J(X,H) indicate that noncontact terms are negligibly small, while for the FC term the difference between a limited CAS calculation and the largest CAS/RAS calculation is larger than 3% only for X = Sn. Results for ^2J(H,H) indicate that noncontact terms can be calculated at the SCF level, but the FC one converges only for the largest CAS/RAS calculation. Agreement with experiment is within 3 Hz for CH_4 and SiH_4 but is much worse between the calculated (1.42 Hz) and experimental (±15.3 Hz) values in SnH_4, perhaps owing to relativistic effects. Calculations of ^1J(Sn,H) in SnH_4 with a larger Sn basis set[172] yielded an absolute value ~300 Hz smaller than that of the experimental coupling, leaving room for significant relativistic effects. Rovibrational corrections calculated at the SCF level were considered to be overestimated by ~50%, which suggests that the geometric dependence surface must be calculated including electron correlation effects.

Convergence of calculated couplings with increasingly large basis sets and/or active spaces was studied by Helgaker *et al.*[157] in C_2H_3F using the seven wavefunctions depicted in Table 2. The study included progressive decontraction of the outermost s and p functions, addition of polarization functions and full decontraction of tight s functions. The lowest-level wavefunction for reliable calculation of each contribution was discussed critically and it was found that for all couplings the DSO contribution, which is significant in ^2J(H,H) couplings, differs by less than 0.1 Hz using different wavefunctions; accordingly, WF1 was considered a good choice. WF2 and WF3 PSO calculations differ by less than 0.3 Hz, except for ^2J(C,F) for which the difference amounts to 1.2 Hz. Therefore, since WF3 differs from WF2 in both the basis set size and the active space size, the PSO term was considered to converge with WF3. The SD term is important only in ^2J(C,F), i.e. 11 Hz out of a total coupling of 20.6 Hz, and a similar criterion was employed to conclude that it converged

Table 2. Quality of wavefunctions employed by Helgaker *et al.*[157] in the convergence analysis of calculated couplings in C_2H_3F

	CGTO	Number of CGTO	Active space	$N(CI)^a$
WF1	[6s4p2d/3s2p]	111	(4,0/0,0/6,2/6,2)	3057
WF2	[6s4p2d/3s2p]	111	(3,0/0,0/7,2/10,4)	11909
WF3	[7s4p2d1f/5s2p1d]	156	(3,0/0,0/7,2/15,8)	31492
WF4	[11s5p2d1f/7s2p1d]	183	(3,0/0,0/7,2/21,10)	57868
WF5	[7s4p2d1f/5s2p1d]	156	(3,0/0,0/7,3/15,7)	776920
WF6	[11s5p2d1f/7s2p1d]	183	(3,0/0,0/7,2/15,8)	31492
WF7	[12s5p2d1f/8s2p1d]	189	(3,0/0,0/7,2/15,8)	31492

[a] Total number of determinants in the MCSCF expansion.

with WF2. The WF4 FC term was considered almost 'saturated', although differences of ~5 Hz were obtained when calculations of ^2J(C,F) and *cis* and *trans* ^3J(F,H) were carried out with WF5. In addition, when using the WF4 active space but decontracting the tight s functions (WF6, WF7), absolute values of most FC terms were practically unaffected, except for ^1J(C,H) and ^1J(C,F) which increased ~8 Hz. When core MOs were included in the active space, differences smaller than 0.3 Hz, except in ^1J(C,F), where it was −1.3 Hz, were obtained. When comparing total couplings with experiment, the largest relative differences were found in *cis* and *trans* ^3J(F,H). Solvent effects were calculated using a dielectric continuum model[173] with $\varepsilon = 20$ (acetone). Differences of ~1–3 Hz in J(C,X) were obtained, yielding a *trans* ^3J(F,H) value closer to the experiment.

Taking HF and H_2O as model compounds, basis set convergence at the MCLR[156] level was discussed.[99] A CAS wavefunction was used with the following basis sets: cc-pVXZ ($2 \leqslant X \leqslant 6$);[174] modified versions, aug-cc-pCVXZ, which include core–valence correlations;[175] those needed for describing the outer regions,[176] aug-cc-pVXZ; and their combination, aug-cc-pCVXZ. In the cc-pVXZ set the s functions were fully decontracted and n, $n = 0$–3, tight s functions were added. FC calculations for this basis with $n = 0$ were as good as those obtained with the remaining basis sets and, interestingly, improved results were obtained by adding $n = 2 - 3$ tight s functions. It was concluded that the poorer performance obtained with the smaller (contracted) cc-pVXZ basis sets was mainly due to the poor description of the MO amplitudes at the coupled nuclear sites. Convergence of the PSO, SD and DSO terms was also discussed, and the transferability of conclusions about the basis set quality was tested by calculating all couplings in HCN.[99]

The MCLR method was extended to calculate triplet response properties taking solvent effects into account[177] through a model in which the molecule is placed in a spherical cavity embedded in a homogeneous medium of dielectric

constant ε. Couplings in H_2Se were studied,[177] analysing the basis set convergence and electron correlation effects. ^1J(Se,H) = 106.3 Hz and ^2J(H,H) = −16.5 Hz *in vacuo* were calculated, including correlation effects, the former being far from experimental values of 63.4 Hz[178] and 65.4 Hz,[179] while the latter is in reasonable agreement with −13.5 Hz.[179] For ε increasing from 1 to 78.54 (water), ^1J(Se,H) increases monotonically by ∼15 Hz but ^2J(H,H) is affected by only 1 Hz in that range of dielectric constant. Such changes in ^1J(Se,H) were shown to originate in the electronic distribution polarization rather than in solvent-induced geometrical effects. Four-component Dirac–Fock calculations at the RPA level[180] yielded a relativistic effect contribution of ∼−50 Hz for ^1J(Se,H), which brings calculated values closer to experiment.

The choice of the basis sets for coupling calculations in CH_4 were thoroughly discussed by studying the effects of a full decontraction of different basis sets and addition of tight s functions on C and H,[106] contraction schemes were obtained from HF-SCF calculations, choosing those that provided practically the same values of J couplings, energy and electron densities as the fully uncontracted basis sets. Following this criterion, a contracted basis set with 63 CGTOs was obtained from an uncontracted basis set with 135 GTOs, yielding deviations smaller than 0.1 Hz in the HF-SCF calculated couplings. The following procedure could be employed in order to obtain accurate FC values. A value J_1 was obtained from an MCLR calculation including up to doubly excited configurations within the largest possible set of active MOs. An estimate of higher-order excitation effects can be obtained as $\Delta = J_2 - J_3$, where J_3 was calculated considering up to doubly excited configurations within a smaller set of active MOs and J_2 is a CAS (or the largest possible RAS calculation) within the same set of active MOs, as it was observed that Δ remains approximately unchanged as the number of active MOs is increased. The total coupling was thus estimated as $J = J_1 + \Delta$. Similar procedures were suggested for evaluating noncontact terms, and the calculation time was thus reduced 15-fold compared with that needed to carry out the larger CAS/RAS calculation within the larger active MOs set. This was achieved with a loss in accuracy of less than 0.3 Hz for both couplings. The best values thus obtained were ^1J(C,H) = 120.63 Hz and ^2J(H,H) = −13.23 Hz, respectively.[106]

Coupled clusters, (CC)-based calculations. A CC-based formulation for the evaluation of the FC term based on the energy derivative (ED) theory[181] was presented by Sekino and Bartlett.[150,182] CC theory can be obtained by imposing stationary conditions on the energy functional, Eq. (10).

$$E(\Lambda, T) = \langle 0 \mid (1 + \Lambda)\exp(-T)H \exp(T) \mid 0\rangle = \langle 0 \mid (1 + \Lambda)\bar{H} \mid 0\rangle \qquad (10)$$

where the similarity-transformed Hamiltonian $\bar{H}$ is introduced. By imposing stationary conditions with respect to independent variations of the T and Λ

operators, the set of CC equations is derived. As a consequence, the first derivative with respect to the nuclear spin in the Hamiltonian that includes the electron–nucleus interactions satisfies a generalized Hellman–Feynman theorem, Eq. (11).

$$E^{\mathrm{A}} = \frac{\partial E}{\partial I_{\mathrm{A}}} = \left\langle 0 \left| (1+\Lambda)\exp(-T)\frac{\partial H}{\partial I_{\mathrm{A}}}\exp(T) \right| 0 \right\rangle \tag{11}$$

Considering a double perturbation expansion of T and Λ with respect to the magnetic spins of nuclei A and B, Eq. (12),

$$\begin{aligned} T &= T^0 + T^{\mathrm{A}} + T^{\mathrm{A,B}} + \cdots \\ \Lambda &= \Lambda^0 + \Lambda^{\mathrm{A}} + \Lambda^{\mathrm{A,B}} + \cdots \end{aligned} \tag{12}$$

an approach to obtain the second-order energy derivative, Eq. (13), is developed.

$$E^{\mathrm{A,B}} = \left.\frac{\partial^2 E}{\partial I_{\mathrm{A}}\,\partial I_{\mathrm{B}}}\right|_{I_A, I_B = 0} \tag{13}$$

The final expression is that given in Eq. (14), where $E^{\mathrm{A}}(E^{\mathrm{B}})$ are the first-order energies, and T^{A}, T^{B} are the first order amplitudes.

$$\begin{aligned} E^{\mathrm{A,B}} = {} & \langle 0 \mid (1+\Lambda^0)(\overline{H}^{\mathrm{A}} - E^{\mathrm{A}})T^{\mathrm{B}} \mid 0\rangle + \langle 0 \mid (1+\Lambda^0)(\overline{H}^{\mathrm{B}} - E^{\mathrm{B}})T^{\mathrm{A}} \mid 0\rangle \\ & + \langle 0 \mid (1+\Lambda^0)(\overline{H}_0 - E_0)T^{\mathrm{A}}T^{B} \mid 0\rangle \end{aligned} \tag{14}$$

Insertion into Eq. (14) of the resolution of the identity and the consideration of a truncated excitation space $|\mathbf{h}\rangle\langle\mathbf{h}|$ leads to Eq. (15).

$$\begin{aligned} E^{\mathrm{A,B}} = {} & \langle 0 \mid (1+\Lambda^0)(\overline{H}^{\mathrm{A}} - E^{\mathrm{A}}) \mid \mathbf{h}\rangle \mathbf{R}_0 \langle \mathbf{h} \mid \overline{H}^{\mathrm{B}} \mid 0\rangle \\ & + \langle 0 \mid (1+\Lambda^0)(\overline{H}^{\mathrm{B}} - E^{\mathrm{B}}) \mid \mathbf{h}\rangle \mathbf{R}_0 \langle \mathbf{h} \mid \overline{H}^{\mathrm{A}} \mid 0\rangle \\ & + \langle 0 \mid (1+\Lambda^0)(\overline{H}_0 - E_0) \mid \mathbf{f}\rangle \langle \mathbf{f} \mid T^{\mathrm{A}}T^{\mathrm{B}} \mid 0\rangle \end{aligned} \tag{15}$$

where $|\mathbf{f}\rangle$ stands for all excitations beyond those explicitly introduced in $|\mathbf{h}\rangle$. The resolvent is given by Eq. (16).

$$\mathbf{R}_0 = \langle \mathbf{h} \mid \overline{H}_0 - E_0 \mid \mathbf{h}\rangle^{-1} \tag{16}$$

The equation of motion (EOM) for the perturbed amplitudes is given in Eq. (17).

$$\langle \mathbf{h} \mid T^{\mathrm{A}} \mid 0\rangle = \mathbf{R}_0 \langle \mathbf{h} \mid \overline{H}^{\mathrm{A}} \mid 0\rangle \tag{17}$$

In eq. (15) the first two terms are those expected from a straightforward generalization of ordinary second-order perturbation theory expressed in the configuration space. EOM-CC[183] introduces a CI-like approximation to excited states, which is often a convenient representation from which the same result can be obtained using an SOS expansion. This procedure was followed[183] to calculate polarizabilities. In the full CC limit both expressions are equivalent, but in a finite configuration space the third term introduces selected effects of higher excitations in analogy to CCD compared with CID. Neglect of the third 'quadratic' term, however, in the truncated case yields to results that are not extensive in the sense of scaling properly with a number of repeated units, as is usually expected for CC methods. Extensivity can be regained by intermediate approximations that allow the quadratic term to cancel the unlinked diagrams that occur in the first two terms, and thus neglect of the residual linked quadratic contribution. This amounts to eliminating the unlinked parts of the first two terms in Eq. (15) and completely neglecting the third term. The CI-like expansion given by these two terms is explicitly shown to be amenable to being written as an SOS expansion in terms of bi-orthogonal eigenstates associated with the EOM-CC eigenvalue problem of the similarity-transformed Hamiltonian $\overline{H}$.[184] Equation (15) is explicitly shown to be consistent with the polarization propagator formalism approach.[185]

The FC component of different couplings in HF, C_2H_4, and several strained cycloalkanes were calculated[182] within the EOM-CC approach, neglecting the last term and keeping only the linked part of the first two terms of Eq. (15). No orbital relaxation was allowed and excellent agreement was found with finite field CCSD results using non-relaxed orbitals, indicating that partial neglect of the quadratic term is unimportant. A Karplus-type relationship for ^3J(H,H) couplings in C_2H_6 was also calculated.[182] Results for ^1J(C,C) couplings were compared with Carmichael's[62] QCISD results. Excellent agreement with experiment was obtained for those couplings known to be dominated by the FC term.

FC, PSO and SD terms were calculated with the EOM-CC method[137] in HF, N_2 and CO, where it is known that noncontact contributions are important, and results were compared with those reported in refs 164,186,187. In the last two cases, couplings were also calculated by Vahtras *et al.*[163] Good agreement with other correlated calculations was obtained. Couplings in H_2O, NH_3 and HCl were also discussed and results were compared with Fukui's MBPT(2),[187] showing that both methods reproduce the experimental ^1J(O,H) and ^1J(N,H) values within ~2%, but for ^2J(H,H) significant differences with experiment were obtained. It is worth noting that $^1J^{RPA}$(H,Cl) = 30.03 Hz, which compares favourably with $^1J^{EOM\text{-}CC}$(H,Cl) = 35.03 Hz and with $^1J^{EXP}$(H,Cl) = 37.7 Hz.[188]

Coupling results of the CI-like calculation (limited to linked terms) and the 'full' EOM-CCSD one, Eq. (15), were compared for a large variety of couplings with different basis sets[189] in order to establish the numerical importance of the quadratic term. The largest FC quadratic contribution was

0.77 Hz for ^1J(C,H) in CH_3CN, the largest SD quadratic contribution was 0.21 Hz for $^1J^{SD}$(C,N), and that to the PSO term was ~0.1 Hz. It was thus concluded that the quadratic term yields only a small correction to different types of couplings and can thus safely be ignored. However, in larger molecules at least, the unlinked part might become more important, as it corrects for the size extensivity error in the CI-like approximation, which is accounted for in the linked CI-like one.

The use of NMR parameters to determine configurations of model carbocations was discussed by Perera and Bartlett.[190,191] In ref. 190, all terms of all couplings for the 'bridged' and 'classical' $H_2C(sp^2)—C(sp^3)H_3^+$ structures of $C_2H_5^+$ were calculated with the EOM-CC approach.[160] Results obtained indicate that J couplings can be confidently used to assess the preferred structure of the $C_2H_5^+$ cation in different chemical environments. For the bridged structure, $^1J(C,H_b) = 13$ Hz for the bridge H_b atom was calculated, which is conspicuously smaller than values of 'normal' C—H bonds (from 120 Hz to 250 Hz). This coupling is thus a fingerprint for such 1,2-hydrogen bridged carbocations. A theoretical discussion of the structure of the 2-norbornyl carbocation[191] indicates that calculated NMR parameters agree quite well with the experimental values if the bridged structure is assumed. Moreover, this was the only stable structure found in the cation geometry optimization.

Bartlett's team[192] presented results with a 'partitioned' version of the EOMCC approach, p-EOMCC, in order to reduce the computational cost and thus extend its applicability, in which the doubles–doubles block of $\bar{H}$ in Eq. (17) is approximated by a diagonal matrix containing the HF orbital energy differences as in MP2 partitioning. In addition, the crude approximation in which T and Λ amplitudes are replaced by MP perturbation theory coefficients was also considered, p-EOMCC-MBPT(2). The agreement between the p-EOM-CC values and the full EOM-CC ones is noteworthy, and important computational cost savings involved in p-EOM-CC were discussed.[192] A conspicuous example is ^1J(C,H) in both CH_3F and CH_3CN, shown in Table 3, where differences from experimental values are most probably due to basis set limitations.

Table 3. Total ^1J(C,H) couplings (in Hz) in CH_3F and CH_3CN as obtained by full EOM-CC[189] and p-EOM[192] approaches

	CH_3F	CH_3CN
p-EOM-CC	137.84	125.77
p-EOM-MBPT	129.33	117.11
Full EOM-CC	138.38	126.20
Exp.	149.1[a]	135.73[b]

[a] Taken from ref. 193.
[b] Taken from ref. 194.

The dependence of all coupling mechanisms in CH_4 upon variation of the H^1—C—H^2 angle while keeping a C_{2v} symmetry was analysed at both the RPA and CCPPA[195] levels in ref. 196. Contrary to bond stretching effects,[197] such dependence is very similar at the RPA and CCPPA levels. The full ^1J(C,H) and ^2J(H,H) coupling surfaces in CH_4, consistent up to second order in symmetry coordinate deviations from equilibrium, were calculated[198] with CCPPA.[195] An 'experimental' $^1J^{FC}$(C,H) = 119.13 Hz at equilibrium was deduced by subtracting the noncontact terms from the experimental ^1J(C,H) value at equilibrium.

The SOPPA equations[199] for triplet response properties have been recently corrected[200] and consequently a modified version of the CCSDPPA method was presented and dubbed SOPPA(CCSD).[201] The full ^1J(C,H) and ^2J(H,H) coupling surfaces in methane were recalculated with this approach.[202] Nuclear motion averages were carried out to study rovibrational as well as isotope effects on those couplings. In subsequent work, nuclear motion effects on J couplings were calculated for H_2O[203] and for H_3O^+ and HO^-.[204] RPA, SOPPA(CCSD) and MCLR results were compared[203,204] and it was concluded that correlated J coupling surfaces for these compounds are significantly different from the RPA ones.

DFT approaches

In recent years the density functional theory, (DFT)[205,206] has been used as a powerful tool for calculating the electronic structure and properties of molecular systems. Extensive reviews have been published on the theory and applications of DFT to computational chemistry,[207,208] making it unnecessary to discuss this theory here.

A critical point of DFT is the search of the exchange-correlation functional, $E_{xc}[\rho]$. Although the exact $E_{xc}[\rho]$ must fulfill certain properties,[209] an approximation to $E_{xc}[\rho]$ that can be systematically improved has not yet been formulated.[208] Therefore, exhaustive tests to prove the validity and accuracy of each approximation when applied to calculating different molecular properties is required. In dealing with magnetic molecular properties, DFT approaches have become the method of choice for calculating NMR chemical shifts in large molecules,[210] but only a few papers have described the calculation of coupling constants during this review period. Malkin *et al.*[211,212] and Malkina *et al.*[213] have developed DFT-based methods for calculating the PSO, FC and DSO terms, disregarding the SD contribution. The authors estimated that the SD term would be the most time-consuming part of the calculations and that its contribution would be smaller than the numerical errors in the DFT calculations of the FC term.[211] They used the FPT approach to calculate the FC term and the DFT/RS-PT for the PSO one. Because the authors do not use any hybrid functional in their work, the RS-PT method, which they originally developed for shielding tensor calculations,[214] allows for the fast noniterative

calculation of the PSO term. The DSO term was calculated using the numerical integration procedures available in the DeMon program for the one-electron integrals.[215]

Results were reported for a large set of molecules including: small molecules such as HF, H_2O, NH_3 and CH_4;[211] a series of hydrocarbons;[211] substituted hydrocarbons;[213] the series XH_4 with X = C, Si, Ge and Sn;[213] and a study of the Karplus equation for ^3J(H,H) and ^3J(C,H) in a model dipeptide.[212] Most of the reported calculations use the IGLO-III basis set[216] and the calculated couplings were compared with experimental and post-HF values, when available. A comparison of the calculated FC terms using different exchange-correlation functionals, VWN,[217] PW[218,219] and PW91,[220] was presented;[211] an excerpt of them[211,213,221] is displayed in Tables 4 and 5. Good agreement with post-HF approaches was obtained for the DFT, PSO and DSO terms regardless of the exchange-correlation functional used. However, the agreement found for DFT FC term is less satisfactory, since its calculated values are strongly sensitive to (a) the choice of the perturbed nucleus in the FPT approach, and (b) the functional employed. For example, for HF, the FC contribution to ^1J(H,F) ranges from 139.2 Hz to 234.3 Hz for the same perturbed nucleus (F) and different choices of functionals; using the PW functional, ^1J(H,F) goes from 198.0 Hz to 217.3 Hz when the choice of the perturbed nucleus changes from H to F. For CH_4, the value of the FC term of ^1J(C,H)[211] ranges from 95.2 Hz to 136.3 Hz for different functionals. Also, this contribution depends on the perturbed nucleus, i.e., 121.9 Hz for H and 135.2 Hz for C. The sensitivity of the FC term to the choice of $E_{xc}[\rho]$ is not

Table 4. Comparison between calculated DFT J(A,B) couplings[221,213] employing the PW exchange-correlation functional and experimental data (in Hz)

Molecule	J(A,B)	Calculated	Exp.	Refs to exp. values
CO	^1J(C,O)	25.9[a]	16.4 ± 0.1	166
N_2	^1J(N,N)	4.7[a]	1.8 ± 0.6	165
C_2H_2	^1J(C,H)	249.1[a]	248.7	223
	^1J(C,C)	184.3[a]	171.5	223
C_6H_6	^1J(C,C)	53.1[a]	56.0	224
	^2J(C,C)	−0.4[b]	2.5	224
CH_3F	^1J(C,F)	−268.1[b]	−157.5	193
CH_2F_2	^1J(C,F)	−343.1[b]	−234.8	193
CHF_3	^1J(C,F)	−390.7[b]	−274.3	193
SiH_3CH_3	^1J(Si,H)	−179.5 (−196.9)[b,c]	−194.3	225
SiH_3F	^1J(Si,H)	−212.1 (−232.7)[b,c]	−229.0	225

[a] Taken from ref. 221.
[b] Taken from ref. 213.
[c] Values in parentheses were calculated with the fully uncontracted basis set of Partridge.[222]

Table 5. Comparison between DFT calculated FC, PSO, SD, and DSO terms of ^1J(A,B) using the PW exchange-correlation functional and the corresponding HF and post-HF calculations (in Hz).

		RPA[a]	SOPPA[a]	CCSDPA[a]	MCLR[b]	DFT[c]	Exp.
HF	FC	467.3	338.3	329.4	–	198.1	
	PSO	119.3	195.7	195.7	–	198.0	
	SD	−12.4	−1.0	−0.6	–	–	
	DSO	−0.1	–	–	–	0.1	
	TOT	654.1	532.9	524.4	–	396.2	500[d]
CH_4	FC	155.6	126.6	122.1	123.5	122.0	
	PSO	1.4	1.5	1.5	1.5	1.7	
	SD	−0.2	0.0	0.0	0.3	–	
	DSO	0.3	–	–	0.0	0.3	
	TOT	157.0	128.3	123.9	125.3	123.9	120.87[e]

[a] Taken from ref. 221.
[b] Taken from refs. 164, 186, 195.
[c] Taken from refs. 163, 156.
[d] Taken from ref. 226.
[e] Taken from ref. 197.

surprising, as it is well known that the FC term is the most sensitive to correlation effects. This sensitivity increases along the series H, C, N, O and F.

With the exception of the calculations using the PW functional for ^1J(H,H) and ^1J(C,H) couplings, none of the other calculations are able to adequately reproduce the most reliable post-HF values. This deficiency seems to originate in the inability of both the LDA and GGA functionals to produce the highly accurate spin density at the coupled nuclei positions, which is required for reproducing the FC interaction. It is noted that the use of the PW functional yields FC terms of ^1J(C,F) that are undervalued by $\sim$110 Hz[213] for all molecules considered. In spite of this systematic deviation from experiment,[211,213] the FC contributions calculated with different $E_{xc}[\rho]$ show the same dependence on the interatomic distance between the coupled nuclei as that found with post-HF methods.[156,163,164,186,195] Similar conclusions were obtained by Dickson and Ziegler,[227] who used the Malkin *et al.* method,[211,213] with an STO basis set instead of GTOs to calculate *geminal* couplings in a series of first- and second-row hydrides, light hydrocarbons and transition-metal carbonyl complexes.[227] In most cases, DFT calculations underestimate the value of the couplings, a trend that seems to originate in the dominant FC term. The results could be improved somewhat by enhancing the quality and flexibility of the basis set used.[227]

It was suggested[213] that the performance of the DFT calculations could be improved using hybrid functionals such as B3LYP.[228,229] In Table 6 a few selected values[12] of the FC term calculated with the FPT scheme and the

Table 6. Comparison between FPT calculated J^{FC} term (in Hz) at the HF, DFT (B3PW91 and B3LYP functionals) and CISD levels of calculation with the 6-311G** basis set. Molecular geometries were optimized at MP2/6-311G** level[a].

	CH_4	CH_3F	CH_2F_2	OCH_2
^1J(C,H)				
HF	140.4	166.7	200.5	270.5
B3PW91	106.2	124.7	153.4	150.5
B3LYP	115.8	134.3	164.1	162.0
CISD	116.5	141.9	180.1	219.0
Exp.	120.87[b]	149.1[c]	184.5[c]	172.0[c]
^1J(C,F)				
HF	–	−197.1	−206.8	–
B3PW91	–	−287.9	−310.2	–
B3LYP	–	−287.8	−309.6	–
CISD	–	−225.8	−240.0	–
Exp.	–	−157.5[c]	−234.8[c]	–

[a] Taken from ref. 12. Calculations were carried out with the Gaussian 94 package of programs[230] which was modified to allow the FC term calculation using the FPT approach.[231]
[b] Taken from ref. 221.
[c] Taken from ref. 193.

6-311G** basis set, employing the B3PW91 and B3LYP functionals, are compared with those calculated with the HF and CISD approaches. It is important to remark that most values shown in Table 6 differ by less than 0.01 Hz when perturbing either coupled nucleus, and that the largest difference found amounted to only 0.2 Hz.

The FPT DFT[213,221] method was also used to calculate couplings in large molecules since its computational cost is similar to the respective HF calculation. In a theoretical and experimental conformational study of 1,3-dimethylated compounds Spencer *et al.*[232] calculated Boltzmann-averaged ^3J(C,C) using the PW exchange-correlation functional and an IGLO-III basis set. Good agreement between experimental and calculated values was found. The FC contribution to J(H,D) in $[Os(NH_3)_4L^z(\eta^2\text{-}H_2)]^{(z+2)+}$ metal complexes with a wide variety of L^z ligands was calculated by Bacskay *et al.*[10] using the FPT method within the DFT approach and the BLYP functional.[229,233] A similar method was used to study the FC contribution to ^3J(C,C) through a C—O—C—C pathway,[11] employing the B3LYP functional.[228,229]

Bour and Budešínský presented SOS/DFT calculations of all the terms in a series of small molecules and in α-pinene, β-pinene and camphor[234] using the B3LYP hybrid HF-DFT functional. In most cases, calculated values were typically two to three times smaller than experimental ones. This may originate in using an uncoupled perturbation scheme with a hybrid functional.

Grayce and Harris have developed a formal 'magnetic-field DFT'[235,236] theory that allows calculation of second-order magnetic response properties directly from the field-free electronic density. In the limit of weak magnetic fields, all the magnetic properties can be calculated by direct convolution of the appropriate interactions with the corresponding universal functional, which depends only on the field-free electronic density. Explicit expressions have been given for all the interesting magnetic properties, i.e. magnetic susceptibility, chemical shifts, and the orbital and spin contributions to the J couplings. Within this approach, the net spin density generated by the Fermi contact perturbation can be obtained by solving a linear partial differential equation whose coefficients are functions of the unperturbed density.[237] These coefficients can be derived analytically for all density functionals currently in use.

A simplified version of magnetic field DFT, namely, an electron gas theory that depends on the sum of the atomic electron densities in the presence of an external field, was used[238] to estimate the FC contribution to the so far unmeasured Xe–H and ^{129}Xe–^{131}Xe couplings as functions of the interatomic distance. Couplings reported are within the order of μHz to mHz for interatomic distances of physical interest.

Relativistic approaches and effects

Since the early relativistic extended Hückel (REX) method of Pyykkö,[239] much progress has been made towards developing methods for performing relativistic calculations of coupling constants. Several approaches were presented during the review period.

A full relativistic theory for coupling tensors within the polarization propagator approach at the RPA level was presented[240] as a generalization of the nonrelativistic theory. Relativistic calculations using the PP formalism have three requirements, namely (i) all operators representing perturbations must be given in relativistic form; (ii) the zeroth-order Hamiltonian must be the Dirac–Coulomb–Breit Hamiltonian, H_{DBC}, or some approximation to it; and (iii) the electronic states must be relativistic spin-orbitals within the particle–hole or normal ordered representation. Aucar and Oddershede[240] used the particle–hole Dirac–Coulomb–Breit Hamiltonian in the no-pair approach as a starting point, Eq. (18),

$$H_{\mathrm{DBC}} = \sum h_{\mathrm{D}}(i) + V \tag{18}$$

where

$$h_{\mathrm{D}}(i) = c\alpha_k p_k + (\beta - 1)mc^2 + V_{\mathrm{nuc}}(\vec{r}_i) + \sum \Lambda_+ U(\vec{r}_i)\Lambda_+ \tag{19}$$

where α_k and β are the 4×4 Dirac matrices, $U(\vec{r}_i)$ is the DHF average potential, and the two-electron part is given in Eq. (20), where g_{ij} is the two-electron

operator that includes the Coulomb and Breit interactions, and Λ_+ is the operator that projects upon the states of positive energy, constructed from the whole set of Dirac one-electron equation solutions.

$$V = \tfrac{1}{2}\sum \Lambda_+ g_{ij} \Lambda_+ - \sum \Lambda_+ U(\mathbf{r}_i)\Lambda_+ \tag{20}$$

Within the second quantization formalism, H_{DBC} is expressed as in Eq. (21), where F is the second-quantized form of h_{D}; u_{ik} are the SCF potential matrix elements, and b_{ijkl} are the Breit interaction matrix elements.

$$\begin{aligned} H_{\mathrm{DBC}} &= F + W \\ &= \sum \varepsilon_k a_k^+ a_k + 1/2 \sum (\langle ij \mid kj \rangle + b_{ijkl}) a_i^+ a_j^+ a_l a_k - \sum u_{ik} a_i^+ a_k \end{aligned} \tag{21}$$

The Breit correction affects mostly the interaction of core electrons and interations between core and valence electrons.[240]

The second-order energy correction corresponding to the indirect coupling between the N and M nuclei is given by Eq. (22), where the relativistic form of the spin–dipole hyperfine interaction operator H is given by Eq. (23), and $\vec{\mathbf{A}}_N$ is the vector potential of the magnetic dipole of nucleus N.

$$E_{NM}^2 = \tfrac{1}{2} Re \langle\langle H_N;\ H_M \rangle\rangle_{E=0} \tag{22}$$

$$\begin{aligned} H_N &= ec\vec{\alpha} \cdot \vec{A}_N \\ &= ecg_N \beta_N \vec{\alpha} \cdot \left(\vec{I}_N \times \frac{\vec{r}_N}{r_N^3} \right) = ecg_N \beta_N \sum_{i=x,y,z} I_{Ni} \kappa_{Ni} \end{aligned} \tag{23}$$

In Eq. (23) the κ_{Ni} operator is $\kappa_{Ni} = \varepsilon_{ikl} \alpha_k r_{Nl} r_N^{-3}$ and ε_{ikl} is the Levi–Civita tensor. With these definitions, the coupling tensor is given by Eq. (24), where the propagator term can be calculated at different levels of approximation. At the RPA level it must be calculated taking into account that the consistent relativistic ground state is the DHF one, i.e. $\mid 0\rangle = \mid \mathrm{DHF}\rangle$. The propagator takes the form of Eq. (25).

$$\vec{J}_{ij}(N,M) = (e^2 c^2 g_N g_M \beta_N^2 / 2h) Re \langle\langle \kappa_{Ni};\ \kappa_{Mj} \rangle\rangle_{E=0} \tag{24}$$

$$\langle\langle \kappa_N;\ \kappa_M \rangle\rangle_E = (\tilde{K}_N, \tilde{K}_N^*) \begin{pmatrix} E\vec{1} - \vec{A} & -\vec{B} \\ -\vec{B}^* & -E\vec{1} - \vec{A}^* \end{pmatrix}^{-1} \begin{pmatrix} K_M \\ K_M^* \end{pmatrix} \tag{25}$$

where $K_{N(M)}$ are the column vectors of the $\kappa_{N(M)}$ operator matrix elements, Eq. (26).

$$\kappa_{N,m\alpha} = \langle m \mid \kappa_N \mid \alpha \rangle \tag{26}$$

where m and α are four-components spinors, which, in split form, are expressed in terms of their small (S) and large (L) components, Eq. (27).

$$|m\rangle = \begin{pmatrix} |m^{L}\rangle \\ |m^{S}\rangle \end{pmatrix} \tag{27}$$

Although Eq. (25) looks like its nonrelativistic counterpart, the $\overleftrightarrow{A}$ and $\overleftrightarrow{B}$ matrices are complex and their elements have to be calculated using $|DHF\rangle$. The κ operator cannot be expressed in terms of the usual singlet and triplet operators and, as the Hamiltonian does not commute with the spin operator, there is only one type of $\overleftrightarrow{A}$ and $\overleftrightarrow{B}$ matrices.

If the MOs are expressed in terms of a set of AOs $\{|r\rangle\}$, the κ operator matrix elements are as in Eq. (28).

$$\langle r \mid \kappa_{Ni} \mid s\rangle = \varepsilon_{ikl}\left[\left\langle r^{L}\left|\frac{r_{NI}\sigma_{\kappa}}{r_{N}^{3}}\right|S^{S}\right\rangle + \left\langle r^{S}\left|\frac{r_{NI}\sigma_{k}}{r_{N}^{3}}\right|S^{L}\right\rangle\right] \tag{28}$$

where σ_k are the Pauli matrices.

Unlike the nonrelativistic case, where the coupling tensor **J** can be decomposed in the FC, PSO, DSO and SD interactions, in the relativistic case, Eq. (24), **J** arises from only one response function that cannot be decoupled in individual mechanisms. The couplings must be calculated using the relativistic propagator, Eq. (25), which has eight times the dimensions of its nonrelativistic counterpart.

Visscher *et al.*[241] have applied this formalism at the RPA level to calculate the **J** coupling tensor in hydrogen halides using the DIRAC code.[180] Only the Coulomb interaction in the two-electron part of the Hamiltonian was considered, disregarding the Breit interaction b_{ijkl}, Eq. (21). Relativistic values were compared with those obtained by applying the Breit scaling factors $B(n,Z)$[242,243] to the FC term:

$$B(n,Z) = \frac{\langle \varphi_{\text{rel}} \mid H_{\text{rel}} \mid \varphi_{\text{rel}}\rangle}{\langle \varphi_{\text{nonrel}} \mid H_{\text{nonrel}}^{\text{FC}} \mid \varphi_{\text{nonrel}}\rangle} \tag{29}$$

where n is the principal quantum number of the atomic s state and H_{rel} includes the nuclear spin–electron orbit, the dipole–dipole and the FC terms. These factors account for the relativistic contraction of s orbitals on both coupled nuclei, and give a simple estimate of the scalar relativistic effects. As the factors corresponding to the outermost s orbitals are applied to the final value of the FC term, it is assumed that this contribution arises mainly from these orbitals. In Table 7 relativistic $^{1}J_{\text{R}}$(H,X) and nonrelativistic $^{1}J_{\text{NR}}$(H,X) (X = F, Cl, Br, I) are compared with the total couplings obtained when the Breit scaling factor is

Table 7. Comparison between RPA calculated ^1J(H,X) couplings (X = F, Cl, Br, I) in hydrogen halides with nonrelativistic (NR), nonrelativistic with a scaled FC contribution (SC)[243] and 4-component relativistic (R) formalisms,[241] and experimental values. All values in Hz

X	$^1J_{NR}$(H,X)	$^1J_{SC}$(H,X)	^1J_R(H,X)	$^1J_{exp}$(H,X)
^{19}F	612.23	616.19	610.42	529[a]
^{35}Cl	32.36	32.98	30.95	37.7[b]
^{79}Br	14.52	8.09	−47.76	±57.36[c]
^{127}I	−31.38	−63.40	−273.94	−79.86[c]

[a] Taken from ref. 244.
[b] Taken from ref. 188.
[c] Taken from ref. 136.

applied to the FC term, $^1J_{SC}$(H,X) and with experimental values. Important relativistic effects are observed for couplings involving the heaviest nuclei. However, for the calculated ^1J(H,I) these effects are notably exaggerated, possibly owing to the neglect of electron correlation. A possible route to overcome this problem could be to add relativistic corrections to correlated nonrelativistic calculations,[241] but, because relativistic and correlation effects are not additive,[245] the relativistic correlated approach is the only adequate way to obtain reliable results. A large discrepancy is also observed between $^1J_{SC}$(H,X) and ^1J_R(H,X) in molecules where relativistic effects are important. This is because, for these couplings, the noncontact contributions are comparable to the FC terms and therefore, a correction including only this last contribution is insufficient. The most conspicuous example is ^1J(H,Br), for which the nonrelativistic FC term is −42.02 Hz, while noncontact terms amount to 56.54 Hz. It must be noted that the Breit scaling factor enlarges the absolute value of the FC term since it increases the electronic density at the nuclear site. Visscher *et al.*[241] carried out nonrelativistic calculations of the FC contribution to ^1K(X,H) in the series of halogen hydrides. The relativistic effect of the contraction of s orbitals was partially taken into account by using experimental geometries, since bond lengths are also affected by such an effect. In this way the following values were calculated, in 10^{19} T^2 J^{-1}: $^1K^{FC}$(H,F) = 37.57, $^1K^{FC}$(H,Cl) = 15.75, $^1K^{FC}$(H,Br) = −13.92 and $^1K^{FC}$(H,I) = −32.74.

A four-component Dirac–Fock RPA calculation of ^1J(H,Se) in hydrogen selenide was also reported by Aucar *et al.*,[177,246] who found a considerable reduction of about 50 Hz from the nonrelativistic coupling.

Aucar *et al.*[246] demonstrated, by means of a four-component relativistic calculation, that the origin of the diamagnetic contribution to any magnetic molecular property is due to contributions from positronic spinors in calculating the response of the system. Several approximations for the calculation of the DSO term were also investigated. As example, the DSO term for the chalcogen hydrides, XH_2 (X = O, S, Se and Te), were calculated.

Kirpekar *et al.*[172] estimated the magnitude of the spin–orbit (SO) correction to one- and two-bond couplings in the series XH_4 (X = C, Si, Ge and Sn),[171] using quadratic response theory, in order to explain the remaining differences between their previous nonrelativistic calculations and experimental values. The SO contributions were calculated with the HERMIT/SIRIUS/RESPONSE MCSCF package of programs[247] at the RPA level. The scalar spin-free mass-velocity and Darwin corrections were not included in this approach because they produce divergences when the corresponding operators are combined with the FC operator, owing to a double δ-function dependence at the site of the nucleus. Assuming a singlet ground state, five spin–orbit corrections to the coupling constants were found. They are given in Eq. (30) in terms of quadratic static ($\omega_1 = \omega_2 = 0$) response functions.[172]

$$\begin{aligned}
&\text{(a)} \quad J^{\mathrm{FC,FC,SO}}(N,M) \propto \langle\langle H_{\mathrm{FC}}(N);\ H_{\mathrm{FC}}(M);\ H_{\mathrm{SO}}\rangle\rangle_{0,0} \\
&\text{(b)} \quad J^{\mathrm{PSO,FC,SO}}(N,M) \propto \langle\langle H_{\mathrm{PSO}}(N);\ H_{\mathrm{FC}}(M);\ H_{\mathrm{SO}}\rangle\rangle_{0,0} \\
&\text{(c)} \quad J^{\mathrm{FC,SD,SO}}(N,M) \propto \langle\langle H_{\mathrm{FC}}(N);\ H_{\mathrm{SD}}(M);\ H_{\mathrm{SO}}\rangle\rangle_{0,0} \\
&\text{(d)} \quad J^{\mathrm{PSO,SD,SO}}(N,M) \propto \langle\langle H_{\mathrm{PSO}}(N);\ H_{\mathrm{SD}}(M); H_{\mathrm{SO}}\rangle\rangle_{0,0} \\
&\text{(e)} \quad J^{\mathrm{SD,SD,SO}}(N,M) \propto \langle\langle H_{\mathrm{SD}}(N);\ H_{\mathrm{SD}}(M); H_{\mathrm{SO}}\rangle\rangle_{0,0}
\end{aligned} \tag{30}$$

where the SO operator, including both the one- and the two-electron contributions is given in Eq. (31).

$$\begin{aligned}
H_{\mathrm{SO}} &= \frac{g_e h e^2}{32\pi^2 \varepsilon_0 m^2 c^2} \left(\sum_N \sum_j \frac{Z_N}{r_{jN}^3} \vec{s}_j \cdot \vec{l}_{jN} - \sum_{i<j} \frac{(2\vec{s}_i + \vec{s}_j) \cdot \vec{l}_{ij}}{r_{ij}^3} \right) \\
&= H_{\mathrm{SO}}^{(1)} + H_{\mathrm{SO}}^{(2)}
\end{aligned} \tag{31}$$

It has been shown,[172] using the Wigner–Eckart theorem, that (a) is identically zero, and (e) could be expected to be negligible owing to the presence of the SD operator twice. The (c) contribution, which involves a combination of three triplet operators, was not calculated since it is expected to be smaller than (b) because it also contains the SD operator.[172] Thus, only the (b) and (d) terms were calculated to estimate the SO correction. Furthermore, an important simplification was obtained taking the effect of the two-electron part of the SO interaction as a shielding of the nucleus field,[248] which reduces the one-electron part. To this end, an effective charge Z_N^{eff} for the N nucleus was introduced, Eq. (32).

$$Z_N^{\mathrm{eff}} = \left(1 + \frac{H_{\mathrm{SO}}^{(2)}}{H_{\mathrm{SO}}^{(1)}} \right) Z_N \tag{32}$$

In Table 8 calculated nonrelativistic ^1J(X,H) and ^2J(H,H) couplings in the XH_4 series[172] at the levels (a) an extended CAS space for CH_4 and SiH_4, and an extended RAS space for GeH_4 and SnH_4,[171] and (b) calculated with a full-uncontracted basis set for the X nucleus[249] are compared with their experimental values, the SO corrections are also displayed. The differences between experimental and nonrelativistic values indicate the existence of appreciable relativistic corrections, which should be smaller than those predicted by Pyykkö.[239] However, only small SO corrections (0.1–1%) were obtained, indicating that relativistic corrections do not originate in SO effects. It is remarked that Z_H^{eff} should be the same whether it is calculated from ^1J(X,H) or from ^2J(H,H) couplings, and values displayed in column 5 in Table 8 differ in some cases notably.

Four-component calculations of J couplings in the same series XH_4 (X = C, Si, Ge and Sn) and in PbH_4 and $Pb(CH_3)_3H$ were performed by Enevoldsen *et al.*[257] at the RPA level, using the DIRAC code.[180] Correlation effects were estimated by means of correction factors obtained from nonrelativistic calculations. Increases of absolute values in ^1J(X,H) of 12% for X = Ge, 37% for X = Sn and 156% for X = Pb with respect to nonrelativistic values

Table 8. Nonrelativistic ^1J(X,H) and ^2J(H,H) couplings (in Hz) and their SO corrections in the series XH_4 (X = C, Si, Ge, Sn). Effective H nuclear charges, Z_H^{eff}, calculated from Eq. (32) are also shown.

X	^nJ(Y,H)	J_{NR}[a]	J_{SO}[b]	Z_H^{eff}	J_{exp}	Refs to exp. values
C	^1J(X,H)	125.30 (135.65)	−0.058	3.63	120.87[c]	197
	^2J(H,H)	−15.30 (−20.75)	0.004	3.32	−12.1[d]	250,202
Si	^1J(X,H)	−186.10 (−209.71)	0.059	9.53	−201.28	251
	^2J(H,H)	−1.63 (−0.38)	0.006	11.07	2.62[e]	252
Ge	^1J(X,H)	−97.56 (−92.96)	0.071	20.46	−97.6	253
	^2J(H,H)	−0.09 (−0.10)	0.530	26.69	7.69[f]	254
Sn	^1J(X,H)	−1891.29 (−1630.31)	21.173	43.31	−1933.3	255
	^2J(H,H)	1.42 (2.32)	0.121	46.80	15.3	256

[a] All four nonrelativistic Ramsey contributions are included. An extended CAS space for X = C, Si and an extended RAS one for X = Ge, Sn, were used. Taken from refs. 171 (X = C) and 156 (X = Si, Ge, Sn). Values calculated with a full uncontracted basis set for the X atom are shown in brackets (taken from ref. 249).

[b] $J^{PSO,FC,SO}$ and $J^{PSO,SD,SO}$ terms, considering one-electron and two-electron SO corrections, Eq. (30), calculated at the RPA level are included.

[c] Estimated value without rovibrational contributions.[197]

[d] Estimated value at equilibrium geometry using a combination of experimental[250] and theoretical data.[202]

[e] In SiH_3D.

[f] In GeH_3D.

were observed. Comparing their results with those of Kirpekar *et al.*,[172] the authors concluded that the main relativistic correction in the series XH_4 is not due to spin–orbit effects but rather to the contraction of the s shells originating in scalar relativistic effects. A large indirect relativistic effect from the heavy atom was also found in ^2J(H,H).

Malkina *et al.*[213] presented DFT calculations of ^1J(X,H) in the same series XH_4, corrected with the Breit scaling factors, Eq. (29) and neglecting the SD contributions. The basis set used was Partridge's large fully uncontracted UP[258] with four additional polarization functions for H, C and Si, and diffuse functions for Ge and Sn. They found good agreement with experimental values as expected since the Breit correction factor affects mainly the FC term, which is, by far, the leading one in these couplings.

Kaupp *et al.*,[259] with the DFT approach, studied the analogy between the transmission mechanisms of the FC term and SO effects on chemical shifts, which has been suggested previously by Nakagawa.[260] Their model is based on the quadratic response calculation of the SO correction to the shielding tensor, which originates in the response of the FC and SD terms to perturbations due to the external magnetic field and the SO interaction. In iodoacetylene the calculated FC contributions to ^1J(I,C) and ^2J(I,C) are -395.5 Hz and -52.6 Hz, respectively,[259] which are in reasonable agreement with recent experimental values of (361 ±11) Hz and (84±14) Hz in trimethylsilylated iodoacetylene.[261]

Relativistic effects were invoked to explain the measured trends in several papers describing experimental work in couplings involving compounds containing heavy atoms. For instance, the change in sign of $^1K(^{207}Pb,M)$ (M = C, Si, Sn, Pb) along the series $Bu^t_3Pb—Me$; $Bu^t_3Pb—SiMe_3$; $Bu^t_3Pb—SnMe_3$ and $Bu^t_3Pb—PbMe_3$, $^1K(^{207}Pb,^{13}C) > 0$; $^1K(^{207}Pb,^{29}Si) > 0$, $^1K(^{207}Pb,^{119}Sn) < 0$, and $^1K(^{207}Pb,^{207}Pb) < 0$, were ascribed to relativistic effects.[49] A similar change in sign was assumed, although it was not determined, in hexaarylated compounds, $Ar_3M—M'Ar'_3$ (M,M′ = Sn, Pb, Ge),[262] where $^1K(^{207}Pb,^{207}Pb)$ covers a wide range of values, while no such variation was found for $^1K(^{207}Pb,^{119}Sn)$ and $^1K(^{119}Sn,^{119}Sn)$ in the same series.

A new series of dileadtrichalcogenide anions $Pb_2S_nCh^{2-}_{3-n}$ (Ch = Se and/or Te), Pb_2SSeTe^{2-} and $M_2Se_3^{2-}$ (M = Sn and/or Pb) were studied[263] that present a trigonal bipyramidal structure with M and M′ (M,M′ = Pb and/or Sn) in the axial positions. $^2J(^{117}Sn,^{119}Sn)$ and $^2J(^{119}Sn,^{207}Pb)$ couplings were observed for the first time and their values are unusually large: 1514 Hz and 1145 Hz, respectively. These values cannot be ascribed to bonding interactions between the axial metal atoms. Owing to their spatial proximity, such large values could be due to a high electron-spin correlation between valence s electron pairs of the axial metal atoms, although large relativistic effects were calculated using the Breit scaling factor, Eq. (29). Significant relativistic effects were also calculated with this method for $^1J(X,^{17}O)$ in tetrahedral perhalate anions XO_4^- (X = Cl, Br and I).[264] However, these estimations of relativistic effect[263,264]

could be quantitatively inaccurate since experimental[265] as well as theoretical[241] evidence indicates that noncontact terms could be significant for couplings involving heavy nuclei.

Semiempirical approaches

The IPPP-CLOPPA approach. The IPPP-CLOPPA (Inner Projections of the Polarization Propagator-Contributions from Localized Orbitals within the Polarization Propagator Approach) method[266] for decomposing second-order contributions to spin–spin couplings and several of its applications have been summarized.[17] In its original version;[266] the ground-state wavefunction was calculated at the INDO level;[231] later it was extended to be used with other kinds of semiempirical ground-state wavefunctions, i.e. MNDO,[267,268] AM1,[96,268,269] and PM3[270], although in this case most results are not encouraging, and *ab initio* calculations.[61,132,135] As the theoretical foundations of the CLOPPA method have been described in some detail in various papers,[1,17,266,271–273] only the final expressions are given here. They are intended to provide an idea of how several empirical trends can be rationalized in terms of transmission mechanisms, provided the approximation used for the wavefunction reproduce the trends observed in the total couplings. It is important to recall that total couplings calculated with the PP approach at the RPA level are exactly the same as those calculated with any of the implementations of the CHF approach, FPT[231] or SCPT.[115] The final expressions for second-order contributions to the **J**(A,B) tensor are:

(i) The Fermi contact contribution, which is isotropic:[2]

$$J^{\mathrm{FC}}(\mathrm{A,B}) = -(4\beta/3)^2\hbar\gamma_{\mathrm{A}}\gamma_{\mathrm{B}} \sum_{ia,jb} U^{\mathrm{FC}}_{ia,\mathrm{A}}({}^3\mathbf{A} - {}^3\mathbf{B})^{-1}_{ia,jb} U^{\mathrm{FC}}_{jb,\mathrm{B}}$$

$$= \sum_{ia<jb} \Omega U^{\mathrm{FC}}_{ia,\mathrm{A}} W_{ia,jb} U^{\mathrm{FC}}_{jb,\mathrm{B}} \tag{33}$$

(ii) The $\alpha\beta$ Cartesian component of the paramagnetic spin–orbital term:

$$J^{\mathrm{PSO},\alpha\beta}(\mathrm{A,B}) = -(4\beta)^2\hbar\gamma_{\mathrm{A}}\gamma_{\mathrm{B}} \sum_{ia,jb} U^{\mathrm{PSO},\alpha}_{ia\mathrm{A}}({}^1\mathbf{A} + {}^1\mathbf{B})^{-1}_{ia,jb} U^{\mathrm{PSO},\beta}_{jb,\mathrm{B}} \tag{34}$$

(iii) The $\alpha\beta$ Cartesian component of the spin–dipolar term:

$$J^{\mathrm{SD},\alpha\beta}(\mathrm{A,B}) = -(2\beta)^2\hbar\gamma_{\mathrm{A}}\gamma_{\mathrm{B}} \sum_{ia,jb} \left[\sum_{\nu} U^{\mathrm{SD},\alpha\nu}_{ia,\mathrm{A}} U^{\mathrm{SD},\beta\nu}_{jb,\mathrm{B}} \right] ({}^3\mathbf{A} - {}^3\mathbf{B})^{-1}_{ia,jb} \tag{35}$$

(iv) The $\alpha\beta$ Cartesian component with the cross term between the Fermi contact and the spin–dipolar one, which is a completely anisotropic tensor since its trace is zero:

$$J^{\mathrm{FC/SD},\alpha\beta}(\mathrm{A},\mathrm{B}) = -\frac{8\beta^2\hbar}{3}\gamma_\mathrm{A}\gamma_\mathrm{B}\sum_{ia,jb}[U^{\mathrm{FC}}_{ia,\mathrm{A}}U^{\mathrm{SD},\alpha\beta}_{jb,\mathrm{B}} + U^{\mathrm{FC}}_{jb,\mathrm{B}}U^{\mathrm{SD},\alpha\beta}_{ia,\mathrm{A}}]({}^3\mathbf{A} - {}^3\mathbf{B})^{-1}_{ja,jb} \tag{36}$$

where *ia* and *jb* stand for occupied (vacant) LMOs; the matrix elements of the perturbative Hamiltonians of Eqs (33–36), which are dubbed the 'perturbators', are, for the FC, PSO and SD, those given in Eqs (37–39), respectively:

$$U^{\mathrm{FC}}_{ia,\mathrm{A}} = \langle i \mid \delta(\vec{r} - \vec{R}_\mathrm{A}) \mid a\rangle \tag{37}$$

$$U^{\mathrm{PSO},\alpha}_{ia,\mathrm{A}} = \left\langle i \left| \frac{L^\alpha_\mathrm{A}}{i\hbar r^3_\mathrm{A}} \right| a \right\rangle \tag{38}$$

$$U^{SD,\alpha\beta}_{ia,\mathrm{A}} = \left\langle i \left| \frac{(3\hat{r}_{\mathrm{A}\alpha}\hat{r}_{\mathrm{A}\beta} - \delta_{\alpha\beta})}{r^3_\mathrm{A}} \right| a \right\rangle \tag{39}$$

At the RPA level the singlet and triplet **A** and **B** matrices can be written in terms of the spatial HF MOs as in Eqs. (40–43).

$${}^1\mathbf{A}_{ia,jb} = (\varepsilon_a - \varepsilon_i)\delta_{ab}\delta_{ij} + 2\langle aj \mid ib\rangle - \langle aj \mid bi\rangle \tag{40}$$

$${}^3\mathbf{A}_{ia,jb} = (\varepsilon_a - \varepsilon_i)\delta_{ab}\delta_{ij} - \langle aj \mid bi\rangle \tag{41}$$

$${}^1\mathbf{B}_{ia,jb} = \langle ab \mid ji\rangle - 2\langle ab \mid ij\rangle \tag{42}$$

$${}^3\mathbf{B}_{ia,jb} = \langle ab \mid ji\rangle \tag{43}$$

Equations (33–36) decompose each term in a sum of bond contributions. Each of them depends at most on two virtual excitations, $i \longrightarrow a$ and $j \longrightarrow b$, and each Cartesian component of each term can be briefly written as

$$J^{\alpha\beta}(\mathrm{A},\mathrm{B}) = \sum_{ia<jb} J^{\alpha\beta}_{ia,jb}(\mathrm{A},\mathrm{B}) \tag{44}$$

and for the isotropic FC term

$$J^{\mathrm{FC}}(\mathrm{A},\mathrm{B}) = \sum_{ia\leqslant jb} J^{\mathrm{FC}}_{ia,jb}(\mathrm{A},\mathrm{B}) \Longrightarrow$$

$$J^{\mathrm{FC}}_{ia,jb}(\mathrm{A},\mathrm{B}) = \Omega W_{ia,jb}(U^{\mathrm{FC}}_{ia,\mathrm{A}}U^{\mathrm{FC}}_{jb,\mathrm{B}} + U^{\mathrm{FC}}_{ia,\mathrm{B}}U^{\mathrm{FC}}_{jb,\mathrm{A}}) \tag{45}$$

If sums in Eqs (44) and (45) are dominated by only a few bond contributions, then interesting physical insight can be obtained on factors defining a given **J**(A,B) tensor, which in many cases it is by far dominated by the FC contribution. This is the case of many $^1J^{FC}$(A,B) couplings through a single bond, which are mainly dominated by the following contributions, (Eq. (45)):[17] The 'bond contribution', J^b, i.e., $i=j$ and $a=b$, where i and a are the LMOs representing respectively the A—B bond and its vacant anti-bonding orbital; the 'other bond contributions', J^{ob}, where i, a and b are the same as in J^b and j corresponds to another σ bond attached either to A or B atoms. If A and/or B bear lone-pairs, then the 'lone-pair contribution', J^{LP} can also be very important, which is similar to J^{ob} but j = LP. While the former, J^b, corresponds to a positive contribution to ^1K(A,B), the latter two, J^{ob} and J^{LP}, correspond to negative contributions to ^1K(A,B).[17] Therefore, $^1K(A,B) > 0$ if $|K^b| > |\Sigma K^{ob} + \Sigma K^{LP}|$ and otherwise $^1K(A,B) < 0$. Examples of the former and the latter are, respectively, $^1K(C,H) > 0$ and $^1K^{FC}(C,F) < 0$.[136] A change in sign of $^1K(^{207}Pb,M)$ (M = C, Si, Sn, Pb) along the series Bu^t_3Pb—Me, Bu^t_3Pb—$SiMe_3$, Bu^t_3Pb—$SnMe_3$ and Bu^t_3Pb—$PbMe_3$ was reported, i.e. $^1K(^{207}Pb,M) > 0$ for the first two, and $^1K(^{207}Pb,M) < 0$ for the latter two.[49] Such behaviour was ascribed to relativistic effects and a CLOPPA description seems to indicate that the relativistic contraction of s orbitals produces a Pb—M bond with lower s character in the latter two members of the series than in the first two, causing a decrease in $^1K^b$ and an increase, in absolute value, of $^1K^{ob}$, in accordance with Bent's rule[274] (see Section 3.3. for further examples).

Substituent, conformational and configurational effects can affect each CLOPPA contribution (Eqs (44) and (45)), in two different ways, namely, through changes in the 'perturbators' and through changes in the PP (Eqs (33–36)). Each perturbator depends only on one occupied and one vacant LMO, while $W_{ia,jb}$ depends on all LMOs belonging to the molecule under study.

The IPPP-CLOPPA approach at the INDO level was applied to study the extremely large (more than three times larger than in the parent compound) substituent effect on ^3J(C1,H) couplings in 1-X derivatives of (**3**).[275] Three main effects contributed to such large effects: (i) the three pathways connecting the coupled nuclei;[276,277] (ii) the strong electron delocalization from a C—C bond to its *vicinal* bridgehead C—H antibond; and (iii) the through-space transmission between the bridgehead carbon atoms.[278]

Using an AM1 ground-state wavefunction, the anisotropy Δ^1**J** of the ^{1}**J**(X,Y) tensor was calculated for compounds of type Me_3X—Y (X = C, Si, Sn, Pb; Y = F, Cl) at the RPA level and Eq. (36) was used to perform a bond contribution analysis of the Fermi contact–spin dipolar cross term, which was calculated as the main contribution to Δ^1**J**(X,Y) in the whole series except for X = Pb. The role played by the X—Y bond, its antibond and the Y lone pairs in determining the cross term as the dominant one was discussed.[96] The RPA-AM1 approach was used to study the ^2J(Sn,Sn) coupling through the

Sn—X—Sn pathway (X = O, S) versus the Sn—X—Sn angle, and in $(H_3Sn)_2N—NH_2$ as a function of the rotation angle around the N—N bond.[269]

A double perturbation expansion of the FC coupling term up to second order in both the magnetic and Coulomb residual interactions was carried out within the CS-INDO method in polymethyne chains.[279] It should be noted, however, that such an expansion usually converges only slowly and, in order for the SOS approach to be equivalent to the FPT and CHF ones, some of the terms in it must be summed to infinite order with respect to the Coulomb interaction.[141] The authors conclude that their calculations 'do not succeed in generating unique effective parameters $s_H^2(0)$ and $s_C^2(0)$' as, for example, $0.1705 \leqslant s_H^2(0) \leqslant 0.5099$ must be taken to bring calculated couplings close to the corresponding experimental values.

CHF calculations of substituent effects on ^1J(C,H) couplings in methane derivatives were reported by Musio and Sciacovelli[280] using MNDO wavefunctions.[281] The CHF approach was implemented following refs 282 and 115 and results were compared with those obtained with the same perturbational approach but using both INDO[231] and MINDO/3[283] wavefunctions. MNDO results describe substituent effects in these methane derivatives much better than those obtained with either of the latter two wavefunctions. However, at this point it should be recalled that MNDO wavefunctions for unsaturated hydrocarbons in general present quasi-instabilities of the non-singlet type.[1,284]

Correlations between coupling constants and other calculated molecular properties

In a series of papers the connection between ^1J couplings and bond parameters was extensively revisited during the review period. The atomic hybridizations of the bonded atoms were described on the basis of MBOHOs (Maximum Bond Order Hybrid Orbitals).[285] The MBOHO approach is based on the maximum bond order principle[286] and the basic idea of the maximum overlap symmetry orbitals. Unitary transformations T and U of the m (orthogonal) AOs on atom A and n AOs on atom B ($n \geqslant m$) can be defined,

$$| g_{iA} \rangle = T_{ij} | \chi_{jA} \rangle \qquad | h_{iB} \rangle = U_{ij} | \chi_{jB} \rangle \tag{46}$$

such that the two-centre off-diagonal block of the one-particle reduced density matrix is

$$M_{1g} |_{i,j} = \langle g_{iA} | \hat{P} | h_{jB} \rangle \tag{47}$$

expressed as a block M_1 of dimension $m \times m$ and a block of dimension $(n - m) \times m$ such that all its elements are zero,

$$M_{1g} = [M_{1m \times m} M_{0(n-m) \times m}] \qquad \text{with} \qquad M_1 = M_1{}^+ \tag{48}$$

Diagonalization of M_1 yields the pairs of MBOHOs,[285] i.e. hybrid orbitals on A and B such that the eigenvalues are extreme values of the bond order for a single pair of hybrid AOs. This method shares with the NBO method[287] the basic idea of obtaining an 'optimum' set of hybrid AOs entering the bonding MOs from considerations of the one-particle density matrix. It is thus applicable to any molecular ground-state wavefunction regardless of the approach employed to calculate it. The NBO counterparts of the MBOHO are the Natural Hybrid Orbitals, NHO. In fact, numerical results for a large series of compounds within the CNDO/2 approximation show excellent agreement between the MBOHO and the NBO approaches, as well as with chemical intuition.[285]

Experimental ^1J(C,H) and ^1J(C,C) couplings in a series of hydrocarbons and heterosubstituted hydrocarbons were related, through regression analysis, to MBOHO parameters obtained with the CNDO/2 approach.[231] A Muller and Pritchard type[288] linear relationship between ^1J(C,H) and the per cent s character of the C—H bond at the C atom, $(s\%)_c$ (Eq. (49)), was found in hydrocarbons with the regression parameters $a = 6.16$, $b = -23.95$, and $\sigma = 3.64$ Hz.

$$^1J(\mathrm{C,H})(\mathrm{Hz}) = a(s\%)_c + b \tag{49}$$

A generalization of Eq. (49) including the 'bond overlap' S_{AB} introduced by Maksic *et al.*[289] was also tested with a slight modification that replaces the bond overlap by the bond order P_{CH} (Eq. (50)). The regression coefficients were $a = 17.063$, $b = -25.01$, and $\sigma = 3.41$ Hz. Only slight changes in the a and b coefficients were found if data from heterosubstituted hydrocarbons were also included, but σ increased from 3.64 to 4.60 Hz for Eq. (49). P_{CH} ranged from 0.9995 to 0.9710[290] in the set of compounds considered. This may be the reason why no significant improvement was obtained with Eq. (50) as compared with Eq. (49). Similarly, a regression analysis with Gil's relationship[291] (Eq. (51)) led to $a = 0.705$, $b = 44.91$ and $\sigma = 5.27$ Hz.

$$^1J(\mathrm{C,H})(\mathrm{Hz}) = a(s\%)_c/[(4/3)^2 + P_{CH}^2] + b \tag{50}$$

$$^1J(\mathrm{C,H})(\mathrm{Hz}) = a(s\%)_c^{3/2} + b \tag{51}$$

Many qualitative trends of ^1J(C,H) couplings can be related to the hybridization of the C atom in the C—H bond and are thus taken into account by these regression analyses. However, many structural and/or substituent effects that are not directly related to the s character may have a magnitude similar to σ, as happens with data collected in Table 9 for ^1J(C,H) in a CH_3 moiety. Also, such correlations are inadequate for substituents of type —I^-;[290] a few conspicuous examples for ^1J(C,H) in CH_nF_{4-n} (n = 1,2,3) are also shown in Table 9.

Table 9. Selected ^1J(C,H) couplings in heterosubstituted hydrocarbons as given by Eq. (49)[290] and Eq. (56)[292] and corresponding experimental values (in Hz)

	Eq. (49)	Eq. (56)	Exp.
CH_4	130.47	–	125
$H_3C—CH_3$	127.0	–	124.9
$H_3C—C{\equiv}CH_3$	128.72	–	131.0
$H_3C—NH_2$	135.6; 131.8	–	133
$H_3C—C{\equiv}N$	126.42	131.75	136
CH_3F	143.72	159.16	149
CH_2F_2	160.57	199.52	184.5
CHF_3	172.13	235.14	239.1

A similar correlation for ^1J(C,C) couplings[290] was sought using Eq. (52); when couplings in single and multiple bonds were included in the regression analysis, $\sigma = 6.43$ Hz was obtained, while for a Maksic-type relationship, Eq. (50), $\sigma = 4.07$ Hz was obtained.

$$^1J(\mathrm{C,C})(\mathrm{Hz}) = a(\mathrm{s}\%)_{\mathrm{C1}}(\mathrm{s}\%)_{\mathrm{C2}} + b \tag{52}$$

When separate regression analyses for single and multiple C—C bonds[290] were considered, σ values of 2.72 Hz and 5.42 Hz were obtained, respectively. Since only ^1J(C,C) values in the range 30–50 Hz were included, substituent and structural effects may well be within the σ limit, as is the case, for instance, for ^1J(C=C) in C_2H_4 and in *trans*-butadiene, for which the respective experimental values are 67.6 Hz and 68.8 Hz and those given by Eq. (52)[290] are 73.74 Hz and 67.53 Hz.

Ab initio STO-3G MBOHO parameters were used[293] to obtain the regression coefficients in Eqs (49) and (52). A similar STO-3G study[294] in the same series of compounds was carried out in terms of Foster and Weinhold's NHOs[287] and only differences in the regression a and b coefficients smaller than 1% were obtained for Eqs (49) and (52) using both approaches[293,294] for ^1J(C,H) and ^1J(C,C) couplings.

Regression coefficients in Eq. (52) adapted to $^1J(C_b,Si)$ couplings between a bridghead C_b nucleus and a Si nucleus in substituted $Si(CH_3)_3$-polycyclic hydrocarbons were also determined, where the s% character for the Si—C bond at each atom was calculated[295] at the AM1 level. In the parent compounds, regression analysis for $^1J(C_b,H)$ couplings was considered using linear relationships between $(s\%)_{C(b)}$ and net charges on both the Si and C atoms. Correlation coefficients of 0.99 and 0.92, respectively, were obtained.

Equations (46–52) were generalized[292] by including ionic terms in a valence-bond two-particle wavefunction representing an AB bond, Eq. (53), where the

λ_A and λ_B coefficients of ionic terms are closely related to the net atomic charges Q_N on A and B, Eq. (54).

$$\Psi_{AB}(1,2) = \phi_A(1)\phi_B(2) + \phi_B(1)\phi_A(2) + \lambda_A\phi_A(1)\phi_A(2) + \lambda_B\phi_B(1)\phi_B(2) \quad (53)$$

$$\lambda_N^2 = a_N Q_N + b_N \quad (54)$$

Assuming that the FC term is largely dominant, Eq. (55) is obtained.

$$^1J(A,B) = k_{AB}(s\%)_A(s\%)_B + (k_A Q_A + I_A)(s\%)_A + (k_B Q_B + I_B)(s\%)_B + I_{AB} \quad (55)$$

The regression analysis should determine six parameters for each kind of chemical bond, but not for C—H bonds since $(s\%)_H = 100$, and for ^1J(C,H) couplings Eq. (55) reduces to Eq. (56).

$$^1J(C,H) = (d_1 + d_2 Q_C)(s\%)_C + d_3 Q_H + d_4 \quad (56)$$

Equation (56) was applied to the same set of compounds as in ref. 290, and the least-square fits were carried out using the CNDO/2 calculated net atomic charges. For ^1J(C,H) couplings in hydrocarbons, only slightly better results than those of ref. 290 were obtained, but for couplings across α-C—H bonds in heterosubstituted hydrocarbons with —I$^-$ substituents, such as CN, C(O)X and NO_2, σ decreases from 18.43 Hz to 6.79 Hz (Eq. (56)). Thus the importance of including 'ionic' terms is emphasized.[292] A selection of calculated couplings[290,292] in the series $CH_{4-n}F_n$ are presented in Table 9.

Equation (55) was applied to ^1J(C,N) couplings[296] using CNDO/2 MBOHO parameters; for single C—N bonds 14 experimental couplings were included in the regression analysis, Eq. (55), yielding $\sigma = 1.24$ Hz. For multiple C—N bonds 12 couplings were included, and $\sigma = 0.70$ Hz was found. Equation (55) was also used for ^1J(P,C) couplings[297] using EHT MBOHO parameters. The six regression coefficients in Eq. (55) were obtained using experimental ^1J(P,C) couplings ranging from −33.6 Hz to +476 Hz, and $\sigma = 3.13$ Hz was obtained.

In ref. 298 the MBOHO approach was reviewed and STO-3G results of Eq. (55) for C–H, C–C, C–N and C–F ^1J couplings were presented. A selection of the regression coefficients for different couplings are shown in Table 10. For ^1J(C,C) couplings no distinction was made[298] between both coupled C nuclei, and therefore assigning different values of k_N and I_N to each of them seems unjustified.

Equation (55) was extended[299] to include the DSO, PSO and SD terms. Considering the two-electron wavefunction in the AB bond, Eq. (53), and assuming that only this pair of electrons makes important contributions, such terms are discussed in terms of the average energy approximation. Introducing the quantities W_{iN} = per cent character of the hybrid AO on atom N associated

Table 10. Regression coefficients corresponding to Eq. (55) for the relationship between ^1J(A,B) couplings and atomic per cent s character $(s\%)_N$ and net atomic charge, Q_N, on each atom of an A—B bond.[298]

A—B	k_{AB}	k_A	I_A	k_B	L_B	I_{AB}	SD
C—H[a]	4.746	4.090	–	–	165.17	15.22	3.98
C—H[b]	5.498	3.493	–	–	197.86	−7.91	3.66
C—C single[c]	0.2967	−0.878	−6.666	0.593	−7.886	575.59	1.74
C—C mult.[d]	0.2858	0.603	−10.91	1.028	−15.43	1286.02	0.16
C—N single[c]	0.0317	−0.335	0.317	0.227	−0.246	−12.54	0.62
C—N mult.[d]	0.6684	1.185	−31.98	3.033	−26.07	114.41	0.74
C—N all[e]	−0.0585	−0.136	2.483	0.197	1.757	−60.71	2.44
C—F	−5.536	5.585	92.41	−27.48	123.87	−1928.51	7.87

SD = standard deviation.
[a] In a series of heterosubstituted hydrocarbons.
[b] Values from hydrocarbons and heterosubstituted hydrocarbons included in the same regression analysis.
[c] Single bonds.
[d] Multiple bonds.
[e] Calculation of regression coefficients where single and multiple CN bonds are included.

with angular momentum quantum number $l = i$, expressions in terms of net atomic charges Q_N and of W_{iN} values were obtained. When the FC, PSO, DSO and SD terms are added, a relationship for the total ^1J(A,B) coupling is obtained. If only s- and p-type AOs make important contributions to MBOHOs of a given A—B bond, Eq. (57) holds and a simplified equation involving only the (s%) character of the hybrid AOs, W_{0N}, and the net atomic charges is obtained, Eq. (58), which was used to carry out actual calculations.[299]

$$W_{sN} + W_{pN} \cong 100 \tag{57}$$

$$^1J(\mathrm{A,B}) = k_{AB} W_{0A} W_{0B} + k_{QA} Q_A W_{0A} + k_A W_{0A} + k_{QB} W_{0B} + k_B W_{0B} + k_{EA} Q_A + k_{EB} Q_B + c_{AB} \tag{58}$$

For each AB bond there are thus eight coefficients, Eq. (58), that must be obtained through a regression analysis. For instance in ^1J(C,F) couplings these coefficients were calculated using a set of 36 experimental J values, Mulliken atomic charges and MBOHO s% characters.[299] The bond parameters were calculated using (i) semiempirical methods, EHT and MNDO, with MNDO optimized geometries and (ii) *ab initio* methods, HF/STO-3G and HF/6-31G*, with HF/STO-3G optimized geometries. Very different regression coefficients were obtained when the two different *ab initio* basis sets were used to calculate bond parameters. In Table 11 these regression coefficients are compared for

Table 11. Regression coefficients, Eq. (58), including 36 experimental ^1J(C,F) couplings,[299] for HF/STO-3G and HF/6-31G* MBOHO bond parameters

Coefficient	HF/STO-3G	HF/6-31G*
k_{CF}	0.64293	8.20187
k_{QC}	−4.3587	30.6132
k_C	−17.8492	−142.1764
k_{QF}	9.7822	−61.8064
k_F	−13.1724	−130.6509
k_{EC}	−137.466	−421.897
k_{EF}	−924.697	216.168
c_{CF}	95.12	1689.89
R	0.981	0.989
σ	8.12	6.28

calculations using bond parameters obtained with the two basis sets quoted above. It is recalled that in both regression analyses the same set of experimental ^1J(C,F) couplings were used; in both cases the correlation coefficients are larger than 0.98 and σ values smaller than 8.5 Hz.

Correlations between ^1J(C,H) couplings and bond parameters have been explored with Eq. (55)[295] and with the sum of the distortions of the internuclear C—C—C bond angle.[300] Experimental ^1J(C,H) couplings were correlated with different bond properties computed with the NBO analyses and optimized geometric structures at the PM3 and HF/6-31G* levels in a set of 38 bi- and polycyclic aliphatic hydrocarbons.[301] Taking into account that such correlations are based on crude approximations, only tertiary C—H bonds were considered. Correlations with the following bond parameters were sought: $(s\%)_C$ of the C—H bond in Muller and Pritchard-type,[288] Maksic-type[289] and Gil-type[291] relationships; atomic charges q_C and q_H intending to take into account ionic terms; internuclear or interbond mean C—C—C angles or mean deviation at the tertiary site. Relationships including both $(s\%)_C$ and ionic terms yielded the smallest standard deviations. The best single parameter correlation at the PM3 level was that involving the H atomic charge q_H ($\sigma = 4.6$ Hz). However, PM3 and HF/6-31G* bond lengths and atomic charges correlate very poorly in spite of the good correlation found with the hybridization at the C atom, and the smallest standard deviation at the *ab initio* level was found for the Zhan and Hu-type relationship, Eq. (55) ($\sigma = 5.5$ Hz). Previously reported correlations were quoted for comparison purposes.[301]

Battacharyya *et al.*[105] linearly correlated the FPT calculated FC term of ^1J(C,H) couplings with the first-order density matrix element between the valence shell s-orbitals of the coupled nuclei in different sets of 4- and 6-heterocyclic compounds.

In a set of organomercury hydrides, RHgH, ^1J(Hg,H) couplings were found[302] to correlate linearly both with the corresponding proton chemical shift

and with the partial charge on the hydrogen atom relative to that in R—H, as calculated with the AM1 approach.[303]

For insight into how the extremely large substituent effects on ^3J(C1,H) observed[275] in 1-X derivatives of bicyclo[1.1.1]pentane (**3**) operate, ^3J(C1,Y) couplings in several 1-X, 3-Y- derivatives were measured and differences in X substituent effects on such couplings between both sets were found to increase with the respective C3—Y bond polarizability as calculated with the *ab initio* IPPP-CLOPPA method.[304]

3. INTRA- AND INTERMOLECULAR INTERACTION EFFECTS ON SPIN–SPIN COUPLING CONSTANTS

3.1. Stereospecific aspects and empirical correlations

Until a few years ago, NMR stereochemical analyses were mainly based on long-range couplings,[3,7,305–307] occupying prominent places in the Karplus equation[153] and its generalization[308] for ^3J(H,H) couplings, Karplus-like relationships for three-bond couplings between different isotopic species,[1] and the Schaefer's 'J method' for studying side-chain conformations in aryl compounds.[309] Perhaps one of the most conspicuous advances in NMR stereochemical analyses that took place during the review period is the extensive use that is now made of one- and two-bond couplings. This is particularly true for studying structures of proteins, nucleic acids and other biological compounds.[11,58,59,62,63,154,310] In general, the main idea is to obtain relationships between a given type of coupling constant and some structural parameter. Such relationships are obtained either theoretically[58,62] or empirically.[311] This possibility was greatly enhanced by the important advances that also took place during the same period in experimental techniques for obtaining isotopically enriched samples, especially in ^{13}C and/or ^{15}N, and by the development of special techniques to detect different couplings and enhance their resolution.[312–318]

The number of studies under this heading published during the six-year review period is so impressive that to attempt to review them exhaustively would lengthen this section unreasonably. Accordingly, only a small selection of papers will be discussed here, to give only a brief overview of this subject. First, some work on one- and two-bond couplings will be quoted; then a few papers dealing with Karplus-like relationships for different isotopic species will be discussed, and finally a few empirical relationships not directly related to structural parameters will be reviewed.

Stereospecific trends

Multidimensional heteronuclear NMR experiments for determining the structure of isotopically labelled RNA were discussed in detail by Pardi.[320]

The utility and potential limitations of using ^{n}J(C,H) coupling for RNA structure determination were discussed in detail by Hines *et al*;[321] $^{1,2,3}J$(C,H) and $^{1,2,3}J$(C,C) couplings were used to study molecular structures of 2′-deoxyribonucleosides labelled with ^{13}C at the 2′ position.[154] The possibility of extracting structural information from NMR of proteins oriented in a strong magnetic field (~17 T) due to their high magnetic anisotropy was discussed by Tolman *et al.*[322] Experimental techniques for accurately determining ^{1}J(C,H) and ^{1}J(N,H) couplings in ^{13}C- and ^{15}N-enriched proteins are continually improving[323] and the use of different ^{3}J and $^{1}J(H_{\alpha},C_{\alpha})$ couplings as restraints in computational structure refinement has been reviewed.[324] Combining different NMR data, e.g. NOEs, coupling constants and chemical shifts, a new approach was developed to obtain accurate structural data in proteins.[325]

Bax *et al.* established empirical correlations between $^{1}J(C_{\alpha},H_{\alpha})$ and the φ and ψ angles defining the backbone conformation in proteins, Eq. (59).[311] The coefficients of the correlation were determined using a large number of coupling values determined for residues of several proteins in which structural data were known from X-ray crystallographic studies.[326,327]

$$^{1}J(C_{\alpha},H_{\alpha}) = A + B\sin(\psi + 138°) + C\cos^{2}(\psi + 138°) + D\cos^{2}(\varphi + 30°) \quad (59)$$

Tvaroska *et al.*[328] studied the angular dependence of ^{1}J(C,H) couplings in β-linked oligosaccharides. Equations relating such coupling with the torsional angles describing the relative orientation of monosaccharide residues and the medium dielectric constant were obtained with the FPT INDO approach.[231] Experimental values were used to adjust the calculated angular dependence. In a series of ^{13}C-labelled methylaldopentopyranosides and aldohexopyranosides, ^{1}J(C,H),^{2}J(C,H) and ^{3}J(C,H) couplings were studied to relate their magnitudes to the aldopyranosyl ring structure.[310] The use of ^{1}J(C,H) and ^{3}J(H,H) couplings to assign the anomeric configuration of *C*-glycopyranosides and *C*-glycofuranosides was discussed by Brakta *et al.*[329] The solvent and concentration dependence of substituent orientational effects in 1-methyl-amino, 2-nitromethane on ^{1}J(C,H) couplings was studied by Kozerski *et al.*[330] ^{1}J(C,H) formyl couplings for s-*cis* and s-*trans* rotamers were compared in a series of alkyl formates.[331]

Both ^{1}J(N,H) and ^{1}J(C,H) couplings were measured to assign different isomers with respect to the amide C(=O)—NH bonds in bis(benzo-15-crown-5) ethers.[332] An approach for measuring the amide $^{1}J(^{15}N,^{1}H)$ couplings in proteins was described by Tolman and Prestegard.[333]

The measurement of ^{1}J(C,H) couplings in carbocations and their comparison with the values in corresponding ketones were used to define the ΔJ parameter and empirical equations were written, Eq. (60), to relate the ^{1}J(C,H) coupling of a group adjacent to a positive charge in a carbocation to the amount of charge and the dihedral angle θ between the C—H orbital and the vacant p_{π} orbital, where the amount of charge at the adjacent carbon is measured by σ^{+}.

Such equations were applied by Kelly *et al.*[334] to polycyclic systems including bicyclo[2.2.1]hept-2-yl cations.

$$\Delta J = 22.5 - 33.1 \cos^2 \theta, \qquad \Delta J = (1 + 0.6\sigma^+)(10.9 - 14.3 \cos^2\theta) \quad (60)$$

The potential of ^2J(C,H) couplings in stereochemical analysis when there are two oxygen substituents along the C—C—H coupling pathway was long known as the 'projection rule'.[140] A modified projection curve appropriate for the stereochemical interpretation of ^2J(C2′,H1′) couplings in various nucleosides was presented.[154] A detailed study on how ^2J(C,H) and ^3J(C,H) couplings depend on factors like the nature, the position and the orientation effects of hydroxyl, carbonyl and bromine substituents was carried out in a series of rigid compounds.[335]

Binding-induced changes in the sugar puckers of DNA determined by measuring ^3J(H,H) couplings in deoxyribose were reported by Szyperski *et al.*[336] The puckering angle of six-membered rings was determined by Haasnoot[337] using the generalized Karplus equation for ^3J(H,H) couplings[308] and his truncated Fourier formalism.[338] The same equation[308] was reparametrized to include empirical group electronegativities.[339] The problem of determining *vicinal* J(H,H) couplings in large molecules where several conformers are differently populated and where such populations can change with solvent and temperature was addressed in several papers.[32,340–342] A new versatile program to apply the Karplus–Altona equation[308] to different classes of chemical compounds was reported.[343]

The angular dependence of ^3J(H,H) in ethane, fluoroethane and 1,1-difluoroethane was explored[344] employing different basis sets at the HF RPA level. The major contribution to these calculated couplings is given by the FC term. Dependence of Karplus-type equation parameters for ^3J(H,H) on substituents were calculated by San Fabián *et al.*[345] in monosubstituted ethanes, CH_3CH_2X (X = CH_3, NH_2, OH and F), employing the 6-31G** basis set at the HF RPA level for the FC term. Calculated substituent effects, ΔJ^X, increase with increasing electronegativity of the substituent. Substituent effects on ^3J(H,H) were also calculated by Guilleme *et al.*[346] in monosubstituted and 1,1-disubstituted ethanes, with substituents containing atoms from rows 2 to 5 of the periodic table. From experimental and calculated data sets, they concluded that experimental couplings as well as calculated substituent effects of monosubstituted ethanes follow a quadratic dependence on the relative electronegativity of the substituent α atom. β-Hydrogen effects on *vicinal* ^3J(H,H) couplings were studied with *ab initio* methods in CH_3CH_2X (X = CH_3, NH_2 and OH).[347]

Schaefer *et al.*[348] studied departures from the Karplus-type relationship ('Barfield effect') to determine the ring pucker in 2-phenyl-1,3-dithiane. The dependence of the ^3J(H,H) Karplus equation on the internal C—C—H angles was given in mathematical form by Barfield *et al.*,[349] who also recalculated the

coefficients using new experimental data for dihedral angles close to 180° in an sp^3—sp^3 system.[350]

^3J(H,H) couplings through the HNCH$^\alpha$ pathway were accurately determined in ^{15}N-enriched proteins and the corresponding Karplus equation was parametrized using residues for which the backbone angle is known.[351] Equation (61) with $A = 6.51$ Hz; $B = -1.76$ Hz and C = 1.60 Hz gives a fit with a rms deviation of 0.73 Hz.

$$^3J(H^N,H^\alpha) = A\cos^2(\varphi - 60°) + B\cos(\varphi - 60°) + C \qquad (61)$$

Experimental ^3J(H,H) couplings in metallapentacycles N—C—C—O—M (M = Rh(III) and Ir(III)) were used to parametrize a Karplus equation for a H—C(sp^3)—N(sp^3)—H pathway.[352]

Taking conformational flexibility into account when studying the structure of different biological compounds requires the use of an adequate force field. Some of them were compared in carbohydrates to see how well several kinds of experimental data are reproduced.[353] Among them, ^3J couplings were considered for H—C—C—H and C—O—C—H coupling pathways using the equations given by Haasnoot *et al.*[308] and Tvaroska *et al.*,[354] respectively. A modified Karplus type equation was presented, where the effect of Gaussian dihedral angle distributions resulting from harmonic dynamics was considered.[355] ^3J(C,H) couplings were used to carry out a conformational analysis of oligosaccharides[356] and such couplings were also used as probes to detect solvent effects on their conformations. Calculations of *vicinal* carbon–proton coupling in propane, 1-fluoropropane and 2-fluoropropane and their angular dependence were carried out by San Fabián *et al.*[357] Employing standard Gaussian-type basis sets enriched with tight s functions on C and H centres, the experimental angular dependence and substituent effects for these couplings in larger compounds were reproduced successfully.

Wang and Bax[358] reparametrized the Karplus equation for $^3J(H^\alpha,N)$ and $^3J(H^N,C')$,[359] and $^3J(H^N,H^\alpha)$ and $^3J(H^\alpha,C')$ for peptides using uniformly $^{13}C/^{15}N$-enriched human ubiquitin.[359]

The possibility of reproducing *vicinal* ^3J(H,F) couplings employing a Karplus-type equation was explored;[360,361] substituent effects and the angular dependence of ^3J(H,F) throughout the series of fluoroethane, difluoroethane and trifluoroethane were studied at the *ab initio* HF RPA level using various basis sets including tight s functions.[360] Large fluorine substituent effects were found to be more significant when the F substituent is bonded to the same carbon atom as the coupled proton, and the effect of substituent interactions on ^3J(F,H) was found to be negligible.[360] Extended Karplus equations for CHXF—CH_3 and CH_2F—CH_2X (X = CH_3, NH_2, OH and F) were developed[361] where the substituent electronegativity effect was incorporated. Individual substituent effects as well as interaction between substituents effects were taken into account.

Bax *et al.*[362] proposed a new pulse scheme for the simultaneous measurement of $^3J(C',C^\beta)$ and $^3J(C',C^\gamma)$ in proteins uniformly enriched with ^{13}C and ^{15}N. For the former they found a Karplus relation by correlating the ubiquitin values with the backbone ϕ angles from its crystal structure, Eq. (62)

$$^3J(C',C^\beta) = 1.59\cos^2(\phi - 120°) - 0.67\cos(\phi - 120°) + 0.27 \text{ Hz} \quad (62)$$

Stereochemical aspects of ^3J(C,H) couplings through a H—C—C=C pathway were discussed in a set of rigid compounds,[363] and differences between *cis* and *trans* ^3J(C,H) couplings through a vinylic moiety H—C=C—C were discussed in propenoic acids.[364] ^3J(C,C) Karplus-type equations for a C—O—C—C pathway were presented.[11,365] The different factors affecting ^3J(C,C) through such a coupling pathway were identified, especially those across the *O*-glycosidic linkages of oligosaccharides; measurements were complemented with DFT calculations of ^3J(C,C) couplings in model mono- and disaccharides.[11] Special techniques were used to detect $^3J(C_\alpha,C_\delta)$ couplings between aliphatic atoms in proteins. These couplings can be used to determine χ_2 in aliphatic side-chains.[366]

The so-called *W* rule for coupled nuclei continued to be used as a powerful tool to detect conformations.[365] The empirical relationships given by Eqs (63) and (64) for long-range ^nJ(H,H) couplings between the α and the aromatic protons in dibenz[*b*,*f*][1,4]oxapine (**7**) can be used to determine the H_α—C_α—C_{ipso}—C1 dihedral angle, θ.[367]

$$^4J(H_\alpha,H_o) = 0.085\sin^2(\theta/2) + 0.828\ {}^6J(H_\alpha,H_p) - 0.352 \quad (63)$$

$$^5J(H_\alpha,H_m) = 0.527\sin^2(\theta/2) + 0.245\sin^2\theta \quad (64)$$

These relationships were taken from Laatikainen *et al.*'s papers.[368,369]

^4J(H,H) couplings through the H—C—S—C—H coupling pathway in 2-phenyl-1,3-dithiane were found to be positive by Schaefer *et al.*[348] RPA AM1

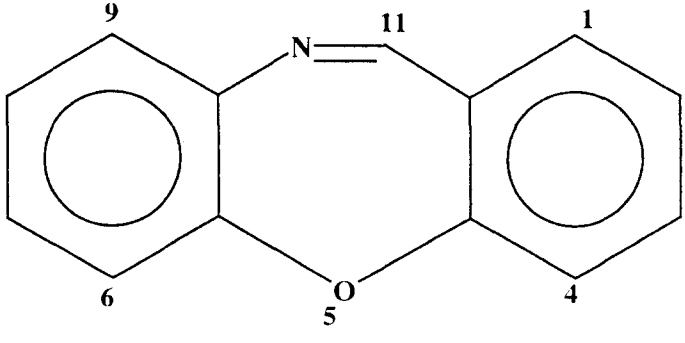

[7]

calculations of ^4J(H,H) involving cyclopropane protons in model compounds were compared with those measured in 17,18-cyclosteroids.[370] In 8-OH-Quinoline $^6J_{2,7}$ and $^6J_{3,6}$ could not be observed.[371] The 6-bond couplings are connected by an extended zig-zag pathway and therefore it can be expected that a positive nonnegligible σ-component is operating. As the corresponding π-transmitted component should be negative, apparently the components compensate each other and this may be the reason why the authors were unable to measure them.[371]

The stereospecific aspects of couplings in difluorodiazine, N_2F_2, were studied, comparing the different couplings in the *cis*- and *trans*-isomers.[372] However, the assignment of different couplings measured in the $^{15}N_2F_2$ isotopomer encountered the problems that are inherent to an $[AX]_2$ spin system. Later, Jaszunski *et al.*[373] performed MCSCF calculations with different degrees of sophistication (different active spaces and different basis sets), reassigning the ^3J(F,F) and ^1J(N,N) couplings in both isomers. In the *trans* isomer, calculations suggest that the experimental assignments of ^1J(N,N) and ^3J(F,F) should be interchanged,[373] leaving an ambiguity in the experimental ^1J(N,N) sign, whose absolute value is $^1J(^{15}N,^{15}N) = 18.5$ Hz. However, calculations[373] yield this coupling as negative, in agreement with values measured[43] in *trans*-azobenzenes, $^1J(^{15}N,^{15}N) = (-15.3 \pm 0.7)$ Hz.

The Si—Si bond force constants in a series of trisilane derivatives were compared with the corresponding ^1J(Si,Si) coupling constants.[374]

In phenyl phosphines, the ^2J(P,C) couplings to the aromatic *ortho* carbon atoms depend on the orientation of the P lone pair; this dependence is given in Eq. (65), where θ is the torsion angle around the C_{ipso}—P bond.[375]

$$^2J(\mathrm{P,C}) = A + B\cos^2(\theta/2) \qquad \text{with} \quad A = (-3.9 \pm 2.0)\ \mathrm{Hz} \qquad \text{and} \quad B = (48.3 \pm 1.8)\ \mathrm{Hz} \tag{65}$$

In phosphanyl ylides, ^2J(P,P) couplings depend strongly on the orientation of the P(III) lone pair with the phosphonio group; they are largest, ~210 Hz, when both moieties are placed with a synperiplanar orientation (**8**).[376,377]

In a set of sulfur diimides bearing the di-*t*-butylphosphinyl substituent, $Bu^t_2(E)P(NSN)R'$ (**9**), Wrackmeyer *et al.*[319] found that both the sign and magnitude of $^1J(^{31}P,^{15}N)$ couplings are predominantly determined by the electronic structure at the N atom. For P(III)—N compounds they found a

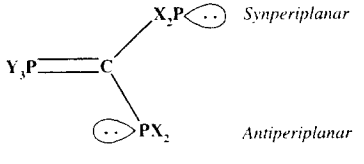

[8]

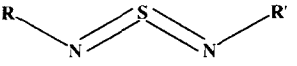

[9]

linear correlation between that coupling and the isotope-induced shift $^1\Delta^{15/14}N(^{31}P)$, Eq. (66).

$$^1J(^{31}P,^{15}N) = -0.85[^1\Delta^{15/14}N(^{31}P)] + 7.13 \qquad (r = 0.98, ^1\Delta \text{ in ppb}, J \text{ in Hz}) \quad (66)$$

New parametrizations for Karplus equations for ^3J(POCH) and ^3J(POCC) couplings were presented by Mooren *et al.*,[378] Eqs (67) and (68). This last differs somewhat from that obtained by Plavec *et al.*,[379] Eq. (69).

$$^3J(\text{POCH}) = 15.3\cos^2\varphi - 6.2\cos\varphi + 1.5 \quad (67)$$

$$^3J(\text{POCC}) = 8.0\cos^2\varphi - 3.4\cos\varphi + 0.5 \quad (68)$$

$$^3J(\text{POCC}) = 9.1\cos^2\varphi - 1.9\cos\varphi + 0.5 \quad (69)$$

New techniques to determine ^3J(P,H) couplings accurately in nucleic acids and protein–nucleic acid complexes were described by Bax *et al.*[380] ^3J(C2′,P) was measured in a 17 kDA protein complex to determine the phosphate conformations of DNA.[381]

In polyoxotungstates ^2J(W,W) couplings were correlated with the sum of both bond lengths, R_1 and R_2, for the vertex W—O—W bridge, and a general trend showing a decrease in ^2J(W,W) with increasing $R_1 + R_2$ was observed.[382]

Linear relationships between the C—Sn—C bond angles of the Me_2Sn moiety and the corresponding $^1J(Sn,C_{Me})$ were presented some years ago by Lockhart and Manders[383] and by Howard *et al.*[384] Caruso *et al.*[385] used such relationships to correlate the C—Sn—C angle, θ, with the magnitude of $^1J(^{119}Sn,^{13}C)$ and $^2J(^{119}Sn,^1H)$ in derivatives of X_2SnQ_2 (X = Me, Ph, benzyl, cyclohexyl, Cl or Bu^t) (Q = 1-R′-3-methyl-4-R″(C=O)-pyrazol-5-one). The former equation gave values of θ for these compounds that are notably different from those measured in solid state for the same compounds. It is interesting to note that in such compounds the tin atom is in a strongly distorted octahedral environment, which causes $^1J(^{119}Sn,^{13}C)$ couplings to be much larger (in absolute value) than those found in a tetrahedral environment. The C—Sn—C angles in tin(IV) and organotin(IV) complexes containing monodentate or bidentate N-donor ligands were estimated[386] using the Lockhart equation,[383] deduced from dimethyltin derivatives[387] and the Holoecek equation, deduced from di-*n*-butyltin(IV) derivatives.[388] Lockhart *et al.*'s equation[383] was also used by Shreeve *et al.*[389] in compounds of type

$R_3SnN(SO_2CF_3)_2$, where at the tin atom a highly flattened tetrahedral geometry was found. On the other hand, such empirical equations applied to the NMR data of diorganotin complexes of 2,2′-bipyrimidine, and similar complexes, suggest that tin atoms have a coordination number between 5 and 6.[390] However, Lockhart and Manders' equation[383] was considered of questionable value by Wrackmeyer *et al.*[391–393]

Experimental data showing that ^3J(Sn,Sn) and ^3J(Sn,Si) couplings satisfy a Karplus-type dependence with the dihedral angles (θ) ^{119}Sn—C—C—^{119}Sn and ^{119}Sn—C—C—^{29}Si, respectively, were given by Mitchell and Kowall,[394] Eqs (70) and (71). Theoretically, at the RPA MNDO level,[268] Karplus type dependences for $^3J(^{119}Sn,^{119}Sn)$ and $^3J(^{119}Sn,^{13}C)$ calculated values were fitted with Eq. (72).

$$^3J(^{119}Sn,^{119}Sn) = 580 - 79\cos\theta + 395\cos 2\theta \quad \text{(in Hz)} \tag{70}$$

$$^3J(^{119}Sn,^{29}Si) = 52 - 9\cos\theta + 45\cos 2\theta \quad \text{(in Hz)} \tag{71}$$

$$^3J(^{119}Sn,M) = A + B\cos\theta + C\sin\theta + D\cos 2\theta + E\sin 2\theta \quad \text{(in Hz)} \tag{72}$$

For M = Sn, $A = 224.1 \pm 12.3$, $B = -136.2 \pm 4.2$, $C = 10 \pm 20.4$, $D = 185.5 \pm 9.2$, and $E = 6.3 \pm 4.6$, which follows a similar trend to the experimental one, but coefficients are undervalued by a factor of ~ 2. In Eq. (72) for M = C, $A = -8.71 \pm 0.43$, $B = 5.31 \pm 0.14$, $C = -0.06 \pm 0.071$, $D = -6.35 \pm 0.33$, and $E = -7.35 \pm 0.16$, which also seem to be undervalued. For both *cis* and *trans* conformations the respective RPA AM1 calculated ^3J(Sn, C) couplings are larger, suggesting a better agreement with experimental values.[268]

Karplus-like behaviour of ^3J(Hg, C) couplings was used in chloromercurio aliphatic acids to determine the Hg—C—C—C dihedral angle preferential conformation.[395]

Other empirical trends

In *o*-substituted acetanilides (**10**), $^1J(C_3,H_3)$ were linearly correlated[396] with the Swain and Lupton *F* parameter,[397] Eq. (73).

$$^1J(C_3,H_3) = (14.5 \pm 2.2)F + (158.3 \pm 0.7) \quad \text{(in Hz)} \tag{73}$$

The stereospecific influence of the N^+—O^- group on ^1J(C,C) couplings in a series of nonaromatic amine oxides was discussed in detail by Potmischil *et al.*,[398] who compared it with the N lone pair orientational effect on that type of coupling.[22,399–401]

Kamienska-Trela *et al.*[402] measured the different ^1J(C,C) couplings in tetramethyl 9a*H*-quinolizine-1,2,3,4-tetracarboxylate and in a series of its alkyl

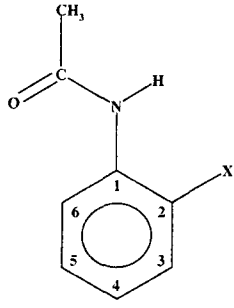

[10]

derivatives and found that such couplings are not correlated with the respective C—C bond lengths. Witanowski *et al.*,[403] when studying nitro group effects on ^1J(C,C) couplings in nitroalkanes, established a linear correlation between ^1J(C,C) couplings in $(CH_3)_2C(X)NO_2$ compounds and the X Pauling electronegativity, E_x, Eq. (74).

$$^1J(C,C) = 3.60E_x + 28.7 \quad \text{(in Hz)} \tag{74}$$

Several structural and electronic effects on $^1J(^{29}Si,^{15}N)$ were studied in *N*-silylated anilines, where the N atom has a planar configuration.[404] Their dependence on the Si—N bond length was also studied.[405] ^1J(Si,Si) couplings in halogenated disilanes are very sensitive to substituents. Interestingly, such couplings do not correlate linearly with the substituent electronegativities,[406–408] but they follow Eq. (75).

$$^1J(Si,Si) = 781.8 - 112.8(\Sigma EN) + 4.51(\Sigma EN)^2 \quad \text{(in Hz)} \tag{75}$$

where ΣEN stands for the sum of the electronegativities of the substituents. This correlation predicts a very large coupling in F_5Si_2H, ^1J(Si,Si) = 491.6 Hz. On the other hand, in halogenate trisilanes ^1J(Si,Si) couplings correlate with valence force constants,[409] paralleling results found previously by Kamienska-Trela[410] for ^1J(C,C) couplings.

Very large substituent effects on ^1J(C,C) couplings were reported previously by Kamienska-Trela *et al.* for substituted ethylenes[411] and for substituted acetylenes.[412] More recently, Kamienska-Trela *et al.*[413] also found a very large sensitivity to substituents in $^1J(C_1,C_2)$ couplings in substituted benzenes. As in the disilanes mentioned above, these substituent effects also do not correlate linearly with the substituent electronegativity. Using least-square fitting, Kamienska-Trela *et al.*[413] found the relationship depicted in Eq. (76).

$$^1J(C1,C2) = 30.57 + 29.82\ln(E_x) \quad \text{(in Hz)} \tag{76}$$

where E_p is the Pauling electronegativity.

The smallest values of ^1J(C,C) couplings so far reported for mono-substituted benzenes are ^1J(C1,C2) = 29.5 Hz[413] and ^1J(C1,C2) = 27.8 Hz.[414]

Additivity of substituent effects on ^1J(C,C) couplings in several substituted nitrobenzenes was reported.[415] Such couplings were also calculated with the INDO-SCPT method[115] and in general a satisfactory agreement with experimental data was found.[415]

3.2. Proximity effects

When there are two moieties, M^1 and M^2, in close proximity belonging either to the same molecule or two different ones, two different phenomena may arise: (a) a coupling constant between two nuclei each belonging to a different moiety, which is described as transmitted through space, J^{TS}; (b) a coupling constant between two nuclei belonging to the same moiety, e.g. M^1, can be affected by the proximity to M^2. A very important case is when the proximity of M^1 and M^2 is through a contact of type X—H...Y. If Y is an electronegative atom, such a contact is known as a hydrogen bond.[416] If Y is a metal atom, the contact is called an agostic interaction.

Various interactions are involved in hydrogen bonding.[417,418] The electrostatic interaction shortens the X—H bond,[61,419] while the charge transfer interaction lengthens it, corresponding, respectively, to a blue shift and a red shift in the IR frequencies. Interestingly, there are cases where there is a very small charge transfer interaction between the two proximate moieties, and, nevertheless, an important J^{TS} component was measured. Exchange interactions, which are repulsive between two proximate moieties, are important in defining some coupling pathways.[231] They could also be important in defining a J^{TS} coupling. This calls for some caution in concluding that the existence of a J^{TS} coupling is an indication that there is a bond with some degree of covalency connecting the moieties.

Through-space transmission between two proximate moieties

One of the interesting features of J^{TS} couplings is that their sign can depend on the relative orientation of bonds containing the coupled nuclei.[420] For this reason it is important to determine their signs experimentally to obtain stereospecific information.

For J^{TS}(H,H) couplings, although the possibility of positive values was theoretically predicted,[421] so far only negative values have been reported. The ^5J(H,H) between the methyl moiety and protons placed *ortho* to the OMe group in aryl methyl ethers continued to be used as probe to detect the preferential conformation of the OMe group.[422] In 2-formylstyrene ^5J(H,H) = −0.16 Hz was measured between the formyl and methine (α) protons and its relationship with the side-chain conformation was discussed.[423]

A brief overview of results obtained with the INDO-IPPP-CLOPPA[66,266] approach was published,[17] in which special attention was paid to the study of J^{TS} couplings. INDO wavefunctions are known to fail in describing several experimental trends of coupling constants. However, they can describe and predict many experimental trends, at least on a qualitative base. Perhaps the most conspicuously successful cases for J^{TS} components are those of J(H,H), J(F,F), J(P,P), J(Se,Se), and those of the indirect through-space transmission of J(C,X) couplings via an intermediate bond, either C—H or C—F (X = H, F, P, Se).[17] But the dependence on θ (see (**11**)) of J^{TS}(F,H) couplings cannot be

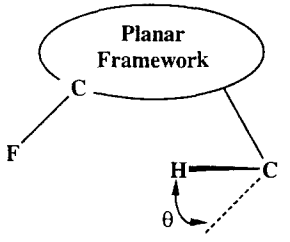

[11]

described correctly at the INDO level. For values of θ smaller than ~30–40°, they are negative, while they are positive for larger angles.[420] Schaefer *et al.*[424] reported ^5J(F,H) = +0.74 Hz in 1,1,1-trifluoro-2-phenylethane. A detailed analysis, based on the INDO MO FPT approach, of the dependence of such coupling with the torsion angle between the C(sp^3)—C(sp^3) bond and the aromatic plane was reported. The corresponding ^4J(C,F) = ±0.70 Hz was measured, but its sign could not be determined.[424] Kane *et al.*[425] reported both J^{TS}(F,H) and J^{TS}(C,F) couplings in 2-phenyl-4-methyl-1,2,4-triazole between the F atom and the methyl moiety. Interestingly, in the corresponding ethyl derivative only the J^{TS}(F,C) coupling was observed. This suggests that in the latter compound the main ethyl conformation corresponds to a θ angle (see (**11**)) where the corresponding J^{TS}(F,H) coupling is close to zero. Under such conditions, the indirect through-space J^{TS}(C,F) coupling via an intermediate C—H bond is not zero.[420] $^7J^{TS}$(H,F) and $^6J^{TS}$(C,F) were reported in α-anomers of 2′,3′-dideoxy-4′-fluoroalkyl nucleosides[426] and (fluoromethyl)nucleosides.[427] The F···H contact is considered a hydrogen bond because such couplings depend on the ability of the solvent to make intermolecular hydrogen bonds.[426,427] In the latter work, both ^7J(F,H) and ^6J(F,C) couplings were measured in different solvents whose Kamlet–Taft solvatochromic parameters β were used as indicators of the empirical hydrogen bond acceptor ability. Values of both types of couplings correlate linearly with that parameter.[427] J^{TS}(C,F) couplings were used by Matsubara *et al.*[428] to assign configurations in trifluomethylvinyl compounds. An example is given where, for the same C···F

distance, the J^{TS}(C,F) coupling could not be observed[428] for a quaternary carbon atom, stressing the importance of a C—H bond in mediating such interaction.[429] A very large $^5J^{TS}$(F,HO) = 9.3 Hz (sign not determined) was reported in (**12**).[430] It is important to note that in this C—F···H—O contact a

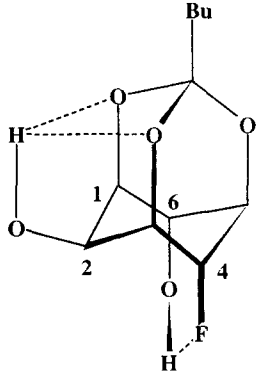

[12]

red shift of the OH IR frequency was reported, indicating that the charge transfer interaction effect on the O—H bond length is more important than the electrostatic interaction. Another interesting example of J^{TS}(F,H) was reported by Polonski *et al.*[431] in the 2,6-bis(2,6-difluorophenyl)piperidine system (**13**). A

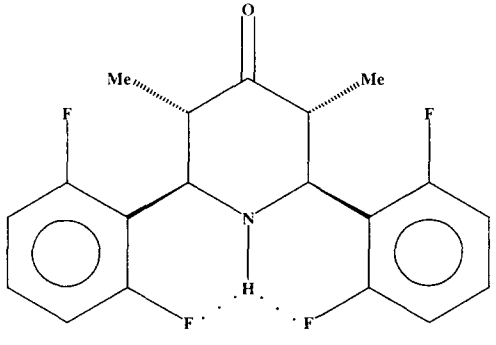

[13]

three-centre CF···HN intramolecular hydrogen-bonding interaction takes place, and $^5J^{TS}$(F,H) = 4.9 Hz was measured (sign not determined). The X-ray structure indicates that the F···H distance is 2.25 Å and a blue shift in ν(NH) was observed compared with the corresponding IR frequency in a similar compound in which the phenyl group does not contain F atoms (3444 cm^{-1} and 3297 cm^{-1}, respectively). This indicates[419] that in this three-

centre CF···HN hydrogen bond the electrostatic effect on the N—H bond length overcomes that of the charge transfer interactions, n(F)→(N—H)*. It is probable that the three-centre $F_a \cdots H \cdots F_b$ interaction inhibits the simultaneous n(F_a)→(N—H)* and n(F_b)→(N—H)* charge transfer interactions while the electrostatic one is reinforced owing to the presence of both F atoms.

In 2-(diphenylphosphino)benzaldehyde, Schaefer *et al.*[375] determined that, for a formyl C—H bond in an all-*cis* conformation to the P lone pair ($\theta = 0°$), $^4J(C\underline{H}O,P) = -7.1$ Hz and $^3J(\underline{C}HO,P) = +29.4$ Hz. Using the INDO MO FPT approach, they found that calculated values for the former closely follow Eq. (77).

$$^4J(C\underline{H}O,P) = -13.8\cos^2\theta \quad \text{Hz} \qquad (0 \leqslant \theta \leqslant 68°) \tag{77}$$

and that for $\theta > 75°$ this coupling becomes positive, resembling the trend known for J^{TS}(F,H) couplings.[420] In 2-(2′,4′-difluoro)-3-alkyl-4,5,6,7-tetrahydroindazoles,[432] the following couplings between the F atom *ortho* to the N atom and atoms in the alkyl moiety (**a**, CH_3; **b**, CF_2H; **c**, CF_3) were reported (signs not given):[432] **a**, ^6J(F,H) = 1.8 Hz and ^5J(C,F) = 3.8 Hz; **b**, ^6J(F,H) = 0.5 Hz, ^6J(F,F) = 3.3 Hz, and ^5J(C,F) = 3.3 Hz; while in **c**, ^6J(F,F) = 4.6 Hz and its corresponding ^5J(C,F) coupling could not be observed. This is in agreement with earlier predictions[429] that indicate that a C—F bond is quite inefficient in mediating in the transmission of J^{TS}(C,F) in a C—F···F—C pathway. J^{TS}(C,F) and J^{TS}(F,H) couplings of like sign in 8-fluoro[2.2]metaparacyclophane[433] and in 4-fluoro[2.2]paracyclophane[434] were reported.

Jones *et al.*[435] reported a ^6J(C,F) = 5.5 Hz in 9,10,11,12-tetrafluoro-5,6-dihydrobenzo[*b*]naphth[2,1-f]oxepine, where the F···H distance between the coupled F nucleus and the H nucleus bonded to the coupled carbon atom was calculated with the MM3 approach as 2.449 Å. They ascribed the origin of such coupling to the n(F)→(C—H)* charge transfer interaction. The important influence of electron delocalizations on coupling constants suggests that a charge transfer interaction between two proximate moieties favours a J^{TS} transmission. For instance, $^4J(N,H_{Me}) = 0.13$ Hz was measured[436] in 2-OMe-pyridine (**14**), and an n(N)→(C_{Me}—H_t)* interaction of 0.95 kcal mol^{-1} was

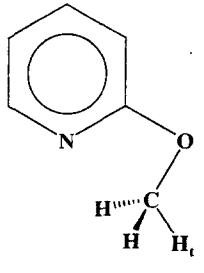

[14]

calculated.[12] However, a charge transfer interaction is not a *sine qua non* condition for transmitting a J^{TS} coupling. Such an observation calls for caution in assigning some covalent character to ionic bonds where couplings through them are observed, for instance $^1J(^{29}Si,^7Li)$ couplings.[437]

Although most J^{TS}(C,X) couplings (X = H, F, P, Se) are indirect couplings via an intermediate C—H bond, other pathways were recently reported. For instance, in tricarbonylchromium complexes of biphenyl derivatives, J^{TS}(C,F) coupling pathways are thought to involve a direct interaction between the p orbital of the F atom and either the π or the π^* orbitals of the CO triple bond.[438] In chelate phosphitodicarbonyl chromium and dicarbonyl(phosphine)chromium complexes with fluorobenzenes, the J^{TS}(F,C) contribution was assumed to dominate the J(C,F) couplings between the aromatic F and the carbonyl C nuclei and its magnitude was taken as a measure of the twist angle of the chromium tripod.[439] A direct C...P pathway was studied by West *et al.*[440] in *in*-phosphaphanes involving C atoms of the basal aromatic ring; effects of ring substituents on such couplings were also discussed. A similar J^{TS}(P,H) = 3 Hz, in a tetrahydroanthracene ruthenium(II) complex, Ru(η^6-$C_{14}H_{14}$)$Cl_2(PPh_3)$ was reported.[441]

In the previous review[1] examples of J^{TS} couplings whose transmission is mediated by an intermediate moiety were quoted. During the period of this review an interesting example was presented by Jirman *et al.*[442] in which the transmission of J^{TS} is assumed to be mediated by the Ni orbitals in square-planar Ni(II) complexes of the Schiff base of (s)-2-(*N*-benzylprolyl)aminobenzophenone and glycine.

Prior to the review period, the FC term of J^{TS} transmitted through the overlap of lone pairs of two proximate atoms was studied using the IPPP approach.[66] The following cases were considered: two *geminal* P atoms;[443] two *vicinal* P atoms;[444] two *vicinal* Se atoms;[445] and the proximity of two F atoms.[271,446] One of the main features found in all of them is that the corresponding K^{TS} is positive, i.e. its sign, as expected, does not depend on the number of formal bonds separating the coupled nuclei. The transmission of J^{TS} by overlap of proximate lone pairs was studied in detail more recently,[447] considering in particular the influence of each bond contribution.[266] J^{TS} depends mainly on the overlap of the two proximate lone pairs, which corresponds to a reduced $K^{TS} > 0$. Subsequently several unusual J(P,P) couplings involving P(III) atoms were published that seem to support that theoretical prediction, i.e. they are large and positive couplings owing to the overlap of their lone pairs. A few examples are as follows. In 1,2-C_6H_4(PRPh)(PPh_2), ^3J(P,P) = 156 Hz (R = Me) and 155 Hz (R = Bu).[448] Kessler *et al.*,[449] for some rhodium complexes, measured several J^{TS}(P,P) couplings, for example, ^4J(P,P) = 243.93 Hz for a P···P distance d(P···P) = 3.35 Å. They assumed that such couplings depend on $1/r^3$, where r is d(P···P),[450] but with the data they had available the plot of J^{TS}(P,P) vs $1/r^3$ was not linear. In 9,9-dimethyl-4,5-bis(diphenylphosphino)xanthene,

^{6}J(P,P) = 27.3 Hz was reported, where an X-ray study showed that d(P...P) is 4.1 Å.[451] ^{8}J(P,P) = 72.8 Hz where d(P···P) = 3.67 Å was reported.[452] ^{8}J(P,P) = 27.5 Hz in a sterically congested bis(phosphite) ligand was reported by Pastor *et al.*[453] ^{7}J(P,P) = 4.8 Hz was reported by Perera *et al.*[454] in an azine diphosphine, and such coupling was not observed in the corresponding dioxide. ^{7}J(P,P) = 22.0 Hz was reported in an (S,*S*),(*R*,*R*)-2,2″-bis[1-(diarylphosphino)ethyl]-1,1″-biferrocene and was taken as evidence of a close proximity between the P lone pairs.[455] The importance of the overlap of P lone pairs between phosphino groups placed *ortho* to each other in substituted benzenes in defining the respective ^{3}J(P,P) coupling was discussed in detail by Hitchcock *et al.*[456] In (**15**), ^{3}J(P,P) = 140.8 Hz, while in (**16**), ^{3}J(P,P) ~20 Hz was measured.[456] Examples where the ^{2}J(P,P) value depends strongly on the overlap of the P lone pairs were discussed by McFarlane *et al.*[457] For instance, in (**17**) for R = H, ^{2}J(P,P) = 98 Hz, while for R = CH_3, ^{2}J(P,P) = 8 Hz, and for R = Ph, ^{2}J(P,P) = 2 Hz. In 1,1′-bis-(diphenylphosphino)octamethylferrocene, J^{TS}(P,P) = 4 Hz was reported.[458] In a set of bis(phosphino)amines where the P lone pairs do not overlap in the preferential conformations, ^{2}J(P,N,P) couplings between 12 and 20 Hz were reported.[459]

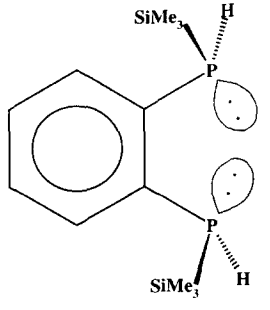

[15]

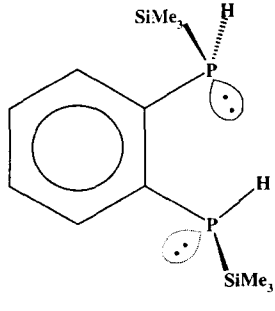

[16]

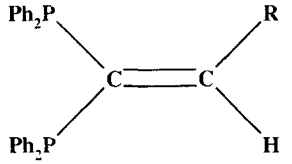

[17]

Several interesting features of J^{TS}(F,F) couplings were discussed by Ernst *et al.*[433,434,460,461] For instance, $J^{TS}(F,F) > 0$ was determined in *syn*-ar,ar′-difluorometacyclophanes and they determined that this sign does not depend on the relative orientation of the C—F bonds containing the coupled nuclei.[461] The dependence of J^{TS}(F,F) on the F···F distance was discussed[460] and compared with earlier estimates.

Distortions in the structure of hexafluorobutadiene upon coordination to ruthenium were gauged, comparing how different J(F,F) couplings measured in [RuCl(η^5-C_5Me_5)(η^4-C_4F_6)][462] are from those measured in free hexafluorobutadiene.[463] The largest change takes place in $^5J(F_M,F'_M)$ (**18**), which increases upon complex formation from 11.31 Hz to 24 Hz, while the corresponding F···F distance in the solid state was measured as 2.78 Å,[462] which is shorter than that measured in the free diene, 3.04 Å.[464]

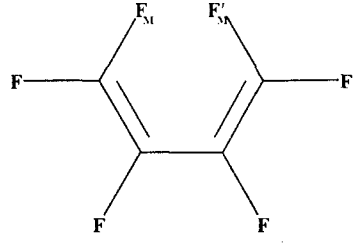

[18]

In $C_3H_7CH(HgCl)COOH$, ^5J(Hg,H) = 125.10 Hz was assumed to be dominated by a J^{TS} component.[395]

Couplings transmitted through a hydrogen bond were reported in several compounds with an OH *peri* to a CHO group, where ^3J(*HO*–C*HO*) couplings of ~1.2 Hz were measured,[465] (**19**). J(C,H) couplings through a C=O···H—O pathway in tautomeric structures like (**20a**) and (**20b**) are such that the sum of J(C3,H) + J(C1,H) correlates linearly with the OH proton chemical shift both for compounds displaying tautomerism and those with localized hydrogen bonds.[466] J(F,H) long-range couplings transmitted through an F...H hydrogen bond were studied in 2-fluoro-*N*-methylbenzamide (**21**).[467] Comparison of the ^3J(F,C) coupling with the carbonyl C atom in *N*-methyl-2-fluorobenzamide

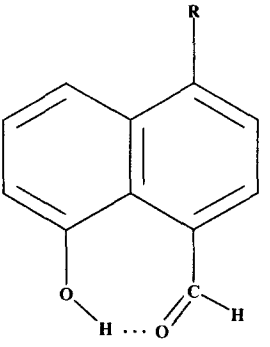

[19]

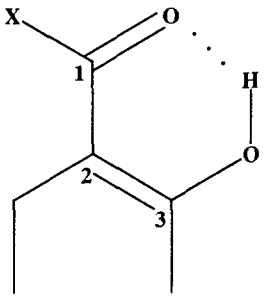

[20a]

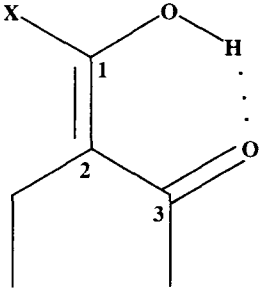

[2ba]

and in *N*,*N*-dimethyl-2-fluorobenzamide (3.3 Hz and 0.0 Hz, respectively) suggests that this coupling is also transmitted through the F...H hydrogen bond.[467] On the other hand, in (**21**) ^4J(F,N) was found to be solvent dependent, taking values of −7.4 Hz ($CDCl_3$), −6.7 Hz (CCl_4), −4.9 Hz (acetone-d_6) and −2.8 Hz (DMSO-d_6).[467] Negative signs were assumed according to IPPP-INDO calculations, which indicate that this is a coupling mainly transmitted

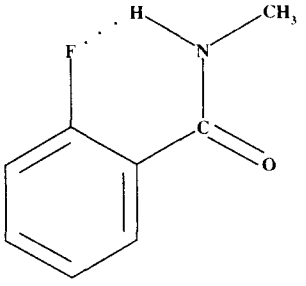

[21]

via the F···H—N hydrogen bond. Recently, J(F,H) couplings transmitted via an F···H—N hydrogen bond were also reported in urolobin difluoroboron complexes.[468]

$^{2}J(^{15}N,^{15}N)$ ~7 Hz were reported in Watson–Crick base pairs in ^{15}N-labelled RNA. They were observed between N3 of uridine (U) and N1 of adenosine (A), (**22**) and between N1 of guanosine (G) and N3 of cytidine (C) (**23**).[469] Such

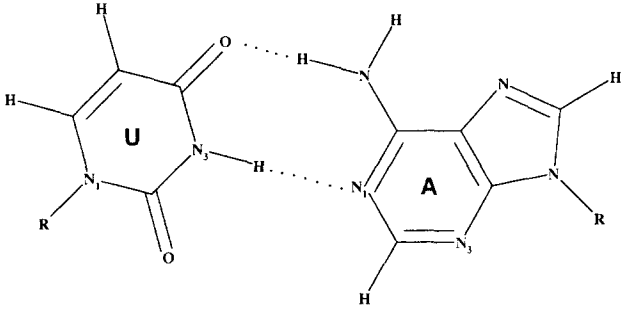

[22]

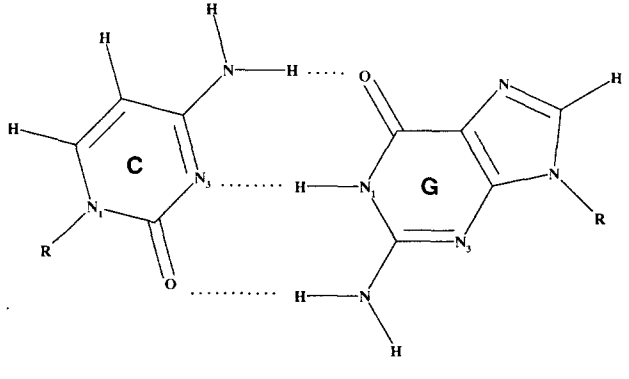

[23]

$^2J(^{15}N,^{15}N)$ coupling is larger than most nitrogen couplings over two bonds. For instance, $^2J(^{15}N,^{15}N) = 5.3$ Hz across the carbonyl carbon atom in $(CH_3NH)_2C{=}O$.[470] Typically this coupling pathway leads to a $^2K > 0$ of a large absolute value.[471] Such $^2J(^{15}N,^{15}N)$ couplings in U···A and G···C are similar to those studied by Galasso[146] in the diazacyclodecyl cation with the EOM approach,[144,145,472–474] for which a theoretical value of $^2J(^{15}N,^{15}N) = +10.1$ Hz was obtained. Galasso stresses the fact that the N—H—N bond is a four-electron three-centre bond, and that it corresponds to a strong hydrogen bond.

Hydrogen-bonding interactions

The effect of steric hindrance around the N atom on $^1J(^{15}N,^1H)$ couplings was discussed by Wong *et al.*[475] Abnormally small $^3J(H,H)$ couplings were reported for H atoms near a *t*-butyl group.[476] They were rationalized as originating in a lengthening of the C—C bond lying along the H—C—C—H coupling pathway owing to the steric demand of this bulky group.[476]

The highly stereospecific inter-proton $^5J(H3,CHO)$ coupling in benzaldehyde derivatives was found to be perturbed by the intramolecular hydrogen bond in salicylaldehyde, reducing such coupling about 25%.[477] Similarly, the fluorine–proton coupling $^5J(F3,CHO)$ in 3-fluorosalicylaldehyde is decreased about 50% from the corresponding value in 3-fluorobenzaldehyde.[477]

$^1J(A,H)$ couplings in A—H···X contacts. For A—H bonds participating in an A—H···X contact, in most cases the electrostatic part yields an increase in the absolute value of the corresponding $^1J(A,H)$ coupling, while a decrease is observed owing to the charge transfer contribution.[419] In addition, the former yields a slight shortening while the latter produces a slight lengthening of the corresponding A—H bond length.[61] However, there does not seem to be a linear correlation between the strength of each interaction and the respective effects on bond length and coupling. Measurements of $^1J(C,H)$ couplings for C—H···X interactions, where X is an electronegative atom, were experimentally reported to yield an increase in that coupling.[134,478,479] For instance, the C—H···N interaction in a large set of hetaryl vinyl ethers where the vinyl H_α proton is proximate to the endocyclic N atom, causes an increase in the $^1J(C_\alpha,H_\alpha)$ coupling in the range 6–7 Hz.[480] A decrease in $^1J(C,H)$ due to the intermolecular interaction in the NCH/H_2O complex was calculated theoretically.[133] Using the *ab initio* version of the CLOPPA approach,[61,135] it was shown that when an electric field is applied along the C—H bond, which in this case is also along the π electronic system, the π-transmitted component decreases algebraically.[61] The effect of the intramolecular electric field on $^1J(C,H)$ couplings was studied in a few 5-substituted salicylaldehydes (**24**), where the conformation of the CHO group is fixed and pointing towards the substituent placed at ring position 5. Changes on $^1J(C,H)$ couplings of the

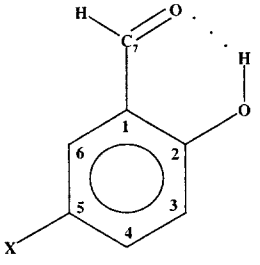

[24]

CHO moiety were reported to correlate linearly with changes of the component of the calculated electric field along the C—H bond at the formyl proton.[481] Kolehmainen *et al.*[482] studied analogous derivatives of salicylaldoximes, (**25**), where similar effects on ^{1}J(C7,H7) are expected. For (**24**) and (**25**) the ^1J(C7,H7) couplings are compared in Table 12 for the same X substituents; given the similarity of both configurations, it is concluded that the electric field effect on ^{1}J(C7,H7) is larger in (**24**) than in (**25**). For X = NO_2 in (**24**), an

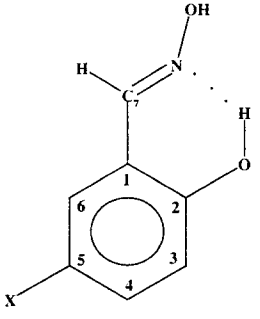

[25]

Table 12. Comparison between ^1J(C7,H7) couplings (in Hz) in (**24**) and (**25**). Changes on ^1J(C7,H7) in (**24**) were linearly correlated with the *ab initio* calculated electric field component along the H7—C7 bond due to the X substituent.[481]

X	(**24**)[a]	(**25**)[b]
H	177.69	166.2
OMe	178.10	166.5
Br	182.13	168.1
Cl	182.02	168.1
NO_2	185.05	170.1

[a] Taken from ref. 481.
[b] Taken from ref. 482.

important substituent effect (~4 Hz) is also observed for ^{1}J(C3,H3) which is similar to that reported by Ibrom and Frahm[483] for a nitro *meta* effect in other aromatic compounds.

An electric field along a C—H bond pointing from the H atom towards the C atom yields a decrease in the corresponding ^1J(C,H) coupling.[484]

How O—H...O interactions affect the respective $^1J(^{17}O,^1H)$ coupling is observed in their concentration and temperature dependence in cyclopentanol (**26**) and related compounds.[485] The observed trends were rationalized[485] as

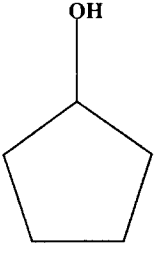

[26]

originating in self-association of cyclopentanol molecules. At 75°C for concentrations ranging from 5 to 0.1 mol l^{-1} in acetonitrile, $^1J(^{17}O,^1H)$ values range from 56.0 Hz to 79.8 Hz. For a fixed concentration, $^1J(^{17}O,^1H)$ increases with increasing temperature; for instance, for 0.5 mol l^{-1} acetonitrile concentration it ranges from 67 Hz at 35°C to 79 Hz at 75°C.[485] Self-associations are defined by hydrogen-bond interactions of type O—H···O where both strong n→(O—H)* charge transfer and electrostatic interactions are operating and, therefore, experimental results suggest that the n→(O—H)* charge transfer effect on this coupling overcomes the corresponding electrostatic effect and yields a reduction of $^1J(^{17}O,^1H)$ (see Section 3.3). The $^1J(^{17}O,^1H)$ values for cyclopentanol should be compared with the corresponding coupling measured in monomeric water, i.e. 79 Hz.[486]

^1J(N,H) in pyridine solutions of proton donor solvents was shown to increase from 12 Hz in *o*-tolylic acid (**27**) to 57 Hz in 2-thiophenecarboxylic

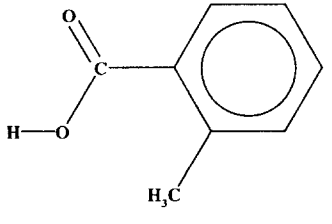

[27]

acid (**28**), and this difference was taken as a measure of the greater acidity on the latter compound.[487] On the other hand, for solutions of pyridine in nitric acid ^1J(N,H) = 90.8 Hz was measured.[487] The possibility of using ^1J(N,H) couplings to study hydrogen bonds was also discussed by Hansen *et al.*[488]

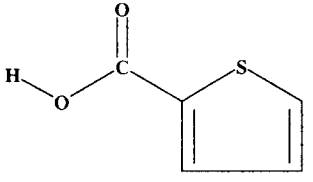

[28]

^1J(N,H) couplings were used as probes to detect the protonation site in *N*-aminoazoles, where absolute values of such couplings are ~104 Hz.[489]

^1J(C,H) couplings in two-electron three-centre C—H—X bonds were reported in several cases. For X = C, EOM-CCSD[137,150,182] calculations were carried out on ethyl carbocations,[190] giving ^1J(C,H) = 13.01 Hz. Galasso,[146] using the EOM approach,[144,145,472–474] obtained values of ^1J(C,H) couplings of ~32.5 Hz, which are in good agreement with experimental results in cyclodecyl cations and related systems. For agostic interactions with ^1J(C,H) = 75 Hz (X = Pt)[490] and ^1J(C,H) = 98 Hz (X = Th)[491] were reported, while for X = Ta, ^1J(C,H) couplings as small as 70 Hz were reported.[492] Similarly, for agostic interactions of type Si—H—Zr, an unusually small value for ^1J(Si,H) of 113.2 Hz was reported,[493] while in silicon hydrides in general coupling of this type ranges from 160 to 200 Hz.[493] For agostic species involving phosphine and phosphite complexes with terminal hydride complexes, J(P,H) are ~12 Hz, and in rhodium ethylene hydride complexes, J(Rh,H) are ~15–18 Hz.[494]

Juranic *et al.*[60,495–497] observed that in protein main-chain amide groups the ^1J(N,C′) coupling constant is a good probe for discriminating between predominantly N—H···O and predominantly C=O···H hydrogen bonds. Absolute values of this coupling smaller than 15 Hz correspond to strong N—H···O hydrogen bonding, while absolute values close to 18 Hz indicate a strong C=O···H hydrogen bond. This N—H···O experimental trend resembles theoretically determined trends for N—H···O and C—H···O interactions in the model systems NH_3/H_2O[498] and CH_4/H_2O,[134] respectively. While there was an increase of ^1K(X,H) in the X—H (X=N,C) bond involved in the X—H···O interaction, decreases were observed in ^1K(X—Y) couplings corresponding to other atoms bonded to X. On the other hand, the experimental trend for the amide ^1J(N,C′) coupling when there is a C=O···H hydrogen bond is in line with theoretical results[419] that show that this hydrogen bond inhibits the strong intracarbonyl group $n(O) \rightarrow (C_C—X)^*$ charge transfer

interactions. An inhibition of charge delocalization into the (N—C′)* antibond causes an increase in the corresponding ^1J(N,C′) coupling.

Geminal J(H,H) and J(P,H) couplings in CH_2 and PCH moieties were reported to increase algebraically when one of the C—H bonds participates in a C—H···LP interaction.[499] This effect was ascribed to an increase in the DSO term due to the larger contribution of electrons inside the sphere whose diameter is defined by both coupled nuclei.[500]

3.3. Intramolecular electron delocalization interactions

In this section, papers will be reviewed that discuss coupling trends where the experimental results can be rationalized in terms of stereospecific interactions involving electron delocalization. In few cases, theoretical approaches that allow decomposition of calculated couplings in terms of different contributions[17] were used to gain insight into the effect of stereoelectronic interactions on couplings. The interactions considered here are: σ conjugation, $\sigma \rightarrow \sigma^*$; hyperconjugation, $\sigma \rightarrow \pi^*$ and $\pi \rightarrow \sigma^*$; anomeric effect, $n \rightarrow \sigma^*$; and other lone pair orientational effects. The last-mentioned effects were discussed by Gil and Philipsborn in their classic review;[400] by Jameson[136] and, using the CLOPPA approach,[266] by Contreras *et al.*[401] For J(C,C) couplings they were discussed by Krivdin and Kalabin,[399] by Krivdin and Della[224] and by Kamienska-Trela.[22]

A few trends relating a variety of couplings with electron delocalization interactions as given by the Weinhold *et al.*'s natural bond orbital (NBO) method[501] have been discussed.[58,59,502] The NBO approach provides a quantitative way to study electron delocalizations and it has the potential for rationalizing several trends of coupling constants. Unfortunately, so far, no approach has been presented where calculations of couplings in terms of electron delocalization interactions are carried out.[503] The characteristics of the electron delocalization interaction are well known from simple PMO theory.[504] They can be used in conjunction with the CLOPPA analysis of couplings[266] (Section 2.2.) to obtain interesting insights into the physicochemical factors affecting the couplings.

NBOs were conceived as a 'chemist's basis set' since they correspond closely to the picture of localized bonds and lone pairs as basic units of molecular structure. The procedure for obtaining them starts from the one-particle density matrix, from which a set of orthonormal NBOs is obtained. The transformation from canonical orbitals to NBOs includes several steps that are not described here, but it is important to stress that the main contribution to the total density matrix comes from a set of one- and two-centred 'occupied' orbitals, ω, the former being identified either as core orbitals or lone pairs and the latter as σ or π bonds. The transformation also yields 'unoccupied' orbitals, ω^*, that are identified as σ or π antibonds (σ^* or π^*) or extra-valence-shell

Rydberg orbitals. The contribution to the total density matrix from unoccupied orbitals is generally small; however, antibonds play an important role since they represent unused valence-shell capacity. The energy of a molecule can be decomposed into two components associated with covalent and noncovalent structures; the former corresponds to the ideal Lewis contributions, and the latter is associated with non-Lewis contributions. The nondiagonal elements of the Fock matrix in the NBO basis are interpreted as the stabilizing interaction between occupied orbitals of the formal Lewis structure and unoccupied ones. Since the corrections to the energy of the Lewis-type picture are usually small, they can be approximated by second-order perturbation theory, Eq. (78),

$$\Delta E^{(2)}_{\omega\omega^*} = -2\,\frac{\langle \omega \,|\, \hat{F} \,|\, \omega^* \rangle}{\varepsilon_{\omega^*} - \varepsilon_{\omega}} \tag{78}$$

where ε_{ω} and ε_{ω^*} stand for the NBO orbital energies. The NBO perturbative framework allows one to apply qualitative concepts of valence theory to describe the noncovalent stabilizing energy.

Weinhold *et al.*[58,59,502] used second-order perturbation theory estimates of NBO orbital interactions, $\Delta E^{(2)}$, to obtain a qualitative description of the physical origin of the angular dependence of several calculated couplings in a model peptide. They compared plots of such estimated interactions with those of the Fermi contact contribution calculated using several *ab initio* SOS approaches.[64] It should be recalled[1] that such an SOS scheme does not take into account the π-transmitted component to the FC interaction in unsaturated compounds. From such comparisons it is apparent that couplings between nuclei separated by different numbers of bonds are differently affected by electron delocalization interactions. From Weinhold *et al.*'s[58] results it is expected that many coupling trends will correlate with electron delocalization interactions, as described by the NBO analysis. It is therefore interesting to identify how couplings between nuclei separated by different numbers of bonds are affected by such interactions. This can be accomplished, at least in several cases, by carefully considering the following: (i) Weinhold *et al.*'s results[58]; (ii) combination of those results with the CLOPPA description[266] of couplings dominated by the FC term, Eq. (45); (iii) results obtained in this laboratory (Buenos Aires) that either have recently been published or will be published in forthcoming papers; (iv) a perusal of experimental values of coupling constants that were rationalized in terms of conjugative interactions; and (v) trends in NBO interactions that can be expected according to simple PMO theory.[504]

Intramolecular NBO interactions between one bond and one antibond are stereospecific[501] and their strength depends on both the ability of the bond to be a good electron donor and that of the antibond to be a good electron acceptor. The main features of these properties can be summarized in a few practical rules that can be rationalized in terms of simple PMO theory.[504] (A) σ *Conjugation*:

$\sigma \rightarrow \sigma^*$ interactions are more efficient for a *vicinal anti* configuration; in general for a dihedral angle smaller than 150° they are very weak, unless the interaction takes place between a σ bond that is a very good electron donor, and a σ^* antibond that is a very good electron acceptor. In this last case for *syn*-arranged *vicinal* bonds, the σ conjugation could be nonnegligible although weaker than in the *trans* case. (B) *Anomeric effect*: $n \rightarrow \sigma^*$ interactions are important for both *syn* and *anti* configurations, being notably stronger in the latter than in the former. (C) *Hyperconjugation*: $\sigma \rightarrow \pi^*$ and $\pi \rightarrow \sigma^*$ interactions are efficient for a σ-type bond placed α to a π-electronic system, and their strength depends on $\sin^2 \theta$, where θ is the dihedral angle determined by the σ bond and the σ-framework associated with the π-electronic system.[505]

It is important to recall that the electron donor ability of a σ-type bond decreases with increasing 'stiffness' of the bond, and that the better the donor ability of a σ-type bond, the poorer the electron acceptor ability of its corresponding antibond.[506] Therefore, an increase in the strain of an X—Y σ bond increases its electron donor ability, while the corresponding (X—Y)* antibond electron acceptor ability decreases. On the other hand, the σ^* antibond electron acceptor ability is larger for a larger difference in electronegativity between the two bonded atoms.

From considerations (i) to (v) quoted above, together with the simple rules (A), (B) and (C), the following trends are expected for the FC term of couplings between nuclei separated by n bonds.

One-bond couplings, $^1J(A,B)$, where the A—B is a single bond: $\sigma \rightarrow \sigma^*$, $\pi \rightarrow \sigma^*$ and $n \rightarrow \sigma^*$ delocalizations

According to the CLOPPA description, the Fermi contact terms of ^1J(A,B) couplings are mainly determined[17] (Eq. (45)), by the 'bond contribution' J^{b}; the 'other bond contributions' J^{ob}; and, for couplings involving lone-pair-bearing atoms, the 'lone-pair contributions' J^{LP}. It should be recalled that 'b' and 'ob' are σ-type bonds and not π-type bonds, since otherwise their 'perturbators' would be zero as they have a node at the site of the coupled nuclei. While the first corresponds to a positive contribution to ^1K(A,B), the latter two correspond to negative contributions to ^1K(A,B). The A—B bond (b), its antibond (A—B)* (b*), the 'other bonds', A—X and B—Y (ob) and their antibonds (A—X)* and (B—Y)* ((ob)*), and the A and B lone pairs (if they are lone-pair-bearing atoms) (n) may be involved in significant electron delocalization interactions. The total trend of a given ^1J(A,B) coupling will depend in general on all these interactions. In most cases the following trends seem to hold, although exceptions can be expected, especially, when the 'perturbators' are affected in the opposite direction to the 'propagator' term, Eq. (33):

(a) Electron delocalizations into the b* antibond yield a decrease in $^1K^{b}$(A,B).

(b) Electron delocalizations from the b bond yield a decrease in $^1K^b$(A,B).
(c) Electron delocalizations into (ob)* antibonds yield a decrease in the absolute value of $^1K^{ob}$(A,B).
(d) Electron delocalization from an ob bond yields a decrease in the absolute value of $^1K^{ob}$(A,B).

Rule (a) is supported,[507–509] for instance, by noting that in 1,3-dioxane, (**29a**), $^1J(C2,H_{eq})$ = 167.5 Hz and $^1J(C2,H_{ax})$ = 158.6 Hz (Perlin effect[510]),

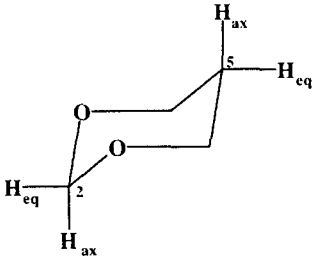

[29a]

while in cyclohexane the corresponding couplings are 126.4 Hz and 122.4 Hz, respectively. The difference was ascribed to the anomeric interaction $n(O) \rightarrow (C1—H_{ax})^*$.[37,507–509,511] A similar effect was observed for $^1J(^{15}N,^{31}P(V))$ couplings in 2-amino-substituted 1,3,2λ^5-oxazaphosphinan-2-ones.[512] On the other hand, in several cases a reverse Perlin effect was reported, for instance in 1,2,4-trioxanes,[508] dithiane,[509] $^1J(C5,H_{eq})$ and $^1J(C5,H_{ax})$ in dioxane (**29a**)[507], etc. This reversed Perlin effect was rationalized assuming a homoanomeric interaction between an oxygen lone pair and the C—H_{eq}, which are in a W configuration.[507] However, instead of the homoanomeric interaction, the reversed Perlin effect could also be rationalized as originating in *vicinal* $(X—C) \rightarrow (C—H_{eq})^*$ and/or $(C—H_{eq}) \rightarrow (X—C)^*$ σ conjugations (X = O, S).[509,513] At least for X = O, the latter interaction should be stronger than the former.[504] Therefore, the reverse Perlin effect should be an example of rule (b). Another example of rule (b) is found in the substituent effects on ^1J(C,Sn) in (**30**), which are transmitted via a 'double hyperconjugation mechanism'[506,514,515] ('double σ conjugation', according to the present notation); for example, for X = H, ^1J(C,Sn) = (−)474 Hz, and for X = F, ^1J(C,Sn) = (−)441 Hz.

One interesting exception to rule (a) is the exoanomeric effect in 3-methoxy-1,2,4,5-tetroxane (**29b**), where an electron delocalization into the (C—H)* antibond causes a significant increase in the $^1J(C,H_{eq})$ coupling corresponding to the highly polar C—H_{eq} bond placed *geminal* to the methoxy group.[516] This is a case where a lengthening of the A—B bond connecting the coupled nuclei yields an increase in the FC contribution to the ^1J(A,B) coupling. According to

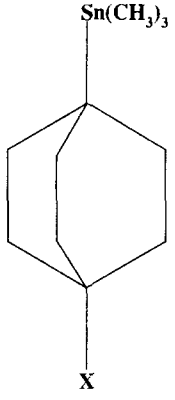

[30]

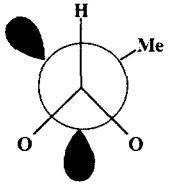

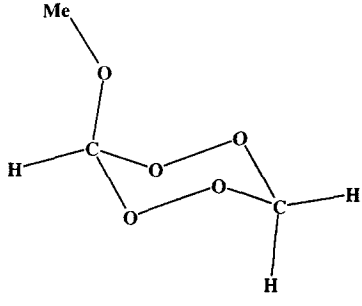

[29b]

the CLOPPA description,[266] the $J_{ia,jb}$ FC contribution depends on the overlap between the occupied (*i,j*) and the vacant (*a,b*) LMOs, Eq. (37), at the sites of both coupled nuclei. Such an effect was described by saying that one-bond couplings depend on both the A and B s-character of the A—B bond as well as on the corresponding s-character of the vacant A—B LMOs.[517] In the current literature, several cases are reported where a lengthening of the A—B bond length yields an increase in the spin–spin interaction[51] and in general such effects are ascribed to noncontact contributions to the corresponding ^1J(A,B) coupling. However, effects similar to that reported in ref. 517 cannot be ruled out. Also, it is frequently accepted that ^1J(A,B) couplings, in general dominated by the FC term, correlate linearly with the A—B bond length, the spin–spin interaction being stronger for shorter A—B distances. However, several interesting counterexamples were published during the review period. For instance, Kamienska-Trela *et al.*[402] found no correlation between ^1J(C,C) couplings and the corresponding C—C bond lengths in alkyl derivatives of tetramethyl 9a*H*-quinozaline-1,2,3,4-tetracarboxylate.[402]

A conspicuous example of the electron delocalization effects on the $^1J^{ob}$ contributions to ^1J(C,H) couplings, rule (c), is given by those corresponding to the bridgehead position in bicyclo[1.1.1]pentane (**3**). It is interesting to compare them with the corresponding effects in bicyclo[2.2.2]octane (**31**); the NBO

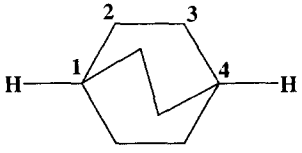

[31]

analysis and the respective couplings are compared in Table 13. The CLOPPA description of the bridgehead ^1J(C,H) coupling trend indicates that the absolute values of the J^{ob} contributions from the cage C—C bonds are notably reduced from those observed in (**3**).[273] The large $\Delta E^{(2)}$ values in (**3**) (Table 13), show the very good electron donor capability of its strained cage (C—C) bonds. Concomitantly, their corresponding antibonds (C—C)* are very poor electron acceptors. In the less strained compound (**31**), these two interactions follow the 'normal' trend, i.e. that which can be expected from simple PMO theory.[504] The difference in strength of these two complementary interactions shows how an increase in the strain of a C—C bond causes an increase in its electron donor ability while it reduces its (C—C)* antibond electron acceptor ability. The three J^{ob} contributions to the ^1J(C1,H1) coupling correspond to the strained C—C bonds, and therefore their absolute values are notably reduced in comparison with a similar situation in unstrained compounds. It should be noted that in (**3**), the (C3—Ci)→(C1—H1)* (i = 2,4,5) interactions are equal to the (C1—Cj)→(C3—H3)* (j = 2,4,5) interactions and the latter correspond to electron delocalizations from ob terms of ^1J(C1,H1) which are consequently notably increased.

Table 13. Comparison of DFT/6-311G** NBO delocalization energies (in kcal mol^{-1}) between cage C—C bonds and antibonds that are *vicinal* to bridgehead C—H antibonds and bonds, respectively, in (**3**) and (**31**); and the respective bridgehead ^1J(C,H) couplings (in Hz)

$E^{(2)}$	(**3**)	(**31**)
(C—C)→(C—H)*[a]	9.29	1.83
(C—H)→(C—C)*[a]	<0.50	3.13
^1J(C,H)[b]	167.8	134.3

[a] Taken from ref. 12.
[b] Taken from ref. 518.

Compound (**3**) is also a very good example for study of electron delocalization effects on ^1J(C,C) couplings, (rule (d)), since there is a strong electron delocalization from the C—C bond containing the coupled nuclei, which must affect its $^1J^b$ contribution. The experimental value for this ^1J(C,C) coupling is 25.1 Hz,[132] which is a small coupling for a saturated C—C bond.[22,399,519] It is interesting that *ab initio* calculations at the RPA level fail notably in reproducing such coupling,[132] indicating that electron correlation effects are very important in strained C—C bonds.[158] In ^1J(C,C) in (**3**), both coupled nuclei are also connected by two equal three-bond coupling pathways, but the configuration of bonds defining such coupling pathways corresponds to very inefficient pathways for transmitting the spin information associated with the FC interaction. It should be noted that in (**3**) there are also important (C—C)→(C—H)* interactions of 4.07 kcal mol^{-1}, where (C—H)* is an antibond of a 'lateral' C—H bond placed *vicinal* to that C—C bond. Another example of a cyclo compound with small ^1J(C,C) where the contribution from one of the two pathways to ^1J(C,C) can be considered negligibly small is 3,5-dimethylcyclobutabenzene ((**32**), $R_1 = R_3$, R_2 = H) where ^1J(C1,C2) = 28.2 Hz.[520]

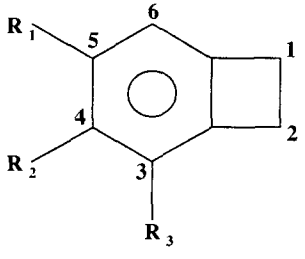

[32]

Abnormally low ^1J(C,C) couplings in small strained cyclic compounds were discussed in detail by Kamienska-Trela.[22] In such strained compounds, couplings across exocyclic bonds are large (for instance, ^1J(C,C) = 43.4 Hz in methyl cyclopropane (**33**)) while those across endocyclic C—C bonds are particularly small (for instance, ^1J(C,C) = 12.4 Hz in cyclopropane (**34**)).[521] The large value in the former can be rationalized in terms similar to those for the bridgehead ^1J(C,H) coupling in (**3**) quoted above, although rehybridization

[33]

effects not related to *vicinal* electron delocalizations should also be operating, like those reported by Oddershede *et al.*[196] when calculating ^1J(C,H) couplings in methane when its geometry is changed in such a way that an H—C—H angle is increased while keeping a C_{2v} symmetry. Therefore, the small couplings through endocyclic bonds originate in at least three different effects, namely (a) electron delocalization interactions from the strained C—C bond into *vicinal* (C—H)* antibonds paralleling the effect described in (**3**); (b) a contribution from the two-bond coupling pathway, as described in detail by Kamienska-Trela,[22] and (c) a rehybridization effect such as that quoted in methane when increasing one of its H—C—H angles.[196] In (**34**) the two-bond contribution is

[34]

expected to be negative and, as described below, two-bond couplings are very sensitive to electron delocalizations from and into the σ-framework of the two-bond pathway: the former causes an algebraic decrease while the latter causes an algebraic increase in the corresponding two-bond coupling. Therefore, in three-membered rings significant spread of ^1J(C,C) couplings is expected depending not only on the strain of the respective C—C bond but also on the relative values of the one- and two-bond pathway contributions. Other interesting examples are, ^1J(C1,C3) < 3 Hz, and ^1J(C2,C3) = 11 Hz in (**35**).[522]

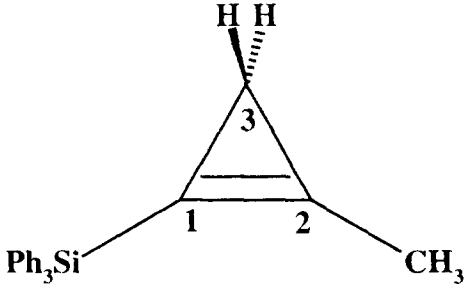

[35]

The conspicuous difference between these two couplings seems to indicate that electron delocalization also plays an important role in defining such a trend. In fact, the electropositive substituent increases the electron donor ability of the C1—C3 bond, although rehybridization effects that cannot be described by electron delocalizations might also be operating.[522] J(C,C) couplings in some

strained compounds were also reported by Krivdin *et al.*[523] No further examples are quoted since the ring size influence on ^1J(C,C) couplings was extensively described by Kamienska-Trela.[22] Another very interesting effect on ^1J(C,C) couplings was discussed by Vogel *et al.*,[524] when going from (**36a**) to (**36b**) and similar pairs of compounds, regardless of the type of substituent in

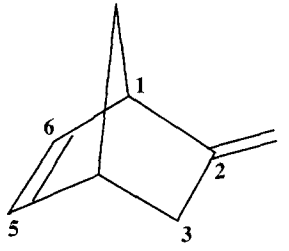

[36a]

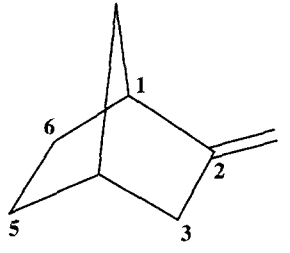

[36b]

position 2, the ethanic ^1J(C2,C3) increases by ~10 Hz, which was rationalized as originating in hyperconjugative interactions.[524]

When only one of both coupled nuclei bears one lone pair, the absolute value of $^1J^{LP}$ of the FC term strongly depends on the lone pair s character, which increases rapidly along the periodic table.[267] That is why it is expected that ^1K(Sn,H) < 0 in SnH_3^-,[267] while for lighter A atoms bearing only one LP ^1K(A,H) > 0.[136] If H is replaced by a methyl group, then $^1K^{ob}$(A,C) contributions from the C—H bonds attached to the coupled carbon atom are expected. They are not present in ^1K(A,H), and therefore it is expected that in many cases while ^1K(A,H) > 0, the corresponding ^1K(A,C) < 0, since the $^1K^{ob}$(A,C) contributions are negative and they will add up to $^1K^{LP}$. In general for ^1K(N,C) couplings the sum of $^1K^{ob}$(A,C) and $^1K^{LP}$(A,C) terms does not overcome the $^1K^{b}$(N,C) positive contribution and, therefore, ^1K(N,C) > 0,[525,526] and the same holds for ^1K(Si,N).[526,527] In arylsilyl-N compounds an increase in the piramidality at the N atom yields a decrease in $^1J(^{29}Si,^{15}N)$ couplings.[528] This is particularly true in compounds like trisilylamines with a planar NSi_3

skeleton.[529] The piramidality effect on $^1J(^{29}Si,^{15}N)$ couplings was studied in methylhydroxylamines[530] with the NBO approach[501] and on the $^1J(N,H)$ coupling in NH_3 using the *ab initio* version[135] of the CLOPPA method.[266] Similarly, an increase in the pyramidality at the N atom leads to a decrease in the absolute value of $^1J(P,N)$ coupling in phosphoric amides.[262] In general $^1K(Sn,N) > 0$ and is of small absolute value,[526,531] but couplings of a negative sign are likely to be found in some cases.[532] A peculiar case is $^1J(^{119}Sn,^{15}N)$ in *N*-triorganostannyl-substituted pyrroles (**37**) and related compounds, where

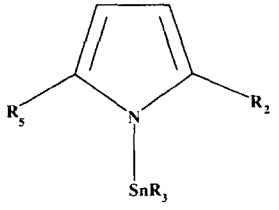

[37]

values of $^1K(^{119}Sn,^{15}N) < 0$ were measured.[533,534] In such compounds the N lone pair is of purely p character and $^1J^{LP} = 0$.[1] In $(Me_3Sn)_3N$, where there is some ambiguity about the structure of the Sn_3N skeleton since IR data suggest a pyramidal structure but electron diffraction studies favour a trigonal planar arrangement, $^1K(^{119}Sn,^{15}N) < 0$ (ref. 535 and references cited therein). In lead compounds, $^1K(^{207}Pb,^{15}N) < 0$,[42,526] this was rationalized by Wrackmeyer *et al.*[534] as originating in the increasing polarity of the M—N bond along the series (M = Si, Sn, Pb). Apparently, in such conditions the absolute value of $^1J^b$ is much decreased while those of $^1J^{ob}$ are much increased. $^1K(Sn,Se) < 0$ was determined in a pentacoordinated tin atom.[536] On the other hand, the larger s character of a P(III) lone pair than of an N(III) lone pair causes the sum of $^1K^{LP}(P,C)$ and the $^1K^{ob}(P,C)$ terms to overcome the positive $^1K^b(P,C)$ contribution, yielding $^1K(P,C) < 0$.[400,537–539] The same seems to hold for $^1K(Si,P(III))$[457] and $^1K(Sn,P(III))$.[531] Similarly, $^1K(P,N) < 0$[538] where both coupled nuclei bear a lone pair. $J(P,C)$ Coupling signs were determined by Gudat *et al.*[540] in several azatriphosphiridines, for low-coordination P atoms, $^1K(P,C) < 0$, while for higher-coordination P atoms, $^1K(P,C) > 0$ were determined. Similarly, for the latter type, both $^1K(P,C) > 0$[136,400] and $^1K(P,Si) > 0$[457] are known. $^1J(^{31}P,^{31}P)$ can be of either sign, in general being positive for high coordination numbers and negative for lower coordination numbers,[51] although in the latter case it also depends on the relative orientation of both P lone pairs, it being important to recall that in P_2H_4 a very large and positive $^1J^{SD}(P,P)$ was calculated.[123] When A bears more than one lone-pair, $^1K(A,H)$ can be positive, but $^1K(A,C) < 0$. For instance $^1J(F,H) = +530$ Hz in FH,[244] and $^1J(C,F) = -157.5$ Hz in FCH_3,[541] that is, in the latter the sum of

the C—H $^1J^{ob}$ and the F $^1J^{LP}$ contributions to the FC term of ^1J(C,F) are larger, in absolute value, than $^1J^b$. The same holds for $^1K(^{35}Cl,H) > 0$ in HCl;[136] and in chloroketosulfones it was found that $^1K(^{35}Cl,^{13}C) < 0$.[542] The sign of ^1K(Br,H) in BrH is not known,[136] but ^1K(C,Br) < 0 was obtained in solid-state NMR measurements for bromobenzene derivatives,[543,544] and in the liquid state for 1-bromo-2-phenylacetylene.[545] If ^1K(A,H) < 0, then ^1K(A,C) is also negative: for example, $^1K(^{127}I,^1H) < 0$[136] and $^1K(^{127}I,^{13}C) < 0$.[259,261]

For couplings involving an F atom n→(ob)*, electron delocalizations operate and they should decrease both the absolute values of the $^1J^{PL}$ and $^1J^{ob}$ contributions. The net result on a given ^1J(C,F) coupling will depend on the strengths of such delocalization interactions. They change the absolute value of ^1J(C,F) couplings but they are negative.[136] Interesting examples are the alkyl fluoride 7-F-norbornane (**38a**), and 7-norbornenyl fluorides (**39**), (**40**) and (**41**), where ^1J(C,F) = (−)192.3 Hz, ^1J(C,F) = (−)210.4 Hz, ^1J(C,F) = (−)199.6 Hz and ^1J(C,F) = (−)228.3 Hz, respectively, were measured,[515] (signs assumed). This trend was rationalized in terms of the following interactions:[546] (a) the homo-hyperconjugation, π→(C—F)*, which is present in compounds (**40**) and (**41**); (b) n(F)→(C1—C7)* and n(F)→(C7—H7)* which increase along this series. Interaction (a) causes an algebraic reduction of ^1J(C,F) coupling

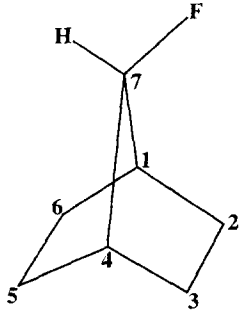

[38a]

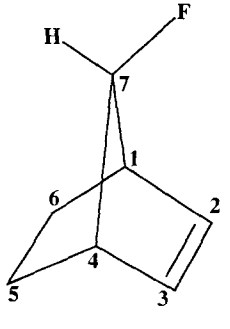

[39]

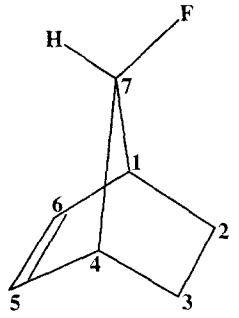

[40]

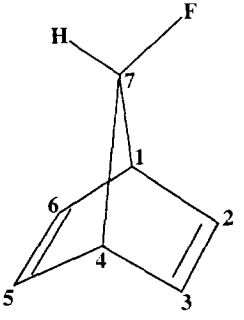

[41]

since this coupling is negative and, therefore, a decrease in its $^1J^b$ contribution yields an increase in its absolute value. Interactions (b), which are of type $n \rightarrow (ob)^*$, in this case yield negative contributions to $^1J(C,F)$ couplings. Similar effects were reported when comparing the *equatorial* and *axial* epimers of cyclohexyl fluorides, where $^1J(C,F) = (-)169.30$ Hz and $(-)164.59$ Hz, respectively, were measured.[546] It is interesting to compare these values with those in *cis*- and *trans*-4-*t*-butyl-2-fluorocyclohexanone of $(-)190.6$ Hz and $(-)176.5$ Hz, respectively.[547,548] Differences in $n \rightarrow (ob)^*$ interactions seem to take into account the opposite behaviours known for the bridgehead $^1J(C,H)$ and $^1J(C,F)$ couplings along the series 1-X-bicyclo[2.2.2]octane, 1-X-bicyclo[2.2.1]heptane, 1-X-bicyclo[2.1.1]hexane and 1-X-bicyclo[1.1.1]pentane for X = H and F, respectively.[273,549]

In SeH_2 $^1K(Se,H) > 0$[178] and frequently, $^1K(^{77}Se,^{13}C) < 0$,[550] as is also the case for $^1K(^{77}Se,^{29}Si) < 0$, for instance in 2,5-dihydro-1,2,5-selenasilaborole derivatives.[551] Similarly, $^1K(^{77}Se,^{15}N) < 0$.[552]

Decrease in the absolute values of $^1K(X,Y)$ couplings owing to electron delocalizations from the X—Y bond seem to take place in norbornane (**38b**), where the difference between $^1J(C,H_{exo}) = 128.85$ Hz and $^1J(C,H_{endo}) = 131.00$ Hz[553] seems to originate[12] in the difference between the

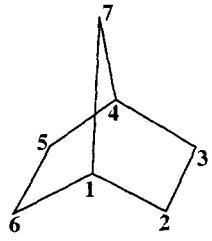

[38b]

$(C3—H_{exo}) \rightarrow (C4—C5)^* = 3.34$ kcal/mol^{-1} and $(C_3—H_{endo}) \rightarrow (C4—C5)^* = 2.51$ kcal mol^{-1} interactions. (The respective $^1J(C,^2H)$ couplings were measured[553] and the values quoted above were obtained as $^1J(C,H) = 6.5144\ ^1J(C,^2H)$).

π-Electron delocalizations

The effects of hyperconjugation on $^1J(C,H)$ couplings corresponding to C—H bonds placed α to a π electronic system were given in the previous review.[1]

Lambert and Singer[554] studied neutral hyperconjugation using as probe the $^1J(C_{CH_2},C_i)$ couplings in some members of the series (**42**), M = C, Si, Ge, Sn;

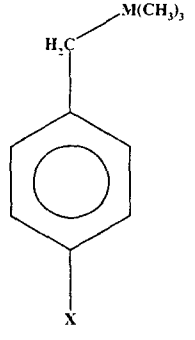

[42]

X = NO_2, CN, H, Me, OMe. They found support for their rationalization in some of the small values measured, for instance for the M = C, X = OMe compound, $^1J(C_{CH_2},C_i) = 36.0$ Hz, but Kamienska-Trela[555] questioned these experimental values because of significant discrepancies observed in the newly measured values when compared with those of ref. 554.

Berger[556] reported that $^1J(C,C)$ couplings in aromatic systems are related to the π-bond order of the corresponding C—C bond. Butenschön *et al.*[520] measured $^1J(C,C)$ couplings in cyclobutabenzene derivatives (**32**) as a probe

to find evidence that π-bonds of the benzene ring have a degree of fixation. The large ^1J(C5,C6) couplings in (**43a**) derivatives were taken as a probe for a certain degree of fixation of the π mobile bond order in the C5—C6 bond.[557] In a series of compounds of type (**43b**), ^1J(N,N) couplings through the N2—N3 and N3—N4 bonds were found to be similar[558] and comparable to that in an N=N double bond, which was taken as an indication that the positive charge is not localized at N3, but delocalized between atoms N2, N3 and N4.

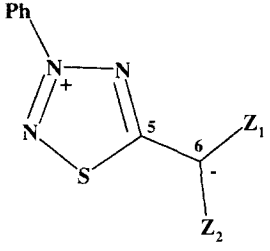

[43a]

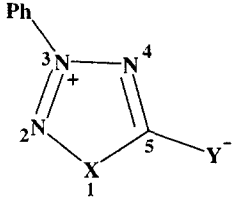

[43b]

Lone-pair orientation

Apparently, most lone pair orientation effects on one-bond couplings[22,136,399,400] can be rationalized in terms of $n \rightarrow \sigma^*$ delocalizations. A case in point is the well-known difference between $^1J^Z$(C,C) = 49.3 Hz and $^1J^E$(C,C) = 41.5 Hz[399] in (**44**) The n(N)$\rightarrow$(C—C^Z)* interaction is notably weaker than the n(N)$\rightarrow$(C—C^E)*, and while the former decreases the $^1J^b$

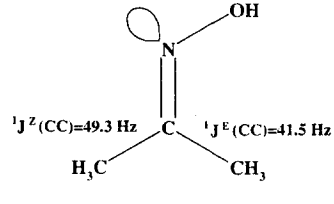

[44]

contribution to $^1J^E$(C,C), the latter decreases its $^1J^{ob}$ contribution from the C—C bond. For $^1J^Z$(C,C) the opposite applies.

An interesting orientational effect of the N lone pair on ^1J(C,H) couplings was reported by Forni *et al.*[559] in *N*-chloroaziridinecarboxylates. The differences of ^1J(C,C) couplings for C—C bonds placed *syn* and *anti* to a lone pair[22,136,224,400] were observed in the *Z* and *E* isomers of ethyl 2-(-2-aminothiazol-4-yl)-2-iminoacetates.[560] Very interesting examples of the orientational N lone pair effect on ^1J[P(V),C] couplings were presented by McKenna *et al.*[561] in trifunctional phosphonate α-oximes and α-arylhydrazones (**45**), where differences between couplings involving the *anti* and *syn* P atoms are as large as ~76 Hz. Examples of the role played by lone pairs in ^1J(P,N) were given by Webb *et al.*[562]

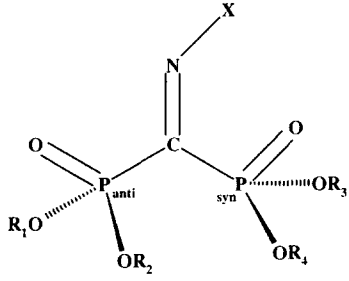

[45]

Two-bond couplings, $^2J(A,B)$, through the A—M—B moiety

^2J(A,B) couplings for any coupled nuclei are known to be spread over a large range of values[2,471] including positive and negative values even for the same type of coupled nuclei.[136,139,140,154] Such large spread of ^2J(A,B) couplings was used to elucidate many structural problems.[58,140,154,310] Some factors affecting two-bond couplings were discussed many years ago.[563] Their non-contact contributions[2,3] can be important and the FC term of ^2J(A,B) couplings is particularly sensitive to electron delocalizations involving any of the bonds or antibonds belonging to the A—M—B moiety. Such sensitivity seems to be one of the main reasons for the surprising range over which these couplings are spread. One of the most conspicuous examples of the influence on ^2J(A,B) couplings of electron delocalization interactions is found in the series (**46**), O = CHC(Cl_nH_{n-3}) (n = 0,1,2,3) where the ^2J(C,H) coupling through the carbonyl group takes values of 26.6 Hz (n = 0),[564] 32.5 Hz (n = 1),[565] 35.8 Hz (n = 2)[564] to 46.3 Hz (n = 3).[564] Such couplings correlate linearly with the sum of the NBO occupation numbers of the (C_c—C)* and (C_c—H)* antibonds (C_c = carbonyl carbon atom).[566] In (**46**), interactions defining the occupation numbers of both antibonds, are n(Cl)→(C_c—C)*, n_p(O)→(C_c—C)* and

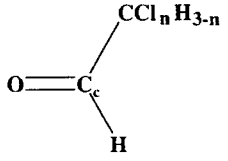

[46]

$n_p(O) \rightarrow (C_c—H)^*$, where n(Cl) stands for the different lone pairs of the Cl atoms, and $n_p(O)$ stands for the oxygen lone pair of purely p character.

The following two simple rules hold for the Fermi contact term and they are important enough to define many observed trends when A—M and B—M are both single bonds, and M does not bear any lone-pair. This does not mean that there are not also other factors that affect ^2J(A,B) couplings: in addition, in the case where both A and B atoms bear lone pairs that overlap, an important positive contribution to ^2K(A,B) arises (see Section 3.2). (a) Electron delocalizations into any of the antibonds, (A—M)* and (B—M)*, yield a positive contribution to the corresponding ^2K(A,B) coupling. (b) Electron delocalizations from any of the two bonds, A—M and B—M, yield a negative contribution to ^2K(A,B).

If the coupling pathway contains at least one double bond, then electron delocalizations from its π bond or into its π^* antibond may also notably affect the respective ^2J(A,B) couplings. However, rules (a) and (b) seem to hold for the σ-type bonds of such pathways, although they may not define the experimental trends.

Perhaps some of the most conspicuous examples of (a) are the surprisingly large ^2J(A,B) (^2K(A,B) > 0) couplings through a carbonyl carbon atom[224,471] (**47**). A few known examples are ^2J(H,H) = 46 Hz (A = B = H);

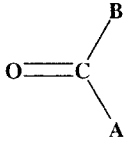

[47]

^2J(C,H) = 26.7 Hz (A = H, B = CH_3); ^2J(C,C) = 15 Hz (A = B = CH_3); ^2J(C,N) = 9.5 Hz (A = CH_3, B = NH_2); and ^2J(C,F) = 61 Hz (A = CH_3, B = F).[471] Recently, $^2J(^{17}O,^{13}C)$ couplings through the carbonyl carbon atom of ~40 Hz were reported in alkyl formates (R = Me, Et, Pr), (**48**).[331] In formamide, ^2J(H{C═O}N) = 15.1 Hz in 3.0 mol l^{-1} acetonitrile solution was reported.[567] In a series of twisted amines the ^2J(C,N) coupling through the carbonyl carbon atom, C_c, was found to correlate linearly with the twist angle

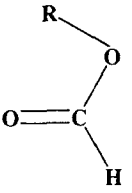

[48]

around the C_c—N bond.[568] These large $^2K(A,B) > 0$ couplings are rationalized as originating in, among other factors, the large $n_p(O) \rightarrow (C_c—A)^*$ and $n_p(O) \rightarrow (C_c—B)^*$ electron delocalizations within the carbonyl moiety.[566] It is recalled that the NBO analysis yields two different types of carbonyl oxygen lone pairs, namely, one in-plane of purely p character and perpendicular to the C=O bond, $n_p(O)$, and another, also in-plane but along the C=O bond, which is hereafter dubbed $n_s(O)$, although it also has p character. The smaller $^2J(C_{ipso},H_f)$ coupling in salicylaldehyde (**49**), (20.13 Hz),[569] than that in benzaldehyde (**50**) (24.11 Hz)[569] is rationalized as originating in the inhibition of the $n_p(O) \rightarrow (C_c—C_{ipso})^*$ and $n(p) \rightarrow (C_c—H_f)^*$ interactions owing to the strong intramolecular hydrogen bond C=O···H—O in the former (**49**),[570] where an important $n_p(O) \rightarrow (O—H)^*$ interaction is present and inhibits the

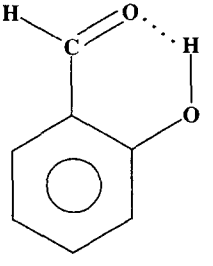

[49]

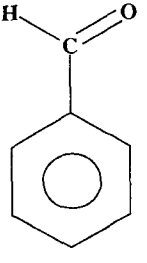

[50]

Table 14. NBO occupation numbers in the $(C_c—C_{ipso})^*$ and $(C_c—H_f)^*$ antibonds in (**49**) and (**50**) and (O—H)* in (**49**). The charge transfer interaction in the hydrogen bond is also shown[a]

	(**50**)	(**49**)
$(C_c—C_{ipso})^*$	0.0503	0.0439
$(C_c—H_f)^*$	0.0510	0.0464
(O—H)*	–	0.0212
n(O)→(O—H)*	–	10.41[b]

[a] Taken from ref. 481.
[b] In kcal mol^{-1}.

$n_p(O)\rightarrow(C_c—C_{ipso})^*$ and $n_p(O)\rightarrow(C_c—H_f)^*$ interactions as shown in the NBO occupation numbers of these antibonds (Table 14).

Unusually large ^2J(X,C) couplings involving a carbonyl carbon atom were also reported, for example ^2J(Hg,C) couplings in chloromercurio aliphatic acids.[395]

Positive and negative ^2K(N,H) and ^2K(N,C)[539] and ^2K(P,H) and ^2K(P,C)[375] couplings were observed depending on the relative orientation between the N or P lone pair and the M—H or M—C bonds, respectively. The antiperiplanar orientation always produces a more positive coupling, paralleling the behaviour of the n(N)→(M—H,C)* or n(P)→(M—H,C)* interactions[136,400,539] and the ability of the (N—M)* or (P—M)* to be good electron acceptors as, for instance, in pyridine (**51**) where $^2J(^{15}N,^1H2) = -10.93$ Hz[571]

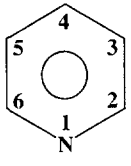

[51]

(see Table 15). Another interesting example is ^2J(N1,C4) < + 0.5 Hz and −4.8 Hz, respectively, in the N3—H and N1—H tautomeric forms in the imidazole ring of the histidine residue (**52**).[572] In the former, a strong $n(N1)\rightarrow\sigma(C4—C5)^*$ interaction takes place. Positive and negative ^2K(P,C) were also observed for P(V) atoms; positive couplings correspond to configurations where strong electron delocalizations either into the (P—M)* or (M—C)* antibonds can be expected.[573] $^2K(C,F) > 0$ in $CF_3(CF_2)_5CH_2CH_2OH$,[574] +21.2 Hz for C2, +31.7 Hz for C3, +34.0 Hz for C7 and +33.1 Hz for C8; i.e. there is a conspicuous difference when the coupled carbon is bonded to two H atoms or to two F atoms. In the latter case, the F atoms bonded to the coupled C nucleus also present n(F)→(C—F)*

Table 15. NBO electron delocalization interactions from the C2—H2 and C3—H3 bonds and into the (C2—H2)* and (C3—H3)* antibonds in pyridine (**51**)[a,b,c]

Donor → acceptor	$E^{(2)}$	Donor → acceptor	$E^{(2)}$
n → (C2—H2)*	4.09	–	–
σ(N—C6) → (C6—H2)*	2.22	σ(N—C2) → (C3—H3)*	1.52
σ(C3—C4) → (C2—H2)*	2.30	σ(C4—C5) → (C3—H3)*	2.72
Sum	8.61	Sum	4.24
(C2—H2) → σ(N—C6)*	4.76	(C3—H3) → σ(N—C2)*	3.42
(C2—H2) → σ(C3—C4)*	2.37	(C3—H3) → σ(C4—C5)*	4.36
Sum	7.13	Sum	7.78
Occupation number (C2—H2)*	0.0239	Occupation number (C3—H3)*	0.0136

[a] NBO analyses and the geometry optimization were performed at the DFT-B3LYP/6-311G** level.[12] $E^{(2)}$ energies are in kcal mol^{-1}.
[b] n → σ(C2—C3)* = 9.06 kcal mol^{-1}.
[c] Occupation number (N—C2)* = 0.0158.

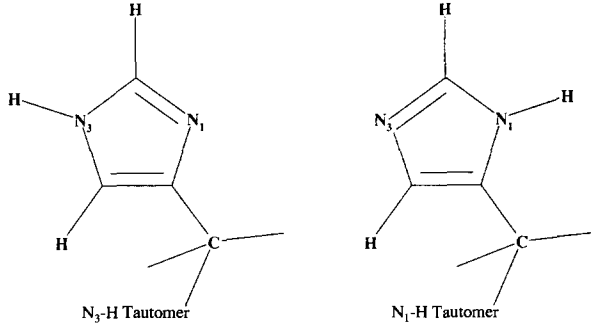

[52]

interactions, where this last antibond contains the coupled F atom. A few other examples are ^2J(C,F) = +19.5 Hz in $CFH_2CH_2CH_3$ and +22.4 Hz in $CFH(Me)_2$,[575] and in general for CF_3—C— fragments,[576] where interactions of type n(F) → (C—C)* are expected, and the (C—C)* antibond belongs to the coupling pathway. Many other cases indicate that for similar F—C—C(CH2) coupling pathways ^2J(C,F) coupling is ~ +20 Hz. However, in $CF_3C(OH)NH_2^+AsF_6^-$,[577] ^2J(C,F) = 46 Hz, which is a typical value for a compound containing a $CF_3C(O)$— moiety.[161] In such a moiety, strong n(F) → (C—C)* and n_p(O) → (C—C)* take place. The increase in the ^2J(C,F) coupling when increasing the number of F atoms bonded to that carbon is nicely exemplified by Abraham *et al.*[548] in the fluoroacetones CH_2FCOCH_3, CHF_2COCH_3 and CF_3COCH_3, i.e. 22.10 Hz, 27.67 Hz and 36.3 Hz, respectively (in CCl_4). It is interesting to note that in the first two compounds ^2J(F,H) = 48.19 Hz and 54.44 Hz, respectively. Another interesting example is

Table 16. Comparison between ^2J(C,F) couplings and the occupation number of both antibonds belonging to the coupling pathway in the *eq*- and *ax*-epimers of cyclohexyl fluoride[546]

	eq-Epimer	*ax*-Epimer
^2J(C,F) (Hz)	(+)17.18	(+)21.06
Occ. (C1—C)*	0.0291	0.0297
Occ. (C1—F)*	0.0343	0.0387

the comparison of ^2J(C,F) couplings in the *axial* and *equatorial* epimers of cyclohexyl fluoride (Table 16). These values should be compared with those in *cis*- and *trans*-4-*t*-butyl-2-fluorocyclohexanone: (+)13.6 Hz and (+)20.6 Hz.[547,548]

Similarly, $^2K(F_a,F_b) > 0$ in a vinyl moiety, (**53**).[578] In this case, strong $n(F_a) \rightarrow (C—F_b)^*$ and $n(F_b) \rightarrow (C—F_a)^*$ interactions take place. Rule (a) is

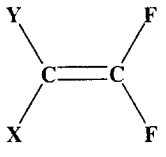

[53]

nicely observed in comparing ^2J(F,F) = 71 Hz in trifluorovinyl aryl derivatives with ^2J(F,F) = 82 Hz in vinyl trifluoride (**54**),[579] where the C—H bond is a

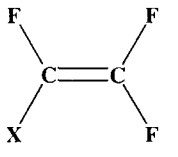

a) X=H
b) X=Ph

[54]

notably better electron donor than the $C—C_{phenyl}$ bond in the phenyl derivatives. A different example of rule (a) is the known asymmetry in pyridine (**51**) between ^2J(C2,H3) = +3.12 Hz and ^2J(C3,H2) = +8.47 Hz.[580] In this case the aromatic C2—C3 bond is shared by both coupling pathways. NBO $\Delta E^{(2)}$ electron delocalization interactions from the C2—H2 and C3—H3 bonds and into the (C2—H2)* and (C3—H3)* antibonds[12] are displayed in Table 15. The sum of $\Delta E^{(2)}$ for the (C2—H2)* antibond is much larger than that for the (C3—H3)* one. On the other hand, the sum of $\Delta E^{(2)}$ electron delocalizations

from the C2—H2 and C3—H3 bonds are similar. The positive sign of these two couplings, ^2J(C2,H3) and ^2J(C3,H2), is due, in part, to the strong n(N)$\rightarrow\sigma$(C2—C3)* = 9.06 kcal mol^{-1} interaction, which affect both of them to the same extent. The π electronic system present in the coupling pathway should also be important in making such couplings positive.[139] Similar asymmetries in $^2J(C_{\beta,\alpha},H_{\alpha,\beta})$ couplings were reported in several isothiazolopyridine systems.[581] The effect of n(N)$\rightarrow$(Sn—C_2)* and n(N)$\rightarrow$(C_2—C_3)* interactions on $^2J(^{119}Sn,C3)$ in 2-stannylpyridine (**55**) is nicely exemplified by comparing that coupling (−93.2 Hz), with the corresponding one (−66.4 Hz) in its borane adduct (**56**), where such interactions are partially inhibited.[393]

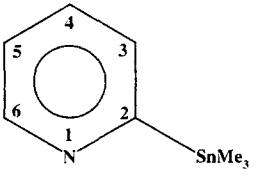

[55]

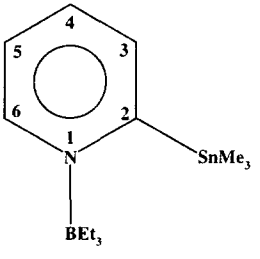

[56]

In furane (**57**), an asymmetry like that in pyridine, although smaller, is also known, ^2J(C2,H3) = +11.03 Hz, while ^2J(C3,H2) = +13.79 Hz.[569,582] This trend is reversed for heavier chalcogen atoms, i.e. thiophene and selenophene[569] and in thiophene-like structures in fused rings, e.g. ^2J(C2,H3) = 6.7 Hz and ^2J(C3,H2) = 3.9 Hz in (**58**).[583]

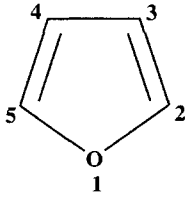

[57]

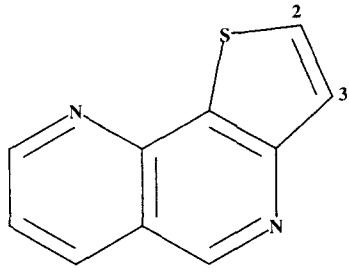

[58]

An interesting comparison was made[584] of ^2J(C1,H2) couplings in benzene, (+1.15 Hz), chlorobenzene (−3.38 Hz), phenol (−2.80 Hz), anisole (−2.78 Hz) and diphenyl ether (−3.48 Hz). According to rules (a) and (b), the last four values should be more positive than in benzene. However, this is a case where the $\pi \rightarrow \pi^*$ seems to define the experimental trend.

In the 2-F-derivative of (**59**), ^2J(C1,F) = 22.5 Hz and ^2J(C3,F) = 25.4 Hz,[585]

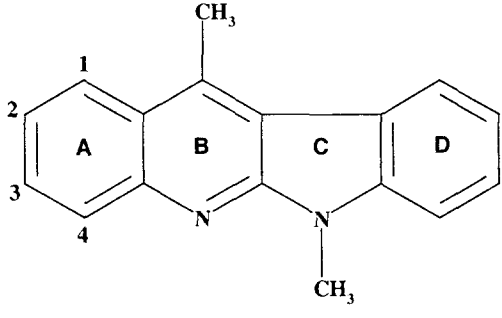

[59]

i.e. the coupling that contains in its coupling pathway the C=C bond with larger bond order, C1—C2, is the smaller coupling. In (**59**), ^1J(C1,C2) = 60.6 Hz and ^1J(C2,C3) = 52.8 Hz were also reported,[585] as expected.[1,22,399] Such asymmetry between ^2J(C1,F) and ^2J(C3,F) suggests that a two-bond pathway like (**60**) introduces a positive contribution to ^2J(A,B) that

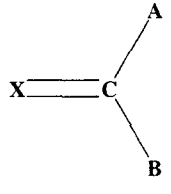

[60]

is larger for larger X=C π bond order. This seems to be the case for ^2J(H,H) = +2.394 Hz in ethylene.[97]

For Sn(IV) atoms, $^2K(^{119}Sn,^{13}C) < 0$ in alkyl tin compounds,[586] and the same holds for ^2J(Sn,Sn) couplings across an sp^3 hybridized carbon atom.[587]

The strong dependence of ^2J(A,B) couplings on various factors made ^2J(C,H) and ^2J(C,N) couplings excellent probes for detecting many local structural problems in proteins, RNA and other biological compounds. To this end, not only selectively enriched but also fully ^{13}C- and ^{15}N-enriched compounds are commonly employed, and new experimental techniques to measure them accurately were developed. A case in point is the stereospecific assignment of H5′ and H5″ in (**61**), which was based on the different signs of $^2J(C4',H5') < 0$ and $^2J(C4',H5'') > 0$.[588] Rules (a) and (b) are useful for predicting them on intuitive grounds.

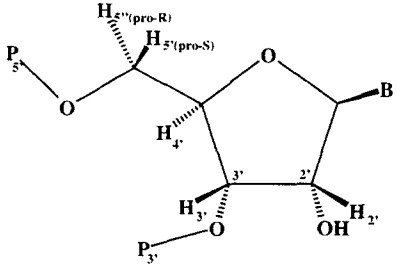

[61]

Perhaps one of the most conspicuous examples of the effect on ^2J(A,B) couplings of electron delocalizations from either or both A—M and B—M bonds are the very well known large and negative ^2J(H,H) couplings in a CH_2 moiety placed α to an unsaturated moiety[264,589] owing to the C—H → π^* hyperconjugative interactions.[348] Also, in cyclic nitrosamines, ^2J(H,H) couplings were observed to be substantially larger in (absolute value) for α-methylene protons *syn* to the nitroso group than for those placed *trans* (**62**).[590]

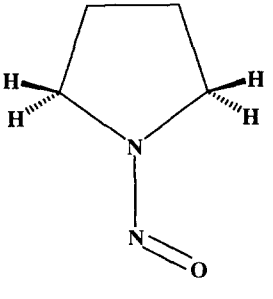

[62]

Apparently, the difference arises from an interaction of the *syn* C—H bonds with the π N═O system.[590] Another example is the similar absolute values but opposite signs between ^2J(C,H) and ^3J(Sn,H), 48.83 Hz and 51.24 Hz, respectively, reported in Bu_4Sn.[591]

Very interesting cases have been discussed when the coupling pathway A—M—B, M bears one or two lone-pair atoms.[592–595] In (**63**) for X = O, ^2J(P,Cl) $\sim$ 0–2 Hz, while for X = N, ^2J(P,Cl) $\sim$ 14–16 Hz. Unfortunately, the signs were not reported.

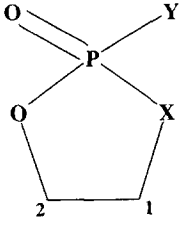

[63]

Very peculiar two-bond couplings were reported[263] in the isostructural $Sn_2Se_3^{2-}$ and $SnPbSe_3^{2-}$ anions, where ^2J[^{119}Sn,^{117}Sn] = 1514 Hz and ^2J[^{119}Sn,^{207}Pb] = 1145 Hz for (**64**) and (**65**), respectively. Both coupled nuclei

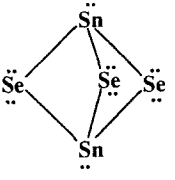

[64]

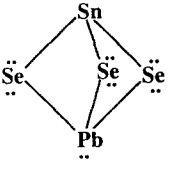

[65]

correspond to atoms bearing one lone pair. In the $Sn_2Se_3^{2-}$ compound the Sn···Sn distance is 3.096 Å, which is significantly shorter than the sum of the van der Waals radii, ~4.4 Å. It would be interesting also to determine the signs of these peculiar couplings.[263]

For F atoms bonded to a Te(IV) atom, ^2J(F,F) couplings ~170 Hz were reported.[466]

Three-bond couplings, $^3J(A,B)$, through the A—M—N—B moiety

The Karplus-like dependence of *vicinal* constants is reviewed in Section 3.1. Although this angular dependence can be traced to stereoelectronic interactions within the molecular fragment containing the coupled nuclei, the main effect to be discussed in this section is the dependence on electron delocalizations both from the A—M and B—N bonds, and into the (A—M)* and (B—N)* antibonds for a fixed dihedral angle. In particular, for a *cis* arrangement, recent results[12] suggest that electron delocalizations into any of the (A—M)* and (B—N)* antibonds produce important decreases. On the other hand, delocalizations from the A—M and B—N bonds seem to produce important increases. This yields to an interesting rationalization of the 'Barfield effect',[596] for example the very well-known difference between $^3J(H_{exo},H_{exo})$ and $^3J(H_{endo},H_{endo})$ in (**38b**), 12.2 Hz and 9.1 Hz, respectively,[597] which has been rationalized using different approaches.[598,599] It can also be rationalized as originating mainly in the different strengths of two pairs of interactions: (1a) (C4—C5)→(C$_3$—H$_{exo}$)* = 2.21 kcal mol^{-1}, (1b) (C4—C7)→(C$_3$→H$_{endo}$)* = 3.11 kcal mol^{-1}; and (2a) (C3—H$_{exo}$)→(C4—C5)* = 3.34 kcal mol^{-1}, (2b) (C3—H$_{endo}$)→(C4—C7)* = 2.51 kcal mol^{-1}. It is important to compare the respective dihedral angles, C5—C4—C3—H$_{exo}$ = 170.1°, and C5—C4—C3—H$_{endo}$ = 156.9°. Despite the latter being ~10° smaller than the former, (1b) is stronger than (1a) and (2b) is stronger than (2a).[12] This shows that the C4—C7 bond is a much better electron donor than the C4—C5 bond, and that the (C4—C5)* antibond is a much better electron acceptor than the (C4—C7)*. Such behaviour parallels the strain in the C—C bonds of the 7 bridge. This suggests that any *cis*-^3J(H,H) coupling with a *vicinal* bridge similar to that in (**38b**) should also be very small. The effect was dubbed the 'Barfield effect'[596] and an empirical correlation between the departure from the generalized Karplus equation[308] and the phase angle of the pseudo-rotation of the envelope conformation was given.[598,600] Similar effects on olefinic ^3J(H,H) couplings were reported; for instance, ^3J(H,H) = 8.6 Hz in cyclohexadiene (**66**),[553] 4.8 Hz in norbornadiene (**67**), 4.7 Hz in norbornene (**68**), and 4.6 Hz in cyclopentene (**69**).[139,601] In all these cycloalkenes the olefinic ^3J(H,H) couplings are notably smaller than in larger members of this series[601] and different geometric and hybridization effects should also be operating. Significant electron delocalization, into one or both (C—H)* antibonds, leads to a very small *vicinal cis*-^3J(H,H) across the olefinic bond of cyclopropene (**6**),

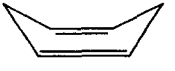

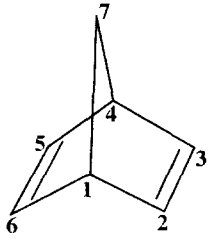

[67]

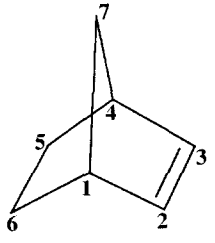

[68]

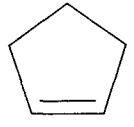

[69]

1.0 Hz.[139] In pyridine (**51**), where this delocalization is inhibited by the strong $n(N) \rightarrow (C_2—H_2)^*$ interaction (NBO $E^{(2)} = 4.09$ kcal mol^{-1}, Table 15) $^3J(H2,H3) = 4.86$ Hz.[602] Similar values have been observed in compounds like (**70**), $^3J(H1,H2) \sim 6$ Hz.[465]

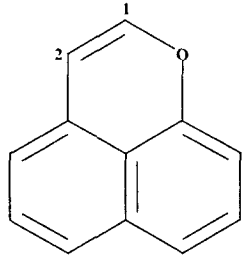

[70]

Examples of an increase in *vicinal* J(H,H) couplings owing to an increase of electron delocalizations from any of the C—H bonds containing the coupled nuclei can be found in the substituent effect on ^3J(H2,H3) in 1-X-benzenes when X is an electronegative substituent group. For instance, in fluorobenzene ^3J(H2,H3) = 8.34 Hz,[603] while in benzene ^3J(H2,H3) = 7.54 Hz.[139] The σ(C1—C2)* and σ(C1—C6)* antibonds are better electron acceptors in the former than in the latter. The dependence of ^3J(C,H) couplings on the orientation of an α-hydroxyl group[527] can also be rationalized in terms of the two types of electron delocalizations that are relevant for *vicinal* couplings. For an O—H conformation *trans* to the Ci—C bond, the O—H bond is a good electron donor. Some conspicuous examples where such an orientational effect was observed were given by Parella *et al.*[604] in norbornene derivatives in which the coupling pathway is not far from a *trans* configuration. This seems to indicate that the rules given above for *vicinal* couplings hold also for a *trans* arrangement. Perhaps two of the best examples are the small *cis* and *trans* ^3J(C,H) couplings in 2-Cl-propene, 4.6 Hz and 8.9 Hz, and in 2-Br-propene (**71**), 4.1 Hz and 8.7 Hz, respectively.[605] In both compounds, strong electron delocalizations from the halogen lone pairs into the (C1—C2)* antibond can be expected.

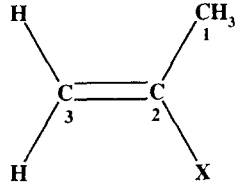

X=Cl, Br

[71]

Notably different ^3J(P,C) couplings through P—C—C—C and P—C—N—C pathways were reported in ref. 606 and were ascribed to the N lone pair, which should enhance the ability of the latter in transmitting the spin information associated with the FC interaction.

The following *cis* three-bond couplings through a vinyl moiety are worthy of note: $^3J(^{199}\text{Hg},^{199}\text{Hg})$ ~8820 Hz in (**72**), and $^3J(^{199}\text{Hg},^{29}\text{Si})$ ~190 Hz in (**73**).[607]

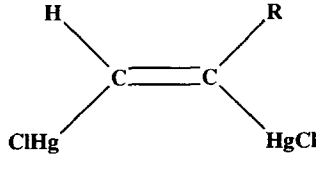

[72]

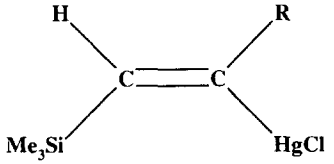

[73]

Longer-range $^nJ(A,B)$ couplings ($n > 3$)

The so called '*J*-coupling method'[309] for the study of side-chain conformations in aromatic compounds was also used during the review period in many interesting examples by Schaefer's team. It is based on the stereospecificity of both σ- and π-transmitted components of long-range couplings, and many of its successful applications are due to the very high accuracy achieved in Schaefer's laboratory in measuring coupling constants. The following examples are noteworthy. The previous study of the barrier to inner rotation in ethylbenzene by the same group[608] was based on the precise measurement of long-range *J*(H,H) couplings between the methylene and ring protons. In a new study,[609] a $^{13}C_\beta$-enriched sample was used and consequently long-range *J*(C,C) couplings between the C_β and ring carbon atoms could be measured accurately. Long-range *J*(H,H) were determined in 1-phenyl-1-butyne and 1-phenyl-1-pentyne to study the corresponding barriers to internal rotation.[610] Similarly, the corresponding barrier in phenylallene was studied using long-range *J*(H,H) and *J*(C,H) couplings.[611] Long-range $J(^{13}C,^1H)$ couplings were used to determine the barrier to internal rotation in fluorothioanisoles.[612]

An interesting effect on the ^4J(C,F) coupling pathway in (**74**) was reported;[613] although it is a W configuration, no coupling was observed.

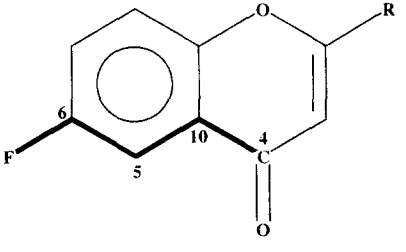

[74]

However, upon protonation of the carbonyl group, ^4J(C,F) ~3 Hz was reported.[613] Upon protonation, the $n_p(O) \rightarrow (C4—C10)^*$ is inhibited, decreasing the $(C4—C10)^*$ occupation number.

Virtual long-range *J*(F,F) were nicely observed in F-bisnoradamantane.[614]

3.4. Complex formation and hybridization effects

In this section only a brief selection of articles in which interesting hybridization effects on couplings were reported is reviewed. Two different types of examples are given, namely (a) hybridization effects that originate in complex formation, and (b) hybridization effects that originate in steric or other intramolecular interactions. Such examples by no means represent an exhaustive account of work reported during this period.

In mesitylene tricarbonyl chromium, $(CH_3)_3C_6H_3Cr(CO)_3$, and mesitylene tricarbonyl tungsten, $(CH_3)_3C_6H_3W(CO)_3$, aromatic ^1J(C,H) couplings of 171.2 Hz and 173.1 Hz, respectively, were measured.[615] These couplings are notably larger than those in the respective uncoordinated arenes. The trend was rationalized as an increase in the s character of the aromatic C—H bonds upon the formation of these complexes. Apparently, the effect originates in a σ-induced effect due to the disturbance of the π arene system by the metal coordination.[615] In $PhCH_2M$ (M = Li, K) as a solvated complex, $^1J(^{13}C,^1H)$ = 151.1 Hz was measured for the methylene group.[616] Accepting the linearity between such coupling and the s character of the C—H bond, an $sp^{2.3}$ hybridization was calculated, supporting the assumption that the CH_2^- group is almost planar.[616]

^1J(C,C) and ^2J(C,H) couplings in vinyllithium were reported by Kamienska-Trela *et al.*[617] A very small value for the former was measured, i.e. ~35.8 Hz. This should be compared with the ^1J(C,C) through the double bond in $(Et_3Sn)_2C{=}CEt(BEt_2)$, of 30.6 Hz.[618] Values of $^1J(^{13}C,^6Li)$ and $^1J(^{15}N,^6Li)$ couplings were measured as a probe of the aggregation behaviour of butyllithium, phenyllithium and lithium diisopropylamide.[619]

^1J(B,H) couplings involving bridging hydrogen atoms are ~43 Hz in (**75**), while for the terminal hydrogen a typical value of ^1J(B,H) ~108 Hz[620] was measured. Calculations of these types of couplings with the EOM-CC approach by Perera *et al.*[189] in B_2H_6 yield 42.69 Hz for the bridging H atom

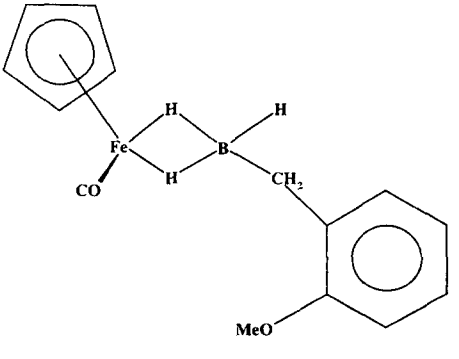

[75]

and 122.17 Hz for the terminal one (the respective experimental values are 46.3 and 133.5 Hz). They are largely dominated by the FC term.[189] Large values of $^{1}J(^{11}B,^{1}H)$ = 199.0 Hz for the apical ^{11}B atom in carboranes, which is formally sp hybridized, were reported.[621]

Increase in the coordination of a Si atom was reported in some cases to decrease a corresponding $^{1}J(Si,H)$ coupling[622,623] and in some cases to increase it, as happens, for instance, in hexacoordinate silicon compounds having a bicapped tetrahedral geometry.[624] $^{n}J(Si,H)$ couplings were found to be more reliable than Si chemical shifts for studying structures in arylsilanes.[625] $^{1}J(Si,H)$ couplings were reported in an interesting set of methyl chlorine disilanes by Herzog *et al.*[626] Coordination of a R_3SiH silicon compound to a highly electronegative ligand is accompanied by a significant increase in $^{1}J(^{29}Si,^{1}H)$, while coordination to an electropositive ligand yields a decrease in $^{1}J(^{29}Si,^{1}H)$.[623] $^{1}J(Si,H)$ couplings were taken as probes of a three-centre bond, W—H—Si, in some complexes of the type $(CO)_{5-n}(L)W(SiHR_3)$.[627]

A coordination bond seems to be very efficient in transmitting spin–spin coupling. This is the case, for instance, in hexacoordinate silicon complexes where two-, three- and four-bond couplings including the dative N→Si bond in the coupling pathway were reported.[628]

Multinuclear couplings involving the Sn nucleus are considered the best probes for detecting pentacoordination of the tin atom.[536] For instance, $^{1}J(Sn,C)$ was used to study the effect of coordinating solvents.[629] $^{1}J(Sn,C)$ and $^{n}J(Sn,P)$ measurements allowed determination of the tin coordination in $Me_2Sn(X)—CH_2—CH_2—P(E)Ph_2$ and $Me_2Sn(X)—CH_2—CH_2—CH_2—P(E)Ph_2$ (X = halogen, E = chalcogen).[630] Examples of $^{1}J(C,C)$ couplings for a pentacoordinate carbon atom were also reported.[631] In brominated trisilylamines, a small value of $^{1}J(^{29}Si,^{15}N)$, of +5.0 Hz, was taken as evidence for Si—Br—Si bridging.[529] Similar bridges are known in tin compounds, e.g. Sn—halogen—Sn.[535,632] In tris(dialkylhalostannyl)amines, similar bridges were also reported and notably larger absolute values of $^{1}J(Sn,C)$ than in tris(trialkylstannyl)amines were observed.[535]

$^{1}J(C,F)$ couplings were used as probes to determine the fluoronium ion character of delocalized arenium ions.[633] Examples of $^{1}J(P,F)$ couplings for hexacoordinate P atoms were measured.[634] $^{1}J(P,P)$ = −405 Hz was determined[51] in the triphenylphosphine phosphadiazonium salt [Mes*NP—PPh_3] [SO_3CF_3] (Mes* = 2,4,6-tri-*t*-butylphenyl). Such a value is surprising since a very long corresponding P—P bond length of 2.625 Å was measured.

In σ-alkyl(pentacarbonyl)manganese complexes and (pentacarbonyl)manganese halides, axial $^{1}J(^{55}Mn,^{13}C)$ couplings are significantly larger than equatorial ones. This is taken as an indication that the *eq*-Mn—C bonds are longer than the axial ones.[635] In a single-crystal molybdenum phosphine complex $^{1}J(^{95,97}Mo,P)$ = 123 Hz was reported (the magnetogyric ratios of the molybdenum isotopes are quite close to each other).[636] $^{1}J(W,P)$ couplings are notably different for the *cis*- and *trans*-isomers of (**76**), for example, in the

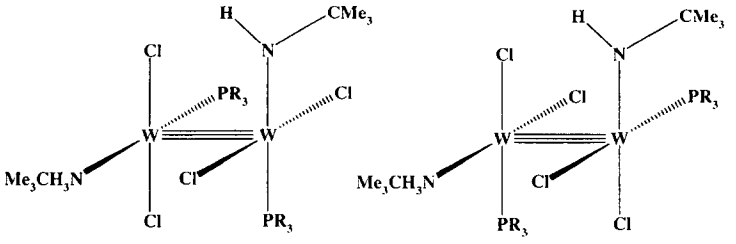

Trans *Cis*

[76]

former ^1J(W,P) is ~110 Hz and in the latter it is ~300 Hz.[637] This difference was rationalized by considering that the $NHCMe_3$ ligands exert a stronger *trans* influence than do Cl ligands, causing the P—W bonds to be stronger in the *cis* than in the *trans* isomers.[637] Couplings involving a ^{183}W nucleus were reported in several other tungsten complexes.[638] $^1J(^{103}Rh,^{15}N)$ for axial and equatorial ligands in rhodoximes of type XRh(III)$(Hdmg)_2L$, X = halide, alkyl, haloalkyl, Hmdg = dimethylgloximate and L = PPh_3 or pyridine, were reported.[639] Increases in axial ^1J(Rh,N) couplings correlate with decreases in the Rh—N distance and therefore such couplings can be taken as a measure of how strong the coordination is with the pyridine ligand. Similar trends were also observed for ^1J(Rh,P) couplings.[640–642] On the other hand, in other rhodium adducts, Kessler *et al.*[449] observed that the Rh—P distances do not correlate with the relative magnitudes of the $J(^{103}Rh,^{31}P)$ couplings. Other rhodium complexes were studied in ref. 643. In *p*-substituted triarylphosphine and triaryl phosphite complexes with Pt(II) and Pt(0), ^1J(Pt,P) couplings were correlated with the Hammett constant and such correlations were rationalized in terms of the σ- and π-bonding components of the Pt—P bonds.[644]

Interligand spin–spin couplings show some interesting features, a few examples of which are presented. In the osmium adduct $(\mu$-H)(H)Os_3-$(CO)_9(C_2H_4)$ ^2J(C,C) = 33 Hz was reported for the *trans* axial carbonyl ligands, while for those in a *cis* configuration the coupling is only 3.5 Hz.[645] ^2J(C,C) coupling through the Cu atom of 21 Hz was reported in Me_2CuLi.[536] Long-range J(C,C) and J(C,N) couplings transferred via the central N(II) atom in square-planar complexes with a Schiff base and glycine were reported.[646] ^2J(P,P) = 200.1 Hz between *trans* axial phosphine ligands in Ru-$\{\eta^3$-$CH_2CHCHCH{=}C(CH_3)_2\}Cl(CO_2)_2(PPr^i_3)$ were measured.[647] Similarly, $^2J(P,P) \geqslant 215$ Hz in *cis*-$[ReCl(NCR)(Ph_2PCH_2CH_2PPh_2)_2]$ (R = alkyl or aryl) complexes with a *cis*-phosphine rhenium(I) centre[648] were reported. Interesting multinuclear couplings were also presented in a variety of complexes, for instance in a trinuclear complex of Pt(II) bridging 1-methylcytosine ligands.[649]

The possibility of measuring a coupling constant between two magnetically equivalent (in the isolated molecule) nuclei was discussed by Wu and Wasylishen.[650] In this way they determined $^2J(P,P) = (250 \pm 15)$ Hz in $Hg(PPh_3)_2(NO_3)_2$ in the solid state. They subsequently determined the absolute sign of the $^2J(P,P)$ coupling as positive using a single crystal in which both phosphino groups are in a *trans* arrangement.[92] Similarly, they measured $^2J(P—Cu—P) = +157$ Hz in $Cu(PPh_3)_2NO_3$[651] and $^2P(^{31}P, ^{31}P)$ in silver complexes.[652]

$^1J(C,C)$ couplings through a triple bond were reported to be reduced by ~23 Hz upon π complex formation.[653,654] The $^1J(^{125}Te, ^{123}Te) = 1603$ Hz coupling in the permethyltitanocene telluride $(C_5Me_5)_2Ti(\eta^2\text{-}Te_2)$ was taken as a probe[655] to detect the presence of an η^2-Te_2 ligand. The Te—Te distance was measured as 2.70 Å, which is longer than that in Te_2, i.e. 2.59 Å. Therefore, in this complex a Te—Te bond order between 1 and 2 was assumed.[655]

Transition metal dihydrogen complexes (**77**) exhibit unique features and were analysed extensively in this review period. NMR parameters are widely

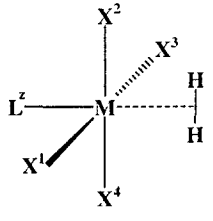

[77]

used probes for studying the nature of the H-bonding to the metal centre, either as a dihydride $(H)_2$ or as an $(\eta_2\text{-}H_2)$ dihydrogen complex, which varies widely depending on the nature of the metal centre and its other ligands, as well as on the nature of the counteranion in charged metal dihydrogen complexes. For instance, the dependence of the H—H distance and $J(H,D)$ coupling of the $(\eta_2\text{-}H_2)$ ligand on the properties of the corresponding *trans* ligand makes them versatile recognition probes for biomolecules.[656]

The relaxation time T_1 of the H resonance is significantly shorter for an $(\eta_2\text{-}H_2)$ structure than that corresponding to a dihydride structure. From the T_1 value, the interatomic H—H distance, r_{HH}, can be obtained, but usually further assumptions are required, especially the rotation rate of the H_2 ligand. Indirect evidence of a more or less intact H_2 bond is taken from the $J(H,D)$ coupling in the HD isotopomer; where values ranging from 10 Hz to 35 Hz are strong evidence of an intact (H_2) ligand.[657] In free H_2, $J(H,D) = 43$ Hz, and $^2J(H,D)$ values as large as 3.3 Hz were found in well-characterized classical dihydrides.[658]

Synthesis and characterization of $[RuH(\eta_2\text{-}H_2)(PP_3Cy)]BPh_4$ (PP_3= $P(CH_2CH_2PPh_2)_3$) were carried out[659] in which $^1J(H,D) = 28$ Hz was measured and taken as evidence for an intact H—D bond. Structural information was also obtained from $J(H,P)$, indicating that the $(\eta_2\text{-}H_2)$ ligand is *trans* to the central P atom. Variable temperature spectra were obtained in solution and the coalescence of the hydride resonances was observed. In $[RuH(\eta_2\text{-}H_2)(DMPE)_2]^+$, evidence for the presence of an intact H—H bond was provided by the facile formation of the HD isotopomer and $J(H,D) = 32.2$ Hz was measured.[660]

In $[(triphos)Re(CO)_2(H_2)]^+$ no coupling of H to P and $J(H,D) = 30.8$ Hz were taken as evidence for the presence of an $(\eta_2\text{-}H_2)$ ligand.[661] The $J(H,D)$ value is among the largest found in this type of complex. In complexes with phosphine coligands, $^2J(H,P)$ values are significantly larger in metal dihydride complexes than in $(\eta_2\text{-}H_2)$ complexes. Large $^2J(H,P)$ couplings and the absence of HD coupling in $[(PP_3)Rh(H_2)]^+$ and $[(PP_3)Co(H_2)]^+$ were indicative of a dihydride structure.[657]

The two D isotopomer rotamers of some Nb dihydrogen complexes have similar $J(H,D) = 15$ Hz, but very different couplings of the H nucleus *cis* to a P ligand, $J(P,H)^{endo} = 50.5$ Hz and $J(P,H)^{exo} < 7$ Hz,[662] indicating that the rotation of the coordinated H—D molecule is slow compared with the NMR timescale. The r_{HH} distance obtained from T_1 was 1.17 Å. At 233 K both signals coalesce and at 273 K a single resonance with $J(H,D) = 16$ Hz and $J(H,P) = 26.4$ Hz appeared. Interestingly, no decoalescence was found for the dihydrogen isotopomer (at 173 K). It was pointed out that this phenomenon could be ascribed either to a very large kinetic isotope effect or (most probably) to the existence of a very large exchange coupling.

The $^1J(H,D) = 22.7$ Hz in $[OsN_4(\eta_2\text{-}H_2)L]^{2+}$ ($N_4 = (NH_3)_4$, L = carbene) was considered the fingerprint for a $(\eta_2\text{-}H_2)$ ligand when the carbene ligand was in a *cis* position.[663] In a study of substitution and geometric isomerization effects of complexes of the type $[Os(en)_2(\eta_2\text{-}H_2)L]^{z+}$ for different L ligands,[664] $J(H,D)$ were measured and employed as structural probes. $J(H,D)$ ranged from 7.2 Hz (L = Cl^-) to 21.1 Hz (L = pyrazine). In $[Os\ H(\eta_2\text{-}H_2)(PPh_2OR)_4]^+$, $J(H,D) = 20$–21 Hz was indicative of a true $(\eta_2\text{-}H_2)$ ligand.[665] The H—H distance obtained from T_1 measurements was 0.90 Å (1.12 Å) assuming fast (slow) spinning of the H_2 ligand. A wide variety of complexes obtained from reactions of $(PPr^i_3)_2OsH_6$ involving addition of protons and removal of electrons were characterized by NMR T_1 and $J(H,D)$ of partially deuterated samples.[666] Interestingly, the product $(PPr^i_3)_2OsH_7{}^+BF_4{}^-$ was characterized as having two $(\eta_2\text{-}H_2)$ ligands with $J(H,D) = 32.6$ Hz and $r_{HH} = 1.00$ Å (0.79 Å) assuming fast (slow) spinning of the H_2 ligands. The dependence of different properties of $[Os(\eta_2\text{-}H_2)(dppe)_2L]$ complexes on the ligand L was analysed experimentally;[667] a consistent correlation of r_{HH} with the bond dissociation energy of the $(\eta_2\text{-}H_2)$ ligand was found and $J(H,D)$ coupling variations were

discussed. These results support the theoretical findings in Os metal complexes.[10,668]

Osmium dihydrogen complexes $[Os(NH_3)_4L^z(\eta_2\text{-}H_2)]^{(z+2)+}$ (L^z = $(CH_3)_2CO$, H_2O, CH_3COO^-, Cl^-, H^-, C_5H_5N and CH_3CN) were analysed theoretically, using SCF and MP2[668] and DFT methods.[10] SCF geometry optimizations were carried out, and the Os—H and H—H distances were optimized at the MP2 level.[668] r_{HH} distances in the range from 1.30 Å (L = C_5H_5N) to 1.40 Å (L = Cl^-) were found. These values were considered to correspond to stretched H_2 bonds, i.e. no dihydrides were found. Inclusion of electron correlation corrections was very important as a consequence of the flatness of the energy surface with respect to H—H bond stretching. Calculated FC contributions to J(H,D) at the SCF and MP2 levels yielded very poor results. An almost inverse linear relationship was found between experimental J(H,D) couplings and MP2 optimized r_{HH} distances. The CSOV method[658] was applied to analyse the interaction of the H_2 ligand with the rest of the complex, and the polarization and charge transfer effects upon complexation were discussed. Electron correlation effects were separated into intramolecular and intermolecular contributions employing Boys' LMOs.[669] Stabilization of the complex was rationalized as originating in σ electron donation from the H_2 bond to an empty d_σ metal AO, and π back-donation from a filled d_π metal AO to the H_2 σ^* antibonding MO. The total energy is thus lowered and the H—H bond is weakened and stretched; the *trans* L ligand may enhance or inhibit this interaction. DFT J(H,D) values[10] for neutral *trans* ligands were in rather good agreement with experimental values, but the calculated value for free H_2, J(H,D) = 51 Hz, indicates either that the basis set was very poor or that the reliability of DFT results needs more extensive analysis. The linear relationship of J(H,D) with r_{HH}, known empirically,[670] was confirmed and theoretical parameters were determined as in Eq. (79),

$$r_{HH} = 1.38 - 0.0187J(H,D) \quad (\pm 0.02) \tag{79}$$

where r_{HH} is in Å and J in Hz. The decrease of J(H,D) as the Os···H_2 interaction strengthens was directly related to the reduction of the hydrogenic 1s character of the H—H bond as a consequence of the above-mentioned σ donation and π back-donation upon complexation.[10] On the other hand, the partial occupation of the H_2 σ^* MO causes an increase in the H—H distance, and the linear dependence of J(H,D) on r_{HH} is thus rationalized. Interestingly, this behaviour is opposite to that found by Bacskay[671] upon bond stretching of free H_2, where a large increase of J(H,D), with a maximum of $\sim 2 \times 10^7$ Hz at r_{HH} around 11 au, was obtained and only for larger distances was a decrease in the coupling found.

Unexpectedly, very similar coefficients of the linear relationship between J(H,D) and r_{HH} were found in 18 electron transition metal (η_2-H_2) complexes

for a wide range of metal centres (Fe, Cr, Ru, Os) and L ligands,[672] Eq. (80), where the r_{HH} distances were determined in the solid state and J(H,D) couplings were measured in solution.

$$r_{HH} = 1.42 - 0.0167J(H,D) \quad (\pm 0.04) \tag{80}$$

Hush[670] made a simple rationalization of Eq. (80); considering only transitions to the first excited triplet state in the SOS expression of J(H,D), a proportionality between J(H,D) and the H—H bond index P_{HH} was found,[673,674] i.e. if J_0 is the value for free H_2, where $P_{HH} = 1$, Eq. (81) holds.

$$J(H,D)^{complex} \cong J_0 P_{HH} \tag{81}$$

On the other hand, r_{HH} and P_{HH} are linearly related through Eq. (82), where r_0 is the equilibrium distance of free H_2. The slope in Eq. (82),

$$r_{HH} = r_0(2 - P_{HH}) \tag{82}$$

is consistent with the calculated values in model compounds, while the intercept was deduced considering that $P_{HH} = 1$ for $r_{HH} = r_0$. Substitution of P_{HH} from Eq. (82) into Eq. (81) yields Eq. (83),

$$r_{HH} = 1.48 - 0.017J(H,D) \tag{83}$$

which is very close to both the empirical relationship, Eq. (80), and that theoretically obtained for Os complexes, Eq. (79), giving support to the generality of the proposed rationalization. Linear correlations of $J(H,D)/J_0$ and r_{HH}/r_0 with the bonding energy of the H_2 ligand were also discussed.[670]

Substituent effects on different coupling constants for different substrates were discussed for many instances and to cite them would be beyond the scope of this work. However, there are a few peculiar cases that seem to be interesting enough to be included here. For instance, 2-X substitution in fluorobenzene (**78**) yielded a negative $^3J(F,C_3)$ coupling depending on the electronic properties of the X substituent; a few cases are shown in Table 17.

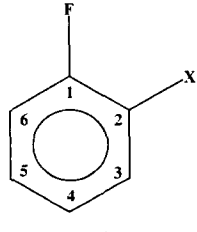

[78]

Table 17. Experimental ^3J(C,F) couplings in 2-X-fluorobenzenes (**78**) (in Hz)

X	$^3J(F,C_3)$	$^3J(F,C_5)$
H[a]	+7.8	+7.8
NH_2[b]	+3.6	+6.8
OCH_3[b]	+1.9	+6.8
I[b]	+1.6	+7.3
NO_2[b]	−2.9	+8.7
CN[b]	−4.0	+7.3
NCS[b]	−4.1	+7.3

[a] Taken from ref. 675
[b] Taken from ref. 52

Ortho- and *meta*-substituted tetra- and triaryltin compounds were studied[676] and *meta* substituents appear to exert electronic effects on ^1J(Sn,C) couplings since better σ-electron acceptors increase such couplings.

Ejchart and Gryff-Keller[261] measured both ^1J(C,X) (halogen) and the ratio $^2J(C,X)/^1J(C,X)$ in $(CH_3)_3SiC{\equiv}CX$. The respective ^1K(C,X) values are 13.2, 34.8 and 60 (in 10^{20} $T^2 J^{-1}$) for X = Cl, Br and I (concerning the sign of such couplings, see Section 3.3), and the ratios are ~0.1–0.2.

In $(CH_3)_3SnR$ (R = alkyl), $\Sigma^1J(Sn,C) = (1350 \pm 47)$ Hz,[515] where Σ stands for the sum of the four ^{1}J(Sn,C) couplings involving the Sn nucleus. This was calculated as the average value for nine substituents including some strained ones like R = bicyclo[1.1.1]pentyl, and individual ^1J(Sn,C) couplings range from 291 Hz to 474 Hz.

J(Te,Te) couplings were used to study the structure of five-membered ring ditellurium derivatives.[677]

The effect of the pyramidality at the N atom on $^1J(^{15}N,^1H)$ in NH_3 was studied using the CLOPPA method[266] with the 6–31G** basis set. As noted above, in this particular case such calculation yields a total $^1J(^{15}N,^1H)$ coupling in close agreement with the experimental value when the optimized geometry at the same level is used.

3.5. Medium effects

A very accurate value of $^1J(^{17}O,^1H)$ coupling in water was measured by Sergeyev *et al.*[678] in a solution of 0.5 mol% in CD_3NO_2. In this way, they obtained $^1J(^{17}O,^1H) = (-)(80.6 \pm 0.1)$ Hz (sign assumed). This should be compared with previous values, which ranged from −73.5 to −96 Hz. It is interesting to note that a concentration dependence was found similar to that quoted in Section 3.3 for $^1J(^{17}O,^1H)$ in cyclopentanol.

The small variations with solvent of long-range J(F,H) and J(H,H) couplings were used[679] to determine how the conformation of the fluoromethyl group in benzyl fluoride (**79**) and some of its derivatives depend on solvent. As both couplings $^6J(H,CH_2)$ and $^6J(H,CH_2F)$ originate in a $\sigma-\pi$ mechanism, the former depends on $\sin^2\theta$ and the latter on $\sin^2\phi$ (**79**). A similar study was performed by Schaefer *et al.*[680] in benzal fluoride.

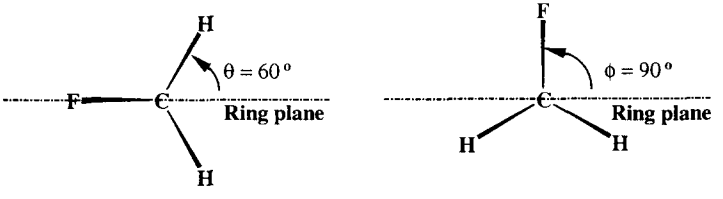

[79]

Important solvent effects on ^1J(C,H) couplings within the side-chain in phenylallene were reported by Schaefer *et al.*[611] They found trends opposite to those expected from the current literature[27] and discussed earlier by Barfield and Johnston[681] and Ando and Webb.[682]

Solvent effects on J(H,H) couplings in (1-^{13}C)benzene in the range of 0.5–1% were reported by Laatikainen *et al.*[683] Magnitudes of couplings increase with the polarity of the solvent. The excellent correlation that those authors found in benzene between $^1J(^{13}C,^1H)$ and Ando's solvation model led Schaefer *et al.*[684] to measure such coupling in benzene in other solutions and to extrapolate the value for gaseous benzene, finding $^1J(^{13}C,^1H)$ = 156.99(2) Hz at 300 K.

In ^{13}C-carbonyl-labelled benzoic acid and benzophenone, Vujanic *et al.*[685] reported $^nJ(^{13}C,^{13}C)$ couplings that depend on solvent. They were rationalized in the former as originating in changes in the intramolecular hydrogen bond in solution, and in the latter in changes in the ring planes dihedral angle.

In a monovalent thallium complex, a ^4J(Tl,F) coupling was found to be extremely solvent dependent. In fact, at room temperature in chloroform a coupling of 850 Hz was measured, which reduced to 0 Hz in methanol, acetonitrile and dimethyl sulfoxide, solvents that promote dissociation.[686]

3.6. Intramolecular dynamics effects

Nuclear motions give rise to isotopic substitution effects and temperature dependence of coupling constants. For rigid molecules, such effects are usually small and their observation requires the use of very accurate experimental techniques.[687] Within the Born–Oppenheimer approximation, both effects may

be described using the J-coupling and energy surfaces as functions of molecular geometric parameters.

During the review period, accurate calculations of rovibrational and geometrical effects of couplings were carried out using the DALTON code.[688] Calculations of the angular dependence of the ^2J(H,H) and ^1J(C,H) couplings in methane were reported[196] at the RPA and CCPPA levels of theory. The H1—C—H2 angle, α, was varied keeping the C_{2V} symmetry, and $\Delta\alpha$ ranged from $-10°$ to $+10°$. It was found that $\Delta\alpha > 0$ leads to an increase in ^1J(C,H1) and a decrease of ^1J(C,H3), with $\Delta^1J(\text{C,H1}) > \Delta^1J(\text{C,H3})$; for $\Delta\alpha < 0$, ^1J(C,H1) decreases and ^1J(C,H3) increases. Δ^1J(C,H3) is numerically larger than Δ^1J(C,H1), an 'anomalous' effect of the same kind as that which was found for bond stretching in methane.[196–198] However, unlike the latter, this unexpected behaviour cannot be attributed to a correlation effect,[197] as RPA results are qualitatively similar to those of CCPPA. The ^2J(H1,H2) coupling was found to change with $\Delta\alpha$ according to a trigonometric law, Eq. (84),

$$\Delta^2J(\text{H1,H2}) = 41.57 \sin \Delta\alpha - 8.90 \sin^2 \Delta\alpha \tag{84}$$

which reproduces all the CCPPA results within 0.025 Hz.

CCSDPPA[689] calculations of the full ^1J(C,H) and ^2J(H,H) coupling surfaces of the methane molecule were reported,[198] consistent to second order in the symmetry displacement coordinates. A total of 51 geometries were selected to fit the coupling surfaces. Equilibrium values for ^1J(C,H) and ^2J(H,H) of 123.865 Hz and -14.308 Hz, respectively, were found. Changes in ^1J(C,H) are mostly due to the FC term behaviour, which exhibits the 'unexpected differential sensitivity' that was found previously[197] because it is more sensitive to the C—H2 than to the C—H1 bond stretching. $^2J^{\text{FC}}$(H,H) becomes less negative as the distance between the coupled nuclei increases. Taking into account that noncontact terms are less dependent on correlation effects than the FC term 'experimental' values of the FC contribution at equilibrium geometry were obtained, $^1J^{\text{FC}}(\text{C,H})^{\text{eq}} = 119.13$ Hz and $^2J^{\text{FC}}(\text{H,H})^{\text{eq}} = -12.9$ Hz, by subtracting the equilibrium value of the noncontact terms from the experimental value.

Wigglesworth *et al.*[202] recalculated the two couplings surfaces of ref. 198 using a grid of 55 points with a similar basis set using the SOPPA(CCSD) method,[690] an improved version of the CCSDPPA. Data obtained were used to calculate values of ^1J(C,H), ^1J(C,D) and ^2J(H,D) in all isotopomers CH_nD_{4-n} for a range of selected temperatures. Calculated values for the equilibrium geometry, $^1J^{\text{eq}}(\text{C,H}) = 123.846$ Hz and $^2J^{\text{eq}}(\text{H,D}) = -2.218$ Hz were compared with those estimated by subtracting the nuclear motion corrections to the experimental values, $^1J^{\text{eq}}(\text{C,H})^{\text{exp}} = (120.78 \pm 0.05)$ Hz and $^2J^{\text{eq}}(\text{H,D})^{\text{exp}} = (-1.84 \pm 0.02)$ Hz.

The same approach as in ref. 202 was used to calculate the ^1J(O,H) and ^2J(H,H) coupling surfaces for an isolated H_2O molecule.[203] In this case, 49 geometries were selected. The 'unexpected differential sensitivity' found

previously in methane does not occur either in H_2O or in NH_3 (results for NH_3 were reported in ref. 691). This was explained taking into account the fact that the electron distribution has more freedom to adjust upon changing a bond length in H_2O than in CH_4 since lone-pair electrons are more polarizable than bond electrons. For ^2J(H,H), bond stretching gives a negative contribution and, hence, a numerically larger coupling, while increasing the HOH angle gives a positive contribution that leads to a numerically smaller coupling. Similar calculations were carried out for OH^- and H_3O^+.[692] Temperature dependence and isotopic substitution were thoroughly discussed (see the next subsection below).

Kirpekar *et al.* calculated the effect of nuclear motion on ^1J(X,H) and ^2J(H,H) in the series XH_4 (X = C, Si, Ge, Sn),[171] up to first order in the normal coordinates, at the RPA, SOPPA and MCLR levels of approximation. The variation of ^2J(H,H) with the X—H distance is dominated by the variation of the FC term. For example, for GeH_4, the FC contribution ranges from −6 Hz to about 25 Hz on varying the Ge—H distance from 1.3 Å to 1.7 Å, while the noncontact contribution varies at most by 5 Hz in the same range.

Temperature dependence

Temperature dependence of J couplings in the liquid phase may originate in both intramolecular nuclear motions and intermolecular interaction effects. In the review period, experimental and theoretical studies of this dependence were reported.

Although in XeF_2 a significant temperature dependence of ^{129}Xe and ^{19}F chemical shifts was found, the corresponding $^1J(^{129}Xe,^{19}F)$ coupling constant was observed to be notably insensitive to temperature changes. In fact, the $^1J(^{129}Xe,^{19}F)$ coupling over the range of temperature from 243 K to 303 K is (5644.2 ± 0.6) Hz.[693]

Laatikainen *et al.*[683] reported that ^5J(H,H) and ^3J(H,H) couplings in (1-^{13}C)benzene decrease ~0.01% K^{-1} and ^4J(H,H) couplings increase ~0.02% K^{-1}.

The change in $^1J(C,^{27}Al)$ coupling with temperature in dimeric ethylaluminium dichloride[694] and in 1 : 2 LiCl–ethylaluminium dichloride[695] was used as a probe to detect the temperature at which a liquid-state phase change takes place.

Very accurate ^2J(H,D) values for water in nitromethane-d_3 were measured by Sergeyev *et al.*[678] at 297 K (−1.127 Hz), 323 K (−1.114 Hz) and 353 K (−1.091 Hz). The couplings were assumed negative on the basis of the Geertsen and Oddershede calculation.[199] Theoretically, ^2J(H,D) for isolated water was calculated[203] to range from −1.231 Hz (260 K) to −1.234 Hz (340 K), and to be $^{16}O/^{17}O/^{18}O$ isotope substitution independent. There is disagreement between calculated and experimental values in the trend of ^2J(H,D) with temperature, which was attributed to intermolecular interaction effects. A

value of $^1J(^{17}O,H) = (-80.62 \pm 0.06)$ Hz was also measured in nitromethane-d_3[678] at 323 K, which is numerically larger than Wasylishen's observed value of (-78.70 ± 0.02) Hz in cyclohexane-d_{12} at 293 K.[696] This difference was also ascribed to intermolecular interactions effects, which were expected to be more important in nitromethane-d_3 than in cyclohexane-d_{12}.[203] The corresponding calculated values for isolated water corroborate this assumption, being −77.187 Hz (323 K) and −77.224 Hz (293 K).[203] However, it should be taken into account that Boykin *et al.*[485] found that $^1J(O,H)$ decreases numerically when the O—H bond acts as acceptor in an intermolecular hydrogen bond interaction, which is consistent with an increase in $|\,^1J(O,H)\,|$ for increasing temperature.

In Wigglesworth *et al.*'s[202] calculations of the temperature dependence of $^1J(C,H)$ and $^2J(H,H)$ in CH_4 and its isotopomers, $^1J(C,H)$ was found to increase by 0.088 Hz on raising the temperature from 180 K to 380 K, which agrees with the observed increase of 0.083 Hz on raising the temperature from 200 K to 370 K.[697] The D primary and secondary isotope effects on $^1J(C,H)$ were predicted to decrease with increasing temperature. Table 18 shows the total values, separated into stretching, bending and the second-order stretch–bend contributions to $^1J(C,H)$ and $^1J^*(C,H)$ in each of the five isotopomers at 300 K, as well as the zero-point corrections. $J^*(X,H)$ is defined as in Eq. (85).

$$J^*(X,H) = \frac{\gamma(H)}{\gamma(D)} J(X,D) \tag{85}$$

The nuclear motion correction is dominated by the positive stretching contribution (~2.5 to 3.5 Hz), followed by the bending contribution (~1.5 to 1.9 Hz), while the stretch–bend contribution is small and negative but not negligible (~−0.2 Hz). $^2J(H,D)$ was found to be practically temperature

Table 18. Calculated vibrational corrections to $^1J(C,H)$ and $^1J^*(C,H)$, for the five deuterated isotopomers of methane at 300 K. All values in Hz[a]

	CH_4	CH_3D		CH_2D_2		CHD_3		CD_4
	$^1J(C,H)$	$^1J(C,H)$	$^1J^*(C,H)$	$^1J(C,H)$	$^1J^*(C,H)$	$^1J(C,H)$	$^1J^*(C,H)$	$^1J^*(C,H)$
Stretch	3.446	3.152	3.442	2.856	3.147	2.557	2.849	2.548
Bend	1.916	1.810	1.778	1.709	1.656	1.618	1.541	1.434
Stretch–bend	−0.227	−0.224	−0.239	−0.222	−0.238	−0.220	−0.238	−0.238
Total	5.134	4.737	4.981	4.343	4.564	3.956	4.152	3.744
Zero-point correction	5.030	4.625	4.890	4.227	4.459	3.844	4.033	3.621

[a] $^1J^*(C,H)$ defined as in Eq. (85), see text.

independent (corrections are two orders of magnitude below the state-of-the-art experimental precision), in agreement with experimental results.[250] Nuclear motion corrections to $^2J^*$(H,H), Eq. (85), at 300 K are displayed in Table 19. As can be expected, the zero-point correction was by far the dominant vibration–rotation contribution to both couplings at any accessible temperature. The same conclusion was obtained in the theoretical analysis of the ^1J(O,H) and ^2J(H,H) coupling surfaces for the isolated H_2O molecule,[203] where, for instance, the zero-point correction was found to account for 3.963 Hz of the 4.340 Hz of the total correction at 300 K for ^1J(O,H).

The temperature dependence on ^1J(X,H) and ^2J(H,H) in the series XH_4 (X = C, Si, Ge, Sn)[171] was calculated by Kirpekar *et al.* at the RPA, SOPPA and MCLR levels of approximation and up to first order in normal coordinates. For ^1J(X,H), the relative importance of the zero-point correction decreases slightly from CH_4 to SnH_4, being about 1–3% of the equilibrium values, i.e. much smaller than the effect of correlation and of the same order as noncontact terms. However, by comparison with refs 198,202, it was pointed out that second-order corrections might be important and could change results by as much as a factor of 2. Since calculated ^2J(H,H) couplings are small (±3–8 Hz), zero-point corrections become significant and up to 25% of the experimental value. The variation of both couplings with temperature in the range 100–500 K is very small, which means that the zero-point correction constitutes by far the largest rovibrational correction to such couplings.

Sauer *et al.*[692] applied the RPA, SOPPA(CCSD) and MCRPA methods using the DALTON program[688] to predict the so far unmeasured temperature dependence and isotope effects of $^1J(^{17}O,H)$, $^1J(^{17}O,D)$ and ^2J(H,H) in the H_3O^+ and OH^- ions. For OH^-, $^1J(^{17}O,H)$ and $^1J(^{17}O,D)$ present a linear dependence with temperature, with almost the same slopes as in H_2O,[203] while the temperature effects for H_3O^+ are very nonlinear, particularly for low temperatures. The difference between $^1J(^{17}O,H)$ in H_3O^+ at 300 K and at 100 K is 0.99 Hz (cf. 0.25 Hz for H_2O[203]), while the corresponding change in ^2J(H,H) is −0.056 Hz (cf. −0.066 Hz for H_2O[203]).

Table 19. Calculated vibrational corrections to J^*(H,H) for the deuterated isotopomers of methane at 300 K. All values in Hz[a]

	CH_3D	CH_2D_2	CHD_3
Stretch	−0.003	−0.029	−0.057
Bend	−0.646	−0.621	−0.594
Stretch–bend	−0.038	−0.038	−0.037
Total	−0.688	−0.689	−0.687
Zero-point correction	−0.686	−0.689	−0.683

[a] J^*(H,H) defined as in Eq. (85), see text.

Isotope effects

In general, isotope effects on coupling constants are very small and they are seldom reported. Their observation requires that measurements be carried out with a very good accuracy.[687] In what follows, primary, Δ_pJ, and secondary, Δ_sJ, isotope effects are defined as in Eqs (86a) and (86b), respectively.

$$\Delta_pJ = |\,(\gamma(^mY)/\gamma(^nY))\,^1J(X^nY)\,|_{(1)} - |\,^1J(X^mY)\,|_{(0)} \tag{86a}$$

$$\Delta_sJ = |\,^1J(X^mY)\,|_{(1)} - |\,^1J(X^mY)\,|_{(0)} \tag{86b}$$

where the subscripts (0,1) indicate the number of deuterium nuclei in the corresponding isotopomer, and superscripts n and m denotes the heavier and lighter isotopes respectively.

Some very interesting cases were reported during the review period. Strelenko and Sergeyev[698] measured $^1J(^{14}N,^{14}N) = (4.233 \pm 0.006)$ Hz in nitrous oxide, NNO. They compared that value with the $^1J(^{15}N,^{15}N)$ coupling measured previously by other authors, i.e. (-9.16 ± 0.3) Hz[699] and (8.9 ± 0.1) Hz,[700] taking into account that the $\gamma(^{14}N)/\gamma(^{15}N) = -0.71288$.

Sergeyev *et al.* measured D/H isotope effects on C–H and C–D couplings in several halomethanes $CH_{2-n}D_nCl_2$ ($n = 0,1,2$),[701,702] and in $CH_mD_nX_{4-n-m}$ (X = Cl,Br,I).[703] The measured ^1J(C,H) and $^1J^*$(C,H), Eq. (85), in halomethanes are displayed in Table 20. Primary and secondary effects for a single deuterium substitution are summarized in Table 21. The Δ_pJ depend almost linearly on the number k of halogen substituents, the extrapolated values for $k = 0$ being close to Δ_pJ in methane (~ -0.07 Hz[250]). For secondary effects, the dependence on k seems to be nonlinear, although it was reported in ref. 701 that Δ_sJ was almost independent of the substituent (cf. -0.30 Hz in CH_4,[250] -0.30 Hz in CH_3Ph,[704] -0.27 Hz in CH_2Cl_2[702] and -0.22 Hz in cyclohexane-d_1[705]). For a fixed k, Δ_pJ increases in magnitude with increasing electronegativity of the substituent. For secondary effects, the influence of the substituent increases in the series Cl, Br, I and seems to be controlled mostly by steric factors.[703] To test the additivity of isotope effects, primary and secondary effects in $CHDCl_2$ were determined and compared with the total observed isotope effect ΔJ_{obs} in CD_2Cl_2, Eq. (87).[701,702]

$$\Delta J_{obs} = |\,(\gamma(H)/\gamma(D))\,^1J(C,D)\,|_{(2)} - |\,^1J(C,H)\,|_{(0)} \tag{87}$$

Results in ref. 702, which were considered more accurate than those of ref. 701, yielded $\Delta J_{obs} = (-0.86 \pm 0.06)$ Hz, $\Delta_sJ = (-0.27 \pm 0.01)$ Hz and $\Delta_pJ = (-0.59 \pm 0.06)$ Hz, showing very good primary and secondary isotope effect additivity.

The secondary isotope effect on $^1J(C,^{19}F)$ in CHF_3 was measured for the first time in ref. 703 as $\Delta_sJ = (+1.56 \pm 0.01)$ Hz. This positive value contrasts with

Table 20. Experimental and some calculated ^1J(C,H) and $^1J^*$(C,H) values in halomethanes. All values in Hz[a]

Compound	n	^1J(C,H)[b]	$^1J^*$(C,H)[b]
$CH_{3-n}D_nI$	0	150.984 ± 0.004 (150.97)[b]	–
	1	150.706 ± 0.004 (150.70)	150.74 ± 0.02 (150.69)
	2	150.420 ± 0.01 (150.42)	150.44 ± 0.02 (150.41)
	3	–	150.13 ± 0.01 (150.13)
$CH_{3-n}D_nBr$	0	151.484 ± 0.002 (151.46)	–
	1	151.175 ± 0.001 (151.17)	151.193 ± 0.010 (151.13)
	2	150.872 ± 0.001 (150.88)	150.86 ± 0.01 (150.83)
	3	–	150.540 ± 0.007 (150.54)
$CH_{2-n}D_nI_2$	0	172.653 ± 0.005	–
	1	172.509 ± 0.002	172.27 ± 0.03
$CH_{2-n}D_nBr_2$	0	178.927 ± 0.001	–
	1	178.735 ± 0.001	178.423 ± 0.007
	2	–	178.23 ± 0.03
$CH_{2-n}D_nCl_2$[c]	0	177.507 ± 0.007	–
	1	177.258 ± 0.010	176.91 ± 0.04
$CH_{1-n}D_nI_3$	0	186.37 ± 0.01	–
	1	–	185.92 ± 0.06
$CH_{1-n}D_nBr_3$	0	204.850 ± 0.005	–
	1	–	204.15 ± 0.10
$CH_{1-n}D_nCl_3$	0	209.10 ± 0.01	–
	1	–	208.18 ± 0.13
$CH_{1-n}D_nF_3$	0	239.10 ± 0.1	–
	1	–	237.45 ± 0.1

[a] $^1J^*$(C,H) defined as in Eq. (85), see text.
[b] Values in parentheses correspond to calculated couplings.
[c] Taken from ref. 427.

secondary effects on ^1J(C,H), which are usually negative. From the very reliable calculation of ref. 203, it was found that the primary isotope effect in HOD is of larger magnitude than the secondary effect (i.e. $\Delta^1_pJ(O,H) = -0.982$ Hz, $\Delta^1_sJ(O,H) = -0.122$ Hz at 343 K, compared with experimental values of (-1.0 ± 0.2) Hz and (0.0 ± 0.1) Hz, respectively[706]), the opposite of what is found in deuterated methane isotopomers.

$^{37}Cl/^{35}Cl$ secondary isotope effects on ^1J(C,H) of order -0.01 Hz were also found by Sergeyev *et al.*[702] in chlorinated methanes CH_3Cl and CH_2Cl_2. Assuming that such isotope effects are due to the 0.000 04 Å shortening of the

Table 21. Experimental primary and secondary isotope effects on C—H couplings due to the substitution by a single D atom in halomethanes $CH_{4-k}X_k$

	$\Delta_p J$(C,H) (Hz)			$\Delta_s J$(C,H) (Hz)	
	$k = 1$	$k = 2$	$k = 3$	$k = 1$	$k = 2$
F	–[a]	–[a]	-1.65 ± 0.1	–[a]	–[a]
Cl	–[a]	0.60 ± 0.02	-0.92 ± 0.13	–[a]	-0.25 ± 0.01
Br	-0.29 ± 0.01	-0.504 ± 0.007	-0.70 ± 0.07	-0.306 ± 0.003	-0.192 ± 0.002
I	-0.25 ± 0.02	-0.38 ± 0.02	-0.45 ± 0.15	-0.285 ± 0.006	-0.144 ± 0.006

[a] Not measured.

C—Cl bond length at room temperature,[702] the authors estimated the derivative for ^1J(C,H) as (Eq. (88))

$$\frac{\partial\, {}^1J(\mathrm{CH})}{\partial r_{\mathrm{C-Cl}}} = 190(\pm 80) \quad \mathrm{Hz\,\AA^{-1}} \tag{88}$$

^1J(C,Cl) were estimated from experimental data, neglecting small primary $^{37}Cl/^{35}Cl$ isotope effects, and it was found to depend strongly on the number of chlorine atoms, ranging from $\sim(11 \pm 2)$ Hz for CH_3Cl to (38 ± 2) Hz for $CHCl_3$.

The primary isotope effect on $^1J(C_\alpha,H)$ in benzaldehyde was measured by Meic *et al.*[707] as (-0.34 ± 0.08) Hz. In the monodeuterated isotopomers of *cis*- and *trans*-stilbene, the primary isotope effects on the vinylic ^1J(C,H) couplings, Eq. (88), were measured as (-0.44 ± 0.37) Hz and (-0.60 ± 0.49) Hz, respectively.[708] For these isotopomers and for other members of this series with different degrees of deuteration, the secondary effects on those ^1J(C,H) couplings as well as on the vinylic ^3J(H,D) couplings were also measured in the same paper.[708] While the former are negative, the latter are positive.

Laatikainen *et al.*[683] measured the ^{1}H NMR spectrum of (1-^{13}C)benzene with high accuracy in a strong magnetic field and found that no isotope effect could be detected for ^3J(H,H) and ^5J(H,H) couplings. On the other hand, for ^4J(H1,H3) and ^{4}J(H2,H4) couplings they measured an isotope effect of (0.7 ± 0.5) mHz, while for ^4J(H3,H5) no effect was observed, and for ^4J(H2,H6) an effect of (0.9 ± 0.5) mHz was reported.

Uvarov *et al.* demonstrated the suitability of the Saunders isotopic perturbation method,[709] applied to *vicinal* C–D couplings, in order to measure the conformational equilibrium of deuterated cycloalkanes.[705] To this end, the secondary isotope effect on ^nJ(C,D) was determined as shown in Eq. (89), where I represents (D_1)cyclohexane, and II represents (1,1-D_2)cyclohexane.

$$\Delta {}^nJ(\mathrm{C,D}) = {}^nJ(\mathrm{C,D})(\mathrm{II}) - {}^nJ(\mathrm{C,D})(\mathrm{I}) \tag{89}$$

This observable isotope effect is given by Eq. (90),

$$\Delta^n J = \tfrac{1}{2}[{}^nJ_{eq}(\mathrm{II}) + {}^nJ_{ax}(\mathrm{II})] - \{[1eq]{}^nJ_{eq}(\mathrm{I}) + [1ax]{}^nJ_{ax}(\mathrm{I})\} \qquad (90)$$

where the subscripts *eq* and *ax* indicate the site of the deuterium substitution, and $[1eq]$ ($[1ax]$) is the equatorial (axial) fraction of the deuterium-substituted compound population. $\Delta^n J$ can be thought of as due to thermodynamic, $\Delta^n J_{\mathrm{th}}$, and intrinsic, $\Delta^n J_{\mathrm{in}}$, contributions, i.e. $\Delta^n J = \Delta^n J_{\mathrm{th}} + \Delta^n J_{\mathrm{in}}$, which are defined as in Eqs (91),

$$\Delta^n J_{\mathrm{th}} = \tfrac{1}{2}[(1-K)/(1+K)][{}^nJ_{eq}(\mathrm{I}) - {}^nJ_{ax}(\mathrm{I})] = \tfrac{1}{2}({}^nJ_{eq}(\mathrm{I}) + {}^nJ_{ax}(\mathrm{I})) - {}^nJ_{\mathrm{obs}}$$

$$\Delta^n J_{\mathrm{in}} = \tfrac{1}{2}[({}^nJ_{eq}(\mathrm{II}) - {}^nJ_{eq}(\mathrm{I})) + ({}^nJ_{ax}(\mathrm{II}) - {}^nJ_{ax}(\mathrm{I}))] \qquad (91)$$

where K is the equilibrium constant, $K = [1eq]/[1ax]$, which can be expressed as $K = ({}^nJ_{\mathrm{obs}} - {}^nJ_{ax})/({}^nJ_{eq} - {}^nJ_{\mathrm{obs}})$,[709] where ${}^nJ_{ax}$ and ${}^nJ_{eq}$ are the values of the limiting forms $1ax$ and $1eq$, and ${}^nJ_{\mathrm{obs}}$ is the averaged (or observable) value of ${}^nJ$.

Thus, $\Delta^n J_{\mathrm{in}}$ may be considered as the average of secondary isotope effects or the averaged value for two equally populated states with equatorial and axial ^{13}C–D couplings. Therefore, if there is no substantial secondary effect on a coupling, $\Delta^n J \approx \Delta^n J_{\mathrm{th}}$ holds, and it is possible to determine the isotope effect on conformational equilibrium in I. It was observed that only for the *vicinal* $^3J(^{13}\mathrm{C,D})$ coupling does the thermodynamic part predominates ($\Delta^3 J_{\mathrm{th}} = -0.0032$ Hz, estimated with $K = 1.014$, from data of ref. 710; $\Delta^3 J_{\mathrm{in}} = -0.0011$ Hz), and therefore this coupling can be used to estimate the conformational equilibrium effect.

ACKNOWLEDGEMENTS

The Argentine authors gratefully acknowledge the financial support from CONICET (grant 4160), UBACYT (grant TX54) and ANPCYT (grant 604). J.E.P. supported by a CONICET fellowship. RHC, C.G.G. and M.C.R.A. are members of the Carrera del Investigader of CONICET.

REFERENCES

1. R. H. Contreras and J. C. Facelli, *Annu. Rep. NMR Spectrosc.*, 1993, **27**, 255.
2. J. Kowalewski, *Prog. NMR Spectrosc.*, 1977, **11**, 1.
3. J. Kowalewski, *Annu. Rep. NMR Spectrosc.*, 1982, **12**, 81.
4. (a) F. Bloch, W. W. Hansen and M. Packard, *Phys. Rev.*, 1946, **69**, 127; (b) E. M. Purcell, H. C. Torrey and R. V. Pound, *Phys. Rev.*, 1946, **69**, 37.
5. M. Barfield and B. Chakrabarti, *Chem. Rev.*, 1969, **69**, 757.
6. J. N. Murrel, *Prog. NMR Spectrosc.*, 1970, **6**, 1.

7. H. Günther and G. Jikeli, *Chem. Rev.*, 1977, **77**, 599.
8. R. H. Contreras, M. A. Natiello and G. E. Scuseria, *Magn. Reson. Rev.*, 1985, **9**, 239.
9. J. Seminario (ed.) *Recent Developments and Applications of Modern Density Functional Theory*, Elsevier, Amsterdam, 1996.
10. G. B. Bacskay, I. Bytheway, N. S. Hush, *J. Am. Chem. Soc.*, 1996, **118**, 3753.
11. B. Bose, S. Zhao, R. Stenutz, *et al.*, *J. Am. Chem. Soc.*, 1998, **120**, 11158.
12. Unpublished results from these laboratories.
13. G. A. Webb (ed.), *Specialist Periodical Reports, Nuclear Magnetic Resonance*, Vols 22–27, Chapters on theoretical aspects of spin–spin couplings. The Royal Society of Chemistry, London, 1993–1998.
14. G. A. Webb (ed.), *Specialist Periodical Reports, Nuclear Magnetic Resonance*, Vols. 22–27, Chapters on applications of spin–spin couplings. The Royal Society of Chemistry, London, 1993–1998.
15. R. H. Contreras, G. A. Aucar, M. C. Ruiz de Azúa and C. G. Giribet, *Folia Chim. Theor. Latina*, 1993, **21**, 83.
16. T. Helgaker, M. Jaszunski and K. Ruud, *Chem. Rev.*, 1999, **99**, 293.
17. R. H. Contreras, M. C. Ruiz de Azúa, C. G. Giribet, G. A. Aucar and R. Lobayán de Bonczok, *J. Mol. Struct. (Theochem)*, 1993, **284**, 249.
18. J. F. Hinton, *Bull. Magn. Reson.*, 1992, **13**, 90.
19. W. Preetz, G. Peters and D. Bublitz, *Chem. Rev.*, 1996, **96**, 977.
20. S. Sabo-Etienne and B. Chaudret, *Chem. Rev.*, 1998, **98**, 2077.
21. S. Szymański, *Annu. Rep. NMR Spectrosc.*, 1998, **35**, 2.
22. K. Kamienska-Trela, *Annu. Rep. NMR Spectrosc.*, 1995, **30**, 131.
23. W. A. Thomas, *Prog. NMR Spectrosc.*, 1997, **30**, 183.
24. *Encyclopedia of Nuclear Magnetic Resonance* (Editors-in-Chief D. M. Grant and R. K. Harris), Wiley, Chichester, 1996.
25. M. Barfield, in ref. 24, p. 2520.
26. J. C. Facelli, in ref. 24, p. 2516.
27. I. Ando, in ref. 24, p. 2512.
28. F. B. Mallory and C. W. Mallory, in ref. 24, p. 1491.
29. R. E. Wasylishen, in ref. 24, p.1685.
30. C. Altona, in ref. 24, p. 4909.
31. J. van Wijk, B. D. Huckriede, J. H. Ippel and C. Altona, *Methods Enzymol.*, 1992, **211**, 286.
32. R. J. Abraham, E. J. Chambers and W. A. Thomas, *Magn. Reson. Chem.*, 1994, **30**, 60.
33. G. A. Webb (ed.), *Specialist Periodical Reports, Nuclear Magnetic Resonance*, Vols. 22–27, Chapters on conformational analysis. The Royal Society of Chemistry, London, 1993–1998.
34. L. B. Krivdin and S. V. Zinchenko, *Current Org. Chem.*, 1998, **2**, 173.
35. N. S. True and C. Suarez, *Adv. Mol. Struct. Res.* 1995, **1**, 115.
36. I. Tvaroska and F. R. Taravel, *Adv. Carbohydr. Chem. Biochem.* 1995, **51**, 15.
37. E. Kleinpeter, *Adv. Heterocyc. Chem.*, 1998, **69**, 217.
38. D. P. Kelly, in *Advances in Carbocation Chemistry* (ed. J. M. Coxon), JAI Press, New York, 1994.
39. L. D. Quin and J. G. Verkade (eds) *Phosphorus-31 NMR Spectral Properties in Compound Characterization and Structural Analysis*, VCH, New York, 1994.
40. D. M. Heinekey and W. J. Oldham, Jr., *Chem. Rev.*, 1993, **93**, 913.
41. M. Hudlicky and M. Pavlath (eds), *Chemistry of Organic Fluorine Compounds II. A Critical Review*, ACS Monograph 187, American Chemical Society, Washington, DC, 1995.
42. B. Wrackmeyer, in *Physical Organometallic Chemistry – Advanced Applications of NMR to Organometallic Chemistry* (eds M. Gielen, R. Willem and B. Wrackmeyer), vol. 1, pp. 87–122, Wiley, Chichester, 1996.
43. A. Lycka, *Annu. Rep. NMR Spectrosc.*, 1993, **26**, 247.
44. D. M. Heinekey, A. S. Hinkle and J. D. Close, *J. Am. Chem. Soc.*, 1996, **118**, 5353.

45. R. M. Claramunt, D. Sanz, C. López, *et al.*, *Magn. Reson. Chem.*, 1997, **35**, 35.
46. R. K. Harris, J. Kowalewski and S. Cabral de Menezes, *Magn. Reson. Chem.*, 1998, **36**, 145.
47. W. T. Raynes and S. J. Stevens, *Magn. Reson. Chem.*, 1992, **30**, 124.
48. S. Ding and C. Ye, *Magn. Reson. Chem.*, 1993, **31**, 185.
49. M. Herberhold, V. Tröbs and B. Wrackmeyer, *J. Organomet. Chem.*, 1997, **541**, 391.
50. R. Eujen and B. Hoge, *Magn. Reson. Chem.*, 1997, **35**, 707.
51. K. Eichele, R. E. Wasylishen, R. W. Schurko, N. Burford and W. A. Whitla, *Can. J. Chem.*, 1996, **74**, 2372.
52. I. D. Rae, J. A. Weigold, D. G. de Kowalewski, R. R. Biekofsky and R. H. Contreras, *Magn. Reson. Chem.*, 1996, **34**, 181.
53. B. Wrackmeyer, K. H. von Locquenghien, E. Kupce and A. Sebald, *Magn. Reson. Chem.*, 1993, **31**, 45.
54. G. Otting, B. A. Messerle and L. P. Soler, *J. Am. Chem. Soc.*, 1997, **119**, 5425.
55. A. Jarid, M. Moreno, A. Lledós, J. M. Lluch and J. Bertrán, *J. Am. Chem. Soc.*, 1993, **115**, 5861.
56. A. Jarid, M. Moreno, A. Lledós, J. M. Lluch and J. Bertrán, *J. Am. Chem. Soc.*, 1995, **117**, 1069.
57. H.-H. Limbach, G. Scherer, M. Maurer and B. Chaudret, *Angew. Chem., Int. Ed. Engl.*, 1992, **31**, 1369.
58. A. S. Edison, J. L. Markley and F. Weinhold, *J. Biomol. NMR*, 1994, **4**, 519.
59. A. S. Edison, F. Weinhold, W. M. Westler and J. K. Markley, *J. Biomol. NMR*, 1994, **4**, 543.
60. N. Juranic, P. K. Ilich and S. Macura, *J. Am. Chem. Soc.*, 1995, **117**, 405.
61. C. G. Giribet, C. V. Vizioli, M. C. Ruiz de Azúa, R. H. Contreras, J. J. Dannenberg and A. Masunov, *J. Chem. Soc., Faraday Trans.*, 1996, **92**, 3029.
62. I. Carmichael, *J. Phys. Chem.*, 1993, **97**, 1789.
63. I. Carmichael, D. M. Chipman, C. A. Podlasek and A. S. Serianni, *J. Am. Chem. Soc.*, 1993, **115**, 10863.
64. A. S Edison, J. L Markley and F. Weinhold, *J. Phys. Chem.*, 1993, **97**, 11657.
65. A. C. de Dios, J. G. Pearson and E. Oldfield, *Science*, 1993, **260**, 1491.
66. A. R. Engelmann and R. H. Contreras, *Int. J. Quantum Chem.*, 1983, **23**, 1033.
67. (a) T. Arliguie, B. Chaudret, J. Devillers and R. Poliblanc, *C. R. Acad. Sci.* 1987, *Ser. II*, **305**, 1523; (b) D. M. Heinekey, N. G. Payne and G. K. Schulte, *J. Am. Chem. Soc.*, 1988, **110**, 2303.
68. B. Chaudret, H.-H. Limbach and C. Moise, *C. R. Acad. Sci.*, 1992, *Ser. II*, **315**, 533.
69. B. Manzano, F. Jalon, J. Mathes, *et al.*, *J. Chem. Soc., Dalton Trans.* 1997, 3153.
70. A. Antiñolo, F. Carrillo-Hermosilla, B. Chaudret, *et al.*, *Inorg. Chem.*, 1996, **35**, 7873.
71. S. Gründemann, H.-H. Limbach, V. Rodriguez, B. Donnadieu, S. Sabo-Etienne and B. Chaudret, *Ber. Bunsenges. Phys. Chem.*, **1998**, 102, 344.
72. M. A. Esteruelas, F. J. Lahoz, A. M. López, *et al.*, *Inorg. Chem.*, 1996, **35**, 7811.
73. S. Sabo-Etienne, B. Chaudret, H. A. el Makarim, *et al.*, *J. Am. Chem. Soc.*, 1995, **117**, 11602.
74. R. Wiedenbruch, M. Schick, A. Pampel, *et al.*, *J. Phys. Chem.*, 1995, **99**, 13088.
75. Y. Guari, S. Sabo-Etienne and B. Chaudret, *J. Am. Chem. Soc.*,1998, **120**, 4228.
76. J. A. Ayllon, S. Sabo-Etienne, B. Chaudret, S. Ulrich and H-H. Limbach, *Inorg. Chim. Acta*, 1997, **259**, 1.
77. A. Antiñolo, F. Carrillo, B. Chaudret, *et al.*, *Inorg. Chem.*, 1994, **33**, 5163.
78. B. Manzano, F. Jalon, S. Sabo-Etienne, B. Chaudret, S. Ulrich and H.-H. Limbach, in press.
79. S. Camanyes, F. Maseras, M. Moreno, A. Lledós, J. M. Lluch and J. Bertrán, *J. Am. Chem. Soc.*, 1996, **118**, 4617.
80. S. Camanyes, F. Maseras, M. Moreno, A. Lledós, J. M. Lluch and J. Bertrán, *Inorg. Chem.*, 1998, **37**, 2334.
81. E. M. Hiller and R. A. Harris, *J. Chem. Phys.*, 1993, **98**, 2077.
82. E. M. Hiller and R. A. Harris, *J. Chem. Phys.*, 1994, **100**, 2522.

83. E. M. Hiller and R. A. Harris, *J. Chem. Phys.*, 1993, **99**, 7652.
84. S. Szymański, *J. Chem. Phys.*, 1996, **104**, 8216.
85. E. Clot, C. Leforestier, O. Eisenstein and M. Pelissier, *J. Am. Chem. Soc.*, 1995, **117**, 1797.
86. H.-H. Limbach, S. Ulrich, S. Gründemann, *et al.*, *J. Am. Chem. Soc.*, 1998, **120**, 7929.
87. R. Kuhlman, E. Clot, C. Leforestier, W. E. Streib, O. Eisenstein and K. G. Caulton, *J. Am. Chem. Soc.*, 1997, **119**, 10153.
88. N. F. Ramsey, *Phys. Rev.*, 1953, **91**, 303.
89. L. A. Latif, *J. Chem. Res., Synop.*, 1995, 264.
90. H.-M. Kao and C. P. Grey, *J. Am. Chem. Soc.*, 1997, **119**, 627.
91. M. D. Lumsden, K. Eichele, R. E. Wasylishen, T. S. Cameron and J. F. Britten, *J. Am. Chem. Soc.*, 1994, **116**, 11129.
92. M. D. Lumsden, R. E. Wasylishen and J. F. Britten, *J. Phys. Chem.*, 1995, **99**, 16602.
93. G. Wu and R. E. Wasylishen, *J. Phys. Chem.*, 1993, **97**, 7863.
94. S. Koeker, J. V. Hanna, R. E. Wasylishen, E. W. Ainscough and A. M. Brodi, *J. Magn. Reson.*, 1998, **135**, 208.
95. K. Eichele, G. Wu, R. E. Wasylishen and J. F. Britten, *J. Phys. Chem.*, 1995, **99**, 1030.
96. J. A. González, G. A. Aucar, M. C. Ruiz de Azúa and R. H. Contreras, *Int. J. Quantum Chem.*, 1997, **61**, 823.
97. J. Kaski, P. Lantto, J. Vaara and J. Jokisaari, *J. Am. Chem. Soc.*, 1998, **120**, 3993.
98. J. Kaski, J. Vaara and J. Jokisaari, *J. Am. Chem. Soc.*, 1996, **118**, 8879.
99. T. Helgaker, M. Jaszunski, K. Ruud and A. Gorska, *Theor. Chem. Acc.*, 1998, **99**, 175.
100. D. M. Chipman and V. A. Rassolov., *J. Chem. Phys.*, 1997, **107**, 5488.
101. J. Fernández Rico, R. López, A. Aguado, I. Ema and G. Ramirez, 1998, **19**, 1284.
102. J. C. Cesco, C. C. Denner, G. O. Guibergia, *et al.*, *J. Comput. Chem.*, 1999, **18**, 604.
103. A. L. Barra and J. B. Robert, *Mol. Phys.*, 1996, **88**, 875.
104. S. P. A. Sauer, *J. Chem. Phys.*, 1993, **98**, 9220.
105. A. Bhattacharyya, R. Nirmala and S. Subramanian, *J. Mol. Struct. (Theochem)* 1995, **339**, 245.
106. J. Guilleme and J. San Fabián, *J. Chem. Phys.*, 1998, **109**, 8168.
107. H. J. Reich and R. R. Dykstra, *Organometallics*, 1994, **13**, 4578.
108. W. Bauer and C. Griesinger, *J. Am. Chem. Soc.*, 1993, **115**, 10871.
109. W. Bauer and P. v. R. Schleyer, in *Advances in Carbanion Chemistry* (ed. V. Snieckus), vol 1, LAI Press, Greenwich, CT, 1992.
110. H. J. Reich and R. R. Dykstra, *J. Am. Chem. Soc.*, 1993, **115**, 7041.
111. D. J. Gallagher, S. T. Kerrick and P. Beak, *J. Am. Chem. Soc.*, 1992, **114**, 5872.
112. T. Koizumi and O. Kikuchi, *Organometallics*, 1995, **14**, 987.
113. T. Koizumi and O. Kikuchi, *Bull. Chem. Soc. Jpn.*, 1995, **68**, 120.
114. T. Koizumi and O. Kikuchi, *J. Mol. Struct. (Theochem)*, 1995, **336**, 39.
115. A. C. Blizzard and D. P. Santry, *J. Chem. Phys.*, 1971, **55**, 959.
116. R. Ditchfield and L. C. Snyder, *J. Chem. Phys.*, 1972, **56**, 5823.
117. T. Koizumi, K. Morihashi and O. Kikuchi, *Organometallics*, 1995, **14**, 4018.
118. T. Koizumi, K. Morihashi and O. Kikuchi, *Bull. Chem. Soc. Jpn.*, 1996, **69**, 305.
119. A. C. Nair and P. Chandra, *Theor. Chim. Acta*, 1994, **89**, 261.
120. A. C. Nair and P. Chandra, *J. Chem. Soc., Faraday Trans.*, 1995, **91**, 23.
121. W. B. Jenkins and W. McFarlane, *J. Chem. Soc., Chem. Commun.*, 1977, 922.
122. M. Chandak and P. Chandra, *Indian J. Chem.*, 1996, **35A**, 4.
123. D. Chakraborty and P. Chandra, *J. Mol. Struct. (Theochem)*, 1998, **434**, 75.
124. A. D. McLean and G. S. Chandler, *J. Chem. Phys.*, 1980, **72**, 5639.
125. E. A. V. Ebsworth and G. M. Sheldrick, *Trans. Faraday Soc.*, 1967, **63**, 1071.
126. G. M. Sheldrick, *Trans. Faraday Soc.*, 1967, **63**, 1077.
127. G. M. Sheldrick, *Trans. Faraday Soc.*, 1967, **63**, 1065.
128. R. M. Lynden-Bell, *Trans. Faraday Soc.*, 1961, **57**, 888.

129. (a) P. Lazzeretti, *Int. J. Quantum Chem.*, 1979, **15**, 181; (b) P. Lazzeretti, *J. Chem. Phys.*, 1979, **71**, 2514; (c) P. Lazzeretti and R. Zanasi, *J. Chem. Phys.*, 1982, **77**, 2448.
130. C. V. McCurdy, Jr, T. N. Rescigno, D. L. Yaeger and V. McKoy, in *Methods of Electron Structure Theory* (ed. H. F. Schaefer, III), vol. 3., p. 339, Plenum Press, New York, 1977.
131. J. Oddershede, *Adv. Quantum Chem.*, 1978, **11**, 275.
132. P. Lazzeretti, M. Malagoli, R. Zanasi, *et al.*, *J. Chem. Soc., Faraday Trans.*, 1995, **91**, 4031.
133. C. Vizioli, M. C. Ruiz de Azúa, C. G. Giribet, *et al.*, *J. Phys. Chem.*, 1994, **98**, 8858.
134. A. V. Afonin, C. V. Vizioli, M. Ruiz de Azúa and R. H. Contreras, *Bull. Acad. Sci. Russia, Div. Chem. Sci.*, 1996, **45**, 1362.
135. M. C. Ruiz de Azúa, C. G. Giribet, C. V. Vizioli and R. H. Contreras, *J. Mol. Struct. (Theochem)*, 1998, **433**, 141.
136. C. J. Jameson, in *Multinuclear NMR* (ed. J. Mason), ch. 4, p. 89, Plenum Press, New York, 1987.
137. S. A. Perera, H. Sekino and R. J. Bartlett, *J. Chem. Phys.*, 1994, **101**, 2186.
138. J. A. Pople and D. P. Santry, *Mol. Phys.*, 1964, **8**, 1.
139. J. L. Marshall, *Carbon–Carbon and Carbon–Proton NMR Couplings: Applications to Organic Stereochemistry and Conformational Analysis*, Verlag Chemie Int., Deerfield Beach, FL, 1983.
140. K. Bock and C. Pedersen, *Acta Chem. Scand.*, 1977, **B31**, 354.
141. H. Fukui, T. Tsuji and K. Miura, *J. Am. Chem. Soc.*, 1981, **103**, 3652.
142. V. Galasso, *Chem. Phys.*, 1994, **184**, 107.
143. (a) T. Shibuya and V. McKoy, *Phys. Rev.* 1970, **A2**, 2208; (b) T. Shibuya, V. Rose and V. McKoy, *J. Chem. Phys.*, 1973, **58**, 500.
144. V. Galasso, *Int. J. Quantum Chem.*, 1996, **57**, 587.
145. V. Galasso, *Chem. Phys. Lett.*, 1994, **230**, 387.
146. V. Galasso, *Int. J. Quantum Chem.*, 1998, **70**, 313.
147. H. Fukui, H. Inomata, T. Baba, K. Miura and H. Matsuda, *J. Chem. Phys.*, 1995, **103**, 6597.
148. H. Fukui, T. Baba, H. Inomata, K. Miura and H. Matsuda, *Mol. Phys.*, 1997, **92**, 161.
149. J. A. Pople, M. Head-Gordon and K. Raghavachari, *J. Chem. Phys.*, 1987, **87**, 5968.
150. R. J. Bartlett and J. F. Stanton, in *Reviews in Computational Chemistry* (eds K. B. Lipkowitz and D. B. Boyd), vol. 5, VCH, New York, 1994.
151. A. S. Serianni, J. Wu and I. Carmichael, *J. Am. Chem. Soc.*, 1995, **117**, 8645.
152. C. A. Podlasek, W. A. Stripe, I. Carmichael, M. Shang, B. Basu and A. S. Serianni, *J. Am. Chem. Soc.*, 1996, **118**, 1413.
153. M. Karplus, *J. Chem. Phys.*, 1959, **30**, 11.
154. T. Bandyopadhyay, J. Wu, W. A. Stripe, I. Charmichael and A. S. Serianni, *J. Am. Chem. Soc.*, 1997, **119**, 1737.
155. T. J. Church, I. Carmichael and A. S. Serianni., *J. Am. Chem. Soc.*, 1997, **119**, 8946.
156. O. Vahtras, H. Agren, P. Jørgensen, H. J. Aa. Jensen, S. B. Padkjaer and T. Helgaker, *J. Chem. Phys.*, 1992, **96**, 6120.
157. T. Helgaker, M. Jaszunski and K. Ruud, *Mol. Phys.*, 1997, **91**, 881.
158. A. Barszczewicz, M. Jaszunski, K. Kamienska-Trela, T. Helgaker, P. Jørgensen and O. Vahtras, *Theor. Chim. Acta*, 1993, **87**, 19.
159. G. Fronzoni and V. Galasso, *J. Magn. Reson.*, 1987, **71**, 229.
160. L. B. Krivdin and I. N. Domnin, *Zh. Org. Khim.*, 1990, **26**, 2229.
161. H. O. Kalinowski, S. Berger and S. Braun, *Carbon-13 NMR Spectroscopy*, pp. 196, 200. Wiley, New York, 1988.
162. J. B. Lambert, A. P. Jovanovich and W. L. Oliver, *J. Chem. Phys.*, 1970, **74**, 2221.
163. O. Vahtras, H. Ågren, P. Jørgensen, T. Helgaker and H. J. Aa. Jensen, *Chem. Phys. Lett.*, 1993, **209**, 201.
164. J. Geertsen, J. Oddershede and G. E. Scuseria, *J. Chem. Phys.*, 1987, **87**, 2138.
165. J. O Friedric and R. E. Wasylishen, *J. Chem. Phys.*, 1985, **83**, 3707.
166. R. E. Wasylishen, J. O. Friedrich, S. Mooibroek and J. B. MacDonald, *J. Chem. Phys.*, 1985, **83**, 548.

167. A. Barszczewicz, T. Helgaker, M. Jaszunski, P. Jørgensen and K. Ruud, *J. Chem. Phys.*, 1994, **101**, 6822.
168. M. Jaszunski, T. Helgaker, K. Ruud, K. L. Bak and P. Jørgensen, *Chem. Phys. Lett.*, 1994, **220**, 154.
169. A. Barszczewicz, T. Helgaken, M. Jaszunski, P. Jørgensen and K. Ruud, *J. Magn. Reson.*, 1995, **A114**, 212.
170. M. Jaszunski, S. Szymanski, O. Christiansen, P. Jørgensen, T. Helgaker and K. Ruud, *Chem. Phys. Lett.*, 1995, **243**, 144.
171. S. Kirpekar, H. J. Aa. Jensen and J. Oddershede, *Chem. Phys.*, 1994, **188**, 171.
172. S. Kirpekar, H. J. Aa. Jensen and J. Oddershede, *Theor. Chim. Acta*, 1997, **95**, 35.
173. P.-O. Åstrand, K. V. Mikkelsen, K. Ruud and T. Helgaker, unpublished results, cited in ref. 157.
174. T. H. Dunning, Jr., *J. Chem. Phys.*, 1989, **90**, 1007.
175. D. E. Woon and T. H. Dunning, Jr., *J. Chem. Phys.*, 1995, **103**, 4572.
176. D. E. Woon and T. H. Dunning, Jr., *J. Chem. Phys.*, 1994, **100**, 2975.
177. P.-O. Åstrand, K. V. Mikkelsen, P. Jørgensen, K. Ruud and T. Helgaker, *J. Chem. Phys.*, 1998, **108**, 2528.
178. T. Birchall, R. J. Gillespie and S. L. Vekris, *Can. J. Chem.*, 1965, **43**, 1672.
179. G. Pfisterer and H. Dreeskamp, *Ber. Bunsenges.*, 1969, **73**, 654.
180. T. Saue, T. Enevoldsen, T. Helgaker, *et al.*, *DIRAC, A Relativistic ab initio Electronic Structure Program*, Release 3.0, 1998. Available upon request at http://assens.chem.ou.dk/dirac.
181. (a) E. A. Salter, G. W. Trucks and R. J. Bartlett, *J. Chem. Phys.*, 1989, **90**, 1752; (b) E. A. Salter and R. J. Bartlett, *J. Chem. Phys.*, 1989, **90**, 1767.
182. H. Sekino and R. J. Bartlett, *Chem. Phys. Lett.*, 1994, **225**, 486.
183. J. F. Stanton and R. J. Bartlett, *J. Chem. Phys.*, 1993, **99**, 5178.
184. (a) D. C. Coineau and R. J. Bartlett, *Chem. Phys. Lett.*, 1993, **207**, 414; (b) J. F. Stanton and R. J. Bartlett, *J. Chem. Phys.*, 1993, **98**, 7029.
185. (a) H. Koch and P. Jørgensen, *J. Chem. Phys.*, 1990, **93**, 3333; (b) H. Koch, H. J. Aa. Jensen, P. Jørgensen and T. Helgaker, *J. Chem. Phys.*, 1990, **93**, 3345.
186. J. Geertsen, J. Oddershede and G. E. Scuseria, *Int. J. Quantum Chem.*, 1987, **S21**, 475.
187. H. Fukui, K. Miura, H. Matsuda and T. Baba, *J. Chem. Phys.*, 1992, **97**, 2299.
188. D. E. O'Reilly and E. M. Peterson, *J. Chem. Phys.*, 1968, **49**, 2872.
189. S. A. Perera, M. Nooijen and R. J. Bartlett, *J. Chem. Phys.*, 1996, **104**, 3290.
190. S. A. Perera, R. J. Bartlett and P. V. Schleyer, *J. Am. Chem. Soc.*, 1995, **117**, 8476.
191. S. A. Perera and R. J. Bartlett, *J. Am. Chem. Soc.*, 1996, **118**, 7849.
192. M. Nooijen, S. A. Perera and R. J. Bartlett, *Chem. Phys. Lett.*, 1997, **266**, 456.
193. E. Breitmaier and W. Voelter, *^{13}C NMR Spectroscopy*, Verlag Chemie, Weinheim, 1978.
194. P. Diehl, J. Jokisaari and J. Amrein, *J. Magn. Reson.*, 1982, **48**, 495.
195. J. Geertsen, J. Oddershede, W. T. Raynes and G. E. Scuseria, *J. Magn. Reson.*, 1991, **93**, 458 and references therein.
196. J. Geertsen, J. Oddershede and W. T. Raynes, *Magn. Reson. Chem.*, 1993, **31**, 722.
197. W. T. Raynes, J. Geertsen and J. Oddershede, *Chem. Phys. Lett.*, 1992, **197**, 516.
198. J. Geertsen, J. Oddershede, W. T. Raynes and T. L. Marvin, *Mol. Phys.*, 1994, **82**, 29.
199. J. Geertsen and J. Oddershede, *Chem. Phys.*, 1984, **90**, 301.
200. T. Enevoldsen, J. Oddershede and S. P. A. Sauer, *Theor. Chem. Acc.*, 1998, **100**, 275.
201. S. P. A. Sauer, *J. Phys.*, 1997, **B30**, 3773.
202. R. D. Wigglesworth, W. T. Raynes, S. P. A. Sauer and J. Oddershede, *Mol. Phys.*, 1997, **92**, 77.
203. R. D. Wigglesworth, W. T. Raynes, S. P. A. Sauer and J. Oddershede, *Mol. Phys.*, 1998, **94**, 851.
204. S. P. A. Sauer, C. K. Møller, H. Koch, I. Paidarová and V. Špirko, *Chem. Phys.*, 1998, **238**, 385.
205. P. Hohenberg and W. Khon, *Phys. Rev.*, 1964, **A136**, 864.
206. W. Kohn and L. J. Sham, *Phys. Rev.*, 1965, **A140**, 1133.

207. J. M. Seminario, in *Modern Density Functional Theory: A Tool for Chemistry*, Theoretical and Computational Chemistry, vol. 2 (eds J. M. Seminario and P. Politzer), Elsevier Science, Amsterdam, 1995.
208. A. St-Amant, in *Reviews in Computational Chemistry* (eds K. B. Lipkowitz and D. B. Boyd), vol. 7, ch. 5, VCH, New York, 1996.
209. (a) M. Levy, *Phys. Rev.*, 1991, **A43**, 4637; (b) H. Oui-Yang and M. Levy, *Phys. Rev.*, 1991, **A44**, 54; (c) A. Görling and M. Levy, *Phys. Rev.*, 1992, **A45**, 1509.
210. J. C. Facelli and A. De Dios (eds). Modeling NMR Chemical Shifts: Gaining Insights into Structure and Environment. ACS Symposium Series, 1999, 732.
211. V. G. Malkin, O. L. Malkina, L. A. Eriksson and D. R. Salahub, in Theoretical and Computational Chemistry, vol. 1, *Density Functional Calculations*, (ed. P. Politzer and J. M. Seminario), Elsevier, Amsterdam, 1994.
212. G. Malkin, O. L. Malkina, L. A. Eriksson and D. R. Salahub, in *Modern Density Functional Theory: A Tool for Chemistry*, Theoretical and Computational Chemistry, vol. 2 (eds. J. M. Seminario and P. Politzer), Elsevier, Amsterdam, 1995.
213. O. L. Malkina, D. R. Salahub and V. G. Malkin, *J. Chem. Phys.*, 1996, **105**, 8793.
214. V. G. Malkin, O. L. Malkina, M. E. Casida and D. R. Salahub, *J. Am. Chem. Soc.*, 1994, **116**, 5898.
215. A. St-Amant and D. R. Salahub, *Chem. Phys. Lett.*, 1990, **169**, 387.
216. W. Kutzelnigg, U. Fleischer and M. Schindler, in *NMR Basic Principles and Progress* (eds P. Diehl, E. Fluck, H. Günther, R. Kosfelt and J. Selig), vol. 23, p. 165, Springer, Berlin, 1990.
217. S. H. Vosko, L. Wilk and M. Nusair, *Can. J. Phys.*, 1980, **58**, 1200.
218. J. P. Perdew and Y. Wang, *Phys. Rev.*, 1986, **B33**, 8800.
219. (a) J. P. Perdew, *Phys. Rev.*, 1986, **B33**, 8822; (b) J. P. Perdew, *Phys. Rev.*, 1986, **B34**, 7406.
220. J. P. Perdew and Y. Wang, *Phys. Rev.*, 1992, **B45**, 13244.
221. V. G. Malkin, O. L. Malkina and D. R. Salahub, *Chem. Phys. Lett.*, 1994, **221**, 91.
222. H. Partridge, *J. Chem. Phys.*, 1989, **90**, 1043.
223. D. L. Beveridge, in *Semiempirical Methods of Electronic Structure Calculation* (ed. G. A. Segal), p. 163, Plenum Press, New York, 1977.
224. L. B. Krivdin and E. W. Della, *Prog. NMR Spectrosc.*, 1991, **23**, 301.
225. E. A. Williams and J. D. Cargioli, *Annu. Rep. NMR Spectrosc.*, 1983, **15**, 235.
226. S. M. Bass, R. L. de León and J. S. Muenter, *J. Chem. Phys.*, 1987, **86**, 4305.
227. R. M. Dickson and T. Ziegler, *J. Phys. Chem.*, 1996, **100**, 5286.
228. A. D. Becke, *J. Chem. Phys.*, 1993, **98**, 5648.
229. C. Lee, W. Yang and R. G. Parr, *Phys. Rev.*, 1988, **B37**, 785.
230. M. J. Frisch, G. W. Trucks, H. B. Schlegel, *et al.*, *Gaussian 94, Revision* D.4, Gaussian, Inc., Pittsburgh, PA, 1995.
231. J. A. Pople and D. L. Beveridge, *Approximate Molecular Orbital Theory*, McGraw-Hill, New York, 1970.
232. M. D. Spencer, P. M. Morese, S. R. Wilson and G. S. Girolami, *J. Am. Chem. Soc.*, 1993, **115**, 2057.
233. A. D. Becke, *Phys. Rev.*, 1988, **A38**, 3098.
234. P. Bour and M. Budešínský, *J. Chem. Phys.*, 1999, **110**, 2836.
235. C. J. Grayce and R. A. Harris, *Phys. Rev.*, 1994, **A50**, 3089.
236. C. J. Grayce and R. A. Harris, *Chem. Phys. Lett.*, 1995, **234**, 319.
237. C. J. Grayce and R. A. Harris, *J. Phys. Chem.*, 1995, **99**, 2724.
238. F. R. Salsbury Jr and R. A. Harris, *Mol. Phys.*, 1998, **94**, 307.
239. P. Pyykkö and L. Wiesenfeld, *Mol. Phys.*, 1981, **43**, 557.
240. G. A. Aucar and J. Oddershede, *Int. J. Quantum Chem.*, 1993, **47**, 425.
241. L. Visscher, T. Enevoldsen, T. Saue, H. J. Aa. Jensen and J. Oddershede, *J. Comp. Chem.*, 1999, **20**, 1262.
242. G. Breit, *Phys. Rev.*, 1930, **35**, 1447.

243. P. Pyykkö, E. Pajanne and M. Inokuti, *Int. J. Quantum Chem.*, 1973, **7**, 785.
244. J. S. Muenter and W. Klemperer, *J. Chem. Phys.*, 1970, **52**, 6033.
245. S. Kirpekar, J. Oddershede and H. J. Aa. Jensen, *J. Chem. Phys.*, 1995, **103**, 2983.
246. G. A. Aucar, T. Saue, L. Visscher and H. J. Aa. Jensen, *J. Chem. Phys.*, 1999, **110**, 6208.
247. (a) P. Jørgensen, H. J. Aa. Jensen and J. Olsen, *J. Chem. Phys.*, 1989, **89**, 3659; (b) J. Olsen, D. L. Yeager and P. Jørgensen, *J. Chem. Phys.*, 1989, **91**, 381; (c) T. Helgaker, P. R. Taylor, K. Ruud, O. Vahtras and H. Koch, HERMIT, a molecular integral program. Available upon request at http://www.kjemi.uio.no/software. (d) H. J. Aa. Jensen, H. Ågren and J. Olsen, SIRIUS, in *Modern Techniques in Computational Chemistry: MOTECC-90* (ed. E. Clementi), ESCOM, Leiden, 1990.
248. W. G. Richards, H. P. Trivedi and D. L. Cooper, *Spin–orbit Coupling in Molecules*, Clarendon Press, Oxford, 1981.
249. S. Kirpekar, T. Enevoldsen, J. Odderhsede and W. T. Raynes, *Mol. Phys.*, 1997, **91**, 897.
250. B. Bennet, W. T. Raynes and C. T. Anderson, *Spectrochim. Acta*, 1989, **45A**, 821.
251. P. W. Fowler, *Mol. Phys.*, 1981, **43**, 591.
252. R. A. Nicholls and W. T. Raynes, unpublished results, 1995.
253. A. L. Wilkins, P. J. Watkinson and K. M. MacKay, *J. Chem. Soc., Dalton Trans.*, 1987, 2365.
254. E. A. V. Ebsworth, S. G. Frankiss and A. G. Robiette, *J. Mol. Spectrosc.*, 1964, **12**, 299.
255. H. Dresskamp, *Z. Naturforsch.*, 1964, **19**, 139.
256. W. Brügel, *Handbook of NMR Spectral Parameters*, London, Heyden, 1979.
257. T. Enevoldsen, L. Visscher, T. Saue, H. J. Aa. Jensen and J. Oddershede, private communication.
258. (a) H. Partridge, *J. Chem. Phys.*, 1989, **90**, 1043; (b) H. Partridge and K. Faegri, *Theor. Chim. Acta*, 1992, **82**, 207; (c) H. Partridge, *J. Chem. Phys.*, 1987, **87**, 6643
259. M. Kaupp, O. L. Malkina, V. G. Malkin and P. Pyykkö, *Chem. Eur. J.*, 1998, **4**, 118.
260. Y. Nomura, Y. Takeuchi and N. Nakagawa, *Tetrahedron Lett.*, 1969, **8**, 639.
261. (a) A. Ejchart and A. Gryff-Keller, *J. Magn. Reson.*, 1996, **A118**, 272; (b) A. Ejchart and A. Gryff-Keller, *Chem. Eur. J.*, 1998, **4**, 2072.
262. H.-J. Koglin, K. Behrends and M. Dräger, *Organometallics*, 1994, **13**, 2733.
263. M. Björgvinsson, H. P. A. Mercier, K. M. Mitchell, G. J. Schrobilgen and G. Strohe, *Inorg. Chem.*, 1993, **32**, 6046.
264. M. F. A. Dove, J. C. P. Sanders and E. H. Appelman, *Magn. Reson. Chem.*, 1995, **33**, 44.
265. R. E. Wasylishen, K. C. Wright, K. Eichele and T. S. Cameron, *Inorg. Chem.*, 1994, **33**, 407.
266. A. C. Diz, C. G. Giribet, C. C. Ruiz de Azúa and R. H. Contreras, *Int. J. Quantum Chem.*, 1990, **37**, 663.
267. G. A. Aucar and R. H. Contreras, *J. Magn. Reson.* 1991, **93**, 413.
268. N. M. Peruchena, L. Sosa, G. A. Aucar and R. H. Contreras, *J. Mol. Struct. (Theochem)*, 1995, **330**, 211.
269. G. A. Aucar, E. Botek, S. Gomez, E. Sproviero and R. H. Contreras, *J. Organomet. Chem.*, 1996, **524**, 1.
270. R. M. Lobayan and G. A. Aucar, *J. Mol. Struct. (Theochem)*, 1998, **452**, 13.
271. M. C. Ruiz de Azúa, A. C. Diz, C. G. Giribet, R. H. Contreras and I. D. Rae, *Int. J. Quantum Chem.* 1986, **S20**, 585.
272. R. H. Contreras, C. G. Giribet, M. C. Ruiz de Azúa and A. C. Diz, in *Recent Advances in Organic NMR Spectroscopy* (eds J. Lambert and R. Rittner), ch. 3, Norell, Landisville, NJ, 1987.
273. R. H. Contreras, C. G. Giribet, M. C. Ruiz de Azúa and M. B. Ferraro, in *Structure, Interactions and Reactivity* (ed. S. Fraga), vol. 77B, ch. 7, Elsevier, Amsterdam, 1992.
274. H. A. Bent, *Chem. Rev.* 1961, **61**, 275.
275. E. W. Della, I. J. Lochert, N. M. Peruchena, G. A. Aucar and R. H. Contreras, *J. Phys. Org. Chem.*, 1996, **9**, 168.

276. G. A. Aucar, M. C. Ruiz de Azúa, C. G. Giribet and R. H. Contreras, *J. Mol. Struct. (Theochem)*, 1990, **205**, 79.
277. E. W. Della, D. K. Taylor, P. E. Pigou, L. B. Krivdin and R. H. Contreras, *Aust. J. Chem.*, 1993, **46**, 63.
278. G. A. Aucar, V. Zunino, M. B. Ferraro, C. G. Giribet, M. C. Ruiz de Azúa and R. H. Contreras, *J. Mol. Struct. (Theochem)*, 1990, **205**, 63.
279. C. Barbier, G. Berthier, I. Baraldi and F. Momicchioli, *J. Mol. Struct. (Theochem)*, 1998, **433**, 231.
280. R. Musio and O. Sciacovelli, *Magn. Reson. Chem.*, 1996, **34**, 348.
281. M. J. S. Dewar and W. Thiel, *J. Am. Chem. Soc.*, 1977, **99**, 4899.
282. P. Lazzeretti, F. Taddei and R. Zanasi, *J. Am. Chem. Soc.*, 1976, **98**, 7989.
283. R. C. Bingham, M. J. S. Dewar and D. H. Lo, *J. Am. Chem. Soc.*, 1975, **97**, 1285.
284. G. E. Scuseria and R. H. Contreras, *Chem. Phys. Lett.* 1982, **93**, 425.
285. C.-G. Zhan and Z.-M. Hu, *Theor. Chim Acta*, 1993, **84**, 511.
286. K. Jug, *J. Am. Chem. Soc.*, 1977, **99**, 7800.
287. J. P. Foster and F. Weinhold, *J. Am. Chem. Soc.*, 1980, **102**, 7211.
288. N. Muller and D. E. Pritchard, *J. Chem. Phys.*, 1959, **31**, 768.
289. Z. B. Maksic, M. Eckert-Maksic and M. Randic, *Theor. Chim. Acta*, 1971, **22**, 70.
290. Z.-M. Hu and C.-G Zhan, *Theor. Chim Acta*, 1993, **84**, 521.
291. V. M. S. Gil, *Theor. Chim. Acta*, 1989, **76**, 291.
292. C.-G. Zhan and Z.-M. Hu, *Magn. Reson. Chem.*, 1994, **32**, 465.
293. C.-G. Zhan, S.-Y. Ye, C.-J. Zhang and J. Wan, *Theor. Chim. Acta*, 1994, **88**, 389.
294. S.-Y. Ye, C.-G. Zhan, J. Wan and C.-J. Zhang, *J. Mol. Struct. (Theochem)*, 1994, **313**, 231.
295. D. Kovacek, Z. B. Maksic, S. Elbel and J. Kudnig, *J. Mol. Struct. (Theochem)*, 1994, **304**, 247.
296. Z.-M. Hu and C.-G. Zhan, *Magn. Reson. Chem.*, 1995, **33**, 249.
297. J. Wan and C.-G. Zhan, *Theor. Chim. Acta*, 1995, **92**, 61.
298. C.-G. Zhan, S.-Y. Ye, W-X. Zhu and C.-J. Zhang, *J. Mol. Struct. (Theochem)*, 1995, **337**, 67.
299. C.-G. Zhan and J. Wan, *Chem. Phys. Lett.*, 1997, **279**, 35.
300. C. Y. Zhao, T. Xiao, X. F. Xu and X. Z. You, *Chem. J. Chin. Univ.*, 1996, **17**, 769.
301. L. Craciun and J. E. Jackson, *J. Phys. Chem.*, 1998, **A102**, 3738.
302. P. J. Craig, M. I. Needham, N. Ostah, G. H. Stojak, M. Symons and P. Teesdale-Spittle, *J. Chem. Soc., Dalton Trans.*, 1996, 153.
303. M. J. S. Dewar, E. G. Zoebisch, E. F. Healey and J. J. P. Stewart, *J. Am. Chem. Soc.*, 1985, **107**, 3902.
304. C. G. Giribet, M. C. Ruiz de Azúa, S. B. Gómez, *et al.*, *J. Comp. Chem.*, 1998, **19**, 181.
305. V. F. Bystrov, *Prog. NMR Spectrosc.*, 1976, **10**, 41.
306. G. Wagner, *J. Biomol. NMR*, 1993, **3**, 375.
307. A. Bax and S. Grzesiek, *Acc. Chem. Res.*, 1993, **26**, 131.
308. C. A. G. Haasnoot, F. A. A. M. de Leeuw and C. Altona, *Tetrahedron*, 1980, **36**, 2783.
309. W. J. E. Parr and T. Schaefer, *Acc. Chem. Res.*, 1980, **13**, 400.
310. C. A. Podlasek, J. Wu, W. A. Stripe, P. B. Bondo and A. S. Serianni, *J. Am. Chem. Soc.*, 1995, **117**, 8635.
311. (a) G. W. Vuister and A. Bax, *J. Biomol. NMR*, 1992, **2**, 401; (b) G. W. Vuister and A. Bax, *J. Magn. Reson.*, 1992, **98**, 428.
312. M. D. Sørensen, S. M. Kristensen, J. J. Led and O. W. Sørensen, *J. Magn. Reson.*, 1993, **A103**, 364.
313. G. W. Vuister, T. Yamazaki, D. A. Torchia and A. Bax, *J. Biomol. NMR*, 1993, **3**, 297.
314. F. Löhr and H. Rüterjans, *J. Am. Chem. Soc.*, 1997, **119**, 1468.
315. G. W. Vuister, A. C. Wang and A. Bax, *J. Am. Chem. Soc.*, 1993, **115**, 5334.
316. J.-S. Hu, S. Grzesiek and A. Bax, *J. Am. Chem. Soc.*, 1997, **119**, 1803.
317. K. V. R. Chary, V. K. Rastogi, G. Govil and H. T. Miles, *J. Chem. Soc., Chem. Commun.*, 1994, 241.

318. B. Brutscher, J. Boisbouvier, A. Pardi, D. Marion and J. P. Simorre, *J. Am. Chem. Soc.*, 1998, **120**, 11845.
319. B. Wrackmeyer, S. Gerstmann and M. Herberhold, *Magn. Reson. Chem.*, 1993, **31**, 499.
320. A. Pardi, *Methods Enzymol.*, 1995, **261**, 350.
321. J. V. Hines, S. M. Landry, G. Varani and I. Tinoco, Jr., *J. Am. Chem. Soc.*, 1994, **116**, 5823.
322. J. R. Tolman, J. M. Flanagan, M. A. Kennedy and J. H. Prestegard, *Proc. Natl. Acad. Sci. USA*, 1995, **92**, 9279.
323. A. Meissner, T. Schulte-Herbrüggen and O. W. Sørensen, *J. Am. Chem. Soc.*, 1998, **120**, 7989.
324. B. Bose, S. Zhao, R. Stenutz, *et al.*, *J. Am. Chem. Soc.*, 1998, **120**, 11158.
325. S. Sherman, S. Sclove, L. Kirnasky, I. Tomchin and O. Shats, *J. Mol. Struct. (Theochem)*, 1996, **368**, 153.
326. G. W. Vuister, F. Delaglio and A. Bax, *J. Biomol. NMR*, 1993, **3**, 67.
327. G. W. Vuister, F. Delaglio and A. Bax, *J. Am. Chem. Soc.*, 1992, **114**, 9674.
328. I. Tvaroska and F. R. Taravel, *J. Biomol. NMR*, 1992, **2**, 421.
329. M. Brakta, R. N. Farr, B. Chaguir, G. Massiot, C. Lavaud, W. R. Anderson Jr, D. Sinou and G. D. Daves Jr, *J. Org. Chem.*, 1993, **58**, 2992.
330. L. Kozerski, P. Krajewski and E. Bednarek, *Magn. Reson. Chem.*, 1995, **33**, 745.
331. D. G. de Kowalewski, V. J. Kowalewski, R. H. Contreras, E. Díez and A. L. Esteban, *Magn. Reson. Chem.*, 1998, **36**, 336.
332. I. Starke, A. Koch, E. Kleinpeter and H.-J. Holdt, *J. Mol. Struct.*, 1995, **356**, 15.
333. J. R. Tolman and J. H. Prestegard, *J. Magn. Reson.*, 1996, **B112**, 269.
334. D. P. Kelly, K. Aherne, F. Delgado, *et al.*, *J. Am. Chem. Soc.*, 1993, **115**, 12010.
335. T. Parella, F. Sánchez-Ferrando and A. Virgili, *Magn. Reson. Chem.*, 1994, **32**, 657.
336. T. Szyperski, C. Fernández, A. Ono, M. Kainosho and K. Wüthrich, *J. Am. Chem. Soc.*, 1998, **120**, 821.
337. C. A. G. Haasnoot, *J. Am. Chem. Soc.*, 1993, **115**, 1460.
338. C. A. G. Haasnoot, *J. Am. Chem. Soc.*, 1992, **114**, 882.
339. C. Altona, R. Francke, R. de Haan, *et al.*, *Magn. Reson. Chem.*, 1994, **32**, 670.
340. L. Fielding and G. H. Grant, *J. Am. Chem. Soc.*, 1993, **115**, 1902.
341. J. T. Martin, P.-O. Norrby and B. Åkermark, *J. Org. Chem.*, 1993, **58**, 1400.
342. R. J. Abraham, P. Leonard, T. A. D. Smith and W. A. Thomas, *Magn. Reson. Chem.*, 1996, **34**, 71.
343. G. Balacco, *J. Chem. Inf. Comput. Sci.*, 1996, **36**, 885.
344. J. San-Fabián, J. Guilleme, E. Díez, P. Lazzeretti, M. Malagoli and R. Zanasi, *Chem. Phys. Lett.*, 1993, **206**, 253.
345. J. San-Fabian, J. Guilleme, E. Díez, *et al.*, *Mol. Phys.*, 1994, **82**, 913.
346. J. Guilleme, J. San-Fabián and E. Díez, *Mol. Phys.*, 1997, **91**, 343.
347. J. San Fabián, J. Guilleme and E. Díez, *An. Quím.*, 1995, **91**, 200.
348. T. Schaefer, J. P. Kunkel, R. W. Schurko and G. M. Bernard, *Can. J. Chem.*, 1994, **72**, 1722.
349. M. Barfield and W. B. Smith, *J. Am. Chem. Soc.*, 1992, **114**, 1574.
350. W. B. Smith and M. Barfield, *Magn. Reson. Chem.*, 1993, **31**, 696.
351. G. W. Vuister and A. Bax, *J. Am. Chem. Soc.*, 1993, **115**, 7772.
352. M. J. Jimeno, J. Elguero, D. Carmona, M. P. Lamata and E. San José, *Magn. Reson. Chem.*, 1996, **34**, 42.
353. S. B. Engelsen, S. Pérez, I. Braccini and C. Hervé du Penhoat, *J. Comput. Chem.*, 1995, **16**, 1096.
354. I. Tvaroska, M. Hricovini and E. Petrakova, *Carbohydr. Res.*, 1989, **189**, 359.
355. R. Brüchweiler and D. A. Case, *J. Am. Chem. Soc.*, 1994, **116**, 11199.
356. T. Rundlöf, A. Kjellberg, C. Damberg, T. Nishida and G. Widmalm, *Magn. Reson. Chem.*, 1998, **36**, 839.
357. J. San Fabián, J. Guilleme and E. Díez, *J. Mol. Struct. (Theochem)*, 1998, **426**, 117.
358. A. C. Wang and A. Bax, *J. Am. Chem. Soc.*, 1995, **117**, 1810.

359. A. C. Wang and A. Bax, *J. Am. Chem. Soc.*, 1996, **118**, 2483.
360. J. San Fabián and J. Guilleme, *Chem. Phys.*, 1996, **206**, 325.
361. J. San Fabián, J. Guilleme and E. Díez, *J. Mag. Reson.*, 1998, **13**, 255.
362. J.-S Hu and A. Bax, *J. Am. Chem. Soc.*, 1997, **119**, 6360.
363. T. Parella, F. Sánchez-Ferrando and A. Virgili, *Magn. Reson. Chem.*, 1997, **35**, 30.
364. H. H. Keah and I. D. Rae, *Aust. J. Chem.*, 1993, **46**, 1413.
365. J. Marton, Z. Szabó, I. Csorvássy, C. Simon, S. Hosztafi and S. Makleit, *Tetrahedron*, 1996, **52**, 2449.
366. M. Hennig, D. Ott, P. Schulte, *et al.*, *J. Am. Chem. Soc.*, 1997, **119**, 5055.
367. M. Mesilaakso, *Magn. Reson. Chem.*, 1996, **34**, 989.
368. S. Suntioinen, R. Laatikainen and V. Král, *Magn. Reson. Chem.*, 1994, **32**, 51.
369. R. Laatikainen and V. Král, *Magn. Reson. Chem.*, 1986, **24**, 498.
370. E. M. Sproviero, A. Ferrara, R. H. Contreras and G. Burton, *J. Chem. Soc., Perkin Trans. 2*, 1996, 933.
371. N. N. Sveshnikov, A. A. Fomichov, I. V. Vystorop and V. G. Kartsev, *Mendeleev Commun.*, 1993, 107.
372. F. Aubke, C. Hägele and H. Willner, *Magn. Reson. Chem.*, 1995, **33**, 817.
373. M. Jaszunski, T. Helgaker and K. Ruud, *Magn. Reson. Chem.*, 1996, **34**, 646.
374. K. Schenzel and K. Hassler, *Spectrochim. Acta*, 1994, **A50**, 127.
375. T. Schaefer, R. Sebastian, R. W. Schurko and F. E. Hruska, *Can. J. Chem.*, 1993, **71**, 1384.
376. A. Schmidpeter, H. Nöth, G. Jochem, H.-P. Schrödel and K. Karaghiosoff, *Chem. Ber.*, 1995, **128**, 379.
377. H. P. Schrödel and A. Schmidpeter, *Magn. Reson. Chem.*, 1996, **34**, 227.
378. M. M. W. Mooren, S. S. Wijmenga, G. A. van der Marel, J. H. van Boom and C. W. Hilbers, *Nucleic Acids Res.*, 1994, **22**, 2658.
379. J. Plavec and J. Chattopadhyaya, *Tetrahedon Lett.*, 1995, **36**, 1949.
380. G. M. Clore, E. C. Murphy, A. M. Gronenborn and A. Bax, *J. Magn. Reson.*, 1998, **134**, 164.
381. T. Szyperski, A. Ono, C. Fernández, *et al.*, *J. Am. Chem. Soc.*, 1997, **119**, 9901.
382. L. P. Kazansky, *Chem. Phys. Lett.*, 1994, **223**, 289.
383. (a) T. P. Lockhart and W. F. Manders, *Inorg. Chem.*, 1986, **25**, 892; (b) T. P. Lockhart and W. F. Manders, *J. Am. Chem. Soc.*, 1987, **109**, 7015.
384. W. F. Howard Jr, R. W. Crecely and W. H. Nelson, *Inorg. Chem.*, 1985, **24**, 2204.
385. F. Caruso, D. Leonesi, F. Marchetti, *et al.*, *J. Organomet. Chem.*, 1996, **519**, 29.
386. C. Pettinari, F. Marchetti and A. Cingolani and S. Bartolini, *Polyhedron*, 1996, **15**, 1263.
387. T. P. Lockhart, W. F. Manders and J. J. Zuckerman, *J. Am. Chem. Soc.*, 1985, **107**, 4546.
388. J. Holoecek, M. Nadvornik, K. Handlir and A. Licka, *J. Organomet. Chem.*, 1986, **315**, 289.
389. A. Vij, Y. Y. Zheng, R. L. Kirchmeier and J. M. Shreeve, *Inorg. Chem.*, 1994, **33**, 3281.
390. F. Caruso, M. Giomini, A. M. Giuliani and E. Rivarola, *J. Organomet. Chem.*, 1996, **506**, 67.
391. B. Wrackmeyer, S. Kerschl, H. E. Maisel and W. Milius, *J. Organomet. Chem.*, 1995, **490**, 197.
392. B. Wrackmeyer, K. Wagner, A. Sebald, L. H. Merwinn and R. Boese, *Magn. Reson. Chem.*, 1991, **29**, S3-10.
393. B. Wrackmeyer, H. E. Maisel and M. Milius, *Z. Naturforsch.*, 1995, **50B**, 809.
394. T. N. Mitchell and B. Kowall, *Magn. Reson. Chem.*, 1995, **33**, 325.
395. B. Korpar-Colig, Z. Popovic, D. Matkovic-Calogovic and D. Vikic-Topic, *Organometallics*, 1993, **12**, 4708.
396. E. Kolehmainen, K. Laihia and R. Kauppinen, D. Rasala and A. Puchala, *J. Phys. Org. Chem.*, 1995, **8**, 577.
397. C. G. Swain and E. C. Lupton, Jr., *J. Am. Chem. Soc.*, 1968, **90**, 4328.
398. F. Potmischil, H. Herzog and J. Buddruss, *Magn. Reson. Chem.*, 1998, **36**, 240.
399. L. B. Krivdin and G. A. Kalabin, *Prog. NMR Spectrosc.*, 1989, **21**, 293.
400. M. S. Gil and W. von Philipsborn, *Magn. Reson. Chem.*, 1989, **27**, 409.

401. R. H. Contreras, G. A. Aucar, C. G. Giribet, M. C. Ruiz de Azúa, C. N. Cavasotto and L. B. Krivdin, *J. Mol. Struct. (Theochem)*, 1990, **210**, 175.
402. K. Kamienska-Trela, L. Kania and E. Bednarek, *Magn. Reson. Chem.*, 1993, **31**, 268.
403. M. Witanowski, Z. Bieddrzycka and K. Grela, *Magn. Reson. Chem.*, 1998, **36**, 356.
404. N. W. Mitzel, K. Angermaier and H. Schmidbaur, *Chem. Ber.*, 1994, **127**, 841.
405. N. W. Mitzel, A. Schier, M. Pauk and H. Schmidbaur, *Chem. Ber.*, 1993, **126**, 2027.
406. K. Hassler, K. W. Köll and K. Schenzel, *J. Mol. Struct.*, 1995, **348**, 353.
407. K. Hassler and G. Bauer, *J. Organomet. Chem.*, 1993, **460**, 149.
408. U. Katzenbeisser and K. Hassler, *Organosilicon Chemistry, From Molecules to Materials* (eds N. Auner and J. Weis), p. 37, VCH, Weinheim, 1994.
409. K. Schenzel and K. Hassler, *J. Mol. Struct.*, 1995, **349**, 161.
410. K. Kamienska-Trela, *Spectrochim. Acta*, 1979, **A36**, 239.
411. K. Kamienska-Trela, Z. Biedrzycka and A. Dabrowski, *Magn. Reson. Chem.*, 1991, **29**, 1216.
412. Z. Biedrzycka and K. Kamienska-Trela, *Spectrochim. Acta*, 1986, **A42**, 1323.
413. K. Kamienska-Trela, A. Dabrowski and H. Januszewski, *Spectrochim. Acta*, 1993, **A49**, 1613.
414. S. Harder, P. F. Ekhart, L. Brandsma, J. A. Kanters, A. J. M. Duisenberg and P. von R. Schleyer, *Organometallics*, 1992, **11**, 2623.
415. W. Domalewski, L. Stefaniak and G. A. Webb, *J. Mol. Struct.*, 1993, **295**, 19.
416. T. Steiner, *Crystallogr. Rev.*, 1996, **6**, 1.
417. A. J. Stone, *Chem. Phys. Lett.*, 1993, **211**, 101.
418. U. Koch and P. L. A. Popelier, *J. Phys. Chem.*, 1995, **99**, 9474.
419. J. E. Peralta, M. C. Ruiz de Azúa and R. H. Contreras, *J. Mol. Struct. (Theochem)*, in press.
420. I. D. Rae, J. A. Weigold, R. H. Contreras and G. Yamamoto, *Magn. Reson. Chem.*, 1992, **30**, 1047.
421. R. H. Contreras, J. C. Facelli and D. G. de Kowalewski, *Org. Magn. Reson.*, 1982, **20**, 40.
422. T. Schaefer and L. B.-L. Lee, *J. Mol. Struct.*, 1993, **296**, 173.
423. T. Schaefer, S. Kroeker and D. M. McKinnon, *Can. J. Chem.*, 1995, **73**, 2208.
424. T. Schaefer, P. Hazendonk and D. M. McKinnon, *Can. J. Chem.*, 1995, **73**, 1387.
425. J. M. Kane, C. R. Dalton, M. A. Staeger and E. W. Huber, *J. Heterocyclic Chem.*, 1995, **32**, 183.
426. A. Mele, G. Salani, F. Viani and P. Bravo, *Magn. Reson. Chem.*, 1997, **35**, 168.
427. A. Mele, B. Vergani, F. Viani, S. V. Meille, A. Farina and P. Bravo, *Eur. J. Org. Chem.*, 1999, 187.
428. K. Matsubara, A. Oba and Y. Usui, *Magn. Reson. Chem.*, 1998, **36**, 761.
429. M. A. Natiello and R. H. Contreras, *Chem. Phys. Lett.*, 1984, **104**, 568.
430. M. A. Biamonte and A. Vasella, *Helv. Chim. Acta*, 1998, **81**, 695.
431. M. Pham, M. Gdaniec and T. Polonski, *J. Org. Chem.*, 1998, **63**, 3731.
432. J. W. Lyga, R. N. Henrie, II, G. A. Meier, R. W. Creekmore and R. M. Patera, *Magn. Reson. Chem.*, 1993, **31**, 323.
433. L. Ernst and K. Ibrom, *Magn. Reson. Chem.*, 1998, **36**, S71.
434. L. Ernst and K. Ibrom, *Magn. Reson. Chem.*, 1997, **35**, 868.
435. C. R. Jones, J. J. Parlow and D. M. Schnur, *J. Heterocyclic Chem.*, 1996, **33**, 1835.
436. W. Städeli, P. Bilger and W. Philipsborn, *Org. Magn. Reson.*, 1981, **16**, 170.
437. A. Heine, R. Herst-Irmer, G. M. Sheldrick and D. Stalke, *Inorg. Chem.*, 1993, **32**, 2694.
438. P. Szczecinski and J. Zachara, *J. Organomet. Chem.*, 1993, **447**, 241.
439. P. Szczecinski, *J. Organomet. Chem.*, 1993, **458**, 119.
440. A. P. West Jr, N. Smyth, C. M. Kraml, D. M. Ho and R. A. Pascal Jr, *J. Org. Chem.*, 1993, **58**, 3502.
441. T. J. Beasley, R. D. Brost, C. K. Chu, S. L. Grundy and S. R. Stobart, *Organometallics*, 1993, **12**, 4599.
442. J. Jirman, M. Nádvorník, J. Sopková and A. Popkov, *Magn. Reson. Chem.*, 1998, **36**, 351.
443. H. O. Gavarini, M. A. Natiello and R. H. Contreras, *Theor. Chim Acta*, 1985, **68**, 171.

444. A. C. Diz, R. H. Contreras, M. A. Natiello and H. O. Gavarini, *J. Comput. Chem.*, 1985, **6**, 647.
445. R. H. Contreras, H. O. Gavarini and M. A. Natiello, *J. Comput. Chem.*, 1987, **8**, 265.
446. M. A. Natiello, R. H. Contreras, H.O. Gavarini and I. D. Rae, *Chem. Phys.* 1985, **98**, 279.
447. C. G. Giribet, M. C. Ruiz de Azúa, R. H. Contreras, R. Lobayán de Bonczok, G. A. Aucar and S. Gomez, *J. Mol. Struct. (Theochem)*, 1993, **300**, 467.
448. G. A. Bowmaker and J. P. Williams, *Aust. J. Chem.*, 1994, **47**, 451.
449. J. M. Kessler, J. H. Nelson, J. Fischer, A. De Cian, W. H. Bearden and N. Fujii, *Inorg. Chem.*, 1994, **33**, 4319.
450. S. Attar, G. A. Bowmaker, N. W. Alcock, J. S. Frye, W. H. Bearden and J. H. Nelson, *Inorg. Chem.*, 1991, **30**, 4753.
451. S. Hillebrand, J. Bruckmann, C. Krüger and M. W. Haenel, *Tetrahedron Lett.*, 1995, **36**, 75.
452. S. D. Pastor, S. P. Shum, R. K. Rodebaugh, A. D. DeBellis and F. H. Clarke. *Helv. Chim. Acta*, 1993, **76**, 900.
453. S. D. Pastor, S. P. Shum, A. D. DeBellis, L. P. Burke and R. K. Rodebaugh, F. H. Clarke and G. Rihs, *Inorg. Chem.*, 1996, **35**, 949.
454. S. D. Perera, B. L. Shaw, M. Thornton-Pett and J. D. Vessey, *Inorg. Chim. Acta*, 1993, **207**, 175.
455. M. Sawamura, H. Hamashima, M. Sugawara, R. Kuwano and Y. Ito, *Organometallics*, 1995, **14**, 4549.
456. P. B. Hitchcock, M. F. Lappert, W.-P. Leung and P. Yin, *J. Chem. Soc., DaltonTrans.*, 1995, 3925.
457. J. L. Bookham, F. Conti, H. C. E. McFarlane, W. McFarlane and M. Thornton-Pett, *J. Chem. Soc., Dalton Trans.*, 1994, 1791.
458. S. R. Ninoreille, R. Broussier, R. Amardeil, M. M. Kubicki and B. Gautheron, *Bull. Soc. Chim. France*, 1995, **132**, 128.
459. T. R. Prout, T. W. Imiolczyk, F. Barthelemy, S. M. Young, R. C. Haltiwanger and A. D. Norman, *Inorg. Chem.*, 1994, **33**, 1783.
460. L. Ernst and K. Ibrom, *Angewandte Chemie, Int. Ed.*, 1995, **34**, 1881.
461. L. Ernst, K. Ibrom, K. Marat, R. H. Mitchell, G. J. Bodwell and G. W. Bushnell, *Chem. Ber.*, 1994, **127**, 1119.
462. R. P. Hughes, P. R. Rose, X. Zheng and A. L. Rheingold, *Organometallics*, 1995, **14**, 2407.
463. S. L. Manatt and M. T. Bowers, *J. Am. Chem. Soc.*, 1969, **91**, 4381.
464. D. A. Dixon, *J. Phys. Chem.*, 1986, **90**, 2038.
465. N. Platzer, J.-P. Buisson and P. Demerseman, *J. Heterocycl. Chem.*, 1992, **29**, 1149.
466. H. Duddeck and A. Biallass, *Magn. Reson. Chem.*, 1994, **32**, 303.
467. I. D. Rae, J. A. Weigold, R. H. Contreras and R. R. Biekofsky, *Magn. Reson. Chem.*, 1993, **31**, 836.
468. A. Gossauer, F. Fehr, F. Nydegger, H. Stöckli-Evans, *J. Am. Chem. Soc.*, 1997, **119**, 1599.
469. A. J. Dingley and S. Grzesiek, *J. Am. Chem. Soc.*, 1998, **120**, 8293.
470. P. Stilbs and S. Forsén, *Org. Magn. Reson.*, 1976, **8**, 384.
471. P. E. Hansen, in *The Chemistry of Double-bonded Functional Groups* (ed. S. Patai), ch. 3, Wiley, New York, 1989.
472. V. Galasso, *J. Chem. Phys.*, 1985, **82**, 899.
473. V. Galasso and G. Fronzoni, *J. Chem. Phys.*, 1986, **84**, 3215.
474. V. Galasso, *Chem. Phys.*, 1987, **117**, 415.
475. T. C. Wong, L. R. Collazo and F. S. Guziec Jr, *Tetrahedron*, 1995, **51**, 649.
476. A. Matallana, A. W. Kruger and C. A. Kingsbury, *J. Org. Chem.*, 1994, **59**, 3020.
477. T. Schaefer, R. Sebastian, D. M. McKinnon, P. W. Spevack, K. J. Cox and C. S. Takeuchi, *Can. J. Chem.*, 1993, **71**, 960.
478. A. V. Afonin, N. M. Peruchena, L. Sosa and R. H. Contreras, *Russ. Chem. Bull.*, 1997, **46**, 251.

479. A. V. Afonin, *Izv. Akad. Nauk., Ser. Khim.*, 1996, 1205.
480. A. V. Afonin, A. V. Vashchenko and H. Fujiwara, *Bull., Chem. Soc. Jpn.*, 1996, **69**, 933.
481. A. Esteban, M. P. Galache, E. Díez, *et al.*, *Magn. Reson. Chem.*, 1999, **37**, 227.
482. E. Kolehmainen, R. Gawinecki, B. Osmialowski and K. Trzebiatowska, *Magn. Reson. Chem.*, 1997, **35**, 778.
483. W. Ibrom and A. W. Frahm, *Magn. Reson. Chem.*, 1996, **34**, 937.
484. A. V. Afonin and A. Esteban, personal communication.
485. S. Chandrasekaran and D. W. Boykin, *Heteroatom. Chem.*, 1992, **3**, 63.
486. H. Kusanagi, *Chem. Lett.*, 1996, 41.
487. S. N. Smirnov, N. S. Golubev, G. S. Denisov, H. Benedict, P. Schah-Mohammedi and H.-H. Limbach, *J. Am. Chem. Soc.*, 1996, **118**, 4094.
488. P. E. Hansen, Aa. E. Hansen, A. Lycka and A. Buvari-Barcza, *Acta Chem. Scand.*, 1993, **47**, 777.
489. R. M. Claramunt, D. Sanz, J. Catalán, F. Fabero, N. A. García, C. Foces-Foces, A. L. Llamas-Saiz and J. Elguero, *J. Chem. Soc., Perkin Trans. 2*, 1993, 1687.
490. N. Carr, L. Mole, A. G. Orpen and J. L. Spencer, *J. Chem. Soc. Dalton Trans.*, 1992, 2653.
491. D. L. Clark, S. K. Grumbine, B. L. Scott and J. G. Watkin, *Organometallics*, 1996, **15**, 949.
492. J. M. Boncella, M. L. Cajigal and K. A. Abboud, *Organometallics*, 1996, **15**, 1905.
493. L. J. Procopio, P. J. Carroll and D. H. Berry, *J. Am. Chem. Soc.*, 1994, **116**, 177.
494. M. Brookhart, E. Hauptman and D. M. Lincoln, *J. Am. Chem. Soc.*, 1992, **114**, 10394.
495. N. Juranic and V. A. Likic, *J. Am. Chem. Soc.*, 1996, **118**, 7859.
496. N. Juranic, M. Moncrieffe, S. Macura and F. G. Prendergast, *Book of Abstracts, 36th Experimental Nuclear Magnetic Conference*, Boston, 1995, p. 152.
497. N. Juranic, M. Moncrieffe, E. Kurian and F. G. Prendergast, *Proceedings, International Conference on Molecular Structural Biology, Vienna*, 1995, p. 21.
498. I. D. Rae, J. Calvar, M. C. Ruiz de Azúa and R. H. Contreras, *12th Conference of the International Society of Magnetic Resonance, Sydney*, 1995, Poster T14.
499. A. V. Afonin, J. E. Pérez, M. C. Ruiz de Azúa, R. H. Contreras and P. Lazzeretti, *Russ. Chem. Bull.*, 1997, **46**, 292.
500. J. E. Pérez, F. S. Ortiz, R. H. Contreras, C. G. Giribet and M. C. Ruiz de Azúa, *J. Mol. Struct. (Theochem)*, 1990, **210**, 193.
501. A. E. Reed, L. A. Curtis and F. Weinhold, *Chem. Rev.*, 1988, **88**, 899.
502. A. S. Edison, J. L. Markley and F. Weinhold, *J. Biomol. NMR*, 1995, **5**, 332.
503. E. Díiez, personal communication.
504. M. J. S. Dewar and R. C. Dougherty, *The PMO Theory of Organic Chemistry*, Plenum Press, New York, 1975.
505. R. A. Hoffman, *Mol. Phys.*, 1958, **1**, 326.
506. W. Adcock and N. A. Trout, *Magn. Reson. Chem.*, 1998, **36**, 181.
507. J. Cai, A. G. Davies and C. H. Schiesser, *J. Chem. Soc., Perkin Trans. 2*, 1994, 1151.
508. J. E. Anderson, A. J. Bloodworth, J. Cai, A. G. Davies and N. A. Tallant, *J. Chem. Soc., Chem. Commun.*, 1992, 1689.
509. E. Juaristi, G. Cuevas and A. Vela, *J. Am. Chem. Soc.*, 1994, **116**, 5796.
510. (a) A. S. Perlin and B. Casu, *Tetrahedron Lett.*, 1969, 2921; (b) S. Wolfe, B. M. Pinto, V. Varma and R. Y. N. Leung, *Can. J. Chem.*, 1990, **68**, 1051.
511. U. Salzner, *J. Org. Chem.*, 1995, **60**, 986.
512. T. Viljanen, K. D. Klika, F. Fülöp and K. Pihlaja, *J. Chem. Soc., Perkin Trans. 2*, 1998, 1479.
513. G. Cuevas, E. Juaristi and A. Vela, *J. Mol. Struct. (Theochem)*, 1998, **418**, 231.
514. W. Adcock, C. I. Clark, A. Houmam, A. R. Krstic and J.-M. Savéant, *J. Org. Chem.*, 1996, **61**, 2891.
515. W. Adcock and A. R. Krstic, *Magn. Reson. Chem.*, 1997, **35**, 663.
516. N. M. Peruchena, PhD thesis, University of La Plata, Argentina, 1997.
517. N. M. Peruchena and R. H. Contreras, *J. Mol. Struct. (Theochem)*, 1995, **338**, 25.

518. C. J. Rhodes, J. C. Walton and E. W. Della, *J. Chem. Soc., Perkin Trans. 2*, 1993, 2125.
519. K. Kamienska-Trela, in *Isotopes in the Physical and Biomedical Studies* (eds E. Buncel and J. R. Jones), vol. 2, p. 297, Elsevier, Amsterdam, 1991.
520. H. Butenschön, B. Gabor, R. Mynott and H. G. Wey, *Z. Naturforsch.*, 1995, **B50**, 483.
521. J. Wardeiner, W. Lüttke, R. Bergholz and R. Machinek, *Angew. Chem. Int. Ed. Engl.*, 1982, **21**, 872.
522. P. Jankowski, K. Kamienska-Trela, K. Minsksztym and J. Wicha, *J. Organomet. Chem.*, 1993, **460**, 15.
523. (a) E. A. Chirkina, O. R. Sergeeva and L. B. Krivdin, *Zh. Org. Khim.*, 1997, **33**, 1144; (b) T. A. Kuznetsova, N. V. Istomina and L. B. Krivdin, *Zh. Org. Khim.*, 1997, **33**, 1703.
524. G. R. Jones, S. Caldarelli and P. Vogel, *Helv. Chim. Acta*, 1997, **80**, 59.
525. E. Kupce and B. Wrackmeyer, *J. Magn. Reson.*, 1993, **A101**, 324.
526. B. Wrackmeyer, G. Kehr, H. Zhou and S. Ali, *Magn. Reson. Chem.*, 1996, **34**, 921.
527. A. A. van Beuzekom, F. A. A. M. de Leeuw and C. Altona, *Magn. Reson. Chem.*, 1990, **28**, 68.
528. N. W. Mitzel, K. Angermaier and H. Schmidbaur, *Organometallics*, 1994, **13**, 1762.
529. B. Wrackmeyer, G. Kehr and D. Wettinger, *Magn. Reson. Chem.*, 1998, **36**, S157.
530. N. W. Mitzel, M. Hofmann, E. Waterstradt, P. v. R. Schleyer and H. Schmidbaur, *J. Chem. Soc., Dalton Trans.*, 1994, 2503.
531. A. Dörr, D. Gudat, D. Hänssgen, H. Hens and E. Stahlhut, *Bull. Soc. Chim. France*, 1994, **131**, 674.
532. B. Wrackmeyer and E. Kupce, in *Topics in Physical Organometallic Chemistry* (ed. M. Gielen), vol. 4, pp. 289–352, Feund Publishing, Tel Aviv, 1992.
533. E. Kupce and B. Wrackmeyer, *J. Magn. Reson.*, 1992, **97**, 568.
534. B. Wrackmeyer, G. Kehr, H. E. Maisel and H. Zhou, *Magn. Reson. Chem.*, 1998, **36**, 39.
535. A. Appel, C. Kober, C. Neumann, H. Nöth, M. Schmidt and W. Storch, *Chem. Ber.*, 1996, **129**, 175.
536. T. N. Mitchell and B. Godry, *J. Organomet. Chem.*, 1995, **490**, 45.
537. J. G. Verkade and J. A. Mosbo, in *Phosphorus-31 NMR Spectroscopy in Stereochemical Analysis* (ed. J. G. Verkade and L. D. Quin), p. 425, VCH, Weinheim, 1989.
538. B. Wrackmeyer and C. Köhler, *Magn. Reson. Chem.*, 1993, **31**, 573.
539. B. Wrackmeyer, C. Köhler and E. Kupce, *Magn. Reson. Chem.*, 1993, **31**, 769.
540. D. Gudat, M. Link and G. Schröder, *Magn. Reson. Chem.*, 1995, **33**, 59.
541. S. G. Frankiss, *J. Chem. Phys.*, 1963, **67**, 752.
542. K. Eichele, R. E. Wasylishen, J. S. Grossert and C. Olivieri, *J. Phys. Chem.*, 1995, **99**, 10110.
543. B. Nagasaka, S. Takeda and N. Nakamura, *Chem. Phys. Lett.*, 1994, **222**, 486.
544. S. H. Alarcon, A. C. Olivieri, S. A. Carss and R. K. Harris, *Magn. Reson. Chem.*, 1995, **33**, 603.
545. A. Ejchart and A. Gryff-Keller, *J. Magn. Reson.*, 1996, **A122**, 233.
546. W. Adcock, D. Lünsman, J. E. Peralta and R. H. Contreras, *Magn. Reson. Chem.*, 1999, **37**, 167.
547. C. R. Kaisen, PhD thesis, Universidade Estadual de Campinas, Campinas, 1982, cited in ref. 548.
548. R. J. Abraham, A. D. Jones, M. A. Warne, R. Rittner and C. F. Tormenta, *J. Chem. Soc., Perkin Trans. 2*, 1996, 533.
549. E. W. Della, E. Cotsaris and P. T. Hine, *J. Am. Chem. Soc.*, 1981, **103**, 4131.
550. W. McFarlane, D. S. Rycroft and C. J. Turner, *Bull. Soc. Chim. Belg.*, 1977, **86**, 457.
551. B. Wrackmeyer, R. Köster and G. Seidel, *Magn. Reson. Chem.*, 1995, **33**, 493.
552. B. Wrackmeyer, B. Distler, S. Gertsmann and M. Herberhold, *Z. Naturforsch.*, 1993, **B48**, 1307.
553. R. Aydin and H. Günther, *Magn. Reson. Chem.*, 1990, **28**, 448.
554. J. B. Lambert and R. A. Singer, *J. Am. Chem. Soc.*, 1992, **114**, 10246.
555. K. Kamienska-Trela, *Magn. Reson. Chem.*, 1995, **33**, 406.

556. S. Berger, *Org. Magn. Reson.* 1984, **22**, 47.
557. W. Bocian, J. Jazwinaki, L. Stefaniak and G. A. Webb, *J. Chem. Soc., Perkin Trans. 2*, 1994, 1467.
558. J. Jazwinski, O. Staszewska, L. Stefaniak and G. A. Webb, *J. Mol. Struct.*, 1996, **377**, 167.
559. A. Forni, I. Moretti, A. Pirondi, F. Prati and L. Schenetti, *J. Chem. Soc. Perkin Trans. 2*, 1994, 1969.
560. J. Jazwinski, J. Pankowski and J. Winiarski, *J. Chem. Soc., Perkin Trans. 2*, 1996, 365.
561. C. E. McKenna, B. A. Kashemirov and J.-Y Ju, *J. Chem. Soc., Chem. Commun.*, 1994, 1211.
562. R. Schmutzler, P. Bernatowicz, W. Schilf, L. Stefaniak and G. A. Webb, *J. Mol. Struct.*, 1998, **442**, 121.
563. J. A. Pople and A. A. Bothner-By, *J. Chem. Phys.*, 1965, **42**, 1335.
564. E. Sackmann and H. Dreeskamp, *Spectrochim. Acta*, 1965, **21**, 2005.
565. O. Yamamoto, M. Watanabe and O. Kikuchi, *Mol. Phys.*, 1969, **17**, 249.
566. A. Esteban, E. Díez, J. E. Peralta and R. H. Contreras, unpublished results.
567. T. D. Ferris, P. T. Lee and T. C. Farrar, *Magn. Reson. Chem.*, 1997, **35**, 571.
568. S. Yamada, M. Nakamura and I. Kawauchi, *Chem. Commun.*, 1997, 885.
569. P. E. Hansen, *Prog. NMR. Spectrosc.*, 1981, **14**, 175.
570. T. Schaefer, *J. Phys. Chem.*, 1975, **79**, 1888.
571. H. J. Jakobsen, P. I. Yang and W. S. Brey, *Org. Magn. Reson.*, 1981, **17**, 290.
572. N. Shimba, H. Takahashi, M. Sakakura, I. Fujii and I. Shimada, *J. Am. Chem. Soc.*, 1998, **120**, 10988.
573. G. Heckmann and E. Fluck, *Magn. Reson. Chem.*, 1995, **33**, 553.
574. A. Ribeiro, *Magn. Reson. Chem.*, 1997, **35**, 215.
575. T. Spoormaker and M. J. A. de Bie, *Rec. Trav. Chim.*, 1978, **97**, 135.
576. A. A. Ribeiro and M. J. Glen, *J. Magn. Reson.*, 1994, **A107**, 158.
577. G. J. Schrobilgen and J. M. Whalen, *Inorg. Chem.*, 1994, **33**, 5207.
578. C. J. Jameson, in *Multinuclear NMR*, (ed. J. Mason), ch. 16, Plenum Press, New York, 1987.
579. H. Koroniak, K. W. Palmer, W. R. Dolbier Jr and H-Q. Zhang, *Magn. Reson. Chem.*, 1993, **31**, 748.
580. M. Jansen and H. J. Jakobsen, *J. Magn. Reson.*, 1975, **20**, 520.
581. S. Chimichi, B. Cosimelli, P. Tedeschi and F. Ponticelli, *Magn. Reson. Chem.*, 1994, **32**, 312.
582. M. Hansen, R. S. Hansen and H. J. Jakobsen, *J. Magn. Reson.*, 1974, **13**, 386.
583. P. Bjork, A.-B. Hornfeldt and S. Gronowitz, *J. Heterocyclic Chem.*, 1994, **31**, 1161.
584. T. Nevalainen, E. Kolehmainen and E. Vilén, *Magn. Reson. Chem.*, 1995, **33**, 355.
585. K. Kamienska-Trela, L. Kania, J. Sitkowski and L. Kaczmarek, *J. Chem. Soc., Perkin Trans. 2*, 1995, 1617.
586. B. Wrackmeyer, U. Klaus, W. Milius, E. Klaus and T. Schaller, *J. Organomet. Chem.*, 1996, **517**, 235.
587. B. Wrackmeyer, U. Klaus and W. Milius, *Chem. Ber.*, 1995, **128**, 679.
588. J. V. Hines, G. Varani, S. M. Landry and I. Tinoco, Jr., *J. Am. Chem. Soc.*, 1993, **115**, 11002.
589. B. S. Reddy, C. D. Reddy and P. M. Reddy, *Heteroat. Chem.*, 1994, **5**, 507.
590. M. J. Milewska and T. Polonski, *Magn. Reson. Chem.*, 1994, **32**, 631.
591. M. Ratier, B. Jousseaume, N. Noiret, N. Petit, J-C. Lartigue and M. Pétraud, *Magn. Reson. Chem.*, 1993, **31**, 176.
592. T. A. Modro, A. M. Modro, P. Bernatowicz, W. Schilf and L. Stefaniak, *Magn. Reson. Chem.*, 1998, **36**, S212.
593. C. Le Roux, A. M. Modro and T. A. Modro, *J. Org. Chem.*, 1995, **60**, 3832.
594. H. Wan and T. A. Modro, *Synthesis*, 1996, **10**, 1227.
595. P. G. Devitt and T. P. Terence, *Tetrahedron*, 1995, **51**, 10987.
596. A. P. Marchand, N. W. Marchand and A. L. Segre, *Tetrahedron Lett.*, 1969, 5207.
597. J. L. Marshall, S. R. Walter, M. Barfield, A. P. Marchand, N. W. Marchand and A. L. Segre, *Tetrahedron*, 1976, **32**, 537.

598. F. A. M. de Leeuw, A. a. van Beuzekom and C. Altona, *J. Comput. Chem.*, 1983, **4**, 438.
599. C. N. Cavasotto, C. G. Giribet, M. C. Ruiz de Azúa and R. H. Contreras, *J. Comput. Chem.*, 1991, **12**, 141.
600. P. P. Lankhorst, T. A. van Beek and C. A. G. Haasnoot, *Magn. Reson. Chem.*, 1993, **31**, 590.
601. R. Radeglia, H. Poleschner and G. Haufe, *Magn. Reson. Chem.*, 1993, **31**, 639.
602. S. Castellano, C. Sun and R. Kostelnik, *J. Chem. Phys.*, 1967, **46**, 327.
603. S. Suntioinen, U. Weber and R. Laatikainen, *Magn. Reson. Chem.*, 1993, **31**, 406.
604. T. Parella, F. Sánchez-Ferrando and A. Virgili, *Magn. Reson. Chem.*, 1995, **33**, 196.
605. U. Vogeli and W. von Philipsborn, *Org. Magn. Reson.*, 1975, **7**, 617.
606. M. Curic, Lj. Tusek'Bozic and Vikic-Topic, *Magn. Reson. Chem.*, 1995, **33**, 27.
607. T. N. Mitchell and B. Kowall, *J. Organomet. Chem.*, 1994, **471**, 39.
608. T. Schaefer, G. H. Penner and R. Sebastian, *Can. J. Chem.*, 1987, **65**, 873.
609. T. Schaefer, W. K. Chan, R. Sebastian, R. Schurko and F. R. Hruska, *Can. J. Chem.*, 1994, **72**, 1972.
610. T. Schaefer, R. W. Schurko and G. M. Bernard, *Can. J. Chem.*, 1994, **72**, 1780.
611. T. Schaefer, S. Kroeker and D. M. Mckinnon, *Can. J. Chem.*, 1995, **73**, 1478.
612. D. Chmielewski, N. H. Werstiuk and T. A. Wildman, *Can. J. Chem.*, 1993, **71**, 1741.
613. A. Habsaoui, J.-C. Wallet and E. M. Gaydou, *Magn. Reson. Chem.*, 1998, **36**, 621.
614. J. L. Adcock and H. Q. Zhang, *J. Org. Chem.*, 1996, **61**, 1975.
615. E. Kolehmainen, K. Laihia, M. I. Rybinskaya, V. S. Kaganovich and Z. A. Kerzina, *J. Organomet. Chem.*, 1993, **453**, 273.
616. D. Hoffmann, W. Bauer, F. Hampel, *et al.*, *J. Am. Chem. Soc.*, 1994, **116**, 528.
617. A. Dabrowski and K. Kamienska-Trela, *J. Organomet. Chem.*, 1993, **460**, C1.
618. B. Wrackmeyer, K. Wagner, A. Sebald, L. H. Merwin and R. Boese, *Magn. Reson. Chem.*, 1991, **29**, S3.
619. K. Bergander, R. He., N. Chandrakumer, O. Eppers and H. Günther, *Tetrahedron*, 1994, **50**, 5861.
620. S. Nlate, P. Guénot, S. Sinbandhit, L. Toupet, C. Lapinte and V. Guerchais, *Angew. Chem., Int. Ed. Engl.*, 1994, **33**, 2218.
621. B. Wrackmeyer and G. Kehr, *J. Organomet. Chem.*, 1995, **501**, 87.
622. D. Kost, I. Kalikhman and M. Raban, *J. Am. Chem. Soc.*, 1995, **117**, 11512.
623. A. R. Bassindale and J. Jiang, *J. Organomet. Chem.*, 1993, 446, C3.
624. C. Breliere, R. J. P. Corriu, G. Royo and J. Zwecker, *Organometallics*, 1989, **8**, 1834.
625. M. Grignon-Dubois, M. Petraud, M. Laguerre and I. Pianet, *Spectrochim. Acta*, 1994, **50A**, 2059.
626. U. Herzog, G. Roewer and U. Pätzold, *J. Organomet. Chem.*, 1995, **494**, 143.
627. U. Schubert and H. Gilges, *Organometallics*, 1996, **15**, 2373.
628. I. Kalikhman, S. Krivonos, D. Stalke, T. Kottke and D. Kost, *Organometallics*, 1997, **16**, 3255.
629. V. Pejchal, J. Holecek, M. Nadvornik and A. Lycka, *Collect. Czech. Chem. Commun.*, 1995, **60**, 1492.
630. (a) T. N. Mitchell and B. Godry, *J. Organomet. Chem.*, 1995, **490**, 45; (b) T. N. Mitchell and B. Godry, *J. Organomet. Chem.*, 1996, **516**, 133.
631. T. R. Forbus Jr and J. C. Martin, *Heteroatom Chem.*, 1993, **4**, 129.
632. C. Kober, H. Noth and W. Storch, *Chem. Ber.*, 1997, **130**, 765.
633. K. K. Laali and P. E. Hansen, *J. Org. Chem.*, 1993, **58**, 4096.
634. C. Y. Wong, R. McDonald and R. G. Cavell, *Inorg. Chem.*, 1996, **35**, 325.
635. (a) V. Torocheshnikov, D. Rentsch and W. von Philipsborn, *Magn. Reson. Chem.*, 1994, **32**, 348; (b) D. Rentsch, W. von Philipsborn and V. Torocheshnikov, *Magn. Reson. Chem.*, 1996, **34**, 955; (c) D. Rentsch, R. Hany and W. von Philipsborn, *Magn. Reson. Chem.*, 1997, **35**, 832.
636. K. Eichele, R. E. Wasylishen, K. Maitra, J. H. Nelson and J. F. Britten, *Inorg. Chem.*, 1997, **36**, 3539.

637. H. Chen, F. A. Cotton and Z. Yao, *Inorg. Chem.*, 1994, **33**, 4255.
638. A. Macchioni, P. S. Pregosin, H. Rüegger, G. van Koten, P. A. van der Shaaf and R. A. T. M. Abbenhius, *Magn. Reson. Chem.*, 1994, **32**, 235.
639. G. H. Rentsch, W. Kozminski, W. von Philipsborn, F. Asaro and G. Pellizer, *Magn. Reson. Chem.*, 1997, **35**, 904.
640. M. Ludwig, L. Öhrström and D. Steinborg, *Magn. Reson. Chem.*, 1995, **33**, 984.
641. F. Asaro, G. Costa, R. Dreos, G. Pellizer and W. von Philipsborn, *J. Organomet. Chem.*, 1996, **513**, 193.
642. I. Potocnak, M. Dunaj-Jurco, M. Ludwig and D. Steinborn, *Acta Crystallogr.*, 1995, **C51**, 1999.
643. M. G. Partridge, B. A. Messerle and L. D. Field, *Organometallics*, 1995, **14**, 3527.
644. C. J. Cobley and P. G. Pringle, *Inorg. Chim. Acta*, 1997, **265**, 107.
645. M. Koike and J. R. Shapley, *J. Organomet. Chem.*, 1994, **470**, 199.
646. J. Jirman, M. Nádvorník, J. Sopková and A. Popkov, *Magn. Reson. Chem.*, 1998, **36**, 351.
647. M. A. Esteruelas, F. Liu, E. Oñate, E. Sola and B. Zeier, *Organometallics*, 1997, **16**, 2919.
648. M. F. C. Guedes da Silva, J. J. R. Fraústo da Silva and A. J. L. Pombeiro, *J. Chem. Soc., Dalton Trans.*, 1994, 3299.
649. L. Schenetti, G. Bandoli, A. Dolmella, G. Trovó and B. Longato, *Inorg. Chem.*, 1994, **33**, 3169.
650. G. Wu and R. E. Wasylishen, *J. Chem. Phys.*, 1993, **98**, 6138.
651. G. Wu and R. E. Wasylishen, *Inorg. Chem.*, 1996, **35**, 3113.
652. C. W. Liu, H. Pan, J. P. Fackler Jr, G. Wu, R. E. Wasylishen and M. Shang, *J. Chem. Soc., Dalton Trans.*, 1995, 3691.
653. K. Nilsson, C. Ullenius and N. Krause, *J. Am. Chem. Soc.*, 1996, **118**, 4194.
654. N. Krause, R. Wagner and A. Gerold, *J. Am. Chem. Soc.*, 1994, **116**, 381.
655. J. M. Fisher, W. E. Piers, L. R. MacGillivray and M. J. Zaworotko, *Inorg. Chem.*, 1995, **34**, 2499.
656. Z. W. Li and H. Taube, *Science*, 1992, **256**, 210.
657. D. M. Heinekey, A. Liegeois and M. v. Roon, *J. Am. Chem. Soc.*, 1994, **116**, 8388.
658. P. S. Bagus, K. Hermann and C. W. Bauschlicher, *J. Chem. Phys.*, 1984, **80**, 4378.
659. G. Jia, S. D. Drouin, P. G. Jessop, A. J. Lough and R. H. Morris, *Organometallics*, 1993, **12**, 906.
660. L. D. Field, T. W. Hambley and B. C. K. Yau, *Inorg. Chem.*, 1994, **33**, 2009.
661. C. Bianchini, A. Marchi, L. Marvelli, *et al.*, *Organometallics*, 1995, **14**, 3203.
662. F. A. Jalón, A. Otero, B. R. Manzano, E. Villaseñor and B. Chaudret, *J. Am. Chem. Soc.*, 1995, **117**, 10123.
663. Z.-W. Li and H. Taube, *J. Am. Chem. Soc.*, 1994, **116**, 11584.
664. Z.-W. Li and H. Taube, *J. Am. Chem. Soc.*, 1994, **116**, 9506.
665. G. Albertin, S. Antoniutti, D. Baldan and E. Bordignon, *Inorg. Chem.*, 1995, **34**, 6205.
666. K.-T. Smith, M. Tilset, R. Kuhlman and K. G. Caulton, *J. Am. Chem. Soc.*, 1995, **117**, 9473.
667. M. Schlaf, A. L. Lough, P. A. Maltby and R. A. Harris, *Organometallics*, 1996, **15**, 2270.
668. J. S. Craw, G. B. Bacskay and N. S. Hush, *J. Am. Chem. Soc.*, 1994, **116**, 5937.
669. S. F. Boys, in *Quantum Theory of Atoms, Molecules and the Solid State: A Tribute to J. C. Slater* (ed. P. O. Löwdin), Academic Press, New York, 1966.
670. N. S Hush, *J. Am. Chem. Soc.*, 1997, **119**, 1717.
671. G. B. Bacskay, *Chem. Phys. Lett.*, 1995, **242**, 507.
672. P. A. Maltby, M. Schlaf, M. Steinbeck, *et al.*, *J. Am. Chem. Soc.*, 1996, **116**, 5937.
673. I. Meyer, *Chem. Phys. Lett.*, 1983, **97**, 270.
674. H. O. Villar and M. Dupuis, *Chem. Phys. Lett.*, 1987, **142**, 59.
675. (a) V. A. Chertkov and N. M. Sergeyev, *J. Magn. Reson.*, 1976, **21**, 159; (b) P. E. Hansen, A. Berg, H. J. Jakobson, A. P. Manzara and J. Michl, *Org. Magn. Reson.*, 1977, **10**, 179.
676. I. Wharf and M. G. Simard, *J. Organomet. Chem.*, 1997, **532**, 1.

677. L. Stefaniak, B. Kamienski, W. Schilf, S. V. Amosova and G. A. Webb, *J. Phys. Org. Chem.*, 1993, **6**, 520.
678. N. M. Sergeyev, N. D. Segeyeva, Yu. A. Strelenko and W. T. Raynes, *Chem. Phys. Lett.*, 1997, **277**, 142.
679. T. Schaefer, R. W. Shurko, R. Sebastian and F. E. Hruska, *Can. J. Chem.*, 1995, **73**, 816.
680. T. Schaefer, G. M. Bernard, Y. Bekkali and D. M. McKinnon, *Can. J. Chem.*, 1996, **74**, 1626.
681. M. Barfield and M. D. Johnston, Jr, *Chem. Rev*, 1973, **73**, 53.
682. I. Ando and G. A. Webb, *Org. Magn. Reson.*, 1981, **15**, 111.
683. R. Laatikainen, J. Ratilainen, R. Sebastian and H. Santa, *J. Am. Chem. Soc.*, 1995, **117**, 11006.
684. T. Schaefer, G. M. Bernard and F. E. Hruska, *Can. J. Chem.*, 1996, **74**, 1524.
685. P. Vujanic, Z. Meic and D. Vikic-Topic, *Spectosc. Lett.*, 1995, **28**, 395.
686. R. Han, P. Ghosh, P. J. Desrosiers, S. Trofimenko and G. Parkin, *J. Chem. Soc., Dalton Trans.*, 1997, 3713.
687. N. M. Sergeyev, in *NMR Basic Principles and Progress* (eds P. Diehl, E. Fluck, R. Kosfield and H. Günther), vol. 22, Springer-Verlag, Berlin, 1990.
688. T. Helgaker, H. J. Aa. Jensen, P. Jørgensen, *et al.*, *DALTON, An Electronic Structure Program, Release 1.0*, 1997. Available upon request at http.//www.kjemi.uio.no/software.
689. J. Geertsen and J. Oddershede, *J. Chem. Phys.*, 1986, **85**, 2112.
690. S. P. A. Sauer, *J. Phys.*, 1997, **B30**, 3773.
691. S. P. A. Sauer, I. Paidarová and W. T. Raynes, personal communication.
692. S. P. A. Sauer, C. K. Møller, H. Koch, I. Paidarová and V. Špirko, *Chem. Phys.*, 1998, **238**, 385.
693. J. P. Jokisaari, L. P. Ingman, G. J. Schrobilgen and J. C. P. Sanders, *Magn. Reson. Chem.*, 1994, **32**, 242.
694. C. E. Keller and W. R. Carper, *J. Magn. Reson.* 1994, **A110**, 125.
695. C. E. Keller, B. J. Piersma, G. J. Mains and W. R. Carper, *Inorg. Chim. Acta*, 1995, **230**, 185.
696. R. E. Wasylishen and J. O. Friidrich, *Can. J. Chem.*, 1987, **65**, 2238.
697. W. T. Raynes, P. Lazzeretti and R. Zanasi, *Chem. Phys. Lett.*, 1986, **132**, 173.
698. Yu. A. Strelenko and N. M. Sergeyev, *J. Mol. Struct.*, 1996, **378**, 61.
699. P. K. Bhattacharyya and B. P. Dailey, *J. Chem. Phys.*, 1973, **59**, 5820.
700. C. J. Jameson, A. K. Jameson, H. Parker, S. M. Cohen and C.-L. Lee, *J. Chem. Phys.*, 1978, **68**, 2861.
701. N. M. Sergeyev, N. D. Sergeyeva and W. T. Raynes, *Magn. Reson. Chem.*, 1994, **32**, 381.
702. N. M. Sergeyev, P. Sandor, N. D. Sergeyeva and W. T. Raynes, *J. Magn. Reson.*, 1995, **A115**, 174.
703. N. D. Sergeyeva, N. M. Sergeyev and W. T. Raynes, *Magn. Reson. Chem.*, 1998, **36**, 255.
704. I. F. Leshcheva, V. N. Torocheshnikov, N. M. Sergeyev, V. A. Chertkov and V. N. Khlopkov, *J. Magn. Reson.*, 1991, **94**, 9.
705. V. A. Uvarov, V. A. Chertkov and N. M. Sergeyev, *J. Chem. Soc., Perkin Trans. 2*, 1994, 2375.
706. N. M. Sergeyev, unpublished results.
707. P. Vujanic, E. Gacs-Baitz, Z. Meic, T. Suste and V. Smrecki, *Magn. Reson. Chem.*, 1995, **33**, 426.
708. P. Novak, Z. Meic and H. Sterk, *J. Chem. Soc., Perkin Trans. 2*, 1996, 2531.
709. M. Saunders, M. H. Jaffé and P. Vogel, *J. Am. Chem. Soc.*, 1971, **93**, 2558.
710. F. A. L. Anet and D. O'Leary, *Tetrahedron Lett.*, 1989, **30**, 1059.

Dipolar Recoupling under Magic-Angle Spinning Conditions

STEPHAN DUSOLD and ANGELIKA SEBALD

Bayerisches Geoinstitut, University of Bayreuth, D-95440 Bayreuth, Germany

Experimental NMR techniques designed to recouple weak homonuclear and heteronuclear dipolar coupling interactions under magic-angle spinning conditions are discussed. Developments and applications of such dipolar recoupling techniques are reviewed, covering the period 1994–early 1999. The various homonuclear and heteronuclear dipolar recoupling pulse sequences are illustrated and explained within the framework of average Hamiltonian theory.

1. INTRODUCTION

When looking back over a period of as little as the past five years and trying to identify the major areas of activity in high-resolution solid-state NMR during

ANNUAL REPORTS ON NMR SPECTROSCOPY
VOLUME 41 ISBN 0-12-505341-X

this period, two topics stand out prominently. The introduction of new multiple-quantum magic-angle spinning (MQ MAS) methods[1,2] has produced a remarkable impact in the area of half-integer, $S > 1/2$, quadrupolar nuclei. In the area of spin-$1/2$ nuclei the predominant theme has been homonuclear and heteronuclear dipolar recoupling under MAS conditions, methodological developments as well as rapid widening of the application of such methods.

In principle, it is easy to understand why dipolar recoupling under MAS conditions should be such an attractive target. Of all NMR interactions, dipolar coupling is the only one that carries direct structural information; that is, information on internuclear distances is encoded in the magnitudes of the corresponding dipolar coupling constants. This useful property is by no means a new discovery. Even in liquid-state NMR, where dipolar coupling is usually not observable directly but only indirectly via relaxation or nuclear Overhauser effects, dipolar interactions play a key role in many structure-determination strategies.[3,4] In solid-state NMR, dipolar coupling usually *is* directly observable. However, taking full advantage of this information requires high spectral resolution, which, for powdered solids, usually only MAS conditions can offer. MAS efficiently improves spectral resolution, but at the same time tends at least to strongly attenuate dipolar coupling-related effects. Being able to retain dipolar coupling information while having the full advantages of high spectral resolution under MAS conditions opens access to selective and, in principle, quantitative structural information. This possibility in itself convincingly explains why dipolar recoupling under MAS conditions qualifies as a generally important topic in high-resolution solid-state NMR. Naturally, it is not a completely new topic within the framework of MAS NMR, but the past few years in particular have brought about an almost explosive growth of activity in this area. It would not do justice to the subject merely to consider this a fashionable trend in high-resolution solid-state NMR. Rather it appears that some broadly shared opinions exist about important problems to be solved by means of contemporary solid-state NMR techniques, about what is currently to be considered as feasible and, hence, should be next on the agenda at a certain time.

The vast topic of homonuclear and heteronuclear dipolar recoupling under MAS conditions was last reviewed comprehensively in 1994.[5] In that article by Bennett, Griffin and Vega, the general principles are fully explained, with a strong emphasis on Floquet theory rather than average Hamiltonian theory (AHT), and all major avenues of homonuclear and heteronuclear dipolar recoupling under MAS conditions known or foreseeable at that time are identified and described. Nothing in this respect needs to be added to their authorative and exhaustive review. Incidentally, the time at which the review article[5] appeared in 1994 approximately coincided with the time when developments in this area started to accelerate strongly and to diversify. We begin our review where the 1994 review by Bennett, Griffin and Vega ends; we cover the period 1994 to early 1999, and attempt to give an overview of the

diversity of MAS dipolar recoupling techniques and their recent applications developed since then. In order to maintain a focus and avoid drowning readers (and the authors) in information overflow, some sacrifices have had to be made. We choose illustrative examples rather than attempt complete coverage of the literature; quadrupolar nuclei are excluded; and neither applications on 'soft' matter nor on ordered and/or partially ordered solids are included.

Having thus excluded a large body of interesting work, we now need to define what we are actually going to describe and how the remainder of the chapter is organized. Section 2 provides a very brief introductory overview of AHT, with the sole purpose of rendering the article conveniently readable without the need to consult the ubiquitous original literature on this subject. Section 3 deals with heteronuclear dipolar recoupling techniques; Section 4 is devoted to homonuclear spin systems. More recent developments where homonuclear and heteronuclear dipolar recoupling techniques are being combined into single, 'hybrid dipolar recoupling' MAS NMR experiments, are described in Section 5.

2. THEORY

The theory describing nuclear spin systems in a strong external magnetic field and subjected to RF irradiation has been thoroughly treated in the literature (for instance, see refs 3,5–8). The following section presents nothing new in this respect; rather it is meant to provide a brief introduction of the basic concepts, definitions and notation used throughout this chapter.

2.1. The Hamiltonian

The Hamiltonian $H(t)$ for a spin system composed of N dipolar coupled spin-1/2 nuclei under MAS conditions may be written

$$H(t) = \sum_{i=1}^{N} H_i^{\mathrm{CS}}(t) + \sum_{i=1}^{N} \sum_{j>i}^{N} H_{ij}^{\mathrm{D}}(t) + \sum_{i=1}^{N} \sum_{j>i}^{N} H_{ij}^{J}(t) + H^{\mathrm{RF}}(t) \qquad (1)$$

where CS refers to chemical shielding, D to direct dipolar coupling (through space), and J to indirect dipolar coupling (through-bond, J-coupling), and where

$$H_i^{\mathrm{CS}}(t) = \omega_i^{\mathrm{CS}}(t) S_{iz} \qquad (2)$$

The terms describing spin–spin coupling interactions are different for homonuclear and heteronuclear spin–spin interactions.

Heteronuclear:

$$H_{ij}^{\mathrm{D}}(t) = \omega_{ij}^{\mathrm{D}}(t) 2 S_{iz} S_{jz} \tag{3}$$

$$H_{ij}^{J} = \omega_{ij}^{J} S_{iz} S_{jz} \tag{4}$$

$$H_{ij}^{J_{\mathrm{aniso}}}(t) = \omega_{ij}^{J_{\mathrm{aniso}}}(t) 2 S_{iz} S_{jz} \tag{5}$$

Homonuclear:

$$H_{ij}^{\mathrm{D}}(t) = \omega_{ij}^{\mathrm{D}}(t)[2 S_{iz} S_{jz} - \tfrac{1}{2}(S_{i+} S_{j-} + S_{i-} S_{j+})] \tag{6}$$

$$H_{ij}^{J} = \omega_{ij}^{J}[S_{iz} S_{jz} + \tfrac{1}{2}(S_{i+} S_{j-} + S_{i-} S_{j+})] \tag{7}$$

Homonuclear anisotropic J-coupling will be ignored throughout the remainder of this article.

The time dependence of the coefficients $\omega^{\tilde{\kappa}}(t)$ ($\tilde{\kappa} = \mathrm{CS}, \mathrm{D}, J$) can be written as a Fourier series,

$$\omega_{i,ij}^{\tilde{\kappa}}(t) = \sum_{m=-2}^{2} \omega_{\kappa}^{(m)} \exp(\mathrm{i} m \omega_{\mathrm{r}} t) \tag{8}$$

where $\kappa = \mathrm{CS}_i, \mathrm{D}_{ij}, J_{ij}$ and

$$\omega_{\kappa}^{(m)} = \omega_{\mathrm{iso}}^{\kappa} \delta_{m0} + \delta^{\kappa} \left\{ D_{0,-m}^{2}(\Omega_{\mathrm{PR}}^{\kappa}) - \frac{\eta^{\kappa}}{\sqrt{6}} [D_{-2,-\mathrm{m}}^{2}(\Omega_{\mathrm{PR}}^{\kappa}) + D_{2,-m}^{2}(\Omega_{\mathrm{PR}}^{\kappa})] \right\} d_{-m,0}^{2}(\beta_{\mathrm{RL}}) \tag{9}$$

with the element $D_{p,q}^{2}(\Omega_{IJ})$ of the Wigner rotation matrix describing the rotation from an axis system I to an axis system J, related by the set of Euler angles $\Omega_{IJ} = \{\alpha_{IJ}, \beta_{IJ}, \gamma_{IJ}\}$ according to

$$D_{p,q}^{2}(\Omega_{IJ}) = \exp(-\mathrm{i}\alpha_{IJ} p) d_{p,q}^{2}(\beta_{IJ}) \exp(-i\gamma_{IJ} q) \tag{10}$$

I,J denote P (principal axis system, PAS), C (crystal axis system, CAS), R (rotor axis system, RAS), or L (laboratory axis system); the definition of the Euler angles $\Omega_{IJ} = \{\alpha_{IJ}, \beta_{IJ}, \gamma_{IJ}\}$ is depicted in Fig. 1. When spinning exactly at

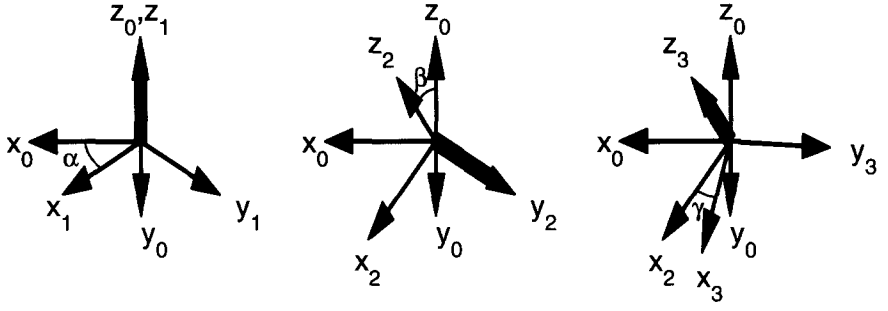

Fig. 1. Definition of the set of Euler angles $\Omega_{IJ} = \{\alpha_{IJ}, \beta_{IJ}, \gamma_{IJ}\}$ relating axis system I to axis system J. Boldface arrows denote the respective axis of rotation and x, y, z are defined in the text.

the angle $\beta_{\mathrm{RL}} = \tan^{-1}\sqrt{2}$ (the 'magic angle') $\omega_\kappa^{(0)} = \omega_{\mathrm{iso}}^\kappa$, and

$$\omega_{\mathrm{iso}}^\kappa = \tfrac{1}{3}(\omega_{xx}^k + \omega_{yy}^k + \omega_{zz}^k) \tag{11}$$

$$\delta^\kappa = \omega_{zz}^\kappa - \omega_{\mathrm{iso}}^\kappa \tag{12}$$

$$\eta^\kappa = \frac{\omega_{yy}^\kappa - \omega_{xx}^\kappa}{\delta^\kappa} \tag{13}$$

with $|\omega_{zz}^\kappa - \omega_{\mathrm{iso}}^\kappa| > |\omega_{xx}^\kappa - \omega_{\mathrm{iso}}^\kappa| > |\omega_{yy}^\kappa - \omega_{\mathrm{iso}}^\kappa|$.[9] For isotropic J-coupling $\omega_{\mathrm{iso}}^J = \pi J_{\mathrm{iso}}$. For direct dipolar coupling $\eta^{\mathrm{D}_{ij}} = \omega_{\mathrm{iso}}^{\mathrm{D}_{ij}} = 0$ and $\delta^{\mathrm{D}_{ij}} = b_{ij} = -\mu_0\gamma_i\gamma_j\hbar/(4\pi r_{ij}^3)$, where γ_i, γ_j are gyromagnetic ratios, and r_{ij} is the internuclear distance between spins S_i and S_j.

2.2. Single transition operators

When selectively exciting single transitions, it is often convenient to introduce single transition operators[3,10–13] defined as

$$S_x^{rs} = \frac{1}{2}(|r\rangle\langle s| + |s\rangle\langle r|) \tag{14}$$

$$S_y^{rs} = \frac{1}{2i}(|r\rangle\langle s| - |s\rangle\langle r|) \tag{15}$$

$$S_z^{rs} = \frac{1}{2}(|r\rangle\langle s| - |s\rangle\langle r|) \tag{16}$$

For a homonuclear pair of 1/2 spins (S_1, S_2), using the eigenbase $|m_1, m_2\rangle$ of the single spin operators S_{1z} and S_{2z}, where

$$S_{iz}\,|m_1, m_2\rangle = m_i\,|m_1, m_2\rangle \tag{17}$$

and employing the numbering system

$$\begin{aligned} |1\rangle &= |+\tfrac{1}{2}, +\tfrac{1}{2}\rangle, \qquad |2\rangle = |+\tfrac{1}{2}, -\tfrac{1}{2}\rangle \\ |3\rangle &= |-\tfrac{1}{2}, +\tfrac{1}{2}\rangle, \qquad |4\rangle = |-\tfrac{1}{2}, -\tfrac{1}{2}\rangle \end{aligned} \tag{18}$$

one obtains

$$\begin{aligned} S_z^{14} &= \tfrac{1}{2}(S_{1z} + S_{2z}), \qquad S_z^{12} - S_z^{34} = 2S_{1z}S_{2z} \\ S_z^{23} &= \tfrac{1}{2}(S_{1z} - S_{2z}), \qquad S_x^{23} = \tfrac{1}{2}(S_{1+}S_{2-} + S_{1-}S_{2+}) \end{aligned} \tag{19}$$

Now the Hamiltonian of a homonuclear pair (S_1, S_2) of spins 1/2 under MAS may be written as

$$H(t) = \omega_\Sigma(t)S_z^{14} + \omega_\Delta(t)S_z^{23} + \omega_A(t)(S_z^{12} - S_z^{34}) + \omega_B(t)S_x^{23} \tag{20}$$

with $\omega_\Sigma(t)$ and $\omega_\Delta(t)$ related to chemical shieldings as

$$\omega_\Sigma(t) = \omega_1^{\mathrm{CS}}(t) + \omega_2^{\mathrm{CS}}(t) \tag{21}$$

$$\omega_\Delta(t) = \omega_1^{\mathrm{CS}}(t) - \omega_2^{\mathrm{CS}}(t) \tag{22}$$

and $\omega_A(t)$, $\omega_B(t)$ related to couplings as

$$\omega_A(t) = \omega_{12}^{\mathrm{D}}(t) + \tfrac{1}{2}\omega_{12}^{J} \tag{23}$$

$$\omega_B(t) = -\omega_{12}^{\mathrm{D}}(t) + \omega_{12}^{J} \tag{24}$$

In addition, it is sometimes useful to define

$$\omega_{\mathrm{iso}}^{\Delta} = \omega_{\mathrm{iso}}^{\mathrm{CS}_1} - \omega_{\mathrm{iso}}^{\mathrm{CS}_2} \tag{25}$$

2.3. Time evolution – average Hamiltonian theory (AHT)[14,15]

The free induction decay can be written as

$$s(t) = \sum_{\Omega_{\mathrm{CR}}} \mathrm{Tr}\left\{ \left(\sum_{i=1}^{N} S_{i+} \right) U(t) \left(\sum_{i=1}^{N} S_{ix} \right) U^{\dagger}(t) \right\} \tag{26}$$

The summation indicates powder averaging; the time evolution is determined by the propagator $U(t)$, which is related to the Hamiltonian in Eq. (1) according to

$$U(t) = \hat{T} \exp\left[-\mathrm{i} \int_0^t H(t)\, \mathrm{d}t\right] \tag{27}$$

where $\hat{T}$ is the Dyson time-ordering operator.

If $H(t)$ is cyclic and periodic with the period τ_c, i.e.

$$H(t) = H(t + \tau_h) \qquad \text{and} \qquad U(t) = U(t + \tau_c) \tag{28}$$

where $\tau_c = m\tau_h$ $(m \in N)$, then

$$U(n\tau_c) = \exp[-\mathrm{i}\bar{H}(\tau_c)\tau_c] \tag{29}$$

with the Magnus expansion

$$\bar{H}(\tau_c) = \sum_{i=0}^{\infty} \bar{H}^i(\tau_c) \tag{30}$$

and

$$\bar{H}^0(\tau_c) = \frac{1}{\tau_c} \int_0^{\tau_c} H(t')\, \mathrm{d}t' \tag{31}$$

$$\bar{H}^1(\tau_c) = -\frac{\mathrm{i}}{2\tau_c} \int_0^{\tau_c} \mathrm{d}t'' \int_0^{t''} \mathrm{d}t' [H(t''), H(t')] \tag{32}$$

$$\bar{H}^2(\tau_c) = -\frac{1}{6\tau_c} \int_0^{\tau_c} \mathrm{d}t''' \int_0^{t'''} \mathrm{d}t'' \int_0^{t''} \mathrm{d}t' \{[H(t'''), [H(t''), H(t')]] + [[H(t'''), H(t'')], H(t')]\} \tag{33}$$

etc.

Note that $\bar{H}^i(\tau_c) \equiv 0$ for $i > 0$ only if $H(t)$ is inhomogeneous in the sense of Maricq and Waugh,[15] that is if $[H(t'), H(t'')] = 0$ $\forall(t'$ and $t'')$. A case where $H(t)$ commutes with itself at different times t', t'' is, for example, a heteronuclear spin pair in the absence of RF irradiation. Further, AHT provides an exact description only for integer multiples of the cycle period τ_c

('stroboscopic observation'). Denoting the lowest-order average Hamiltonian as $\bar{H}^0(\tau_c)$ has been the most common approach in the literature, but alternative notation is used occasionally where the lowest-order average Hamiltonian is denoted $\bar{H}^1(\tau_c)$.[16,17]

Higher-order terms are usually difficult or impossible to calculate. Accordingly, the most common pulse-sequence design procedures take only lower-order terms actively into account. Keeping this in mind, the importance of experimentally checking the actual performance of a pulse sequence under realistic conditions (as well as by numerical methods, where appropriate) is self-evident.

2.4. The average Hamiltonian in the rotating frame

Additional transformation to a suitable rotating frame is usually necessary to achieve convergence of an average Hamiltonian series. As this is often practised, a step-by-step illustration will be given here. As an example, we consider a heteronuclear spin pair (S_1, S_2), and assume application of RF irradiation ω_2^{RF} according to $H^{\mathrm{RF}}(t) = n\omega_{\mathrm{r}} S_{2x}$ and absence of chemical shielding anisotropy (CSA) (this situation is equivalent to a rotary resonance experiment (R^3, see Section 3.1) without CSA). The corresponding Hamiltonian in the Zeeman-interaction frame is $H(t) = \omega_{12}^{\mathrm{D}}(t) 2S_{1z}S_{2z} + n\omega_{\mathrm{r}} S_{2x}$ $(n \in N)$. The Magnus expansion (Eqs (31)–(33)) cannot be applied successfully to the Hamiltonian in this form. The rotation operator $U_R = \exp(in\omega_{\mathrm{r}} t S_{2x})$ transforms $H(t)$ to an appropriate interaction frame where $H^{\mathrm{RF}}(t)$ vanishes. In a second step, the average Hamiltonian in this rotating frame needs to be calculated.

1. The rotating frame Hamiltonian

Transformation of $H(t)$ to the above-defined rotating frame gives[3]

$$H_{\mathrm{R}}(t) = \omega_{12}^{\mathrm{D}}(t) 2S_{1z}[S_{2z}\cos(n\omega_{\mathrm{r}} t) + S_{2y}\sin(n\omega_{\mathrm{r}} t)] \tag{34}$$

$$= \omega_{12}^{\mathrm{D}}(t) S_{1z}[S_{2z}(\exp(in\omega_{\mathrm{r}} t) + \exp(-in\omega_{\mathrm{r}} t)) - \mathrm{i}S_{2y}(\exp(in\omega_{\mathrm{r}} t) - \exp(-in\omega_{\mathrm{r}} t))] \tag{35}$$

which, after insertion of Eq. (8), is

$$H_{\mathrm{R}}(t) = \sum_{m=-2}^{2} \{\omega_{\mathrm{D}_{12}}^{(m)}[\exp(\mathrm{i}(m+n)\omega_{\mathrm{r}} t) + \exp(\mathrm{i}(m-n)\omega_{\mathrm{r}} t)] S_{1z}S_{2z} - \mathrm{i}\omega_{\mathrm{D}_{12}}^{(m)}[\exp(\mathrm{i}(m+n)\omega_{\mathrm{r}} t) - \exp(\mathrm{i}(m-n)\omega_{\mathrm{r}} t)] S_{1z}S_{2y}\} \tag{36}$$

2. The lowest-order average Hamiltonian in the rotating frame

The cycle for the chosen example is the rotation period. Hence, to calculate the lowest-order average Hamiltonian one has to average over one rotation period. The time-dependent terms in Eq. (36) are $\omega_\kappa^{(m)} \exp(\mathrm{i}(m \pm n)\omega_r t)$; the average of these over a rotation period is given by

$$\frac{1}{\tau_r} \int_0^{\tau_r} \mathrm{d}t\, \omega_\kappa^{(m)} \exp(\mathrm{i}(m \pm n)\omega_r t) = \begin{cases} 0, & \text{if } m \pm n \neq 0 \\ \omega_\kappa^{(\mp n)}, & \text{if } m \pm n = 0 \end{cases} \tag{37}$$

leading to the lowest-order average Hamiltonian

$$\bar{H}_R^0 = (\omega_{D_{12}}^{(-n)} + \omega_{D_{12}}^{(n)}) S_{1z} S_{2z} - \mathrm{i}(\omega_{D_{12}}^{(-n)} + \omega_{D_{12}}^{(n)}) S_{1z} S_{2y} \tag{38}$$

where $n = -2, \ldots, +2$. Equation (38) immediately reveals that the dipolar interaction is recoupled if $n = \pm 1, \pm 2$ (compare Section 3.1). The crucial point of this example is Eq. (37): similar kinds of equations, arising from similar transformation procedures, usually 'select' the recoupled terms for a given pulse sequence as described within the framework of AHT. How well the description/selection corresponds to a particular experimental situation depends on how well the chosen average Hamiltonian approximates the properties of the particular spin system and pulse sequence.

3. THE HETERONUCLEAR DIPOLAR INTERACTION

3.1. Rotary Resonance Recoupling, R^3

Continous-wave (CW) irradiation at the Larmor frequency of one spin species S_2 to decouple it from another type of spin S_1 is widely used in NMR spectroscopy.[3] While a high RF field strength ω_2^{RF} is important to decouple the two spin species from each other, a small RF amplitude ω_2^{RF} matching an integer multiple of the spinning frequency ($\omega_2^{RF} = n\omega_r$) will result in recoupling of the dipolar interaction between the two spins. This so called 'rotary resonance recoupling' (R^3)[18,19] recouples not only the dipolar interaction between the two spins but also the chemical shielding interaction of spin S_2. This might come as a disadvantage if the information one is seeking is internuclear distances only. Alternatively, it may be considered an advantage if additional orientational information can be extracted simultaneously from the same experiment.

As the theory for R^3 has been covered in detail in the literature, applying both AHT[18,19] and Floquet methods,[5] we introduce only a brief theoretical

description to provide an illustration of the principal ideas of the cause and results of the R^3 recoupling effect.

We shall assume an isolated heteronuclear two-spin system, with spin S_1 observed and CW RF applied at the Larmor frequency of spin S_2; the R^3 experiment is schematically depicted in Fig. 2. The complete Hamiltonian in the rotating frame of the Zeeman interaction is then given by

$$H(t) = \omega_1^{CS}(t)S_{1z} + \omega_2^{CS}(t)S_{2z} + \omega_{12}^{D}(t)2S_{1z}S_{2z} + \omega_2^{RF}S_{2x} \tag{39}$$

where isotropic and anisotropic J coupling between spins S_1 and S_2 has been neglected.

In a rotating frame defined by the transformation operator[19]

$$U_R = \exp(-in\omega_r t S_{2z})\exp(i(\pi/2)S_{2y}) \tag{40}$$

the Hamiltonian becomes

$$\begin{aligned} H_R(t) = {} & \omega_1^{CS}(t)S_{1z} \\ & - \tfrac{1}{2}\omega_2^{CS}(t)[S_{2-}\exp(in\omega_r t) + S_{2+}\exp(-in\omega_r t)] \\ & - \tfrac{1}{2}\omega_{12}^{D}(t)2S_{1z}[S_{2-}\exp(in\omega_r t) + S_{2+}\exp(-in\omega_r t)] \\ & + (\omega_2^{RF} - n\omega_r)S_{2z} \end{aligned} \tag{41}$$

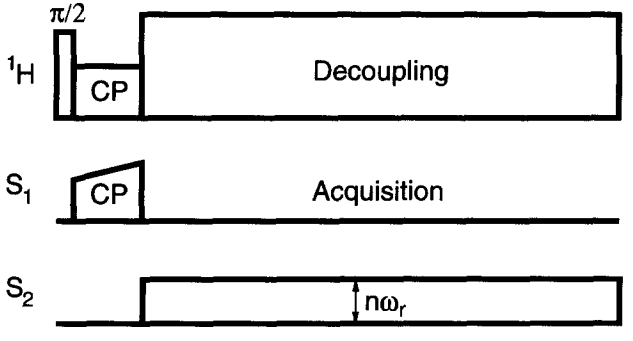

Fig. 2. Pulse sequence of the rotary resonance recoupling experiment (R^3) where the amplitude of ω_2^{RF} matches an integer multiple of ω_r. Here we have assumed a spin system with additional presence of ^{1}H spins in the sample, hence the pulse sequence includes (ramped) cross polarization $^1H \rightarrow S_1$ and ^{1}H decoupling during acquisition. This assumption will be made throughout as this represents the most typical circumstance. However, replacing CP by direct single-pulse S_1 excitation and omitting the ^{1}H decoupling, the R^3 pulse sequence and all sequences discussed in the following are also applicable to (S_1,S_2) spin systems in the absence of ^{1}H spins.

The lowest-order average Hamiltonian in this frame is

$$\begin{aligned}\bar{H}_R^0 = {} & \omega_{CS_1}^{(0)} S_{1z} \\ & - \tfrac{1}{2}(\omega_{CS_2}^{(n)} + \omega_{D_{12}}^{(n)}) S_{1\alpha} S_{2-} - \tfrac{1}{2}(\omega_{CS_2}^{(n)} - \omega_{D_{12}}^{(n)}) S_{1\beta} S_{2-} \\ & - \tfrac{1}{2}(\omega_{CS_2}^{(-n)} + \omega_{D_{12}}^{(-n)}) S_{1\alpha} S_{2+} - \tfrac{1}{2}(\omega_{CS_2}^{(-n)} - \omega_{D_{12}}^{(-n)}) S_{1\beta} S_{2+} \\ & + (\omega_2^{RF} - n\omega_r) S_{2z} \end{aligned} \tag{42}$$

where $S_{1\alpha} = \frac{1}{2}(1 + 2S_{1z})$ and $S_{1\beta} = \frac{1}{2}(1 - 2S_{1z})$ are the projection operators for the two states of the S_1 spin.

As the coefficients $\omega_\kappa^{(\pm n)}$ (Eq. (9)) are only defined for $|n| \leqslant 2$, one has to distinguish two different cases (apart from the trivial case where $n = 0$).

(1) $n > 2$: In this limit the terms containing the Fourier coefficients $\omega_\kappa^{(\pm n)}$ in $\bar{H}_R^0$ vanish, resulting in one single resonance line for spin S_1 at $\omega_{CS_1}^{(0)}$ (i.e. $\omega_{iso}^{CS_1}$ when spinning the sample exactly at the magic angle). This is equivalent to the result one would have found without applied CW RF within the lowest-order AHT approach. It is, however, important to note that this is a largely oversimplified picture, as it fails to explain higher-order rotary-resonance conditions ($n = 3, 4, \ldots$). Those require calculation of higher-order terms, or application of Floquet theory.[5]

(2) $n = 1, 2$: When the rotary-resonance condition is fulfilled, the $(\omega_{CS_2}^{(\pm n)} \pm \omega_{D_{12}}^{(\pm n)}) S_{1\alpha} S_{2\pm}$ and $(\omega_{CS_2}^{(\pm n)} \pm \omega_{D_{12}}^{(\pm n)}) S_{1\beta} S_{2\pm}$ terms in $\bar{H}_R^0$ give rise to recoupling of the dipolar interaction as well as S_2 chemical shielding (and, in fact, anisotropic J-coupling interaction, where applicable).

For a single crystallite, the S_1-spin spectrum consists of four lines at the frequencies $\omega_{iso}^{CS_1} \pm |\omega_{CS_2}^{(n)} + \omega_{D_{12}}^{(n)}| \pm |\omega_{CS_2}^{(n)} - \omega_{D_{12}}^{(n)}|$,[19] depending on the orientations of the two interaction tensors with respect to the magnetic field. If the chemical shielding interaction of the coupled spin S_2 can be neglected, only two resonance lines, separated by a splitting $\omega_\Delta^n = 2|\omega_{D_{12}}^{(n)}|$ will be observed. For $n = 1$ the splitting $\omega_\Delta^1 = |\sqrt{2} b_{12} \sin\beta_{PR}^{D_{12}} \cos\beta_{PR}^{D_{12}}|$ has a maximum of $b_{12}/\sqrt{2}$ at $\beta_{PR}^{D_{12}} = \pi/4$; and for $n = 2$ the maximum of $\omega_\Delta^2 = |1/2\, b_{12} \sin^2 \beta_{PR}^{D_{12}}|$ is $b_{12}/2$ at $\beta_{PR}^{D_{12}} = \pi/2$.

The dependence of the S_1-spin dynamics on the S_2 chemical shielding tensor will in general increase the number of spin parameters, which have to be known or determined for a meaningful evaluation of the experimental results. This is certainly a disadvantage when the only goal is extraction of dipolar coupling information. But even for cases where it is feasible to extract all dipolar *and*

CSA parameters from a single R^3 experiment, it still remains an advantage to have a complementary experimental option to reduce the number of unknowns, by recoupling the dipolar interaction alone.

Costa *et al.*[20] have shown that it is possible to eliminate the S_2 chemical shielding term from $\bar{H}^0_R$ by inverting the phase of the recoupling pulse every second rotation period. The pulse sequence of this SPI-R^3 experiment is shown in Fig. 3. When dropping the non-affected S_1 chemical shielding term for convenience, assuming that the R^3 condition $\omega_2^{RF} = n\omega_r$ is met, and switching to a rotating frame defined by the transformation operator $U_{R\pm} = \exp(\pm in\omega_r t S_{2x})$, the Hamiltonian (Eq. (39)) becomes

$$H_{R_\pm}(t) = \omega_2^{CS}(t)[\tfrac{1}{2}(S_{2z} - iS_{2y})\exp(\pm in\omega_r t) + \tfrac{1}{2}(S_{2z} + iS_{2y})\exp(\mp in\omega_r t)]$$
$$+ \omega_{12}^{D}(t)2S_{1z}[\tfrac{1}{2}(S_{2z} - iS_{2y})\exp(\pm in\omega_r t) + \tfrac{1}{2}(S_{2z} + iS_{2y})\exp(\mp in\omega_r t)] \quad (43)$$

The lowest-order average Hamiltonian calculated over one rotation period in this frame is

$$\bar{H}^0_{R_\pm} = \tfrac{1}{2}\omega_{CS_2}^{(\pm n)}(S_{2z} - iS_{2y}) + \tfrac{1}{2}\omega_{CS_2}^{(\mp n)}(S_{2z} + iS_{2y})$$
$$+ \tfrac{1}{2}\omega_{D_{12}}^{(\pm n)}S_{1z}(S_{2z} - iS_{2y}) + \tfrac{1}{2}\omega_{D_{12}}^{(\mp n)}S_{1z}(S_{2z} + iS_{2y}) \quad (44)$$

The overall average Hamiltonian over the complete cycle period (two rotation periods) of the SPI-R^3 pulse sequence is just the average over two successive rotation periods:

$$\bar{H}^0_R = \tfrac{1}{2}(\bar{H}^0_{R_+} + \bar{H}^0_{R_-}) \quad (45)$$
$$= \tfrac{1}{2}(\omega_{CS_2}^{(n)} + \omega_{CS_2}^{(-n)})S_{2z} + \tfrac{1}{2}(\omega_{D_{12}}^{(n)} + \omega_{D_{12}}^{(-n)})S_{1z}S_{2z} \quad (46)$$

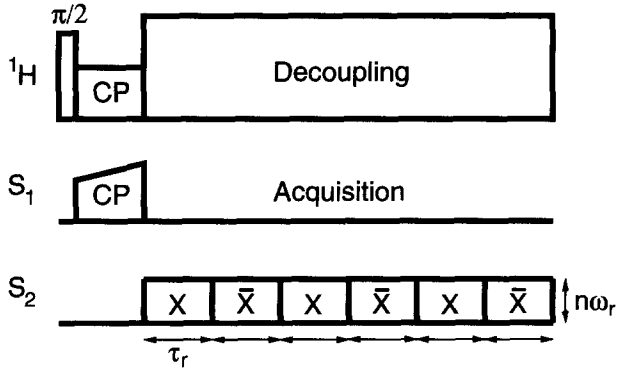

Fig. 3. Pulse sequence of the SPI-R^3 experiment[20] where the phase of ω_2^{RF} is altered every other rotation period τ_r.

As the S_2 chemical shielding term now commutes with the dipolar term, only the latter will affect the S_1 spin dynamics:

$$\bar{H}_{\mathrm{R}}^{0}(S_1) = \tfrac{1}{2}(\omega_{\mathrm{D}_{12}}^{(n)} + \omega_{\mathrm{D}_{12}}^{(-n)})S_{1z}S_{2z} \tag{47}$$

$$= \omega_{\Delta}^{n}(\beta_{\mathrm{PR}}^{D_{12}})\cos(\gamma_{\mathrm{PR}}^{D_{12}})S_{1z}S_{2z} \tag{48}$$

SPI-R^3 accordingly provides recoupling of the heteronuclear dipolar interaction, without recoupling of the S_2 chemical shielding terms to this order of AHT approximation. A similar cancellation of terms can be shown to yield compensation of RF inhomogeneity ($\omega_2^{\mathrm{RF}} = n\omega_{\mathrm{r}} + \delta\omega$) and isotropic chemical shielding offsets, if the condition $\omega_{\mathrm{r}}/2 \gg \delta\omega$ is fulfilled.[20]

It has been pointed out[5,18,19] that R^3 experiments are susceptible to RF inhomogeneity, owing to the requirement that the amplitude of ω_2^{RF} must be matched to a small integer multiple of ω_{r} over the entire sample volume. In practice, we have not come across severe experimental problems of this kind[21,22] but satisfactory experimental R^3 conditions may require restriction of the sample volume. A modification of the R^3 experiment aiming at reducing RF inhomogeneity problems has been proposed. In this modulatory resonance recoupling experiment (MORE)[23,24] the R^3 condition $\omega_2^{\mathrm{RF}} = n\omega_{\mathrm{r}}$ is replaced by a recoupling condition in which the amplitude of ω_2^{RF} is modulated with a frequency $\omega_{\mathrm{mod}} = n\omega_{\mathrm{r}}$ matching multiples of the spinning frequency. Another recently proposed scheme, using simultaneous frequency and amplitude modulation (SFAM)[25] to achieve heteronuclear dipolar recoupling, is shown in Fig. 4. SFAM simultaneously modulates the amplitude of ω_2^{RF} sinusoidally and the carrier frequency of ω_2^{RF} cosinusoidally, with a modulation frequency $\omega_{\mathrm{mod}} = k\omega_{\mathrm{r}}/(2m-1)$, where m is a positive integer and $k = 1, 2$. With careful selection of the parameters for the frequency and amplitude modulation, the SFAM recoupling approach should be flexible and able to cater for a wide range of experimental conditions, in particular including fast spinning conditions.

While lowest-order AHT is suitable to illustrate R^3 recoupling effects in a simplified and intuitive fashion, this is obviously not a viable method for general lineshape analysis of experimental R^3 NMR spectra. Full, numerically exact lineshape simulations have to be carried out instead. This necessity for full analysis of R^3 NMR spectra may partially explain why, in the past, R^3 NMR experiments have not been widely used in practice. Full lineshape simulations no longer present a serious obstacle.[21,22] In contrast to REDOR (see Section 3.2), R^3 and related experiments, such as MORE or SFAM, are not restricted to (relatively) slow MAS conditions, and unwanted simultaneous recoupling of S_2 chemical shielding in R^3 experiments may be eliminated to a certain extent if need arises (see Section 3.2). R^3 (and related schemes) is thus taking shape for solving heteronuclear dipolar-recoupling tasks at high fields and fast MAS conditions, where REDOR will eventually fail. R^3-type

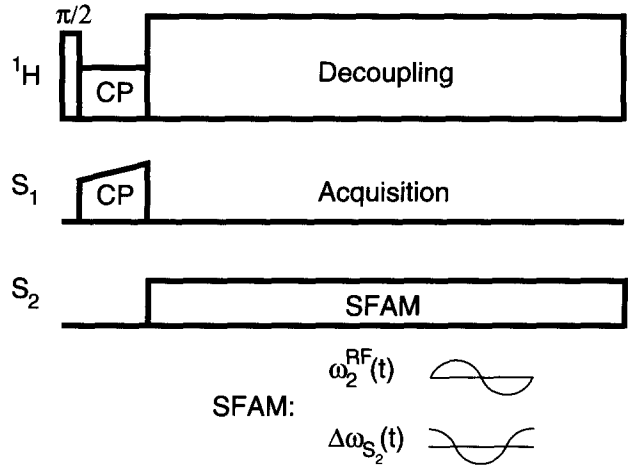

Fig. 4. Pulse sequence of the SFAM experiment[25] where the amplitude of $\omega_2^{RF}(t)$ is modulated sinusoidally, simultaneously with cosinusoidal modulation $\Delta\omega_{S_2}(t)$ of the carrier frequency.

experiments where ω_2^{RF} is applied during acquisition of the S_1 free induction decay require efficient separation of the two (or three) RF channels by suitable RF filters. Especially for applications on S_1, S_2 combinations with similar Larmor frequencies and when working at low magnetic field strengths, the necessary RF filtering may turn out to be experimentally demanding. For high-field applications, with larger frequency separations of the S_1, S_2 RF channels, these R^3 hardware requirements will in general be less demanding.

Otherwise one may adopt an alternative view and consider simultaneous recoupling of S_2 chemical shielding as a favourable property of R^3. The following two examples illustrate how this attitude may be put to work. R^3 experiments can be helpful to determine accurately chemical shielding tensor orientations in a fairly common situation, that is where the single-crystal X-ray structure of a compound is known and polycrystalline powder material is available, but no realistic isotope-labelling or single-crystal NMR option exists to determine chemical shielding tensor orientation parameters. In this situation, magnitudes of chemical shielding tensors will be known (or can be determined easily from standard MAS NMR spectra), the corresponding dipolar coupling constants can be calculated from the known internuclear distances, and only the relative chemical shielding tensor orientations of S_1, S_2 remain to be determined from R^3 experiments. An example where this approach was taken is the trisammonium salt of phosphoenol pyruvate, $(NH_4)_3$PEP, with ^{13}C in natural abundance.[21] ^{13}C (S_1) CP/MAS NMR spectra of $(NH_4)_3$PEP, obtained with slow magic-angle spinning and the ^{31}P (S_2) $n = 1$ R^3 condition fulfilled, are shown in Fig. 5, together with the corresponding

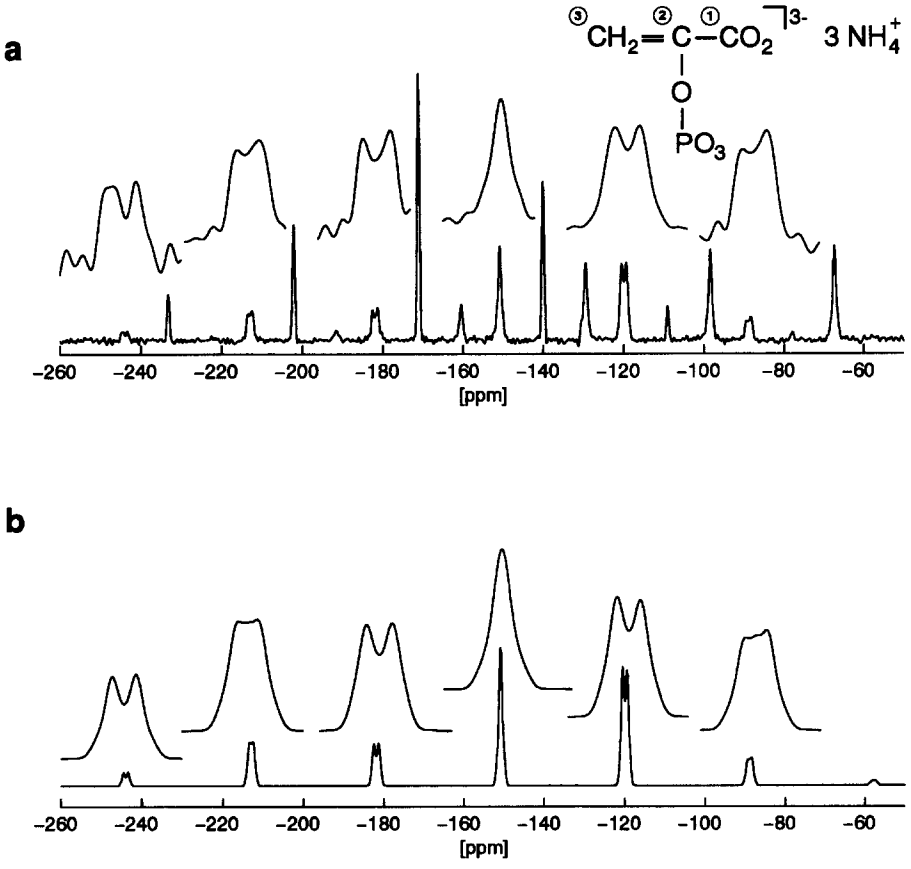

Fig. 5. Experimental (a) and best-fit simulated (b) ^{13}C (S_1) R^3 spectra with $n = 1$ ^{31}P (S_2) recoupling of trisammonium phosphoenol pyruvate, $(NH_4)_3PEP$; only the simulation for $^{13}C2$ is shown, the lineshapes of $^{13}C1$ and $^{13}C3$ are not significantly affected.[21]

best-fit simulated spectra. A $^{31}P-^{13}C2$ internuclear distance of 267 pm ($b_{12}/2\pi = 645$ Hz) in the PEP moiety is sufficient to permit accurate determination of the orientation of the ^{31}P and $^{13}C2$ chemical shielding tensors in the molecular frame. The internuclear $^{31}P-^{13}C1$, $^{31}P-^{13}C3$ distances in the PEP moiety are too large to yield sufficiently characteristic R^3 ^{13}C spectral lineshapes for meaningful analysis. The resulting ^{31}P and $^{13}C2$ chemical shielding tensor orientations in the PEP moiety of $(NH_4)_3PEP$ are shown in Fig. 6.

R^3 experiments are not by definition restricted to isolated heteronuclear spin pairs and can be extended to larger isolated spin systems. Evaluation of the

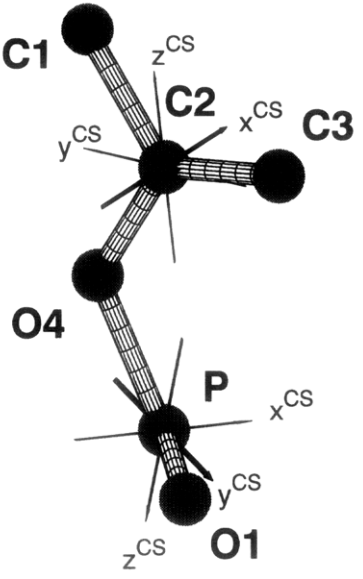

Fig. 6. The orientation of the ^{31}P and $^{13}C2$ chemical shielding tensors in the PEP moiety of $(NH_4)_3PEP$ as derived from experimental ^{13}C NMR data (see Fig. 5).[21]

experimental data then requires *n*-spin system numerical simulations; certain (computational) limits arise from this requirement. Take, for instance, a three-spin system $S_1(S_2)_2$ for which, in principle, the complete geometry of the corresponding molecular fragment could be determined from fully analysing a single R^3 experiment. A recent example of a three-spin system $S_1(S_2)_2$ investigated by means of R^3 experiments is the $^{113}Cd(^{31}P)_2$ spin system in a Cd(II)–phosphane complex $Cd(NO_3)_2 \cdot 2PMe_2Ph$.[22] This $^{113}Cd(^{31}P)_2$ spin system has less common properties, as neither homonuclear $J(^{31}P,^{31}P)$ nor heteronuclear $J(^{113}Cd,^{31}P)$ coupling can be neglected. In particular, $^1J_{iso}(^{113}Cd,^{31}P) = 2285$ Hz is sizeable and of a similar order of magnitude to typical MAS frequencies. Figure 7 displays ^{113}Cd MAS NMR spectra of $Cd(NO_3)_2 \cdot Me_2Ph$. For this particular $^{113}Cd(^{31}P)_2$ spin system it turns out that determination of the geometry of the P—Cd—P moiety from ^{113}Cd–^{31}P R^3 experiments is not possible: the anisotropy of the heteronuclear ^{113}Cd–^{31}P *J*-coupling is such that the corresponding heteronuclear dipolar coupling is essentially cancelled.[22] Anisotropy of heteronuclear *J*-coupling will not often have such a striking effect as for the $^{113}Cd(^{31}P)_2$ spin system shown here, but even 'milder' forms of anisotropic *J* coupling will invariably result in incorrectly determined internuclear distances from *any* heteronuclear dipolar-recoupling experiments if not taken into account properly. Nonvanishing, or rather nonnegligible *J*-coupling effects are most likely to occur for spin systems

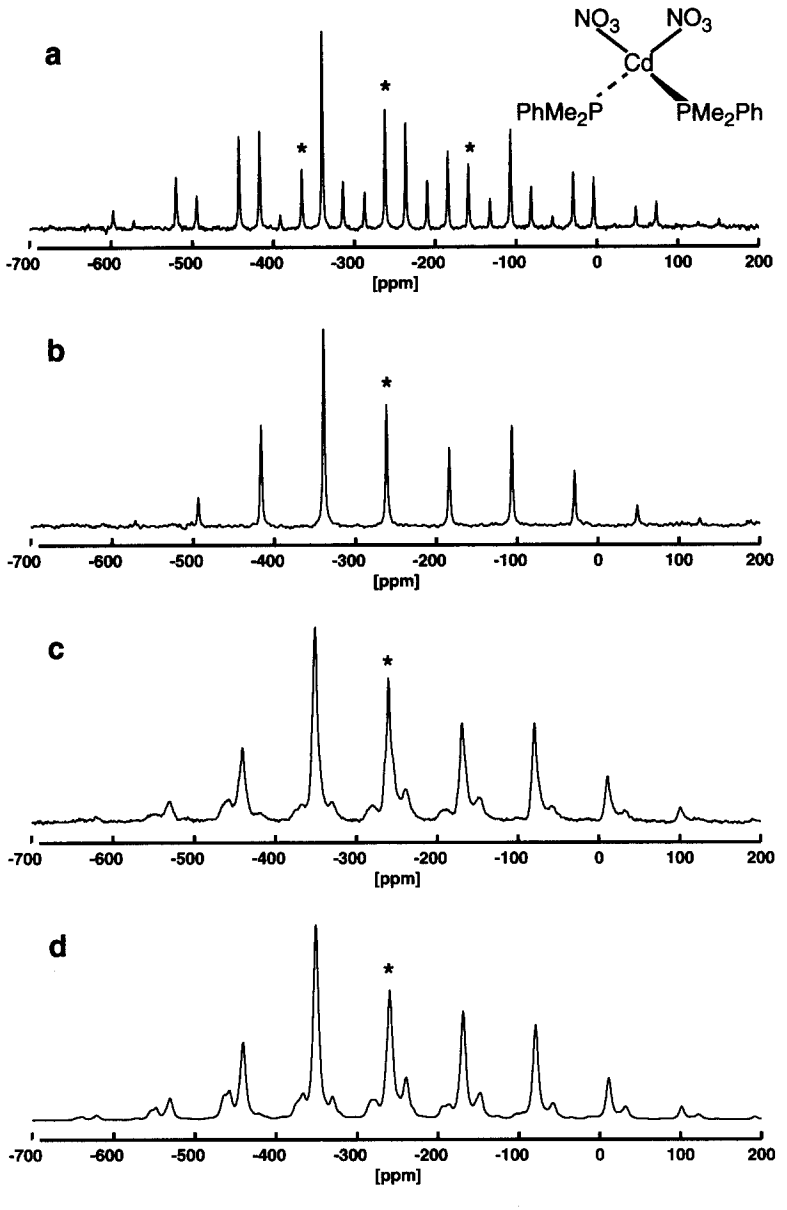

Fig. 7. ^{113}Cd MAS NMR spectra of $Cd(NO_3)_2 \cdot 2PMe_2Ph$; * marks centre bands. (a) Conventional ^{113}Cd MAS spectrum, note splittings due to $^1J(^{113}Cd,^{31}P)$. (b) ^{113}Cd MAS spectrum with simultaneous ^{1}H and ^{31}P high-power decoupling. (c) ^{113}Cd (S_1) MAS spectrum with simultaneous ^{1}H high-power decoupling and ^{31}P (S_2) $n = 1$ R^3 recoupling. (d) Best-fit simulated spectrum corresponding to (c).[22]

involving heavy elements and spin pairs in directly chemically bonded sites in nonorganic chemicals. For the vast majority of applications of heteronuclear dipolar-recoupling experiments (using less heavy isotopes, and inspecting non-directly bonded sites), neither isotropic nor anisotropic J-coupling will probably be of much concern. Viewing anisotropy of heteronuclear J-coupling from a slightly different angle and placing this otherwise evasive quantity at the centre of attention, R^3 experiments offer one of the few possibilities to determine this NMR interaction tensor experimentally.

Finally, the SPECIFIC CP (spectrally induced filtering in combination with CP) experiment recently introduced by Baldus *et al.*[26] can be seen as an expansion of R^3 towards selective cross polarization. SPECIFIC applies weak RF fields ω_1^{RF} and ω_2^{RF} at both Larmor frequencies of a heteronuclear (S_1, S_2) spin system, leading to chemical shielding-dependent zero-, single- or double-quantum transfer. When neglecting CSA terms, the condition

$$\sqrt{(\omega_{iso}^{CS_1})^2 + (\omega_1^{RF})^2} \pm \sqrt{(\omega_{iso}^{CS_2})^2 + (\omega_2^{RF})^2} = n\omega_r \tag{49}$$

can be determined to establish zero-quantum (ZQ, negative sign) or double-quantum (DQ, positive sign) transfer, respectively.[26] Single-quantum transfer occurs if one of the conditions $\omega_1^{RF} = n\omega_r$ or $\omega_2^{RF} = n\omega_r$ is fulfilled. If one arbitrarily chooses $\omega_{iso}^{CS_2} = 0$, Eq. (49) predicts ZQ or DQ transfer, when the condition $|\omega_{iso}^{CS_1}| = ((n\omega_r \pm \omega_2^{RF})^2 - (\omega_1^{RF})^2)^{1/2}$ is met. This is illustrated by the experimental and numerically simulated SPECIFIC transfer curves in Fig. 8. There are various conceivable applications of SPECIFIC, such as dipolar filtering or combination with homonuclear recoupling techniques, for example in order to determine molecular torsion angles directly.

3.2. Rotational-Echo Double Resonance, REDOR

Rotational-echo double resonance (REDOR)[27] experiments follow another strategy to achieve recoupling of weak heteronuclear dipolar coupling interactions under MAS conditions, quite different from the R^3 approach. REDOR experiments prevent the refocusing of weak heteronuclear dipolar coupling interactions under MAS by applying rotation-synchronized trains of π pulses. Figure 9 depicts some (of many possible) versions of REDOR sequences. The theory of REDOR has been treated extensively in the literature.[5,28–31]

We take an isolated heteronuclear spin pair (S_1, S_2), where S_1 represents the observed nucleus, and rotation-synchronized π pulses are applied at the S_1 and S_2 Larmor frequencies. In the Zeeman interaction frame, the Hamiltonian

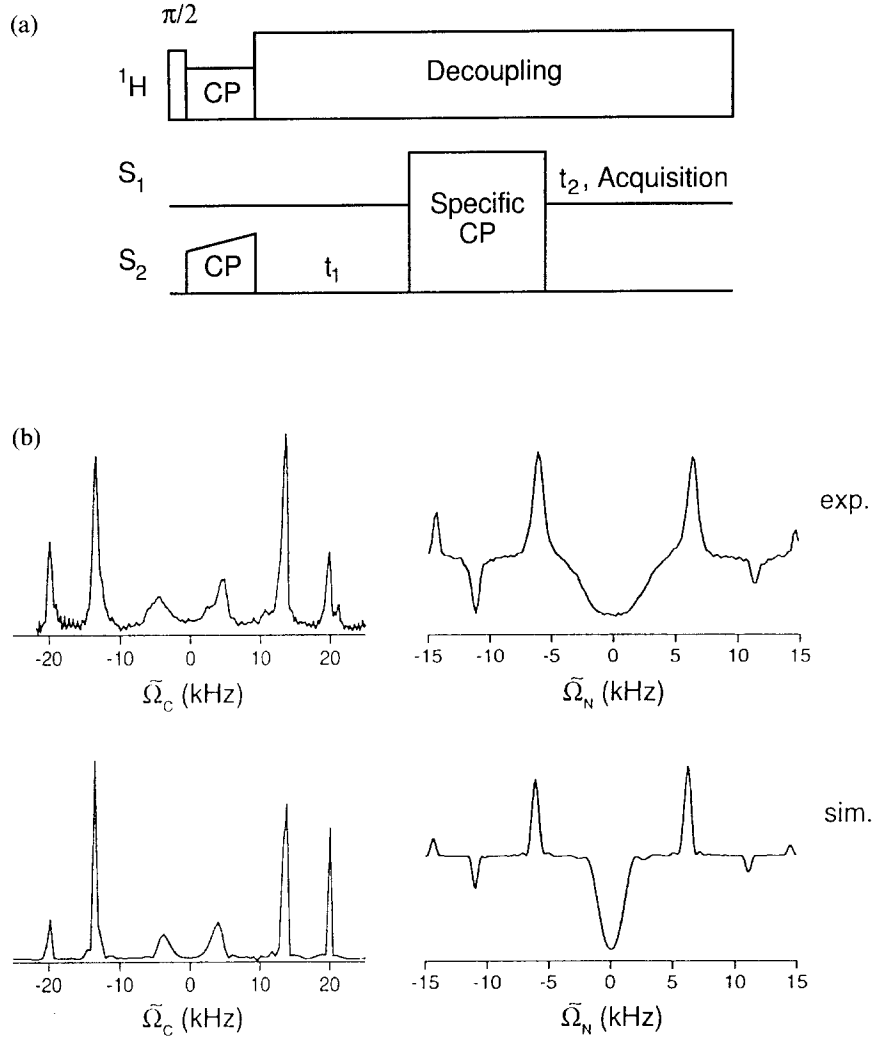

Fig. 8. (a) SPECIFIC[26] pulse sequence for one-dimensional (omitting the t_1 period) and two-dimensional experiments; conditions for the S_1 and S_2 RF fields denoted as 'SPECIFIC CP' are described in the text. (b) Comparison of experimental (upper traces) and simulated (lower traces) ZQ SPECIFIC transfer curves ($n = 1$, $\Omega s_1 = 0$) obtained on a sample of (1-^{15}N-*acetyl*-1,2-^{13}C2)valine. Left, transfer curves for $S_1 = {}^{15}$N; right, transfer curves for $S_1 = {}^{13}$C. (Part (b) reproduced with permission from ref. 26. © 1998 Taylor and Francis.)

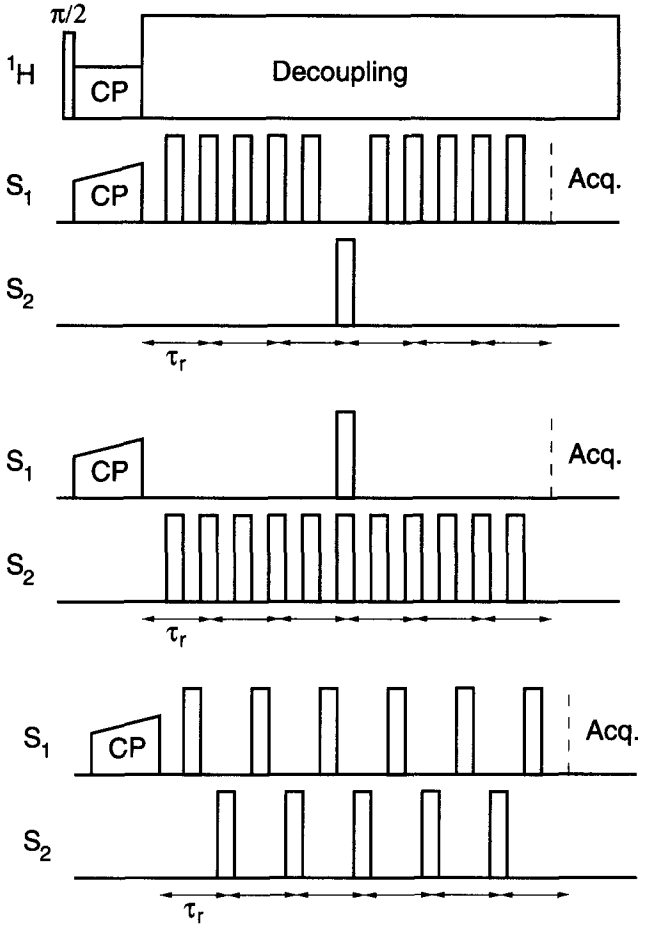

Fig. 9. Some common REDOR sequences[31] where all unspecified S_1, S_2 pulses denote π pulses.

(neglecting J-coupling) is given by

$$H(t) = \omega_1^{CS}(t)S_{1z} + \omega_2^{CS}(t)S_{2z} + \omega_{12}^{D}(t)2S_{1z}S_{2z} + H^{RF}(t) \tag{50}$$

After transformation to a toggling frame defined by the sequence of π pulses and in the limit of δ-shaped π pulses, the Hamiltonian assumes the simple form

$$H_T(t) = \omega_{12}^{D}(t)2S_{1z}S_{2z} \tag{51}$$

with

$$\omega_{12}^{D}(t) = \frac{b_{12}}{2} [\sin^2 \beta_{PR}^{D_{12}} \cos(2(\gamma_{PR}^{D_{12}} + \omega_r t)) - 2\sqrt{2} \sin \beta_{PR}^{D_{12}} \cos \beta_{PR}^{D_{12}} \cos(\gamma_{PR}^{D_{12}} + \omega_r t)] \quad (52)$$

π pulses applied at the S_2 Larmor frequency invert the sign of the dipolar evolution and thus prevent refocusing of the dipolar coupling interaction. The effective dipolar coupling $\bar{\omega}_{12}^{D}$ over one rotation period τ_r for a single crystallite is obtained by summation of the integrals over $\omega_{12}^{D}(t)$. If, for instance, a single S_2 π pulse is applied at $\tau_r/2$, we get

$$\bar{\omega}_{12}^{D} = \frac{1}{\tau_r} \left[\int_0^{\tau_r/2} \omega_{12}^{D}(t)\, dt - \int_{\tau_r/2}^{\tau_r} \omega_{12}^{D}(t)\, dt \right] \quad (53)$$

$$= \frac{2\sqrt{2}}{\pi} b_{12} \sin \beta_{PR}^{D_{12}} \cos \beta_{PR}^{D_{12}} \sin \gamma_{PR}^{D_{12}} \quad (54)$$

The so-called dephasing angle $\Delta\Phi$ depends linearly on the number n of rotation periods over which the π pulses are applied and after n rotation periods is given by

$$\Delta\Phi_n = 4\sqrt{2}\lambda_n \sin \beta_{PR}^{D_{12}} \cos \beta_{PR}^{D_{12}} \sin \gamma_{PR}^{D_{12}} \quad (55)$$

with the dimensionless parameter $\lambda_n = n b_{12} \tau_r/(2\pi)$. The normalized REDOR signal $S(t)$ is finally obtained after averaging over all crystallite orientations as

$$S(t) = \frac{S_R}{S_0} = \frac{1}{4\pi} \int_0^{2\pi} \int_0^{\pi} \cos(\Delta\Phi_n) \sin \beta_{PR}^{D_{12}}\, d\beta_{PR}^{D_{12}}\, d\gamma_{PR}^{D_{12}} \quad (56)$$

where S_R denotes the signal amplitude of S_1 in the presence of S_2-dephasing π pulses, and S_0 is the full S_1-echo amplitude in the absence of S_2 π pulses. For increasing numbers of rotation periods $S(t)$ approaches zero. Plots of $S(t)$ as a function of λ_n are the well-known REDOR dephasing curves, which are unambiguously determined by b_{12} and the applied pulse sequence. In practice, b_{12} is extracted numerically from experimental REDOR dephasing curves.

The REDOR approach has become very popular for determining internuclear distances S_1–S_2, and REDOR applications (usually employing the most common REDOR sequences (see Fig. 9) with xy-8 or xy-4 phase cycling[31]) covering wide ranges of 'chemistry' and combinations of spin-1/2

isotopes have been reported. An impression of the enormous diversity of circumstances in which REDOR experiments are currently being used may be gained from the summary in Table 1.

Practical requirements for obtaining reliable and accurate internuclear distances from REDOR experiments on isolated (S_1, S_2) spin pairs have been investigated systematically for ^{13}C (S_1)–^{15}N (S_2) spin pairs in some specifically labelled crystalline peptide samples, covering a range of internuclear ^{13}C–^{15}N internuclear distances of ~320 pm to 560 pm.[47–49] Minimization of ω_2^{RF} inhomogeneity by restriction of the sample volume and π-pulse durations not exceeding 10% of the rotation period are recommended.[48] The use of undiluted selectively ^{13}C,^{15}N-labelled samples tends to systematically underestimate target ^{13}C–^{15}N internuclear distances by up to 10%.[47,49] While excessive dilution of the labelled sample is undesirable owing to the negative side-effects of a poor signal-

Table 1. Recent REDOR applications; S_1 denotes observed spin(s)

S_1	S_2	Systems investigated/problems addressed	ref.
^{19}F	^{113}Cd	Fluoride disorder in inorganic oxyfluorides; e.g. $CdWO_3F_2$	32
^{19}F, ^{31}P	^{31}P, ^{19}F	Fluoridation of hydroxyapatite	33
^{29}Si	^{19}F	Location of fluoride anion in silicate-framework structure; octadecasil	34
^{31}P	^{113}Cd	Crystalline and amorphous forms of Cd-phosphide, Cd_3P_2	35
^{13}C, ^{19}F	^{19}F, ^{13}C	Residue location in protein; tryptophan synthase	36
^{13}C	^{19}F	Interface of heterogeneous polymer blend; polycarbonate–polyfluorostyrene	37
^{13}C	^{19}F	Molecular structure and packing; benzyl ether dendrimers	38
^{15}N	^{19}F	Amorphous regions in HF-doped polyaniline powders	39
^{13}C, ^{15}N	^{15}N, ^{13}C	Antiplasticizer in cross-linked epoxy resins	40
^{13}C	^{15}N	Structure of silk fibroin	41
^{13}C	^{15}N	Structure of spider dragline silk	42
^{13}C, ^{15}N	^{15}N, ^{13}C	Incorporation of catecholamine in insect cuticle	43
^{13}C	^{15}N	Molecular conformation of acetyl-L-carnitine	44
^{15}N	^{13}C	Peptide conformation; pheromone	45
^{15}N	^{13}C	Mixture of cyclic peptides	46
^{13}C, ^{15}N	^{15}N, ^{13}C	Molecular structure of tripeptide; *N*-acetyl-Pro-Gly-Phe	47,48
^{13}C	^{15}N	Molecular structure of pentapeptide; Tyr-Gly-Gly-Phe-Leu	49
^{15}N	^{31}P	Binding of guanosine diphosphate in 43 kDa bacterial protein; elongation factor T_u	50
^{31}P	^{19}F	Binding sites in 46 kDa enzyme; EPSP	51
^{13}C	^{31}P	Detection of transient intermediates in enzyme reactions	52,53

to-noise ratio on the accuracy of the experimental REDOR data, a protocol employing successive milder forms of dilution experiments, followed by extrapolation to infinite dilution, appears more promising.[49] Satisfactory isolation of the (S_1, S_2) spin pairs from surrounding ^{1}H spins, where applicable, by means of ^{1}H decoupling is crucial for the success of REDOR experiments in the majority of applications. Application of improved ^{1}H decoupling schemes such as TPPM[54] instead of ^{1}H CW decoupling has been shown to improve the practical performance of REDOR experiments.[55] Where desirable for reasons of spectral resolution, the TOSS sequence (total suppression of spinning sidebands[56]) may be incorporated as an accessory in REDOR experiments.[57,58] Two-dimensional HETCOR experiments providing heteronuclear S_1, S_2 chemical shielding correlations are an important tool for purposes of spectral assignment. Among other $S_2 \rightarrow S_1$ polarization transfer schemes,[59,60] REDOR sequences are suitable building blocks for establishing heteronuclear dipolar recoupling in, e.g., 2D ^{13}C–^{15}N HETCOR experiments.[61,62]

The time-domain FID and the frequency-domain spectrum of any NMR experiment contain identical information. Still, it is almost always the spectrum that is evaluated to retrieve this information, as the frequency domain is more directly related to the properties and the dynamics of the spin system. In analogy, it would be advantageous to transform the time-domain REDOR curve $S(t)$ to the frequency domain in such a manner that a peak is produced at the frequency b_{12} of the S_1–S_2 dipolar coupling. In the presence of more than one spin pair, this would be even more preferable, as it would allow for easy extraction of multiple dipolar coupling constants by simple inspection of the 'dipolar spectrum' $S(b_{ij})$. The linearity of the transform will be assured by the fact that multiple dipolar couplings b_{ij} will contribute additively to the REDOR signal, as long as the individual spin pairs are well separated from each other. It is important to note here that *homonuclear* dipolar coupling between different spin pairs is not readily averaged by MAS for cases where a homonuclear rotational resonance (R^2) condition ($\omega_{\mathrm{iso}}^{\Delta} = n\omega_{\mathrm{r}}$, $n = 1, 2, \ldots$) is fulfilled (or nearly so; see Section 4.1). It will usually be possible to avoid such homonuclear $n = 1, 2$ R^2 conditions for cases of large homonuclear isotropic shielding differences $\omega_{\mathrm{iso}}^{\Delta}$. For $\omega_{\mathrm{iso}}^{\Delta} \simeq 0$, however, $n = 0$ or $n \simeq 0$ R^2 conditions may severely violate the validity of this 'linearity assumption'.

Inspection of Eq. (56) immediately shows that Fourier transformation is not suitable to produce the 'dipolar spectrum' $S(b_{ij})$ from $S(t)$, as the time-domain signal is not oscillating harmonically with the frequency of the dipolar coupling. Vogt *et al.*[63] have shown that application of the so-called REDOR asymptotic rescaling (REDOR-AR) permits use of Fourier transformation to generate $S(b_{ij})$ from the asymptotic form of $S(t)$ for $t \rightarrow \infty$, which they calculated as

$$S_{\mathrm{a}}(t) = \frac{\sin(\sqrt{2}b_{12}t/\pi)}{2\sqrt{2}b_{12}t/\pi} \tag{57}$$

This asymptotic form then requires multiplication by time and a subsequent phase shift of $\pi/2$ to generate $S(b_{ij})$ by Fourier transformation. REDOR-AR thus allows fast numerical calculation of $S(b_{ij})$ for the price of using an asymptotic form of $S(t)$ that is strictly valid only for $t = \infty$.

Fourier transformation cannot be applied for transformation of the *general* form of the time-domain signal. Instead, a kernel $K(b_{ij}, t)$ for the Fredholm integral equation of the first kind[64,65]

$$S(t) = \int_{\omega_1}^{\omega_2} K(b_{12}, t) S(b_{12})\, \mathrm{d}\omega \tag{58}$$

has to be found in order to calculate the 'dipolar spectrum' $S(b_{ij})$ according to

$$S(b_{12}) = \int_{t_1}^{t_2} K^{-1}(b_{12}, t) S(t)\, \mathrm{d}t \tag{59}$$

provided the analytical inverse of the kernel $K^{-1}(b_{12}, t)$ is known. Mueller and co-workers[64,65] have found an analytical inverse kernel for REDOR transform given by

$$\begin{aligned} K^{-1}(b_{12}, t) = \frac{b_{12}^2 t^2}{2\pi^2} & \left[J_{-3/4}\left(\frac{b_{12}t}{\sqrt{2}\pi}\right) J_{1/4}\left(\frac{b_{12}t}{\sqrt{2}\pi}\right) - J_{-5/4}\left(\frac{b_{12}t}{\sqrt{2}\pi}\right) J_{-1/4}\left(\frac{b_{12}t}{\sqrt{2}\pi}\right) \right. \\ & \left. + J_{-1/4}\left(\frac{b_{12}t}{\sqrt{2}\pi}\right) J_{3/4}\left(\frac{b_{12}t}{\sqrt{2}\pi}\right) + J_{1/4}\left(\frac{b_{12}t}{\sqrt{2}\pi}\right) J_{5/4}\left(\frac{b_{12}t}{\sqrt{2}\pi}\right) \right] \\ & + \frac{b_{12}t}{\sqrt{2}\pi} \left[\left(J_{1/4}\left(\frac{b_{12}t}{\sqrt{2}\pi}\right) \right)^2 - \left(J_{-1/4}\left(\frac{b_{12}t}{\sqrt{2}\pi}\right) \right)^2 \right] \end{aligned} \tag{60}$$

where the $J_\nu(x)$ are Bessel functions of the first kind.

Owing to the large number of noninteger Bessel functions in Eq. (60), the actual numerical calculation of Eq. (59) is slow. Using identical numbers of points and time increments, this problem may be reduced by calculating the inverse kernel once and storing it for subsequent use. There is, however, a second drawback of the analytical transform method – its instability to experimental noise. It can be shown[63] that very small perturbations $\varepsilon(t)$ added to Eq. (58) lead to a large number of unrelated (and physically meaningless) solutions.

Vogt *et al.* have therefore made use of Tikhonov regularization[63] to handle both of the problems of the analytical transform method, i.e. instability to

experimental noise and the need to apply the numerically cumbersome inverse kernel $K^{-1}(b_{12}, t)$. The Tikhonov method in general selects the simplest member of a set of solutions, in the present case represented by the number of solutions of Eq. (58) in the presence of noise. Application of Tikhonov regularization is therefore equivalent to the assumption that the simplest is also the physical solution.

The basic principle of the method is to minimize the function

$$\Psi(\lambda) = \sum_{j=1}^{n} \frac{1}{\sigma_j} \left\| f_k + \varepsilon_k - \sum_{k=1}^{n} K_{kj} F_j \right\|_2 + \lambda \, || \, DF_j \, ||_2 \tag{61}$$

where

$$f_k = \sum_{k=1}^{n} K_{kj} F_j \tag{62}$$

is the discrete version of Eq. (58) with n points of data, ε_k represents experimental noise, D is the second derivative operator, and the σ_j are determined by the noise model, which has to be chosen together with the regularization operator λ for successful application of the method. Note that Eq. (61) makes use of the kernel itself instead of its inverse, and it does not involve direct transformation of the time-domain data to a frequency-domain spectrum, but uses numerical minimization.

d'Espinose de la Caillerie and Fretigny[66] have chosen an approach similar to REDOR-AR in which they use an asymptotic expansion of the inverse kernel[67] instead of the time signal. They find best overall agreement between the exact inverse kernel and the first two terms of the expansion

$$K^{-1}(b_{12}, t) \simeq \frac{8 b_{12} t}{\pi^2} \sin(\sqrt{2} b_{12} t/\pi) - \frac{3}{2\sqrt{2}\pi^2} \cos(\sqrt{2} b_{12} t/\pi) \tag{63}$$

This again allows application of Fourier transformation, as insertion of Eq. (63) into Eq. (59) yields

$$S(b_{12}) \simeq -4 b_{12} \frac{\partial}{\partial b_{12}} C[S(t)] - \tfrac{3}{2} C[S(t)] \tag{64}$$

where $C[S(t)]$ represents the cosine transform.

All REDOR transform methods require well-separated spin pairs, but fail for systems where one spin S_1 of a certain spin species is coupled to n spins S_i of another species. The pulse sequences in Fig. 10 represent conventional REDOR

experiments if the pulse angle $\theta = \pi$. Gullion and Pennington[68] have suggested applying a pulse angle θ smaller than π (θ-REDOR) for systems where one spin S_1 is coupled to multiple spins S_i. Taking the top pulse sequence of Fig. 10 as an example, this has the following consequence for the dipolar dephasing of spin S_1. The contribution to the dephasing of spin S_1 from a spin S_i during the first half of the evolution period will be reversed during the second half if spin S_i does not change its spin state during the θ pulse and if contributions from the homonuclear coupling between the S_i spins can be neglected. The probability for the spin state to change during a θ pulse is given by[7]

$$p(\theta) = \tfrac{1}{2}(1 - \cos\theta) \tag{65}$$

which is a small value for small angles θ. Accordingly, on average, no more than one spin S_i will contribute to the dephasing of spin S_1 when a sufficiently small

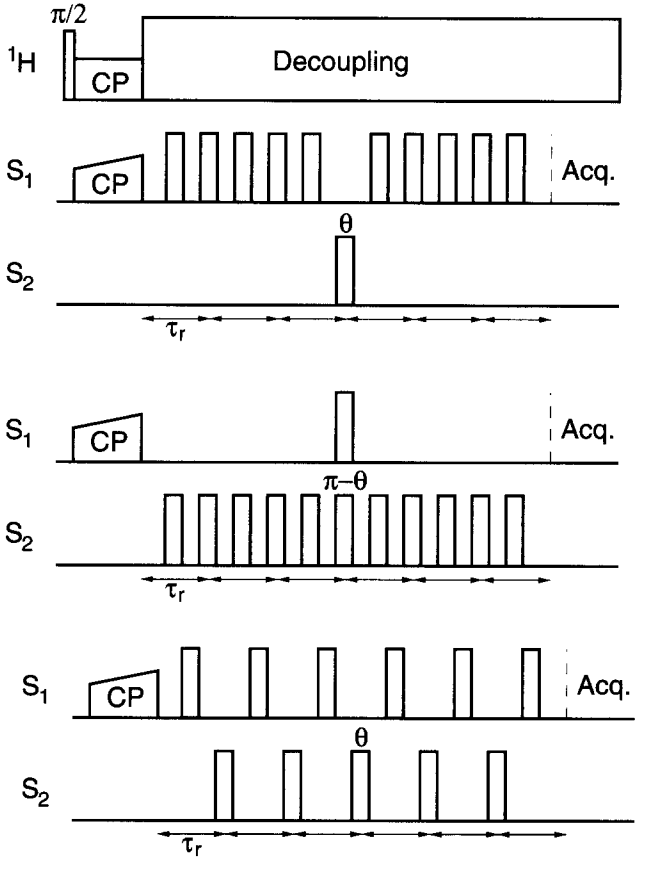

Fig. 10. Some θ-REDOR sequences[68] where all unspecified S_1, S_2 pulses denote π pulses.

pulse angle θ is applied. However, if θ is chosen too small, practically no spins S_i will contribute to the dephasing of S_1. As a compromise, Gullion and Pennington suggest $\theta = 40°$. The implications for a system composed of, for instance, four spins S_i coupled to one spin S_1 are that for 61% of all spin systems none of the S_i spins will contribute to the dephasing; for 32% it will be one spin S_i; for 6% two spins S_i; and for 1% three spins S_i.[68] Assuming that only S_1-S_i pairs contribute to the dephasing, and taking account of the portion of spin systems not contributing to the dephasing at all, one can then apply REDOR transform methods to extract the individual S_1-S_i dipolar coupling constants.

The basic principle of θ-REDOR can also be directly utilized for purposes of spin counting, as the dephasing of spin S_1 as a function of the flip angle θ depends on the number of spins S_i coupled to S_1. Cull *et al.*[69] have recently followed this approach to determine the number of ^{13}C (S_i) spins coupled to ^{15}N (S_1) in multiply ^{13}C-labelled DL-alanine and the number of ^{15}N (S_i) spins coupled to ^{13}C (S_1) in U-^{13}C,^{15}N-labelled urea.

The FDR (frequency-selective dipolar recoupling) experiment[70,71] utilizes a pulse sequence (Fig. 11a) similar to the REDOR sequence. The major difference is that $\pi/2$ pulses are applied at the Larmor frequency of the nonobserved spin S_2 instead of π pulses as applied in REDOR. In the FDR experiment, dipolar dephasing of the S_1 spin depends on the chemical shielding of the S_2 spin, as will be shown. Using AHT, Bennett *et al.*[71] have calculated the evolution of the magnetization of the S_1 spin under the influence of the pulse sequence depicted in Fig. 11a as

$$S(t) = \frac{(\omega_{\text{iso}}^{\text{CS}_2})^2}{(\omega_{\text{iso}}^{\text{CS}_2})^2 + (\bar{\omega}_{12}^{\text{D}})^2} + \frac{(\bar{\omega}_{12}^{\text{D}})^2}{(\omega_{\text{iso}}^{\text{CS}_2})^2 + (\bar{\omega}_{12}^{\text{D}})^2} \cos\left(\sqrt{\tfrac{1}{2}((\omega_{\text{iso}}^{\text{CS}_2})^2 + (\bar{\omega}_{12}^{\text{D}})^2)}t\right) \quad (66)$$

which is valid for synchronous sampling at $t = 2n\tau_{\text{r}}$ and where $\bar{\omega}_{12}^{\text{D}}$ denotes the effective dipolar coupling constant

$$\bar{\omega}_{12}^{\text{D}} = \frac{\sqrt{2}b_{12}}{\pi} \sin(2\beta_{\text{PR}}^{\text{D}_{12}}) \sin(\gamma_{\text{PR}}^{\text{D}_{12}}) \quad (67)$$

At exact resonance, where $\omega_{\text{iso}}^{\text{CS}_2} = 0$, Eq. (66) becomes

$$S(t) = \cos\left(\frac{\bar{\omega}_{12}^{\text{D}}t}{\sqrt{2}}\right) \quad (68)$$

and for $\omega_{\text{iso}}^{\text{CS}_2} \gg \omega_{12}^{\text{D}}$ one gets $S(t) = 1$. This dependence of the dephasing on the isotropic chemical shielding of the S_2 spin can, for example, be utilized to reduce multiple-spin effects in systems composed of more than two spins by

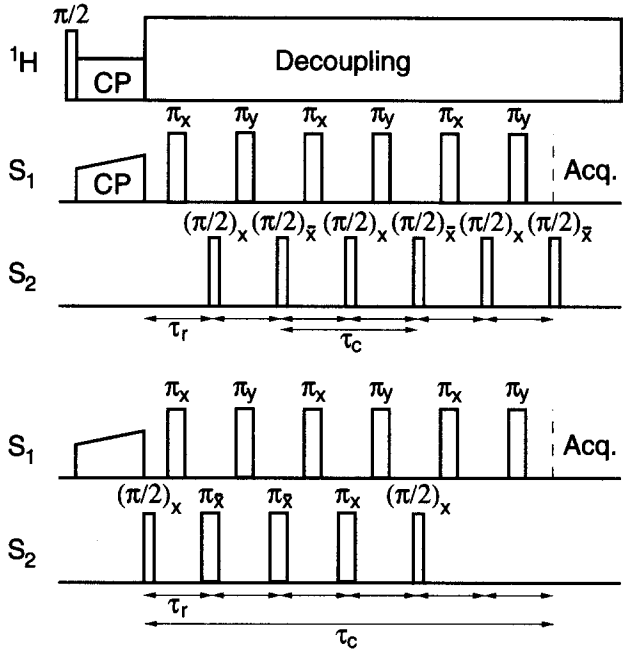

Fig. 11. FDR[70,71] pulse sequences; top, the basic sequence; bottom, a better-compensated FDR version.

suitable adjustment of the transmitter offset. The sensitivity of the pulse sequence in Fig. 11 (top) to experimental imperfections can be circumvented by the better-compensated pulse sequence in Fig. 11 (bottom), for the price of a slightly smaller effective dipolar coupling constant $(2/3)\bar{\omega}_{12}^{\mathrm{D}}$ compared to $(1/\sqrt{2})\bar{\omega}_{12}^{\mathrm{D}}$ for the less-compensated sequence.[71]

4. THE HOMONUCLEAR DIPOLAR INTERACTION

For the following section, dealing with dipolar recoupling experiments on homonuclear spin systems, we will use an isolated pair of 1/2 spins (S_1, S_2), for general purposes of illustration. The Hamiltonian of such a spin pair is derived from Eq. (1) as

$$H(t) = \omega_1^{\mathrm{CS}}(t)S_{1z} + \omega_2^{\mathrm{CS}}(t)S_{2z} + \omega_{12}^{\mathrm{D}}(t)[2S_{1z}S_{2z} - \tfrac{1}{2}(S_{1+}S_{2-} + S_{1-}S_{2+})]$$
$$+ \omega_{12}^{J}[S_{1z}S_{2z} + \tfrac{1}{2}(S_{1+}S_{2-} + S_{1-}S_{2+})] + H^{\mathrm{RF}}(t) \qquad (69)$$

or, with the use of fictitious spin-1/2 operators,

$$H(t) = \omega_\Sigma(t)S_z^{14} + \omega_\Delta(t)S_z^{23} + \omega_A(t)(S_z^{12} - S_z^{34}) + \omega_B(t)S_x^{23} + H^{RF}(t) \quad (70)$$

Other than for heteronuclear spin pairs, the Hamiltonian of a homonuclear spin pair is in general homogeneous in the sense of Maricq and Waugh.[15] $H(t)$ does not commute with itself at different times t', t'' ($[H(t'), H(t'')] \neq 0$) and MAS does not readily average out the effects of homonuclear dipolar coupling.

There is no single, clear-cut criterion for subdividing the numerous existing homonuclear dipolar recoupling approaches into subgroups or 'families'. Criteria such as similarities or equalities of the lowest-order average Hamiltonians appropriate to describe the different pulse experiments, excitation of zero-quantum versus double-quantum coherences, or laboratory-frame versus rotating-frame experiments, lead to quite different subgroups and stress different relationships among the various homonuclear dipolar recoupling approaches. Somewhat arbitrarily, we have chosen to follow a 'zero-quantum versus double-quantum coherences' approach as a rough pattern for a topic that essentially resists such simple, single-criterion classifications.

4.1. Rotational Resonance, R^2

At the rotational resonance (R^2) conditions, where $\omega_{iso}^{\Delta} = n\omega_r$, the homonuclear dipolar interaction is reintroduced to the MAS experiment without the necessity to apply additional RF irradiation to the spin system. It is not surprising that this very direct access to structural information has been analysed in great detail in the literature.[5,12,72–74] We will, therefore, not discuss the theory of the basic R^2 experiment in any detail here, but rather continue the approach of only sketching a very brief, lowest-order AHT description for general purposes of illustration.

Neglecting CSA and J-coupling, the homonuclear two-spin Hamiltonian (Eq. (69)) becomes

$$H(t) = \omega_{iso}^{CS_1} S_{1z} + \omega_{iso}^{CS_2} S_{2z} + \omega_{12}^{D}(t)[2S_{1z}S_{2z} - \tfrac{1}{2}(S_{1+}S_{2-} + S_{1-}S_{2+})] \quad (71)$$

When switching to a rotating frame defined by

$$U_R = \exp(i(\omega_{iso}^{CS_1} S_{1z} + \omega_{iso}^{CS_2} S_{2z})t) \quad (72)$$

to remove the isotropic chemical shielding terms, the rotating-frame Hamiltonian becomes

$$H_R(t) = \omega_{12}^{D}(t)\{2S_{1z}S_{2z} - \tfrac{1}{2}(S_{1+}S_{2-} \exp(-i\omega_{iso}^{\Delta}t) + S_{1-}S_{2+} \exp(i\omega_{iso}^{\Delta}t))\} \quad (73)$$

which, averaged over one rotation period, results in the lowest-order average Hamiltonian

$$\bar{H}_{\mathrm{R}}^{0} = -\tfrac{1}{2}\{\omega_{\mathrm{D}_{12}}^{(n)} S_{1+} S_{2-} + \omega_{\mathrm{D}_{12}}^{(-n)} S_{1-} S_{2+}\} \tag{74}$$

if the R^2 condition is fulfilled and $n = \pm 1, \pm 2$. We have pointed out already that this description gives only a rough picture of the R^2 phenomenon and fails to explain some important features of the experiment, such as the occurrence of higher-order recoupling conditions ($n > 2$), the dependence of the R^2 lineshapes on magnitudes and orientations of the chemical shielding tensor interactions, and the $n = 0$ R^2 condition, which leads to dipolar recoupling at virtually all MAS frequencies for spin pairs with identical isotropic chemical shielding but differing orientations of the two chemical shielding tensors. By now, there are basically two well-established ways to retrieve information from the R^2 phenomenon: iterative lineshape fitting, or monitoring longitudinal magnetization exchange as a function of mixing time τ_{m} after selective inversion of one of the two resonances initially[75] (see Fig. 12).

The $n = 0$ R^2 condition is a rather special case with few experimental limitations, with spectral lineshapes sensitive to orientational parameters and to interactions of relatively small magnitudes. $n = 0$ R^2 lineshapes are equally suitable for determining internuclear distances or spin parameters (or both) by lineshape simulations. Spin parameters may include homonuclear J-coupling constants, even of small magnitude, where the absolute sign of the J-coupling constant can be determined from $n = 0$ R^2 lineshape simulations.[76,77] $n = 0$ R^2 lineshapes usually are highly sensitive to CSA orientations and thus offer a route to determining chemical shielding tensor orientations in the molecular frame, but will leave an assignment ambiguity for reasons of symmetry.[77] Spatially isolated homonuclear spin pairs fulfilling the $n = 0$ R^2 condition occur for different isotopes in many different chemical environments. Such (S_1, S_2) spin pairs range from one extreme, such as the ^{1}H spin pair in $Ba(ClO_3)_2 \cdot H_2O$[78] (where b_{12} is the interaction of largest magnitude and the ^{1}H chemical shielding anisotropy is very small), through pairs of ^{13}C spins in selectively ^{13}C-labelled compounds[79] (where b_{12} and ^{13}C chemical shielding anisotropies have similar magnitudes), to the other extreme of, e.g., ^{31}P spin pairs,[77] where ^{31}P chemical shielding anisotropy is the predominant interaction tensor within the spin pair. However different the relative magnitudes (and orientations) of the various interaction tensors for this range of $n = 0$ R^2 spin pairs may be, all these circumstances yield the complete set of parameters describing the spin pair from numerically exact lineshape simulations. Experimental and best-fit simulated ^{31}P MAS NMR spectra of $Na_4P_2O_7 \cdot 10H_2O$[77] are shown as an example in Fig. 13.

$n = 1, 2, 4$ R^2 conditions for various (S_1, S_2) spin pairs have been considered, predominantly aiming at internuclear distance determinations in organic solids.

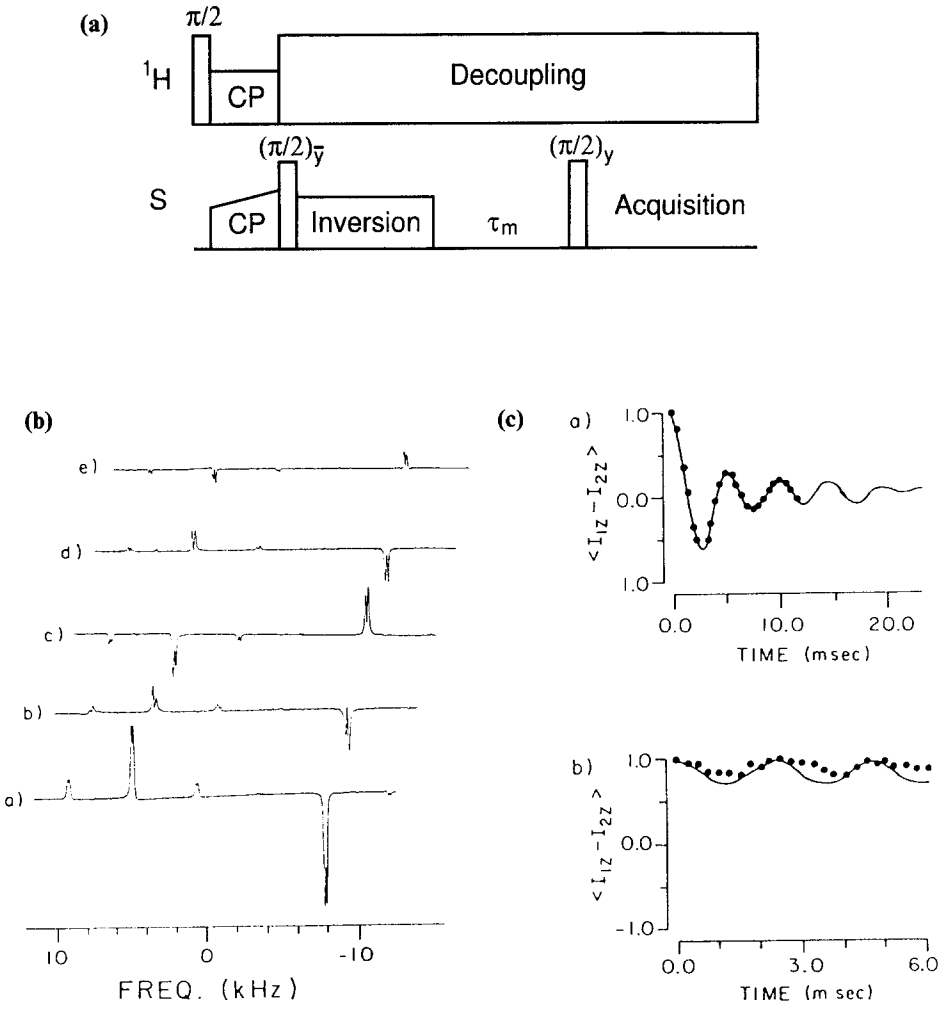

Fig. 12. The R^2 magnetization-exchange experiment.[75] **(a)** R^2 magnetization-exchange pulse sequence; **(b)** $n = 3$ ^{13}C R^2 magnetization-exchange spectra of doubly ^{13}C-labelled zinc acetate at different mixing times τ_m; **(c)** simulated (solid lines) and experimental (·) magnetization-exchange curves on (top) and off (bottom) the R^2 condition. (Parts **(b)** and **(c)** reproduced from ref. 75, © 1988, with permission from Elsevier Science.)

The splitting patterns arising in the centre-band region of $n = 1$ R^2 spectra have been used to estimate $^{15}N-^{15}N$[80] and $^{13}C-^{13}C$[81] internuclear distances from one-dimensional as well as from two-dimensional $^{13}C-^{13}C$ correlation experiments;[82] these one- and two-dimensional approaches have in common that they represent a direct application of the lowest-order AHT results to the

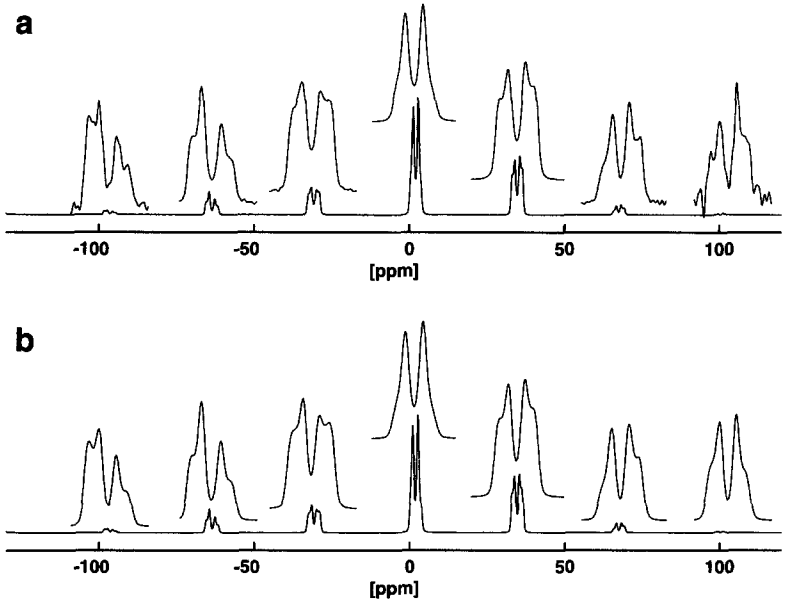

Fig. 13. $n=0$ R^2 ^{31}P MAS NMR spectra of the isolated ^{31}P spin pair in the P_2O_7 moiety of $Na_4P_2O_7 \cdot 10H_2O$. (a) Experimental; (b) best-fit calculated spectrum. $^2J_{iso}(^{31}P,^{31}P) = -19.5$ Hz is well defined from spectral lineshape simulations.[77]

experimental data to extract distance information. Studies of internuclear ^{13}C–^{13}C distances in a variety of organic and biochemically relevant compounds, such as retinals or peptides, using longitudinal magnetization exchange at the $n=1$ R^2 condition (see Fig. 12) have been reported.[83–87] Extraction of internuclear distances from $n=1$ R^2 longitudinal magnetization-exchange curves relies on numerical simulations, with b_{12} and a T_2^{ZQ}-decay constant as adjustable parameters. It has been pointed out[5,87] that accurate determination of internuclear distances from small values of b_{12} is problematic, in particular in the absence of knowledge of T_2^{ZQ}. Recently a method to determine T_2^{ZQ} experimentally has been introduced[88] (see below); precise knowledge of this parameter becomes increasingly important when aiming at the determination of long internuclear distances.

Higher-order, $n=2$[89] and $n=4$[90] R^2 conditions, in conjunction with longitudinal magnetization exchange, have been employed to study conformational properties of biologically relevant molecules. Higher-order ($n>1$) R^2 conditions appear generally less attractive for internuclear distance determination, since chemical shielding tensor orientations are more strongly reflected for $n>1$ than for $n=1$. Hence, $n>1$ R^2 conditions are the preferred choice for study of molecular conformations, based on chemical shielding tensor orientations.

It will often be necessary to eliminate 'non-spin-pair background' from experimental R^2 spectra. Unwanted background resonances may be present for a number of reasons. One may have to work with natural-abundance, dilute S_1, S_2 isotopes and observe the rare (S_1, S_2) spin-pair isotopomers.The target (S_1, S_2) spin pair may be 100% selectively isotopically enriched, but the sample has to be diluted with natural-abundance material for reasons of spatially isolating the (S_1, S_2) spin pairs. Even for a 100% selectively enriched (S_1, S_2) spin-pair sample there may be additional contributions from the nonenriched remainder of the molecule in the spectral region of interest. The latter two circumstances typically arise for ^{13}C spin pairs in organic solids, while the first is more typical for non-^{13}C spin systems. Double-quantum filtration at the $n = 1$ R^2 condition *via* *J*-coupling by the INADEQUATE experiment has been demonstrated for a ^{119}Sn (S_1, S_2) spin pair in an organotin compound with ^{119}Sn in natural abundance (8.58%).[91] Double-quantum *J*-filtering requires a sufficient magnitude of J_{iso} but has the distinct advantage that no further orientation dependence is introduced. A difference-spectroscopy approach to achieving filtering uses the strongly differing zero-quantum relaxation characteristics of coupled spin pairs at the R^2 condition compared to the dynamics of noncoupled spins.[92] Two spectra at the R^2 condition with selective inversion (see Fig. 12) are recorded, one with zero mixing time τ_m, one with a 'long' mixing time τ_m. Only the non-spin-pair magnetization survives the latter condition, and after subtraction the difference spectrum displays only the lineshape of the (S_1, S_2) spin-pair resonances in antiphase. Application of both these filter methods is straightforward for fast spinning conditions. Yet another alternative to achieve filtration is the excitation of double-quantum coherence through dipolar coupling at the R^2 condition[93] (see below).

Anomalous spectral lineshapes in ^{13}C R^2 spectra of organic solids, obtained under conditions of CW ^1H decoupling, have been observed repeatedly. This appearance of additional features in these ^{13}C R^2 spectral lineshapes has recently been explained in terms of differential transverse relaxation, caused by insufficient CW ^1H decoupling performance.[94] According to this explanation, ^1H decoupling-related distortions in ^{13}C R^2 spectral lineshapes are expected to affect mainly the centre-band region of nonprotonated ^{13}C sites and to be more severe at higher external magnetic field strengths and/or MAS frequencies. It has also been shown that application of improved ^1H decoupling schemes, such as TPPM[54] strongly minimizes this problem and leads to ^{13}C R^2 spectral lineshapes suitable for purposes of iterative lineshape fitting, even for experimental spectra obtained at high external magnetic field strengths:[79] in this way all parameters of the four-^{13}C spin system of the maleate moiety in the monoammonium salt of maleic acid have been determined by lineshape fitting of various ^{13}C R^2 spectra. Figure 14 displays an experimental ^{13}C R^2 spectrum of this compound and the corresponding best-fit calculated spectrum. Also shown is a simulated spectrum, assuming 'typical' ^{13}C chemical shielding tensor orientations for this moiety. Even though these 'typical' orientations do not

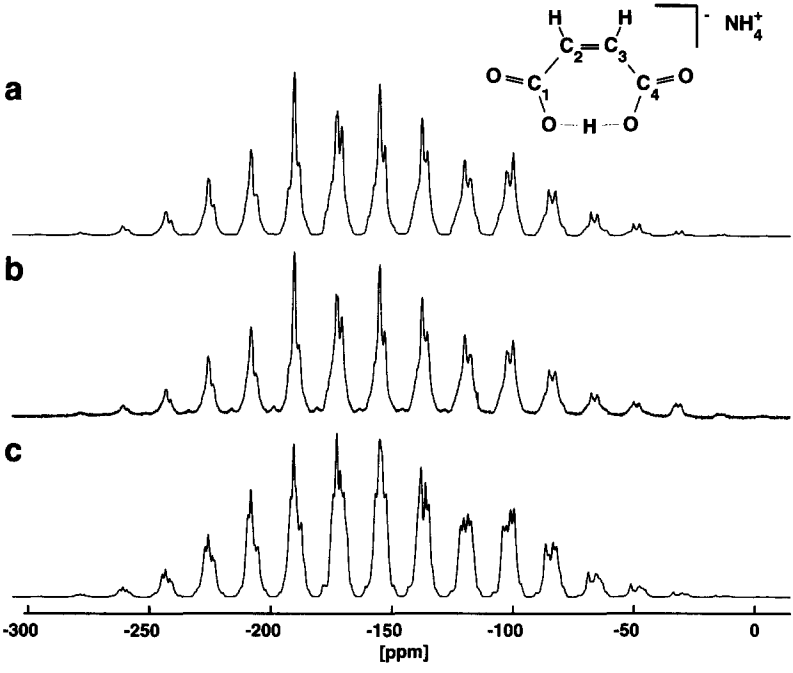

Fig. 14. ^{13}C MAS NMR spectra of U-^{13}C-labelled monoammonium maleate. The experimental spectrum (b) is obtained at a MAS frequency where the $n = 2$ R^2 condition between the $^{13}C{=}O$ and the $^{13}C{=}$ resonances is fulfilled. In (a) the corresponding best-fit simulated spectrum is shown; (c) represents a simulated spectrum assuming 'typical' ^{13}C chemical shielding tensor orientations.[79]

deviate much from the precise orientational parameters, this minor deviation is enough to cause major changes in the lineshapes. Given that high-resolution solid-state NMR experiments are carried out at increasingly higher magnetic field strengths, CSA parameters are bound to play an increasingly important role in the near future. In this sense, Fig. 14 serves as an illustrative example that roughly estimating 'typical' chemical shielding tensor orientations (and using those as fixed input parameters in numerical simulation procedures) may not be good enough when aiming at accurate determination of internuclear distances: in fortunate cases numerical analysis procedures will merely be less sensitive, while in less fortunate cases wrong distance parameters will result.

The APRR (adiabatic polarization transfer under rotational resonance conditions) experiment[95] is essentially an R^2 polarization transfer experiment, with the difference that the spinning rate is not kept constant but is ramped adiabatically through the R^2 condition (Fig. 15). This leads to a more complete transfer and a more broadband resonance condition, rendering the experiment less sensitive to distributions of isotropic chemical shielding in disordered systems.

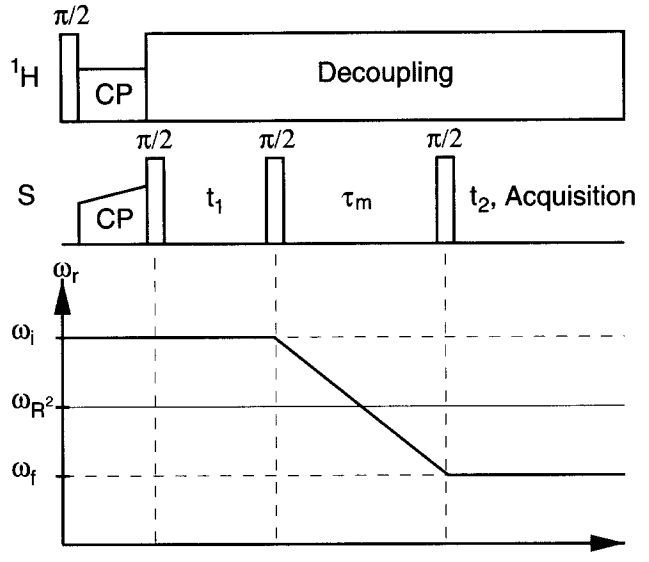

Fig. 15. The APPR pulse sequence[95] where ω_r is adiabatically ramped through the R^2 condition such that the R^2 condition is met at $\tau_m/2$.

As the spinning speed ω_r itself is no longer constant during the course of the APRR experiment, Eq. (8) acquires an additional time dependence and becomes

$$\omega_{l,ij}^{\kappa}(t, T) = \sum_{m=-2}^{2} \omega_{\kappa}^{(m)} \exp(im\omega_r(T)t) \tag{75}$$

Under the assumption that the initial polarization resides on spin S_1, the initial density operator is given by $\rho(0) = S_z^{23} + S_z^{14}$. Because the sum polarization is a constant of the motion, only the 'zero-quantum Hamiltonian'

$$H^{23}(t) = \omega_\Delta(t) S_z^{23} - \omega_B(t) S_x^{23} \tag{76}$$

has to be considered in this context.[13,95]

After transformation to a time-dependent interaction frame defined by

$$U = \exp\left(-i \int_0^t \omega_\Delta(t', T) S_z^{23} \, dt' \right) \tag{77}$$

where $T = \tau/2$ marks the point in time at which the exact R^2 condition is met, and after application of an additional crystallite-orientation-dependent

rotation around the z-axis of the interaction frame, the lowest-order average Hamiltonian becomes[95]

$$\bar{H}^0_{23}(T) = (\omega^{\text{iso}}_{\Delta} - n\omega_r(T))S^{23}_z + \omega^{(n)}_{\text{eff}} S^{23}_x \tag{78}$$

where $\omega^{(n)}_{\text{eff}} = \sum^{2}_{M=-2} \omega^{(M)}_{D_{12}} I_{n-M}$. I_k denotes the intensity of the kth spinning sideband of the chemical-shielding-difference interaction $\omega_{\Delta}(t, T)$. For vanishing CSA ($\omega^{(n)}_{\text{eff}} = \omega^{(n)}_{D_{12}}$) Eq. (78) therefore predicts the recoupling conditions $n = \pm 1, \pm 2$, while in the presence of a sizeable chemical shielding anisotropy higher-order recoupling conditions are also expected.

At $T = \tau/2$ the coefficient $(\omega^{\text{iso}}_{\Delta} - n\omega_r(T))$ passes through zero. If the passage is slow enough to be adiabatic, this causes an inversion of the initial magnetization during the course of the experiment: $\langle S^{23}_z \rangle(\tau) = -\langle S^{23}_z \rangle(0)$. There are two requirements to ensure adiabatic passage. First, the initial Hamiltonian $\bar{H}^0(0)$ has to be approximately parallel with S^{23}_z and, second, the change of the angle between the Hamiltonian and S^{23}_z has to be small compared with the effective field strength $\omega_{\text{eff}} = ((\omega^{\text{iso}}_{\Delta} - n\omega_r(T))^2 + (\omega^{(n)}_{\text{eff}})^2)^{1/2}$. Assuming a linear sweep of the spinning speed ($\omega_r(T) = \omega_r(0) + \lambda T$), this would require $n\lambda \ll (\omega^{(n)}_{\text{eff}})^2$ to achieve adiabatic behaviour. Experimentally, Verel *et al.* found that $n\lambda \cong (\omega^{(n)}_{\text{eff}})^2$ is sufficient to ensure an adiabatic passage and to reach a transfer efficiency of 75% between the two ^{31}P resonances in $[PCl^{+}_{4}][PCl^{-}_{6}]$.[95]

Another strategy to extend the range of spin systems accessible to rotational resonance recoupling is followed by the R2TR (rotational resonance in the tilted rotating frame) experiment.[96,97] It applies a weak RF field during the mixing time of a polarization exchange experiment (see Fig. 16), resulting in new and more easily adjustable resonance conditions. This allows, for example, the investigation of spin systems with isotropic chemical shielding differences

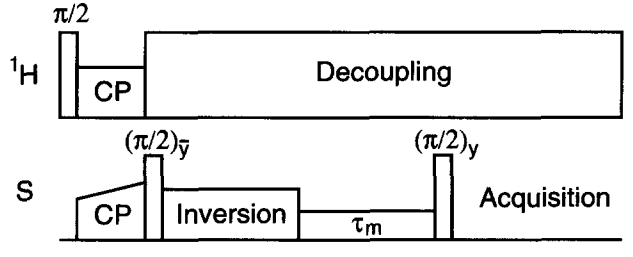

Fig. 16. The basic R2TR pulse sequence[96] where a weak RF field at the S Larmor frequency is applied during τ_m; several one- and two-dimensional versions of the R2TR experiment are feasible.[97]

too small for standard R^2 experiments. Furthermore, because RF fields can be changed in a much more flexible manner than the spinning speed, R2TR may also be extended to perform homonuclear two-dimensional correlation experiments.[97a]

The Hamiltonian of a homonuclear spin pair (Eq. (69)) subjected to an on-resonance RF field defined by the RF Hamiltonian $H^{RF} = \omega^{RF}(S_{1x} + S_{2x})$ and transformed to a doubly tilted frame defined by $U_T = \exp(i(\theta_1 S_{1y} + \theta_2 S_{2y}))$ and $\theta_{1,2} = \tan^{-1}(\omega^{RF}/\omega^{CS}_{1,2})$ is given by

$$\begin{aligned} H_T(t) = {} & \omega^e_1 S_{1z} + \omega^e_2 S_{2z} + \omega^D_{12}(t)[AS_{1z}S_{2z} + B(S_{1+}S_{2-} + S_{1-}S_{2+}) \\ & + R(S_{1z}S_{2+} + S_{1z}S_{2-}) + S(S_{1+}S_{2z} + S_{1-}S_{2z}) \\ & + Q(S_{1+}S_{2+} + S_{1-}S_{2-})] \end{aligned} \tag{79}$$

where the chemical shielding anisotropy has been neglected,

$$\omega^e_{1,2} = \sqrt{(\omega^{RF})^2 + (\omega^{CS_{12}}_{iso})^2} \tag{80}$$

and

$$A = 2\cos\theta_1\cos\theta_2 - \sin\theta_1\sin\theta_2 \tag{81}$$

$$B = -\tfrac{1}{4}(1 + \cos\theta_1\cos\theta_2 - 2\sin\theta_1\sin\theta_2) \tag{82}$$

$$R = -\tfrac{1}{2}(\sin\theta_1\cos\theta_2 + 2\cos\theta_1\sin\theta_2) \tag{83}$$

$$S = -\tfrac{1}{2}(\cos\theta_1\sin\theta_2 + 2\sin\theta_1\cos\theta_2) \tag{84}$$

$$Q = \tfrac{1}{4}(1 - \cos\theta_1\cos\theta_2 + 2\sin\theta_1\sin\theta_2) \tag{85}$$

Switching to the interaction frame defined by $U_I = \exp(i(\omega^e_1 S_{1z} + \omega^e_2 S_{2z})t)$, we get

$$\begin{aligned} H_I(t) = {} & \omega^D_{12}(t)\{AS_{1z}S_{2z} \\ & + B[S_{1+}S_{2-}\exp(-i\Delta t) + S_{1-}S_{2+}\exp(i\Delta t)] \\ & + R[S_{1z}S_{2+}\exp(-i\omega^e_2 t) + S_{1z}S_{2-}\exp(i\omega^e_2 t)] \\ & + S[S_{1+}S_{2z}\exp(-i\omega^e_1 t) + S_{1-}S_{2z}\exp(i\omega^e_1 t)] \\ & + Q[S_{1+}S_{2+}\exp(-i\Sigma t) + S_{1-}S_{2-}\exp(i\Sigma t)]\} \end{aligned} \tag{86}$$

where $\Delta = \omega_1^e - \omega_2^e$ and $\Sigma = \omega_1^e + \omega_2^e$. Note that for $\omega^{RF} = 0$ (where $A = 2$, $B = -1/2$, and $R = S = Q = 0$) this is equivalent to the average Hamiltonian (Eq. (74)) of the conventional R^2 experiment. Calculation of the average Hamiltonian leads only to contributions from those terms for which one of the Fourier frequencies from the Fourier expansion of ω_{12}^D (Eq. (8)) matches with the corresponding frequency in Eq. (86). If, for example, $\Delta = n\omega_r$ ($n = 1, 2$) the 'flip-flop' term is not averaged to zero, which corresponds to the standard R^2 experiment. If $\Sigma = n\omega_r$ the 'flop-flop' term remains, which has no analogue in the conventional R^2 experiment. It can be shown[97a] that the so far neglected CSA interactions are also recoupled for the $\omega_i^e = n\omega_r$ ($i = 1, 2$) conditions and may affect the lineshapes for the other conditions, but are expected to have a minor impact on polarization transfer experiments. A detailed investigation on the practical requirements and the experimental performance of the R2TR experiment by applying it to induce polarization transfer between different pairs of ^{13}C spins in triply ^{13}C-labelled L-alanine under the $\Delta = n\omega_r$ and $\Sigma = n\omega_r$ conditions is given in ref. 97a.

The R^2T (rotational resonance tickling) experiment[98] essentially represents a ramped R2TR experiment (see Fig. 17), where the ramp is applied to compensate for RF inhomogeneity and distributions of the isotropic chemical shielding. R^2T investigations on doubly ^{13}C-labelled tyrosine ethyl ester and glycylglycine hydrochloride, employing the double-quantum recoupling condition $\Sigma = n\omega_r$, point to a reduced sensitivity to double-quantum-relaxation effects and hence should allow for more accurate determination of internuclear ^{13}C–^{13}C distances in the range 450–500 pm. This improved distance range should be compared to the slightly more 'shortsighted' properties of spectral lineshapes in standard R^2 experiments, where for ^{13}C–^{13}C spin pairs significant R^2 lineshape effects are observed for distances up to 300–350 pm.[79] Both the R2TR and the R^2T approaches utilize low-power RF amplitudes to generate new and adjustable resonance conditions. The idea of generating such new R^2 conditions by applying additional RF irradiation has been outlined earlier, in an approach where short cycles of high-power RF pulses, together with

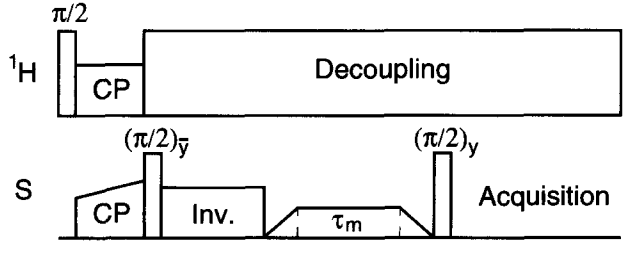

Fig. 17. The R^2T pulse sequence[98] where a ramped weak RF field at the S Larmor frequency is applied during τ_m.

stroboscopic signal observation once per rotation period, lead to a scaled range of (adjustable) zero-, single- and double-quantum R^2 conditions.[99]

The concept of R^2 in conjunction with short cycles of high-power RF pulses has been developed further in a slightly different direction. Karlsson *et al.*[100] have introduced a scheme to reverse the spin evolution at rotational resonance, which leads to the formation of echoes of transverse or differential longitudinal magnetization (Fig. 18). The principal idea is to apply a short RF-pulse sequence, which suspends the spin evolution for an incomplete fraction of a rotation period and therefore represents a cycle in the sense of Haeberlen and Waugh.[14] After the cycle, the spin system has accordingly returned to its initial state, the spin dynamics are reversed, and an echo is formed. In the absence of chemical shielding anisotropy and in the limit of $|\omega_B| \ll |\omega_\Delta|$ it has been shown that a full echo is formed at $\tau_1 = \tau_2 = \tau$ for difference longitudinal magnetization, which is illustrated in Fig. 18. For transverse magnetization the echo maximum

$$S = [\exp(i\omega_{iso}^{CS_1}\tau) + \exp(i\omega_{iso}^{CS_2}\tau)]\ \cos(\omega_{iso}^{J_{12}}\tau) \tag{87}$$

is modulated by the isotropic J-coupling $\omega_{iso}^{J_{12}}$. The value for $\omega_{iso}^{J_{12}}$ extracted from transverse R^2-echo experiments on doubly ^{13}C-labelled zinc acetate, for example, compares well with the value determined by liquid-state NMR.

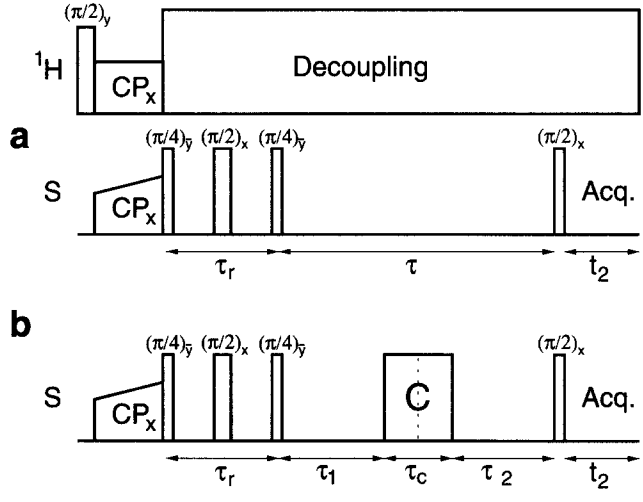

Fig. 18. Pulse sequences for monitoring longitudinal magnetization exchange (a) and longitudinal magnetization echoes (b) at the $n = 1$ R^2 condition where the duration of the three-pulse sub-sequence amounts to one rotation period. In (b) the cycle C represents two RF-pulses of opposite phase and of total duration $\tau_r/2$; to avoid unwanted Hartmann–Hahn CP in practice the ^1H decoupling is interrupted during C.[100]

In addition to this possibility of determining isotropic J-coupling constants, the R^2-echo concept has been extended to address two further aspects of general interest in the context of R^2 experiments: experimental determination of zero-quantum relaxation characteristics,[88] and excitation of double-quantum coherence through dipolar coupling.[93]

The zero-quantum relaxation time constant T_2^{ZQ} is one of the parameters necessary to describe R^2 longitudinal magnetization exchange experiments, widely used for determination of internuclear distances, as has been discussed already. In order to experimentally determine T_2^{ZQ}, it is necessary to isolate the contributions from this zero-quantum relaxation process from inhomogeneous contributions arising simultaneously under rotational resonance. This isolation can be achieved by R^2 echoes, which permit the desired isolation of the homogeneous decay to a good approximation by refocusing of inhomogeneous contributions. Following this strategy, Karlsson and Levitt found experimentally for doubly ^{13}C-labelled zinc acetate that the model of a single exponential ^{13}C T_2^{ZQ} decay holds quite well for high ^{1}H decoupling field strengths or without ^{1}H decoupling, but fails for intermediate decoupling fields, where a superposition of exponential decays is necessary to fit the experimental data.[88]

The principal possibility for exciting double-quantum coherence under rotational resonance conditions was demonstrated in 1992 by Nielsen *et al.*:[101] transverse magnetization evolving under the $n = 1$ R^2 condition was converted into double-quantum coherence by application of a $\pi/2$ pulse, resulting in a theoretical DQ efficiency (i.e. the ratio of the signal amplitude passed through DQ coherence to the signal amplitude in a conventional MAS experiment) of 50% and an experimental efficiency of 25% for the ^{13}C-spin pair in doubly ^{13}C-labelled zinc acetate. The pulse scheme shown in Fig. 19[93] excites DQ coherence in a different and more efficient way by making use of R^2 echoes.

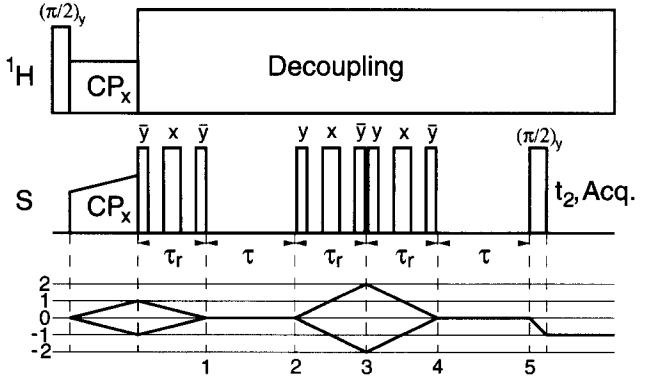

Fig. 19. Pulse sequence for R^2-echo DQ filtration at the $n = 1$ R^2 condition. The individual three-pulse sub-sequences last for one rotation period and consist of sets of equally spaced $\pi/4-\pi/2-\pi/4$ pulses; see text for further explanations.[93]

First, cross-polarization creates transverse magnetization of the observed spins, which is transformed into longitudinal magnetization by the following three-pulse sequence, which is partially compensated for chemical shielding anisotropy of one of the two spins. The longitudinal difference magnetization is then converted into ZQ coherence under the influence of the homonuclear dipolar coupling, recoupled by rotational resonance. The second three-pulse sequence selectively inverts one of the two spins and thus creates double-quantum coherence, which is converted back to zero-quantum coherence by the subsequent three-pulse sequence. During the following interval τ, the zero-quantum coherence is converted back to longitudinal magnetization, which forms an echo at time point 5. Finally, a strong nonselective $\pi/2$ pulse converts the longitudinal difference magnetization to observable transverse difference magnetization. Appropriate phase cycling[3] selects the signal that has passed through DQ coherence at time point 3. The theoretical efficiency of this approach is 73% and experimentally up to 40% have been reached.[93] Figure 20 shows the application of this R^2-echo DQ filter to a sample of (11,20-$^{13}C_2$)retinal at the $n = 1$ R^2 condition.

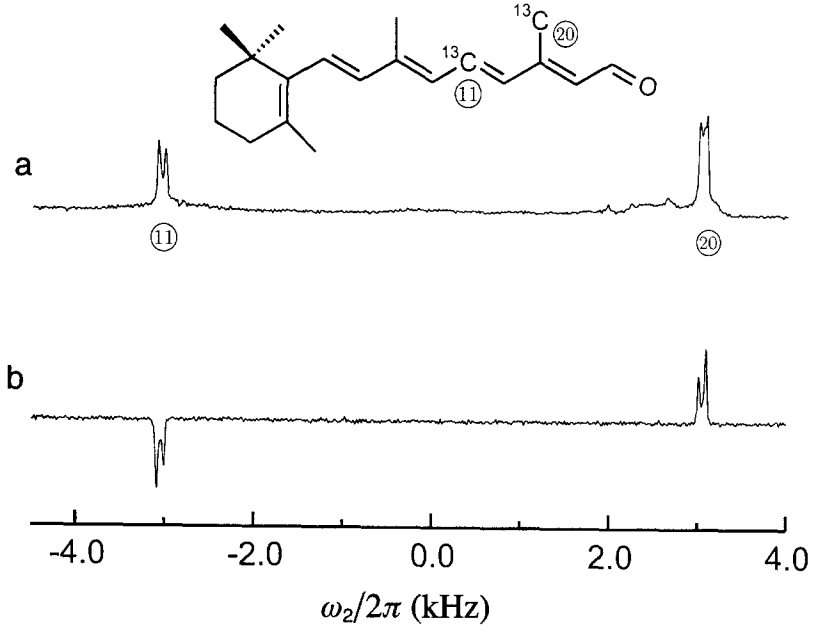

Fig. 20. ^{13}C $n = 1$ R^2 MAS NMR spectra of (11,20-$^{13}C_2$)retinal. (a) 'Conventional' $n = 1$ R^2 MAS NMR spectrum after subtraction of natural ^{13}C-abundance background. (b) $n = 1$ R^2 MAS NMR spectrum, obtained with the R^2-echo DQ-filtering technique (see Fig. 19) with an efficiency of 40%.[93] (Fig. 20 courtesy of T. Karlsson and M. H. Levitt.)

4.2. RFDR and SEDRA

The SEDRA (simple excitation for the dephasing of the rotational echo amplitudes')[102] and RFDR (RF-driven dipolar recoupling)[103] experiments can be seen as closely related not only to each other but in a more general sense also to the REDOR sequence. All of these spin-echo schemes apply rotation-synchronized π pulses to recouple the dipolar interaction. The term SEDRA is used if the train of π pulses is applied to obtain 'dephasing curves' similar to REDOR dephasing curves; the corresponding pulse sequence is shown in Fig. 21a. If the sequence is applied during the mixing time of a two-dimensional correlation experiment (Fig. 21b) it is referred to as RFDR.

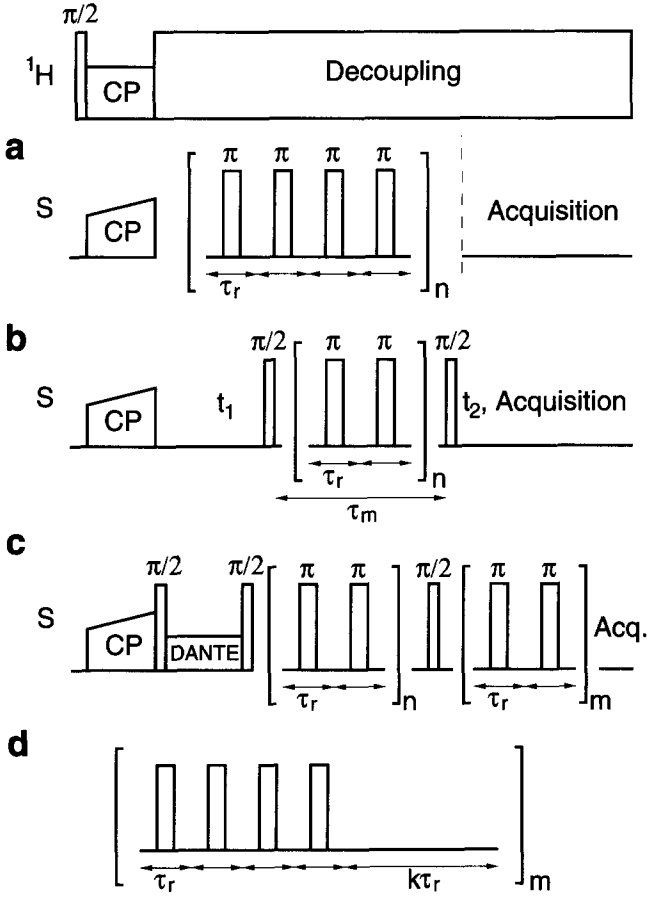

Fig. 21. Pulse sequences of (a) SEDRA,[102] (b) RFDR,[103] (c) CEDRA,[106] and (d) modified version of the basic RFDR sequence where delays of duration $k\tau_r$ are inserted between sets of π pulses.[104]

The RFDR/SEDRA sequence is not compensated for isotropic or anisotropic chemical shieldings: for spinning speeds not greatly exceeding the anisotropy of the chemical shielding interactions, the effectively recoupled dipolar Hamiltonian of RFDR/SEDRA becomes a relatively complicated function of the CSA terms. But even in the limit of $\omega_r \gg \delta^{CSA}$ the average Hamiltonian of the dipolar interaction is a function of the difference between the isotropic chemical shieldings. In the $\omega_r \gg \delta^{CSA}$ limit it can be written in the toggling frame of the pulse sequence (representing the appropriate frame for a multiple-pulse sequence like RFDR/SEDRA) as[103]

$$\bar{H}^0_{D_{12}} = \bar{\omega}_D(S_{1x}S_{2x} + S_{1y}S_{2y}) \tag{88}$$

$$= \bar{\omega}_D \tfrac{1}{2}(S_{1+}S_{2-} + S_{1-}S_{2+}) \tag{89}$$

with the scaling factor

$$\bar{\omega}_D = \frac{2}{\pi} \sum_{m=1}^{2} \tilde{\omega}^{(m)}_{D_{12}}(\beta^{D_{12}}_{PR}) \cos(m\gamma^{D_{12}}_{PR}) \frac{\omega^{\Delta}_{iso}/\omega_r}{m^2 - (\omega^{\Delta}_{iso}/\omega_r)^2} (-1)^{m-1} \sin\left(\pi \frac{\omega^{\Delta}_{iso}}{\omega_r}\right) \tag{90}$$

In Eq. (90) we have defined $\tilde{\omega}^{(m)}_{D_{12}}(\beta^{D_{12}}_{PR})$ as

$$\omega^{(m)}_{D_{12}}(\beta^{D_{12}}_{PR}, \gamma^{D_{12}}_{PR}) = \tilde{\omega}^{(m)}_{\kappa}(\beta^{D_{12}}_{PR}) \exp(im\gamma^{D_{12}}_{PR}) \tag{91}$$

which leads to

$$\tilde{\omega}^{(1)}_{D_{12}}(\beta^{D_{12}}_{PR}) = -\frac{b_{12}}{\sqrt{2}} \sin(\beta^{D_{12}}_{PR}) \cos(\beta^{D_{12}}_{PR}) \tag{92}$$

$$\tilde{\omega}^{(2)}_{D_{12}}(\beta^{D_{12}}_{PR}) = \frac{b_{12}}{4} \sin^2(\beta^{D_{12}}_{PR}) \tag{93}$$

assuming exact magic-angle spinning. At exactly rotational resonance conditions (i.e. $\omega^{\Delta}_{iso} = n\omega_r$, $n = 1, 2$) the scaling factor reduces to

$$\bar{\omega}_D = \tilde{\omega}^{(n)}_{D_{12}}(\beta^{D_{12}}_{PR}) \cos(n\gamma^{D_{12}}_{PR}) \tag{94}$$

The $S_{1z}S_{2z}$ part of the dipolar coupling vanishes over each cycle and only the flip-flop part is recovered in the average Hamiltonian of Eq. (89) by the train of π pulses. Bennett *et al.* have pointed out[104] that only dephasing of transverse and exchange of longitudinal magnetization occurs under this regime. The first option is followed by the SEDRA experiment, the latter by RFDR. Exchange of transverse magnetization may be introduced, however, by additionally applied $\pi/2$ pulses (t-SEDRA[105]).

The acquisition of SEDRA dephasing curves S/S_0 requires observation of rotational echoes with (S) and without (S_0) dephasing pulses. The homogeneous nature of the homonuclear dipolar coupling will, however, prevent the formation of full echoes even in the absence of the dephasing pulses. This effect will be most pronounced close to the R^2 conditions ($\omega_{iso}^{\Delta} = n\omega_r$, $n = 0, 1, 2, ...$) but will be reduced if one of the 'off-R^2' conditions $\omega_{iso}^{\Delta} = (n + 1/2)\omega_r$ ($n = 0, 1, 2, ...$) is fulfilled. This is utilized by the CEDRA (controlled SEDRA)[106] and T-CEDRA[107] experiments. CEDRA applies the 'off-R^2' conditions to obtain SEDRA dephasing curves; the T-CEDRA sequence generates exchange of longitudinal magnetization between selectively excited spins with differing isotropic chemical shieldings in a one-dimensional experiment (Fig. 21c). The goal of both CEDRA experiments is to obtain dipolar coupling constants b_{12} from the resulting dephasing (CEDRA) or coherence transfer (T-CEDRA) curves. They differ, however, with respect to sensitivity to CSA parameters: it was shown experimentally for the ^{13}C two-spin system in L-(1,3-$^{13}C_2$)alanine that T-CEDRA in general and CEDRA under the conditions $n = 0$ or 1 should be relatively insensitive to orientational parameters, while the sensitivity of CEDRA to CSA parameters increases at higher orders of n.[106,107] CEDRA and other homonuclear dephasing experiments like DRAMA (see below) have been applied for investigations on $^{13}C-^{13}C$ distances in the 500–600 pm range in carbonyl-^{13}C-labelled polycarbonate and a blend of different polycarbonates[108] in order to suggest a local-order structural model.

Bennett *et al.* have given a thorough discussion of SEDRA/RFDR-type experiments in ref. 104, where they covered influences from finite pulses, insufficient proton decoupling, and multi-spin interactions, and introduced a modified version of the basic RFDR sequence with delays of duration $k\tau_r$ incorporated between sets of four π pulses (see Fig. 21d). This modification recouples weak dipolar coupling interactions only at the conditions $\omega_{iso}^{\Delta} = (n/k)\omega_r$, which avoids the R^2 conditions ($\omega_{iso}^{\Delta} = n\omega_r$) if n/k is not an integer. This is reflected in the average Hamiltonian as[104]

$$\bar{H}_{D_{12}}^{0} = \frac{k}{4+k}\left[\omega_{iso}^{\Delta} - \frac{n}{k}\omega_r\right]\frac{1}{2}(S_{1z} - S_{2z}) - \frac{4}{4+k}\bar{\omega}_D\frac{1}{2}(S_{1+}S_{2-} + S_{1-}S_{2+}) \tag{95}$$

and can be applied to multi-spin systems to selectively recouple weak dipolar interactions in the presence of stronger couplings. In conclusion, they stress the robustness of RFDR/SEDRA-type experiments with respect to pulse imperfections and the applicability at relatively high MAS frequencies, and demonstrate these advantages of 2D RFDR correlation experiments for obtaining backbone $^{13}C-^{13}C$ connectivities in peptides and proteins for the model tetrapeptide (U-^{13}C,^{15}N)achatin-II (Gly-Phe-Ala-Asp).

Another route to the study of peptide-backbone conformations is double-quantum experiments incorporating RFDR recoupling, which are sensitive not only to internuclear distances but also to the orientations of the CSA tensors: combined results from RFDR exchange and RFDR double-quantum-filtration experiments allowed the dihedral angles relating the ^{13}C-labelled Gly-3 and Ala-4 carbonyl sites in the backbone of the 26-residue helical peptide melittin (diluted in a frozen glycerol/water solution) to be obtained that were in good agreement with the values known for crystalline melittin.[109]

Of all the various SEDRA/RFDR-type experiments the 'conventional' 2D RFDR correlation experiment has so far found the widest range of applications. For instance, it has been applied to probe spatial connectivities and to assign resonances for compounds ranging from inorganic phosphate phases and ceramics,[110,111] to organic polymers,[112] to peptides and proteins.[113–115] Quantitative determination of internuclear ^{13}C–^{13}C distances (between the singly methyl-^{13}C-labelled carbon sites of *p*-xylene and the naturally abundant ^{13}C nuclei of the host molecules in a *p*-xylene/Dianin inclusion complex) has also been demonstrated;[116] the quantitation step takes advantage of the isotopically dilute ^{13}C spin system.

4.3. USEME and RIL

When dealing with homonuclear multiple-spin systems, polarization transfer in the zero-quantum subspace of the effective dipolar Hamiltonian is advantageous as the spin dynamics of the process may be described by a kinetic matrix.[117] The USEME (unified spin echo and magic echo)[118] and RIL (rotating/laboratory frame)[119] sequences follow this zero-quantum-subspace philosophy and aim at 'broadband' properties of the pulse sequence.

The model pulse sequence representing the basic principle of both the USEME[118] and the RIL[117,119] experiment is depicted in Fig. 22a. The RF irradiation during the first half of the rotation period (the 'R part') scales the average Hamiltonian of the dipolar interaction by $-1/2$ in the limit of an infinite amplitude $\omega^{RF} \rightarrow \infty$.[120–122] This scaling prevents cancellation (which would occur without applying the RF irradiation) of the dipolar contributions arising during the first and the second halves of the rotation period. The lowest-order average Hamiltonian $\bar{H}_D^0$ in a tilted frame, related to the standard rotating frame by a $\pi/2$ rotation around the *y*-axis, then becomes[117]

$$\bar{H}_D^0 = \sum_{i=1}^{N} \sum_{j>i}^{N} \left[-\frac{1}{2\tau_r} \int_0^{\tau_r/2} H_{ij}^D(t)\mathrm{d}t + \frac{1}{\tau_r} \int_{\tau_r/2}^{\tau_r} H_{ij}^D(t)\mathrm{d}t \right] \tag{96}$$

$$= \sum_{i=1}^{N} \sum_{j>i}^{N} \frac{-3b_{ij}}{2\sqrt{2}\pi} \sin(2\beta_{PR}^{D_{ij}}) \sin(\gamma_{PR}^{D_{ij}})[2S_{iz}S_{jz} - \tfrac{1}{2}(S_{i+}S_{j-} + S_{i-}S_{j+})] \tag{97}$$

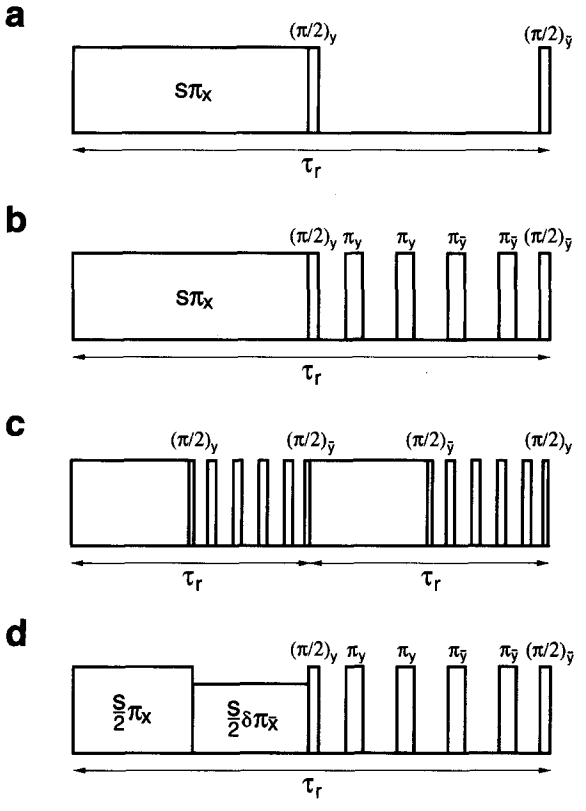

Fig. 22. (a) The basic principle of the USEME[118] and RIL[117,119] experiment. (b) The basic scheme with π pulses applied during the 'L part' for better CSA compensation. (c) Additional supercycle for elimination of remaining chemical shielding contributions. (d) The complete RIL sequence with additional amplitude attenuation during the 'R part' to compensate for finite RF-field strength.[119]

Equation (97) represents the complete average Hamiltonian for an isolated spin system in the absence of chemical shielding interactions. If chemical shielding contributions cannot be neglected, the basic sequence has to be modified in order to cancel isotropic and anisotropic chemical shielding terms, which are suppressed by the RF irradiation during the first half of the sequence but still contribute to the average Hamiltonian as they are not suppressed during the second half of the rotation period (the 'L part'). Both schemes (RIL and USEME) apply π pulses to refocus the chemical shielding interactions in the second half of the rotation period (Fig. 22b) which, in the limit of an infinite number of δ-shaped pulses, would lead to complete refocusing. Application of the supercycle shown in Fig. 22c finally averages out remaining chemical shielding contributions for a finite number of pulses in

lowest-order AHT, and adding a phase shift in the middle of the R part also cancels the first-order term $\overline{H}^1_{\mathrm{CS}\times\mathrm{CS}}$.

Equation (97) assumes infinite RF amplitudes. For a finite RF amplitude during the R part, the average Hamiltonian of the dipolar coupling can be calculated as

$$\overline{H}^0_{\mathrm{D}} = \sum_{i=1}^{N}\sum_{j>i}^{N} \frac{-3b_{ij}}{2\sqrt{2}\pi} \sin(2\beta^{\mathrm{D}_{ij}}_{\mathrm{PR}})\{\sin(\gamma^{\mathrm{D}_{ij}}_{\mathrm{PR}})[2S_{iz}S_{jz} - 1/2(S_{i+}S_{j-} + S_{i-}S_{j+})$$

$$+ \varepsilon(S_{i+}S_{j-} + S_{i-}S_{j+})] - \varepsilon'\cos(\gamma^{\mathrm{D}_{ij}}_{\mathrm{PR}})(S_{ix}S_{jy} + S_{iy}S_{jx})\} \tag{98}$$

with $\varepsilon = 1/(16s^2 - 4)$ and $\varepsilon' = 4s/(12s^2 - 3)$ where $s = \omega^{\mathrm{RF}}/\omega_{\mathrm{r}}$. These additional contributions are expected to be small in practical applications and can be further minimized by an additional amplitude attenuation in the middle of the R part (Fig. 22d), which should fulfil one of the conditions[117]

$$\delta = 1 - \frac{1}{s} \tag{99}$$

or

$$\delta = 1 - \frac{3}{s} \tag{100}$$

As for applications of most homonuclear recoupling schemes, decoupling from heteronuclear spins (most commonly ^{1}H), where necessary, plays a crucial role also for a successful execution of RIL experiments. Application of frequency-switched Lee–Goldburg decoupling has been shown to provide good ^{13}C-RIL performance for uniformly (^{13}C,^{15}N)-labelled arginine.[117]

Including the aforementioned approximations, the average Hamiltonian of the final RIL-ZQT ('RIL zero-quantum transfer') sequence (Fig. 22d) consists only of the sum of dipolar ($\overline{H}^0_{\mathrm{D}}$) and isotropic J-coupling ($\overline{H}^0_{J_{\mathrm{iso}}}$) terms. If $\overline{H}^0_{J_{\mathrm{iso}}}$ happens to be absent or small compared to $\overline{H}^0_{\mathrm{D}}$, one finally arrives at the desired result of a 'purely dipolar' average Hamiltonian

$$\overline{H}^0 \simeq \overline{H}^0_{\mathrm{D}} \tag{101}$$

As mentioned already, this type of 'purely dipolar' average Hamiltonian leads to conservation of the sum polarization. This permits one to describe the polarization-transfer dynamics under the regime of such a Hamiltonian by a simple kinetic matrix K, where the elements of the matrix are proportional to the squared value of the dipolar coupling constant between the individual spins

or, in terms of the corresponding internuclear distances, to $K_{kl} = \text{const.}\ r_{kl}^{-6}$ where r_{kl} denotes the internuclear distance. If a pulse sequence generating an average Hamiltonian such as in Eq. (101) is applied during the mixing time τ_m of a two-dimensional experiment, the time-domain signal can be written as[3]

$$s(t_1, \tau_m, t_2) = -\sum_k \sum_l \exp(i\Omega_k t_2)[\exp(K\tau_m)]_{kl} \exp(i\Omega_l t_1) M_{l0} \qquad (102)$$

where M_{l0} denotes the equilibrium magnetization of the lth spin, weighted by the number of equivalent spins. The integrated intensity I_{kl} of a peak with frequency coordinates (Ω_l, Ω_k) is obtained from Eq. (102) after two-dimensional Fourier transformation as

$$I_{kl} = a_{kl}(\tau_m) M_{l0} \qquad (103)$$

with

$$a_{kl}(\tau_m) = [\exp(K\tau_m)]_{kl} \qquad (104)$$

Equations (103) and (104) allow one to obtain the complete intensity distribution of a 2D experiment by calculation of a single matrix exponential. It is also evident that for long mixing times τ_m a quasi-equilibrium with equal intensity for all diagonal and cross peaks will be reached, and that for short mixing times τ_m the cross-peak intensity I_{kl} will depend approximately linearly on the matrix elements K_{kl}. Though quite different in physical origin, such an 'initial rate' regime bears some seeming similarity with the so-called initial rate regime encountered in, e.g., 2D NOE solution-state NMR experiments.[3]

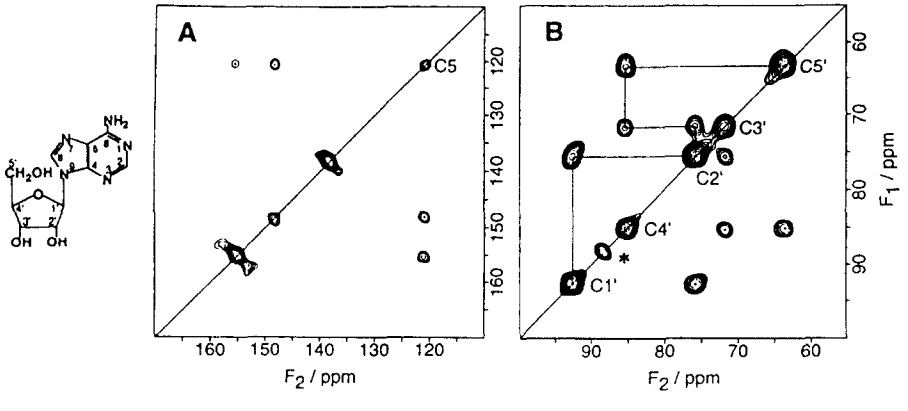

Fig. 23. ^{13}C 2D USEME correlation experiment on U-^{13}C,^{15}N-labelled adenosine, using a short mixing time $\tau_m = 1.2$ ms. (A) Purine and (B) ribose regions of the contour plots. (Reproduced with permission from ref. 123 © 1995 American Chemical Society.)

There are two principal possibilities for extracting information from ZQ dipolar correlation experiments. One can either probe distance connectivities by acquiring experiments with short mixing times and thus obtain an effective polarization transfer predominantly between spins in spatial proximity to each other; or one may try to extract distance information from series of 2D experiments with different mixing times τ_m and using Eqs (103) and (104). The first approach has been applied to fully ^{13}C-labelled adenosine using the USEME sequence[123] and yields complete assignment of all ^{13}C resonances (see Fig. 23; in combination with a 2D ^{13}C–^{15}N correlation experiment all ^{15}N resonances have been assigned). Similarly, a short mixing time regime RIL approach has been used to identify and distinguish intramolecular and intermolecular distance connectivities in doubly ^{13}C-labelled calcium-acetate monohydrate.[124]

Extracting distance information from ZQ dipolar correlation experiments requires acquisition of a series of 2D experiments with different mixing times and fitting of the theoretical intensities corresponding to a matrix K to the experimentally obtained build-up curves as a function of τ_m. For an *isolated n*-spin system the matrix elements K_{kl} can be converted directly to internuclear distances from $K_{kl} = \text{const.}\ r_{kl}^{-6}$ if the constant scaling factor can be determined from other sources, such as one known internuclear distance within the spin system. If the spin system does not consist of isolated subsystems, direct calculation of internuclear distances is prohibited as multiple *different* distances r_{kl} will contribute to a single matrix element K_{kl}. Such a *non-isolated* spin system is represented by the ^{31}P spin system in $Cd_3(PO_4)_2$. There are six crystallographically inequivalent P sites in the asymmetric unit, but dipolar coupling between ^{31}P spins in different asymmetric units cannot be neglected. The best-fit build-up curves from a series of 2D ^{31}P RIL ZQ dipolar correlation experiments are in excellent agreement with theoretical build-up curves calculated from the known single-crystal X-ray structure of $Cd_3(PO_4)_2$ (see Fig. 24),[125] demonstrating the validity of the approximation of a purely dipolar RIL average Hamiltonian for this particular ^{31}P spin system. Accordingly, for this spin system it is possible to obtain the matrix K experimentally with high accuracy (and hence assign all ^{31}P resonances), but direct conversion to internuclear distances is not possible owing to the nonisolated nature of this spin system.

4.4. DRAMA, DRAWS, MELODRAMA and BABA

The first experiment to reintroduce homonuclear dipolar coupling under MAS conditions by applying a multiple-pulse sequence was DRAMA (dipolar recovery at the magic angle).[126,127] The basic sequence of DRAMA consists of two $\pi/2$ pulses in each rotation period to spoil the averaging of the dipolar coupling interaction by MAS. In the complete DRAMA sequence (Fig. 25)

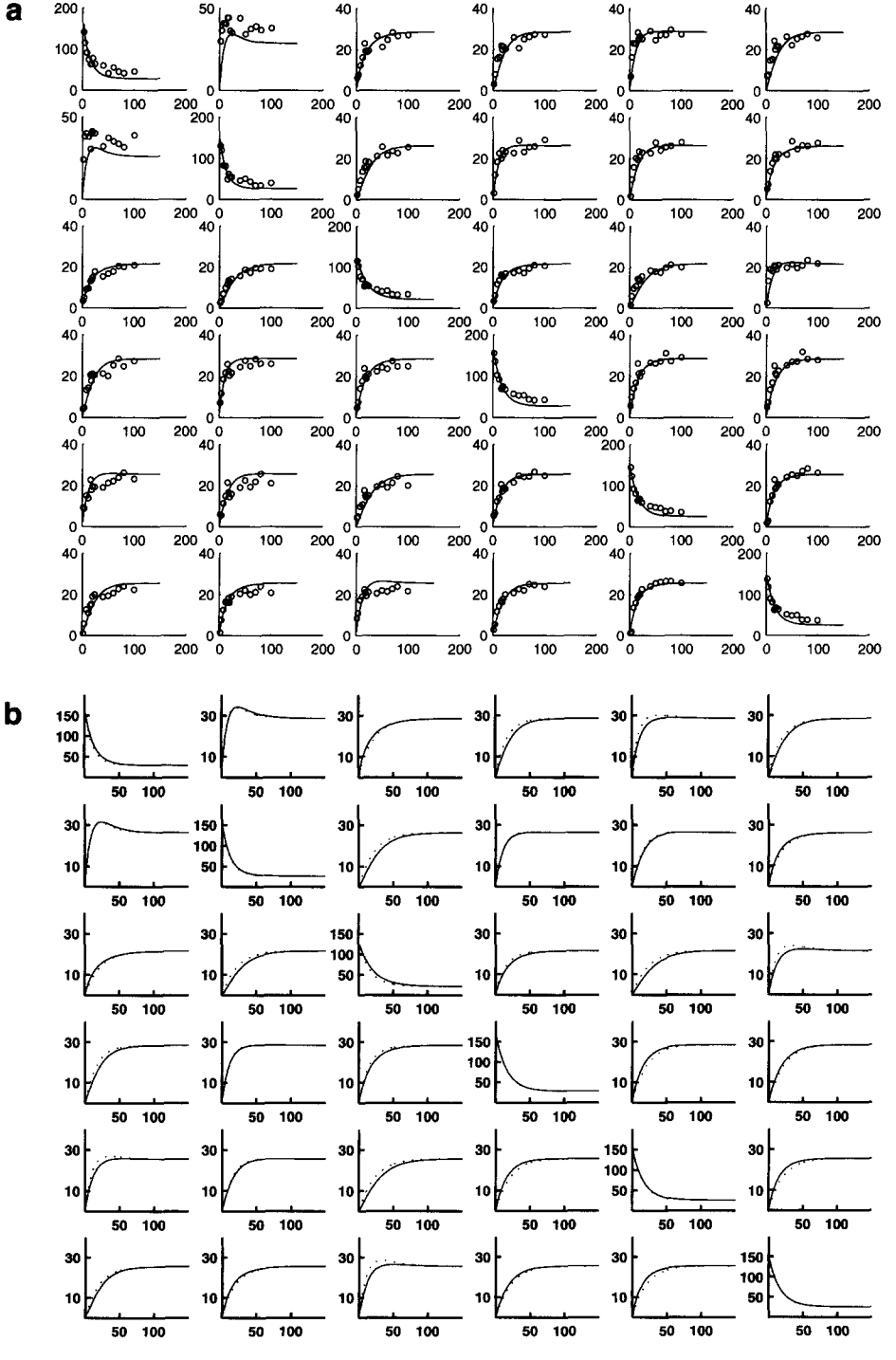
a
b

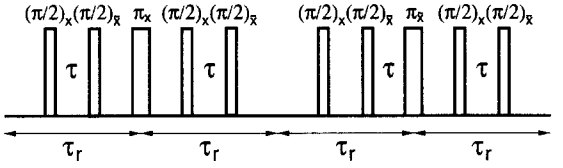

Fig. 25. The DRAMA pulse sequence, complete over four rotation periods.[126,127]

extending over four rotation periods, two π pulses are included after every second rotation period to reduce influences from chemical shielding. The resulting average Hamiltonian for a spin pair in the toggling frame of the pulse sequence calculated over four rotation periods is[126,127]

$$\bar{H}_{\mathrm{T}}^{0} = \frac{3\sqrt{2}}{2\pi} b_{12} \sin(2\beta_{\mathrm{PR}}^{\mathrm{D}_{12}}) \cos(\gamma_{\mathrm{PR}}^{\mathrm{D}_{12}})[S_{1z}S_{2z} - S_{1y}S_{2y}] \tag{105}$$

where J-coupling has again been neglected and τ has been set to $\tau = \tau_{\mathrm{r}}/2$, leading to the maximum obtainable scaling factor of the average Hamiltonian. No recoupling, however, occurs for $\tau = 0$. The possibility of scaling the magnitude of the dipolar scaling factor by altering τ was utilized by Geen *et al.*[128] for investigations on the ^{1}H spin system of polycarbonate under fast MAS conditions. The insensitivity of DRAMA to chemical shielding effects predicted by Eq. (105) is not achieved in practice, where also a relatively strong sensitivity to RF field inhomogeneities is found. xy-8-Phase cycling, applied to the refocusing π pulses was suggested to remedy this problem[129,130] but results in a very long cycle of 16 rotation periods.

We will not discuss the basic DRAMA experiment in any greater depth, as this was treated in detail in the review by Bennett *et al.*[5] in 1994. Since then DRAMA has, for instance, been employed to investigate experimentally the internuclear ^{31}P–^{31}P distance in a 12-residue helical peptide[131] and to

---

Fig. 24. 2D MAS ^{31}P RIL experiments on $Cd_3(PO_4)_2$; there are six crystallographically independent P sites 1 to 6, corresponding to six ^{31}P resonances A to F (see Fig. 34 for 1D ^{31}P MAS spectrum and numbering scheme). (a) Comparison of experimental (O) and calculated (solid line) build-up curves as a function of mixing time. The arrangement of the curves is such that top left curve = diagonal peak AA, bottom right curve = diagonal peak FF. On the x-axis in each curve the mixing time is given in ms; the y-axis gives the integrated intensities of the respective peaks, with the y-axes defined such that the total integrated spectral intensity is 1000. (b) Comparison of the best-fit experimental build-up curves (solid line) with build-up curves calculated (dotted line) from the single-crystal X-ray structure. The comparison in (b) yields unambiguous assignment of the six ^{31}P resonances A to F to the six crystallographic P sites 1 to 6; see Fig. 34 for assignment. (Reproduced with permission from ref. 125, © 1997, American Chemical Society.)

determine $^{13}C-^{13}C$ distances in crystalline and amorphous domains of doubly ^{13}C-labelled polyethylene.[132]

Various pulse schemes have evolved from DRAMA, mainly with the goal of overcoming the rather strong sensitivity of DRAMA to chemical shielding and RF inhomogeneities. The DRAWS (dipolar recovery with a windowless sequence)[133] sequence (Fig. 26) applies additional trains of 2π pulses between the $\pi/2$ pulses of the basic DRAMA sequence to improve compensation for chemical shielding terms. The RF field amplitude during the DRAWS sequence has to match 8.5 times the MAS frequency ($\omega^{RF} = 8.5\omega_r$), as eight 2π pulses and two $\pi/2$ pulses are applied over one rotation period. The appropriate frame for calculating the average Hamiltonian for a sequence with continuous RF irradiation such as DRAWS (and in fact all sequences discussed in the following) is the interaction frame of the RF field defined by

$$U_{RF} = \hat{T}\exp\left(-i\int_0^t H^{RF}(\tau)\,d\tau\right) \tag{106}$$

where $\hat{T}$ represents the Dyson time ordering operator. Calculation of the average Hamiltonian in this frame over one DRAWS cycle (again ignoring J-coupling) leads to[133]

$$\begin{aligned}\bar{H}_I^0 \simeq \frac{b_{12}}{17\pi}\,[&c_{DQ}\tfrac{1}{2}(S_{1+}S_{2+} + S_{1-}S_{2-}) \\ &+ c_{ZQ}(2S_{1z}S_{2z} - \tfrac{1}{2}(S_{1+}S_{2-} + S_{1-}S_{2+}))] \\ &+ \bar{H}_{CS}^0\end{aligned} \tag{107}$$

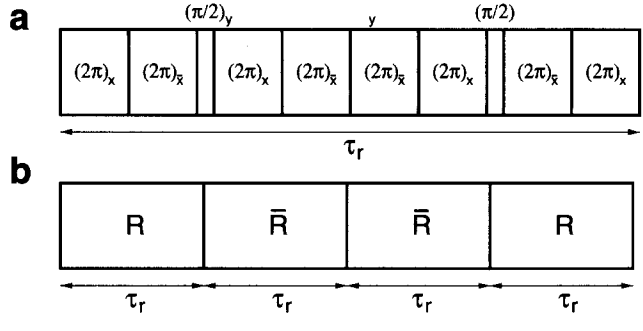

Fig. 26. The basic DRAWS pulse sequence. (a) Pulses over one rotation period with the requirement $\omega^{RF} = 8.5\omega_r$. (b) Complete DRAWS cycle over four rotation periods.[133]

with

$$c_{DQ} = 9.0\cos(\beta_{PR}^{D12})\sin(\beta_{PR}^{D12})\left[\sin\left(\gamma_{PR}^{D12}+\frac{8\pi}{17}\right)+\cos\left(\gamma_{PR}^{D12}+\frac{\pi}{34}\right)\right]$$

$$-4.8\sin^2(\beta_{PR}^{D12})\left[\sin\left(2\gamma_{PR}^{D12}+\frac{\pi}{17}\right)+\cos\left(2\gamma_{PR}^{D12}+\frac{15\pi}{34}\right)\right] \quad (108)$$

$$c_{ZQ} = -9.0\cos(\beta_{PR}^{D12})\sin(\beta_{PR}^{D12})\left[\sin\left(\gamma_{PR}^{D12}+\frac{8\pi}{17}\right)+\cos\left(\gamma_{PR}^{D12}+\frac{\pi}{34}\right)\right]$$

$$-1.6\sin^2(\beta_{PR}^{D12})\left[\sin\left(2\gamma_{PR}^{D12}+\frac{\pi}{17}\right)+\cos\left(2\gamma_{PR}^{D12}+\frac{15\pi}{34}\right)\right] \quad (109)$$

The residual chemical shielding contributions $\overline{H}_{CS}^{0}$ are suppressed by the supercycle shown in Fig. 26. The average Hamiltonian of the DRAWS scheme (Eq. (107)) consists of zero-quantum and double-quantum terms with similar magnitudes (Eqs. (108) and (109)) and shows a rather strong dependence on the angles connecting PAS and RAS of the dipolar coupling tensor.

Monitoring the decay of transverse sum magnetization as a function of the number of applied DRAWS cycles leads to 'DRAWS decay curves', similar to the well-known 'REDOR or SEDRA decay curves' (see Sections 3.2 and 4.2). Application of this method to three doubly ^{13}C-labelled dicarboxylic acids ((1,2-$^{13}C_2$)oxalic acid dihydrate, (1,3-$^{13}C_2$)malonic acid, and (1,4-$^{13}C_2$)succinic acid) allowed determination of a considerable range of internuclear $^{13}C-^{13}C$ distances.[133] It was also demonstrated that DRAWS decay curves are relatively insensitive to isotropic chemical shielding effects by comparing the ^{13}C two-spin systems in 2′-deoxy(4,6-^{13}C)thymidine and L-(1,3-$^{13}C_2$)alanine: these two ^{13}C spin pairs are characterized by similar internuclear $^{13}C-^{13}C$ distances (about 250 pm) but quite different isotropic chemical shielding differences of about 30 ppm and 160 ppm, respectively.[133] The method was also employed to obtain $^{13}C-^{13}C$ distances in five doubly ^{13}C-labelled DNA dodecamers,[134] and in singly ^{13}C-labelled β-amyloid peptides where the 'single-label approach' was chosen to determine *inter*molecular distances.[135] Effects of DQ relaxation on DRAWS decay curves have been discussed in ref. 135.

The DRAWS sequence (and a modified version thereof with twice the number of 2π pulses incorporated between the $\pi/2$ pulses[136]) has been further utilized for DQ filtering experiments, for which the theoretical filtering efficiency is limited to about 50% by the orientational dependence of the sequence. Experimental efficiencies between 7% and 25% allowed determination of $^{13}C-^{13}C$

connectivities in selectively ^{13}C-labelled DNA molecules[136] and in ^{13}C-labelled β-amyloid peptides.[135] The DQ part of the average Hamiltonian of DRAWS may also be used to determine the relative orientations of chemical shielding tensors by analysis of DQ sideband patterns. The orientations of three ^{13}C CSA tensors in selectively ^{13}C-labelled 2′-deoxythymidine determined in this way compared well with results obtained from R^2 exchange experiments.[137]

DRAWS represents a direct modification of the DRAMA pulse sequence which, however, results in a relatively large change of the resulting average Hamiltonian. The correspondence between DRAMA and MELODRAMA (melding of spin-locking and DRAMA)[138] is more directly related to the spin dynamics. There is little similarity between these two pulse sequences (see Figs 25 and 27) as MELODRAMA applies continuous RF irradiation to minimize the influences from chemical shielding and resonance offsets (hence 'spin locking'). The analogy between DRAMA and MELODRAMA results from the average Hamiltonians of the two sequences. These are closely related when calculated in the respective appropriate frames, which in the case of MELODRAMA (like in the case of DRAWS) is the interaction frame of the RF field. Calculating the average Hamiltonian for MELODRAMA in this frame over the cycle time of four rotation periods ($\tau_c = 4\tau_r$) leads to[138]

$$\bar{H}_I^0 = \bar{\omega}_D(S_{1y}S_{2y} - S_{1x}S_{2x}) \tag{110}$$

$$= -\bar{\omega}_D \tfrac{1}{2}(S_{1+}S_{2+} + S_{1-}S_{2-}), \qquad \text{for even } N \tag{111}$$

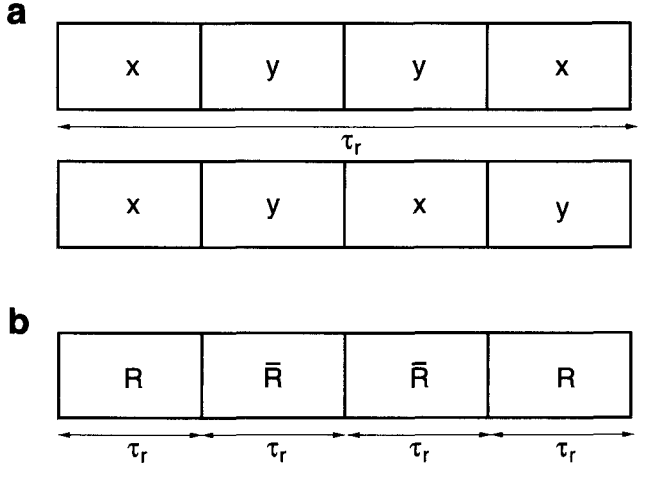

Fig. 27. The basic MELODRAMA pulse sequence. (a) Basic sequence over one rotation period for the recoupling of components modulated at ω_r (top) or at $2\omega_r$ (bottom). (b) Complete MELODRAMA cycle over four rotation periods. Slight modifications of the basic sequence with improved compensation for RF inhomogeneity have been implemented.[138]

or

$$\bar{H}_I^0 = \bar{\omega}_D(S_{1z}S_{2z} + S_{1x}S_{2x}) \qquad \text{for odd } N \tag{112}$$

where $N = \omega^{RF}/\omega_r$ and

$$\bar{\omega}_D = \frac{3\sqrt{2}b_{12}}{4\pi[1-(1/4N^2)]} \sin(2\beta_{PR}^{D_{12}})\cos(\gamma_{PR}^{D_{12}}) \tag{113}$$

No simple 'dipolar average Hamiltonian' is obtained unless N is an integer. The average Hamiltonian for odd N is related to that for even N by a $\pi/2$ rotation about the x-axis. Appropriate initial conditions ($S_{1z} + S_{2z}$ for even N and $S_{1y} + S_{2y}$ for odd N), which can be selected by an optional $\pi/2$ pulse after cross polarization, result in identical spin dynamics for odd and even N.

The dipolar scaling factor of the MELODRAMA sequence amounts to about half the scaling factor of DRAMA. However, for MELODRAMA the chemical shielding terms are completely averaged out at all orders of AHT in the limit of an infinite RF field amplitude. RF inhomogeneities and the limitation to finite RF amplitudes in practice prohibit complete averaging of chemical shielding terms in MELODRAMA experiments.[138]

Incorporating the MELODRAMA sequence in the mixing time of a two-dimensional correlation experiment, one finds negative cross-peak intensities for a two-spin system. This is due to the double-quantum nature of the exchange process and has been demonstrated for the ^{13}C-spin system of a doubly ^{13}C-labelled peptide.[138] For larger spin systems, both positive and negative 2D-MELODRAMA cross peaks occur, depending on the exchange pathways correlating two spins with each other. If the exchange is dominated by an even (odd) number of steps, the corresponding cross peaks will be positive (negative). This negative/positive cross-peak pattern has been shown for the ^{13}C spin systems in uniformly ^{13}C-labelled L-arginine[138] and adenosine monophosphate[139] and represents a useful property for purposes of assignment. The 2D homonuclear MELODRAMA correlation experiment has been further extended to a third dimension, by incorporating a second, heteronuclear dipolar recoupling mixing time. This 3D experiment has been applied successfully to the $^{15}N-^{13}C$ spin system in (U-^{15}N,^{13}C)-labelled histidine by combining ^{13}C MELODRAMA homonuclear recoupling and $^{15}N-^{13}C$ (RFDR or APHH) cross polarization.[139] Analytical expressions for the cross-peak intensities in a 2D MELODRAMA experiment have been calculated, based on the two spin average Hamiltonian of Eq. (112). Good agreement is found between experimental and calculated build-up curves for the $^{13}C-^{13}C$ two-spin system in 90% ^{13}C-labelled sodium(2-3-$^{13}C_2$)propionate. The approach has been suggested for the determination of several internuclear distances in a single experiment on low-level, multiply

^{13}C-labelled compounds and has been applied to 36% uniformly ^{13}C-labelled glucose.[140]

Spiess and co-workers have suggested another pulse sequence for the excitation of multiple-quantum coherences. The basic BABA (back-to-back) sequence is built from four $\pi/2$ pulses as shown in Fig. 28a. It was first applied to the heteronuclear ^{1}H–^{13}C spin system in different singly ^{13}C-labelled L-alanine samples to obtain two-dimensional correlations of a single-quantum ^{13}C ω_1-dimension with a ^{1}H double-quantum ω_2-dimension.[141] The lowest-order average Hamiltonian for a homonuclear spin system subjected to the basic BABA sequence consists not only of a dipolar term but also of contributions from isotropic and anisotropic chemical shieldings. The super-cycle depicted in Fig. 28b inverts the sign of the chemical shielding terms every second rotation period. This leads to a purely dipolar average Hamiltonian given by[142]

$$\bar{H}_{\mathrm{D}}^{0} = \left(\frac{3}{2\pi\sqrt{2}}\right) b_{12} \sin(2\beta_{\mathrm{PR}}^{\mathrm{D}_{12}}) \sin(\gamma_{\mathrm{PR}}^{\mathrm{D}_{12}})[S_{1+}S_{2+} + S_{1-}S_{2-}] \qquad (114)$$

BABA (Fig. 28b) as the DQ excitation–reconversion sequence in ^{31}P DQ MAS experiments has been used to probe ^{31}P–^{31}P distance connectivities in various crystalline inorganic phosphates. The presence of two crystalline polymorphs has been detected for a sample of $Mg_2P_2O_7$.[142,143] For more highly condensed crystalline phosphate phases such as MgP_4O_{11} and $Ca_2P_6O_{17}$, the ability of the DQ experiment also to reveal 'self-connectivities', that is spatial proximity between ^{31}P spins with equal chemical shielding, comes as an advantage for the characterization of structural motifs as compared to ^{31}P RFDR experiments.[142,143] This property of the ^{31}P DQ approach has been further exploited

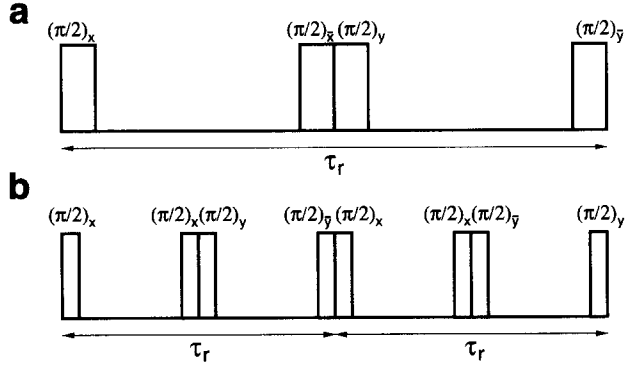

Fig. 28. (a) The basic BABA pulse sequence over one rotation period. (b) Supercycle for the elimination of chemical shielding contributions over two rotation periods.[141]

for the study of local structures in calcium phosphate glasses $(CaO)_x$–$(P_2O_5)_y$ with different ratios $x:y$ of Ca:P composition.[144] Further improvements in spectral resolution of ^{1}H DQ MAS NMR experiments by combining BABA with homonuclear dipolar decoupling (semi-windowless WHH-4) applied during the evolution and/or detection periods have been demonstrated for L-alanine[145] and have been used to investigate aspects of hydrogen-bonding in several solid benzoxazine derivatives.[146]

4.5. HORROR and C7

Within the framework of AHT there are two criteria for discussing the performance of a dipolar recoupling experiment: the size of the effective dipolar scaling factor and the efficiency of the recoupling. For powder samples, the latter is determined by the number of orientational angles the average Hamiltonian depends on. For the sequences discussed so far this number is two, as two such angles ($\beta_{PR}^{D_{12}}$ and $\gamma_{PR}^{D_{12}}$) appear in the lowest-order average Hamiltonian. The unifying principle of the 'rotation frame' sequences HORROR (homonuclear rotary resonance)[147] and C7,[148] which will be discussed now, is the dependence of the amplitude of the effective dipolar coupling constant on only one angle, $\beta_{PR}^{D_{12}}$, leading to a higher theoretical recoupling efficiency of 73%.

The pulse sequence for a double-quantum filtration experiment utilizing the HORROR sequence[147] is shown in Fig. 29. The weak on-resonance RF field leads to recoupling of the homonuclear dipolar interaction under MAS if the DQ-HORROR condition $\omega_r = 2\omega^{RF}$ is fulfilled (which may be seen as equivalent to a (homonuclear) '$n = 1/2$ R^3' experiment). This resonance condition leads to a purely dipolar double-quantum average Hamiltonian which has to be calculated by averaging over two rotation periods. Similarly to

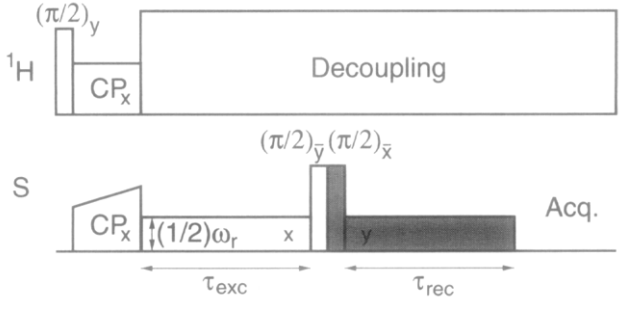

Fig. 29. Pulse sequence for DQ-HORROR filtration with $\omega_r = 2\omega^{RF}$;[147] shading indicates phase cycling appropriate for DQ selection.

the R^3 case, it turns out to be useful to transform the two-spin Hamiltonian (Eq. (69)) into a rotating frame to remove the spin evolution caused by H^{RF}. Transformation to H_R is then defined by

$$U_R = \exp(i\omega^{RF}(S_{1x} + S_{2x})t) = \exp(i\tfrac{1}{2}\omega_r(S_{1x} + S_{2x})t) \tag{115}$$

where $\omega_r = 2\omega^{RF}$ has been assumed already. This transformation of the homonuclear Hamiltonian produces a rather complicated transformed Hamiltonian H_R. Since by far the largest part of H_R does not contribute to the lowest-order average Hamiltonian anyway, we simply give some general ideas about the 'surviving' terms. After transformation to the rotating frame, the Hamiltonian will consist of terms proportional to $\exp(\pm i(1/2)\omega_r t)$ and terms proportional to $\exp(\pm i(1/2)\omega_r t)\exp(\pm i(1/2)\omega_r t) = \exp(\pm i\omega_r t)$. A comparison with the R^3 example given in the Introduction, immediately reveals that only the latter terms, which will be connected to terms of the type $S_{1k}S_{2l}$ $(k, l = x, y, z, +, -)$, will not be cancelled. It follows that the single-spin chemical shielding terms will be averaged to zero and only the $n = \pm 1$ Fourier components of the dipolar coupling $\omega_{12}^D(t)$ will contribute to the average Hamiltonian. Exact (and straightforward) calculation results in

$$\bar{H}_R^0 = \tfrac{3}{4}(\omega_{D_{12}}^{(1)} S_{1-} S_{2-} + \omega_{D_{12}}^{(-1)} S_{1+} S_{2+}) \tag{116}$$

$$= \frac{3b_{12}}{4\sqrt{2}} \sin(2\beta_{PR}^{D_{12}})\tfrac{1}{2}(S_{1-} S_{2-} \exp(i\gamma_{PR}^{D_{12}}) + S_{1+} S_{2+} \exp(-i\gamma_{PR}^{D_{12}})) \tag{117}$$

$$= \bar{\omega}_D(\beta_{PR}^{D_{12}})(\tfrac{1}{2} S_-^{14} \exp(i\gamma_{PR}^{D_{12}}) + \tfrac{1}{2} S_+^{14} \exp(-i\gamma_{PR}^{D_{12}})) \tag{118}$$

Here we have assumed exact MAS in the second step; single-transition operators and the DQ nutation frequency

$$\bar{\omega}_D(\beta_{PR}^{D_{12}}) = \frac{3}{4\sqrt{2}} b_{12} \sin(2\beta_{PR}^{D_{12}}) \tag{119}$$

have been introduced in the last step. This corresponds to an effective dipolar scaling factor of

$$|\bar{\omega}_D(\beta_{PR}^{D_{12}})| \simeq |0.53\, b_{12} \sin(2\beta_{PR}^{D_{12}})| \tag{120}$$

Equation (118) implies that only the phase, but not the amplitude, of the effective, double-quantum nutation field depends on $\gamma_{PR}^{D_{12}}$. Thus, powder averaging will result in the higher theoretical efficiency of 73% for the excitation of double-quantum coherence if the experiment is performed on a

powder sample. In practice, the DQ-HORROR experiment is relatively sensitive to RF-amplitude mismatch and chemical shielding offsets.

While the $\omega_r = 2\omega^{RF}$ DQ-HORROR condition selectively recouples dipolar interactions, the homonuclear rotary resonance condition $\omega_r = \omega^{RF}$ leads to single-quantum and double-quantum recoupling, including recoupling of CSA. Accordingly, the homonuclear $n = 1$ R^3 condition with $\omega_r = \omega^{RF}$ has also been called MSD-HORROR (mixed single- and double quantum HORROR)[149] and has been employed to determine the orientation of the two ^{13}C chemical shielding tensors in 2,3-$^{13}C_2$-labelled L-alanine. However, the homonuclear $\omega_r = \omega^{RF}$ resonance condition simultaneously represents a heteronuclear $n = 1$ R^3 condition (see Section 3.1) for recoupling of the residual ^{13}C–^{14}N dipolar coupling in L-alanine as well. Taking a third spin, that is the ^{14}N nucleus, into account it is then possible to determine the absolute orientation of the two ^{13}C chemical shielding tensors in the molecular frame of L-alanine.[149] Obviously, recoupling of the chemical shielding interaction does not necessarily have to be a disadvantage in the context of the homonuclear $n = 1$ R^3/ MSD-HORROR experiment. In fact, it can be utilized to directly determine chemical shielding parameters also in the absence of dipolar coupling interaction(s).[150] The pulse sequence for such a 2D experiment with the $\omega_r = \omega^{RF}$ resonance condition fulfilled is shown in Fig. 30a. During the t_1 period a RF field fulfilling the homonuclear $n = 1$ R^3 condition is applied, leading to recoupling of the chemical shielding interaction of the spins S_i, which are observed during t_2. The resulting 2D spectrum separates the chemical shielding powder patterns of different spins S_i in the ω_1 dimension from isotropic chemical shielding in the ω_2 dimension, thus offering the possibility of determining multiple chemical shielding tensors in a single experiment. Experimental results compared with computer simulations applying AHT and Floquet theory are shown in Fig. 30b. The main advantage of this experiment is its applicability at spinning speeds exceeding the size of the chemical shielding anisotropies, where standard MAS NMR spectra would be virtually free of spinning sidebands. This regime of operation also allows for relatively accurate numerical simulations using the AHT approach (see Fig. 30b).

Sweeping the RF amplitude through the $\omega_r = 2\omega^{RF}$ HORROR condition (similar to the R^2 case with an adiabatically swept MAS frequency) creates an adiabatic version of the HORROR experiment with a theoretical recoupling efficiency of 100%. The DREAM (dipolar recoupling enhancement through amplitude modulation) experiment[151] shares the basic principle with the adiabatic version of the R^2 experiment, APRR[95] (see Section 4.1), but here the RF amplitude gains an additional time dependence ($\omega^{RF} = \omega^{RF}(T)$) which can be considered slow compared to the time dependence of the sample spinning. In an appropriate tilted interaction frame one finds again an average Hamiltonian of the general form[151]

$$\bar{H}^0_{\vartheta} = \chi S^{\vartheta}_z + \omega_{\text{eff}} S^{\vartheta}_x \tag{121}$$

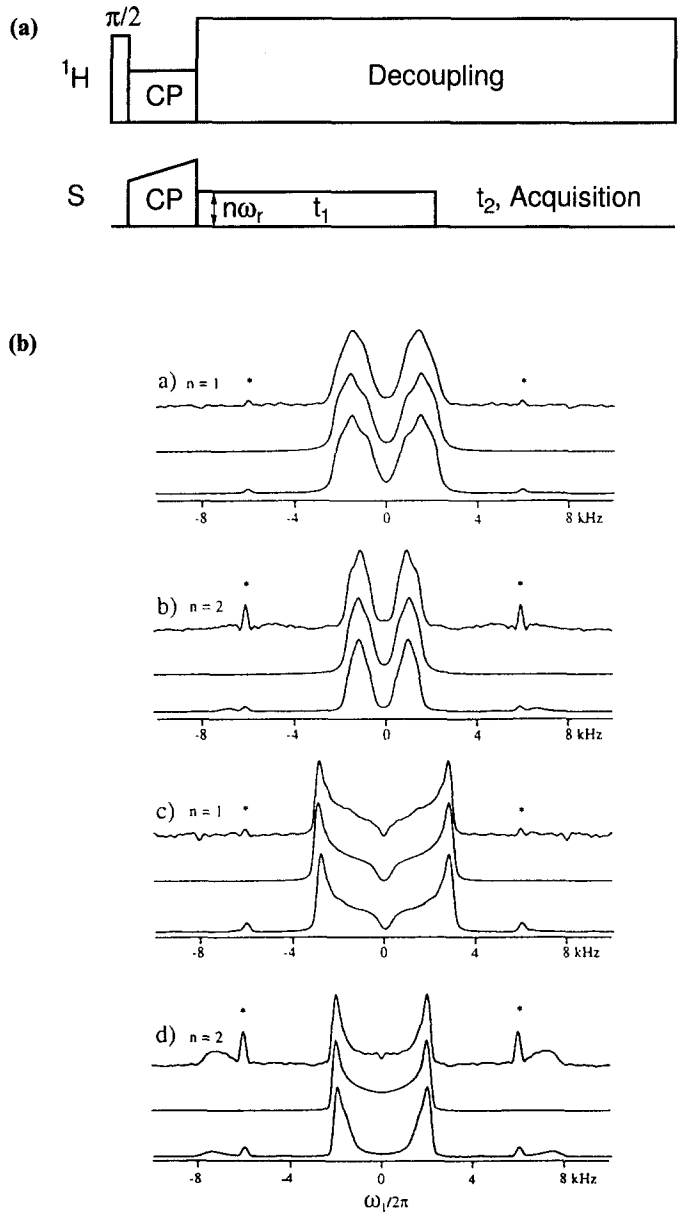

Fig. 30. (a): Pulse sequence of the 2D homonuclear R^3 experiment (where $\omega^{RF} = n\omega_r$) for recoupling of CSA. **(b)**: Experimental and simulated ^{13}C R^3 spectra at the $n = 1, 2$ conditions, obtained for calcium formate (a, b) and hexamethyl benzene (c, d); top traces are experimental spectra, middle and bottom traces are simulated spectra using AHT (middle) or Floquet theory (bottom). (Part (b) reproduced from ref. 150, © 1996, with permission from Elsevier Science.)

where $\chi = \chi(T)$ is weakly time dependent, is large compared to ω_{eff} at $T = 0$ ($\chi(0) \gg \omega_{\text{eff}}$), and changes from $\chi(0)$ to $-\chi(0)$ during the course of the experiment. If the initial density operator is prepared proportional to S_z^{ϑ} and the variation of $\chi(T)$ is performed adiabatically, the density operator will remain parallel to the Hamiltonian during the experiment and end up proportional to $-S_z^{\vartheta}$. The average Hamiltonian for APRR (Eq. (78)) resembles the general Hamiltonian from Eq. (121) for $\vartheta = 23$ (representing a 'zero-quantum Hamiltonian'), while for DREAM one finds $\vartheta = 14$ (i.e. a 'double-quantum Hamiltonian'). The coefficients for DREAM are[151]

$$\chi = \Delta_1(T) + \Delta_2(T) \tag{122}$$

$$\omega_{\text{eff}} = \frac{-3b_{12}}{4\sqrt{2}} \sin(2\beta_{\text{PR}}^{\text{D}_{12}}) Q(\beta_1, \beta_2) \tag{123}$$

where $\Delta_i(T) = \omega_i^{\text{eff}}(T) - \bar{\omega}_i^{\text{eff}}$ represents the generalized HORROR condition with the amplitude of the instantaneous effective fields $\omega_i^{\text{eff}}(T) = ((\omega_{\text{iso}}^{CS_i})^2 + (\omega^{\text{RF}}(T))^2)^{1/2}$ and $\bar{\omega}_i^{\text{eff}} = \omega_i^{\text{eff}}(\tau/2)$. The scaling function

$$Q = \tfrac{1}{3}(1 - \cos(\beta_1)\cos(\beta_2) + 2\sin(\beta_1)\sin(\beta_2)) \tag{124}$$

depends on the tilt angles

$$\beta_i(T) = \tan^{-1}\left(\frac{\omega^{\text{RF}}(T)}{\omega_{\text{iso}}^{\text{CS}_i}}\right) \tag{125}$$

of the effective field and approaches unity if the applied RF field strength is much larger than the isotropic chemical shielding difference ($\omega^{\text{RF}}(T) \gg \omega_{\text{iso}}^{\Delta}$).

Application of the amplitude sweep depicted in Fig. 31a (left trace) to a coupled spin pair will therefore lead to a change of sign of the density operator during the course of the experiment ($\rho(\tau) = -\rho(0)$, see above), while the 'final' density operator after the sweep shown in Fig. 31a (right trace) will be identical to the 'initial' density operator ($\rho(\tau) = \rho(0)$). It follows that subtraction of the first experiment from the second will result in a $2\rho(0)$ difference for a pair of coupled spins. The effective Hamiltonian for uncoupled spins $\bar{H}_{\vartheta}^{0} = \chi S_z^{\vartheta}$, however, commutes at all times with the initial density operator $\rho(0) \sim S_z^{\vartheta}$, so no time evolution takes place ($\rho(\tau) = \rho(0)$) during either of the two amplitude-modulation versions and the difference between the two experiments vanishes for uncoupled spins. Experiments comparing the performance of this so-called DREAM-SPS filter ('DREAM spin-pair selection') with more conventional DQ-DREAM and HORROR filters consisting of excitation and reconversion

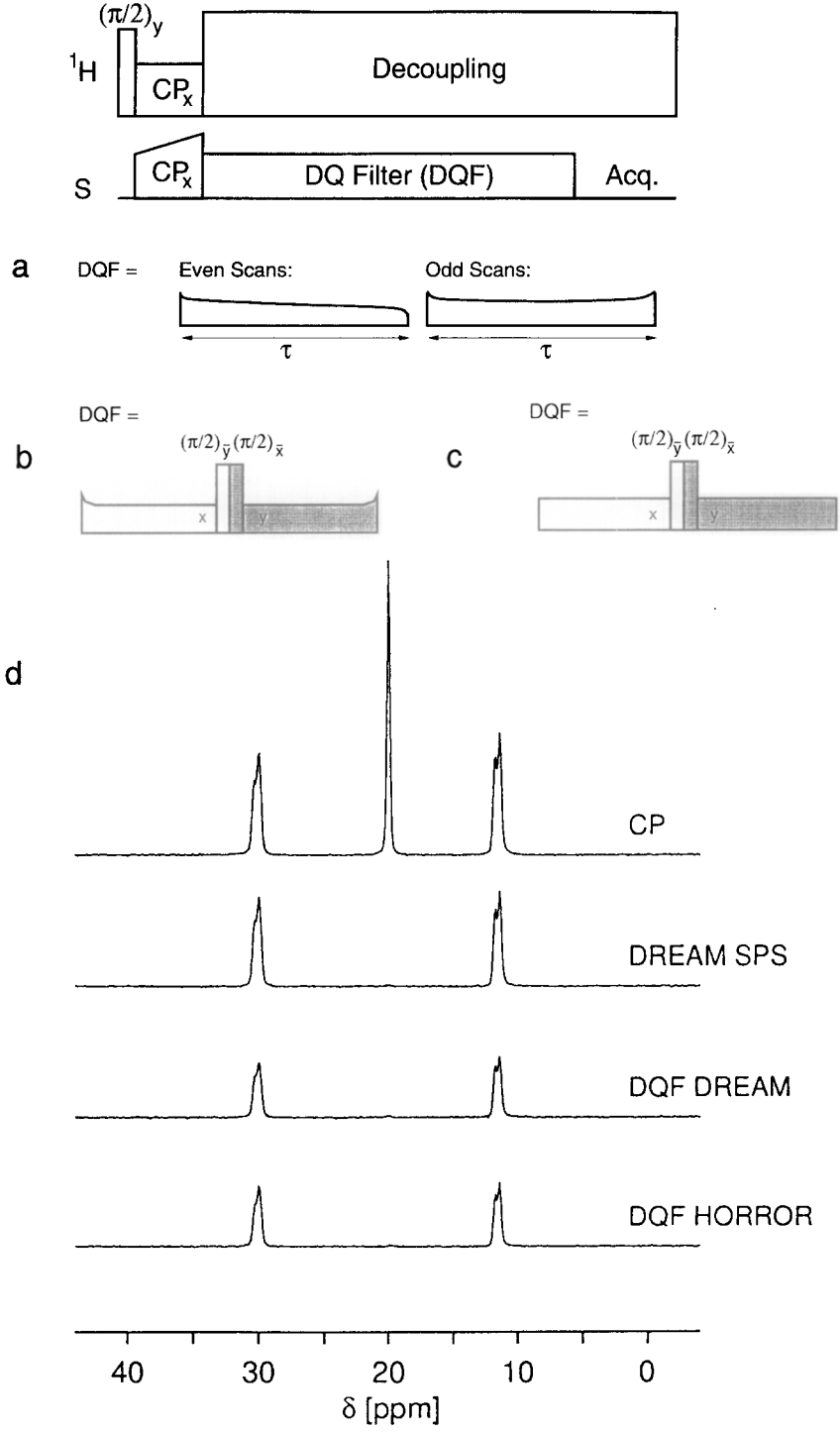

Fig. 31. Pulse sequences for (a) DREAM SPS, (b) DQ-DREAM filtration, (c) DQ-HORROR filtration. The experimental performance of the sequences shown in (a) to (c) is displayed in (d), where experimental ^{13}C NMR data obtained on a mixed sample consisting of 100% 2,3-$^{13}C_2$-labelled sodium propionate and 10% 3-^{13}C-labelled alanine are shown. (Reproduced from ref. 151, © 1998 with permission from Elsevier Science.)

periods (see Figs 31b,c) on a mixture of 100% 2,3-$^{13}C_2$-labelled sodium propionate and 10% labelled (3-$^{13}C_1$)alanine have demonstrated good suppression of single-spin contributions for all three DQ filters, while an efficiency of 80% for DREAM SPS, compared to only 53% efficiency for the two conventional DQ filters, has been achieved (Fig. 31d). Improved stability against mismatches of the DQ-HORROR condition has been found for DREAM-SPS, and it has been pointed out that DREAM-SPS will perform best with increasing spinning frequencies.[151]

Reduced sensitivity to RF mismatch and chemical shielding contributions is also provided by the general pulse sequence shown in Fig. 32a, which allows selections of 'wanted' and suppression of 'unwanted' interaction terms in the average Hamiltonian by adjusting the number n of phase-shifted elements that are implemented over N rotation periods. The Hamiltonian of such a Cn

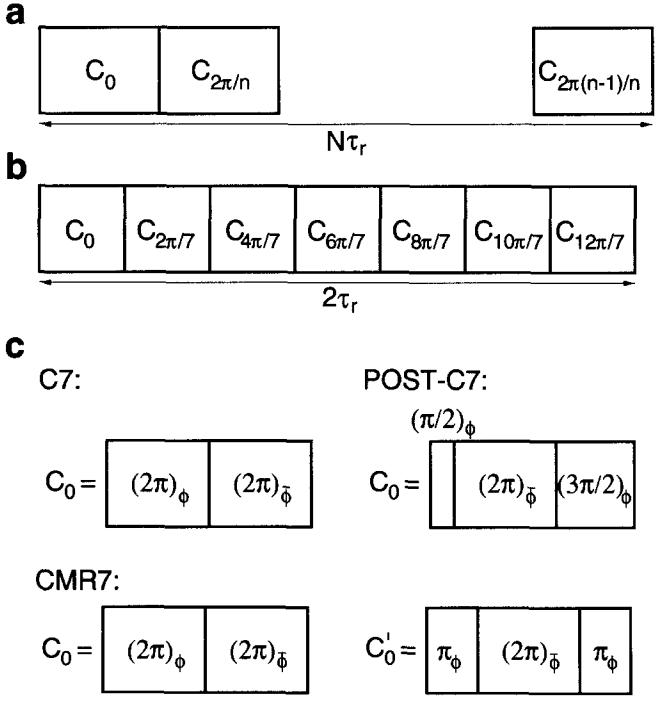

Fig. 32. (a) General Cn-pulse sequence with n phase-shifted elements implemented over N rotation periods. (b) The C7 sequence with $n = 7$ and $N = 2$.[148] (c) The cycles shown represent the C elements of the original C7 sequence,[148] the POST-C7 sequence,[152] and the CMR7 sequence,[153] respectively.

experiment in the interaction frame of the RF field may be written as[148]

$$H_{\mathrm{I}} = \sum_{\kappa} \sum_{\lambda\mu lm} \tilde{\omega}^{\kappa}_{\lambda\mu lm}(t - t_p^0) \exp(\mathrm{i}2\pi(Nm - \mu)p/n) T^{\kappa}_{\lambda\mu} \tag{126}$$

where

$$\tilde{\omega}^{\kappa}_{\lambda\mu lm}(\tau) = i^{\mu} d^{\lambda}_{\mu 0}(-\beta^{\mathrm{RF}}(\tau)) \omega^{\kappa}_{\lambda\mu \mathrm{lm}} \exp(im\omega_{\mathrm{r}}(\tau + t^0)) \tag{127}$$

and β^{RF} is the overall spin-rotation angle induced by the RF field. The spin tensor operators $T^{\kappa}_{\lambda\mu}$[3,8,13] and the coefficients $\omega^{\kappa}_{\lambda\mu lm}(t)$ in Eqs (126) and (127) represent the spin and spatial parts, respectively of the Hamiltonian

$$H^{\kappa}(t) = \sum_{\lambda\mu lm} \omega^{\kappa}_{\lambda\mu lm}(t) T^{\kappa}_{\lambda\mu} \tag{128}$$

of the interaction.

The average over the pth cycle can easily be calculated as

$$\bar{H}^0_{\mathrm{I},p} = \sum_{\kappa} \sum_{\lambda\mu lm} \bar{\omega}^{\kappa}_{\lambda\mu lm} \exp(\mathrm{i}2\pi(Nm - \mu)p/n) T^{\kappa}_{\lambda\mu} \tag{129}$$

with

$$\bar{\omega}^{\kappa}_{\lambda\mu lm} = \frac{1}{\tau_{\mathrm{c}}} \int_0^{\tau_{\mathrm{c}}} \tilde{\omega}^{\kappa}_{\lambda\mu lm}(\tau)\, \mathrm{d}\tau \tag{130}$$

The chemical shift terms $\bar{\omega}^{\mathrm{CS}_i}_{1\mu 0}$ are averaged to zero already for the individual cycles and the average Hamiltonian over the complete cycle becomes

$$\bar{H}^0_{\mathrm{I}} = \sum_{\kappa} \sum_{\lambda\mu lm} \bar{\omega}^{\kappa}_{\lambda\mu lm} T^{\kappa}_{\lambda\mu} \delta(Nm - \mu = nk) \tag{131}$$

where k is an arbitrary integer and the δ function is 1 if the condition is fulfilled and zero otherwise. As the number of cycles n and the number of rotation periods N are experimentally adjustable parameters, one can now utilize Eq. (131) to select the required interaction terms. The MELODRAMA[138] sequence, for instance, corresponds to $N = 2$ and $n = 4$, which leads to an average Hamiltonian containing DQ terms only. The DQ-nutation frequency, however, still depends on the angle $\gamma^{\mathrm{D}_{12}}_{\mathrm{PR}}$ for this choice of $N = 2$ and $n = 4$. The smallest pair of numbers selecting solely DQ terms *and* depending on $\beta^{\mathrm{D}_{12}}_{\mathrm{PR}}$ only,

is $N=2$ and $n=7$ (i.e. C7[148] (Fig. 32b)). The complete average Hamiltonian for $N=2$ and $n=7$ (ignoring J-coupling) is

$$\bar{H}_I^0 = \bar{\omega}_{2221}^{D_{12}} T_{22}^{D_{12}} + \bar{\omega}_{2-22-1}^{D_{12}} T_{2-2}^{D_{12}} \tag{132}$$

with

$$\bar{\omega}_{2\pm 22\pm 1}^{D_{12}} = \frac{343(i+\exp(i\pi/14))}{520\pi\sqrt{2}}\, b_{12}\, \exp(i(\omega_r t^0 - \gamma_{PR}^{D_{12}}))\, \sin(2\beta_{PR}^{D_{12}}) \tag{133}$$

If we choose $t^0=0$ and use single-transition operators for ease of comparison, we can rewrite this as

$$\bar{H}_I^0 = \bar{\omega}_D(\beta_{PR}^{D_{12}})(\tfrac{1}{2} S_-^{14} \exp(-i\gamma_{PR}^{D_{12}}) + \tfrac{1}{2} S_+^{14} \exp(-i\gamma_{PR}^{D_{12}})) \tag{134}$$

with

$$\bar{\omega}_D(\beta_{PR}^{D_{12}}) = \frac{343(i+\exp(i\pi/14))}{520\pi\sqrt{2}}\, b_{12}\, \sin(2\beta_{PR}^{D_{12}}) \tag{135}$$

The lowest-order average Hamiltonian for C7 (Eq. (135)) is identical with that for DQ-HORROR, except that the effective dipolar scaling factor

$$|\,\bar{\omega}_D(\beta_{PR}^{D_{12}})\,| \simeq |\,0{\cdot}23\, b_{12}\, \sin(2\beta_{PR}^{D_{12}})\,| \tag{136}$$

is smaller by a factor of 2.3 than for DQ-HORROR. The C7 sequence, however, is better compensated for chemical shielding effects and RF inhomogeneities. This can in part be explained by the fact that the more important chemical shielding terms are averaged over a single cycle C. Calculation of higher-order terms[152] not only provides a deeper analysis but also enables the design of even better compensated sequences by utilizing yet another degree of freedom. To obtain the average Hamiltonian of Eq. (134) it was only required that the C elements represent a cycle.[14,148] For the conventional C7 sequence, the cycle consists of two 2π pulses with opposite phase ($2\pi_\phi 2\pi_{\phi+\pi}$). However, other cycles leading to even better-compensated sequences have been derived (Fig. 32c).

The POST-C7 (permutationally offset stabilized C7) sequence[152] applies the cycle $(\pi/2)_\phi 2\pi_{\phi+\pi}(3\pi/2)_\phi$, which effectively cancels isotropic resonance offsets up to fourth order and cross terms between isotropic resonance offsets and RF inhomogeneity up to third order. POST-C7 thus represents an improvement by two perturbation orders compared to the original $2\pi_\phi 2\pi_{\phi+\pi}$ cycle regarding both resonance-offset and cross-term compensation. The effective dipolar

scaling factor for POST-C7, however, remains the same as for C7 (Eq. (136)) as the number of cycles ($n = 7$) and the number of rotation periods ($N = 2$) are unchanged. The same is true for the CMR7 (combined MLEV refocusing and C7) sequence.[153] CMR7 employs a supercycle combining the original $2\pi_\phi 2\pi_{\phi+\pi}$ cycle with a $\pi_\phi 2\pi_{\phi+\pi}\pi_\phi$ cycle (Fig. 32c), which again results in a better-compensated sequence. A comparison of experimentally determined offset dependences for C7, POST-C7 and CMR7 is shown in Fig. 33. The robust practical performance of CMR7 has been demonstrated in a 2D ^{13}C–^{13}C correlation experiment on the antibiotic (U-^{13}C)erythromycin A. This compound consists of a 14-membered lactone ring with two sugar ligands attached, amounting to 21 fully assigned ^{13}C resonances.[153]

When applied to longitudinal magnetization, the C7 sequence in general excites even-order multiple (double)-quantum coherences. Applying C7 to transverse magnetization, in general leads to excitation of odd-order multiple-quantum coherences. Using POST-C7, ^{13}C triple-quantum coherence in fully ^{13}C-labelled L-alanine has been excited in this way, with a triple-quantum filter efficiency of ~8% for the central and ~4% for the two peripheral ^{13}C spins.[154]

The original C7 sequence[148] has served as the basic building block for excitation and reconversion of DQ coherence in a number of 2D correlation experiments. Operating in a regime of relatively short C7 excitation periods, several ^{31}P SQ–DQ correlation experiments on anhydrous inorganic solids have been reported. These applications include the distinction of different polymorphs in a $Mg_2P_2O_7$ sample,[155] the demonstration of major structural reorganization during the crystallization of vitreous $Li_4P_2S_7$ to $Li_4P_2S_6$,[156] and the assignment of all ^{31}P resonances to the six crystallographically distinct P sites in polycrystalline $Cd_3(PO_4)_2$.[157] The contour plot of a ^{31}P 2D SQ–DQ correlation experiment on $Cd_3(PO_4)_2$ is shown in Fig. 34. Also aiming at spectral assignment, this 2D approach employing short excitation periods has recently been applied to ^{13}C spin systems in multiply ^{13}C-labelled organic solids.[158] ^1H SQ-DQ correlation experiments have been used to investigate the extent of cross linking in a series of differently prepared elastomers[159] and to study the chain dynamics in a polybutadiene melt.[160] These C7-based ^1H and ^{31}P experiments have all been executed at relatively high spinning frequencies, in the MAS range 10–15 kHz. For single-frequency experiments without the need to apply high-power ^1H decoupling throughout the pulse sequence, the constraints of prohibitively high power-level input to the probe at higher MAS frequencies are much relaxed as compared to ^{13}C C7 applications on organic solids.

A pulse sequence aiming at reducing the power-level limitations for applications of C7-type experiments on organic solids at higher MAS frequencies has recently been introduced. We have pointed out already that $N = 2$ and $n = 7$ is the minimum requirement to construct a Cn sequence that selects only DQ terms and is independent of $\gamma_{PR}^{D_{12}}$, as is exploited in C7, POST-C7 and CMR7. Experimentally, $n = 7$ is a problematic aspect of these

sequences since at higher MAS frequencies prohibitively high ^{1}H-decoupling levels become necessary. SPC-5 (supercycled POST C5)[161] relaxes these limitations by reducing n to 5 without sacrificing the favourable $\gamma_{PR}^{D_{12}}$-encoded and CSA-compensation properties of the C7 sequences. Circumventing the 'magic' number $n = 7$ becomes possible by concatenating two C7-type cycles

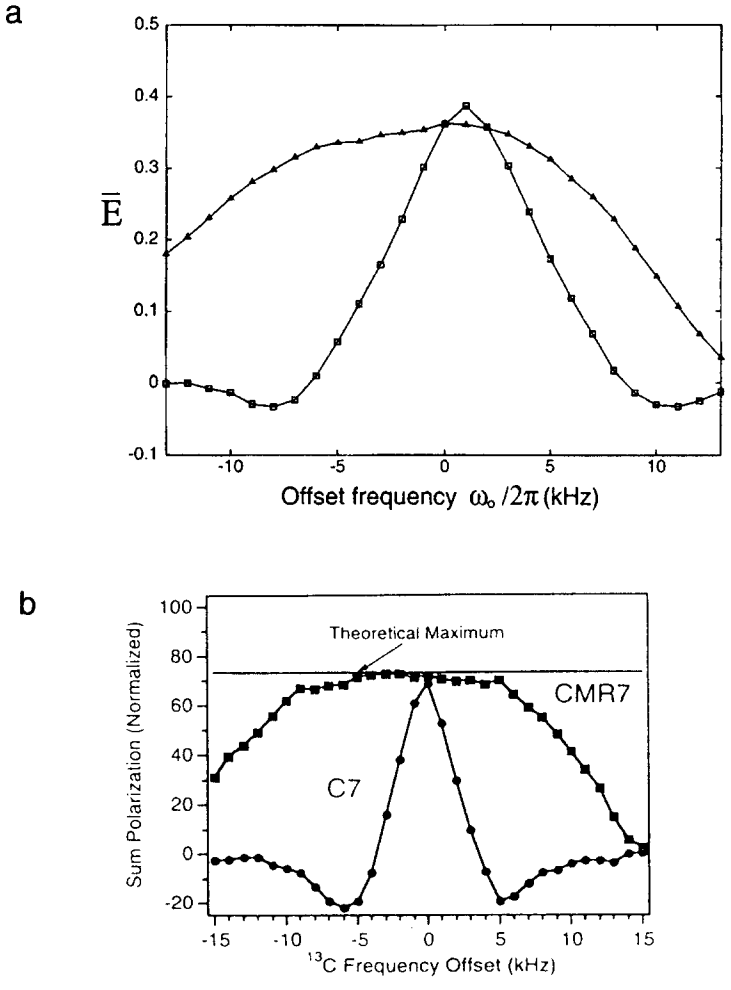

Fig. 33. Comparison of DQ-transfer efficiencies as a function of offset frequency for C7,[148] POST-C7,[152] and CMR7.[153] (a) Comparison of C7 (squares) vs POST-C7 (triangles), based on experimental ^{13}C NMR data acquired on a sample of 2,2′-$^{13}C_2$-labelled diammonium fumarate, DAF (see Fig. 37).[152] (b) Comparison of C7 (circles) vs. CMR7 (squares), based on experimental ^{13}C NMR data acquired on a sample of U-^{13}C,^{15}N-labelled glycine.[153] (Reproduced with permission from ref. 152, © 1998, American Institute of Physics and ref. 153, © 1998, American Chemical Society.)

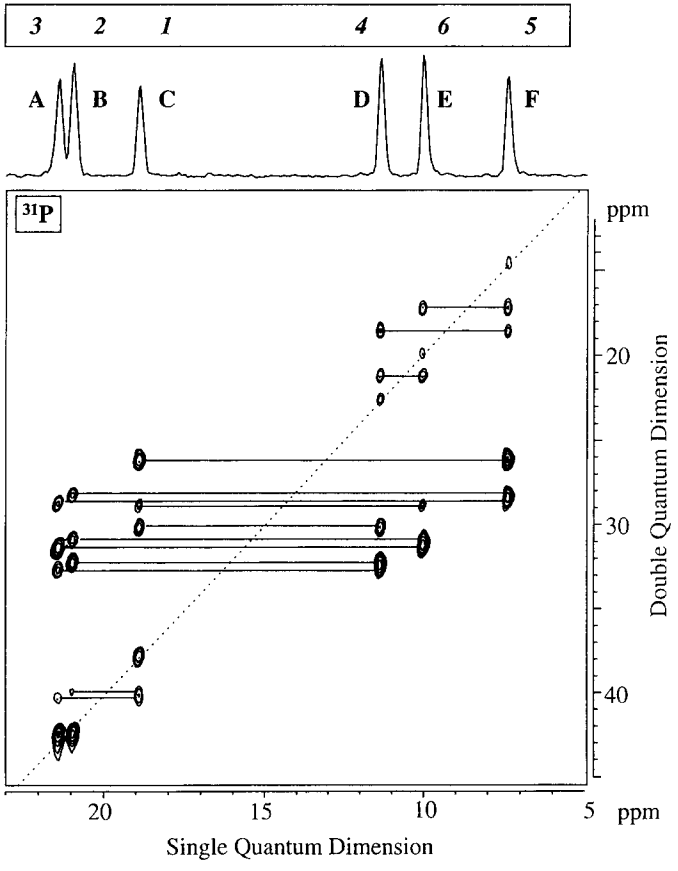

Fig. 34. Contour plot of an SQ-DQ MAS 2D ^{31}P correlation experiment on $Cd_3(PO_4)_2$ where the C7 sequence[148] has been used to excite and reconvert ^{31}P DQ coherences. DQ coherences between ^{31}P resonances A to F are indicated; note 'self connectivities' displayed along the diagonal. The resulting assignment of ^{31}P resonances A to F to the six crystallographic P sites 1 to 6 is identical to the assignment derived from ^{31}P RIL experiments on $Cd_3(PO_4)_2$ (see Fig. 24). (Reproduced with permission from ref. 157, © 1997, American Chemical Society.)

with an overall phase shift Φ, as illustrated in Fig. 35. Overall, SPC-5 thus reduces the matching requirement from $\omega_S^{RF} = 7\omega_r$ for the C7 sequences to $\omega_S^{RF} = 5\omega_r$ and accordingly also reduces the power requirements for sufficiently off-match ^1H decoupling. The experimental performance of SPC-5 has been demonstrated on U-^{13}C-labelled samples of sucrose and L-alanine.[161]

To conclude this section on recoupling of homonuclear dipolar interactions under MAS conditions, a few general remarks seem in place. The performances of some of the homonuclear dipolar recoupling sequences discussed here have

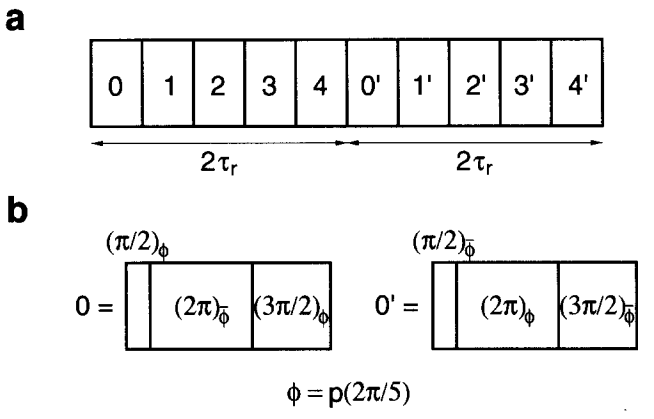

Fig. 35. The SPC-5 pulse sequence (a), incorporating phase-shifted POST-C7 cycles (b).[161]

recently been compared by numerical methods,[162] with an emphasis on 'broadbandedness' and off-set compensation properties of the various recoupling sequences. Indeed, it is fortunate that the currently existing collection of recoupling methods ranges from extremely narrowband/selective (such as R^2) to quite broadband (such as POST-C7, RIL). This leaves us with the problem of choosing the most promising experimental technique to solve a given task. Obviously, this best choice depends on the properties of the spin system at hand and on the nature of the problem to be solved. In this context, 'broadbandedness' of the recoupling sequence is only one of several selection criteria. For more than purely aesthetic reasons, the recoupling sequence should provide a 'clean' Hamiltonian, either for the zero-quantum or the double-quantum subspace, as this avoids unnecessary approximations. Also with a view to the Hamiltonian, low orientation dependence is desirable as this promises the highest theoretical recoupling efficiency. This point is, however, closely linked to the effective dipolar scaling factor of a recoupling sequence. There may be application circumstances where fast build-up rates provided by a large effective scaling factor outweigh the argument of high recoupling efficiency – but there may equally well be circumstances where a slower build-up rate in conjunction with high recoupling efficiency is more desirable. From an experimental point of view, the RF-power requirements of a recoupling sequence at a given necessary MAS frequency are an important consideration: little is gained if, for instance, good CSA compensation can only be obtained at the price of burning the probe (or sample). *The* ideal homonuclear recoupling sequence would have to combine high efficiency with a large effective scaling factor, while working well at modest power levels. *The* ideal, all-purpose homonuclear recoupling sequence does not (yet) exist; for the time being we have no choice but sometimes to choose between two evils.

Given the rapid developments in this area, however, it takes only little optimism to predict that some or many of the remaining evils will disappear over the next few years.

5. HYBRID EXPERIMENTS AND OTHER BORDERLINE CROSSINGS

The progress made with both homonuclear and heteronuclear MAS dipolar recoupling techniques has triggered further developments. By combining homonuclear and heteronuclear dipolar recoupling sequences into single experiments, new families of 2D and pseudo-2D experiments have been created. These 'hybrid' experiments follow the spirit of separated local field (SLF) spectroscopy[3] and generally aim at correlating two interaction tensors with each other. More specifically, the goal is to directly obtain information on molecular conformational properties, such as torsion angles around specific chemical bond directions, in a model-free manner by experimentally determining the mutual orientation of, e.g., two dipolar coupling tensors.

Strategies have been developed to experimentally determine the mutual orientation of Y–X or Z–Y dipolar coupling tensors in Y–X–X–Y or Y–X–Z–Y fragments in order to directly derive molecular torsional angles. We will take the pulse sequence depicted in Fig. 36[163] as the prototype example for a whole range of experiments, all dedicated to directly correlating Y–X or Z–Y dipolar coupling tensors in molecular fragments under MAS conditions. The pulse scheme as depicted in Fig. 36 is applicable to $^{1}H—^{13}C\cdots{}^{13}C—^{1}H$ fragments. In this scheme, C7 is used to excite and reconvert ^{13}C DQ coherence under MAS conditions and ^{1}H MREV-8 decoupling serves to establish local heteronuclear $^{1}H-^{13}C$ dipolar couplings under which the ^{13}C DQ coherence evolves. Accordingly, this type of experiment is referred to as

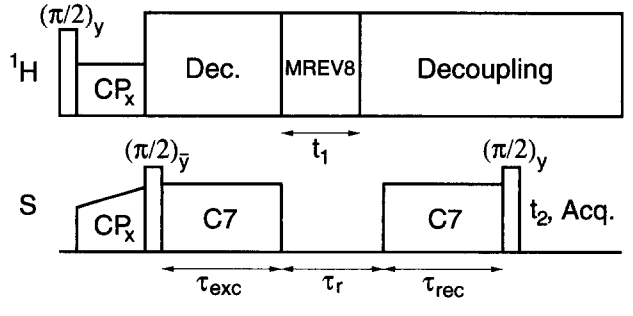

Fig. 36. Pulse sequence for direct determination of $^{1}H—^{13}C\cdots{}^{13}C—^{1}H$ molecular torsion angles by heteronuclear $^{1}H-^{13}C$ dipolar modulation of ^{13}C DQ coherence.[163] The scheme employs the C7 sequence[148] for excitation and reconversion of DQ coherence; homonuclear ^{1}H MREV-8 decoupling is applied during the variable period t_1; see text for explanation.

double-quantum heteronuclear local field spectroscopy (DQ-HLF).[163] Note that alternative approaches to determining torsional angles in $^{1}H—^{13}C...^{13}C—^{1}H$ moieties have been proposed (combining the USEME sequence with BLEW-12 ^{1}H decoupling in a 3D experiment).[164] Liquid-state NMR versions[165] and schemes applicable to static powder samples,[166] closely related to the pulse sequence depicted in Fig. 36 also exist.

The ^{13}C spin dynamics evolving under the regime of the pulse sequence shown in Fig. 36 are as follows. A $\pi/2$ pulse rotates the ^{13}C transverse magnetization, obtained after cross polarization, to the z-axis. The C7 sequence converts this z-magnetization in the next step to double-quantum coherence, which then evolves for an interval $\tau = \tau_r$. A subsequent C7 interval reconverts the double-quantum coherence back to z-magnetization, which is finally converted to observable magnetization by another $\pi/2$ pulse. The relevant double-quantum spin dynamics take place in the interval τ, which is divided into two parts. During the first sub-interval of variable duration t_1 homonuclear ^{1}H MREV-8 decoupling is applied, while during the second sub-interval of duration $\tau_r - t_1$ the ^{13}C spins are decoupled from ^{1}H spins by high-power ^{1}H decoupling. DQ coherence evolves independently from homonuclear couplings at the sum of the chemical shieldings in the high-field limit, the ^{13}C CSA is averaged to zero over a full rotation period, and effects from isotropic chemical shieldings may be removed by setting the ^{13}C RF carrier frequency to the mean of the two isotropic chemical shielding frequencies. This leaves heteronuclear $^{1}H-^{13}C$ dipolar couplings (scaled by a factor $\kappa < 1$ owing to MREV-8 ^{1}H decoupling) as the only interactions to be taken into account to describe the evolution of the ^{13}C DQ coherence during the variable interval t_1, while in the second interval $(\tau_r - t_1)$ heteronuclear $^{1}H-^{13}C$ couplings are also suppressed. It follows that the resulting double-quantum-filtered ^{13}C signal amplitudes depend only on the heteronuclear $^{13}C-^{1}H$ couplings. The following equation for the modulated signal amplitudes $a(t_1)$ has been given[163] as

$$a(t_1) = \langle \tfrac{1}{2} \sin^2(\bar{\omega}_D \tau_{exc})[\cos(\Phi^{\frac{1}{2},\frac{1}{2}}(t_1)) + \cos(\Phi^{\frac{1}{2},-\frac{1}{2}}(t_1))] \rangle \qquad (137)$$

where $\langle ... \rangle$ denotes powder averaging, $\bar{\omega}_D$ is given for the C7 sequence by Eq. (135) and the phase angles $\Phi^{m_1 m_2}$ are

$$\Phi^{m_1,m_2}(t) = 2\kappa \int_0^t \{m_1[\omega_{21}^D(t') + \omega_{24}^D(t') + \omega_{31}^D(t') + \omega_{34}^D(t')]\}\, dt' \qquad (138)$$

where we have used the numbering scheme 1 to 4 for the $^{1}H—^{13}C2—^{13}C3—^{1}H4$ moiety. Figure 37 shows experimentally acquired plots of amplitudes $a(t_1)$ for the two model compounds ammonium (2,2′-$^{13}C_2$)maleate (AHM) and diammonium (2,2′-$^{13}C_2$)fumarate (DAF) where the $^{1}H—^{13}C=^{13}C—^{1}H$ moieties are in *cis* and *trans* conformation, respectively. The *trans* geometry of

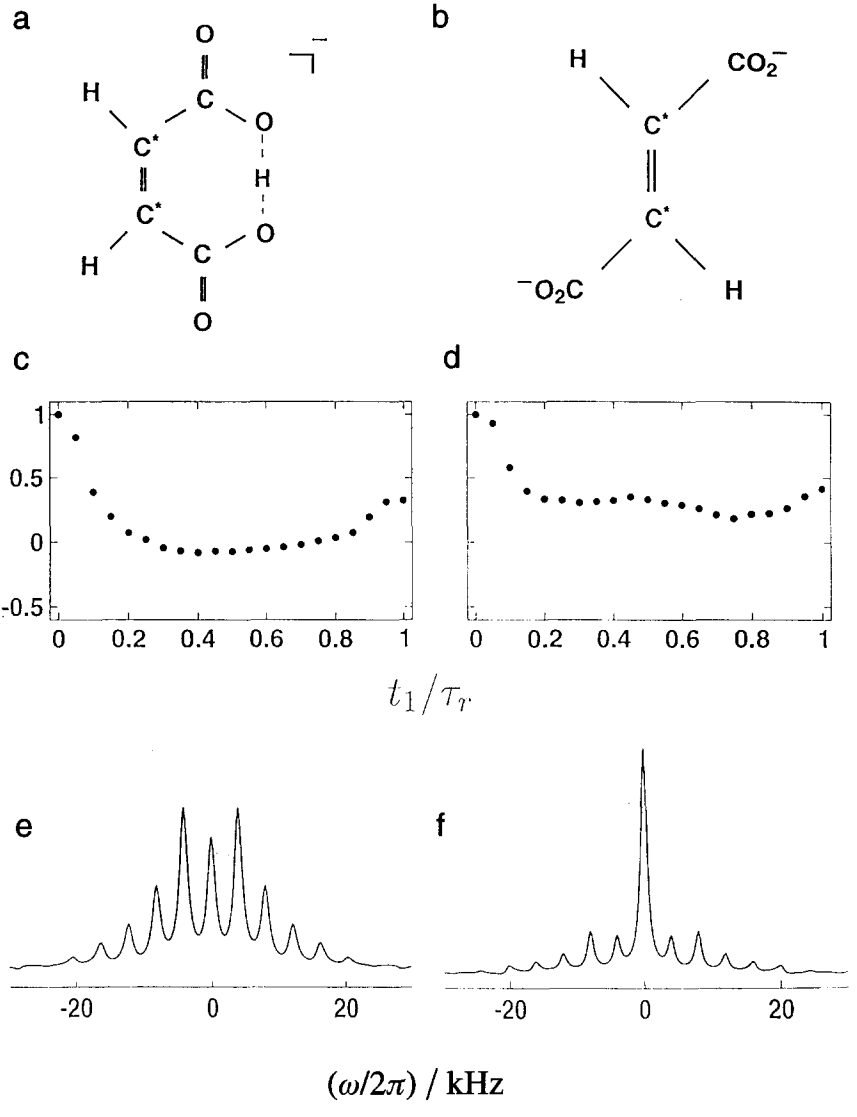

Fig. 37. Experimental ^{13}C NMR results, applying the pulse sequence shown in Fig. 36 to determine the $^{1}H—^{13}C=^{13}C—^{1}H$ torsion angles in (a) mono-ammonium maleate (AHM) and (b) diammonium fumarate (DAF). Plots of DQ-filtered signal amplitudes $a(t_1)$ for AHM (c) and DAF (d). DQ spinning sideband patterns for AHM (e) and DAF (f), obtained after Fourier transformation of the time-domain data shown in (c, d) as described in ref. 163. (Reproduced from ref. 163, © 1996, with permission from Elsevier Science.)

DAF was found within an error of $\pm 10°$ and the *cis* geometry of AHM within $\pm 20°$ by adjusting $a(t_1)$ curves calculated according to Eq. (137) to the experimental data.[163] The method allowed determination of the $^1H—^{13}C10—^{13}C11—^1H$ torsional angle in the retinylidene chromophore of rhodopsin as $160° \pm 10°$.[167]

The principles of DQ-HLF spectroscopy are not only applicable to $^1H—X\cdots X—^1H$ fragments; similar approaches can be taken to determine torsional angles in other $Y—X\cdots X—Y$ fragments such as $^{15}N—^{13}C\ldots{}^{13}C—^{15}N$. For example, C7 to excite/reconvert ^{13}C DQ coherence, in combination with REDOR for recoupling of the $^{15}N-^{13}C$ heteronuclear dipolar couplings during t_1, has been used to determine a $^{15}N—^{13}C—^{13}C—^{15}N$ torsional angle in the backbone of a $^{15}N_2,^{13}C_2$-labelled tripeptide (GlyGly-Gly) · HCl.[168] Similarly, another set of homonuclear and heteronuclear recoupling sequences (MELODRAMA combined with SPI-R^3) serves the same purpose and has been applied to determine the backbone $^{15}N—^{13}C—^{13}C—^{15}N$ torsional angle in GlyGly · HCl.[20] The DQ-HLF approach has been further extended to include $^1H—X\cdots Z—^1H$ fragments where heteronuclear X–Z DQ coherence, evolving under the influence of the $X-^1H$ and $Z-^1H$ dipolar interactions is monitored to directly obtain molecular torsional angles. Examples of this approach relate to the $^1H—^{15}N\cdots{}^{13}C—^1H$ fragment where REDOR-like $^{15}N-^{13}C$ dipolar recoupling is combined with ^1H MREV-8 decoupling.[169,170] A direct extraction of the dihedral angle relating the $^1H-^{15}N$ and $^1H-^{13}C$ dipolar coupling tensors was also performed by correlating the two tensors in a 2D correlation experiment, incorporating ramped $^{15}N-^{13}C$ cross polarization in the mixing time and the RHEDS[171] homonuclear decoupling sequence during the t_1 and t_2 periods.[172]

The dipolar coupling interaction is directly and unambiguously related to molecular structure. Knowledge of the mutual orientation of dipolar coupling tensors is therefore equivalent to knowledge about molecular geometry. The same is not quite true for the chemical shielding interaction in general. Chemical shielding tensors are not *a priori* oriented along certain molecular axes. Determination of molecular torsion angles, based on correlations of CSA with dipolar coupling tensors, therefore requires additional information regarding the orientation of chemical shielding tensors in the molecular frame. 2D experiments following a CSA/dipolar coupling tensor correlation approach also have been developed. By combining selective ^{13}C excitation, USEME homonuclear recoupling and BLEW-12 ^1H decoupling, the mutual orientation of the carboxyl-^{13}C CSA and the $^1H_\alpha-^{13}C_\alpha$ dipolar coupling tensor in ^{13}C-labelled alanine has been determined.[173] The backbone torsion angle Φ in the model peptide *N*-acetyl-DL-valine has been derived from a correlation of the amide-^{15}N CSA and the $^1H_\alpha-^{13}C_\alpha$ dipolar coupling tensor, with MREV-8 ^1H decoupling and $^{13}C-^{15}N$ REDOR recoupling providing the building blocks of the 2D correlation experiment.[174] Recently, $2\pi/5$ phase-shifted frequency-switched Lee–Goldburg irradiation schemes, applicable at either the ^1H or ^{13}C Larmor

frequency, have been introduced.[175] Depending on the irradiation mode chosen, these pulse schemes recouple the CSA and/or heteronuclear dipolar interactions while simultaneously leading to homonuclear decoupling of the irradiated spin species. Accordingly, such phase- and frequency-shifted Lee-Goldburg irradiation schemes provide a possibility to extend 'torsion-angle' $^{1}H/^{13}C$ MAS NMR experiments from selectively to multiply labelled samples.[175]

Another area in which the borderlines between the worlds of homonuclear and heteronuclear dipolar interactions under MAS conditions begin to gradually smear out is the topic of heteronuclear dipolar (predominantly ^{1}H) decoupling under (fast) MAS conditions. To illustrate the intricate relationships between decoupling and recoupling under MAS conditions, take the heteronuclear R^3 experiment as an example: application of a sufficiently strong, on-resonance RF field ω_2^{RF} results in decoupling of S_2 from S_1, while an RF field ω_2^{RF} matched to an integer multiple of the spinning frequency ($\omega_2^{RF} = n\omega_r$) leads to recoupling of the dipolar coupling and CSA S_1-S_2 interactions. Moving to higher MAS frequencies and external magnetic field strengths, the limitations and shortcomings of heteronuclear CW ^{1}H decoupling have become more obvious. Satisfactory ^{1}H decoupling performance, however, is a necessary prerequisite for the vast majority of MAS NMR applications. The importance of the homogeneous nature of the ^{1}H spin system in achieving efficient heteronuclear ^{1}H decoupling has repeatedly been pointed out.[8,54,176–179] Fast MAS conditions and high external magnetic field strengths tend to diminish the homogeneous character of the ^{1}H spin systems in typical solids and lead to residual broadening or even splitting in rare-spin NMR spectra obtained under MAS and CW ^{1}H-decoupling conditions. Phase-modulated[54,176] as well as frequency- and phase-modulated[178] decoupling schemes have been introduced to remedy this CW ^{1}H-decoupling problem. In practice, the TPPM[54] scheme in particular has so far been employed successfully. In addition to the occurrence of off-resonance decoupling effects, the origin of residual broadening or splitting in rare-spin MAS NMR spectra under on-resonance CW ^{1}H-decoupling conditions has been traced back to second-order recoupling between the heteronuclear dipolar coupling tensors and the (irradiated) ^{1}H chemical shielding tensors.[177] Consistent with this explanation, modulated decoupling schemes usually provide improved decoupling performance compared to CW decoupling by restoring (some of) the homogeneous ^{1}H spin system characteristics. The beneficial side-effects of active homonuclear $^{1}H-^{1}H$ recoupling on the ^{1}H heteronuclear decoupling performance of modulated decoupling schemes has been demonstrated.[180]

Notes added in proof

Since the submission of this manuscript several further papers related to various subjects of this review (REDOR,[181–187] Rotational Resonance,[188–191]

DRAWS,[192–194] BABA,[195] and C7[196,197]) have appeared in the literature. The accuracy of distance determinations by homonuclear or heteronuclear dipolar recoupling experiments in complex spin systems has been investigated.[198]

ACKNOWLEDGEMENTS

Support of our work by the Deutsche Forschungsgemeinschaft, the Fonds der Chemischen Industrie, and the Swedish Natural Science Research Foundation is gratefully acknowledged. We are grateful to the Division of Physical Chemistry, Stockholm University, for the hospitality extended to us during the writing of this article. We would like to thank M. Bechmann (Bayreuth), A. Brinkmann, M. Edén, T. Karlsson, and M. H. Levitt (Stockholm) for their suggestions and for scientific discussions, and J. Kümmerlen (Bayreuth) for his logistical support. Proof-reading in 'pedantic mode' of the manuscript by M. Edén (Stockholm), X. Helluy (Bayreuth), and C. Marichal (Mulhouse) is much appreciated.

REFERENCES

1. L. Frydman and J. S. Harwood, *J. Am. Chem. Soc.*, 1995, **117**, 5367.
2. A. Medek, J. S. Harwood and L. Frydman, *J. Am. Chem. Soc., 1995*, **117**, 12779.
3. R. R. Ernst, G. Bodenhausen and A. Wokaun, *Principles of Nuclear Magnetic Resonance in One and Two Dimensions*, Clarendon Press, Oxford, 1987.
4. W. R. Croasmun and R. M. K. Carlson, *Two-Dimensional NMR Spectroscopy*, VCH, New York, 1994.
5. A. E. Bennett, R. G. Griffin and S. Vega, Recoupling of homo- and heteronuclear dipolar interactions in rotating solids, in *NMR Basic Principles and Progress*, vol. 33, pp. 3–77, Springer-Verlag, Berlin, 1994.
6. A. Abragam, *The Principles of Nuclear Magnetism*, Clarendon Press, Oxford, 1961.
7. C. P. Slichter, *Principles of Magnetic Resonance*, 3rd edn, Springer-Verlag, Berlin, 1990.
8. M. Mehring, *Principles of High Resolution NMR in Solids*, Springer-Verlag, Berlin, 1983.
9. U. Haeberlen (Waugh, J. S., ed), *Adv. Magn. Reson.*, Suppl. 1, 1976.
10. A. Wokaun and R. R. Ernst, *J. Chem. Phys.*, 1977, **67**, 1752.
11. S. Vega, *J. Chem. Phys.*, 1978, **68**, 5518.
12. M. H. Levitt, D. P. Raleigh, F. Creuzet and R. G. Griffin, *J. Chem. Phys.*, 1990, **92**, 6347.
13. B. H. Meier, '*Polarization Transfer and Spin Diffusion in Solid-State NMR*', in: *Advances in Magnetic and Optical Resonance*, vol. 18, pp. 1–116, Ed. W. S. Warren, Academic Press, New York, 1994.
14. U. Haeberlen and J. S. Waugh, *Phys. Rev.*, 1968, **175**, 453.
15. M. M. Maricq and J. S. Waugh, *J. Chem. Phys.*, 1979, **70**, 3300.
16. M. Hohwy and N. C. Nielsen, *J. Chem. Phys.*, 1997, **106**, 7571.
17. M. Hohwy and N. C. Nielsen, *J. Chem. Phys.*, 1998, **109**, 3780.
18. M. H. Levitt, T. G. Oas and R. G. Griffin, *Isr. J. Chem.*, 1988, **28**, 271.
19. T. G. Oas, M. H. Levitt and R. G. Griffin, *J. Chem. Phys.*, 1988, **89**, 692.
20. P. R. Costa, J. D. Gross, M. Hong and R. G. Griffin, *Chem. Phys. Lett.*, 1997, **280**, 95.

21. M. Bechmann, S. Dusold, H. Förster, U. Haeberlen, T. Lis, A. Sebald and M. Stumber, *Mol. Phys.*, 2000, in press.
22. S. Dusold and A. Sebald, *Mol. Phys.*, 1998, **95**, 1237.
23. K. Takegoshi, K. Takeda and T. Terao, *Chem. Phys. Lett.*, 1996, **260**, 331.
24. T. Terao, *J. Mol. Struct.*, 1998, **441**, 283.
25. R. Fu, S. A. Smith and G. Bodenhausen, *Chem. Phys. Lett.*, 1997, **272**, 361.
26. M. Baldus, A. T. Petkova, J. Herzfeld and R. G. Griffin, *Mol. Phys.*, 1998, **95**, 1197.
27. T. Gullion and J. Schaefer, *J. Magn. Reson.*, 1989, **81**, 196.
28. A. Schmidt and S. Vega, *Isr. J. Chem.*, 1992, **32**, 215.
29. T. Gullion and J. Schaefer, *Adv. Magn. Reson.*, 1989, **13**, 57.
30. E. R. H. van Eck and W. S. Veeman, *Solid State Nucl. Magn. Reson.*, 1993, **2**, 307.
31a. T. Gullion, *Magn. Reson. Rev.*, 1997, **17**, 83.
31b. T. Gullion, *Concepts in Magn. Reson.*, 1998, **10**, 277.
32. L.-S. Du, F. Wang and C. Grey, *J. Solid State Chem.*, 1998, **140**, 285.
33. Y. Pan, *Solid State Nucl. Magn. Reson*, 1995, **5**, 263.
34. C. A. Fyfe, A. R. Lewis, J. M. Chézeau and H. Grondey, *J. Am. Chem. Soc.*, 1997, **119**, 12210.
35. S. M. Holl, T. Kowalewski and J. Schaefer, *Solid State Nucl. Magn. Reson.* 1996, **6**, 39.
36. L. M. McDowell, M. Lee, R. A. McKay, K. S. Anderson and J. Schaefer, *Biochemistry*, 1996, **35**, 3328.
37. G. Tong and J. Schaefer, *Macromolecules*, 1997, **30**, 7522.
38. K. L. Wooley, C. A. Klug, K. Tasaki and J. Schaefer, *J. Am. Chem. Soc.*, 1997, **119**, 53.
39. M. P. Espe, B. R. Mattes and J. Schaefer, *Macromolecules*, 1997, **30**, 6307.
40. M. E. Merritt, J. M. Goetz, D. Whitney, C.-P. P. Chang, L. Heux, J. L. Halary and J. Schaefer, *Macromolecules*, 1998, **31**, 1214.
41. T. Asakura, A. Aoki, M. Demura, J. M. Moers, R. C. Rosanske and T. Gullion, *Polymer J.*, 1994, **26**, 1405.
42. C. A. Michal and L. W. Jelinski, *J. Biomol. NMR*, 1998, **12**, 231.
43. M. E. Merritt, A. M. Christensen, K. J. Kramer, T. L. Hopkins and J. Schaefer, *J. Am. Chem. Soc.*, 1996, **118**, 11278.
44. R. C. Anderson, T. Gullion, J. M. Joers, M. Shapiro, E. B. Villhauer and H. P. Weber, *J. Am. Chem. Soc.*, 1995, **117**, 10546.
45. J. R. Garbow, M. Breslav, O. Antohi and F. Naider, *Biochemistry*, 1994, **33**, 10094.
46. T. P. Jarvie, G. T. Went and K. T. Mueller, *J. Am. Chem. Soc.*, 1996, **118**, 5330.
47. A. Naito, K. Nishimura, S. Tuzi and H. Saito, *Chem. Phys. Lett.*, 1994, **229**, 506.
48. A. Naito, K. Nishimura, S. Kimura, S. Tuzi, M. Aida, N. Yasuoka and H. Saito, *J. Phys. Chem.*, 1996, **100**, 14995.
49. K. Nishimura, A. Naito, S. Tuzi, H. Saito, C. Hashimoto and M. Aida, *J. Phys. Chem. B*, 1998, **102**, 7476.
50. L. M. McDowell, D. Barkan, G. E. Wilson and J. Schaefer, *Solid State Nucl. Magn. Reson*, 1996, **7**, 203.
51. D. R. Studelska, C. A. Klug, D. D. Beusen, L. M. McDowell and J. Schaefer, *J. Am. Chem. Soc.*, 1996, **118**, 5476.
52. D. R. Studelska, L. M. McDowell, M. P. Espe, C. A. Klug and J. Schaefer, *Biochemistry*, 1997, **36**, 15555.
53. D. Mitchell, D. L. Jakeman, T. I. Igumenova, W. A. Shuttleworth, K. D. Miller and J. N. S. Evans, *Chem. Commun.*, 1997, 1019.
54. A. E. Bennett, C. M. Rienstra, M. Auger, K. V. Lakshmi and R. G. Griffin, *J. Chem. Phys.*, 1995, **103**, 6951.
55. D. J. Mitchell and J. N. S. Evans, *Chem. Phys. Lett.*, 1998, **292**, 656.
56. W. T. Dixon, *J. Chem. Phys.*, 1982, **77**, 1800.
57. Y. Li and J. N. S. Evans, *J. Magn. Reson.*, 1994, **A109**, 256.
58. Y. Li and J. N. S. Evans, *J. Chem. Phys.*, 1994, **101**, 10211.

59. B. Q. Sun, P. R. Costa and R. G. Griffin, *J. Magn. Reson.*, 1995, **A112**, 191.
60. M. Baldus, D. G. Geurts, S. Hediger and B. H. Meier, *J. Magn. Reson.*, 1996, **A118**, 140.
61. C. A. Michal and L. W. Jelinski, *J. Am. Chem. Soc.*, 1997, **119**, 9059.
62. M. Hong and R. G. Griffin, *J. Am. Chem. Soc.*, 1998, **120**, 7113.
63. F. G. Vogt, D. J. Aurentz and K. T. Mueller, *Mol. Phys.*, 1998, **95**, 907.
64. K. T. Mueller, *J. Magn. Reson.*, 1995, **A113**, 81.
65. K. T. Mueller, T. P Jarvie, D. J. Aurentz and B. W. Roberts, *Chem. Phys. Lett.*, 1995, **242**, 535; K. T. Mueller, T. P Jarvie, D. J. Aurentz and B. W. Roberts, *Chem. Phys. Lett.*, 1996, **254**, 281.
66. J.-B. d'Espinose de la Caillerie and C. Fretigny, *J. Magn. Reson.*, 1998, **133**, 273.
67. M. Abramowitz and I. A. Stegun, *Handbook of Mathematical Functions*, Dover, New York, 1965.
68. T. Gullion and C. H. Pennington, *Chem. Phys. Lett.*, 1998, **290**, 88.
69. T. S. Cull, J. M. Joers, T. Gullion, R. E. Norberg and M. S. Conradi, *J. Magn. Reson.*, 1998, **133**, 352.
70. A. E. Bennett, L. R. Becerra and R. G. Griffin, *J. Chem. Phys.*, 1994, **100**, 812.
71. A. E. Bennett, C. M. Rienstra, P. T. Lansbury Jr and R. G. Griffin, *J. Chem. Phys.*, 1996, **105**, 10289.
72. A. Schmidt and S. Vega, *J. Chem. Phys.*, 1992, **96**, 2655.
73. T. Nakai and C. A. McDowell, *Mol. Phys.*, 1992, **77**, 569.
74. T. Nakai and C. A. McDowell, *J. Chem. Phys.*, 1992, **96**, 3452.
75. D. P. Raleigh, M. H. Levitt and R. G. Griffin, *Chem. Phys. Lett.*, 1988, **146**, 71.
76. S. Dusold, E. Klaus, A. Sebald, M. Bak and N. C. Nielsen, *J. Am. Chem. Soc.*, 1997, **119**, 7121.
77. S. Dusold, W. Milius and A. Sebald, *J. Magn. Reson.*, 1998, **135**, 500.
78a. P. Tekely, P. Palmas and P. Mutzenhardt, *J. Magn. Reson.*, 1997, **127**, 238.
78b. P. Tekely, D. E. Demco, D. Canet, and C. Malveau, *Chem. Phys. Lett.*, 1999, **309**, 101.
79. S. Dusold, H. Maisel and A. Sebald, *J. Magn. Reson.*, 1999, **141**, 78.
80. R. Challoner and R. K. Harris, *Chem. Phys. Lett.*, 1994, **228**, 589.
81a. P. J. E. Verdegem, M. Helmle, J. Lugtenburg and H. J. M. de Groot, *J. Am. Chem. Soc.*, 1997, **119**, 162.
81b. X. Feng, P. J. E. Verdegem, Y. K. Lee, M. Helmle, S. C. Shekar, H. J. M. de Groot, J. Lugtenburg and M. H. Levitt, *Solid State Nucl. Magn. Reson.*, 1999, **14**, 81.
82. J. M. Koons, G. E. Pavlovskaya, A. A. Jones and P. T. Inglefield, *J. Magn. Reson.*, 1997, **124**, 499.
83. A. E. McDermott, F. Creuzet, R. Gebhard, K. van der Hoef, M. H. Levitt, J. Herzfeld, J. Lugtenburg and R. G. Griffin, *Biochemistry*, 1994, **33**, 6129.
84. O. B. Peersen, M. Groesbeek, S. Aimoto and S. O. Smith, *J. Am. Chem. Soc.*, 1995, **117**, 7228.
85. J. M. Griffiths, T. T. Ashburn, M. Auger, P. R. Costa, R. G. Griffin and P. T. Lansbury Jr, *J. Am. Chem. Soc.*, 1995, **117**, 3539.
86. S. O. Smith, K. Aschheim and M. Groesbeek, *Q. Rev. Biophys.*, 1996, **29**, 395.
87. J. Heller, R. Larsen, M. Ernst, A. C. Kolbert, M. Baldwin, S. P. Prusiner, D. E. Wemmer and A. Pines, *Chem. Phys. Lett.*, 1996, **251**, 223.
88. T. Karlsson and M. H. Levitt, *J. Chem. Phys.*, 1998, **109**, 5493.
89. P. R. Costa, D. A. Kocisko, B. Q. Sun, P. T. Lansbury Jr and R. G. Griffin, *J. Am. Chem. Soc.*, 1997, **119**, 10487.
90. Y. Tomita, E. J. O'Connor and A. McDermott, *J. Am. Chem. Soc.*, 1994, **116**, 8766.
91. R. Challoner and A. Sebald, *J. Magn. Reson.*, 1996, **A122**, 85.
92. T. Nakai and C. A. McDowell, *J. Magn. Reson.*, 1995, **A112**, 199.
93. T. Karlsson, M. Edén, H. Luthman and M. H. Levitt, *J. Magn. Reson.*, 1999, submitted.
94. M. Helmle, Y. K. Lee, P. J. E. Verdegem, X. Feng, T. Karlsson, J. Lugtenburg, H. J. M. de Groot and M. H. Levitt, *J. Magn. Reson.*, 1999, **140**, 379.
95. R. Verel, M. Baldus, M. Nijman, J. W. M. van Os and B. H. Meier, *Chem. Phys. Lett.*, 1997, **280**, 31.

96. K. Takegoshi, K. Nomura and T. Terao, *Chem. Phys. Lett.*, 1995, **232**, 424.
97a. K. Takegoshi, K. Nomura and T. Terao, *J. Magn. Reson.*, 1997, **127**, 206.
97b. K. Nomura, K. Takegoshi, T. Terao, K. Uchida and M. Kainosho, *J. Am. Chem. Soc.*, 1999, **121**, 4604.
98. P. R. Costa, B. Sun and R. G. Griffin, *J. Am. Chem. Soc.*, 1997, **119**, 10821.
99. R. G. S. Spencer, K. W. Fishbein, M. H. Levitt and R. G. Griffin, *J. Chem. Phys.*, 1994, **100**, 5533.
100. T. Karlsson, M. Helmle, N. D. Kurur and M. H. Levitt, *Chem. Phys. Lett.*, 1995, **247**, 534.
101. N. C. Nielsen, F. Creuzet, R. G. Griffin and M. H. Levitt, *J. Chem. Phys.*, 1992, **96**, 5668.
102. T. Gullion and S. Vega, *Chem. Phys. Lett.*, 1992, **194**, 423.
103. A. E. Bennett, J. H. Ok, R. G. Griffin and S. Vega, *J. Chem. Phys.*, 1992, **96**, 8624.
104. A. E. Bennett, C. M. Rienstra, J. M. Griffiths, W. Zhen, R. P. T. Lansbury Jr and R. G. Griffin, *J. Chem. Phys.*, 1998, **108**, 9463.
105. O. Weintraub, S. Vega, C. Hoelger and H. H. Limbach, *J. Magn. Reson.*, 1994, **A109**, 14.
106. W. Zhu, C. A. Klug and J. Schaefer, *J. Magn. Reson.*, 1994, **A108**, 121.
107. C. A. Klug and J. Schaefer, *J. Magn. Reson.*, 1996, **A122**, 251.
108. C. A. Klug, W. Zhu, K. Tasaki and J. Schaefer, *Macromolecules*, 1997, **30**, 1734.
109. A. E. Bennett, D. P. Weliky and R. Tycko, *J. Am. Chem. Soc.*, 1998, **120**, 4897.
110. P. Hartmann, C. Jana, J. Vogel and C. Jäger, *Chem. Phys. Lett.*, 1996, **258**, 107.
111. I. Abrahams, G. E. Hawks and J. Knowles, *J. Chem. Soc., Dalton Trans.*, 1997, 1483.
112. W. Heinen, C. B. Wenzel, C. H. Rosenmöller, F. M. Mulder, G. J. Boender, J. Lugtenburg, H. J. M. de Groot, M. van Duin and B. Klumpermann, *Macromolecules*, 1998, **31**, 7404.
113. T. S. Balaban, A. R. Holzwarth, K. Schaffner, G.-J. Boender and H. J. M. de Groot, *Biochemistry*, 1995, **34**, 15259.
114. T. A. Egorova-Zachernyuk, B. van Rossum, G.-J. Boender, E. Franken, J. Ashurst, J. Raap, P. Gast, A. J. Hoff, H. Oschkinat and H. J. M. de Groot, *Biochemistry*, 1997, **36**, 7513.
115. B.-J.van Rossum, G. J. Boender, F. M. Mulder, J. Raap, T. S. Balaban, A. Holzwarth, K. Schaffner, S. Prytulla, H. Oschkinat and H. J. M. de Groot, *Spectrochim. Acta*, 1998, **A54**, 1167.
116. E. Zaborowski, H. Zimmermann and S. Vega, *J. Magn. Reson.*, 1999, **136**, 47.
117. M. Baldus and B. H. Meier, *J. Magn. Reson.*, 1997, **128**, 172.
118. T. Fujiwara, A. Ramamoorthy, K. Nagayama, K. Hioka and T. Fujito, *Chem. Phys. Lett.*, 1993, **212**, 81.
119. M. Baldus, M. Tomaselli, B. H. Meier and R. R. Ernst, *Chem. Phys. Lett.*, 1994, **230**, 329.
120. S. Zhang, B. H. Meier and R. R. Ernst, *Phys. Rev. Lett.*, 1992, **69**, 2149.
121. W. K. Rhim, A. Pines and W. S. Waugh, *Phys. Rev. Lett.*, 1970, **25**, 218.
122. W. K. Rhim, A. Pines and W. S. Waugh, *Phys. Rev.*, 1971, **B3**, 684.
123. T. Fujiwara, K. Sugase, M. Kainosho, A. Ono, A. M. Ono and H. Akutsu, *J. Am. Chem. Soc.*, 1995, **117**, 11351.
124. M. Baldus, R. Iuliucci and B. H. Meier, *J. Am. Chem. Soc.*, 1997, **119**, 1121.
125. S. Dusold, J. Kümmerlen, T. Schaller, A. Sebald and W. A. Dollase, *J. Phys. Chem.*, 1997, **B101**, 6359.
126. R. Tycko and G. Dabbagh, *Chem. Phys. Lett.*, 1990, **173**, 461.
127. R. Tycko and S. O. Smith, *J. Chem. Phys.*, 1993, **98**, 932.
128. H. Geen, J. J. Titman, J. Gottwald and H. W. Spiess, *Chem. Phys. Lett.*, 1994, **227**, 79.
129. C. A. Klug, W. Zhu, K. Tasaki and J. Schaefer, *Macromolecules*, 1997, **30**, 1734.
130. C. A. Klug, W. Zhu, M. E. Merritt and J. Schaefer, *J. Magn. Reson.*, 1994, **109**, 134.
131. C. A. Klug, D. R. Studelska, G. Chen, S. R. Gilbertson and J. Schaefer, *Solid State Nucl. Magn. Reson.*, 1996, **7**, 173.
132. R. Graf, D. E. Demco, J. Gottwald, S. Hafner and H. W. Spiess, *J. Chem. Phys.*, 1997, **106**, 885.
133. D. M. Gregory, D. J. Mitchell, J. A. Stringer, S. Kiihne, J. C. Shiels, J. Callahan, M. A. Metha and G. P. Drobny, *Chem. Phys. Lett.*, 1995, **246**, 654.

134. M. A. Mehta, D. M. Gegory, S. Kiihne, J. D. Mitchell, M. E. Hatcher, J. C. Shiels and G. P. Drobny, *Solid State Nucl. Magn. Reson.*, 1996, **7**, 211.
135. D. M. Gregory, T. L. S. Benzinger, T. S. Burkoth, H. Miller-Auer, D. G. Lynn, S. C. Meredith and R. E. Botto, *Solid State Nucl. Magn. Reson.*, 1998, **13**, 149.
136. D. M. Gregory, G. M. Wolfe, T. P. Jarvie, J. C. Shiels and G. P. Drobny, *Mol. Phys.*, 1996, **89**, 1835.
137. D. M. Gregory, M. A. Metha, J. C. Shiels and G. P. Drobny, *J. Chem. Phys.*, 1997, **107**, 28.
138. B.-Q. Sun, P. R. Costa, D. Kosisko, P. T. Lansbury Jr and R. G. Griffin, *J. Chem. Phys.*, 1995, **102**, 702.
139. B.-Q. Sun, C. M. Rienstra, P. R. Costa, J. R. Williamson and R. G. Griffin, *J. Am. Chem. Soc.*, 1997, **119**, 8540.
140. H. C. Jarrell, D. Lu and D. J. Siminovitch, *J. Am. Chem. Soc.*, 1998, **120**, 10453.
141. W. Sommer, J. Gottwald, D. E. Demco and H. W. Spiess, *J. Magn. Reson.*, 1995, **A113**, 131.
142. M. Feike, D. E. Demco, R. Graf, J. Gottwald, S. Hafner and H. W. Spiess, *J. Magn. Reson.*, 1996, **A122**, 214.
143. M. Feike, R. Graf, I. Schnell, C. Jäger and H. W. Spiess, *J. Am. Chem. Soc.*, 1996, **118**, 9631.
144. R. Witter, P. Hartmann, J. Vogel and C. Jäger, *Solid State Nucl. Magn. Reson.*, 1998, **13**, 189.
145. I. Schnell, A. Lupulescu, S. Hafner, D. E. Demco and H. W. Spiess, *J. Magn. Reson.*, 1998, **133**, 61.
146. I. Schnell, S. P. Brown, H. Y. Lee, H. Ishida and H. W. Spiess, *J. Am. Chem. Soc.*, 1998, **120**, 11784.
147. N. C. Nielsen, H. Bildsoe, H. J. Jakobsen and M. H. Levitt, *J. Chem. Phys.*, 1994, **101**, 1805.
148. Y. K. Lee, N. D. Kurur, M. Helmle, O. G. Johannessen, N. C. Nielsen and M. H. Levitt, *Chem. Phys. Lett.*, 1995, **242**, 304.
149. M. Bak and N. C. Nielsen, *J. Chem. Phys.*, 1997, **106**, 7587.
150. Z. Gan, D. M. Grant and R. R. Ernst, *Chem. Phys. Lett.*, 1996, **254**, 349.
151. R. Verel, M. Baldus, M. Ernst and B. H. Meier, *Chem. Phys. Lett.*, 1998, **287**, 421.
152. M. Hohwy, H. J. Jakobsen, M. Edén, M. H. Levitt and N. C. Nielsen, *J. Chem. Phys.*, 1998, **108**, 2686.
153. C. M. Rienstra, M. E. Hatcher, L. J. Mueller, B. Sun, S. W. Fesik and R. G. Griffin, *J. Am. Chem. Soc.*, 1998, **120**, 10602.
154. M. Edén and M. H. Levitt, *Chem. Phys. Lett.*, 1998, **293**, 173.
155. H. Geen, J. Gottwald, R. Graf, I. Schnell, H. W. Spiess and J. J. Titman, *J. Magn. Reson.*, 1997, **125**, 224.
156. J. Schmedt auf der Günne and H. Eckert, *Chemistry*, 1998, **4**, 1762.
157. W. A. Dollase, M. Feike, H. Förster, T. Schaller, I. Schell, A. Sebald and S. Steuernagel, *J. Am. Chem. Soc.*, 1997, **119**, 3807.
158. M. Hong, *J. Magn. Reson.*, 1999, **136**, 86.
159. R. Graf, D. E. Demco, S. Hafner and H. W. Spiess, *Solid State Nucl. Magn. Reson.*, 1998, **12**, 139.
160. R. Graf, A. Heuer and H. W. Spiess, *Phys. Rev. Lett.*, 1998, **80**, 5738.
161. M. Hohwy, C. M. Rienstra, C. P. Jaroniec and R. G. Griffin, *J. Chem. Phys.*, 1999, **110**, 7983.
162. M. Baldus, D. G. Geurts and B. H. Meier, *Solid State Nucl. Magn. Reson.*, 1998, **11**, 157.
163. X. Feng, Y. K. Lee, D. Sandström, M. Edén, H. Maisel, A. Sebald and M. H. Levitt, *Chem. Phys. Lett.*, 1996, **257**, 314.
164. T. Fujiwara, T. Shimomura, Y. Ohigashi and H. Akutsu, *J. Chem. Phys.*, 1998, **109**, 2380.
165. B. Reif, M. Henning and C. Griesinger, *Science*, 1997, **276**, 1230.
166. K. Schmidt-Rohr, *J. Am. Chem. Soc.*, 1996, **118**, 7601.
167. X. Feng, P. J. E. Verdegem, Y. K. Lee, D. Sandström, M. Edén, P. Bovee-Geurts, W. J. de Grip, J. Lugtenburg, H. J. M. de Groot and M. H. Levitt, *J. Am. Chem. Soc.*, 1997, **119**, 6853.

168. X. Feng, M. Edén, A. Brinkmann, H. Luthman, L. Eriksson, A. Gräslund, O. N. Antzutkin and M. H. Levitt, *J. Am. Chem. Soc.*, 1997, **119**, 12006.
169a. M. Hong, J. D. Gross and R. G. Griffin, *J. Phys. Chem. B*, 1997, **101**, 5869.
169b. M. Hong, *J. Magn. Reson.*, 1999, **139**, 389.
170. M. Hong, J. D. Gross, C. M. Rienstra, R. G. Griffin, K. K. Kumashiro and K. Schmidt-Rohr, *J. Magn. Reson.*, 1997, **129**, 85.
171. Y. Ishii, T. Terao and M. Kainosho, *Chem. Phys. Lett.*, 1996, **256**, 133.
172. Y. Ishii, K. Hirao, T. Terao, T. Terauchi, M. Oba, K. Nishiyama and M. Kainosho, *Solid State Nucl. Magn. Reson.*, 1998, **11**, 169.
173. T. Fujiwara, T. Shimomura and H. Akutsa, *J. Magn. Reson.*, 1997, **124**, 147.
174. M. Hong, J. D. Gross, W. Hu and R. G. Griffin, *J. Magn. Reson.*, 1998, **135**, 169.
175. J. D. Gross, P. R. Costa and R. G. Griffin, *J. Chem. Phys.*, 1998, **108**, 7286.
176. P. Tekely, P. Palmas and D. Canet, *J. Magn. Reson.*, 1994, **A107**, 129.
177. M. Ernst, S. Bush, A. C. Kolbert and A. Pines, *J. Chem. Phys.*, 1996, **105**, 3387.
178. Z. Gan and R. R. Ernst, *Solid State Nucl. Magn. Reson.*, 1997, **8**, 153.
179. D. L. van der Hart and G. C. Campbell, *J. Magn. Reson.*, 1998, **134**, 88.
180. M. Edén and M. H. Levitt, *J. Chem. Phys.*, 1999, **111**, 1511.
181. J. Schaefer, *J. Magn. Reson.*, 1999, **137**, 272.
182. K. Nishimura, A. Naito, S. Tuzi and H. Saito, *J. Phys. Chem. B*, 1999, **103**, 8398.
183. M. E. Merritt, S. T. Sigurdsson and G. P. Drobny, *J. Am. Chem. Soc.*, 1999, **121**, 6070.
184. V. Schimming, C.-G. Hoelger, G. Buntkowsky, I. Sack, J.-H. Fuhrhop, S. Rocchetti, and H.-H. Limbach, *J. Am. Chem. Soc.*, 1999, **121**, 4892.
185. J. M. Goetz, B. Polikis, D. R. Studelska, M. Fischer, K. Kugelbrey, A. Bacher, M. Cushman and J. Schaefer, *J. Am. Chem. Soc.*, 1999, **121**, 7500.
186. B. Arshava, M. Breslav, O. Antohi, R. E. Stark, J. R. Garbow, J. M. Becker and F. Naider, *Solid State Nucl. Magn. Reson.*, 1999, **14**, 117.
187. K. Saalwächter, R. Graf and H. W. Spiess, *J. Magn. Reson.*, 1999, **140**, 471.
188. Y. S. Balazs and L. K. Thompson, *J. Magn. Reson.*, 1999, **139**, 371.
189. D. Kuwahara, T. Nakai, J. Ashida and S. Miyajima, *Chem. Phys. Lett.*, 1999, **305**, 35.
190. W. S. Maas, A. Bielecki, M. Ziliox, F. H. Laukien and D. C. Cory, *J. Magn. Reson.*, 1999, **141**, 29.
191. K. Takegoshi, S. Nakamura and T. Terao, *Chem. Phys. Lett.* 1999, **307**, 295.
192. S. Kiihne, M. A. Mehta, J. A. Stringer, D. M. Gregory, J. C. Shiels and G. P. Drobny, *J. Phys. Chem. A*, 1998, **102**, 2274.
193. S. R. Kiihne, K. B. Geahigan, N. A. Oyler, H. Zebrowski, M. A. Mehta and G. P. Drobny, *J. Phys. Chem. A*, 1999, **103**, 3890.
194. P. V. Bouwer, N. Oyler, M. A. Mehta, J. R. Long, P. S. Stayton and G. P. Drobny, *J. Am. Chem. Soc.*, 1999, **121**, 8873.
195. S. P. Brown, I. Schnell, J. D. Brand, K. Müllen and H. W. Spiess, *J. Am. Chem. Soc.*, 1999, **121**, 6712.
196. H. Geen, R. Graf, A. S. D. Heindrichs, B. S. Hickman, I. Schnell, H. W. Spiess and J. J. Titman, *J. Magn. Reson.*, 1999, **138**, 167.
197. T. Karlsson, A. Brinkmann, P. J. E. Verdegen, J. Lugtenburg and M. H. Levitt, *Solid State Nucl. Magn. Reson.*, 1999, **14**, 43.
198. P. Hodginson and L. Emsley, *J. Magn. Reson.*, 1999, **139**, 46.

Characterization of Porous Media Using NMR Methods

PATRICK J. BARRIE

Department of Chemical Engineering, University of Cambridge, Pembroke Street, Cambridge CB2 3RA, UK

1. INTRODUCTION

Porous media play an important role in a wide number of disciplines. Geologists are interested in the flow of water through aquifers, and the flow of oil in reservoirs. Chemical engineers are interested in the effectiveness of porous catalyst particles and in multiphase flow in packed columns. Biologists are interested in the flow of blood through organ tissues. Porous media are also important in the fields of soil science (transport of water and nutrients to roots), environmental science (soil remediation and wastewater treatment),

ANNUAL REPORTS ON NMR SPECTROSCOPY
VOLUME 41 ISBN 0-12-505341-X

food science (food cryopreservation) and separation technologies (processes such as filtration, gas separation using membranes, and liquid chromatography). Other examples in which the characterization of porous media is important are in the construction industry (e.g. the hydration of cement) and in polymer science (e.g. the dehydration of contact lenses). As well as scientists in these disciplines, mathematicians and physicists are interested in the various ways of modelling porous media and flow behaviour within them from a purely scientific point of view. In most of the applications mentioned, it is the transport of fluids within the porous media that is of interest. There is thus an extensive literature on modelling transport within porous media.[1–6]

The main advantages of NMR methods in the study of porous media are that they are noninvasive and nondestructive. They can investigate both static and dynamic systems: for instance, pore space can be characterized using magnetic resonance imaging, and then local transport velocities measured using an NMR flow imaging technique. A wide range of different NMR methods is available. As a result of this, NMR techniques are capable of probing both microscopic and macroscopic phenomena. These range from studying molecular reorientations at adsorption sites in microporous solids, to studying bulk fluid flow through sedimentary rocks. Similarly, the variety of NMR methods can look at changes in a sample over a wide range of timescales, ranging from milliseconds to days. Another advantage of NMR methods is that measurements may be selectively made on one component of a multiphase mixture, for instance by using chemical shift selectivity or relaxation contrast techniques.

Porous media are routinely characterized by techniques such as gas adsorption and mercury porosimetry, as well as by NMR methods.[7–10] A number of parameters are normally used to describe porous media. The *surface area* is normally found by adsorption measurements and gives the available surface area of the pore space. The *porosity*, ϕ, gives the ratio of the pore volume to the total volume. It may be obtained by a variety of methods, including measuring the NMR signal intensity from a fluid that is saturating the sample. The formation factor and tortuosity give information on how the pores are connected together. The *formation factor*, F, is defined as the ratio between the conductivity of a bulk fluid and the conductivity of the porous medium when saturated with that fluid (assuming that the solid phase does not contribute to the conductivity). Different authors use slightly different definitions of the tortuosity. Here we shall take *tortuosity*, α, to be the product of the formation factor and porosity, i.e. $\alpha = F\phi$. Tortuosity can be used to relate the actual distance that an element of fluid travels in a porous medium compared with the net distance moved. The *permeability* is a transport property giving the fluid superficial velocity in a pressure gradient. The permeability is a function solely of the pore structure for viscous flow of Newtonian fluids.[3] The *wettability* expresses the affinity of a porous matrix for one fluid in preference to another when more than one fluid is present.

Together with these parameters, it is important to gain information about the *pore dimensions* (e.g. the surface area to volume ratio), the *pore size distribution* and the *pore connectivity*. All of these factors will, in general, have some influence on fluid transport within a porous structure.

However, modelling fluid transport in porous media is not a straightforward task even for pure components, let alone multiphase mixtures. Within each individual pore, differential equations can be written down expressing the conservation of mass, energy and momentum, and these could in principle be solved. However, this would require a detailed knowledge of the solid–fluid boundary conditions of all pores, information which is not normally available, and it would be extremely demanding computationally. Therefore, models for transport processes in porous media have been developed. These may be classified into continuum models and discrete models.[11] Continuum models employ a macroscopic description at a length scale much larger than the dimension of the individual pores. Macroscopic transport properties are defined as the average of microscopic quantities over the specified volume, and transport equations, such as Darcy's law, are employed over this averaged space. On the other hand, discrete models employ a microscopic approach. In this case, the volume under consideration can become that of an individual pore. However, only simplified geometrical representations of the pore space (e.g. a bundle of capillary tubes) can currently easily be modelled. Such pore network models can be used to predict macroscopic transport coefficients that can then be compared with experimental values. However, a fundamental understanding of how local microstructural variations can influence macroscopic transport is still lacking. Thus, a key area of research is to establish which microstructural parameters are influencing macroscopic flow properties, and it is in this regard that NMR techniques have considerable potential.[12]

This review concentrates on characterization of the actual pore space, and transport within the pore space, using NMR methods. Thus, it neglects several areas. For instance the adsorption properties of a porous solid are of considerable interest in the fields of gas separation and catalysis. Adsorption and catalytic properties depend critically on the surface chemistry of the solid phase, and NMR studies of this topic have been widely reviewed elsewhere.[13–19] We shall, however, consider NMR studies of adsorbates when they specifically give information on the pore space.

It is important to appreciate the range of porous materials that have been studied, and the different challenges that they pose the NMR spectroscopist. The pore spaces will range from microporous systems (pore diameters less than 20 Å), through mesoporous systems (pore diameters in the range 20–500 Å), up to macroporous systems (pore diameters greater than 500 Å).[20] For instance, zeolites have pore diameters less than 10 Å, while sandstones tend to have pore sizes in the range 0.1–100 μm. The precise NMR technique used to characterize pore spaces or transport within these materials will be different. Some samples will have fairly well-defined pore sizes (such as zeolites and

certain silicas), while others will have a broad range of pore size (such as sedimentary rocks). It will be important to distinguish between 'homogeneous' and 'heterogeneous' pore structures. In homogeneous pore structures, the pore size distribution is relatively constant throughout the sample, while in heterogeneous pore structures there may be considerable variation in pore characteristics across the sample. The use of NMR methods to characterize real porous media is often handicapped by problems associated with magnetic susceptibility differences between the solid phase and the fluid in the pore space. These can be particularly severe when paramagnetic species are present. For this reason, many studies are performed on model porous systems (such as a packed bed of glass beads) to try to ascertain the fundamental science occurring. In other cases, a genuine system of interest, such as an oil-containing rock, is studied even though detailed interpretation of the results becomes more difficult.

Some information can be obtained on porous media from conventional NMR spectroscopy, and this is discussed in Section 2. Relaxation time measurements have been widely used to characterize porous solids, and this technique is discussed in Section 3. Pulsed field gradient (PFG) methods may be used to probe the local structure of the pore space and to characterize transport within it, and these are discussed in Section 4. Magnetic resonance imaging (MRI) techniques can also be used to characterize the pore space and to measure transport, and applications are discussed in Section 5. The bulk of this review will be concerned with mesoporous and macroporous materials, as it is for these systems that NMR is particularly useful in characterizing the pore space. However, some applications of NMR techniques to probe the pore space and transport within microporous materials will be mentioned in Section 6. Finally, some general conclusions are given in Section 7.

2. SPECTROSCOPY OF ADSORBATES WITHIN THE PORE SPACE

The key parameters in NMR spectroscopy when used for chemical structure identification are the chemical shift, the intensity and the linewidth. However, less information is available from these parameters towards the characterization of porous media than might at first be expected. The reason for this is that fluids in porous media tend to give broad resonance peaks, concealing evidence that different environments are present.

One reason for the broadening is that there are differences in magnetic susceptibility between the solid phase and the fluid within it. This means that different parts of a pore space will be feeling different apparent magnetic fields, and so spectral linewidths will be broad. This is particularly the case when the sample contains trace amounts of paramagnetic ions. For instance, the linewidths of ^{1}H spectra from rock core samples saturated with water may be 5 ppm for carbonates, but can exceed 50 ppm for sandstones.[21,22] Magnetic

susceptibility differences are also responsible for an increase in linewidth for adsorbed water in porous silica as the water loading is increased.[23]

Another factor causing line broadening in porous media is that the fluid will normally have lower mobility than in a bulk fluid. In particular, the fluid at the pore surface will have greatly reduced mobility. Fluid at the wall surface normally has a very short spin–spin relaxation time, and this will influence the relaxation time of the entire fluid present in the pore space, as discussed in Section 3. Thus, even when differences in magnetic susceptibility are small, there may be significant line broadening simply due to relaxation effects. Again this may be severe when the solid contains significant amounts of paramagnetic species. There are, however, some special cases when the simple NMR experiment does yield information on the pore structure, and these will be considered in this section.

2.1. Chemical shift resolution of species in different pores

NMR spectroscopy does not normally distinguish between a fluid present in pores of different dimensions in mesoporous or macroporous solids. In some cases this is due to rapid exchange on the NMR timescale between the environments. In other cases, the linewidth of the spectra is greater than the difference in chemical shift due to the different environments. However, in a few cases the NMR signal from adsorbates in different pores may be resolved.

One example is small organic molecules adsorbed within certain porous carbons. The ^1H NMR spectra of Fig. 1 show several peaks for acetonitrile (CH_3CN) dissolved in carbon tetrachloride (CCl_4) adsorbed within a carbonaceous adsorbent, A-572.[24] This particular adsorbent is mainly mesoporous with a maximum in its pore size distribution plot of 580 Å as determined by gas adsorption measurements. It does, however, also contain some micropores. The NMR spectra shown in Fig. 1 can be resolved into bands assigned to acetonitrile adsorbed in small pores, medium pores and large pores. Similar results were obtained using dichloromethane (CH_2Cl_2) or benzene (C_6H_6) as the probe molecule. The results can be interpreted to yield thermodynamic properties for the adsorption process in the different sized pores.[25]

In the case when spectral lines are normally too broad to resolve individual species, it may still be possible to achieve high-resolution spectra using line-narrowing techniques such as magic-angle spinning. This has recently been demonstrated to be an effective way of resolving spectral peaks arising from oil and water in a sandstone sample.[26]

Another approach to gaining information from spectroscopy about pore sizes is to adsorb a mixture of different size molecules. Comparison of the peak intensities from the adsorbed molecules with those from the starting mixture will reveal the extent to which the different size species present have been

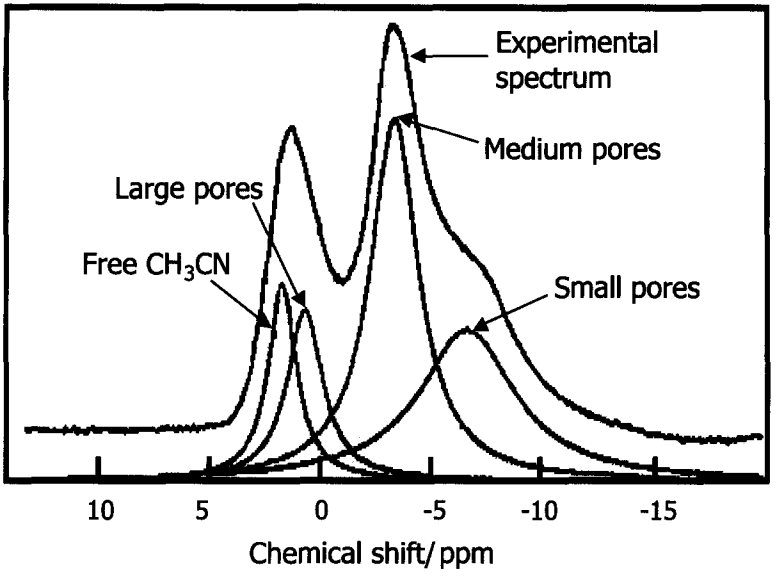

Fig. 1. ^1H NMR spectrum of 1.25 moll^{-1} CH_3CN in CCl_4 adsorbed into a porous carbon. (Reproduced with permission from ref. 24, © 1995, American Chemical Society.)

adsorbed. There would be too much overlap between peaks in ^1H NMR spectra for this to be a useful method of investigation. However, the chemical shift range of ^{19}F is sufficiently large that signals from the different species present may be resolved, and this method has been applied to measure chromatographic column void volumes and the porosities of several bulk resins.[27]

2.2. Freezing point depression

It has long been known that the freezing point of a liquid inside a porous solid is lower than that of the bulk liquid. A number of expressions may be derived to predict the actual freezing point based on the Kelvin equation.[28,29] One such expression is[30]

$$\Delta T = \frac{T_{obs}}{L}\frac{2M}{r}\left(\frac{\gamma_l}{\rho_l} - \frac{\gamma_s}{\rho_s}\right) \tag{1}$$

where ΔT is the depression of the freezing point and r is the pore radius. Thus there is a relationship between melting point and pore size. The other terms in Eq. (1) are the observed freezing point, T_{obs}, the molecular weight, M, the

latent heat of fusion, L, and the surface energy, γ, and density, ρ, of the liquid (l) and solid (s) measured at the normal bulk melting temperature. If the physical parameters in Eq. (1) are not all known, then a modified form of the Gibbs–Kelvin equation may be used to analyse the data:

$$\Delta T = \frac{K}{r + d} \tag{2}$$

where K and d are constants that depend on the fluid. These may be obtained from freezing point depression measurements on samples of known pore sizes. Equations (1) and (2) contain only a single pore size, r. Work is continuing to establish expressions for the freezing point depression in pores of more complicated geometries.[31,32]

The NMR peak area from an adsorbate saturating the solid can be measured as a function of temperature. As the frozen adsorbate is solid, nuclei in this phase will have very short spin–spin relaxation times. Hence, signal from the frozen adsorbate can easily be eliminated by using a spin-echo pulse sequence, or by increasing the specified dead-time after the excitation pulse. This means that the relative amount of liquid present in the pores can be measured by variable-temperature NMR methods. An intensity correction to allow for the change in the Boltzmann equilibrium population of energy levels with temperature is also required:

$$\frac{N_{\text{upper}}}{N_{\text{lower}}} = \exp\left(\frac{-\gamma\hbar B_0}{kT}\right) \tag{3}$$

Here N_{upper} is the population of the upper energy level, N_{lower} is the population of the lower energy level, γ is the gyromagnetic ratio, B_0 is the magnetic field strength, and k is Boltzmann's constant. The signal intensity is proportional to the difference in energy level population, and so is proportional to $1/T$ (because $\gamma\hbar B_0 \gg kT$). Care is needed over temperature calibration, and checks need to be made that the probe tuning remains constant over the temperature range studied. In combination with the Kelvin equation, the liquid intensity measurements enable a pore size distribution plot to be made from the results. The method is particularly appropriate for studying pore sizes in the mesoporous range (i.e. 20–500 Å). However, caution is needed when strong surface adsorption effects occur.

NMR measurements of the freezing of water in mesoporous solids such as silica and activated charcoal have been shown to be a reliable measure of pore volume, provided that allowance for strong adsorption on hydroxyl groups of the silica surface is taken into account.[33] Strong adsorption at the surface becomes more difficult to model as the pore size becomes smaller. For instance,

a number of water phase transitions are observed during freezing of water in mesoporous silica MCM-41 (which can be prepared with regular channels with pore radii in the range 20–80 Å).[34,35] There is a transition below 209 K independent of pore size, and one or more transitions above 222 K that depend on pore size. The low-temperature transition is assigned to water strongly bonded to the channel surface. The pore size of MCM-41 can be predicted on the basis of the ^{1}H NMR results provided that the appropriate transition temperature is used.[36,37] NMR measurements of the freezing point of water have also been used to estimate the pore size in gypsum and cement pastes.[38–40]

It might be expected that probe molecules that do not interact strongly with the surface would provide more reliable results. For instance, the pore size distribution of porous silicas has been determined using NMR measurements of the freezing point of cyclohexane within porous silicas, and the results have been confirmed by comparison with gas adsorption measurements (Fig. 2).[41] Further, it has been found that the freezing points of cyclohexane and benzene are more sensitive to the pore size than is that of water.[42,43] Cyclohexane has also been used to probe the pore structure of a porous carbon adsorbent.[44]

In a recent study, the melting point of frozen water or cyclohexane in a porous silica was measured using NMR at different adsorbate loadings.[45] Different behaviour was found for the two fluids. It was found that water

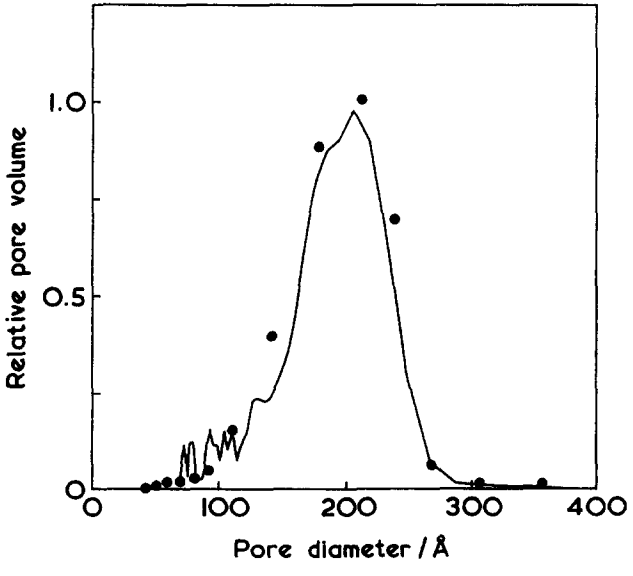

Fig. 2. Pore size distribution of a silica with nominal pore diameter of 200 Å. The solid line gives that determined from variable-temperature ^{1}H NMR spectra of adsorbed cyclohexane, while the points give that determined by conventional gas adsorption/desorption measurements. (Reproduced with permission from ref. 41, © 1993, American Physical Society.)

forms 'puddles' that are smaller than the pore size at low filling fractions, and that these puddles become larger at higher filling fractions until all the pore volume is filled. By contrast, cyclohexane completely fills the smaller pores at low loadings, and fills the larger pores at high loadings. Thus different behaviour is observed for wetting and nonwetting fluids when the pores are not saturated. It also means that pore size determinations using the freezing point depression method will be more reliable for water than for cyclohexane if the sample is not fully saturated.

The method of measuring the freezing point of liquids in porous media has recently been combined with relaxation time measurements and NMR imaging techniques. The relaxation time measurements show unusual structural behaviour for the nanosized particles of frozen solid cyclohexane in silica.[46,47] The imaging experiments can potentially determine the pore size distribution at any point within the sample (subject to the resolution of the image), and can reveal heterogeneities within the sample.[48–50] Magnetic resonance imaging of the freezing/melting of water in concrete has also been performed.[51,52]

3. NMR RELAXATION TIMES OF ADSORBATES WITHIN THE PORE SPACE

3.1. Introduction

An NMR experiment can provide more information than simply a spectral resonance frequency (chemical shift) and associated linewidth. The various NMR relaxation times can be particularly useful parameters, particularly in the characterization of pore spaces. This is because they prove to be sensitive to molecular motion and are affected by the pore geometry. There are three NMR relaxation times to consider.

First, the spin–lattice relaxation time, T_1, quantifies the time that it takes for nuclear spins to return to Boltzmann equilibrium after a perturbation. The spin–lattice relaxation time(s) of fluids in porous media may readily be measured using the standard $180° - \tau - 90°$-acquire inversion-recovery pulse sequence. Secondly, the spin–spin relaxation time, T_2, governs the dephasing of nuclear spins in a direction perpendicular to the applied static magnetic field. For fluids in porous media, T_2 may be measured using a $90°-\tau-180°-\tau$-acquire spin-echo sequence such as the Carr–Purcell–Meiboom–Gill (CPMG) method.[53] However, as will be discussed below, in order to obtain accurate T_2 values it is necessary to use fairly low static magnetic fields and use short echo spacings in order to reduce complications due to diffusion in the presence of local magnetic field gradients. The third relaxation time, $T_{1\rho}$, corresponds to relaxation in a rotating frame of reference and will not be discussed further here.

In order for spin–lattice relaxation to occur, the nuclei need to experience a fluctuating magnetic field of the correct frequency. There are a number of

different relaxation mechanisms for this to occur.[54,55] The most important of these are relaxation due to dipolar coupling, in which the relative motion of other nuclear spins in the proximity causes relaxation; coupling to paramagnetic ions; and the quadrupolar interaction (which is relevant only for nuclei with spin $I \geqslant 1$). These interactions will be different for molecules adsorbed at the pore wall surface compared to those in bulk fluid. They will also depend on the rate of molecular reorientation.

The vast majority of work on relaxation times in porous media has been performed on macroporous materials and rocks such as sandstones. This is because of the commercial significance of well logging. In this technique, 'inside-out' NMR equipment is used: large static magnetic fields and high-frequency oscillating magnetic fields have to be projected into the surrounding rock formations.[56–58] The amplitude of the ^{1}H NMR signal provides a measurement of the fluid content of the rock, while the relaxation times are used to gain information on the pore size distribution as discussed below. Nonuniformity of the static magnetic field prevents the acquisition of chemical shift spectra. However, in some cases, the water and oil have significantly different relaxation times, and in these cases the amount of oil in the rock can be estimated.[58] It has been found that hydrostatic pressure does not have a major influence on relaxation times.[59]

Relaxation times are commonly measured for porous media that have been saturated with a fluid such as water or an aqueous brine solution. The observed relaxation times are strongly dependent on the pore size, the distribution of pore sizes, the type of material (e.g. content of paramagnetic ions) and the water content. While relaxation times in porous media have been modelled using random walk methods and finite-element methods,[60,61] simplified models are usually needed to obtain information on pore space. Section 3.2 reviews the standard model used to analyse relaxation behaviour of fluid in macroporous samples such as rocks. Mesoporous materials such as porous silica will be discussed in Section 3.3.

3.2. Relaxation in macroporous materials

It has long been known that the NMR relaxation times of fluids in porous media are shorter than in bulk fluids. A simple model is that water molecules may be either adsorbed at the wall surface, where they will have particular relaxation times (T_{1S} and T_{2S}), or they will be located in the middle of the pore, in which case they will have relaxation times associated with bulk water (T_{1B} and T_{2B}).[62–64] Incorporation of diffusion between the two water environments follows from work of Brownstein and Tarr who developed a model rationalizing the relaxation behaviour of water in biological cells.[65,66] In the case of rocks, the enhanced relaxation rate of water at the wall surface is principally due to paramagnetic species in the solid phase.[67,68] In some other

porous systems, such as cements, the dipolar interactions between bound water and surface hydroxyl groups may be the most significant relaxation mechanism.[68,69] A reduced rate of reorientation of molecules at the pore surface may also play a role in some systems. This idealized two-site model has been widely used to interpret the NMR relaxation behaviour of water in the pores of rocks and other macroporous media.[67,70–73]

In macroporous systems, there is normally fast exchange of the water molecules between the surface and bulk environments owing to rapid diffusion. In that case, the water molecules within the pore will experience an average environment with a single relaxation time, T_1, that obeys

$$\frac{1}{T_1} = \frac{x}{T_{1S}} + \frac{(1-x)}{T_{1B}} \tag{4}$$

where x is the fraction of water molecules that is present at the surface sites. If the thickness of the water surface layer is h, the pore surface area is S, and the pore volume is V (see Fig. 3), then Eq. (4) may be rearranged to give

$$\frac{1}{T_1} = \frac{1}{T_{1B}} + \frac{Sh}{V}\left(\frac{1}{T_{1S}} - \frac{1}{T_{1B}}\right) \tag{5}$$

This is normally written in the form

$$\frac{1}{T_1} = \frac{1}{T_{1B}} + \rho_1 \frac{S}{V} \tag{6}$$

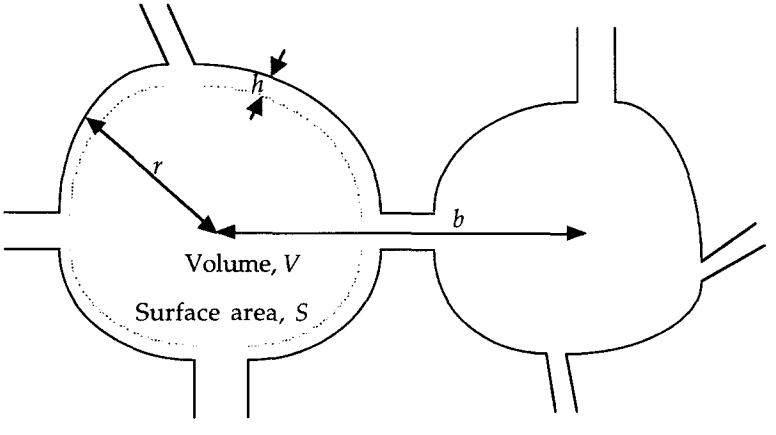

Fig. 3. Schematic representation of a pore space, showing a surface layer h, the pore radius r, and the interpore spacing b.

where ρ_1 is called the 'surface relaxivity parameter' for spin–lattice relaxation and has units of velocity. An expression for T_2 may be derived in the same fashion:

$$\frac{1}{T_2} = \frac{1}{T_{2B}} + \rho_2 \frac{S}{V} \tag{7}$$

In many cases, the relaxation time of water in porous media is far smaller than that of bulk water, and so only the second term on the right-hand side of Eqs (6) and (7) is significant:

$$\frac{1}{T_1} \approx \rho_1 \frac{S}{V} \tag{8}$$

$$\frac{1}{T_2} \approx \rho_2 \frac{S}{V} \tag{9}$$

Experiments may be performed in the laboratory to obtain both T_1 and T_2 for fluids in porous media. It is possible to measure T_2 in a single experiment using the CPMG spin-echo method. This is faster than performing a series of inversion-recovery experiments to measure T_1. For this reason, time constraints in well logging applications usually mean that only T_2 can be determined. From Eqs (8) and (9) it can be seen that measurements of T_1 and T_2 may be used to obtain surface area to volume ratios of the pores present. If spherical pores are assumed, then the pore radius, r, may be obtained as $S/V = 3/r$. However, the actual pores of rocks are not spherical and are interconnected. We shall simply use the term 'pore size' to imply a quantity inversely proportional to S/V at a particular location in the pore space.

Figure 4 shows a plot of the T_2 distribution for water in a sedimentary rock.[58] The solid line corresponds to the case when the rock is fully saturated, and there is a distribution of relaxation times spanning three orders of magnitude. The dashed line in Fig. 4 shows the T_2 distribution after the rock has been centrifuged. It can be seen that there is a reduction in the relative amount of fluid having large values of T_2, and this corresponds to the fact that centrifugation selectively removes water from the larger pores.

However, there are a number of important limitations to this method, which will be discussed in the next subsections. First, the mathematical analysis to obtain the distribution of relaxation times is itself a problem. Secondly, the surface relaxivity parameter is required in order to obtain a pore size distribution. Thirdly, the model assumes that diffusion within the pore is rapid and that interpore coupling can be neglected. Finally, differences in magnetic susceptibility between the solid and fluid phase complicate the interpretation of

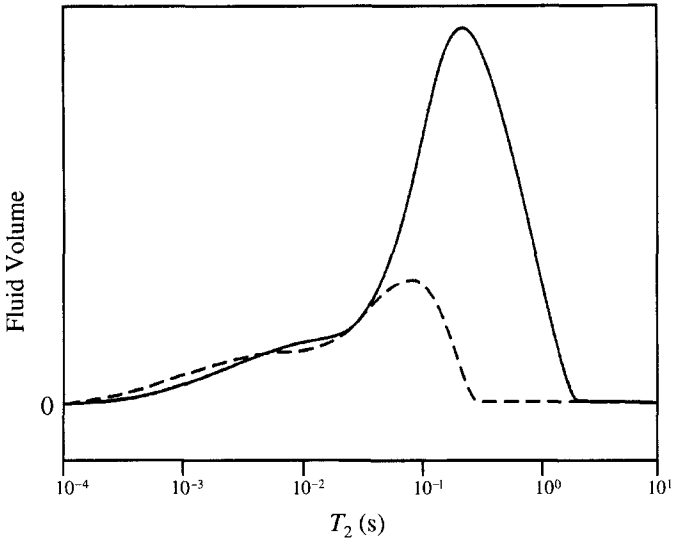

Fig. 4. Distribution of relaxation times for water in a sedimentary rock. The solid curve is for the rock fully saturated with water. The dashed curve shows results after centrifugation. (Reproduced with permission from ref. 58, © 1996, John Wiley & Sons.)

spin-echo data used to obtain the T_2 distribution. It is also possible that surface irregularities play a significant role in modifying the relaxation behaviour.[74]

Analysis of data to obtain distribution of relaxation times

Rocks tend to have a very broad distribution of pore sizes, and there is therefore a distribution of observed relaxation times. In general, the magnetization signal, $M(t)$, from a spin-echo experiment (used to determine the T_2 distribution) is expected to obey (based on Eq. (9))

$$M(t) = \sum_i m_i \exp\left[-\rho_2 \left(\frac{S}{V}\right)_i t\right] \tag{10}$$

for pores, i, with different S/V ratios, where m_i is proportional to the volume of fluid in pore i. Note that this assumes ρ_2 is independent of S/V.

However, extraction of the desired pore information from the magnetization data poses significant mathematical problems, and a number of papers have discussed different methods of analysing the data.[75–87] The experimental data often only justify fitting using a limited number of exponential components, and this would only provide a very limited number of points in a plot of pore

size distribution. Stretched exponential functions, which start by assuming a particular form of pore size distribution, have been used to circumvent this problem.[77] Modified stretched exponential functions have also been proposed and these have the advantage, compared to the basic stretched exponential function, that they can provide quantitative intensity information by back-extrapolation of the NMR data.[78] An alternative approach is simply to calculate the fractional power average relaxation time $T_2^{(p)} = \langle T_2^p \rangle^{1/p}$, where p may be specified separately. Emphasis may be given to data at short or long times depending on the choice of p, and thus different properties of the porous medium may be correlated with a particular fractional power average.[79,80]

Direct inversion of Eq. (10) to obtain the pore size distribution is also possible, for instance using inverse Laplace transform techniques, but in the presence of noise this produces a physically unrealistic distribution of pore sizes featuring many spikes.[81] It is therefore common to treat the data with a regularization function first to smooth out the noise,[82] preferably using an algorithm that selects the degree of regularization based on the signal-to-noise ratio of the measured data.[83,84] This treatment does, however, cause a small amount of broadening of the peaks in the pore size distribution plot, and may give misleading results if the actual pore distribution of the sample contains both broad and narrow peaks. An algorithm employing a variable, rather than fixed, data smoothing function has recently been implemented using an iterative feedback scheme to give 'uniform-penalty' data inversion throughout the spectrum.[85] Other inversion methods that do not suffer unduly from regularization problems have also been proposed.[86,87]

The surface relaxivity parameters

A major drawback in using NMR relaxation times to obtain pore size distributions is a lack of knowledge of the surface relaxativity parameters ρ_1 and ρ_2 in Eqs (8) and (9). It is usually assumed that the surface relaxivity is constant for a particular sample, though some workers have allowed it to vary within a sample.[88] In the case when surface relaxivity is a constant, differentiation of Equation (10) shows that the initial slope of the spin-echo magnetization data will obey:

$$\left.\frac{\mathrm{d}M}{\mathrm{d}t}\right|_{t=0} = -\rho_2 \sum_i m_i \left(\frac{S}{V}\right)_i \tag{11}$$

This permits measurement of ρ_2 provided that an independent measurement of S/V ratios is available. A similar method can be applied to estimate ρ_1 using inversion-recovery data. However, different values of the surface relaxivity parameters are obtained depending on the technique used to determine S/V ratios. For instance, pore size distributions for sandstones using BET surface

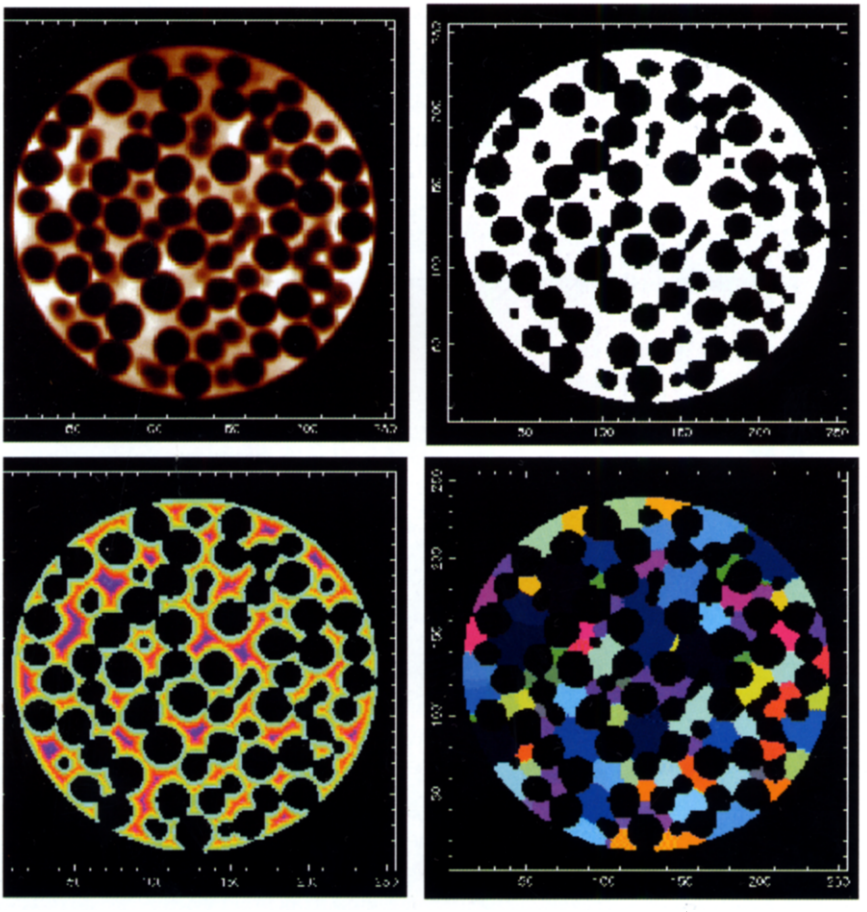

Plate 1. Application of the morphological thinning algorithm showing the processing steps. [233, 234] The image in the top left-hand corner is converted into a map of discrete pores in the bottom right-hand corner. The colouring in the pore map is used to distinguish between the individual pores assigned by the algorithm.

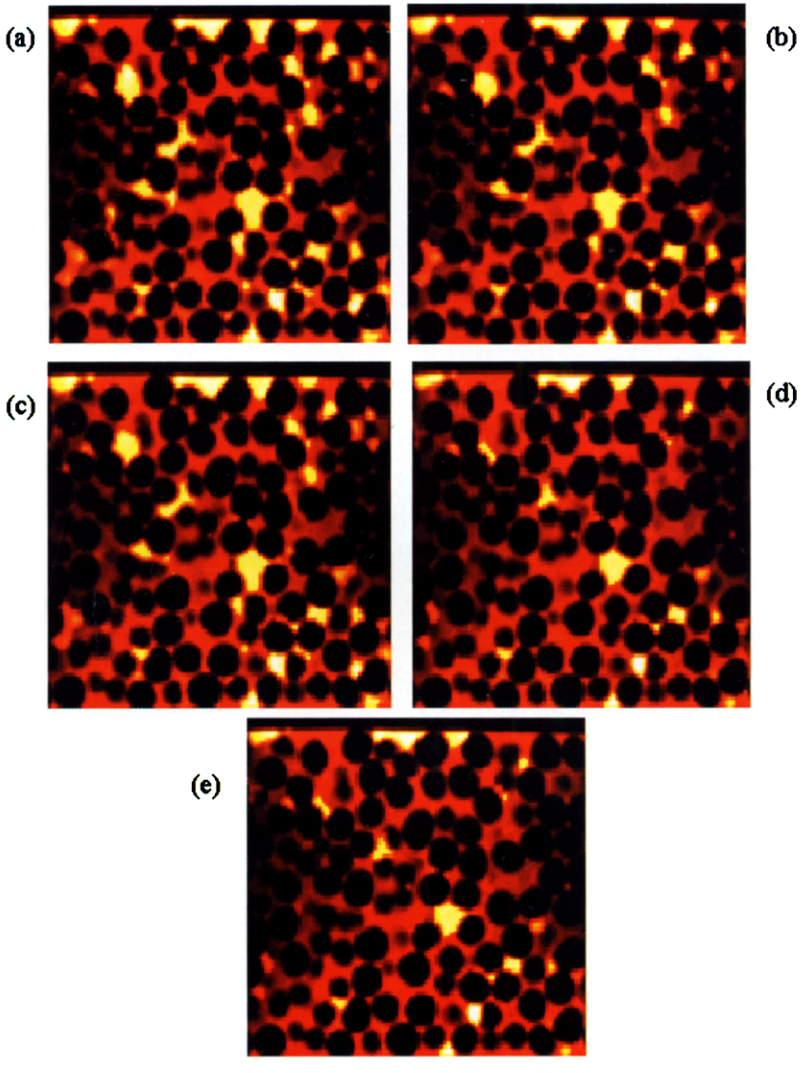

Plate 2. A slice taken from three-dimensional images recorded as a function of time. The bright regions correspond to ganglia of octanol trapped inside a packed bed of glass spheres of diameter 5 mm. Water is flowing through the packed bed, and so gradual dissolution of the hydrocarbon is taking place. The images were recorded after times of (a) 0; (b) 14.5h (c) 24.5 h; (d) 56.5h and (e) 69 h after the commencement of dissolution. (Reproduced with permission from ref. 260, © 1999, Academic Press.)

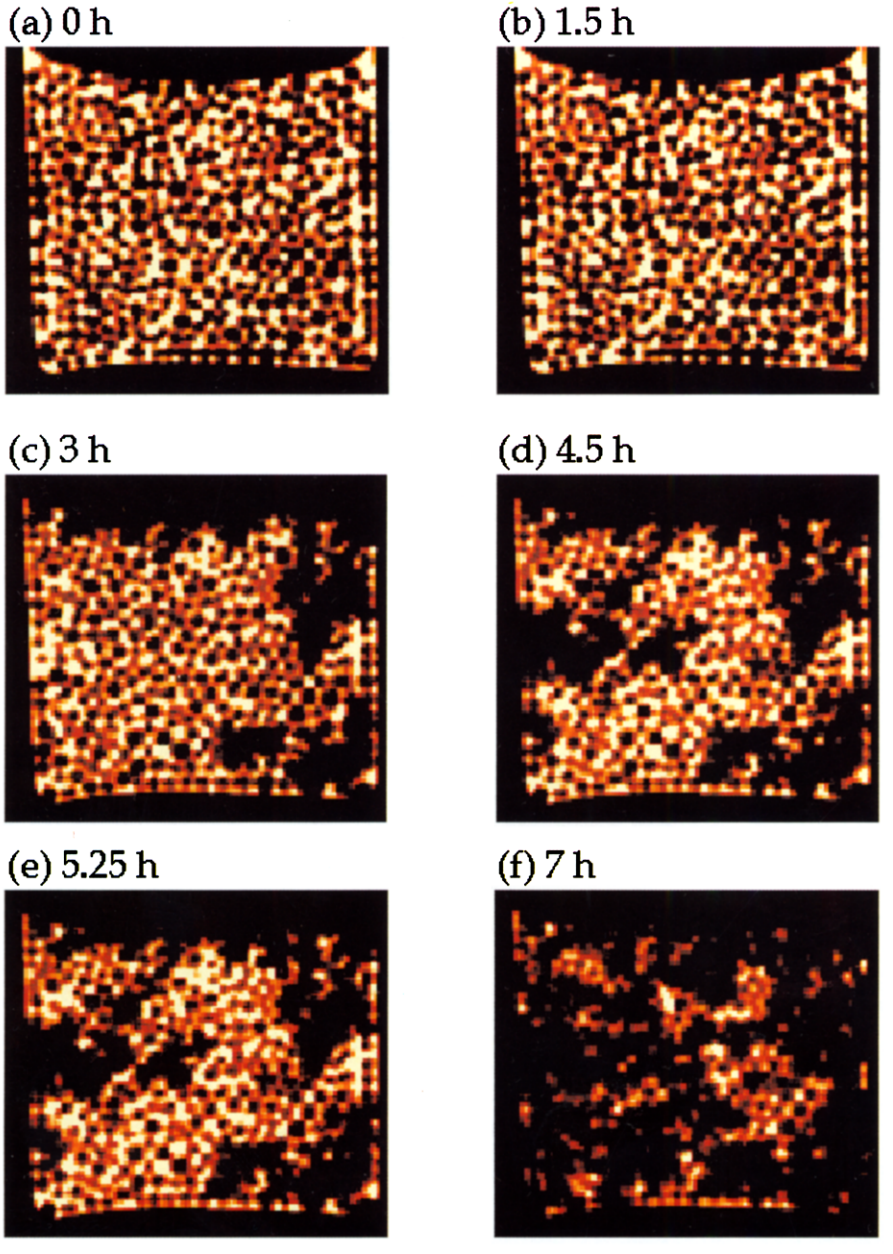

Plate 3. A slice taken from three-dimensional images of water in a packed bed of 1 mm-diameter glass spheres recorded as a function of drying time. (Reproduced with permission from ref. 272, © 1999, Academic Press.)

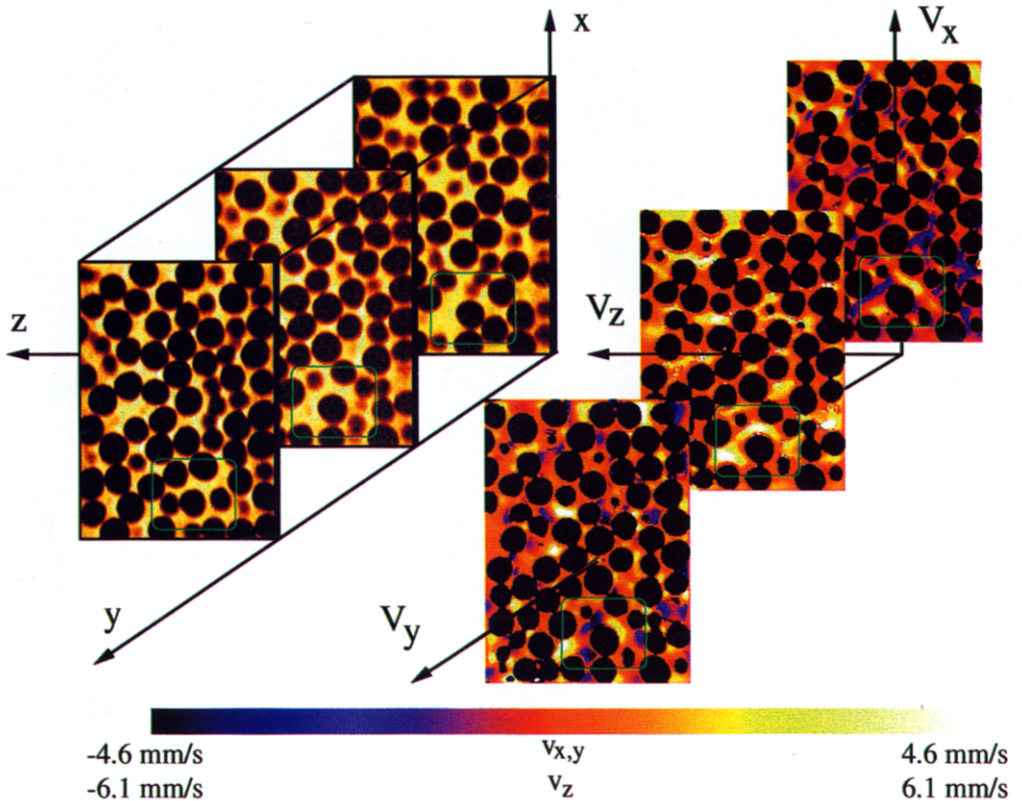

Plate 4. Spin-density and velocity images taken from water flowing in a packed bed of 5mm-diameter glass spheres. The left-hand images are slices, separated by 1 mm, from a three-dimensional spin-density image. The right-hand images are velocity images taken from the central slice on the left-hand side, and give the flow speed in the *x, y* and *z* directions. The net direction of flow is in the *z* direction. (Reproduced with permission from ref. 236, © 1997, Elsevier Science.)

areas usually give $\rho_1 = 0.1 - 0.8\ \mu m\ s^{-1}$ while those from mercury porosimetry give $\rho_1 \approx 4\ \mu m\ s^{-1}$.[58] Thin section image analysis has also been used to obtain the surface relaxivity.[89] One recent advance has been the utilization of pulsed field gradient (PFG) NMR methods to measure the surface relaxivity, as discussed in Section 4 of this review.[86,90] This method has been used successfully to determine pore size and fluid phase distributions in sandstone and carbonate samples, and the results are comparable to those estimated by mercury porosimetry.[90] A further complication to the analysis is that the actual S/V ratio may depend on the length scale of the measurement owing to the fractal nature of porous media. Despite these limitations, surface relaxivity parameters have now been measured for a range of materials with a wide distribution of pore sizes, and so in favourable cases reasonable predictions of pore size distributions can be made from NMR relaxation data alone.[91]

Diffusion and pore coupling

The simple two-site model discussed above assumes fast diffusion between bulk and surface water, and neglects the possibility of water transport to neighbouring pores of different dimensions. Thus a more general relaxation model also needs to include the rate of diffusion within a pore, and the rate of exchange of the fluid between pores (pore coupling). Thus, there are four rates to consider. These may all be written in units of s^{-1} in the following way:[92]

(1) $w_B = 1/T_{1B}$, the bulk relaxation rate of the fluid.
(2) $w_\rho = \rho/r$, the relaxation rate in the vicinity of the pore wall.
(3) $w_D = D/r^2$, the rate of molecular diffusion to the pore wall, where D is the bulk diffusion coefficient.
(4) $w_C = SD/Vb$, the rate for pore coupling, where b is the distance between the centres of neighbouring pores (Fig. 3). This expression needs modifying if the pore throat linking neighbouring pores is so small that it imposes a resistance to diffusion through it.

The model described earlier assumed that w_D was very large and w_C was very small. Relaxation time measurements for water in rocks found that T_1 and T_2 were almost independent of temperature in the range 25–175 °C.[93] This suggests that diffusion is not playing a significant role, and so supports the fast-exchange assumption. It thus appears that molecules sample only a limited volume of pore space before they are relaxed in the case of water in rocks. However, the diffusion and pore-coupling rates may be important in other systems.

The effect of diffusion within isolated pores (allowing w_D to vary) was first considered by Brownstein and Tarr.[66] In the event that diffusion within a pore is not rapid, then more than one relaxation time will be observed for that pore, with values dependent on the detailed pore geometry (rather than simply the S/V ratio of that pore). The mean relaxation lifetime under conditions when

diffusion is a limiting factor has been calculated for different pore geometries.[94] While multicomponent relaxation behaviour due to slow diffusion is observed for water in biological cells, it is not normally observed for fluids in porous solids.

The effect of pore coupling on relaxation times has been modelled.[92,95] If the rate of pore coupling is small, then a distribution of relaxation times is obtained corresponding to the distribution of S/V ratios of individual pores as discussed earlier. Faster rates of pore coupling between pores of different sizes initially cause a broadening of the relaxation time distribution.[92] Eventually the rate of coupling may become so fast that most of the sample experiences uniform magnetization behaviour. In the limit of very rapid pore coupling, a single relaxation time would be observed, related to the S/V ratio of the whole sample (rather than to those of individual pores).[92,95] The case when the rate of pore coupling is intermediate is, however, complicated to analyse in detail. Therefore, relaxation time studies of porous media are likely to continue to assume weak pore coupling for simplicity, even in those cases where this assumption is not fully justified.

Complications for spin-echo measurements

As stated earlier, T_2 is measured using a spin-echo pulse sequence. However, analysis is complicated by the fact that there will be magnetic susceptibility differences between the solid phase and the fluid filling the pore space. This leads to a background magnetic field gradient within the pore space. It is well established that diffusion of molecules in a constant field gradient during a spin-echo causes a signal decay:[96]

$$E = \exp\left(-\frac{1}{12} D\gamma^2 g^2 t^3\right) \tag{12}$$

where E is the attenuation, D is the diffusion coefficient, γ is the gyromagnetic ratio, g is the field gradient, and t is the spin-echo time. This decay is in addition to the decay due to pure spin–spin relaxation, which is the property that we wish to measure. Analysis of spin-echo data in the presence of a constant background field gradient thus gives an apparent relaxation time, T_2^{app}, that differs from the true spin–spin relaxation time, T_2^{true}:

$$\frac{1}{T_2^{\text{app}}} = \frac{1}{T_2^{\text{true}}} + \frac{1}{12} D\gamma^2 g^2 t^2 \tag{13}$$

Thus attenuation due to magnetic susceptibility effects has to be minimized if measured T_2 relaxation times are to be reliable. For this reason, T_2 experiments

on porous media are best performed in fairly small static magnetic fields because the internal gradient, g, due to magnetic susceptibility differences is proportional to B_0. It is also best to use only short echo delays, t. In well logging applications, the ^{1}H resonance frequency is typically 2 MHz, and echo delays less than 70 μs are used. Under these conditions it has been shown that the errors in T_2 determination are small even in the presence of large static magnetic field gradients.[58,97]

For spin-echo measurements at higher magnetic fields, it is found that the apparent T_2 depends on the echo time, t. However, experimentally the apparent rate of relaxation does not follow Eq. (13) but has an approximately linear dependence with t. One reason for this is that the magnetic field gradient is not constant within these materials, and the conditions for the quasi-linear variation with t have been discussed.[22,98,99] It is also worth pointing out that there is a problem with defining diffusion coefficients in a bounded space, as will be discussed in Section 4, and so Eq. (12) is not strictly valid in confined geometries.[100] As a result of this, dephasing in the presence of field inhomogeneities due to magnetic susceptibility differences has been shown to depend on pore size.[101] In the particular case of isolated spherical pores, analytical solutions for the spin-echo intensity including the effect of diffusion in a field gradient have been obtained.[102]

Applications of relaxation times to the characterization of porous rocks

Despite the limitations discussed in earlier Subsections, relaxation time data are useful for characterizing porous media. For instance, NMR well logging experiments provide valuable information that may be critical in determining whether a particular borehole will be profitable. As well as pore size information, other parameters characterizing the pore space have also been obtained from relaxation data.

A number of correlations between permeability and relaxation time have been proposed.[71,80,83,103–107] Measurements may also be made on porous systems that are not fully saturated with fluid. Such experiments can provide an estimation of capillary pressures and residual fluid content after drainage at a given pressure.[108,109] Drainage experiments show that relaxation times change with the degree of saturation owing to the fluid being distributed in different sized pores for different saturation states.[110] Experiments as the fluid content is reduced can also be used to probe the degree of sample homogeneity at different length scales, as the term due to surface relaxation at the wall will become more increasingly dominant over the bulk water relaxation term.[111]

When two immiscible fluids are present in the pores, relaxation time measurements provide information on the fluid locations and can be used to estimate the wettability, i.e. to quantify the affinity of the surface of the pores towards one fluid in preference to another.[112–114] The irreducible water

saturation (the fraction of water in porous media that remains trapped in the solid matrix after displacement with a nonwetting phase) may also be estimated from relaxation data.[80,106,115]

There have been comparatively few studies of the NMR relaxation times of gases within porous structures, despite the importance of this in well logging applications. Preliminary measurements on methane show that surface relaxation affects T_1 when the gas alone is present, but has little effect when water is also present.[116] Fast gaseous diffusion means that T_2 measurements of gases are dominated by the internal field gradients due to magnetic susceptibility. Indeed, it has been suggested that measurements of the inhomogeneous susceptibility by this method might actually prove a useful method for characterizing porous media.[117]

Applications of relaxation times to the characterization of other macroporous media

A number of systems besides porous rocks have been investigated. For instance, the two-site fast-exchange model has been applied successfully to measure the pore space of cement pastes during hydration.[118] Results show that two distinct pore volume components are present.[39,119]

Characterization of the pore spaces of soils is an area of importance in hydrology. Spin–lattice relaxation time measurements have successfully been made on saturated beds of nonporous silica particles to characterize the interparticle pore size distribution. However, the interparticle pore sizes predicted by NMR relaxation times were underestimated when highly porous silica particles were used.[120] It thus appears that interparticle information from relaxation times may only be reliable if the solid phase has low to moderate surface area. Despite this limitation, the pore sizes derived from NMR relaxation time data for Borden Aquifer material agree well with those observed in scanning electron micrographs.[120] Other work has found that T_2 of water in saturated soils varies significantly from sample to sample and is affected by magnetic susceptibility and the presence of free iron oxides, clay, sand, exchangeable cations and organic matter. Using a spin-echo pulse sequence with an echo delay of 1 ms, only 0.4–66% of the water present is detected, and this probably represents the water present in large pores.[121]

NMR relaxation times have also proved useful in probing water mobility in foodstuffs. In some cases, exchange between three water sites, corresponding to bulk, surface and bound water, is used to explain observed relaxation behaviour.[122] Another interesting area is using NMR relaxation times to study the water that does not freeze at the temperatures normally used in cryopreservation.[123]

3.3. Relaxation in mesoporous materials

Porous silicas are usually mesoporous materials and they can be made with a variety of pore dimensions. In particular, silica glasses can be made with well-defined pore diameters, typically in the range 30–250 Å, using sol-gel methods. Such a system provides a good model for testing the models of relaxation behaviour of fluids in porous solids. It is normally found that the two-site fast-exchange model for relaxation described above for macroporous systems is still valid.[124,125] For instance, ^{1}H and ^{2}H relaxation times have been measured during both adsorption and desorption of water in a porous silica. Despite hysteresis in the observed adsorption isotherms, it was found that the relaxation times depended solely on water content.[126] For deuterated water in some porous silicas, multicomponent ^{2}H relaxation behaviour for T_2 and $T_{1\rho}$ has been observed, and this has been attributed to the fractal nature of the pore structure.[127]

Relaxation time studies of the filling process of porous silica with water and cyclohexane have been used to establish whether the adsorption is homogeneous.[128] It was found that water initially collected in small puddles at interstices in the structure, and then formed a surface layer over the silica surface before the remaining pore volume was filled. On the other hand, cyclohexane appeared to fill the smaller pores completely before spreading to the larger pores. A similar effect was observed for water adsorbing in a silica that had been chemically treated to make the surface hydrophobic. Thus, the fluid location in mesoporous materials at low loadings depends critically on the wettability of the surface.

Some interesting effects have been observed in a series of ^{1}H and ^{2}H relaxation time experiments using different organic liquids within silicas of known pore size under saturation conditions. It was observed that the relaxation times of polar molecules, such as pyridine, aniline and nitrobenzene, obeyed:[129,130]

$$\frac{1}{T_1} = a + \frac{b}{r} \tag{14}$$

where r is the pore radius, and a and b are constants. A similar result was obtained for the other relaxation times, $T_{1\rho}$ and T_2. This is as predicted by Eqs (6) and (7), and indicates that the two-site fast-exchange model continues to be effective even at a pore radius as low as 18 Å in the cases studied. However, nonwetting adsorbates (i.e. those with only weak interactions with the surface) such as cyclohexane, decalin and toluene were found to deviate from this behaviour, particularly in the smaller pores (see Fig. 5).[130,131]

The explanation for this is that translational diffusion in a confined geometry can cause relaxation even in the absence of a surface relaxation

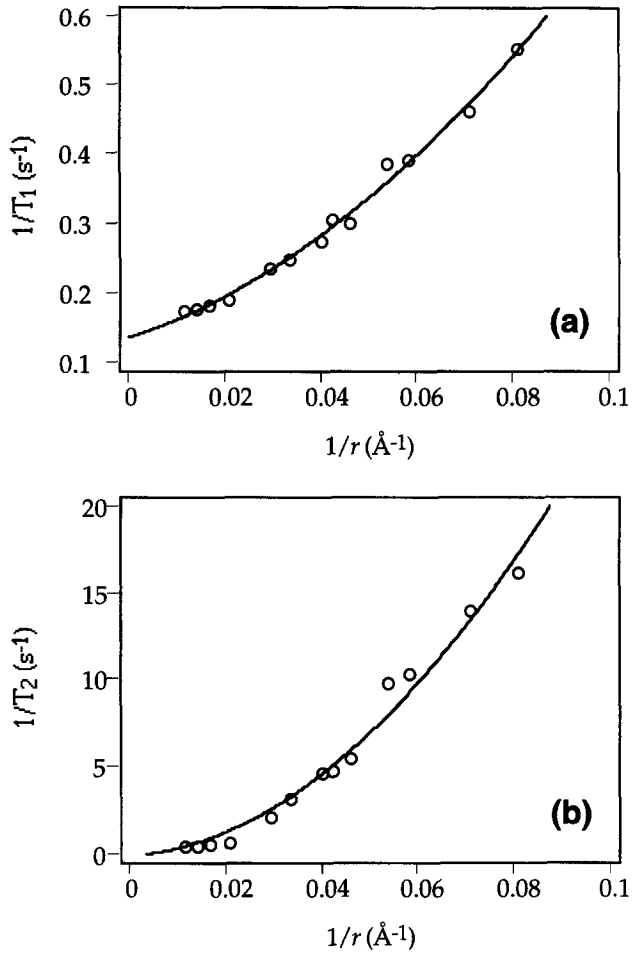

Fig. 5. ^{1}H relaxation time measurements at 300 K and 180 MHz of methylcyclohexane in silica sol-gel glasses as a function of 1/pore radius: (a) $1/T_1$; (b) $1/T_2$. (Reproduced with permission from ref. 131, © 1994, American Institute of Physics.)

mechanism.[130] For instance, the reorientational dynamics of adsorbates such as toluene within silica are no longer isotropic, indicating that the confined geometry is playing an important role.[132] Evidence for nonisotropic motion, such as for a two-dimensional system, also comes from the fact that a logarithmic dependence of $1/T_1$ on spectral frequency is observed for weakly interacting adsorbates in small pores.[130] The relaxation rate ($1/T_1$) in a two-dimensional spin system within spherical pores is expected to be proportional to $1/r^2$.[133] Thus, in small mesopores (with $r < 30$ Å) the relaxation data for

nonwetting fluids obey:[130,131]

$$\frac{1}{T_1} = a + \frac{b}{r} + \frac{c}{r^2} \tag{15}$$

where c is a constant. The first term can be treated as being due to bulk relaxation, the second term as due to surface relaxation, and the third term arises from purely geometrical effects. The curves shown in Fig. 5 are fits to the experimental data for methylcyclohexane in silica using Eq. (15).

Relaxation time measurements have also been used to gain more information on the dynamics of molecules in the adsorbed surface layer. For instance, the temperature variation of the ^2H spin–lattice relaxation time of deuterated pyridine in porous silica gives information on the rotational dynamics of the surface layer.[134] Spin–lattice relaxation time measurements made in different magnetic fields have also been used to gain information on the dynamics of molecules at the surface of porous silica. The adsorbate molecules are found to have a preferential orientation relative to the local surface, which may be expressed as an 'orientational structure factor'.[135,136] Relaxation by the dipolar coupling mechanism is then possible in two different ways. The first method is translational diffusion at the surface, as this will cause molecular reorientation. The second method is bulk-mediated surface diffusion, in which desorption and readsorption steps occur in a Lévy walk mechanism. The combination of these leads to an efficient spin–lattice relaxation mechanism when the adsorption is strong.[135,137] Some interesting work performed field-cycling relaxation time measurements on frozen adsorbates within porous media.[138–140] While the adsorbate is rigid in the centre of the pore, that at the surface forms a 'nonfrozen layer' owing to the incommensurability of the adsorbate crystal structure and the matrix surface. Surface diffusion continues to occur by the translational diffusion mechanism, and may be surprisingly rapid. Field-cycling relaxation time measurements under these conditions may become another method suitable for the determination of pore size.[138]

4. PULSED FIELD GRADIENT (PFG) NMR METHODS

Pulsed field gradient methods may be used in combination with a spin-echo pulse sequence to measure average molecular displacements in a time Δ.[141–143] In liquids, PFG methods can therefore be used to measure self-diffusion coefficients (i.e. the rate of diffusion due to Brownian motion in the absence of a concentration gradient). In porous media, there is the possibility of obtaining information about the pore geometry because the pore boundaries will influence molecular transport. PFG techniques can measure restricted diffusion and thus provide valuable information on pore sizes in the range 5–100 μm.

This is beyond the resolution of the NMR imaging techniques that are discussed in Section 5. In this section, we shall consider the theory behind the application of PFG methods to measure diffusion coefficients, and then go on to consider how diffusion coefficients in porous media reveal structural information. Some PFG pulse sequences that overcome particular problems experienced for porous media are discussed. PFG methods on samples in which there is bulk flow of fluid will be considered in Section 6.

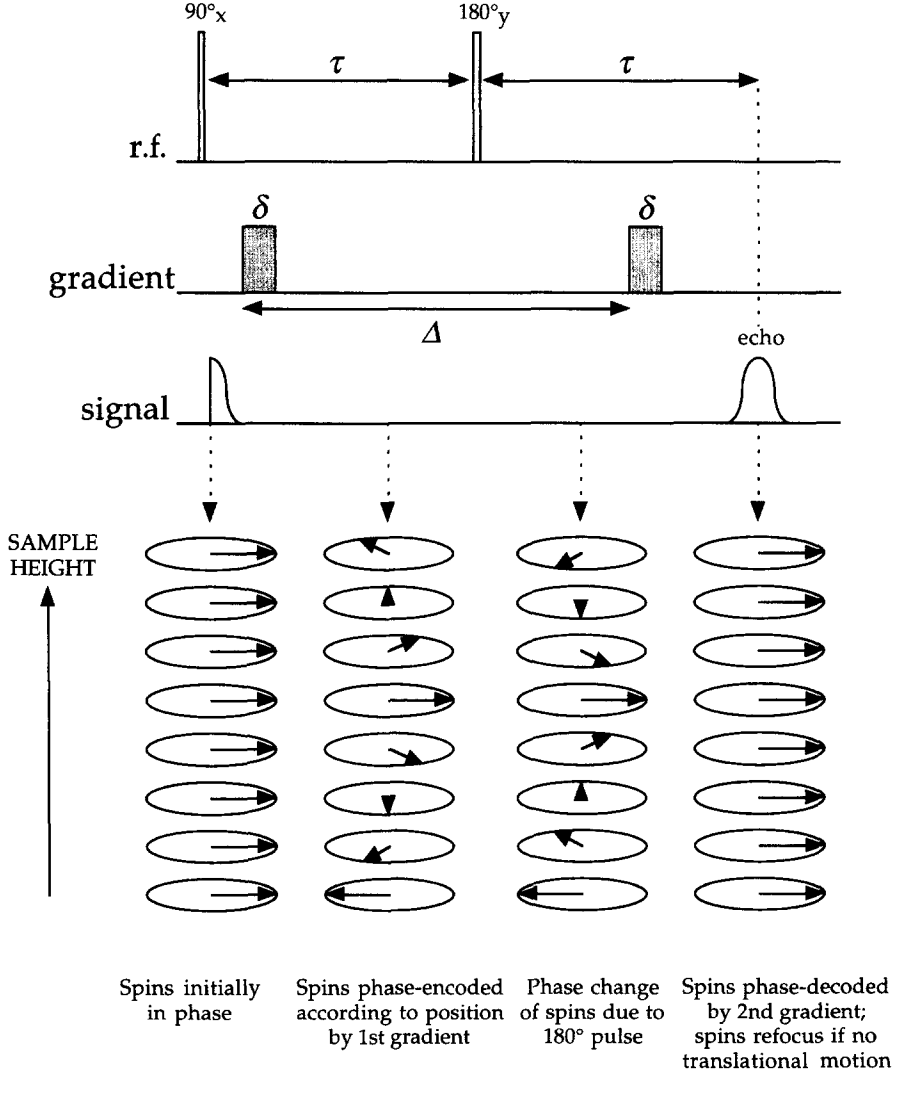

Fig. 6. The pulsed field gradient (PFG) spin-echo pulse sequence.

4.1. Diffusion measurements using the PFG technique

Consider the pulse sequence shown in Fig. 6. Two magnetic field gradient pulses of magnitude g, duration δ and separation Δ are applied during the dephasing and rephasing sections of a spin-echo pulse sequence. The use of pulsed field gradients, rather than a continuous background gradient, retains chemical shift information and ensures that the entire sample volume is measured. The nuclear spins during the magnetic field gradient pulses will have different Larmor precession frequencies, ω, depending on their spatial location according to the equation:

$$\omega(\mathbf{r}) = \gamma B_0 + \gamma \mathbf{g} \cdot \mathbf{r} \tag{16}$$

where $\mathbf{r}$ is the position, B_0 is the static magnetic field and $\mathbf{g}$ is the magnetic field gradient. As a result of this, at the end of the first field gradient pulse, the nuclear spins will have been encoded with a particular phase depending on their location. During the rephasing part of the spin-echo, an identical field gradient is encountered. In the absence of any molecular motion, the second gradient will exactly rephase all spins so that no attenuation in the echo signal will be observed, other than that from spin–spin relaxation (Fig. 6).

However, molecular motion may have occurred in the interval Δ between the two pulsed field gradients. The phase shift of a nucleus that moves from location $\mathbf{r}$ to $\mathbf{r}'$ in time Δ is given by

$$\text{Phase shift} = \gamma \delta \mathbf{g} \cdot (\mathbf{r}' - \mathbf{r}) \tag{17}$$

If the conditional probability of this displacement is $P_s(\mathbf{r} \mid \mathbf{r}', \Delta)$, then the echo signal E for the ensemble will be

$$E(\mathbf{g}, \Delta) = \int\int \rho(\mathbf{r}) P_s(\mathbf{r} \mid \mathbf{r}', \Delta) \exp[i\gamma \delta \mathbf{g} \cdot (\mathbf{r}' - \mathbf{r})] \, d\mathbf{r} \, d\mathbf{r}' \tag{18}$$

It is useful to define the *average propagator*, $\bar{P}_s(\mathbf{R}, \Delta)$ as the ensemble-averaged probability for a molecule to displace by $\mathbf{R} = \mathbf{r}' - \mathbf{r}$ irrespective of starting position.[144] Thus,

$$\bar{P}_s(\mathbf{R}, \Delta) = \int \rho(\mathbf{r}) P_s(\mathbf{r} \mid \mathbf{r} + \mathbf{R}, \Delta) \, d\mathbf{r} \tag{19}$$

Combining Eqs (18) and (19) gives

$$E(\mathbf{g}, \Delta) = \int \bar{P}_s(\mathbf{R}, \Delta) \exp[i\gamma \delta \mathbf{g} \cdot \mathbf{R}] \, d\mathbf{R} \tag{20}$$

This is normally expressed in '**q**-space' by defining[141]

$$\mathbf{q} = \gamma\delta\mathbf{g}/2\pi \tag{21}$$

Hence the spin-echo signal is

$$E(\mathbf{q}, \Delta) = \int \bar{P}_s(\mathbf{R}, \Delta) \exp[2\pi i\mathbf{q} \cdot \mathbf{R}]\, d\mathbf{R} \tag{22}$$

Note that the spin-echo signal intensity will also be affected by NMR relaxation during the pulse sequence. However, the time taken for echo formation may be kept constant while varying **q**, and this enables the average propagator to be determined through the inverse Fourier relationship:

$$\bar{P}_s(\mathbf{R}, \Delta) = \int E(\mathbf{q}, \Delta) \exp(-2\pi i\mathbf{q} \cdot \mathbf{R})\, d\mathbf{q} \tag{23}$$

For fluids in porous media, this propagator contains information on the diffusion coefficient of the fluid, and information on the pore geometry, as will now be discussed.

Unrestricted diffusion

In the case of unrestricted diffusion (i.e. when diffusion is not affected by pore walls), the Einstein equation gives the mean square displacement of molecules in a time Δ:

$$\langle \mathbf{r}^2(\Delta) \rangle = 6D\Delta \tag{24}$$

where D is the self-diffusion coefficient. In this case, the average propagator $\bar{P}_s(\mathbf{R}, \Delta)$ is a Gaussian function and Equation (22) can be used to show that

$$E(q, \Delta) = \exp(-4\pi^2 q^2 D\Delta) \tag{25}$$

where q is the magnitude of **q**. In the case of the pulse sequence shown in Fig. 6, this equation can be modified to allow for the effects of finite-length gradient pulses to give[145]

$$E(q, \Delta) = \exp(-4\pi^2 q^2 D(\Delta - \delta/3)) \tag{26}$$

This provides a means of measuring the diffusion coefficient of a fluid. The spin-echo intensity is measured while q is varied (by changing **g** or δ). A plot of $\ln(E(q, \Delta))$ against $4\pi^2 q^2(\Delta - \delta/3)$ will be linear with gradient $-D$. Some

applications of measuring diffusion coefficients in this manner for adsorbates in microporous solids are given in Section 6. There are also a number of refinements to this basic PFG spin-echo pulse sequence, and these will be discussed in Section 4.2.

Restricted diffusion in isolated pores

In an isolated pore, collisions of molecules with the pore wall during the time Δ mean that the apparent diffusion rate will be influenced by the pore geometry. The average propagator will still be Gaussian if the distance moved by molecules in the time Δ is less than the pore size (i.e. when $\Delta \ll r^2/D$ for a spherical pore), and the measured diffusion coefficient will then be the same as for the case of unrestricted diffusion (i.e. Eqs (25) and (26) can be applied). The pore wall will, however, have an effect if $\Delta > r^2/D$. In the case of isolated pores, the pore walls impose a limit to the distance that molecules can diffuse. Figure 7 shows a schematic plot of $\ln(E(q, \Delta))$ against $4\pi^2 q^2 \Delta$ for the cases of free diffusion and restricted diffusion. In the case of restricted diffusion, analytical expressions for $E(q, \Delta)$ neglecting the effect of relaxation at the wall can only be obtained for simple geometries such as diffusion in a rectangular box.[146,147] These calculations predict that minima in $E(q, \Delta)$ will occur when $q \approx 1/r$ in a process analogous to that causing diffraction peaks in light-scattering experiments.[147–149] An alternative view of the phenomenon is as a discord of spin phase structure.[150] Such diffusive diffraction effects were first observed experimentally for connected pores (discussed below in the next subsection), but have since been observed for pentane constrained between two parallel plates and for water in a cylinder.[151,152]

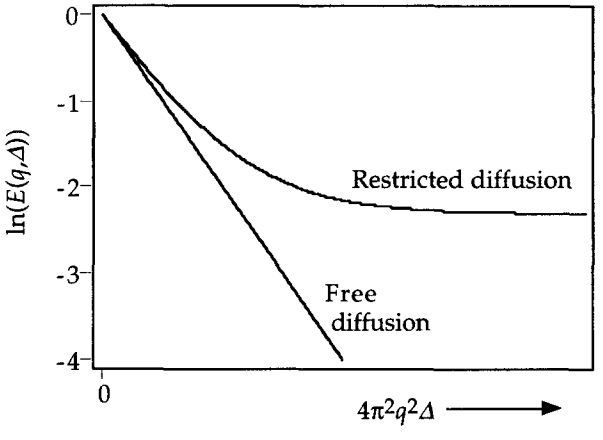

Fig. 7. Schematic log-attenuation plot comparing free and restricted diffusion behaviour.

Calculations of the spin-echo intensity are complicated by the fact that surface relaxation may play a significant role. A general formalism for calculating PFG spin-echo attenuation for restricted diffusion in isolated pores has recently been proposed that allows for wall relaxation effects.[153] Expressions have been obtained for the cases of diffusion within a sphere,[102,154] and for planar and cylindrical geometries.[155,156] These show that diffraction effects are still apparent even when surface relaxation is rapid. Also, the locations of the minima in the spin-echo intensities are not particularly affected by varying the surface relaxation parameter, ρ.[155,156] Analysis of PFG spin-echo data that feature diffraction effects thus enables a characteristic pore size to be determined. For instance, PFG spin-echo data on water in a cylindrical capillary tube (with the field gradient applied perpendicular to the axis) can be used to determine the inner diameter.[152]

Another complication is the fact that gradient pulses have a finite length. Unlike the case of free diffusion, it is not straightforward to predict the influence of this factor on PFG spin-echo intensity measurements. Finite gradient pulses have been considered during diffusion between two parallel plates.[153,157,158] Numerical solutions of this case have also been obtained.[159] For other geometries, the effects may be approximated by treating the finite gradient pulses as a sequence of narrow pulses, and this method has been shown to agree with numerical simulations.[160,161]

Restricted diffusion in connected pores

Diffusion in the case of interconnected pores is more complicated to analyse in detail. On the basis of pore-hopping models, diffusive diffraction effects are predicted at values of $q \approx 1/b$, $2/b$ and so on (where b is the distance between pore centres).[147,149,162] Experimental evidence for this is shown in Fig. 8, which shows spin-echo signal intensities from water saturating a randomly packed bed of polystyrene spheres with diameter 15.8 μm. The data were recorded at four different Δ times as a function of q. At signal intensities less than 1% of the original, a maximum in signal can indeed be seen at a spacing corresponding to the expected interpore spacing.[147] Realistic parameters for interpore spacings have been obtained from PFG spin-echo measurements on water saturating close-packed polymer spheres of different sizes.[163] Similarly, simulations of disordered porous media have shown that the echo-diffraction pattern still detects the dominant length scale.[164] Predictions of PFG spin-echo intensities have also been made for diffusion in fractal spaces.[165] Another similarity between PFG spin-echo intensities and optical scattering is that it has been shown that spin-echo intensities become proportional to $1/q^4$ when q becomes large; this is analogous to the Debye–Porod law.[166,167]

Correct interpretation of diffusion constants in porous materials depends critically on the measurement time Δ.[168] In the case when Δ is large, more than one pore will be sampled during the measurement (i.e. when $\Delta > b^2/D$, where b

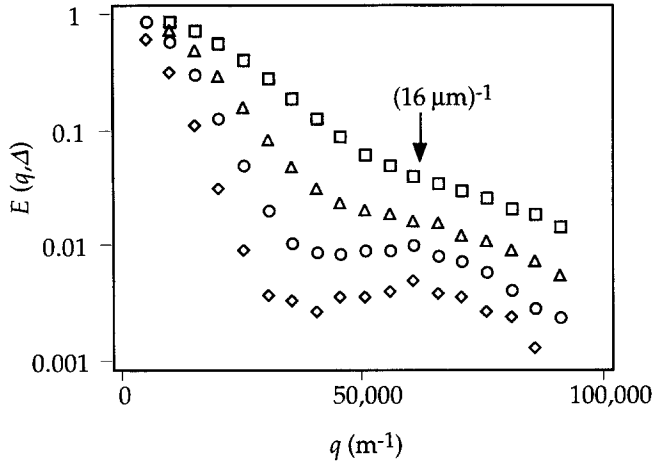

Fig. 8. Plot of spin-echo intensity (on a logarithmic scale) against the gradient wave vector q for water in a randomly packed bed of polystyrene spheres with average diameter 15.8 μm. The diffusion time Δ was 20 ms (squares), 40 ms (triangles), 70 ms (circles) and 110 ms (diamonds). A coherence peak is observed at a position corresponding to the average interpore spacing. (Reproduced with permission from ref. 147, © 1992, American Institute of Physics.)

is the distance separating pores, Fig. 3). In this case, the propagator will be Gaussian, and an effective long-range diffusion coefficient D_{eff} can then be defined by analogy with Eq. (24):

$$D_{\text{eff}} = \lim_{t \to \infty} \frac{\langle \mathbf{r}^2(t) \rangle}{6t} \tag{27}$$

Note that in some cases direct measurement using PFG NMR of this quantity by increasing Δ to large values may be hindered by loss of signal intensity due to nuclear relaxation during the spin-echo measurement. The effective diffusivity is related to the bulk diffusion coefficient through the relation

$$D_{\text{eff}} = D/\alpha \tag{28}$$

where α is the tortuosity (defined in Section 1).

There is an important intermediate case, which occurs just at the point when more than one pore is being sampled during the diffusion time. In this case, an apparent diffusion coefficient D_{app} may be defined on the basis of Eq. (25) (assuming that $\delta \ll \Delta$):

$$D_{\text{app}}(\Delta) = -\frac{1}{4\pi^2 q^2} \frac{\mathrm{d} \ln[E(q, \Delta)]}{\mathrm{d}\Delta} \tag{29}$$

Measurements of D_{app} by PFG NMR reveal different information about the pore structure depending on the choice of Δ.[169]

Random walk simulations assuming a smooth surface and allowing for surface relaxation have derived the following equation for short Δ times:[170,171]

$$\frac{D_{app}}{D} = 1 - \frac{4}{9\sqrt{\pi}} \left(\frac{S}{V}\right) (D\Delta)^{1/2} + O(D\Delta) \tag{30}$$

Thus measurements of D_{app} at short Δ times may be used to measure the surface area to volume ratio of the pores.[90,172–175] This is a particularly useful measurement, as it may be compared with the results of relaxation time measurements (discussed in Section 3), and thus provide an independent measurement of the surface relaxivity parameters ρ_1 and ρ_2.[90,173–175]

In the case when Δ is large, several pores may be sampled, and it would be expected that $D_{app} = D_{eff}$ in the limit of large Δ. Thus PFG measurements may be used to obtain D_{eff}, and thus to obtain the tortuosity of the pore structure through Eq. (28).[173,176,177] Tortuosity results obtained on porous media using this method are somewhat variable. Good results may be obtained on model porous media consisting of glass spheres, but less reliable results are obtained on rock samples in which there is a broad range of pore sizes.[174,178] One approach to obtaining pore space information from PFG spin-echo data when there is a broad distribution of pore sizes present is to calculate the probability of diffusing molecules returning to their initial positions after a given diffusion time.[179–181] This 'return-to-origin' probability quantifies the dynamic connectivity of a pore space, and it has been used to characterize natural rock samples with widely different pore connectivities.[179]

In general it is clear that PFG spin-echo data can provide information on the pore structure at both the gradient length scale, $1/q$, and the diffusion length scale, $\sqrt{(D\Delta)}$. The NMR data can be analysed to obtain simple structure factors, which may then be related to particular pore network models.[169,182]

4.2. PFG pulse sequences

The basic spin-echo pulse sequence shown in Fig. 6 is not normally used in practice for PFG measurements as it has a number of disadvantages. First, there would be significant loss of signal in the time Δ owing to spin–spin relaxation. Therefore it is normal to use a stimulated echo pulse as shown in Fig. 9a.[183] This stores the magnetization in the z-direction once the spins have been phase-encoded. The advantage of this is that, during this period, signal losses will only be due to spin–lattice relaxation, and it is normally found that $T_1 \gg T_2$ for fluids in porous media.

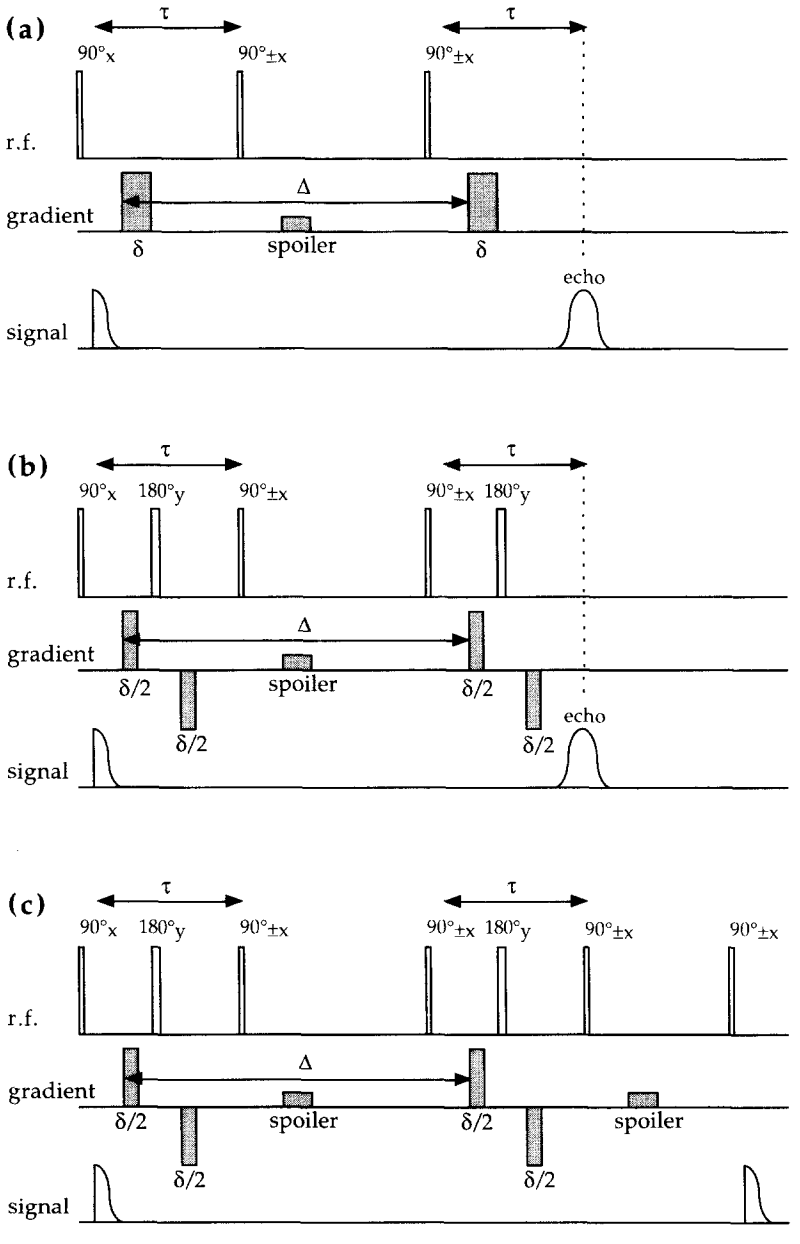

Fig. 9. Modifications to the basic PFG spin-echo pulse sequence: (a) stimulated echo; (b) addition of alternating pulse gradients; (c) addition of longitudinal eddy-current delay period.

Another problem is that spin-echo measurements are affected by background field gradients that will be present when there are magnetic susceptibility inhomogeneities within the sample. For instance, this reduces the general applicability of proposed continuous field gradient techniques.[184–186] The magnetic susceptibility problem can be reduced by applying very large field gradients,[187,188] but these are not always achievable or appropriate to the system under investigation. The influence of background field gradients when the pulsed field gradients are not switched on may be minimized using the stimulated echo method, or by employing a multiple spin-echo technique.[189–191] Background field gradients will also be felt during the applied field gradients, and this superposition will affect the spin-echo intensities. This effect can be reduced by using alternating bipolar phase field gradients.[192–194] One such pulse sequence that is appropriate when large static field gradients are present is the alternating pulsed gradient (APG) method, also known as the bipolar pulse pair (BPP) method, shown in Fig. 9b.[195]

A further problem is that strong pulsed field gradients generate eddy currents within the coil of the probe, and these can distort the signal obtained. It is therefore often desirable to have a reasonable delay between the last pulsed field gradient and the signal acquisition. This may be achieved by storing the magnetization in the z-direction for a time after the last pulsed field gradient before detection.[196] The combined PFG pulse sequence employing a stimulated echo (STE), alternating phased gradients (APG) and a longitudinal eddy-current delay (LED) is shown in Fig. 9c, and this corresponds to the 13-interval sequence previously suggested.[193] Analysis of this sequence has shown that the signal intensity, allowing for finite-length field gradients, obeys[195a,b]

$$E(q, \Delta) = \exp(-4\pi^2 q^2 D(\Delta - t/2 - \delta/3)) \tag{31}$$

where t denotes the time interval between the opposite polarity gradient pulses.

The role of the spoiler field gradients in the STE and LED sequences is to destroy unwanted magnetization in the $x - y$ plane, and this helps suppress signal from unwanted coherence pathways. Full phase cycling is particularly important with the pulse sequences shown in Fig. 9 in order to remove unwanted echo formation. In some cases, bipolar gradients of different strengths may be used if the phase cycling is insufficient to remove unwanted signal,[197] but this will create errors if the background field gradients are large. Another factor that is critical in obtaining reliable results is that the pulsed field gradient areas need to be equal in order for the spins to be refocused completely. For some NMR probes, this can be facilitated by using dummy gradients at the correct intervals before the RF pulse sequence is started. For other probes, small adjustments may need to be made to the length of the decoding field gradient in order to maximize the observed signal; this is normally a trial-and-error process.

4.3. Transport measurements using PFG techniques

We have so far discussed PFG methods that characterize porous media when there is no net flow of liquid through the sample. However, PFG techniques may still be applied when there is bulk fluid flow through the porous medium. The signal for the spin-echo signal (Eq. (22)) and the average propagator (Eq. (23)) are still applicable in the case of flowing fluid. Hence PFG spin-echo measurements may be used to obtain the average propagator $\bar{P}_s(R, \Delta)$, which is the ensemble-averaged probability for a molecule to be displaced by the vector **R** in time Δ.

One interesting phenomenon that has been observed is that the echo signal intensity may show maxima due to 'flow-diffraction' in a similar process to that discussed for diffusion in Fig. 8.[198,199] This arises when the mean displacement ($v_{ave}\Delta$, where v_{ave} is the average velocity) is comparable to the average pore separation.

Figure 10 shows some experimentally determined propagators from PFG spin-echo measurements on 3 wt% aqueous sodium chloride solution in Fontainebleau sandstone.[200] The aqueous phase was pumped through the sample at a flow rate of 400 ml h^{-1}. The upper graph shows propagators in the axial direction, which corresponds to the direction of flow, at four different Δ times. When $\Delta = 67$ ms, the propagator is approximately Gaussian, and the molecular transport within this timescale is largely confined to single pores. When $\Delta = 417$ ms, an asymmetric peak is observed with reproducible oscillatory features. At this timescale, molecular transport is over more than one pore, and the detailed shape of the propagator will depend on the pore sizes and geometry. When $\Delta = 813$ ms, the propagator is becoming close to Gaussian again, as would be expected for bulk flow over a long length scale with a degree of dispersion. The lower graph in Fig. 10 shows propagators in the radial direction, perpendicular to the direction of net flow.[200] As expected, the propagators are symmetric about zero net flow in this direction, and the shape is Gaussian at short Δ times. At longer Δ times, the propagator becomes broadened, and some features on the curves can be observed that are related to the pore structure. Similar experiments have also been made on packed beds of glass spheres.[201–205] Transport in a chromatographic column has also been studied using the PFG propagator approach.[206] The propagator curves obtained for fluids within porous media have been simulated numerically, assuming appropriate pore network models.[200,202–204] The PFG NMR approach is thus a valuable tool in identifying which pore network models are physically realistic at this length scale.

Propagators have also recently been measured for multiphase flow in Fontainebleau sandstone by the PFG approach using flows of water, dodecane and nitrogen gas. In an extensive series of experiments, both water and dodecane propagators were measured at different degrees of water saturation to reveal information on the physical importance of parameters such as

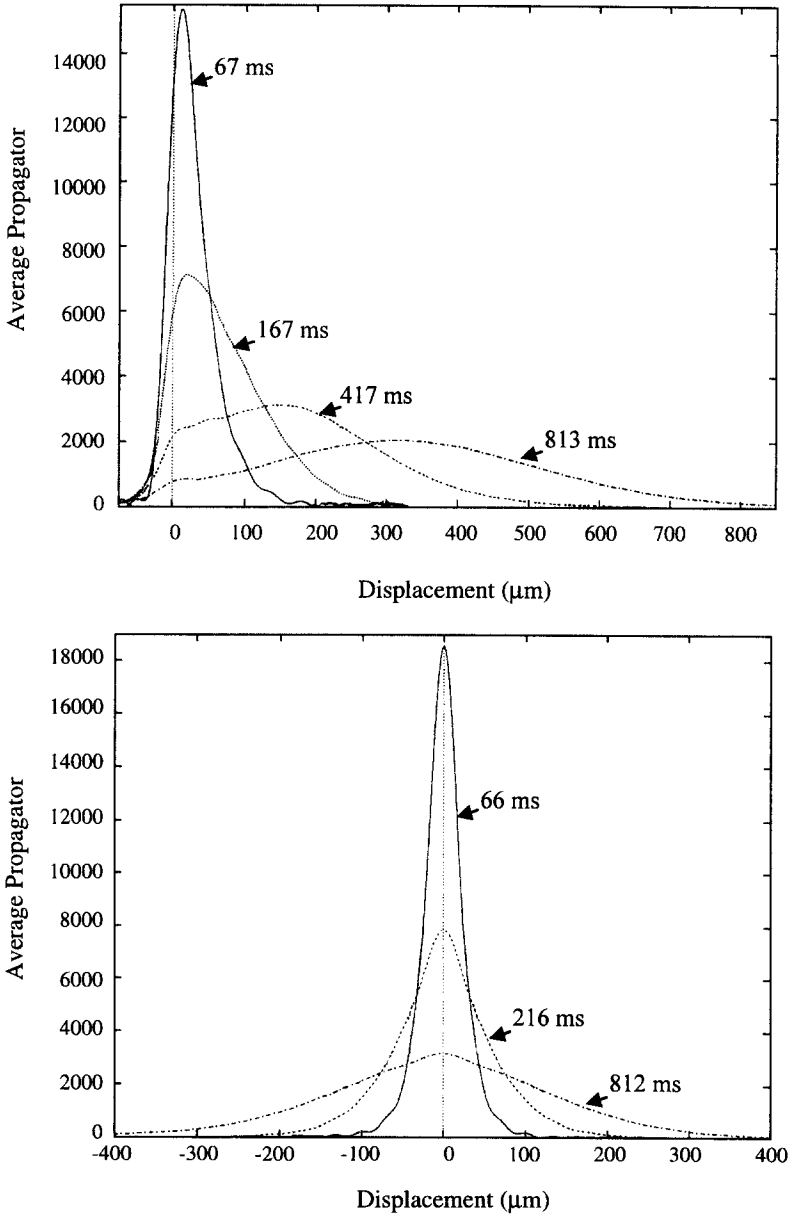

Fig. 10. Average propagators at the Δ times indicated for a flow of 3 wt% NaCl aqueous solution through Fontainebleau sandstone at a rate of 400 ml h^{-1}. The top figure corresponds to propagators in the direction of the net flow. The bottom figure corresponds to propagators perpendicular to the direction of net flow. (Reproduced with permission from ref. 200, © 1996, Taylor & Francis, http://www.tandf.co.uk/journals/mph.htm).

wettability, spreading and phase saturation on transport phenomena.[207] In particular, the effect of a wetting phase on transport may be shown by obtaining propagators in the presence and the absence of that phase, and inspecting the difference between them (termed the difference propagator).[208] Useful reference propagators for comparison are those in the two limiting cases where single-phase flow is occurring (i.e. at the irreducible water saturation, and at the residual oil saturation).[209]

It is also possible to perform a two-dimensional PFG spin-echo experiment employing two orthogonal magnetic field gradients. This yields a two-dimensional propagator $\bar{P}_s(X, Y, \Delta)$ that corresponds to the joint probability for molecular displacements X and Y in time Δ. Results have been obtained on a packed bed of glass spheres and on a sandstone, and have been compared with those predicted by numerical simulation of the flow assuming pore network models.[210,211]

An important parameter in quantifying flow in porous media is the dispersion. This is a measure of the 'spreading out' of an element of fluid as it travels through the medium, and it is analogous to diffusion for stagnant fluids. As in the case of the diffusion coefficient, apparent dispersion coefficients can vary with the measurement time in porous media. The effective dispersion coefficient may be obtained directly from a plot of $\ln(E(q, \Delta))$ against $4\pi^2 q^2 \Delta$ in the low-q limit.[212,213] It may prove possible to correlate the dispersion factor with the local pore structure.[199,214] The dispersion coefficients obtained can be compared to established models for dispersion in the literature. Dispersion in a bed of spheres can occur by three principal processes, which scale differently with the Peclet number $Pe = v_{ave}d/D$ where v_{ave} is the average fluid velocity, d is the sphere diameter and D is the self-diffusion coefficient.[215] Mechanical dispersion arises from stochastic variations of the velocity field due to the arrangement of the pores, and scales as Pe. Taylor dispersion[216] is due to the diffusion of molecules across streamlines and scales as Pe^2. Holdup dispersion is caused by blocked pores, and is expected to scale as $Pe \log Pe$. PFG NMR experiments have been performed using a range of Peclet numbers, and it has been found that non-Fickian effects are important in the flow direction, even for flow within a single pore. Dispersion transverse to the direction of superficial flow, on the other hand, is dominated by Taylor dispersion.[199]

5. MAGNETIC RESONANCE IMAGING (MRI) METHODS

Magnetic resonance imaging (MRI) methods have considerable potential towards the characterization of porous media. The location of a fluid within a porous system may be studied noninvasively, and there is the possibility of discriminating between different species present on the basis of mobility or

chemical identity. The time taken to record an image depends on the amount of fluid present in a sample, its relaxation properties, and the resolution required. Typically MRI techniques enable one-dimensional profiles of fluid within a material to be obtained in a matter of seconds, two-dimensional slice images to be obtained in a matter of minutes, or full three-dimensional volume images to be obtained in a matter of hours. The resolution of images of porous media is usually limited by magnetic susceptibility effects. The resolution attainable for model porous structures, such as water within a packed bed of glass spheres, may be 100 μm, but it will be considerably worse than this for other porous media such as rocks.

In this section, we shall briefly consider the principles behind MRI, and then go on to consider applications of the technique to the characterization of porous media. These include characterization of the pore space and components within it, time-resolved imaging studies, and the measurement of velocity images.

5.1. Theory

It is appropriate here to provide only brief details of the principles behind MRI methods. An excellent book on the subject, particularly with regard to porous media, is that of Callaghan.[141] Nuclear spins in a magnetic field gradient **G** will have different Larmor precession frequencies depending on their spatial location. Thus, during a field gradient, the local Larmor frequency will be

$$\omega(\mathbf{r}) = \gamma B_0 + \gamma \mathbf{G} \cdot \mathbf{r} \tag{32}$$

where **r** is the position, B_0 is the static magnetic field and **G** is the magnetic field gradient. This provides the basis for imaging as it implies a linear relationship between spatial position and NMR frequency. If the local spin density at a position **r** is given by $\rho(\mathbf{r})$, then the signal intensity $\mathrm{d}S$ from a particular volume element $\mathrm{d}V$ will be

$$\mathrm{d}S(\mathbf{G}, t) = \rho(\mathbf{r}) \exp[\mathrm{i}\omega(\mathbf{r})t]\, \mathrm{d}V \tag{33}$$

If necessary, a term allowing for nuclear relaxation can also be included in Eq. (33). The frequency distribution detected by the spectrometer is the difference between γB_0 and the sample resonance frequencies. Hence the detected signal will be

$$S(t) = \int\int\int \rho(\mathbf{r}) \exp[\mathrm{i}\gamma \mathbf{G} \cdot \mathbf{r}t]\, \mathrm{d}\mathbf{r} \tag{34}$$

The concept of **k**-space is normally employed by defining[141,217,218]

$$\mathbf{k} = \gamma \mathbf{G} t / 2\pi \tag{35}$$

In this case, it can be seen that $S(\mathbf{k})$ and $\rho(\mathbf{r})$ form a conjugate pair with

$$S(\mathbf{k}) = \int\int\int \rho(\mathbf{r}) \exp[2\pi i \mathbf{k} \cdot \mathbf{r}] \, d\mathbf{r} \tag{36}$$

$$\rho(\mathbf{r}) = \int\int\int S(\mathbf{k}) \exp[-2\pi i \mathbf{k} \cdot \mathbf{r}] \, d\mathbf{k} \tag{37}$$

Thus, measurements of signal intensity as a function of the **k**-vector enables the spin density $\rho(\mathbf{r})$ to be obtained by the inverse Fourier relation. A finite number of points in **k**-space are measured in the time domain either by varying the gradient strength (phase encoding) or by varying the time during which the gradients are applied (frequency encoding).

There is a wide variety of different imaging pulse sequences that fully sample **k**-space and so can be used to give the spin density function.[141] Imaging sequences can be modified to provide information other than a spin density image. For instance, images of relaxation times or diffusion coefficients can be obtained. Chemical shift imaging is also possible, in which chemical shift information is retained for each element of the image. In most cases, ^{1}H is the nucleus investigated owing to its high sensitivity, but other nuclei have been studied.

A drawback to MRI is that experiments become very difficult if the spin–spin relaxation time of the sample becomes too short. Thus imaging of solids is only possible using special methods involving line-narrowing techniques or exceptionally large gradients (such as in stray-field imaging).[219–221] Short spin–spin relaxation times may also be a problem with imaging fluids in porous media. Another major problem is that large magnetic field inhomogeneities within the sample severely limit the achievable resolution and can even make imaging impossible in some cases. One way of minimizing the effects of magnetic susceptibility is to use very high gradient strengths.[222] The effect of magnetic susceptibility on images obtained using different pulse sequences has been considered.[223]

A further problem with imaging fluids in porous media is that the images may contain artefacts due to restricted molecular diffusion within the pores.[224,225] For imaging sequences employing a spin-echo, this effect has been shown to be due to diffusive attenuation.[226] This is normally a problem but in some cases can provide a useful image contrast that emphasizes the location of the pore boundaries. A generalized calculation of this effect has been presented, which may lead to its use in characterizing the pore morphology.[227,228]

5.2. Pore space characterization

Imaging of a single component

Conventional images may readily be obtained of a fluid within porous rocks provided that the concentration of paramagnetic impurities is not too high. A feature of the images is that they may show spatial inhomogeneities within the samples, and they may be used to obtain local porosity values.[229,230] The correct evaluation of porosity and the saturation distribution from the image does, however, require allowance for relaxation effects if quantitative data are required. This will require knowledge of the local relaxation times, or alternatively extrapolation of data from several acquired images may give reasonable results.[231,232] Unfortunately, the resolution achievable in images of rocks is not sufficient to be able to resolve individual pores.

It is of considerable interest to gain more detailed information about the structure of a pore space, and the parameters that can be used to characterize it. Three-dimensional NMR images of water in model porous media such as beds of glass spheres may be obtained at a resolution of 100 μm, which is sufficient to resolve individual pores. It is therefore possible to measure structural parameters at a local level from the three-dimensional image, and use these to characterize the pore space. One algorithm that does this is based on a variant of morphological thinning.[233] In this analysis, a pore is considered to be a portion of the void space bounded by a solid surface and by planes erected where the hydraulic radius of the void space exhibits local minima.[3] Application of the algorithm is shown for a slice through a three-dimensional NMR image in Plate 1.[234] As can be seen, the void space becomes partitioned into a discrete and well-defined collection of individual pores, from which pore size distributions, pore surface areas and coordination numbers may be obtained.[233–237] The constriction area of the throats between neighbouring pores may also be established. It is worth noting that analysis of images of random packed glass spheres shows that the pore space has a fractal character.[233,236]

MRI techniques other than imaging of spin density have been applied to the study of porous media. An image of spin–lattice relaxation times may be obtained by prefacing the conventional imaging sequence with an inversion-recovery or saturation-recovery pulse sequence, and repeating the experiment at different recovery times. Spatially resolved T_1 and T_2 images have been recorded in this manner for water in porous rocks.[238–240] It has also been found that with flowing water there is a correlation between the T_1 and the local rate of flow.[240] Diffusion imaging has been performed by combining pulsed field gradients with an imaging sequence. This enables a local map of diffusion coefficients to be obtained.[241] This method has been used to study diffusion in brine-saturated reservoir cores, and it is observed that there is a general tendency for the average diffusivity to be larger in those pixels that show

greatest signal intensity.[242] It is difficult, though, to draw definite conclusions from diffusion maps as there are variations in porosity, pore size and relaxation time over the sample investigated.

MRI is capable of detecting macroscopic heterogeneities in porous solids. For instance, images (including relaxation time images) have been used to show the presence of structural inhomogeneities over length scales of 0.1–1 mm in alumina catalyst pellets.[243,244] The impact of heterogeneities on this length scale on transport within the medium has been investigated using both PFG and imaging methods.[245] It should also be pointed out that such heterogeneities may need to be included in any pore network model that is going to be physically realistic. For this reason, simulation of diffusion has been performed on pore network lattices that have been derived from NMR images.[246] Imaging studies have also shown that a fractal representation of the pore space is often appropriate, and this can be incorporated into transport models.[247,248]

Phase discrimination in images

There is considerable interest in being able to distinguish clearly between different phases, such as oil and water, in images of porous media. There are a variety of ways in which this might be accomplished.

In the event that the spectral peaks from the individual components are well resolved, then chemical shift contrast can be used. This may employ selective excitation of a single species using a soft 90° pulse, or alternatively use a selective suppression method such as presaturation of one component.[249,250] Alternatively, a chemical shift imaging pulse sequence may be employed. Here phase-encoding field gradients are used to provide spatial information, but the signal is recorded in the absence of magnetic field gradients to retain chemical shift information. The chemical shift axis is then effectively another dimension to the image. The result is an image in which a normal NMR spectrum is available for each pixel. An example of a chemical shift image is shown in Fig. 11.[251] Here two sandstone samples have been separately saturated with water and dodecane and then placed together. It can be seen that peaks from the two fluids are resolved both on the spatial and on the chemical shift axis. Thus, in favourable cases, chemical shift imaging can be an extremely powerful technique in determining the location of different species in porous media.[252] However, chemical shift images are very time consuming to acquire, particularly if three-dimensional spatial information is required. Another possible approach to separating signals from oil and water locations is to image nuclei other than ^{1}H. For instance, ^{7}Li from LiCl dissolved in water within sandstone pores can be imaged, as can ^{19}F from trifluorotoluene present in an organic phase.[253]

The NMR resonances from oil and water in most natural rock samples cannot be fully separated because of line broadening arising from the magnetic field inhomogeneities within the sample, and this limits the applicability of

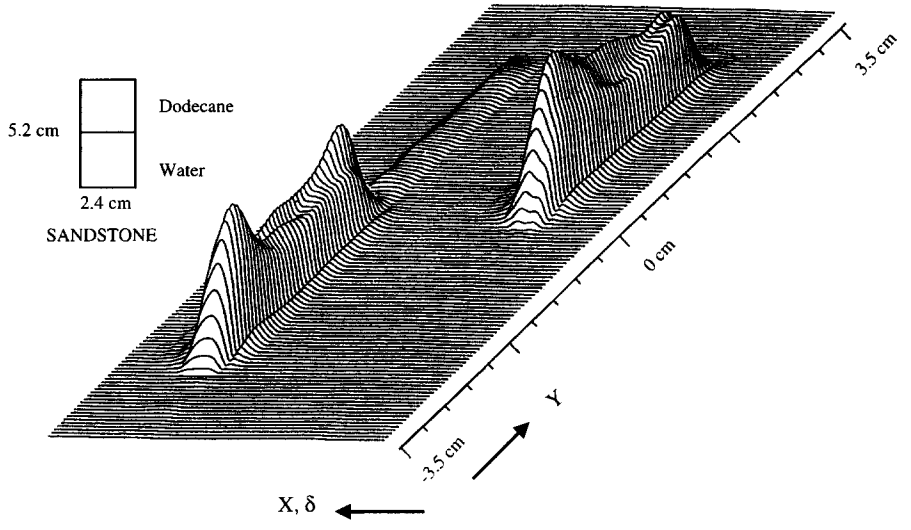

Fig. 11. Chemical-shift resolved image of two sandstone samples saturated with water and dodecane separately, and then placed together. (Reproduced with permission from ref. 251, © 1986, Academic Press.)

imaging based on chemical shift contrast. If the separate oil and water resonances have previously been characterized, then numerical estimation methods may be applied to quantify the oil/water mixture even when there is some peak overlap by analysing images recorded under different acquisition conditions.[254] A general algorithm for resolving chemical species in images that have signals that partially overlap has been proposed by recording the image under different gradient strengths.[255]

The other method of obtaining images selectively from one component is to exploit relaxation time differences. For instance, the NMR signal from a component with a short T_2 will be reduced during a spin-echo pulse sequence, and this may be exploited in some cases to obtain separate images from oil and water in porous rocks.[256] Relaxation times may be influenced by the addition of relaxation contrast agents such as paramagnetic ions. For instance, Mn^{2+}, Ni^{2+} or Cu^{2+} may be added to the water phase, thus reducing its spin–spin relaxation time. The effect of this can be to reduce significantly the signal from water without affecting the signal from oil that is present.[257–259] Differences in T_1 between components may also be exploited. For instance, a fast recycle delay between scans will discriminate against any component with a long T_1. Alternatively, it is possible to preface the imaging sequence with an inversion recovery period ($180\,^\circ - \tau$), and to choose the value of τ such that there is zero magnetization for one of the components (the condition for which is $\tau = T_1 \ln 2$). This method has been used to quantify the amount and location of oil and water phases in carbonate rocks.[252] However, it should be pointed

out that the relaxation times of crude oils in porous media can vary widely depending on paramagnetic content, pore size, degree of saturation and presence of water.[57] As a consequence, it is not normally possible to predict relaxation times for fluid in rocks, and so the possibility of obtaining a selective image by this method needs to be assessed separately for each individual case.

An example showing selective imaging of water and hydrocarbon species is shown in Plate 2.[260] Here ganglia of octanol trapped in a packed bed of glass spheres are detected in the presence of flowing water. The chemical selectivity between the hydrocarbon and water has been obtained using a T_1-weighted method. The figure shows a set of images obtained as a function of time of water flow, and gradual dissolution of the hydrocarbon ganglia can be observed. The images allow the interfacial area of the hydrocarbon ganglia to be obtained, and it is found that the dissolution is a mass-transfer-limited process. It should be noted that some ganglia dissolve faster than others, and this can be related to the local water flow rate, which can be obtained from NMR velocity images (as discussed in Section 6).[260] This work has obvious applications in the field of understanding soil remediation, and other MRI work relating to the removal of hydrocarbons from porous media has also appeared.[261–263]

5.3. Time-resolved studies

When the rate of fluid transport is slow, it may be sufficient to follow a process by recording successive NMR images. For instance, this approach has been applied to visualize water infiltration into soils.[264–266] One-dimensional profiles can be obtained rapidly, and these can follow the changes in the moisture profile with time. Two-dimensional images can detect preferential flow phenomena and air entrapment within the soil.[265] Another approach to understanding transport in a porous media using a time-resolved study is to add a paramagnetic tracer into the sample, and observe its progress into the sample.[267]

However, the acquisition time for conventional two- and three-dimensional images is often too long to allow one to follow the changes occurring in the sample. In these cases, there is the possibility of performing a rapid imaging technique. One method of rapid scanning is echo-planar imaging (EPI), which can obtain a full two-dimensional image from a single excitation effectively using a multiple spin-echo sequence.[268] However, variation in magnetic susceptibility over the sample leads to distortions and blurring of images for fluids in porous media. This problem is partially overcome by the π-EPI sequence which has additional 180° pulses to refocus the magnetization that has been dephased by the field inhomogeneities.[269,270] The method may be extended to give a three-dimensional imaging sequence with an acquisition time of several minutes, and this has been applied to fluids in porous solids.[271] A

modification of the sequence is the use of composite 180° pulses in order to reduce cumulative errors in the RF field.[272]

An example of the application of three-dimensional π-EPI is the investigation of drying in porous media.[272] Plate 3 shows slices taken from three-dimensional images of water in a packed bed of 0.5 mm glass spheres as a function of time. The resolution is 94 μm. In these images, drying is occurring from the top surface only. It can be seen that the drying process is inhomogeneous, with different parts of the bed drying at very different rates. Work is ongoing to relate the evaporation rate to the three-dimensional bed structure. Drying of porous catalyst pellets has also been investigated, and again inhomogeneous drying occurs.[273,274]

The main limitations of the π-EPI variants are that a reasonably long T_2 is required (>100 ms), the phase and timing of the RF pulses needs to be accurate, and the gradient strength must not be too high (to prevent eddy current formation). However, in favourable cases, it is possible to record full three-dimensional images in a matter of minutes, depending on the desired resolution.

5.4. Velocity imaging of flowing fluid

NMR may be used to measure fluid velocity by time-of-flight techniques or by detecting phase shifts based on the flow.[275,276] The phase-shifting method is based on the PFG spin-echo pulse sequence shown earlier in Fig. 6. For a flowing liquid, there will be net translation of molecules during the Δ interval, which means that the magnetic field felt by molecules during the second gradient pulse will be different from that felt during the first pulse. The result of this for coherent motion will be a phase shift of all the spins when the echo is formed. Thus, a pair of pulsed field gradients may be used to create a phase shift that depends on fluid velocity. It is possible to include the pulsed field gradients into a conventional imaging sequence, and by varying the strength of the velocity-encoding gradients it is possible to acquire an image (one-dimensional, two-dimensional or three-dimensional) in which each pixel contains the fluid velocity in the gradient direction.[277] Different authors refer to the technique as flow imaging, velocity imaging, velocimetry or as a form of dynamic NMR microscopy. Flow images have been obtained on model systems such as flow in a pipe (for both Newtonian and non-Newtonian fluids), in a curved tube, and at abrupt contractions and expansions.[278–281] Good agreement between the local flow found from the imaging technique and simulations based on the Navier–Stokes equation has been found. The ability of NMR to measure fluid velocity non-invasively has led to it being used as a rheological tool to study fluid flow as a function of shear.[282–286] It also has the potential to measure vascular flow in living plants.[287]

Velocity images may readily be obtained on water flowing through model porous media with net velocities in the range 1–2 mm s^{-1}, and good agreement is obtained between flow rates obtained from images and those obtained by direct measurement.[288–290] A high-resolution three-dimensional velocity image in a packed bed of 5 mm-diameter glass spheres is shown in Plate 4.[236] Here the three left-hand images are slices, separated by 1 mm, from a three-dimensional spin-density image. This may be used to characterize the pore space as discussed in Section 5. The three right-hand images give the flow speed in the x, y and z directions for the central zx-slice shown. The overall flow direction in the packed bed is in the z-direction, and the velocity image in this direction shows enhanced flow in certain channels, and reverse flow in certain parts of the bed. In the highlighted region, the velocity images in the x and y directions show positive and negative components corresponding to flow over and around the glass sphere obstacle.

While the images shown in Plate 4 are very time consuming to acquire, they are of great value when trying to understand the relationship between local structure and local flow.[234,236,237] Significant heterogeneity in the flow is observed. For instance, in one slice, it is found that approximately 8% of the pores carry 40% of the volumetric flow. The topology of the bed plays a crucial role in determining the mean flow velocity through a given pore, and various correlations between structure and flow have been explored.[234] For instance, Fig. 12 shows a plot of volumetric flow rate between neighbouring pores as a function of the cross-sectional area of the constriction between them. Two limiting cases can be observed. At the lowest local Reynolds number (corresponding to laminar flow), the flow rate scales as the square of cross-

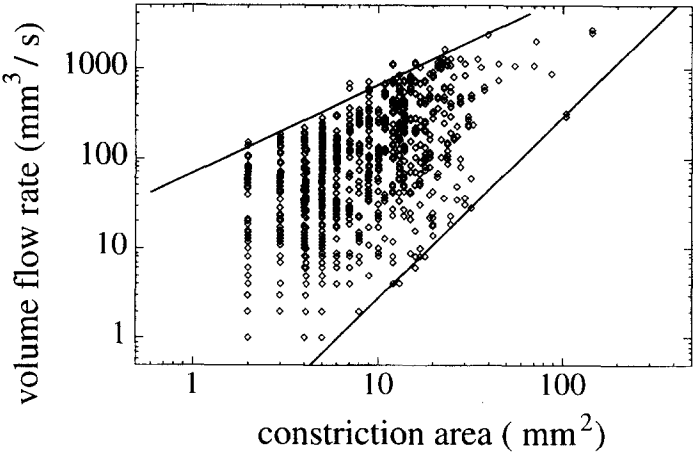

Fig. 12. Graph of the volume flow rate as a function of the constriction area between pores. The two solid lines show the limiting cases when the gradient is 1, and when the gradient is 2. (Reproduced with permission from ref. 236, © 1997, Elsevier Science.)

sectional area, while at the highest local Reynolds numbers (corresponding to turbulent flow), the flow rate scales with the cross-sectional area.[236] Flow imaging experiments in a bed of packed glass spheres have also been used to obtain the velocity covariance as a test of stochastic transport theory.[291]

A number of alternative schemes for obtaining velocity images and processing the data have been proposed. Faster image acquisition is possible using echo-planar imaging (EPI) methods.[269,271,292] It is also possible to perform chemically selective velocity imaging, and this has been demonstrated for an oil/water emulsion flowing in a pipe and through an abrupt contraction and expansion.[293] It has been suggested that Bayesian analysis of the data may be appropriate for obtaining velocities when a limited number of velocity-encoding gradient data points have been sampled.[294]

Velocity imaging is more difficult to perform in natural porous rocks, but is still possible when the paramagnetic content is low.[295] As stated earlier, the resolution is not sufficient to resolve individual pores in this case. Early studies found that the average flow velocity inside a brine-filled sandstone is a linear function of porosity.[296,297] EPI studies showed that the velocity of water in a sandstone was randomly distributed around a mean value that corresponded to Darcy's law.[298] The fact that the velocity map changes when the identical experiment is repeated, while the general characteristics of the velocity distribution remain unaltered, supports a stochastic model of the flow. Rapid imaging using π-EPI has allowed the transient changes in flow patterns in porous rocks when the bulk flow rate is altered to be investigated.[299] Oil flow at a velocity of 0.04 mm s^{-1} in a sandstone has also been imaged.[300]

6. CHARACTERIZING THE PORE SPACE OF MICROPOROUS MATERIALS

This review has concentrated on the application of NMR methods to the characterization of mesoporous and macroporous materials. However, transport within microporous materials such as zeolites is also an area of immense commercial potential. While similar NMR techniques may be applied, the interpretation of the results is often very different for microporous solids because the adsorbate is essentially always in contact with the solid surface. Thus, spectra are normally dominated by surface adsorption effects.

One technique that does reveal some information about the pore size in microporous materials is ^{129}Xe NMR spectroscopy. Xenon is inert and highly polarizable, and so the chemical shift of ^{129}Xe is sensitive to the size of its environment. Several reviews on the use of ^{129}Xe NMR spectroscopy in characterizing microporous materials have appeared.[13,301–306] The variation of ^{129}Xe chemical shift with xenon concentration can normally be fitted to

$$\delta = \delta_S + C_1\rho_{Xe} + C_2\rho_{Xe}^2 \tag{38}$$

where ρ_{Xe} is the density of xenon, and C_1 and C_2 are constants. In the absence of strong surface adsorption sites, it is normally found that $C_2 \approx 0$, and there is thus an approximately linear dependence of chemical shift on concentration. In this case, the value of δ_S, reflecting interactions with the surface, has been found to be an indication of pore size, with large values of δ_S suggesting that the xenon is present in small cavities.[301,302] However, when strong surface adsorption sites are present, the dependence of chemical shift on xenon concentration is no longer linear. Adsorption sites will also modify δ_S to reflect the interaction between xenon and the adsorption site rather than giving any information about the pore size. For instance, xenon has significant interactions with divalent cations, and thus in many cases the primary use of ^{129}Xe NMR spectroscopy is to characterize cations sites in zeolites rather than to obtain pore space information.[307,308] A number of studies calculating the ^{129}Xe chemical shift in zeolites using Monte Carlo or molecular dynamics simulations have appeared.[309–315]

Deuterium NMR spectroscopy is another technique that can reveal information about adsorption sites and transport in microporous materials. An adsorbate molecule will not necessarily be able to undergo isotropic reorientational motion in a microporous material. Owing to the quadrupolar interaction, a lineshape will therefore be observed that will depend on the molecular mobility.[316] Lineshape experiments at various temperatures may thus be used to help characterize molecular motion. For instance, ^{2}H NMR lineshapes from deuterated benzene in zeolite Y have been used to obtain activation energies for hopping between neighbouring cages.[317,318] Information on the activation energies for hopping between adsorption sites is also available from ^{2}H relaxation time measurements performed at different temperatures.[318–320] Measurements of the rate of transport between adsorption sites may then be used in simulations to obtain diffusion coefficients.[321,322]

Direct measurement of diffusion within microporous materials is possible using PFG spin-echo techniques. There have been extensive measurements of diffusion of hydrocarbons within zeolites.[323] One factor that is worth noting is that the particle size of many zeolites is often very small (typically 1–50 μm). Thus, the length scale of the PFG experiment may be larger than the particle size, and so the echo signal intensity will be affected by both the intraparticle and interparticle diffusion coefficients. A plot of $\ln(E(q, \Delta))$ against $4\pi^2 q^2(\Delta - \delta/3)$ using Eq. (26) will not be linear in this case, and will show a curve similar to that depicted for restricted diffusion in Fig. 7 (but arising for a completely different reason). The initial slope of the curve depends on the interparticle diffusivity and the relative weighting of how long the adsorbed molecule spends in each region, while the final slope gives the intraparticle diffusivity only.[324] There has been particular attention paid recently to using NMR to measure multicomponent diffusion in zeolites, in which the presence of one adsorbate influences the diffusion coefficient of another.[325,326]

Anomalous diffusion is also possible in microporous solids. For instance, it is possible for molecules to be confined in a channel system in which they cannot pass each other, and this will obviously affect molecular displacement in a time interval. This case is termed 'single-file diffusion', and the mean square displacement in a time t is then given by[327,328]

$$\langle \mathbf{r}^2(t) \rangle = 2F\sqrt{t} \tag{39}$$

where F is the single-file mobility factor and is analogous to the normal diffusion coefficient. The square-root dependence on t may be contrasted with the normal linear dependence as given in Eq. (24). Single-file diffusion has recently been confirmed to occur by PFG NMR for CF_4 in the channels of the molecular sieve $AlPO_4$-5.[329,330]

7. CONCLUSIONS

NMR methods offer a noninvasive method of characterizing porous media. A variety of different techniques may be used to obtain useful information on the pore space. For instance, pore sizes may be measured using the freezing point depression technique for mesoporous solids or by relaxation time measurements for macroporous solids. Other pore space information comes from PFG techniques, while direct imaging of the pore space is possible for large pores. The information from studying the pore space can then be incorporated into appropriate pore network models.

Transport of fluids within porous materials may also be studied using NMR techniques. The PFG spin-echo technique enables diffusion to be measured at a local scale, thus allowing the effect of the pore space on transport, including dispersion, to be measured. Imaging techniques are also useful in studying transport in porous media. Time-resolved imaging can be used to follow slow changes in fluid content, while velocity imaging can be used to obtain fluid velocities at a microscopic level. This allows correlations between structure and flow to be explored.

In conclusion, NMR techniques have led to improved knowledge of porous media at a local level, and there is now potential for understanding how microscopic structure affects macroscopic transport properties. Further developments in NMR hardware and techniques are likely to ensure progress in this research area for many years to come.

REFERENCES

1. J. Bear, *Dynamics of Fluids in Porous Media*, Dover, New York, 1988.
2. J. Bear and Y. Bachmat, *Introduction to Modeling of Transport Phenomena in Porous Media*, Kluwer Academic, Dordrecht, 1991.

3. F. A. L. Dullien, *Porous Media: Fluid Transport and Pore Structure*, Academic Press, San Diego, 1992.
4. P. M. Adler, *Porous Media: Geometry and Transport*, Butterworth-Heinemann, Boston, 1992.
5. C. M. Case, *Physical Principles of Flow in Unsaturated Porous Media*, Clarendon Press, Oxford, 1994.
6. M. Sahimi, *Flow and Transport in Porous Media and Fractured Rock: From Classical Methods to Modern Approaches*, VCH, Weinheim, 1995.
7. S. J. Gregg and K. S. W. Sing, *Adsorption, Surface Area and Porosity*, Academic Press, London, 1982.
8. S. Lowell and J. E. Shields, *Powder Surface Area and Porosity*, Chapman and Hall, London, 1991.
9. K. Meyer, P. Lorenz, B. Bohlkuhn and P. Klobes, *Cryst. Res. Technol.*, 1994, **29**, 903.
10. C. K. Lee, A. S. T. Chiang and C. S. Tsay, *Key Eng. Mater.*, 1996, **115**, 21.
11. M. Sahimi, *Rev. Mod. Phys.*, 1993, **65**, 1393.
12. A. T. Watson and C. T. P. Chang, *Prog. Nucl. Magn. Reson. Spectrosc.*, 1997, **31**, 343.
13. P. J. Barrie, *Annu. Rep. NMR Spectrosc.*, 1995, **30**, 37.
14. M. Hunger, *Catal. Rev. Sci. Eng.*, 1997, **39**, 345.
15. M. E. Smith and J. H. Strange, *Measurement Sci. Technol.*, 1996, **7**, 449.
16. L. F. Gladden, *Chem. Eng. Sci.*, 1994, **49**, 3339.
17. J. Klinowski, *Chem. Rev.*, 1991, **91**, 1459.
18. J.-P. Ansermet, C. P. Slichter and J. H. Sinfelt, *Prog. Nucl. Magn. Reson. Spectrosc.*, 1990, **22**, 401.
19. V. M. Mastikhin, I. L. Mudrakovsky and A. V. Nosov, *Progr. Nucl. Magn. Reson. Spectrosc.*, 1991, **23**, 259.
20. IUPAC Manual of Symbols and Terminology, *Pure Appl. Chem.*, 1972, **31**, 579.
21. M. Peyron, G. K. Pierens, A. J. Lucas, *et al.*, *Magn. Reson. Imaging*, 1994, **12**, 295.
22. M. Hürlimann, *J. Magn. Reson.*, 1998, **131**, 232.
23. S. Allen, M. Mallett, M. E. Smith and J. H. Strange, *Magn. Reson. Imaging*, 1998, **16**, 597.
24. R. S. Drago, D. C. Ferris and D. S. Burns, *J. Am. Chem. Soc.*, 1995, **117**, 6914.
25. R. S. Drago, D. S. Burns and T. J. Lafrenz, *J. Phys. Chem.*, 1996, **100**, 1718.
26. T. M. de Swiet, M. Tomaselli, M. D. Hürlimann and A. Pines, *J. Magn. Reson.*, 1998, **133**, 385.
27. T. W. Perkins, T. W. Root and E. N. Lightfoot, *Anal. Chem.*, 1997, **69**, 3293.
28. W. Thomson, *Phil. Mag.*, 1871, **42**, 448.
29. J. R. Blanchere and J. E. Young, *J. Am. Ceram. Soc.*, 1972, **55**, 306.
30. R. W. Batchelor and A. G. Foster, *Trans. Faraday Soc.*, 1944, **40**, 300.
31. K. E. Gubbins, M. Sliwinsk-Bartkowiak and S. H. Suh, *Mol. Simul.*, 1996, **17**, 333.
32. H. Dominguez, M. P. Allen and R. Evans, *Mol. Phys.*, 1999, **96**, 209.
33. K. Overloop and L. Van Gerven, *J. Magn. Reson. Ser. A*, 1993, **101**, 179.
34. D. Akporiaye, E. W. Hansen, R. Schmidt and M. Stocker, *J. Phys. Chem.*, 1994, **98**, 1926.
35. E. W. Hansen, M. Stocker and R. Schmidt, *J. Phys. Chem.*, 1996, **100**, 2195.
36. R. Schmidt, E. W. Hansen, M. Stocker, D. Akporiaye and O. H. Ellestad, *J. Am. Chem. Soc.*, 1997, **117**, 4049.
37. E. W. Hansen, E. Tangstad, E. Myrvold and T. Myrstad, *J. Phys. Chem. B*, 1997, **101**, 10709.
38. A. V. Filippov, M. G. Altykis, M. I. Khaliullin, R. Z. Rachimov and V. M. Lantsov, *J. Mater. Sci.*, 1996, **31**, 4369.
39. J. Y. Jehng, D. T. Sprague and W. P. Halperin, *Magn. Reson. Imaging*, 1996, **14**, 785.
40. F. Milia, M. Fardis, G. Papavassiliou and A. Leventis, *Magn. Reson. Imaging*, 1998, **16**, 677.
41. J. H. Strange, M. Rahman and E. G. Smith, *Phys. Rev. Lett.*, 1993, **71**, 3589.
42. J. H. Strange and E. G. Smith, *Magn. Reson. Imaging*, 1994, **12**, 257.

43. E. W. Hansen, R. Schmidt and M. Stocker, *J. Phys. Chem.*, 1996, **100**, 11396.
44. A. V. Filippov and R. S. Vartapetyan, *Colloid J.*, 1997, **59**, 226.
45. S. G. Allen, P. C. L. Stephenson and J. H. Strange, *J. Chem. Phys.*, 1998, **108**, 8195.
46. H. F. Booth and J. H. Strange, *Mol. Phys.*, 1998, **93**, 263.
47. H. F. Booth and J. H. Strange, *Magn. Reson. Imaging*, 1998, **16**, 501.
48. J. H. Strange, J. B. W. Webber and S. D. Schmidt, *Magn. Reson. Imaging*, 1996, **14**, 803.
49. J. H. Strange and J. B. W. Webber, *Appl. Magn. Reson.*, 1997, **12**, 231.
50. J. H. Strange and J. B. W. Webber, *Measur. Sci. Technol.*, 1997, **8**, 555.
51. P. J. Prado, B. J. Balcom, S. D. Beyea, R. L. Armstrong and T. W. Bremner, *Solid State Nucl. Magn. Reson.*, 1997, **10**, 1.
52. P. J. Prado, B. J. Balcom, S. D. Beyea, *et al.*, *J. Phys. D: Appl. Phys.*, 1998, **31**, 2040.
53. S. Meiboom and D. Gill, *Rev. Sci. Instrum.*, 1958, **29**, 688.
54. R. K. Harris, *Nuclear Magnetic Resonance Spectroscopy: A Physicochemical View*, Pitman Books, London, 1983.
55. H. W. Spiess, *NMR Basic Principles and Progress*, 1978, **15**, 55.
56. J. Jackson and M. Mathews, *Log Analyst*, 1993, **34**, 35.
57. W. E. Kenyon, *Nucl. Geophys.*, 1992, **6**, 153.
58. R. L. Kleinberg, in *Encyclopedia of Nuclear Magnetic Resonance* (eds D. M. Grant and R. K. Harris), Vol. **3**, p. 4960, Wiley, New York, 1996.
59. R. S. Chen, P. E. Stallworth, S. G. Greenbaum and R. L. Kleinberg. *J. Magn. Reson. Ser.* A, 1994, **110**, 77.
60. M. Leibig, *J. Phys. A: Math Gen.*, 1993, **26**, 3349.
61. S. H. Nguyen and S. Mardon, *Comput. Geosci.*, 1995, **21**, 51.
62. J. R. Zimmerman and W. E. Brttin, *J. Phys. Chem.*, 1957, **61**, 1328.
63. J. Korringa, D. O. Seevers and H. C. Torrey, *Phys. Rev.*, 1962, **127**, 1143.
64. S. D. Senturia and J. D. Robinson, *Soc. Petroleum Eng. J.*, 1970, **249**, 237.
65. K. R. Brownstein and C. E. Tarr, *J. Magn. Reson.*, 1977, **26**, 17.
66. K. R. Brownstein and C. E. Tarr, *Phys. Rev. A*, 1979, **19**, 2446.
67. R. L. Kleinberg, W. E. Kenyon and P. P. Mitra, *J. Magn. Reson. Ser. A*, 1994, **108**, 206.
68. I. Foley, S. A. Farooqui and R. L. Kleinberg, *J. Magn. Reson. Ser.* A, 1996, **123**, 95.
69. K. S. Mendelson, W. P. Halperin, J. Y. Jehng and Y. Q. Song, *Magn. Reson. Imaging*, 1994, **12**, 207.
70. D. P. Gallegos, K. Munn, D. M. Smith and D. L. Stermer, *J. Colloid Interface Sci.*, 1987, **119**, 127.
71. J. J. Howard, W. E. Kenyon and C. Straley, *SPE Formation Evaluation*, 1993, **8**, 194.
72. M. Y. Su and O. Nalcioglu, *J. Colloid Interface Sci.*, 1993, **160**, 332.
73. F. D'Orazio, S. Bhattacharja, W. P. Halperin, K. Eguchi and T. Mizusaki, *Phys. Rev. B*, 1990, **42**, 9810.
74. B. Sapoval, S. Russ, D. Petit and J.-P. Korb, *Magn. Reson. Imaging*, 1996, **14**, 863.
75. K. Munn and D. M. Smith, *J. Colloid Interface Sci.*, 1987, **119**, 117.
76. G. C. Borgia, V. Bortolotti, R. J. S. Brown, P. Castaldi, P. Fantazzini and U. Soverini, *Magn. Reson. Imaging*, 1994, **12**, 209.
77. W. E. Kenyon, P. I. Day, C. Straley and J. F. Willemsen, *SPE Formation Evaluation*, 1988, **3**, 622.
78. M. Peyron, G. K. Pierens, A. J. Lucas, L. D. Hall and R. C. Stewart, *J. Magn Reson. Ser. A*, 1996, **118**, 214.
79. G. C. Borgia, V. Bortolotti, R. J. S. Brown and P. Fantazzini, *Magn. Reson. Imaging*, 1998, **16**, 625.
80. G. C. Borgia, R. J. S. Brown and P. Fantazzini, *Magn. Reson. Imaging*, 1998, **16**, 613.
81. C. Straley and L. M. Schwartz, *Magn. Reson. Imaging*, 1996, **14**, 999.
82. D. P. Gallegos and D. M. Smith, *J. Colloid Interface Sci.*, 1988, **122**, 143.
83. R. L. Kleinberg, *Magn. Reson. Imaging*, 1996, **14**, 761.

84. E. J. Fordham, A. Sezginer and L. D. Hall, *J. Magn. Reson. Ser. A*, 1995, **113**, 139.
85. G. C. Borgia, R. J. S. Brown and P. Fantazzini, *J. Magn. Reson.*, 1998, **132**, 65.
86. H. K. Liaw, R. Kulkarni, S. H. Chen and A. T. Watson, *AIChE J.*, 1996, **42**, 538.
87. A. Miller, S. H. Chen, D. T. Georgi and K. Vozoff, *Magn. Reson. Imaging*, 1998, **16**, 617.
88. S. Davies, K. J. Packer, D. R. Roberts and F. O. Zelaya, *Magn. Reson. Imaging*, 1991, **9**, 681.
89. M. B. Carr, R. Ehrlich, M. C. Bowers and J. J. Howard, *J. Petroleum Sci. Eng.*, 1996, **14**, 115.
90. M. D. Hürlimann, L. L. Latour and C. H. Sotak, *Magn. Reson. Imaging*, 1994, **12**, 325.
91. G. C. Borgia, R. J. S. Brown and P. Fantazzini, *J. Appl. Phys.*, 1996, **79**, 3656.
92. K. R. McCall, D. L. Johnson and R. A. Guyer, *Phys. Rev. B*, 1991, **44**, 7344.
93. L. L. Latour, R. L. Kleinberg and A. Sezginer, *J. Colloid Interface Sci.*, 1992, **150**, 535.
94. D. J. Wilkinson, D. L. Johnson and L. M. Schwartz, *Phys. Rev. B*, 1991, **44**, 4960.
95. M. H. Cohen and K. S. Mendelson, *J. Appl. Phys.*, 1982, **53**, 1127.
96. H. C. Torrey, *Phys. Rev.*, 1956, **101**, 363.
97. G. Goelman and M. G. Prammer, *J. Magn. Reson. Ser. A*, 1995, **113**, 11.
98. P. Le Doussal and P. N. Sen, *Phys. Rev. B*, 1992, **46**, 3465.
99. R. J. S. Brown and P. Fantazzini, *Phys. Rev. B*, 1993, **47**, 14823.
100. T. M. de Swiet and P. N. Sen, *J. Chem. Phys.*, 1994, **100**, 5597.
101. M. D. Hürlimann, K. G. Helmer and C. H. Sotak, *Magn. Reson. Imaging*, 1998, **16**, 535.
102. P. W. Kuchel, A. J. Lennon and C. Durrant, *J. Magn. Reson. Ser. B*, 1996, **112**, 1.
103. C. Straley, A. Matteson, S. Feng, L. M. Schwartz, W. E. Kenyon and J. R. Banavar, *Appl. Phys. Lett.*, 1987, **51**, 1146.
104. P. N. Sen, C. Straley, W. E. Kenyon and M. S. Whittingham, *Geophysics*, 1990, **55**, 61.
105. B. Issa and P. Mansfield, *Magn. Reson. Imaging*, 1994, **12**, 213.
106. G. C. Borgia, R. J. S. Brown and P. Fantazzini, *J. Appl. Phys.*, 1997, **82**, 4197.
107. K. J. Dunn, G. A. La Torraca and D. J. Bergman, *Magn. Reson. Imaging*, 1998, **16**, 553.
108. G. C. Borgia, A. Brancolini, R. J. S. Brown, P. Fantazzini and G. Ragazzini, *Magn. Reson. Imaging*, 1994, **12**, 191.
109. G. C. Borgia and P. Fantazzini, *J. Appl. Phys.*, 1994, **75**, 7562.
110. S. H. Chen, H. K. Liaw and A. T. Watson, *Magn. Reson. Imaging*, 1994, **12**, 201.
111. W. P. Halperin, S. Bhattacharja and F. D'Orazio, *Magn. Reson. Imaging*, 1991, **9**, 733.
112. J. J. Howard, *Magn. Reson. Imaging*, 1994, **12**, 197.
113. J. J. Howard, *Magn. Reson. Imaging*, 1998, **16**, 529.
114. I. Bonalde, M. Martinlandrove, A. Benavides, R. Martin and J. Espidel, *J. Appl. Phys.*, 1995, **78**, 6033.
115. G. C. Borgia and P. Fantazzini, *J. Appl. Phys.*, 1994, **75**, 7562.
116. P. Hari, C. T. P. Chang, R. Kulkarni, J. R. Lien and A. T. Watson, *Magn. Reson. Imaging*, 1998, **16**, 545.
117. M. E. Smith and S. N. Stuart, *J. Phys. D: Appl. Phys.*, 1995, **28**, 229.
118. K. S. Mendelson, W. P. Halperin, J. Y. Jehng and Y. Q. Song, *Magn. Reson. Imaging*, 1994, **12**, 207.
119. S. Bhattacharja, M. Moukwa, F. D'Orazio, J. Y. Jehng and W. P. Halperin, *Advanced Cement Based Materials*, 1993, **1**, 67.
120. Z. R. Hinedi, A. C. Chang, M. A. Anderson and D. B. Borchardt, *Water Resources Res.*, 1997, **33**, 2697.
121. L. D. Hall, M. H. G. Amin, E. Dougherty, *Geoderma*, 1997, **80**, 431.
122. B. P. Hills, C. E. Manning, Y. Ridge and T. Brocklehurst, *J. Sci. Food. Agric.*, 1996, **71**, 185.
123. B. P. Hills and G. Lefloch, *Food Chem.*, 1994, **51**, 331.
124. F. D'Orazio, J. C. Tarczon, W. P. Halperin, K. Eguchi and T. Mizusaki, *J. Appl. Phys.*, 1989, **65**, 742–751.
125. G. Liu, Y.-Z. Li and J. Jonas, *J. Chem. Phys.*, 1989, **90**, 5881.

126. P. Porion, A. M. Faugere, P. Levitz, *et al.*, *Magn. Reson. Imaging*, 1998, **16**, 679.
127. S. Wonorahardjo, G. Ball, J. Hook and G. Moran, *Magn. Reson. Imaging*, 1998, **16**, 511.
128. S. G. Allen, P. C. L. Stephenson and J. H. Strange, *J. Chem. Phys.*, 1997, **106**, 7802.
129. G. Liu, Y. Li and J. Jonas, *J. Chem. Phys.*, 1991, **95**, 6892.
130. J.-P. Korb, S. Xu and J. Jonas, *J. Chem. Phys.*, 1993, **98**, 2411.
131. J.-P. Korb, A. Delville, S. Xu, G. Demeulenaere, P. Costa and J. Jonas, *J. Chem. Phys.*, 1994, **101**, 7074.
132. G. Liu, M. Mackowiak, Y. Li and J. Jonas, *J. Chem. Phys.*, 1991, **94**, 239.
133. J.-P. Korb, M. Winterhalter and H. M. McConnell, *J. Chem. Phys.*, 1984, **80**, 1059.
134. J.-P. Korb, L. Malier, F. Cros, S. Xu and J. Jonas, *Phys. Rev. Lett.*, 1996, **77**, 2312.
135. S. Stapf, R. Kimmich and J. Niess, *J. Appl. Phys.*, 1994, **75**, 529.
136. R. Kimmich and H. W. Weber, *Phys. Rev. B, Condensed Matter*, 1993, **47**, 11788.
137. T. Zavada, S. Stapf, U. Beginn and R. Kimmich, *Magn. Reson. Imaging*, 1998, **16**, 711.
138. S. Stapf and R. Kimmich, *J. Chem. Phys.*, 1995, **103**, 2247.
139. T. Zavada and R. Kimmich, *J. Chem. Phys.*, 1998, **109**, 6929.
140. T. Zavada, S. Stapf and R. Kimmich, *Magn. Reson. Imaging*, 1998, **16**, 695.
141. P. T. Callaghan, *Principles of Nuclear Magnetic Resonance Microscopy*, Clarendon Press, Oxford, 1991.
142. W. S. Price, *Concepts Magn. Reson.*, 1997, **9**, 299.
143. W. S. Price, *Concepts Magn. Reson.*, 1998, **10**, 197.
144. J. Kärger and W. Heink, *J. Magn. Reson.*, 1983, **51**, 1.
145. E. O. Stejskal and J. E. Tanner, *J. Chem. Phys.*, 1965, **42**, 288.
146. J. E. Tanner and E. O. Stejskal, *J. Chem. Phys.*, 1968, **49**, 1768.
147. P. T. Callaghan, A. Coy, T. P. J. Halpin, D. MacGowan, K. J. Packer and F. O. Zelaya, *J. Chem. Phys.*, 1992, **97**, 651.
148. P. T. Callaghan, D. MacGowan, K. J. Packer and F. O. Zelaya, *J. Magn. Reson.*, 1990, **90**, 177.
149. P. T. Callaghan, A. Coy, D. MacGowan, K. J. Packer and F. O. Zelaya, *Nature*, 1991, **351**, 467.
150. J. Stepisnik, *J. Magn. Reson.*, 1998, **131**, 339.
151. A. Coy and P. T. Callaghan, *J. Chem. Phys.*, 1994, **101**, 4599.
152. S. J. Gibbs, *J. Magn. Reson.*, 1997, **124**, 223.
153. P. T. Callaghan, *J. Magn. Reson.*, 1997, **129**, 74.
154. P. T. Callaghan, *J. Magn. Reson. Ser. A*, 1995, **113**, 53.
155. P. P. Mitra and P. N. Sen, *Physica A*, 1992, **186**, 109.
156. P. T. Callaghan, *J. Magn. Reson. Ser. A*, 1995, **113**, 53.
157. A. Coy and P. T. Callaghan, *J. Chem. Phys.*, 1994, **101**, 4599.
158. P. P. Mitra and B. I. Halperin, *J. Magn. Reson. Ser. A*, 1995, **113**, 94.
159. M. H. Blees, *J. Magn. Reson. Ser. A*, 1994, **109**, 203.
160. L. Z. Wang, A. Caprihan and E. Fukushima, *J. Magn. Reson. Ser. A*, 1995, **117**, 209.
161. A. Caprihan, L. Z. Wang and E. Fukushima, *J. Magn. Reson. Ser. A*, 1996, **118**, 94.
162. P. T. Callaghan, A. Coy, D. MacGowan and K. J. Packer, *J. Mol. Liq.*, 1992, **54**, 239.
163. A. Coy and P. T. Callaghan, *J. Colloid Interface Sci.*, 1994, **168**, 373.
164. A. Bhattacharya and S. D. Mahanti, *Phys. Rev. B: Condensed Matter*, 1997, **55**, 11230.
165. R. A. Damion and K. J. Packer, *Proc. R. Soc. London Ser. A*, 1997, **453**, 205.
166. P. N. Sen, M. D. Hürlimann and T. M. de Swiet, *Phys. Rev. B: Condensed Matter*, 1995, **51**, 601.
167. M. D. Hürlimann, T. M. de Swiet and P. N. Sen, *J. Non-Cryst. Solids*, 1995, **182**, 198.
168. P. Callaghan, D. MacGowan, K. J. Packer and F. O. Zelaya, *Magn. Reson. Imaging*, 1991, **9**, 663.
169. P. P. Mitra, *Physica A*, 1997, **241**, 122.
170. P. P. Mitra, P. N. Sen, L. M. Schwartz and P. Le Doussal, *Phys. Rev. Lett.*, 1992, **68**, 3555.
171. P. P. Mitra, P. N. Sen and L. M. Schwartz, *Phys. Rev. B*, 1993, **49**, 8565.

172. L. L. Latour, P. P. Mitra, R. L. Kleinberg and C. H. Sotak, *J. Magn. Reson. Ser. A*, 1993, **101**, 342.
173. P. N. Sen, L. M. Schwartz and P. P. Mitra, *Magn. Reson. Imaging*, 1994, **12**, 227.
174. E. J. Fordham, S. J. Gibbs and L. D. Hall, *Magn. Reson. Imaging*, 1994, **12**, 279.
175. M. D. Hürlimann, K. G. Helmer, L. L. Latour and C. H. Sotak, *J. Magn. Reson. Ser A*, 1994, **111**, 169.
176. P. N. Sen, L. M. Schwartz, P. P. Mitra and B. I. Halperin, *Phys. Rev. B: Condensed Matter*, 1994, **49**, 215.
177. A. J. Lucas, S. J. Gibbs, M. Peyron, G. K. Pierens, L. D. Hall, R. C. Stewart and D. W. Phelps, *Magn. Reson. Imaging*, 1994, **12**, 249.
178. L. L. Latour, R. L. Kleinberg, P. P. Mitra and C. H. Sotak, *J. Magn. Reson. Ser. A*, 1995, **112**, 83.
179. P. P. Mitra, L. L. Latour, R. L. Kleinberg and C. H. Sotak, *J. Magn. Reson. Ser. A*, 1995, **114**, 47.
180. M. D. Hürlimann, L. M. Schwartz and P. N. Sen, *Phys. Rev. B: Condensed Matter*, 1995, **51**, 14936.
181. L. M. Schwartz, M. D. Hürlimann, K. J. Dunn, P. P. Mitra and D. J. Bergman, *Phys. Rev. E*, 1997, **55**, 4225.
182. P. N. Sen and M. D. Hürlimann, *J. Chem. Phys.*, 1994, **101**, 5423.
183. J. E. Tanner, *J. Chem. Phys.*, 1970, **52**, 2523.
184. M. D. Hürlimann, K. G. Helmer, T. M. de Swiet and P. N. Sen, *J. Magn. Reson. Ser. A*, 1995, **113**, 260.
185. K. G. Helmer, M. D. Hürlimann, T. M. de Swiet, P. N. Sen and C. H. Sotak, *J. Magn. Reson. Ser. A*, 1995, **115**, 257.
186. J. E. M. Snaar and B. P. Hills, *Magn. Reson. Imaging*, 1997, **15**, 983.
187. J. Kärger, H. Pfeifer and S. Rudtsch, *J. Magn. Reson.*, 1989, **85**, 381.
188. P. T. Callaghan, M. E. Komlosh and M. Nyden, *J. Magn. Reson.*, 1998, **133**, 177.
189. K. J. Packer, C. Rees and D. J. Tomlinson, *Mol. Phys.*, 1970, **18**, 421.
190. D. van Dusschoten, P. A. de Jager and H. Van As, *J. Magn. Reson. Ser. A*, 1995, **112**, 237.
191. R. W. Mair, D. G. Cory, S. Peled, C. H. Tseng, S. Patz and R. L. Walsworth, *J. Magn. Reson.*, 1998, **135**, 478.
192. R. F. Karlicek Jr and I. J. Lowe, *J. Magn. Reson.*, 1980, **37**, 75.
193. R. M. Cotts, M. J. R. Hoch, T. Sun and J. T. Markert, *J. Magn. Reson.*, 1989, **83**, 252.
194. L. L. Latour, L. Li and C. H. Sotak, *J. Magn. Reson. Ser. B*, 1993, **101**, 72.
195a. A. J. Lucas, S. J. Gibbs, E. W. G. Jones, M. Peyron, J. A. Derbyshire and L. D. Hall, *J. Magn. Reson. Ser. A*, 1993, **104**, 272.
195b. D. Wu, A. Chen and C. S. Johnson Jr., *J. Magn. Reson. Ser. A*, 1995, **115**, 260.
196. S. J. Gibbs and C. S. Johnson Jr., *J. Magn. Reson.*, 1991, **93**, 395.
197. G. H. Sørland, B. Hafskjold and O. Herstad, *J. Magn. Reson.*, 1997, **124**, 172.
198. J. D. Seymour and P. T. Callaghan, *J. Magn. Reson. Ser. A*, 1996, **122**, 90.
199. B. Manz, P. Alexander and L. F. Gladden, *Phys. Fluids*, 1999, **11**, 259.
200. K. J. Packer and J. J. Tessier, *Mol. Phys.*, 1996, **87**, 267.
201. L. Lebon, J. Leblond, J. P. Hulin, N. S. Martys and L. M. Schwartz, *Magn. Reson. Imaging*, 1996, **14**, 989.
202. L. Lebon, L. Oger, J. Leblond, J. P. Hulin, N. S. Martys and L. M. Schwartz, *Phys. Fluids*, 1996, **8**, 293.
203. L. Lebon, J. Leblond and J. P. Hulin, *Phys. Fluids*, 1997, **9**, 481.
204. J. J. Tessier, K. J. Packer, J. F. Thovert and P. M. Adler. *AIChE J.*, 1997, **43**, 1653.
205. M. H. G. Amin, S. J. Gibbs, R. J. Chorley, K. S. Richards, T. A. Carpenter and L. D. Hall. *Proc. R. Soc. London Ser. A.*, 1997, **453**, 489.
206. U. Tallarek, D. van Dusschoten, H. Van As, E. Bayer, G. Guiochon, *J. Phys. Chem. B*, 1998, **102**, 3486.

207. J. J. Tessier and K. J. Packer, *Phys. Fluids*, 1998, **10**, 75.
208. P. T. Callaghan, W. Kockenberger and J. M. Pope, *J. Magn. Reson. Ser. B*, 1994, **104**, 183.
209. K. J. Packer, S. Stapf, J. J. Tessier and R. A. Damion, *Magn. Reson. Imaging*, 1998, **16**, 463.
210. S. Stapf, K. J. Packer, R. G. Graham, J. F. Thovert and P. M. Adler, *Phys. Rev. E*, 1998, **58**, 6206.
211. S. Stapf and K. J. Packer, *Appl. Magn. Reson.*, 1998, **15**, 303.
212. P. T. Callaghan and J. Stepisnik, *Adv. Magn. Opt. Reson.*, 1996, **19**, 325.
213. J. D. Seymour and P. T. Callaghan, *AIChE J.*, 1997, **43**, 2096.
214. B. Manz, P. Alexander, P. B. Warren and L. F. Gladden, *Magn. Reson. Imaging*, 1998, **16**, 673.
215. D. L. Koch and J. F. Brady, *J. Fluid Mech.*, 1985, **154**, 399.
216. G. Taylor, *Proc. R. Soc. London Ser. A*, 1953, **219**, 186.
217. P. Mansfield and P. K. Grannell, *J. Phys. C: Solid State Phys.*, 1973, **6**, L422.
218. A. Sodickson and D. G. Cory, *Prog. Nucl. Magn. Reson.*, 1998, **33**, 77.
219. P. Blümler and B. Blümich, *NMR Basic Principles and Progress*, 1994, **30**, 209.
220. J. B. Miller, *Prog. Nucl. Magn. Reson.*, 1998, **33**, 273.
221. P. J. McDonald, *Prog. Nucl. Magn. Reson.*, 1997, **30**, 69.
222. C. J. Rofe, J. Van Noort, P. J. Back and P. T. Callaghan, *J. Magn. Reson. Ser. B*, 1995, **108**, 125.
223. P. T. Callaghan, L. C. Forde and C. J. Rofe, *J. Magn. Reson. Ser. B*, 1994, **104**, 34.
224. W. B. Hyslop and P. C. Lauterbur, *J. Magn. Reson.*, 1991, **94**, 501.
225. B. Pütz, D. Barsky and K. Schulten, *J. Magn. Reson.*, 1992, **97**, 27.
226. P. T. Callaghan, A. Coy, L. C. Forde and C. J. Rofe, *J. Magn. Reson. Ser. A*, 1993, **110**, 347.
227. P. T. Callaghan and S. L. Codd, *Magn. Reson. Imaging*, 1998, **16**, 471.
228. J. Stepisnik, A. Duh, A. Mohoric and I. Sersa, *J. Magn. Reson.*, 1999, **137**, 154.
229. P. A. Osment, K. J. Packer, M. J. Taylor, *et al.*, *Phil. Trans. R. Soc. London Ser. A*, 1990, **333**, 441.
230. M. R. Merrill, *Appl. Magn. Reson.*, 1993, **5**, 317.
231. S. H. Chen, F. F. Qin, K. H. Kim and A. T. Watson, *AIChE J.*, 1993, **39**, 925.
232. S. H. Chen, F. F. Qin and A. T. Watson, *AIChE J.*, 1994, **40**, 1238.
233. C. A. Baldwin, A. J. Sederman, M. D. Mantle, P. Alexander and L. F. Gladden, *J. Colloid Interface Sci.*, 1996, **181**, 79.
234. A. J. Sederman, M. L. Johns, P. Alexander and L. F. Gladden, *Chem. Eng. Sci.*, 1998, **53**, 2117.
235. L. F. Gladden and P. Alexander, *Measur. Sci. Technol.*, 1996, **7**, 423.
236. A. J. Sederman, M. L. Johns, A. S. Bramley, P. Alexander and L. F. Gladden, *Chem. Eng. Sci.*, 1997, **52**, 2239.
237. A. J. Sederman, M. L. Johns, P. Alexander and L. F. Gladden, *Magn. Reson. Imaging*, 1998, **16**, 497.
238. J. J. Attard, T. A. Carpenter, L. D. Hall, S. Davies, M. J. Taylor and K. J. Packer, *Magn. Reson. Imaging*, 1991, **9**, 815.
239. G. K. Pierens, M. Peyron, A. J. Lucas, *et al.*, *Magn. Reson. Imaging*, 1994, **12**, 323.
240. P. Mansfield and B. Issa, *Magn. Reson. Imaging*, 1994, **12**, 275.
241. S. J. Gibbs, T. A. Carpenter and L. D. Hall, *J. Magn. Reson.*, 1992, **98**, 183.
242. S. J. Gibbs, J. J. Attard and L. D. Hall, *AIChE J.*, 1993, **39**, 689.
243. M. P. Hollewand and L. F. Gladden, *J. Catal.*, 1993, **144**, 254.
244. L. F. Gladden, M. P. Hollewand and P. Alexander, *AIChE J.*, 1995, **41**, 894.
245. M. Hollewand and L. F. Gladden, *Chem. Eng. Sci.*, 1995, **50**, 327.
246. S. P. Rigby and L. F. Gladden, *J. Catal.*, 1998, **173**, 484.
247. S. P. Rigby and L. F. Gladden, *Chem. Eng. Sci.*, 1996, **51**, 2263.
248. S. Rigby, K. Y. Cheah and L. F. Gladden, *Appl. Catal. A: General*, 1996, **144**, 377.
249. W. A. Edelstein, H. J. Vinegar, P. N. Tutunjian, P. B. Roemer and O. M. Mueller, *Proceedings 63rd Annual Technology Conference, Society of Petroleum Engineers*, 1988, p. 101.

250. J. J. Dechter, R. A. Komoroski and S. Ramaprasad, *J. Magn. Reson.*, 1991, **93**, 142.
251. L. D. Hall, V. Rajanayagam and C. Hall, *J. Magn. Reson.*, 1986, **68**, 185.
252. S. Davies, A. Hardwick, D. Roberts, K. Spowage and K. J. Packer, *Magn. Reson. Imaging*, 1994, **12**, 349.
253. S. N. Sarkar, J. J. Dechter and R. A. Komoroski, *J. Magn. Reson. Ser. A*, 1993, **102**, 314.
254. M. A. Horsfield, C. Hall and L. D. Hall, *J. Magn. Reson.*, 1990, **87**, 319.
255. C. A. Baldwin, P. Alexander and L. F. Gladden, *J. Magn. Reson. Ser. A*, 1995, **112**, 169.
256. P. Majors, P. Li and E. Peters, *SPE Formation Evaluation*, 1997, **12**, 164.
257. J. D. Chen, M. M. Dias, S. Patz and L. M. Schwartz, *Phys. Rev. Lett.*, 1988, **61**, 1489.
258. B. A. Baldwin and W. S. Yamanashi, *SPE Reservoir Eng.*, 1989, **4**, 207.
259. P. D. Majors, J. L. Smith, F. S. Kovarik and E. Fukushima, *J. Magn. Reson.*, 1990, **89**, 470.
260. M. L. Johns and L. F. Gladden, *J. Colloid Interface Sci*, 1999, **210**, 261.
261. C. A. Baldwin and L. F. Gladden, *AIChE J.*, 1996, **42**, 1341.
262. M. L. Johns and L. F. Gladden, *Magn. Reson. Imaging*, 1998, **16**, 655.
263. M. Pervizpour, S. Pamukcu and H. Moo-Young, *J. Comput. Civil Eng.*, 1999, **13**, 96.
264. H. Van As and D. van Dusschoten, *Geoderma*, 1997, **80**, 389.
265. M. H. G. Amin, R. J. Chorley, K. S. Richards, L. D. Hall, T. A. Carpenter, M. Cislerova and T. Vogel, *Hydrol. Processes*, 1997, **11**, 471.
266. M. H. G. Amin, L. D. Hall, R. J. Chorley and K. S. Richards, *Prog. Phys. Geography*, 1998, **22**, 135.
267. A. E. Fischer, B. J. Balcom, E. J. Fordham, T. A. Carpenter and L. D. Hall, *J. Phys. D: Appl. Phys.*, 1995, **28**, 384.
268. P. Mansfield, *J. Phys. C: Solid State Phys.*, 1977, **10**, L55.
269. D. N. Guilfoyle, P. Mansfield and K. J. Packer, *J. Magn. Reson.*, 1992, **97**, 342.
270. A. M. Peters, P. S. Robyr, R. W. Bowtell and P. Mansfield, *Magn. Reson. Imaging*, 1996, **14**, 875.
271. D. N. Guilfoyle, B. Issa and P. Mansfield, *J. Magn. Reson., Ser. A*, 1996, **119**, 151.
272. B. Manz, P. S. Chow and L. F. Gladden, *J. Magn. Reson.*, 1999, **136**, 226.
273. M. P. Hollewand and L. F. Gladden, *Magn. Reson. Imaging*, 1994, **12**, 291.
274. I. V. Koptyug, V. B. Fenelonov, L. Y. Khitrina, R. Z. Sagdeev and V. N. Parmon, *J. Phys. Chem. B*, 1998, **102**, 3090.
275. A. Caprihan and E. Fukushima, *Phys. Rep.*, 1990, **192**, 195.
276. E. Fukushima, *Annu. Rev. Fluid Mech.*, 1999, **31**, 95.
277. P. T. Callaghan and Y. Xia, *J. Magn. Reson.*, 1991, **91**, 326.
278. K R. Jeffrey, P. T. Callaghan and Y. Xia, *Food Res. Int.*, 1994, **27**, 199.
279. Y. Xia, P. T. Callaghan and K. R. Jeffrey, *AIChE J.*, 1992, **38**, 1408.
280. K. Y. Chung, G. Belfort, W. A. Edelstein and X. M. Li, *AIChE J.*, 1993, **39**, 1592.
281. B. Newling, S. J. Gibbs, J. A. Derbyshire, *et al.*, *J. Fluids Eng.: Trans. ASME*, 1997, **119**, 103.
282. J. D Seymour, J. E. Maneval, K. L. McCarthy, R. L. Powell and M. J. McCarthy, *J. Texture Stud.*, 1995, **26**, 89.
283. S. J. Gibbs, K. L. James, L. D. Hall, D. E. Haycock, W. J. Frith and S. Ablett, *J. Rheol.*, 1996, **40**, 425.
284. M. M. Britton, P. T. Callaghan, M. L. Kilfoil, R. W. Mair and K. M. Owens, *Appl. Magn. Reson.*, 1998, **15**, 287.
285. S. J. Gibbs, D. E. Haycock, W. J. Frith, S. Ablett and L. D. Hall, *J. Magn. Reson.*, 1997, **125**, 43.
286. A. D. Hanlon, S. J. Gibbs, L. D. Hall, D. E. Haycock, W. J. Frith and S. Ablett, *Magn. Reson. Imaging*, 1998, **16**, 953.
287. W. Kockenberger, J. M. Pope, Y. Xia, K. R. Jeffrey, E. Komor and P. T. Callaghan, *Planta*, 1997, **201**, 53.
288. V. Rajanayagam, S. G. Yao and J. M. Pope, *Magn. Reson. Imaging*, 1995, **13**, 729.

289. Y. E. Kutsovsky, L. E. Scriven, H. T. Davis and B. E. Hammer, *Phys. Fluids*, 1996, **8**, 863.
290. C. T. P. Chang and A. T. Watson, *AIChE J.*, 1999, **45**, 437.
291. N. C. Irwin, S. A. Altobelli, J. H. Cushman and R. A. Greenkorn, *Magn. Reson. Imaging*, 1998, **16**, 493.
292. J. A. Derbyshire, S. J. Gibbs, T. A. Carpenter and L. D. Hall, *AIChE J.*, 1994, **40**, 1404.
293. B. Newling, S. J. Gibbs, L. D. Hall, D. E. Haycock, W. J. Frith and S. Ablett, *Chem. Eng. Sci.*, 1997, **52**, 2059.
294. D. Xing, S. J. Gibbs, J. A. Derbyshire, E. J. Fordham, T. A. Carpenter and L. D. Hall, *J. Magn. Reson. Ser. B*, 1995, **106**, 1.
295. S. Davies, A. Hardwick, K. Spowage and K. J. Packer, *Magn. Reson. Imaging*, 1994, **12**, 265.
296. M. R. Merrill, *AIChE J.*, 1994, **40**, 1262.
297. M. R. Merrill and Z. S. Jin, *Magn. Reson. Imaging*, 1994, **12**, 345.
298. P. Mansfield and B. Issa, *J. Magn. Reson. Ser. A*, 1996, **122**, 137.
299. B. Issa, M. A. Al Mugheiry and P. Mansfield, *Magn. Reson. Imaging*, 1996, **14**, 933.
300. R. A. Waggoner and E. Fukushima, *Magn. Reson. Imaging*, 1996, **14**, 1085.
301. J. Fraissard and T. Ito, *Zeolites*, 1988, **8**, 350.
302. P. J. Barrie and J. Klinowski, *Prog. Nucl. Magn. Reson. Spectrosc.*, 1992, **24**, 91.
303. C. Dybowski, N. Bansal and T. M. Duncan, *Annu. Rev. Phys. Chem.*, 1991, **42**, 433.
304. D. Raftery and B. Chmelka, *NMR Basic Principles and Progress*, 1994, **30**, 111.
305. M. A. Springuel-Huet, J. L. Bonardet and J. Fraissard, *Appl. Magn. Reson.*, 1995, **8**, 427.
306. J. A. Ripmeester and C. I. Ratcliffe, *Anal. Chim. Acta*, 1993, **283**, 1103.
307. S.-B. Liu, B. M. Fung, T. C. Yang, *et al.*, *J. Phys. Chem.*, 1994, **98**, 4393.
308. B. Boddenberg and A. Seidel, *J. Chem. Soc., Faraday Trans.*, 1994, **90**, 1345.
309. T. T. P. Cheung, *J. Phys. Chem.*, 1995, **99**, 7089.
310. C. J. Jameson, *Annu. Rev. Phys. Chem.*, 1996, **47**, 135.
311. C. J. Jameson, A. K. Jameson, R. E. Gerald and H. M. Lim, *J. Phys. Chem. B*, 1997, **101**, 8418.
312. J. H. Kantola, J. Vaara, T. T. Rantala and J. Jokisaari, *J. Chem. Phys.*, 1997, **107**, 6470.
313. F. Vigné-Maeder, *J. Phys. Chem.*, 1994, **98**, 4666.
314. V. Gupta, H. T. Davis and A. V. McCormick, *J. Phys. Chem.*, 1996, **100**, 9824.
315. V. Gupta, D. Kim, H. T. Davis and A. V. McCormick, *J. Phys Chem. B*, 1997, **101**, 129.
316. R. J. Schadt, E. J. Cain and A. D. English, *J. Phys. Chem.*, 1993, **97**, 8387.
317. L. M. Bull, N. J. Henson, A. K. Cheetham, J. M. Newsam and S. J. Heyes, *J. Phys. Chem.*, 1993, **97**, 11776.
318. L. M. Bull, A. K. Cheetham, B. M. Powell, J. A. Ripmeester and C. I. Ratcliffe, *J. Am. Chem. Soc.*, 1995, **117**, 4328.
319. S. M. Auerbach, L. M. Bull, N. J. Henson, H. I. Metiu and A. K. Cheetham, *J. Phys. Chem.*, 1996, **100**, 5923.
320. P. Alexander and L. F. Gladden, *Zeolites*, 1997, **18**, 38.
321. S. M. Auerbach, *J. Chem. Phys.*, 1997, **106**, 7810.
322. L. F. Gladden, J. A. Sousa Gonçalves and P. Alexander, *J. Chem. Phys. B*, 1997, **101**, 10121.
323. J. Kärger and D. M. Ruthven, *Diffusion in Zeolites and Other Microporous Solids*, Wiley, New York, 1992.
324. J. Kärger, H. Pfeifer and W. Heink, *Adv. Magn. Reson.*, 1988, **12**, 1.
325. U. Hong, J. Kärger and H. Pfeifer, *J. Am. Chem. Soc.*, 1991, **113**, 4812.
326. R. Q. Snurr and J. Kärger, *J. Phys. Chem. B*, 1997, **101**, 6469.
327. J. Kärger, M. Petzold, H. Pfeifer, H. Ernst and J. Weitkamp, *J. Catal.*, 1992, **136**, 283.
328. C. Rödenbeck, J. Kärger and K. Hahn, *Phys. Rev. E*, 1997, **55**, 5697.
329. V. Kukla, J. Kornatowski, D. Demuth, *et al.*, *Science*, 1996, **272**, 702.
330. K. Hahn, J. Kärger and V. Kukla, *Phys. Rev. Lett.*, 1996, **76**, 2762.

Index

Note — Page numbers in *italic* type refer to figures and tables.